Evolutionary Adaptation of Developmental Plasticity in the Nematode *Pristionchus pacificus*

Dissertation

der Mathematisch-Naturwissenschaftlichen Fakultät

der Eberhard Karls Universität Tübingen

zur Erlangung des Grades eines

Doktors der Naturwissenschaften

(Dr. rer. nat.)

vorgelegt von

Penghieng Theam

aus Phnom Penh, Kambodscha

Tübingen

2026

Gedruckt mit Genehmigung der Mathematisch-Naturwissenschaftlichen Fakultät der Eberhard Karls Universität Tübingen.

Tag der mündlichen Qualifikation:	24.06.2026
Dekan:	Prof. Dr. Thilo Stehle
1. Berichterstatter/-in:	Prof. Dr. Ralf J. Sommer
2. Berichterstatter/-in:	Prof. Dr. Karl Forchhammer

Table of Contents

I. Summary ..... **i**
II. Zusammenfassung ..... **ii**
III. List of publications ..... **iii**
1. Introduction **1**
1.1. Phenotypic plasticity: a common phenomenon, a contentious concept, and an important driver of evolution **1**
1.1.1. The nature of phenotypic plasticity 1
1.1.2. Mounting empirical evidence for plasticity-led evolution in the age of molecular biology 7
1.2. Nematode systems: abundant in nature, versatile for biological research, and emerging models for phenotypic plasticity research **10**
1.2.1. Nematodes as model organisms 10
1.2.2. Phenotypic plasticity in nematodes 12
1.2.3. *Pristionchus pacificus* as lab rats for resource polyphenism studies 14
2. Research objectives **20**
3. Results **21**
3.1. Thousands of *Pristionchus pacificus* orphan genes were integrated into developmental networks that respond to diverse environmental microbiota **21**
3.1.1. Synopsis 21
3.1.2. Own contribution 21
3.2. Description of two new *Pristionchus* species from South Korea **22**
3.2.1. Synopsis 22
3.2.2. Own contribution 22
3.3. *Pristionchus kravanhensis* n. sp., the first *Pristionchus* species reported from Cambodia **23**
3.3.1. Synopsis 23
3.3.2. Own contribution 23
3.4. Biosynthesis of modular signaling molecules requires functional diversification of carboxylesterases in *Pristionchus pacificus* **24**
3.4.1. Synopsis 24
3.4.2. Own contribution 24
3.5. Bacterial diet influences mutation rate in *Pristionchus pacificus* **25**
3.5.1. Synopsis 25
3.5.2. Own contribution 25
3.6. The dynamics of coexistence and succession in a decaying ecosystem **26**
3.6.1. Synopsis 26
3.6.2. Own contribution 26
3.7. Evidence of a predator-prey co-evolutionary arms race within a nematode microhabitat **27**
3.7.1. Synopsis 27
3.7.2. Own contribution 27

3.8. Plasticity in nonsense-mediated decay and translation initiation regulate polyphenism 28
3.8.1. Synopsis 28
3.8.2. Own contribution 28
4. Discussion 29
5. References 34
6. Appendix 63

Acknowledgements

First and foremost, I would like to express my sincere gratitude to the German taxpayers for supporting research through the Max Planck Society. I am also deeply grateful to my supervisor, Prof. Dr. Ralf J. Sommer, for his guidance, mentorship, and support throughout the years. His supervising style—providing significant research freedom—is also highly appreciated as it has allowed me to dive into various research directions and grow as a scientist. My Thesis Advisory Committee members, Prof. Dr. Karl Forchhammer and Dr. Honour C. McCann, are also thanked for their input across project meetings.

My thanks are also extended to former and current members of the Sommer Lab over the course of my PhD journey for countless memories to be looked back at and the collaborative interdisciplinary research environment. Scientific input from Dr. Matthias Herrmann, Dr. Christian Rödelsperger, Dr. Cátia Igreja and Dr. Adrian Streit has contributed to my scientific skills. Thank you, Matthias and Chris W., for imparting your fieldwork skills to me as well as good memories during beetle-nematode collection trips to the tropical Réunion, Laos and Cambodia. Thank you, Christian, Cátia and Matthias, for wide-ranging and stimulating scientific discussions. These have shaped my scientific thinking.

I would like to specially thank lab 17 crew versions 1 and 2 during my time at the Sommer Lab including Shuai, Sara and Veysi (v1) and Rebecca, Berke and Jiajia (v2) for friendship, scientific and non-scientific discussions, and great times inside and outside the lab. Hanh, thank you very much for always having my back and I will miss you dearly. Veroni, Radhika, Chris, Marina, Tobi, Yinan and Victor, thank you for the great times. Thank you, Hanh, Heike, Walli, Chris, Tobi and Doro, for your assistance with my PhD research. I also would like to thank lab technical support staff, Steffi, Aida, Saskia and Alex. Support from scientific facilities including the Genome Center, Electron Microscopy, Mass Spectrometry and BioOptics are also appreciated. I would like to thank Prof. Dr. Chuanfu Dong, Dr. Ata Kalirad and Dr. James W. Lightfoot for project collaborations.

My thanks also go to the Research Support Team and International Office for support with administrative matters.

During this period, emotional support from friends outside the MPI including Regina Betz and her Kürzinger family, Bram Ulrichts, Martina Cassanmagnago, Luca Giurdanella and Lukas Fäßler is also appreciated.

Finally, I would like to wholeheartedly thank my wife Sunheng Yon and our families for unwavering support during this stage of my life.

I dedicate this work to the very small number of past and present scientists of Cambodian origin. I also humbly hope it can help to inspire others in the country to join the field of science.

I. Summary

Developmental or phenotypic plasticity refers to the ability of living organisms to execute varying phenotypes in response to changes in the environment. This phenomenon has been implicated to play an important role in the plasticity-led evolution concept, where it gives rise to trait novelty and ultimately speciation. The nematode *Pristionchus pacificus* has been important model system to study developmental plasticity at the mechanistic level. This species has a discrete feeding dimorphism. While the narrow-mouthed stenostomatous (St) morph possesses a single tooth and is able to feed strictly on bacteria, the wide-mouthed eurystomatous (Eu) morph has two teeth enabling them to become omnivorous feeding on both bacteria and nematodes. Over the past decade, efforts to study the genetic and molecular control of the mouth-form decision have resulted in a robust mouth-form plasticity gene regulatory network (GRN) from the most upstream to the most downstream modules. In this GRN, the sulfation pathway, especially the sulfatase enzyme EUD-1, plays a central role in the phenotype switching. Additionally, the environmental stimuli influencing this feeding plasticity have also been determined, for example, pheromones. However, there are still certain knowledge gaps to be filled. For instance, the evolutionary adaptation of this developmental plasticity remains to be further investigated. In my PhD dissertation, the contribution in addressing this question is fourfold. 1) The main mouth-form switch protein, EUD-1, in the *P. pacificus* mouth-form GRN evolves repeatedly at the microevolutionary timescale. Interestingly, there exist N-terminal proteoforms, i.e., the two first exons have a start codon each, which serve as an evolutionary 'back-up' strategy in the genetic drift events of exon 1 or exon 2 deleterious alleles in the wild. 2) This GRN has evolved to be robust in dictating the mouth-form fate. It acts downstream of the pheromonal signals and reliably executes the mouth-form decision even when the pheromone biosynthesis is disrupted. 3) In the metacommunity settings, wherein *P. pacificus* coexists with other nematodes, its ability to have and employ the plastic intraguild feeding plays out in its advantage in the species succession and coexistence. This finding conforms with the notion that developmental plasticity is evolutionary important in ecological interactions. 4) Across a larger phylogenetic context of the whole *Pristionchus* genus, the adaptive mouth-form plastic trait is evolutionarily labile. While some species have secondarily lost the plasticity, i.e., the feeding structure has become monomorphic, this trait has evolved to be more complicated, for example, the transition from dimorphism to trimorphism. Overall, this dissertation serves as an additional cornerstone in progressing our understanding of the evolutionary adaptation of an adaptive plastic trait with supporting empirical data.

II. Zusammenfassung

Phänotypische Plastizität beschreibt die Fähigkeit von Lebewesen als Reaktion auf Veränderungen in ihrer Umgebung unterschiedliche Phänotypen bzw. Erscheinungsformen anzunehmen. Dieses Phänomen spielt eine wichtige Rolle im Konzept der plastizitätsgesteuerten Evolution, das zur Entstehung neuer Merkmale und letztlich zur Artbildung führt. Der Fadenwurm *Pristionchus pacificus* ist ein wichtiges Modellsystem und Versuchstier um phänotypische Plastizität auf molekularer Ebene zu untersuchen. Diese Art weist einen ausgeprägten Ernährungs-Dimorphismus auf. Während die schmalmündige 'stenostomate' Form (St) einen einzigen Zahn besitzt und sich ausschließlich von Bakterien ernährt, hat die breitmündige 'eurystomate' Form (Eu) zwei Zähne, wodurch sie sich sowohl von Bakterien als auch von anderen Fadenwürmern ernähren kann. In den letzten zehn Jahren haben Bemühungen zur Erforschung der genetischen und molekularen Steuerung der Entscheidung über die Mundform zu einem robusten Genregulationsnetzwerk (GRN) für die Mundformplastizität geführt, welches zahlreiche gut charakterisierte Module umfasst. In diesem GRN spielt der Sulfatierungsweg, insbesondere das Sulfatase-Enzym EUD-1, eine zentrale Rolle bei der Merkmalsausprägung und wird deshalb als 'switch' Gen bezeichnet. Darüber hinaus wurden auch die Umweltreize bestimmt, die diese Plastizität beeinflussen, beispielsweise Pheromone. Es gibt jedoch noch zahlreiche Wissenslücken, die geschlossen werden müssen, so z.B. die evolutionäre Anpassung dieser phänotypischen Plastizität. In meiner Doktorarbeit trage ich in vier Punkten zur Beantwortung mehrerer bisher ungelöster Fragen bei. 1) Das wichtigste Protein für den Wechsel der Mundform, EUD-1, im GRN von *P. pacificus* entwickelt sich auf mikroevolutionärer Zeitskala wiederholt weiter. Interessanterweise gibt es N-terminale Proteoformen, d. h. die ersten beiden Exons haben jeweils ein Startcodon, die als evolutionäre „Backup"-Strategie bei genetischen Drift-Ereignissen von schädlichen Allelen in Exon 1 oder Exon 2 in der Natur dienen. 2) Dieses GRN hat sich zu einem robusten Faktor entwickelt, der das Schicksal der Mundform bestimmt. Es wirkt downstream der Pheromonsignale und führt die Entscheidung über die Mundform auch dann zuverlässig aus, wenn die Pheromonbiosynthese gestört ist. 3) In der Metagemeinschaft, in der *P. pacificus* mit anderen Nematoden koexistiert, spielt sich seine Fähigkeit, das plastische räuberische Verhalten zu nutzen, zu seinem Vorteil in der Artenfolge und Koexistenz aus. Diese Erkenntnis steht im Einklang mit der Vorstellung, dass phänotypische Plastizität in ökologischen Interaktionen wichtig ist. 4) Im größeren phylogenetischen Kontext der gesamten Gattung *Pristionchus* ist das adaptive plastische Merkmal der Mundform evolutionär labil. Während einige Arten die Plastizität sekundär verloren haben, d. h. die Fressstruktur monomorph geworden ist, hat sich dieses Merkmal zu einer komplexeren Form entwickelt, beispielsweise durch den Übergang vom Dimorphismus zu einem Trimorphismus. Insgesamt leistet diese Dissertation einen weiteren wichtigen Beitrag, unser Verständnis der evolutionären Anpassung eines adaptiven plastischen Merkmals durch unterstützende empirische Daten voranzutreiben.

III. List of publications

1. Athanasouli, M., N. Akduman, W. Röseler, **P. Theam**, and C. Rödelsperger. 2023. Thousands of *Pristionchus pacificus* orphan genes were integrated into developmental networks that respond to diverse environmental microbiota. *PLoS Genet.* 19:e1010832.

2. Herrmann, M., N. Kanzaki, C. Weiler, **P. Theam**, C. Rödelsperger, and R. J. Sommer. 2024. Description of two new *Pristionchus* species from South Korea. *J. Nematol.* 56:20240032.

3. **Theam, P.**, N. Kanzaki, M. Herrmann, C. Weiler, C. Rödelsperger, and R. J. Sommer. 2025. *Pristionchus kravanhensis* n. sp., the first *Pristionchus* species reported from Cambodia. *Nematology* 27:651–663.

4. Zhang, P.[#], **P. Theam**[#], W. Xu[#], S. Ye, H. Witte, T. Liu, R. J. Sommer, and C. Dong. 2025. Biosynthesis of modular signaling molecules requires functional diversification of carboxylesterases in *Pristionchus pacificus*. *Commun. Biol.* 8:1213. (# denotes co-first authors)

5. Wang, Y.[#], **P. Theam**[#], S. P. Quiobe[#], W. Röseler, H. Witte, C. Rödelsperger, and R. J. Sommer. 2026. Bacterial diet influences mutation rate in *Pristionchus pacificus*. *G3* 16:jkag038. (# denotes co-first authors)

6. Kalirad, A., **P. Theam**, and R. J. Sommer. 2025. The dynamics of coexistence and succession in a decaying ecosystem. *bioRxiv* 2025.04.28.650976.

7. Goetting, D. L., K. K. Sarai, **P. Theam**, R. J. Sommer, and J. W. Lightfoot. 2026. Evidence of a predator-prey co-evolutionary arms race within a nematode microhabitat. *bioRxiv* 2026.04.02.716111.

8. **Theam, P.**, H. Witte, R. Liu, T. Loschko, C. Rödelsperger, C. Igreja, and R. J. Sommer. 2026. Plasticity in nonsense-mediated decay and translation initiation regulate polyphenism. *bioRxiv* 2026.03.27.714762.

Manuscripts not included in this dissertation:

1. Wighard, S., **P. Theam**, C. Rödelsperger, and R. J. Sommer. Multiple evidence for environmental sex determination in the hermaphroditic nematode *Allodiplogaster sudhausi*. *In preparation*.

2. **Theam, P.**, P. Vaninetti, B. Güner, R. Liu, D.-L. Vu, C. Igreja, and R. J. Sommer. Evolution and biosynthesis of sulfated lipids in *Pristionchus* nematodes. *In preparation*.

3. **Theam, P.**, B. Güner, N. Kanzaki, and R. J. Sommer. Description of a new nematode genus in the family Rhabditidae. *In preparation*.

1. Introduction

"*Nothing in evolution or ecology makes sense except in the light of the other.*"
Pelletier et al. (2009)

1.1. Phenotypic plasticity: a common phenomenon, a contentious concept, and an important driver of evolution

1.1.1. The nature of phenotypic plasticity

Virtually, all living organisms need to flexibly respond within certain ranges to both abiotic and biotic environmental factors for their survival (Grime and Pierce 2012). The ability of a single genotype to express distinct phenotypes depending on environmental stimuli is commonly referred to as 'phenotypic plasticity' (also dubbed 'developmental plasticity'). This common phenomenon includes all aspects of traits including physiology, morphology, behaviour, and life history (West-Eberhard 1989; Pigliucci 2005). Not unlike or maybe more than other concepts in biology, the universal acceptance of what the term phenotypic plasticity entails has not been smooth due to the existence of various historical terminologies and definitions and their corresponding methodological pipelines (Sultan 2021; Gómez et al. 2025). Another and arguably more important aspect hindering the proper appreciation of phenotypic plasticity is rather conceptual: is phenotypic plasticity just a mere noise in the gene-centric world, and, if at all it is relevant, does it contribute to evolution? These are indeed some of the core questions in the ongoing phenotypic plasticity studies (Wund 2012; Pfennig 2021; Schlichting 2021).

In her impactful monograph *Developmental Plasticity and Evolution*, West-Eberhard (2003) significantly contributed to the 'plasticity-led evolution' concept. She presented a four-step synthesis of adaptive evolution. First, *an alternative trait variant originates* from the pre-existing phenotype due to a genetic mutation or a novel environmental input. Second, the newly arisen trait goes through a '*phenotypic accommodation*' phase in which immediate and further adjustments of development take place and improve the functioning of that trait. Third, the *recurrence of mutational or environmental initiating factor* induces a subpopulation of individuals expressing the trait. Lastly, there exists a '*genetic accommodation*' phase in which gene frequencies are affected by selection on the regulation, shape, and/or side-effects of the novel trait persisting in the above-mentioned subpopulation. It should be noted that the 'genetic accommodation' step can be followed by a 'genetic assimilation' step wherein the novel trait becomes 'genetically fixed' and is expressed without the need for the novel environmental signal anymore. Of note, oftentimes Conrad H. Waddington also interchangeably referred to 'genetic assimilation' as 'canalisation' (Waddington 1953; Pigliucci et al. 2006; Sommer 2020).

Despite providing a conceptual framework for the role of phenotypic plasticity in evolution, West-Eberhard's hypothesis would not go unquestioned. For example, starting from the definition of 'phenotypic plasticity' used by West-Eberhard itself,

Nicoglou (2013) emphasised that it is still restricted by failing to cover the plasticity in 'embryological tradition' and, in essence, is not really an inclusive operative concept for 'developmental plasticity' as claimed. The constraints of phenotypic plasticity due to their associated costs and limits have also been a question (DeWitt et al. 1998; van Kleunen and Fischer 2005). de Jong (2005) acknowledged that phenotypic plasticity, just as genetic variation, can lead to trait optimum and be favoured by selection if it is not physiologically constrained. However, phenotypic plasticity per se is not a mechanism in evolution. Additionally, the concept of genetic assimilation has been sidelined (Simpson 1953; Williams 1966; Orr 1999). Above all, the main pushback for the plasticity-led evolution concept may have to do with the fact that it has been perceived that there are not enough supporting empirical data (Wray et al. 2014). Nevertheless, this view has been challenged by the ever-emerging body of both theoretical and empirical evidence over the last decade with the 'plasticity-led evolution' theory, which will be discussed in greater detail below, earning its rightful place in a modern-day evolutionary biology book (Levis and Pfennig 2016, 2019; Uller et al. 2020, 2024; Lala et al. 2024).

To account for these concerns and to fully appreciate the role of phenotypic plasticity in evolution, we have to look at the nature of phenotypic plasticity.

First, this phenomenon is widespread across literally all living organisms as Moczek (2015) put it:

> *Developmental plasticity is everywhere, from microtubule and synapse formation to allometries and learning. To develop is to be plastic. To make traits come into being is to utilize developmental plasticity. Research in developmental plasticity thus deserves to be recognized for what it really is—an investigation of phenomena of fundamental importance to the genesis of all traits, in all organisms.*

Indeed, the list of documented phenotypically plastic traits comprises of cases across the tree of life, for instance, responses to the availability of nitrogen and stress in archaea (Hackley and Schmid 2019; Hwang et al. 2019), cell elongation in nutrient-poor environments, functional dimorphism, and cooperative trait in iron-scavenging in bacteria (Akhurst 1980; Kümmerli et al. 2009; Delaby et al. 2025), environmentally-stimulated morphological and behavioural changes in protists (Hamilton 1975; Mulot et al. 2017; Pan et al. 2024), predator-induced polyphenolic production and aging-associated expression of varying ecomorphs in algae (Van Alstyne 1988; Trainor and Egan 1991), sex reversal and body size changes in response to nutrient levels in nematodes (Papadopoulou and Triantaphyllou 1982; Fonderie et al. 2013), phenotypic switching and inducible defence strategies in fungi (Jain et al. 2008; Döll et al. 2013), expression of distinct leaf morphologies in submerged or ambient growth condition and biomass allocation alterations in response to changing environments in plants (Bruni et al. 1996; Sultan 2003), defensive behavioural changes in response to chemical cues and tactile input and morphological variation across environments in mobile crustaceans and changes in genital and feeding-leg length in response to

differences in density and wave-exposure and settlement-site-induced shape variation in sessile crustaceans (Hazlett and McLay 2000; Haye et al. 2010, Neufeld 2011; De Filippo et al. 2025), phase variation, horn size differences, and reproductive mode changes in insects (Ananthakrishnan 2005), environmentally induced morph variation in coral reefs (Dubé et al. 2017; Ducret et al. 2026), prey-induced shell colouration adjustments and predatory-induced variations in shell shape, growth rate, and life-history traits in mollusks (Manríquez et al. 2009; Bourdeau et al. 2015), morphological changes due to the presence of predators or environmental fluctuations in fish (Brönmark and Miner 1992; Imre et al. 2002; Crispo and Chapman 2010; Meuthen et al. 2018), diet-induced plumage colour changes and predator-induced changes in nest site selection and feeding rates in birds and plastic reproductive traits attributed to prey availability and environmentally-driven changes in the growth and survival rates in reptiles (Ford and Seigel 1989; Sorci et al. 1996; Price 2006; Susana et al. 2008), environmentally-cued hatching and predator- and prey-induced alternative feeding morphs in amphibians (Kishida et al. 2006; Warkentin 2011; Maher et al. 2013; Katayama et al. 2021), and differences in calving dates and numbers influenced by the varying amounts of rainfall and population density and temperature-induced changes in morphology and metabolic rates in mammals (Nussey et al. 2005; Riek and Geiser 2012).

Second, upon experiencing a novel environment, plastic traits need not to be exclusively adaptive. They can also be neutral, non-adaptive, or maladaptive (Merilä and Hendry 2014; Murren et al. 2015; Palacio-Lopez et al. 2015; Acasuso-Rivero et al. 2019). Whereas adaptive phenotypic plasticity can lead to adaptive evolution, the roles of non-adaptive and/or maladaptive phenotypic plasticity in evolution remain controversial (Nettle and Bateson 2015; Levis and Pfennig 2019, 2020; Ng and Kinjo 2023; Gómez et al. 2024; Garaffa 2025). Nevertheless, both modelling and empirical data suggest that non-adaptive and/or maladaptive phenotypic plasticity still contribute to adaptive evolution (Ghalambor et al. 2007, 2015; Fitzpatrick 2012; Morris and Rogers 2013; Fischer et al. 2016; Leonard and Lancaster 2020). Of note, an important commonly used experimental parameter to measure the performance of plastic traits across distinct environments is ‘reaction norms’ or ‘norm of reaction’ (from the original German term ‘Reaktionsnorm’). This term was first coined by the German zoologist Richard Woltereck in 1909 based on his work on the change in head ‘helmet’ size of the water flea *Daphnia* based on the availability of the algal food source—a form of phenotypic plasticity and later formally termed cyclomorphosis (Woltereck 1909; Coker and Addlestone 1938; *sensu* Sarkar 1999). There has been variation in the interpretation and usage of reaction norm, but the core point is that it refers to quantitative readout of the phenotype in a certain environment of certain genotype (Platt and Sanislow 1988; Morrissey and Liefting 2016). While this concept is widely used in different fields in biology, it has been an important working concept in phenotypic plasticity studies (Roff 1997; David et al. 2004). For example, Dodson (1989) compiled his colleagues’ and own works on predator-induced cyclomorphosis in *Daphnia* and made a link to the use of reaction norms for the measurements of

head-helmet-associated defence character values. Such a link had been made across other systems too, including the modelling of plasticity in character traits and fitness across abiotic environment gradients in the thale cress *Arabidopsis* (Pigliucci et al. 1995; Pigliucci and Schlichting 1996), plasticity in wing length and pigmentation in the fruit fly *Drosophila* and wing pattern elements in the butterfly *Bicyclus anynana* across temperature regimes (Holloway and Brakefield 1995; David et al. 1997), and plasticity in litter size and weight in varying food availabilities in Trinidadian guppies *Poecilia reticulata* (Gordon et al. 2017). There are many more phenotypic plasticity studies employing reaction norms without explicitly mentioning the term (*sensu* Roff 1997). The importance of reaction norms as a method for character measurements in these studies and as a concept for the understanding of the evolution of phenotypic plasticity is immense. Therefore, it has resulted in in-depth conceptual reviews and a landmark book titled *Phenotypic Evolution: A Reaction Norm Perspective* by Carl D. Schlichting and Massimo Pigliucci (Stearns 1989; Pigliucci et al. 1996; Schlichting and Pigliucci 1998; Pigliucci et al. 2006). However, it is important to consider that the sole reliance on the classical 'phenotypic reaction norms' to distinguish the types of adaptability such as neutral, adaptive, non-adaptive or maladaptive can be misleading (Gotthard and Nylin 1995; Bonser 2021; Eriksson et al. 2023). Thus, whenever possible, it is recommended to study the plastic responses at the whole-organism level and across generations and as various environmental conditions as possible (Araya-Ajoy et al. 2015; Forsman 2015; Schneider 2022). The temporal dynamics of the plastic responses should also be considered (Dupont et al. 2024). Regarding the environmental conditions tested, it should also be noted that while most studies have focused on the adaptability and/or non-adaptability to novel environments, the readaptation to the ancestral environments can be overlooked (Ho et al. 2020).

Third, besides its effect on fitness, phenotypic plasticity can be categorised by the onset (*immediate or delayed*), period (*short or long*), mode (*active or passive*), inheritance (*genetic or non-genetic*), reversibility (*reversible or irreversible*), or form (*continuous or discrete*) of the response. These broad categorisations are not mutually exclusive as plastic responses can be described by multiple terms (Fusco and Minelli 2010; Schneider 2022). Although these classifications can be useful for phenotypic plasticity studies in their own right, it is perhaps the existence of discrete plasticity (also referred to as 'polyphenism') that provides a unique feature to progress our understanding of phenotypic plasticity at the mechanistic level (Projecto-Garcia et al. 2017; Yang and Pospisilik 2019). Polyphenism, as opposed to continuous plasticity, refers to the extreme form of plasticity wherein one genome gives rise to alternative and discontinuous phenotypes in response to varying environmental inputs (Michener 1961; Mayr 1963; Sakamoto and Innan 2024). Such a discrete bi- or multifurcation of the phenotypes makes epigenetic, genetic, and molecular dissections of any polyphenic traits possible (Levis and Ragsdale, 2022; Wighard and Sommer 2024; Dearden 2025). Numerous empirical data for the genetic basis of polyphenic traits have emerged over the years and across systems. For example, in Atlantic salmon which have male alternative mating tactics: large-bodied anadromous males or small-

bodied male parr, one main quantitative trait locus (QTL) was identified to be the most significant in explaining this trait (Lepais et al. 2017). Various flowering plants bear both chasmogamous flowers, which are open permitting cross pollination, and cleistogamous flowers, which are closed and significantly smaller than the chasmogamous ones, and are thus strictly self-pollinated (Joly and Schoen 2021). In barley, cleistogamy is regulated by the effects of a dominant gene *Cly2* on a recessive gene *cly1* (Wang et al. 2013). In another domain of life, the bacterium *Photorhabdus*, which is the endosymbiont of the entomopathogenic nematode *Heterorhabditis*, can switch between small-cell mutualistic form (M-form) to get associated with its nematode partner or large-cell pathogenic form (P-form) to kill its host insect. This switch occurs through an on-or-off fashion of a major subunit in the promoter region, named *madswitch*, upstream of the *mad* (maternal adhesion fimbriae) genes (Somvanshi et al. 2012). These genes play an indispensable role in this nematode-bacterial symbiosis through the adherence to maternal nematode intestine followed by the transmission to the nematode progeny (Somvanshi et al. 2010). Another form of phenotypic plasticity in bacteria is the switch between motility and sessility. The latter form of bacterial life is also referred to as biofilm (Verstraeten et al. 2008). The transition between sessility to motility in *Escherichia coli*, *Salmonella* and *Pseudomonas aeruginosa* is attributed to the nucleotide signaling molecule cyclic-di-GMP (c-di-GMP) (Simm et al. 2004). Later, more factors have been shown to be involved in the biofilm production including another nucleotide signaling molecule cyclic-di-AMP (c-di-AMP), toxin-antitoxin modules, and a transcriptional regulator BolA (Sadiq et al. 2017).

Collectively, insects might be the champion for the cases of polyphenism, hence there exists ample mechanistic understanding of this phenomenon in these systems (Simpson et al. 2011). As wing polymorphism is widespread in insects across various orders, various breakthrough molecular findings have been uncovered (Zhang et al. 2019). In the pea aphid *Acyrthosiphon pisum*, a single gene named *aphicarus* (*api*) was identified as a switch gene governing the wing polymorphism in males (Braendle et al. 2005). In the brown planthopper *Nilaparvata lugens*, two insulin receptors, InR1 and InR2, were shown to function as a switch in the long- and short-winged morphs. They antagonistically regulate the Forkhead transcription factor (FoxO) activity. When InR2 is inactive, InR1 acts through the phosphatidylinositol-3-OH kinase (PI(3)K)–protein kinase B (Akt)-FoxO signalling cascade leading to the long-winged morph. Opposingly, when InR2 is more activated, it compromises the InR1-Akt-FoxO signalling pathway resulting in the short-winged morph instead (Xu et al. 2015). The butterfly *Bicyclus anynana* has been an important model organism in studying seasonal wing spot polymorphism, in which hot wet or cold dry season increases or decreases the size of hindwing eyespots, respectively (Brakefield et al. 1996). This derived plastic trait is controlled in a lineage-specific manner by the temperature-sensitive production of 20-hydroxyecdysone (20E), an insect ecdysteroid hormone, and the sensing of this molecule by the 20E receptor (EcR) during the wandering developmental stages (Monteiro et al. 2015; Bhardwaj et al. 2020).

Recently, Tian et al. (2025) demonstrated that the *cis*-regulation of the promoter of a Hox gene *Antennapedia* (*Antp*) acts upstream in the gene regulatory network (GRN) controlling the eyespot polyphenism in the subfamily to which *B. anynana* belongs. The underlying regulatory network of phase transition polyphenism between gregarious and solitary phases in locusts has been extensively dissected over the years at the epigenetic, genetic, and molecular levels (Guo and Kang 2024).

Insects have evolved sociality from solitary ancestors. At least three insect orders including Hymenoptera (e.g., ants, bees, and wasps), Blattodea (e.g., termites) and Coleoptera (e.g., ambrosia beetles) have independently evolved an even more complicated form of sociality termed 'eusociality' by the American entomologist Suzanne Batra in 1966. Insect eusociality has led to a diverse collection of plastic traits such as caste determination and its associated behavioural, physiological, and morphological alterations (Batra 1966; Gadagkar 1997; Toth and Rehan 2017; Abbot 2022; Mikhailova et al. 2024). Undoubtedly, our understanding of the molecular pathways underlying these polyphenic characters is extensive (Smith et al. 2008; Corona et al. 2016; Weitekamp et al. 2017). For instance, in the termite *Reticulitermes speratus* having XY sex determination, its castes are genetically controlled by an X-linked locus named *worker* (*wk*) with two alleles A and B. Females having two copies of A (wk^{AA}) develop as nymphs and are fated to be future queens while individuals inheriting a copy of A and B (wk^{AB}) become workers. Those inheriting two copies of B (wk^{BB}) are lethal. Males having a copy of A (wk^{A}Y) become workers while individuals inheriting a copy of B (wk^{B}Y) develop as nymphs and are fated to be future kings (Hayashi et al. 2007). Similarly, in the red harvester ant *Pogonomyrmex barbatus*, at least one caste-determination locus, dubbed *caste*, is involved in caste determination. Progeny that arise from crosses of different lineages are heterozygous at the *caste* locus and become workers, while those of parents from the same lineage are homozygous at this locus and become queens (Volny and Gordon 2002). The plasticity in behaviour in eusocial insects, also referred to as 'polyethism', signifies the functional division of daily colony tasks among non-reproducing castes (Beshers and Fewell 2001). A circadian clock pathway gene, *period*, was cloned from the harvester ant *P. occidentalis* and shown to be important for the age-related polyethism in this species (Ingram et al. 2009). Studying the GRN underlying wing polymorphism, which is an important morphological trait for caste differentiation, across different ant genera, Abouheif and Wray (2002) found that the expression of various genes is evolutionarily conserved in the winged reproductive castes across genera. These gene orthologues in *D. melanogaster*, including *Ultrabithorax* (*Ubx*), *extradenticle* (*exd*), *engrailed* (*en*), *wingless* (*wg*), *scalloped* (*sd*), *spalt* (*sal*), and *distal-less* (*dll*), also regulate wing development in fruit flies. However, in the wingless sterile castes, the interruption in the wing-patterning gene network occurs at different points, and thus is evolutionarily labile among ants.

Lastly, there has been a growing support for the roles of phenotypic plasticity in evolution in various organisms (Levis and Pfennig 2021). Nevertheless, the

acceptance of such an evolutionary importance that phenotypic plasticity conveys has been contentious and there has also been a perception that the body of evidence is not strong enough (Wund 2012; Wray et al. 2014). There are multiple mechanisms by which plasticity impacts evolution and it would not be correct to assume any single study can completely cover this diversity (Price et al. 2003; Nonaka et al. 2015; Bailey et al. 2021). By comparing mechanisms of phenotypic plasticity-facilitated evolution to the mechanisms of speciation, Wund (2012) wrote:

> *Despite relatively few demonstrations of all mechanisms of speciation from inception to completion, we are collectively convinced that speciation occurs, and we base our understanding on a large body of evidence, with individual studies filling in pieces of a much larger puzzle.*

Diversification and incipient speciation are ultimate steps to which phenotypic plasticity leads (Pfennig et al. 2010). This is supported by both simulations and empirical data (Magalhaes et al. 2009; Thibert-Plante and Hendry 2011; Schneider and Meyer 2017). Recently, Jarrett et al. (2025) performed a meta-analysis of 34 speciation studies and found that pre-mating barrier can be attributed to phenotypic plasticity. Additionally, plastic traits also allow species to be well off in the coexistence with others and have broader ecological implications (Miner et al. 2005; Pfennig et al. 2006; Lundsgaard-Hansen et al. 2014; Pérez-Ramos et al. 2019; Hess et al. 2022).

Taken together, phenotypic plasticity is a widespread phenomenon that is important in evolution. It is indeed not just a negligible nuance in biology. Leveraging on the advantages that molecular biology has to offer, we can dive deeper into the discussion of genetic assimilation and evolution (Kelly et al. 2012).

1.1.2. Mounting empirical evidence for plasticity-led evolution in the age of molecular biology

Genetic assimilation refers to the process whereby a plastic trait originally responsive to environmental inputs becomes nonsensitive and invariant. This newly arisen and phenotypically fixed population will exhibit certain genetic reconfigurations after some generations and become stably inherited (Waddington 1953; *sensu* Pigliucci et al. 2006). This phenomenon plays a central role in the plasticity-led evolution concept (Nanjundiah 2003; Pigliucci and Murren 2003; Braendle and Flatt 2006; Nijhout 2025). Its implications for evolution include the rise of trait diversification and speciation (Pál and Miklós 1999; Pfennig et al. 2010). Despite genetic assimilation being a controversial process, various examples have emerged to support its evolutionary significance in nature (Simpson 1953; Williams 1966; Orr 1999; de Jong 2005). In plants, maize domestication (Lorant et al. 2017), sexual expression in the nightshade genus *Solanum* (Diggle and Miller 2013), and adaptation to zinc contamination in the sea campion *Silene uniflora* (Wood et al. 2023) all have some signature of genetic assimilation. In animal systems, this evolutionary attribute is involved in the pelvic fin loss in the extremophile Devils Hole pupfish *Cyprinodon diabolis* (Martin et al 2016), evolution of genital sidedness in anablepid fishes (Torres-

Dowdall et al. 2022), diet-dependent colouration in birds (Badyaev et al. 2017), wing shape evolution in the non-migratory monarch butterfly *Danaus plexippus* (Nixon and Parzer 2024), head size evolution in the island tiger snake *Notechis scutatus* (Aubret and Shine 2009), and the evolution of menstruation in higher primates and some other mammals (Emera et al. 2011). In addition to these examples in nature, there are also experimental works on genetic assimilation, for instance, the contributions by the British developmental biologist Conrad H. Waddington who coined the term 'genetic assimilation'. He exposed the fruit fly *Drosophila melanogaster* pupae to heat shock and early embryos to ether and selected for *crossveinless* and *bithorax* phenotypes, respectively. In both cases, it was shown that the selected phenotypes were reliably inherited without further need of environmental inductions (Waddington 1953, 1956). Recently, there emerged a theoretical model supporting these findings (Raju et al. 2023). Two experimental insights from nematode species in the genus *Caenorhabditis*, namely *C. elegans* and *C. remanei*, also exemplified the genetic assimilation process in phenotypically plastic traits such as sensory imprinting and heat sensitivity, respectively (Remy 2010; Sikkink et al. 2014).

Despite being important examples for this evolutionarily relevant process, the above-mentioned evidence still lacks the molecular support, which is the gold standard in modern biological research. Identifying associated molecular principles would likely catalyse the widespread acceptance of this concept (Gilbert 2003; Espinosa-Soto et al. 2021). Chavhan et al. (2023) demonstrated that both gram-negative (e.g., *Escherichia coli*, *Citrobacter freundii*, and *Pseudomonas aeruginosa*) and gram-positive bacteria (e.g., *Staphylococcus aureus*) can reveal phenotypic plasticity in the elongation of cell clustering in response to high salt conditions. By employing an experimental evolution setup using *E. coli*, this plastic trait was proven to be amenable to genetic assimilation wherein the evolved lines grew as undifferentiated elongated cells without the stimulation by high salinity any longer. The authors further pinpointed an overwhelming number of genetic mutations (e.g., *mrcB*, *mrdA*, *mrdB*, *mreB*, and *murF*) accompanying this assimilated trait in the peptidoglycan biosynthesis, which is a pathway directly involved in the maintenance of the cell wall. Most importantly, 70% of the sequenced genetically assimilated *E. coli* clones independtly had a single nonsynonymous or frameshift mutation in the gene *mraY* which encodes an essential enzyme for the biosynthesis of peptidoglycan. Separately, Walworth and colleagues (2016) worked on the genetic assimilation of the response to elevated CO_2 conditions by a marine nitrogen-fixer cyanobacterium *Trichodesmium*. They discovered that this process required changes from the upstream transposition and regulatory networks to downstream metabolic pathways. In a molecular study on the diet-induced low pharyngeal jaw plasticity in East African cichlid fishes, two candidate genes, *gif* and *alas1*, were identified to may have undergone genetic assimilation (Gunter et al. 2017). Two investigations related to high-altitude adaptations also provided additional support for this evolutionary feature. By performing transcriptomic comparisons between the toad-headed agama *Phrynocephalus vlangalii*, which are true high-altitude dwellers, to its low-altitude

congeners, *P. axillaris and P. forsythii*, Yang and coworkers (2021) found that essential genes in the fatty acid metabolism pathway became genetically assimilated in the former species. This process was inferred to support the successful survival of *P. vlangalii* in the high-altitude conditions. In the hypoxia adaptation of the Tibetan antelope *Panthelops hodgsonii*, Signore and Storz (2020) delicately demonstrated that this species has evolved the upregulation of a high-affinity juvenile haemoglobin isoform (isoHb) to displace low-affinity adult isoHb. The latter is highly prevalent in the red blood cells of adults in other bovine species. This mode of biochemical paedomorphosis enables Tibetan antelope to elevate its haemoglobin-oxygen affinity, hence adaptive evolution in the hypoxic environment. Research on heat stress adaptation in the splash pool copepod *Tigriopus californicus* revealed that peptidases showed traces of genetic assimilation (Neylan et al. 2026). In response to low nutrient status, the self-fertilising hermaphroditic nematode *C. elegans* can opt for matricidal hatching by sacrificing their own life to secure the survival of their non-feeding, stress-resistant, and dispersal-stage larvae, known as dauer larvae. This is a form of adaptive phenotypic plasticity because even if one dauer larva survives, it will be able to establish the next generation through self-fertilisation when it gets dispersed to a new environment with food (Chen and Caswell-Chen 2003). Leveraging on the plethora of available wild isolates of this species that are still either plastic or have opted for constitutive matricidal hatching even in the presence of food, Vigne et al. (2021) found a single nonsynonymous mutation in the KCNL-1, a small-conductance calcium-activated potassium (SK) channel protein, would be enough to lead to trait assimilation. The common buckeye butterfly *Junonia coenia* changes their wing colour in different seasons. By artificially selecting for lines with the reduced wing colour plasticity, van der Burg et al. (2020) identified three genes which are involved in this process such as *cortex*, *trehalase*, and *herfst*. The genuinely monophenic green tobacco hornworm *Manduca sexta* could be induced by heat-shock experiments to have larval colour polyphenism: *black* (mutant) and green. In one of the follow-up studies, molecular mechanisms underlying the differences between monophenic and polyphenic strains were explored. Noticeably, DNA methylation and juvenile hormone (JH) signaling showed signs of genetic assimilation (Suzuki and Nijhout 2006; Suzuki et al. 2025). Finally, to go full circle to *D. melanogaster* which was the system that Conrad H. Waddington worked on when the term ‘genetic assimilation’ was dubbed, more modern studies uncovered extra trait assimilations even at the mechanistic level. Using a number of natural fly populations, Sabarís et al. (2025) worked on the genetic assimilation of the *ectopic veins* phenotype. They discovered that the underlying mechanisms for this process is mainly due to the insertion of a transposable element in the 3’ untranslated region (3’ UTR) of the receptor tyrosine kinase gene *Cad96Ca*. In another study that followed Waddington’s original experimental procedure by exposing the fly population to heat-stress, researchers could isolate four phenotypes that became genetically fixed including modified eye colour, melanotic tumours, and two separate forms of bristle defects. They could also nail down the underlying molecular mechanisms of these defects

(Fanti et al. 2017; Kasinathan et al. 2017).

In sum, originally phenotypically plastic traits can evolve and lose their responsiveness to the environmental inductions and certain genetic rewiring follows. This process of genetic assimilation indeed has molecular support. Thus, the studies of phenotypic plasticity should be appreciated for its relevance for evolution. Among various biological systems that can help to progress our mechanistic understanding of phenotypic plasticity, nematodes represent an important model group owing to many known cases of plastic traits and ease of culturing and genetic manipulation. These biological models are further discussed below.

1.2. Nematode systems: abundant in nature, versatile for biological research, and emerging models for phenotypic plasticity research

1.2.1. Nematodes as model organisms

Nematodes, also known as roundworms especially in health sciences, have gained fame in the field of experimental biology due to one specific champion model system: the soil free-living bacterivorous nematode *C. elegans* (Witkowski 1988; Müller and Grossniklaus 2010; Irion and Nusslein-Volhard 2022). The selection of this one-millimetre-long species as a model organism by the South African biologist Sydney Brenner in 1965 was due to its short generation time, ease of culturing on *E. coli* as food source, self-fertilising reproduction with the presence of spontaneous males allowing additional cross-fertilisation, and relatively small and invariant number of cells and neurons. More importantly, the system is amenable to genetic analysis (Brenner 1974). The original research focus was on organismal and neural development (Riddle et al. 1997). Later, as *C. elegans* became the first multicellular organism to have its whole genome sequenced, further studies could incorporate genetic information and evolutionary aspects (The *C. elegans* Sequencing Consortium 1998). The availability of the complete genome has also made reverse genetics more feasible on a larger scale (Ahringer 2006). Notably, highly important discovery milestones in biology were achieved in the studies on this tiny worm species. They include genetics of apoptosis, or commonly known as programmed cell death, and the discovery of microRNAs (miRNAs) and their roles in gene regulation (Ellis and Horvitz 1986; Lee et al. 1993). Nowadays, what can be studied with this model system has evolved to cover almost every aspect in biological research, for instance, genetics (Zhong and Sternberg 2006), physiology (Strange 2007; Miranda-Vizuete and Veal 2017), evolution (Gray and Cutter 2014), disease model (Kaletta and Hengartner 2006), microbiome (Zhang et al. 2017; O'Donnell et al. 2020), and neural system and behaviour (Hobert 2003).

As nematodes are the most abundant animals in the soil playing intricate roles in virtually all trophic levels, it should not come as a surprise that many topics can also be studied in other nematode systems (van den Hoogen et al. 2019). For example,

due to their transparent body, large sperm cells, and the small number of chromosomes, observations in the parasitic nematodes *Ascaris* have already in the late 19th and early 20th centuries described early development from fertilisation and meiosis onward (*sensu* Nigon and Félix 2017). Using a species from a related genus, *Parascaris univalens* (formerly known as *A. megalocephala*), Boveri (1887) observed the somatic programmed DNA elimination (PDE) for the first time. This is a process in which portions of DNA are eliminated during development of the soma, a phenomenon that exists across many phyla of both invertebrates and vertebrates (Mochizuki 2024). This process also occurs in the free-living nematode *Oscheius tipulae*, a relative of *C. elegans* belonging to the same Rhabditidae family. Additionally, PDE was recently discovered in members of 12 out of 17 genera tested in the family Rhabditidae and among which many studies have been conducted in the genus *Mesorhabditis* (Rey et al. 2023; Launay et al. 2025 *preprint*). Interestingly, while PDE is absent in *C. elegans*, this phenomenon exists in the early-diverging members of the genus *Caenorhabditis* (Launay et al. 2025 *preprint*; Stevens et al. 2025 *preprint*). Another biological trait that comes with the diversity of nematodes is the various modes of reproduction including sexual, asexual, and hermaphroditic reproductions (Rödelsperger 2024). Among the various lineages from plant-parasitic to free-living nematodes that have independently evolved to reproduce by parthenogenesis, a form of asexual reproduction, two divergent genera *Panagrolaimus* and *Diploscapter* have been extensively used as model systems (Lewis et al. 2009; Fradin et al. 2017). *Diploscapter* nematodes have one of the most extreme forms of genome arrangement in nematodes with the entire genome assembled into a single pair of highly heterozygous chromosomes. This feature allows mechanistic observations of chromosome evolution to be conducted (Chung et al. 2026). The genus *Panagrolaimus*, including individuals thawed back to life from Siberian permafrost samples, has also been used to study extreme desiccation or anhydrobiosis (Shannon et al. 2005; Schiffer et al. 2019; Shatilovich et al. 2023). Two closely related rhabditid genera *Tokorhabditis* and *Auanema*, which interestingly have three sexes including males, females, and hermaphrodites, have been utilised to study the evolution of vivipary and sex determination, respectively (Yamashita et al. 2023, 2025; Adams et al. 2025). In the phylum Nematoda, two genera, *Heterorhabditis* and *Steinernema*, have convergently evolved to have a strict high-fidelity symbiosis with bacteria. These nematode taxa need to vector their bacterial symbionts into insect hosts to complete their life cycle. Recently, the genus *Steinernema* has been established as a genetically tractable model to study symbiosis and parasitism (Blaxter et al. 1998; Cao et al. 2022; Schwartz et al. 2024; Schwarz et al. 2025).

Another model nematode system, *Pristionchus pacificus*, was established in the historical context of the quest to understand the evolution of developmental processes (evo-devo) (Sternberg 2015). In a specific evo-devo theme of vulva development, molecular comparative analysis of *P. pacificus* with *C. elegans* revealed a signature of developmental system drift, a phenomenon of convergent regulatory mechanisms leading to the same development (Haag and True 2021). Indeed, vulva

development in *P. pacificus* and *C. elegans* requires EGF/Ras and Wnt signalings, respectively (Sommer 2012). Over the years, the model nematode *P. pacificus* has evolved from being a satellite model of *C. elegans* to being a model system in its own right. The former species has certain features that are absent in the latter including morphological coupled with behavioural plasticity related to predation, which will be discussed in more detail in the following sections, and kin-recognition system (Sommer and Lightfoot 2022; Sommer 2025).

All in all, as the most abundant animals on earth, a plethora of nematode systems can be used to address various biological questions. Additionally, since phenotypic plasticity is a common phenomenon, as discussed earlier, this topic could also be studied in nematodes.

1.2.2. Phenotypic plasticity in nematodes

Phenotypic plasticity in nematodes includes life-history traits, development, morphology, and behaviour. In at least three divergent groups of plant-parasitic nematodes, the body shape of females is plastic in relation to the feeding stage. Root-knot nematodes of the genus *Meloidogyne* and cyst nematodes, comprising eight cyst-forming genera such as *Heterodera*, *Globodera*, *Cactodera*, *Dolichodera*, *Paradolichodera*, *Betulodera*, *Punctodera*, and *Vittatidera*, are vermiform in the free-living immature adult stage. However, when they start to initiate the feeding site inside plant roots, the mature females will develop into an obese and sedentary shape. Whereas the root-knot nematodes lay eggs into the protective glycoprotein matrix egg masses produced and secreted by rectal glands, cyst nematodes' shape plasticity involves another major change, namely cuticle hardening, and their whole body becomes a cyst housing a large number of eggs. In some species of cyst nematodes, a certain number of eggs are also laid into external egg masses (Moens et al. 2009, 2018). The third plant-parasitic nematode group exhibiting this shape plasticity is the reniform nematodes of the genus *Rotylenchulus*. Just like the other above-mentioned nematodes, *Rotylenchulus* females are also vermiform. However, the mature females develop into a reniform shape and become sedentary. Their eggs are deposited in the protective gelatinous matrix produced by vaginal glands instead of rectal glands in *Meloidogyne* (Cohn and Mordechai 1988; Ganji et al. 2013). In the bumblebee-parasitic nematode *Sphaerularia bombi*, there exists a developmental plasticity of the female reproductive system. When they initiate the infection, the whole reproductive system is expelled through the vulva into the body cavity of the host. This structure then develops to be around 100 times larger than that of the free-living form. This everted uterine sac also involves ultrastructural changes to serve as nutrient uptake apparatus to nourish the developing embryos (Poinar and Hess 1972; Poinar and van der Laan 1972).

Along the line of diet-induced plasticity, many discoveries have also been made in the fungus-feeding genus *Bursaphelenchus*. In this genus, two congener species, the red ring nematode *B. cocophilus* and pinewood nematode *B. xylophilus*, have

evolved to also feed on plants (Kanzaki 2008). Living in the alternating environments between being a mycophagous or phytophagous organism, *B. xylophilus* has to change the ultrastructure of their cuticle and intestinal microvilli (Ekino et al. 2020). In a related species feeding of fungi, *B. sinensis*, there also exists a predatory morph with accompanying morphological changes at the lip and pharyngeal regions. The presence of monoxenic fungal food sources and the duration of nematode culturing were shown to influence the ratio of predatory individuals in the population (Kanzaki et al. 2019). In a completely different nematode family, it was shown that body size and many other morphometric values of the bacterivorous genus *Halicephalobus* change drastically in response to food and temperature. These changes are so significant that two isogenic populations raised in different environments can be wrongly considered as 'two species' (Fonderie et al. 2013).

Another form of plasticity is related to reproduction. In hermaphroditic nematodes, self-produced sperm cells are one of the main factors for population success. In different genetic backgrounds of *B. okinawaensis*, the type of fungal food source can affect the number of sperm cells produced. Additionally, this environmental stimulus can influence the sex determination as some hermaphrodites become females instead (Fujimori et al. 2022). Sperm production was also observed to be a plastic trait in *C. elegans* (Gimond et al. 2025). In the root-knot nematode *Meloidogyne incognita*, there exists a plastic trait in the form of sex reversal in response to the population density. When too many larvae infest plant roots, larvae fated to become females can switch to develop as males instead, retaining remnants of the female reproductive tracts (Triantaphyllou 1960, 1973; Papadopoulou and Triantaphyllou 1982).

Nematode dauer formation is probably one of the most extensively studied examples of developmental plasticity at the genetic, molecular, biochemical, and neuronal levels. *C. elegans* has four larval stages (L1-L4) with the corresponding three moults before the final moult to reach adulthood, which then lays eggs to complete the life cycle. Cassada and Russell (1975) formally described the discovery of the dauer larval stage (from German for 'enduring larvae') in *C. elegans* as an alternative arrested developmental stage after the first two moults in response to harsh environmental conditions. Already in the early L1 stage and with a certain threshold of environmental stimuli, *C. elegans* has to decide which developmental pathway to go for between normal development to L3 or dauer development. In case of the latter, the nematodes have to adjust their morphology to be dauer-like before the second moult and these animals are called pre-dauer larvae (L2d) (Golden and Riddle 1984). As early as two years after the description of the dauer stage, genetic screens revealed that two types of dauer mutants can readily be isolated, dauer-formation constitutive (Daf-c) and dauer-formation defective (Daf-d) mutants (Riddle 1977). Further studies over the years have resulted in the understanding of underlying pathways of this developmental plasticity including guanylyl cyclase, TGFβ-like, insulin-like, and steroid hormone pathways (Hu 2007; Fielenbach and Antebi 2008). Noticeably, this

alternative developmental stage also exists in other nematodes of both free-living and parasitic life cycles (Crook 2014; Gilabert et al. 2016). Additionally, in the trioecious genus *Auanema*, in which males, females, and hermaphrodites coexist, the plasticity in female-hermaphrodite sex determination involves passing through the dauer stage. Individuals recovering from the dauer stage will strictly become hermaphrodites (Chaudhuri et al. 2011; Adams et al. 2025). Similarly, in the entomopathogenic nematode *Heterorhabditis*, there is also a switch between female and hermaphroditic reproductive modes. Larvae that go through the pre-dauer juvenile stage (J2d = L2d in *C. elegans*) will become hermaphrodites (Strauch et al. 1994; Johnigk and Ehlers 1999).

To summarise, phenotypic plasticity is a common phenomenon in the phylum Nematoda. The types of plasticity observed cover a broad range from sex determination to behaviour. As the facultatively predatory nematode *P. pacificus* has been a hotbed for studies related to mouth-morph and behavioural plasticity, it will be discussed in greater extent below.

1.2.3. *Pristionchus pacificus* as lab rats for resource polyphenism studies

The model nematode *P. pacificus* belongs to the monophyletic family Diplogastridae, which is the sister of the paraphyletic family Rhabditidae (Rödelsperger et al. 2024; Qing et al. 2025). The diplogastrid family has evolved morphological and behavioural novelties in the form of predatory mouth morph compared to that of their sister family. This morph arose to complement the ancestral bacterivorous morph, representing a case of resource polyphenism. This plastic trait also showed signatures of being secondarily lost in the evolution of the family Diplogastridae (Susoy et al. 2015).

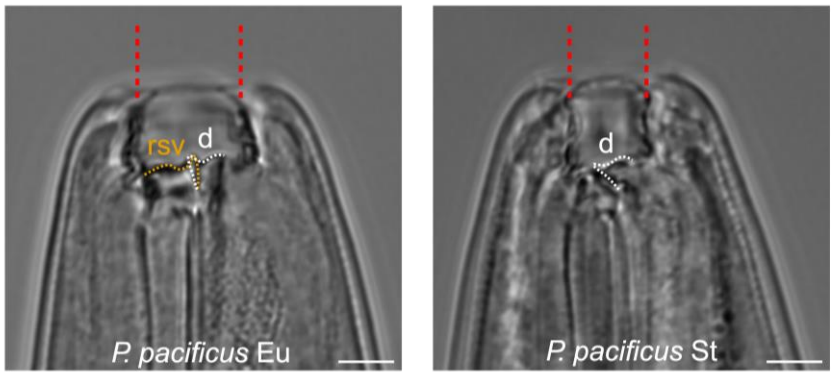


Figure 1 Mouth-form dimorphism in *P. pacificus*. The eurystomatous (Eu) morph has a bigger and more sclerotised stoma (spaces between red dashed lines) than the stenostomatous (St) morph. Whereas both morphs have a dorsal (d) tooth (highlighted by white dashed lines), the Eu morph is decorated with a second tooth on the right subventral (rsv) sector of the stoma (highlighted by orange dashed lines). Scale bars denote 5 µm.

While the mouth dimorphism in Diplogastridae was alluded to by the British zoologist Frank Armitage Potts in the early 20th century, it was the German-born American nematologist Hedwig Hirschmann who later showed that the mouth-form plasticity is genuine by culturing *Pristionchus lheritieri* (formerly known as *Diplogaster*

lheritieri) isofemale progeny and revealing they represented two discrete phenotypes (*sensu* Ragsdale 2015). Hirschmann (1951) called the wide-mouthed and narrow-mouthed forms 'eurystomatous (Eu)' and 'stenostomatous (St)', respectively (**Figure 1**). *P. pacificus* also exhibits this irreversible mouth-form plasticity at the adult stage with the St form being strictly bacterivorous and the Eu form being omnivorous and able to predate on other nematodes (Bento et al. 2010). In addition to the width, there are more morphological differences in the stoma between these two morphs. Both morphs have a moveable dorsal tooth which is flint-shaped and large and claw-like in the St and Eu forms, respectively. While the Eu individuals have their right subventral sector of the stoma decorated with a large and claw-like tooth, St individuals only possess a small denticle. The stoma is generally more sclerotised in the Eu morph (Ragsdale et al. 2015). Even though the plasticity is only observed in the adult stage, the decision of the worms to be Eu or St is already made in the early juvenile stages (Sun et al. 2023; Werner et al. 2023). Environmental factors influencing the mouth-form decision include pheromones (Bose et al. 2012), temperature (Lenuzzi et al. 2023), and diet (Namdeo et al. 2018; Piskobulu et al. 2025).

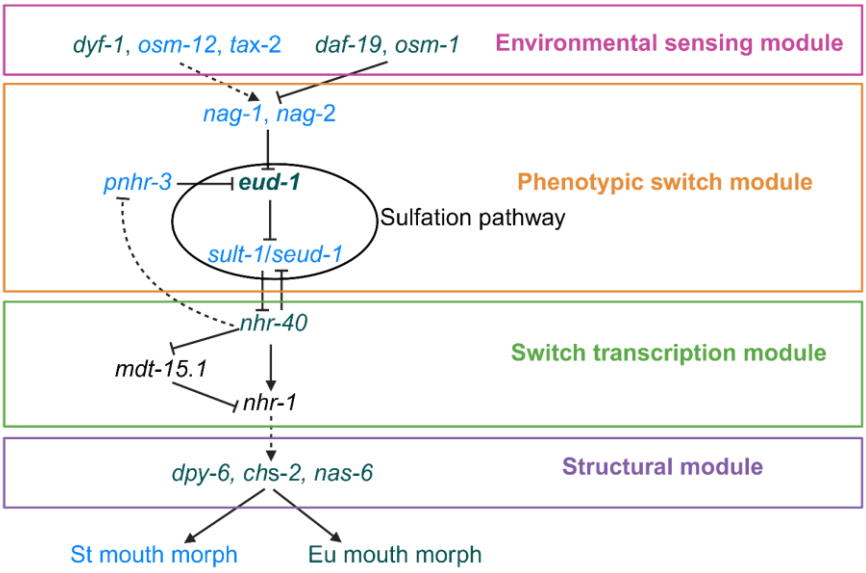


Figure 2 Mouth-form gene regulatory network (GRN) in *P. pacificus*. This GRN comprises four modules arranged hierarchically from upstream to downstream: environmental sensing, phenotypic switch, switch transcription, and structural modules. The sulfation pathway (in black circle) plays a central role in the mouth-form GRN with the sulfatase-encoding gene *eud-1* (in bold) acting as the main switch gene. Genes important for the Eu and St morphs are in green and blue, respectively. Genes in black may regulate both phenotypes. Solid lines denote gene orders with epistatic support while dashed lines represent untested epistasis. Arrowhead and T-shaped lines represent positive and negative regulations, respectively. Adapted from Katsougia et al. (2025) and Reich et al. (2025).

The existence of such a discrete polymorphism in a genetically tractable system like *P. pacificus* has enabled the discovery of the underlying gene regulatory network (GRN) of the mouth-form decision (*sensu* Reich et al. 2025). The first gene identified in this mouth-form GRN was *eud-1* (*eu*rystomatous form *d*efective) which encodes

sulfatase and plays a central role as a switch gene between Eu and St morph. This gene is necessary for the Eu morph, i.e., when it is knocked out, *P. pacificus* becomes 100% St (Ragsdale et al. 2013a). Additionally, the *eud-1* locus is flanked by two α-N-acetylglucosaminidase-encoding genes, *nag-1* and *nag-2*, which act oppositely to *eud-1*, i.e., both *nag* genes are needed for St morph formation. This genomic arrangement of the multi-gene locus controlling mouth-form plasticity is only observed in the genus *Pristionchus* (Sieriebriennikov et al. 2018). Interestingly, the *sult-1*/*seud-1* gene encoding a sulfotransferase, the complementary part of sulfatases in the sulfation pathway, was also found to be involved in the mouth-form decision—it is required for the St phenotype (Bui et al. 2018; Namdeo et al. 2018). The sulfation enzymes are in the centre of the GRN for mouth-form control (Igreja and Sommer 2022) (**Figure 2**). Acting upstream of this 'phenotypic switch module' is the 'environmental sensing module'. As nematodes can use ciliated neurons to sense the environmental inputs, *P. pacificus*' cilia-related genes were indeed shown to play a role in the mouth-form decision. These include genes such as *daf-19*, *osm-1*, *dyf-1*, *osm-12* and *tax-2* (Roggen et al. 1966; Moreno et al. 2019; Lenuzzi et al. 2023; Nechipurenko and Sengupta 2025). A 'switch transcription module' then acts downstream of these two modules. This module includes two nuclear hormone receptors (NHRs), *nhr-40* and *nhr-1*, and a transcription coregulator *mdt-15.1* (Kieninger et al. 2016; Sieriebriennikov et al. 2020; Casasa et al. 2023). Recently, Katsougia et al. (2025) identified another NHR, *pnhr-3*, to be also involved in the mouth-form plasticity. This NHR is different from *nhr-40* and *nhr-1* on two points. First, it is not a conserved NHR. While *nhr-40* and *nhr-1* have 1:1 homology in *C. elegans*, *pnhr-3* is found only in *P. pacificus* and not even in its sister congener, *P. exspectatus*, due to the species-specific gene duplication. Second, *pnhr-3* is rather situated in the 'phenotypic switch module' and *eud-1* is proven to be epistatic over this gene. Finally, the most downstream 'structural module' involved in the execution of the mouth forms through changes to the stoma and teeth include *dpy-6* (encoding Mucin-type hydrogel-forming protein) (Sun et al. 2022), *chs-2* (encoding chitin-synthase) (Sun et al. 2023) and *nas-6* (encoding astacin metalloprotease) (Ishita et al. 2023) (**Figure 2**).

The available understanding of the mouth-form GRN is indeed important; however, there are still standing questions, such as (i) how does the GRN evolve in nature; (ii) how do the environmental signals such as pheromones get integrated into the mouth-form GRN; (iii) what is the nature of mouth-form accommodation/assimilation in the genus *Pristionchus*; and (iv) what are the interactions of *P. pacificus* with other nematodes in nature.

The soil nematode *P. pacificus* is entomophilic and necromenic. They can reliably be found in association specifically in the dauer stage with insects, especially scarab beetles. In nature, these nematodes resume development, a phenomenon known as dauer recovery, once they sense the food signal from the proliferating microbes on the dead hosts (Hong 2015; Ragsdale et al. 2015). With this host

association determined, more than 2,000 *P. pacificus* strains have been collected worldwide enabling various natural variation studies to be conducted. Noticeably, *P. pacificus* strains can be split into well-supported lineages or clades (Herrmann et al. 2007, 2010; McGaughran and Morgan 2015; Rödelsperger et al. 2017). This strain collection serves as an entry point to study the differences in mouth-form preference as *P. pacificus* strains have varying degrees of mouth-form ratios (Ragsdale et al. 2013a). By performing quantitative trait locus (QTL) mapping of recombinant inbred lines (RILs) generated from parental strains from the same clade with contrasting mouth-form ratios, i.e., one being predominantly Eu and the other one being predominantly St, Dardiry et al. (2023a) identified rapid evolution of *cis*-regulatory elements in the mouth-form switch gene *eud-1*. Importantly, this study provided direct evidence for the evolution of a gene controlling the phenotypic plasticity, which is in itself evolvable at a different scale as discussed above (Susoy et al. 2015). Given the plethora of available strains, more studies can be carried out using other *P. pacificus* clades to understand the evolution of mouth-from GRN. Such a project represents a main part of my PhD work.

Both plastic traits, dauer formation and mouth-form polyphenism, are controlled by population density, which is itself sensed through pheromones. These communication signals, also known as ascarosides, exist in various nematodes from free-living to parasitic lifestyles and play a role in other important behaviours such as mating repulsion and attraction, aggregation, and foraging (Choe et al. 2012; Bhar et al. 2020; Machado and von Reuss 2022).One of the early discoveries pointing towards the potential use of pheromones in biological communication in nematodes dates back to the 1960s. Greet (1964) used a cellulose barrier to split males and females of the free-living nematode *Panagrolaimus rigidus* on culture agar plate and discovered that they get attracted to each other at the barrier. The same phenomenon was not observed for the same sexes. This indicated that sex pheromones were released and sensed by the opposite sexes. Later, Golden and Riddle (1982) reported a fatty-acid like pheromone that could control the dauer entry and exit in *C. elegans*. The molecular structures of nematode pheromones had remained enigmatic until 2005 when the first chemical characterisation of a *C. elegans* dauer pheromone, originally named daumone, took place (Jeong et al. 2005). This was soon followed by the discoveries of additional dauer-inducing pheromones indicating that a cocktail of ascarosides, and not just one single compound, is important for this developmental plasticity in *C. elegans* (Butcher et al. 2007; Pungaliya et al. 2009). It should be pointed out that there are two standard nomenclatures in the field of nematode pheromones. They can be named based on the modular structure in a 4-letter nematode gene-style format and followed by a number indicating the order of discovery. Alternatively, they can be named based on the structure in this format: head group-asc-(ω)(Δ)C#-terminus group, where ω specifies attachment at the terminal (ω), instead of the penultimate (ω-1) carbon, and Δ denotes a double bond at the α–β position. This second system is highly suitable for naming complex ascarosides. As an example for the ascaroside nomenclature, the first characterised *C. elegans* dauer pheromone is now commonly

known as ascr#1 or asc-C7 (Ludewig and Schroeder 2012; Butcher 2017).

Ascaroside pheromones can be broadly categorised into two groups: simple and complex ascarosides (von Reuss 2018). Simple ascarosides are glycolipids composed of a dideoxysugar L-ascarylose attached with a short to medium fatty acid side chain of varying lengths. Two other related sugars, the 2'-epimerised L-ascarylose called L-paratose and the 4'-epimerised L-ascarylose called L-caenorhabdose, are also utilised as pheromone building in *P. pacificus* and *Caenorhabditis nigoni*, respectively (Bose et al. 2012; Bergame et al. 2019). Complex ascarosides have simple ascarosides as the 'backbone' building block that is further decorated with a variety of moieties originating from diverse metabolic pathways at the terminus of fatty acid side chain and/or 2' or 4' position of the sugar. Historically, the term 'ascarosides' was erected to refer to non-pheromone unsaponifiable lipid molecules made up of an ascarylose sugar and a long aliphatic side chain of between 29 to 33 carbons originally found in the egg shell of parasitic nematode family Ascarididae more than 100 years ago (von Reuss and Schroeder 2015; Butcher 2017; Bhar et al. 2020; Hille-Rehfeld 2025).

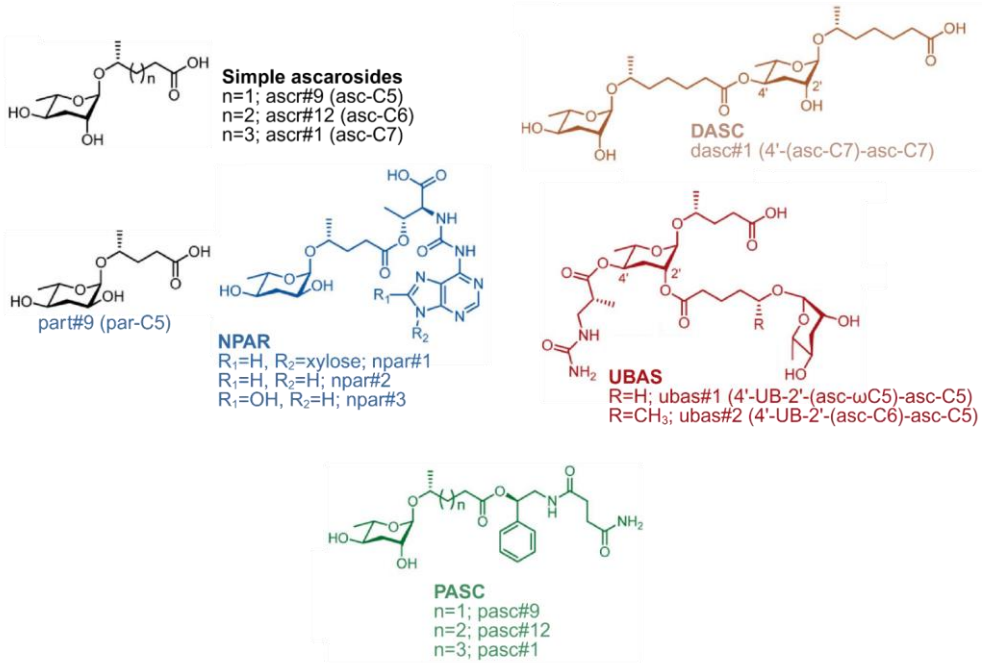


Figure 3 *P. pacificus* pheromones. These communication chemicals in *P. pacificus* are composed of simple ascarosides and four groups of complex ascarosides: UBAS (3-ureidoisobutyrate ascarosides), DASC (dimeric ascaroside), PASC (phenylethanolamide ascaroside), and NPAR (nucleoside-based paratoside). Adapted from Dong et al. (2020) and Zhang, Theam et al. (2025).

In *P. pacificus*, in addition to simple ascarosides, there are four types of complex ascarosides including UBAS (3-ureidoisobutyrate ascarosides), DASC (dimeric ascaroside), PASC (phenylethanolamide ascaroside), and NPAR (nucleoside-based paratoside) (Bose et al. 2012; Dong et al. 2020) (**Figure 3**). To understand the integration of pheromones into the mouth-form phenotype execution,

each type of pheromones should be ideally inhibited from being biosynthesised. Leveraging the available *P. pacificus* strains, Falcke et al. (2018) performed a genome-wide association study (GWAS) for the production of pheromones. They found that a carboxylesterase-encoding gene named *uar-1* (*u*bas *a*scaroside required) is specifically involved in the production of UBAS compounds. In relation to mouth-form plasticity, dasc#1 (4'-(asc-C7)-asc-C7), which is a DASC type pheromone, was shown to have the strongest influence on the Eu phenotype (Bose et al. 2012; Werner et al. 2018). Another part my PhD work was to uncover the biosynthesis of dasc#1 and study how *P. pacificus* mutants defective for the production of this ascaroside influence the mouth-form decision. This work was conducted in collaboration with Prof. Dr. Chuanfu Dong's lab at Beijing Normal University and built on the previous discovery of the biosynthesis pathway of UBAS ascarosides.

Well-supported phylogenies are important for the understanding of gene-or-plasticity-first debate and evolution in general (Lee and Doughty 1997; Schwander and Leimar 2011). In model organisms such as zebrafish (*Danio*), thale cress (*Arabidopsis*), fruit fly (*Drosophila*) baker's yeast (*Saccharomyces*), and mouse (*Mus*), the existence of robust phylogenetic trees supports comparative studies (Tucker 2007; Hittinger 2013; Koenig and Weigel 2015; O'Grady and DeSalle 2018; Lu et al. 2025 *preprint*). The same is true for the nematode genus *Caenorhabditis* (Stevens et al. 2019; Devi et al. 2025; Rockman et al. 2026). In the context of the mouth-form plasticity in the genus *Pristionchus*, such a quest to find new species has resulted in important findings. For example, there has been discovery of a clade with an additional form of the predatory mouth morph, dubbed 'megastomatous (Mg)', in addition to the canonical Eu and St phenotypes. Separately, species with trait assimilation, i.e., mouth-form plasticity is secondarily lost resulting in species being monomorphic, were also found (Kanzaki et al. 2012, 2013; Ragsdale et al. 2013b). I joined forces with the entomo-nematology group in my lab, led by Dr. Matthias Herrmann with the support from his research technician Mr. Christian Weiler, to describe new *Pristionchus* species with mouth morphs that can be used to understand phenotypic transitions.

Lastly, as *Pristionchus* nematodes can be found in coexistence with other nematodes in the beetle system, this metacommunity is appropriate to address ecological questions (Herrmann et al. 2006; Weller et al. 2010). Interestingly, the dimorphic *P. pacificus* has been found together with its relative species *P. mayeri*, which is preferentially St-biased, and a completely different diplogastrid genus *Acrostichus* having only the St morph on the same host beetle *Gymnogaster buphthalma*. This feature permits the study on competition and dynamics of coexistence with the potential implications for further understanding of the metacommunity and species succession theories. This work was conducted in collaboration with Dr. Ata Kalirad, a postdoctoral researcher in my lab.

2. Research objectives

The overall goal of my dissertation is to further elucidate the evolutionary adaptation of stomatal plasticity in the omnivorous *P. pacificus*. Specifically, I tried to fill knowledge gaps regarding (i) how the mouth-form GRN itself evolves; (ii) how the biosynthesis of complex pheromones is controlled and the potential role of these pheromones in the mouth-form GRN; and (iii) how mouth-form developmental plasticity in *P. pacificus* contributes in nature in the context of metacommunity ecology and species succession. Additionally, I wanted to contribute to the understanding of the evolution of this plastic trait in a larger phylogenetic context of the genus *Pristionchus*. To achieve these aims, I conducted various projects as following:

1. I sampled *Adoretus* beetles on Réunion island to isolate extra *P. pacificus* strains for mouth-form phenotyping. After determining that previously and newly collected strains from the same host beetles and locality had contrasting mouth-form biases, I generated RILs and mapped the underlying QTL explaining this difference. This project led to the understanding on how mouth-form GRN itself evolves in nature.

2. I generated CRISPR/Cas9-mediated *P. pacificus* mutants in the most closely related homologues of carboxylesterase-encoding gene *uar-1*, which is specifically involved in the production of a class of pheromones. Together with the collaborators in China, we screened these mutants for the loss of the production of dasc#1, a pheromone that induces the predatory phenotype. We found such mutants which could be used to answer how pheromonal communication is regulated downstream in the mouth-form GRN.

3. I collected *G. buphthalma* beetles on Réunion island and observed their emergence and determined the number of nematodes (*P. pacificus* and their potential competitors) exiting dauer stage. I isolated and determined fecundity, sex ratio, and mouth-form preferences of *P. pacificus*, *P. mayeri*, and *Acrostichus* sp. that co-infested the same host beetles. These empirical data were complemented with model simulations from a postdoctoral colleague. This project contributed to the understanding on how mouth-form plasticity in *P. pacificus* helps it in nature in the context of metacommunity ecology and species succession.

4. I joined my colleagues, Dr. Matthias Herrmann and Mr. Christian Weiler, in the beetle collection trips to Asia, which is the biodiversity hotspot and speciation hub of the genus *Pristionchus*. We could isolate new *Pristionchus* species with mouth-form features implicated for important evolutionary/comparative understanding of trait evolution.

The results of these projects and other collaborative works are described in more detail below.

3. Results

3.1. Thousands of *Pristionchus pacificus* orphan genes were integrated into developmental networks that respond to diverse environmental microbiota

Athanasouli, M., N. Akduman, W. Röseler, **P. Theam**, and C. Rödelsperger. 2023. *PLoS Genet.* 19:e1010832. DOI: 10.1371/journal.pgen.1010832

3.1.1. Synopsis

Orphan genes are taxonomically restricted genes and there are no homologues detected in any taxa. One third of the model nematode *P. pacificus* genes are made up of orphan genes. While previous works have uncovered the origins and patterns of this gene class, their functionality in the organism has not been well characterised except for two genes. *dau-1* was the first *P. pacificus* orphan gene shown to have a function in dauer formation and life-history competition and *self-1*, the second characterised orphan gene, was linked to kin recognition. To assign potential functionalities to the rest of the orphan genes, *P. pacificus* was monoxenically raised in 24 bacterial diets and the coexpression modules with at least 50 genes each were assigned. Such an approach revealed that thousands of *P. pacificus* orphan genes are environmentally responsive and, among the 28 identified coexpression modules, the largest ones are potentially associated with reproduction, nervous system, and intestine. This research supports the notion that newly arisen orphan genes are integrated into the life-history responses to environments.

3.1.2. Own contribution

I performed developmental speed experiments and wrote the corresponding part. My contribution is approximately 10%.

3.2. Description of two new *Pristionchus* species from South Korea

Herrmann, M., N. Kanzaki, C. Weiler, **P. Theam**, C. Rödelsperger, and R. J. Sommer. 2024. Description of two new *Pristionchus* species from South Korea. *J. Nematol.* 56:20240032. DOI: 10.2478/jofnem-2024-0032

3.2.1. Synopsis

The genus *Pristionchus* represents an important group for evo-devo studies, especially for the plasticity of their stomatal morphology. This plasticity is in the form of bacterivorous and predatory mouth morphs. In the quest to isolate more *Pristionchus* species for comparative studies over the past two decades across different continents, there are at least two important findings. First, biogeography of the species clades has become evident and Asia seems to be the origin of the genus as it is the most species-rich continent for *Pristionchus* and the sister genus *Parapristionchus* was also isolated from there. Second, there are signatures of *Pristionchus* species in one of the clades with the secondary loss of plasticity and the mouth morph becomes monomorphic providing an opportunity to study the genetic assimilation. In this study, further collection trips were carried out in South Korea to isolate extra *Pristionchus* species as it is situated between two countries with many novel *Pristionchus* species found: Japan and China. Two novel species were found from different scarab beetles and described. Essentially, one of the new species, *P. coreanus* n. sp., has only one mouth morph representing another species with the secondary loss of mouth-form plasticity in a separate clade from what was known earlier. The finding of the other species, *P. hangukensis* n. sp., helps clarify the biogeography of a subclade between *pacificus* and *maupasi* clades with Asian and American origins, respectively. This subclade is now clearly separated from the American-*maupasi* clade and is most likely of Asian origin. Taken together, this work contributed important materials for genetic assimilation and biogeography of the genus *Pristionchus*.

3.2.2. Own contribution

I measured the morphometrics of these species and contributed to the revision of the manuscript. My contribution is approximately 15%.

3.3. *Pristionchus kravanhensis* n. sp., the first *Pristionchus* species reported from Cambodia

Theam, P., N. Kanzaki, M. Herrmann, C. Weiler, C. Rödelsperger, and R. J. Sommer. 2025. *Nematology* 27:651–663. DOI: 10.1163/15685411-bja10413

3.3.1. Synopsis

The model nematode *P. pacificus* has two mouth forms including single-toothed and narrow-mouthed bacterivorous 'stenostomatous (St)' and two-teethed and wide-mouthed omnivorous 'eurystomatous (Eu)' morphs, providing a clear example of phenotypic plasticity. The canonical morphs are present across the whole genus, except for some species with secondary loss of plasticity and one clade that has a third mouth form. This form is known as 'megastomatous (Mg)' morph, which is similar to the Eu morph. One of the main differences between these two morphs is that Eu and Mg phenotypes have 6 and up to 12 cheilostomatal plates, respectively. The presence of this trimorphism has been so far observed only in the *triformis* clade of *Pristionchus*. In this paper, we set out to find new *Pristionchus* species in a less explored part of Asia for *Pristionchus*, which is Southeast Asia. We isolated one novel species, *P. kravanhensis* n. sp., which turned out to be the sister of all described species in the *triformis* clade. Of note, this species has only two mouth morphs: St and Eu. In a portion of the population, some splits in the 6 cheilostomatal plates in the Eu form were observed, but they are essentially not Mg. Hence, this species represents an interesting biological attribute for the study of the transitions from dimorphism to trimorphism.

3.3.2. Own contribution

I initiated the project, joined the field collection, measured the morphometrics of this species, and revised the manuscript. My contribution is approximately 35%.

3.4. Biosynthesis of modular signaling molecules requires functional diversification of carboxylesterases in *Pristionchus pacificus*

Zhang, P.[#], **P. Theam**[#], W. Xu[#], S. Ye, H. Witte, T. Liu, R. J. Sommer, and C. Dong. 2025. *Commun. Biol.* 8:1213. DOI: 10.1038/s42003-025-08641-4

# denotes co-first authors

3.4.1. Synopsis

Nematodes utilise ascaroside pheromones to communicate and make life-history decisions, for example dauer entry or exit. These compounds are made up of an ascarylose sugar attached with a wide range of short fatty acid side chains. These simple ascarosides can be further decorated with various moieties on the 2'- or 4'-position of the sugar of the terminus of the fatty acid side chains making them become complex ascarosides. In *P. pacificus*, the complex ascarosides include UBAS (3-ureidoisobutyrate ascarosides), DASC (dimeric ascaroside), PASC (phenylethanolamide ascaroside), and NPAR (nucleoside-based paratoside). A carboxylesterase enzyme, UAR-1, was discovered to be specifically involved in the production of UBAS. The same enzyme class was also shown to be important for *C. elegans* pheromone biosynthesis. This project was initiated to identify a carboxylesterase-encoding gene involved in the production of a DASC-type ascaroside, dasc#1, which is important for predatory mouth-form fate. We found that the *uar-12* gene is specifically needed for the production of this chemical. Importantly, by assaying the dasc#1-deficient mutants and wild-type individuals, we showed that the mouth-form decision genes can override the pheromone signal. Additionally, we also discovered that *uar-6* and *uar-5* are essential for the production of the NPAR and 2'-decorated UBAS pheromones, respectively. *uar-12* and *uar-6* were demonstrated to be expressed in the epidermal cells and intestine. In sum, the findings in this paper supported the importance of carboxylesterases in the production of complex ascarosides with the intestine serving as a main hub for the biosynthesis.

3.4.2. Own contribution

I isolated CRISPR/Cas9-engineered mutants, performed phylogenetic and protein domain analyses, and wrote parts of the manuscript. My contribution is approximately 30%.

3.5. Bacterial diet influences mutation rate in *Pristionchus pacificus*

Wang, Y.[#], **P. Theam**[#], S. P. Quiobe[#], W. Röseler, H. Witte, C. Rödelsperger, and R. J. Sommer. 2026. *G3* 16:jkag038. DOI: 10.1093/g3journal/jkag038

# denotes co-first authors

3.5.1. Synopsis

Mutation is one of the main attributes for evolution across the tree of life. The rates of mutation can be influenced by both abiotic and biotic environmental factors and genetic backgrounds. While various studies have shown the effects of temperature on mutation rates, diets which represent another important and direct factor influencing the organisms has not been observed more widely. In this paper, we addressed exactly this question in the backdrop of different *P. pacificus* strains over 100 generations using the mutation accumulation line approach. We found that there was approximately 1.4-fold mutation-rate difference between *P. pacificus* fed with various monoxenic bacterial diets. While this stark difference was observed, the mutation spectra themselves did not vary much. These results together demonstrated that the environmental inputs can affect the mutation rates, but the mutation spectra are relatively comparable.

3.5.2. Own contribution

I cultured mutation accumulation lines on three monoxenic diets for 100 generations, extracted their DNA for whole-genome sequencing, and wrote the corresponding parts. My contribution is approximately 30%.

3.6. The dynamics of coexistence and succession in a decaying ecosystem

Kalirad, A., **P. Theam**, and R. J. Sommer. 2025. *bioRxiv* 2025.04.28.650976. DOI: 10.1101/2025.04.28.650976

3.6.1. Synopsis

Pristionchus nematodes including *P. pacificus* can be found in association with scarab beetles together with other nematodes as dauers, the non-feeding, stress-resistant, and dispersal stage of nematodes. Upon the natural death of the hosts, these nematodes exit dauer in response to the food cues from the growing microbes on the beetle carcass. Specifically, in the melolonthine beetle system *Gymnogaster buphthalma*, there exist three species of nematodes including *P. pacificus*, *P. mayeri* and *Acrostichus* sp. Whereas *P. pacificus* and *P. mayeri* are androecious hermaphrodites, *Acrostichus* sp. is gonochoristic. The two *Pristionchus* species have mouth-form dimorphism allowing them to be capable of killing and feeding on other nematodes. However, under lab conditions, while *P. pacificus* is preferentially predatory, *P. mayeri* tends to be more bacterivorous. *Acrostichus* sp. is strictly bacterivorous. In this study, we observed the emergence time and the number of emerging nematodes on the sacrificed beetles every 24 h. These triple species were isolated to determine their fecundity. Combining the data of reproduction strategies, mouth-form biases, emergence time, nematodes exiting dauer, and brood size with model simulations, we could provide evidence for species coexistence. Overall, this work could contribute to our understanding of the metacommunity and species succession.

3.6.2. Own contribution

I collected the beetles, observed the nematode succession on the beetle carcasses, and determined the fecundity, sex ratio, and mouth-form biases of the nematodes. My contribution is approximately 40%.

3.7. Evidence of a predator-prey co-evolutionary arms race within a nematode microhabitat

Goetting, D. L., K. K. Sarai, **P. Theam**, R. J. Sommer, and J. W. Lightfoot. *bioRxiv* 2026.04.02.716111. DOI: 10.64898/2026.04.02.716111

3.7.1. Synopsis

Interactions between cohabiting organisms including predators and their prey can result in the arms race in the form of evolutionary trajectories that would be optimal for survival of each organism. While there exist various cases of interspecific interactions in nature, the possibility to study such interactions in-depth at the mechanistic level is scarce. The predatory nematode *P. pacificus* has served as a well-established predator model system in predatory-prey interactions; however, to date, the prey side has been studied using *C. elegans*, which *P. pacificus* rarely encounters in the wild. To fill this knowledge gap, in this study, we set out to find potential natural prey of *P. pacificus* from their necromenic beetle environment. We found that *Oscheius myriophilus*, which are distantly related to *C. elegans*, could be isolated from the same beetle hosts together with *P. pacificus*. Thus, *O. myriophilus* likely represents potential natural prey of *P. pacificus*. Indeed, using predatory assays, automated tracking, and machine-learning-based behavioural analysis, it was shown that *O. myriophilus* nematodes are killed and consumed by *P. pacificus* isolated from the same host beetles. However, the predation rates on *O. myriophilus* were observed to be lower than those in the *C. elegans* prey control experiments. This finding indicates that *O. myriophilus* might have evolved some level of resistance to their naturally co-occurring predators. We further showed that, *O. myriophilus* possesses a mixed reproductive strategy: early oviposition coupled with ovoviviparity and matricide later in mature hermaphrodites. This strategy could have evolved as a bet-hedging strategy maximising early dispersal and growth in the protected environment of the mother cuticle in the presence of *P. pacificus* predators. Together, this work establishes a naturally occurring nematode predator-prey highly amenable to genetic manipulations potentially progressing our deeper understanding of co-evolutionary arms race.

3.7.2. Own contribution

I collected beetle and nematode specimens, genotyped the nematodes and analysed their phylogenetic relationships, and wrote the corresponding parts. My contribution is approximately 10%.

3.8. Plasticity in nonsense-mediated decay and translation initiation regulate polyphenism

Theam, P., H. Witte, R. Liu, T. Loschko, C. Rödelsperger, C. Igreja, and R. J. Sommer. *bioRxiv* 2026.03.27.714762. DOI: 10.64898/2026.03.27.714762

3.8.1. Synopsis

Developmental plasticity plays an important role in plasticity-led evolution. The execution of such alternative phenotypes is under the control of a robust gene regulatory network (GRN). How genes in these GRNs themselves evolve in nature has not been well elucidated. The model nematode *P. pacificus*, which can be found on scarab beetles, exhibits mouth morph plasticity in adult individuals. These animals can grow as strict bacterivores known as St form or facultative predators known as Eu form. The underlying GRN controlling the decision between these two morphs has been characterised with the sulfatase-encoding gene *eud-1* acting as the central switch gene. Leveraging on the available plethora of *P. pacificus* strains with varying mouth-form ratios and the possibility to isolate extra strains from beetles, we conducted a study to understand how mouth-form GRN genes evolve in the wild. We isolated new strains from the same beetle group at the same locality of previously isolated strains with the St-form bias, which were collected more than a decade earlier. We found that there was a stark shift in the mouth-form preference with the newly isolated strains being highly Eu instead. We generated recombinant inbred lines (RILs) and mapped the quantitative trait locus (QTL) and found that there is an exonic difference in the *eud-1* with the St parent having a 19-bp deletion in the first exon. Further experiments involving allele swappings, qPCR, polysome profiling, and steroid sulfatase inhibitor pointed towards the plasticity in nonsense-medicated decay efficiency coupled with alternative N-terminal proteoforms of the EUD-1 protein consisting of two methionines: one on exon 1 and the other one on exon 2. All in all, this study provides evidence for the microevolution of plasticity GRN in nature.

3.8.2. Own contribution

I conceived the project with my supervisor, collected the beetles, isolated *P. pacificus* strains, generated RILs and extracted their DNA for QTL mapping, isolated CRISPR/Cas9-mediated allele-swapping mutants, and obtained all the mouth-form ratio data. My contribution is approximately 80%.

4. Discussion

Phenotypic plasticity has been increasingly accepted to not only have ecological relevance but also evolutionary importance (Thompson 1991; Agrawal 2001; Pigliucci 2001; Miner et al. 2005). The model nematode *P. pacificus* has become one of the important systems in phenotypic plasticity studies (Moczek et al. 2011; Gilbert et al. 2015; Gibert 2017; Schlichting 2021). The uniqueness of this biological system is twofold. Firstly, owing to its self-fertilising hermaphroditic reproduction, its irreversible feeding polyphenism, i.e., bacterivorous (St) and omnivorous (Eu) mouth morphs can be studied in isogenic backgrounds. These works have contributed to our understanding of the adaptive value and cost of alternative phenotypes and the effects of abiotic and biotic environmental stimuli on phenotypic execution (Bose et al. 2012; Serobyan et al. 2014; Dardiry et al. 2023b; Lenuzzi et al. 2023; Kalirad and Sommer 2024; Piskobulu et al. 2025). Secondly, as a highly genetically tractable system, this feeding structure plasticity has been extensively studied at the genetic and molecular levels resulting in a robust mouth-form GRN (Sommer et al. 2017; Reich et al. 2025; FitzGerald et al. 2025 *preprint*). While these discoveries have accelerated our understanding of phenotypic plasticity, certain knowledge gaps still exist, for example, the evolutionary adaptability of *P. pacificus* mouth-form plasticity. To address this big question, my overall PhD dissertation led to four main findings such as (i) the microevolution of mouth-form GRN; (ii) the evolutionary robustness of mouth-form GRN in interpreting the environmental inputs, for instance, pheromones; (iii) the adaptive role of mouth-form plasticity in metacommunity ecology and species succession; and (iv) the evolutionary flexibility of mouth-form plasticity in a larger phylogenetic context, i.e., across the whole genus *Pristionchus*.

Firstly, leveraging the well-established *P. pacificus*-beetle association enabling easy isolation of the nematodes, I could study the natural variation and evolution of mouth-form GRN at the microevolutionary timescale (Sommer 2025). By experimenting on *P. pacificus* strains with contrasting mouth-form preferences but sampled one decade apart from the same locality and host beetle genus, my QTL mapping study revealed that the main mouth-form switch gene in the GRN, *eud-1*, has a frameshift deletion in the coding region in the St-biased parent. Additionally, amino acid substitution, qPCR, and polysome profiling experiments unequivocally indicated that the EUD-1 protein can be translated either from the first or second exon (Theam et al. 2026 *preprint*). This work led to three main conclusions: (i) natural variation in the mouth-form GRN exists in the natural populations of *P. pacificus*; (ii) *eud-1* is a mutational hotspot in *P. pacificus* natural populations; and (iii) the N-terminal proteoforms of EUD-1 buffer the potential deleterious mutations in exon 1 or 2 in *P. pacificus* populations in the wild. The first two conclusions corroborate the earlier findings by Dardiry et al. (2023a), wherein they also found natural variation in *eud-1* among *P. pacificus* strains with contrasting mouth-form biases. Noticeably, *P. pacificus* genotypes in their study belong to a different phylogenetic clade from my study. With these pieces of evidence, it would be worthwhile to study the natural

variation in the mouth-form phenotype across the worldwide collection of *P. pacificus* employing quantitative genetic techniques, for instance, genome-wide association study (GWAS) (Ragsdale et al. 2013a; Rödelsperger et al. 2017; Widmayer et al. 2022). Such a work could potentially uncover natural variation in other genes in the mouth-form GRN and/or other variants in *eud-1* locus extending our understanding of genetic variation and evolution at the mechanistic level (Dobzhansky 1959; Mitchell-Olds et al. 2007; Latta 2010). For example, in other biological systems such as humans, the standing variation has implications for the evolution of disease susceptibility and resistance (Ashley et al. 2012; Gomez et al. 2014; Quintana-Murci 2016). In the bacterial kingdom, cryptic genetic variation contributes to evolution of biosynthetic gene clusters (Chevrette et al. 2020). In plants such as *Arabidopsis* and rice *Oryza sativa*, flowering time can be attributed to polymorphisms. Genetic variation also explains the production of flavonoids and apocarotenoids in rice and citrus (e.g., tangerine *Citrus reticulata* and trifoliate orange *Poncirus trifoliata*), respectively (Johanson et al. 2000; Xue et al. 2008; Peng et al. 2017; Zheng et al. 2019). Regarding the evolutionary adaptation in the form of alternative translations of EUD-1, the main switch protein for mouth-form decision, this finding contributes to the mounting known cases of proteoforms in phenotypic plasticity across various systems such as sex determination plasticity in *Drosophila*, the American alligator *Alligator mississippiensis* and the red-eared slider turtle *Trachemys scripta*, wing pattern plasticity in the butterfly *B. anynana*, and castes in the buff-tailed bumble bee *Bombus terrestris* (Price et al. 2018; Steward et al. 2022; *reviewed in* Wright et al. 2022). Additionally, the existence of alternative translations of such an important gene in a dimorphic trait provides direct evidence for the evolutionary adaptation in the events of the genetic drift of deleterious alleles in exon 1 or 2. Going forward, as mentioned earlier, since *P. pacificus* is highly amenable to genetic studies, it would be an interesting avenue to decipher the transcriptional and/or translational mechanisms of N-terminal proteoforms of EUD-1 in greater detail. All in all, the *P. pacificus* system has a great potential in progressing our understanding of polymorphisms of trait polyphenism and its evolutionary adaptation at the mechanistic level.

Secondly, while it has been clearly proven that ascaroside pheromones (e.g., an Eu-morph-inducing dimeric ascaroside dasc#1) are essential in the mouth-form dimorphism in *P. pacificus*, how robust has the mouth-form GRN evolved to interpret these communication signals still remains enigmatic (Bose et al. 2012; Werner et al. 2018). One of the approaches to address this question is to ideally interrupt the biosynthesis of each pheromone class and study the 'indirect epistasis' of mouth-form GRN over pheromone biosynthetic genes. Two important findings were discovered: (i) carboxylesterase-encoding genes, called *uar* genes in *P. pacificus* and *cest* in *C. elegans*, are important for specific production of each group of pheromones and (ii) the mouth-form decision gene network can override the pheromone signals, i.e., the *P. pacificus* reference strain can still form the Eu morph in the absence of dasc#1 (Zhang, Theam et al. 2025). Three implications can be drawn from these results. Firstly, the mouth-form GRN has evolved to be robust (MacNeil and Walhout 2011;

Sieriebriennikov and Sommer 2018). Secondly, while it is clear that the mouth-form GRN acts downstream of the *uar* genes in the mouth-form phenotype decision, the pheromone receptors still remain to be identified and their epistatic relationships with mouth-form genes needs to be formally analysed (McGrath and Ruvinsky 2019). Pheromone receptors have also been characterised in other systems with known phenotypic plasticity. For instance, in *Drosophila*, the plasticity in mating choice among females was shown to act via Or47b olfactory receptor neuron for the response to a male pheromone (Kohlmeier et al. 2021). In the migratory locust *Locusta migratoria*, an important pheromone for aggregation behaviour was elucidated as 4-vinylanisole (4VA) and it is sensed through the OR35 olfactory receptor (Guo et al. 2020). Thirdly, the discovery that carboxylesterase-encoding genes are essential for the biosynthesis of complex pheromones in *P. pacificus* like in *C. elegans* might serve as a potential means to control plant- and animal-parasitic nematodes by inhibiting this class of enzymes (Falcke et al. 2018; Faghih et al. 2020; Le et al. 2020). Indeed, there seems to be an expansion of carboxylesterase-encoding genes in parasitic nematode clades (Wrobel and Schroeder 2023). However, to date, there have only been simple pheromones discovered in a small number of parasitic nematodes with their pheromones profiled. Pheromone compositions of many other important parasitic nematode groups such as animal and human parasites of the genus *Strongyloides*, ruminant parasites of the genus *Haemonchus*, and animal parasites of the genus *Ancylostoma* still remain to be characterised (Choe et al. 2012; Manosalva et al. 2015).

Thirdly, another aspect of evolutionary adaptation of feeding dimorphism in *P. pacificus* awaiting elucidation is how this plastic trait plays out in the advantage of this species in the natural coexistence environment with other nematode groups. Using the co-infestation on the same beetle carrier *G. buphthalma*, of *P. mayeri*, a congener of *P. pacificus*, and a novel *Acrostichus* species, a member of a distantly related genus of *Pristionchus*, Renahan and Sommer (2021) showed that this setting could lead to the competition-induced predatory feeding plasticity in the preferentially bacterivorous *P. mayeri*. In our study, this system was taken forward, specifically by studying it in the context of species coexistence in disequilibrium combining life-history traits with agent-based modeling. We found that: (i) *P. pacificus* also naturally coexists with *P. mayeri* and *Acrostichus* sp. on *G. buphthalma* beetles and (ii) nematode coexistence is possible across various scenarios, i.e., double and triple co-infestations (Kalirad, Theam, and Sommer 2025 *preprint*). Given that *P. pacificus* is a well-established model system, the discovery of coexistence in nature would serve as an important entry point to study the nematode interactions at a mechanistic depth, for example, the role of neuronal activity and biochemical communication in the interplay of interactions in addition to the topic of this current study (Hsueh et al. 2014; Liu et al. 2018; Quach and Chalasani 2020; Eren et al. 2026). As for the nematode species coexistence in disequilibrium, we found that they distinctly employ various metacommunity-level strategies including plastic characters (i.e., mouth-form and dauer), dispersal timing, and life-history traits (e.g., fecundity). In *P. pacificus*, the

existence of the mouth-form dimorphism provides an evolutionary advantage offsetting the relatively later dispersal timing whereas the preferentially bacterivorous *P. mayeri* and strictly bacterivorous *Acrostichus* sp. instead opt for high fecundity and faster dispersal, respectively. Noticeably, various nematodes can evolve to utilise different processes altering coexistence. For example, while the coexistence of the bacterivorous marine nematode *Litoditis marina* is shaped by density- and interspecific interaction-induced dispersal, this phenomenon is affected by asymmetric sperm-induced harm in sympatric the *Caenorhabditis* nematodes (De Meester et al. 2015; Schalkowski et al. 2024). In this context, our work contributes a unique system with various levels of interactions and life-history strategies for further observations in the framework of metacommunity ecology and species succession.

Lastly, while the presence of the plastic intraguild predation trait is evolutionarily beneficial for *P. pacificus*, the evolutionary lability of this trait across the genus, for example, in the context of genetic assimilation or genetic accommodation remains to be addressed (Serobyan et al. 2014; Renahan and Sommer 2022; Kalirad, Theam, and Sommer 2025 *preprint*). By joining forces with the entomo-nematology group in my department, I contributed to the descriptions of three novel *Pristionchus* species, two of them being important for the understanding of trait evolvability. Whereas the mouth of *P. coreanus*, belonging to a dimorphic clade, has become monomorphically St, this phenotype in *P. kravanhensis*, a sister species to all species of the only known trimorphic clade in the genus *Pristionchus*, is dimorphic (Herrmann, Kanzaki, Weiler, Theam et al. 2024; Theam et al. 2025). These results provide additional evidence for the genetic assimilation (i.e., secondary loss of plasticity) as observed in various nematode genera in the family Diplogastridae, to which *Pristionchus* belongs, and the emergence of trait novelty, for example, in spadefoot toads (Susoy et al. 2015; Levis et al. 2018). The secondary loss of plasticity in *P. coreanus* represents the third case of such a phenomenon in the genus. *P. elegans* and *P. bucculentus* are monomorphic for the feeding structure having only the St and Eu morph, respectively (Kanzaki et al. 2012, 2013). These convergently repeated losses of plasticity at the genus level provide a treasure trove for the understanding of genetic assimilation theories. Additionally, studies can also be devised to uncover the adaptive value as well as life-history strategies of these taxa possessing monomorphic feeding structure. The discovery of a dimorphic species being a sister to all known trimorphic *Pristionchus* species to date serves as a key experimental material to study the trait evolution, i.e., the evolutionary transition from dimorphism to trimorphism (Brommer 2013; DeWitt 2016; Levis et al. 2018). Thus, the genus *Pristionchus* is a potential hotbed for progressing our understanding of plastic trait evolution, especially with regard to the macroevolution context.

In conclusion, my dissertation contributed towards further understanding of the evolutionary adaptation of developmental plasticity using the model nematode *P. pacificus* with four main findings: (i) the mouth-form GRN evolves at the microevolutionary timescale, specifically the main plasticity switch gene, *eud-1*, has

evolved to have N-terminal proteoforms as a ‘back-up’ strategy in events of genetic drift of deleterious alleles in one of the first two exons; (ii) the mouth-form GRN has evolved to be robust in controlling the mouth-form decision downstream of the pheromone communication; (iii) the existence of intraguild predatory morph plays an essential role for the coexistence of *P. pacificus* with other nematode species, which are able to utilise other life-history strategies in this metacommunity ecology; and (iv) this plastic feeding trait is evolutionarily labile. Overall, this dissertation provides empirical data for further understanding of the evolutionary adaptation of adaptive phenotypic plasticity.

5. References

Abbot, P. 2022. Defense in social insects: diversity, division of labor, and evolution. *Annu. Rev. Entomol.* 67:407–436.

Abouheif, E., and G. A. Wray. 2002. Evolution of the gene network underlying wing polyphenism in ants. *Science* 297:249–252.

Acasuso-Rivero, C., C. J. Murren, C. D. Schlichting, and U. K. Steiner. 2019. Adaptive phenotypic plasticity for life-history and less fitness-related traits. *Proc. R. Soc. B* 286:20190653.

Adams, S., S. Tandonnet, and A. Pires-daSilva. 2025. Balancing selfing and outcrossing: the genetics and cell biology of nematodes with three sexual morphs. *Genetics* 229:iyae173.

Agrawal, A. A. 2001. Phenotypic plasticity in the interactions and evolution of species. *Science* 294:321–326.

Ahringer, J. 2006. Reverse genetics. In The *C. elegans* Research Community, ed., WormBook: The Online Review of *C. elegans* Biology. Pasadena, CA.

Akhurst, R. J. 1980. Morphological and functional dimorphism in *Xenorhabdus* spp., bacteria symbiotically associated with the insect pathogenic nematodes *Neoaplectana* and *Heterorhabditis*. *J. Gen. Microbiol.* 121:303–308.

Ananthakrishnan, T. N. 2005. Perspectives and dimensions of phenotypic plasticity in insects. In T. M. Ananthakrishnan, and D. Whitman, eds., *Insect Phynotypic Plasticity: Diversity of Responses.* Science Publishers, Plymouth, UK.

Araya-Ajoy, Y. G., K. J. Mathot, and N. J. Dingemanse. 2015. An approach to estimate short-term, long-term and reaction norm repeatability. *Methods Ecol. Evol*. 6:1462–1473.

Ashley, N. T., Z. M. Weil, and R. J. Nelson. 2012. Inflammation: mechanisms, costs, and natural variation. *Annu. Rev. Ecol. Evol. Syst.* 43:385–406.

Aubret, F., and R. Shine. 2009. Genetic assimilation and the postcolonization erosion of phenotypic plasticity in island Tiger snakes. *Curr. Biol.* 19: 1932–1936.

Badyaev, A. V., A. L. Potticary, and E. S. Morrison. 2017. Most colorful example of genetic assimilation? Exploring the evolutionary destiny of recurrent phenotypic accommodation. *Am. Nat.* 190:266–280.

Bailey, N. W., C. Desjonquères, A. Drago, J. G. Rayner, S. L. Sturiale, and X. Zhang. 2021. A neglected conceptual problem regarding phenotypic plasticity's role in adaptive evolution: the importance of genetic covariance and social drive. *Evol. Lett.* 5:444–457.

Batra, S. W. T. 1966. Nests and social behavior of halictine bees of India

(Hymenoptera: Halictidae). *Indian J. Entomol.* 28:375–393.

Bento, G., A. Ogawa, and R. J. Sommer. 2010. Co-option of the hormone-signalling module dafachronic acid–DAF-12 in nematode evolution. *Nature* 466:494–497.

Bergame, C. P., C. Dong, S. Sutour, and S. H. von Reuß. 2019. Epimerization of an ascaroside-type glycolipid downstream of the canonical *β*-oxidation cycle in the nematode *Caenorhabditis nigoni*. *Org. Lett.* 21:9889–9892.

Beshers, S. N., and J. H. Fewell. 2001. Models of division of labor in social insects. *Annu. Rev. Entomol.* 46:413–440.

Bhar, S., D. H. Perez, and R. A. Butcher. 2020. Chemical ecology of nematodes. In H.-W. Liu, and T. P. Begley, eds., *Comprehensive Natural Products III: Chemistry and Biology*. Elsevier, London, UK.

Bhardwaj, S., L. S.-H. Jolander, M. R. Wenk, J. C. Oliver, H. N. Nijhout, and A. Monteiro. 2020. Origin of the mechanism of phenotypic plasticity in satyrid butterfly eyespots. *eLife* 9:e49544.

Blaxter, M. L., P. De Ley, J. R. Garey, L. X. Liu, P. Scheldeman, A. Vierstraete, J. R. Vanfleteren, L. Y. Mackey, M. Dorris, L. M. Frisse, J. T. Vida, and W. K. Thomas. 1998. A molecular evolutionary framework for the phylum Nematoda *Nature* 392:71–75.

Bonser, S. P. 2021. Misinterpreting the adaptive value of phenotypic plasticity in studies on plant adaptation to new and variable environments. *Plant Biol.* 23:683–685.

Bose, N., A. Ogawa, S. H. von Reuss, J. J. Yim, E. J. Ragsdale, R. J. Sommer, and F. C. Schroeder. 2012. Complex small-molecule architectures regulate phenotypic plasticity in a nematode. *Angew. Chem. Int. Ed. Engl.* 51:12438–12443.

Bourdeau, P. E., R. K. Butlin, C. Brönmark, T. C. Edgell, J. T. Hoverman, and J. Hollander. 2015. What can aquatic gastropods tell us about phenotypic plasticity? A review and meta-analysis. *Heredity* 115:312–321.

Boveri, T. 1887. Über Differenzierung der Zellkerne während der Furchung des Eies von *Ascaris megalocephala*. *Anat. Anz.* 2:688–693.

Braendle, C., M. C. Caillaud, and D. L. Stern. 2005. Genetic mapping of *aphicarus* – a sex-linked locus controlling a wing polymorphism in the pea aphid (*Acyrthosiphon pisum*). *Heredity* 94:435–442.

Braendle, C., and T. Flatt. 2006. A role for genetic accommodation in evolution? *Bioessays* 28:868–873.

Brakefield, P. M., J. Gates, D. Keys, F. Kesbeke, P. J. Wijngaarden, A. Monteiro, V. French, and S. B. Carroll. 1996. Development, plasticity and evolution of

butterfly eyespot patterns. *Nature* 384:236–242.

Brenner, S. 1974. The genetics of *Caenorhabditis elegans*. *Genetics* 77:71–94.

Brommer, J. E. 2013. Phenotypic plasticity of labile traits in the wild. *Curr. Zool.* 59:485–505.

Brönmark, C., and J. G. Miner. 1992. Predator-induced phenotypical change in body morphology in crucian carp. *Science* 258:1348–1350.

Bruni, N. C., J. P. Young, and N. G. Dengler. 1996. Leaf developmental plasticity of *Ranunculus flabellaris* in response to terrestrial and submerged environments. *Can. J. Bot.* 74:823–837.

Bui, L. T., N. A. Ivers, and E. J. Ragsdale. 2018. A sulfotransferase dosage-dependently regulates mouthpart polyphenism in the nematode *Pristionchus pacificus*. *Nat. Commun.* 9:4119.

Butcher, R. A., M. Fujita, F. C. Schroeder, and J. Clardy. 2007. Small-molecule pheromones that control dauer development in *Caenorhabditis elegans*. *Nat. Chem. Biol.* 3:420–422.

Butcher, R. A. 2017. Small-molecule pheromones and hormones development. *Nat. Chem. Biol.* 13:577–586.

Cao, M., H. T. Schwartz, C.-H. Tan, and P. W. Sternberg. 2022. The entomopathogenic nematode *Steinernema hermaphroditum* is a self-fertilizing hermaphrodite and a genetically tractable system for the study of parasitic and mutualistic symbiosis. *Genetics* 220:iyab170.

Casasa, S., E. Katsougia, and E. J. Ragsdale. 2023. A Mediator subunit imparts robustness to a polyphenism decision. *Proc. Natl. Acad. Sci. U.S.A.* 32:e2308816120.

Cassada, R. C., and R. L. Russell. 1975. The dauerlarva, a post-embryonic developmental variant of the nematode *Caenorhabditis elegans*. *Dev. Biol.* 46:326–342.

Chaudhuri, J., V. Kache, and A. Pires-daSilva. 2011. Regulation of sexual plasticity in a nematode that produces males, females, and hermaphrodites. *Curr. Biol.* 21:1548–1551.

Chavhan, Y., S. Dey, and P. A. Lind. 2023. Bacteria evolve macroscopic multicellularity by the genetic assimilation of phenotypically plastic cell clustering. *Nat. Commun.* 14:3555.

Chen, J., and E. P. Caswell-Chen. 2003. Why *Caenorhabditis elegans* adults sacrifice their bodies to progeny. *Nematology* 5:641–645.

Chevrette, M. G., K. Gutiérrez-García, N. Selem-Mojica, C. Aguilar-Martínez, A.

Yañez-Olvera, H. E. Ramos-Aboites, P. A. Hoskisson, and F. Barona-Gómez. 2020. Evolutionary dynamics of natural product biosynthesis in bacteria. *Nat. Prod. Rep.* 37:566.

Choe, A., S. H. von Reuss, D. Kogan, R. B. Gasser, E. G. Platzer, F. C. Schroeder, and P. W. Sternberg. 2012. Ascaroside signaling is widely conserved among nematodes. *Curr. Biol.* 22:772–780.

Chung, G., L. Stevens, X. Dai, S. Hickey, K. Kiontke, P. Rughani, M. R. Kieninger, J. C. Collins, S. Juul, F. Piano, D. H. A. Fitch, M. Blaxter, and K. C. Gunsalus. 2026. Genome evolution in parthenogenetic nematodes shaped by chromosome rearrangements and introgression. *Genome Res.* (ahead of print).

Cohn, E., and M. Mordechai. 1988. Morphology and parasitism of the mature female of *Rotylenchulus macrosomus*. *Revue Nématol.* 11:385–389.

Coker, R. E., and H. H. Addlestone. 1938. Influence of temperature on cyclomorphosis of *Daphnia longispina*. *J. Elisha Mitchell Sci. Soc.* 54:45–75.

Corona, M., R. Libbrecht, and D. E. Wheeler. 2016. Molecular mechanisms of phenotypic plasticity in social insects. *Curr. Opin. Insect Sci.* 13:55–60.

Crispo, E., and L. J. Chapman. 2010. Geographic variation in phenotypic plasticity in response to dissolved oxygen in an African cichlid fish. *J. Evol. Biol.* 23:2091–2103.

Crook, M. 2014. The dauer hypothesis and the evolution of parasitism: 20 years on and still going strong. *Int. J. Parasitol.* 44:1–8.

Dardiry, M., G. Eberhard, H. Witte, C. Rödelsperger, J. W. Lightfoot, and R. J. Sommer. 2023a. Divergent combinations of *cis*-regulatory elements control the evolution of phenotypic plasticity. *PLoS Biol.* 21:e3002270.

Dardiry, M, V. Piskobulu, A. Kalirad, and R. J. Sommer. 2023b. Experimental and theoretical support for costs of plasticity and phenotype in a nematode cannibalistic trait. *Evol. Lett.* 7:48–57.

David, J. R., P. Gibert, E. Gravot, G. Petavy, J.-P. Morin, D. Karan, and B. Moreteau. 1997. Phenotypic plasticity and developmental temperature in *Drosophila*: analysis and significance of reaction norms of morphometrical traits. *J. Therm. Biol.* 22:441–451.

David, J. R., P. Gibert, and B. Moreteau. 2004. Evolution of reaction norms. In T. J. DeWitt, and S. M. Scheiner, eds., *Phenotypic Plasticity: Functional and Conceptual Approaches*. Oxford University Press, New York, NY.

Dearden, P. K. 2025. Polyphenisms: a developmental perspective. *Development* 152:dev204693.

De Filippo, T., S. Siciliano, M. R. Werneck, A. C. Colosio, P. H. Ott, H. A. Benítez, R.

V. Missagia, and T. Iwasa-Arai. 2025. Phenotypic plasticity in shell morphometrics of the barnacle *Coronula diadema* (Linnaeus, 1767) reflects cetacean hydrodynamics. *Evol. Ecol.* 39:547–562.

de Jong, G. 2005. Evolution of phenotypic plasticity: patterns of plasticity and the emergence of ecotypes. *New Phytol.* 166:101–117.

Delaby, M., L. Yang, M. Jacq, K. A. Gallagher, D. T. Kysela, V. Hughes, F. Pulido, F. J. Veyrier, M. S. VanNieuwenhze, and Y. V. Brun. 2025. Phenotypic plasticity in cell elongation among closely related bacterial species. *Nat. Commun.* 16:5099.

De Meester, N., S. Derycke, A. Rigaux, and T. Moens. 2015. Active dispersal is differentially affected by inter- and intraspecific competition in closely related nematode species. *Oikos* 124:561–570.

Devi, M. P., E. Haryoso, E. I. Rais, A. Karuniawan, M. Q. Yahya, A. Richaud, J. Wang, M. V. Rockman, H. Tarno, and M.-A. Félix. 2025. Five new *Caenorhabditis* species from Indonesia provide exceptions to Haldane's rule and partial fertility of interspecific hybrids. *G3* 15:jkaf134.

DeWitt, T. J., A. Sih, and D. S. Wilson. 1998. Costs and limits of phenotypic plasticity. *Trends Ecol. Evol.* 13:77–81.

DeWitt, T. J. 2016. Expanding the phenotypic plasticity paradigm to broader views of trait space and ecological function. *Curr. Zool.* 62:463–473.

Diggle, P. K., and J. S. Miller. 2013. Developmental plasticity, genetic assimilation, and the evolutionary diversification of sexual expression in *Solanum*. *Am. J. Bot.* 100:1050–1060.

Dobzhansky, T. 1959. Variation and evolution. *Proc. Am. Philos. Soc.* 103:252–263.

Dodson, S. 1989. Predator-induced reaction norms: cyclic changes in shape and size can be protective. *Bioscience* 39:447–452.

Döll, K., S. Chatterjee, S. Scheu, P. Karlovsky, and M. Rohlfs. 2013. Fungal metabolic plasticity and sexual development mediate induced resistance to arthropod fungivory. *Proc. R. Soc. B* 280:20131219.

Dong, C., C. J. Weadick, V. Truffault, and R. J. Sommer. 2020. Convergent evolution of small molecule pheromones in *Pristionchus* nematodes. *eLife* 9:e55687.

Dubé, C. E., E. Boissin, J. A. Maynard, and S. Planes. 2017. Fire coral clones demonstrate phenotypic plasticity among reef habitats. *Mol. Ecol.* 26:3860–3869.

Ducret, H., C. R. Suchocki, C. J. Lewis, H. Dierssen, E. J. Hochberg, D. W. H. Schar, M. Kochzius, I. F. George, R. J. Toonen, and J.-F. Flot. 2026. Nature vs. nurture? Light availability drives phenotypic plasticity within a reef coral species. *Limnol. Oceanogr.* 71:e70368.

Dupont, L., M. Thierry, L. Zinger, D. Legrand, and S. Jacob. 2024. Beyond reaction norms: the temporal dynamics of phenotypic plasticity. *Trends Ecol. Evol.* 39:41–51.

Ekino, T., H. Kirino, N. Kanzaki, and R. Shinya. 2020. Ultrastructural plasticity in the plant-parasitic nematode, *Bursaphelenchus xylophilus*. *Sci. Rep.* 10:11576.

Ellis, H. M., and H. R. Horvitz. 1986. Genetic control of programmed cell death in the nematode *C. elegans*. *Cell* 44:817–829.

Emera, D., R. Romero, and G. Wagner. 2011. The evolution of menstruation: a new model for genetic assimilation. *Bioessays* 34:26–35.

Eren, G. G., L. Böger, M. Roca, F. Hiramatsu, J. Liu, L. Alvarez, D. L. Goetting, L. A. Cockram, N. Zorn, Z. Han, M. Okumura, M. Scholz, and J. W. Lightfoot. 2026. Predatory aggression evolved through adaptations to noradrenergic circuits. *Nature* 651:154–163.

Eriksson, M., A. Kinnby, P. De Wit, and M. Rafajlović. 2023. Adaptive, maladaptive, neutral, or absent plasticity: hidden caveats of reaction norms. *Evol. Appl.* 16:486–503.

Espinosa-Soto, C., U. Hernández, and Y. S. Posadas-García. 2021. Recombination facilitates genetic assimilation of new traits in gene regulatory networks. *Evol. Dev.* 23:459–473.

Faghih, N., S. Bhar, Y. Zhou, A. R. Dar, K. Mai, L. S. Bailey, K. B. Basso, and R. A Butcher. 2020. A large family of enzymes responsible for the modular architecture of nematode pheromones. *J. Am. Chem. Soc.* 142:13645–13650.

Falcke, J. M., N. Bose, A. B. Artyukhin, C. Rödelsperger, G. V. Markov, J. J. Yim, D. Grimm, M. H. Claassen, O. Panda, J. A. Baccile, Y. K. Zhang, H. H. Le, D. Jolic, F. C. Schroeder, and R. J. Sommer. 2018. Linking genomic and metabolomic natural variation uncovers nematode pheromone biosynthesis. *Cell Chem. Biol.* 25:787–796.

Fanti, L., L. Piacentini, U. Cappucci, A. M. Casale, and S. Pimpinelli. 2017. Canalization by selection of *de novo* induced mutations. *Genetics* 206:1995–2006.

Fielenbach, N., and A. Antebi. 2008. *C. elegans* dauer formation and the molecular basis of plasticity. *Genes Dev.* 22:2149–2165.

Fischer, E. K., C. K. Ghalambor, and K. L. Hoke. 2016. Can a network approach resolve how adaptive vs nonadaptive plasticity impacts evolutionary trajectories? *Integr. Comp. Biol.* 56:877–888.

FitzGerald, C. E., S. Reich, V. Agaba, A. Mathur, M. S. Werner, and N. M. Mangan. 2025. Practical indistinguishability in a gene regulatory network inference

problem, a case study. *arXiv* 2508.21006.

Fitzpatrick, B. M. 2012. Underappreciated consequences of phenotypic plasticity for ecological speciation. *Int. J. Ecol.* 2012:256017.

Fonderie, P., H. Steel, T. Moens, and W. Bert. 2013. Experimental induction of intraspecific morphometric variability in a single population of *Halicephalobus* cf. *gingivalis* may surpass total interspecific variability. *Nematology* 15:529–544.

Ford, N. B., and R. A. Seigel. 1989. Phenotypic plasticity in reproductive traits: evidence from a viviparous snake. *Ecology* 70:1768–1774.

Forsman, A. 2015. Rethinking phenotypic plasticity and its consequences for individuals, populations and species. *Heredity* 115:276–284.

Fradin, H., K. Kiontke, C. Zegar, M. Gutwein, J. Lucas, M. Kovtun, D. L. Corcoran, L. R. Baugh, D. H. A. Fitch, F. Piano, and K. C. Gunsalus. 2017. Genome architecture and evolution of a unichromosomal asexual nematode. *Curr. Biol.* 27:2928–2939.

Fujimori, Y., T. Ekino, and R. Shinya. 2022. Reproductive plasticity in response to food source in the fungal-feeding nematode *Bursaphelenchus okinawaensis*. *Nematology* 24:631–638.

Fusco, G., and A. Minelli. 2010. Phenotypic plasticity in development and evolution: facts and concepts. *Phil. Trans. R. Soc. B* 365:547–556.

Gadagkar, R. 1997. The evolution of caste polymorphism in social insects: genetic release followed by diversifying evolution. *J. Genet.* 76:167–179.

Ganji, S., M. J. Wubben, and J. N. Jenkins. 2013. Two simple methods for the collection of individual life stages of reniform nematode, *Rotylenchulus reniformis*. *J. Nematol.* 45:87–91.

Garaffa, L. 2025. Plasticity-led (not first) evolution: a matter of causal relevance. *Biol. Theory* 20:175–188.

Ghalambor, C. K., J. K. McKay, S. P. Carroll, and D. N. Reznick. 2007. Adaptive versus non-adaptive phenotypic plasticity and the potential for contemporary adaptation in new environments. *Funct. Ecol.* 21:394–407.

Ghalambor, C. K., K. L. Hoke, E. W. Ruell, E. K. Fischer, D. N. Reznick, and K. A. Hughes. 2015. Non-adaptive plasticity potentiates rapid adaptive evolution of gene expression in nature. *Nature* 525:372–375.

Gilabert, A., D. M. Curran, S. C. Harvey, and J. D. Wasmuth. 2016. Expanding the view on the evolution of the nematode dauer signalling pathways: refinement through gene gain and pathway co-option. *BMC Genomics* 17:476.

Gibert, J.-M. 2017. The *flexible stem hypothesis*: evidence from genetic data. *Dev.*

Genes Evol. 227:297–307.

Gilbert, S. F. 2003. The role of predator-induced polyphenism in the evolution of cognition: a Baldwinian speculation. In B. H. Weber, and D. J. Depew, eds., *Evolution and Learning: The Baldwin Effect Reconsidered*. The MIT Press, Cambridge, MA.

Gilbert, S. F., T. C. G. Bosch, and C. Ledón-Rettig. 2015. Eco-Evo-Devo: developmental symbiosis and developmental plasticity as evolutionary agents. *Nat. Rev. Genet.* 16:611–622.

Gimond, C., N. Poullet, A. Vielle, E. Demoinet, and C. Braendle. 2025. Developmental plasticity of hermaphrodite sperm production across environments in *Caenorhabditis elegans*. *PLoS One* 20:e0336162.

Golden, J. W., and D. L. Riddle. 1982. A pheromone influences larval development in the nematode *Caenorhabditis elegans*. *Science* 218:578–580.

Golden, J. W., and D. L. Riddle. 1984. The *Caenorhabditis elegans* dauer larva: developmental effects of pheromone, food, and temperature. *Dev. Biol.* 102:368–378.

Gomez, F., J. Hirbo, and S. A. Tishkoff. 2014. Genetic variation and adaptation in Africa: implications for human evolution and disease. *Cold Spring Harb. Perspect. Biol.* 6:a008524.

Gómez, J. M., A. González-Megías, C. Armas, E. Narbona, L. Navarro, and F. Perfectti. 2024. Selection maintains a nonadaptive floral polyphenism. *Evol. Lett.* 8:610–621.

Gómez, J. M., F. Perfectti, A. González-Megías, and C. Armas. 2025. Quantifying phenotypic plasticity: a call for consistency. *Funct. Ecol.* 39:2974–2984.

Gordon, S. P., A. P. Hendry, and D. N. Reznick. 2017. Predator-induced contemporary evolution, phenotypic plasticity, and the evolution of reaction norms in guppies. *Copeia* 105:514–522.

Gotthard, K., and Nylin, S. 1995. Adaptive plasticity and plasticity as an adaptation: a selective review of plasticity in animal morphology and life history. *Oikos* 74:3–17.

Gray, J. C., and A. D. Cutter. 2014. Mainstreaming *Caenorhabditis elegans* in experimental evolution. *Proc. R. Soc. B* 281:20133055.

Greet, D. N. 1964. Observations on sexual attraction and copulation in the nematode *Panagrolaimus rigidus* (Schneider). *Nature* 204:96–97.

Grime, J. P., and S. Pierce. 2012. *The Evolutionary Strategies that Shape Ecosystems*. John Wiley & Sons, Chichester, UK.

Gunter, H. M., R. F. Schneider, I. Karner, C. Sturmbauer, and A. Meyer. 2017. Molecular investigation of genetic assimilation during the rapid adaptive radiations of East African cichlid fishes. *Mol. Ecol.* 26:6634–6653.

Guo, X., Q. Yu, D. Chen, J. Wei, P. Yang, J. Yu, X. Wang, and L. Kang. 2020. 4-Vinylanisole is an aggregation pheromone in locusts. *Nature* 584:584–588.

Guo, X., and L. Kang. 2024. Phenotypic plasticity in locusts: trade-off between migration and reproduction. *Annu. Rev. Entomol.* 70:23–44.

Haag, E. S., and J. R. True. 2021. Developmental system drift. In L. Nuño de la Rosa, and G. B. Müller, eds., *Evolutionary Developmental Biology*. Springer, Cham, Switzerland.

Hackley, R. K., and A. K. Schmid. 2019. Global transcriptional programs in archaea share features with the eukaryotic environmental stress response. *J. Mol. Biol.* 431:4147–4166.

Hamilton, T. C. 1975. Behavioral plasticity in protozoans. In E. M. Eisenstein, ed., *Aneural Organisms in Neurobiology*. Springer, Boston, MA.

Hayashi, Y., N. Lo, H. Miyata, and O. Kitade. 2007. Sex-linked genetic influence on caste determination in a termite. *Science* 318:985–987.

Haye, P. A., P. Salinas, E. Acuña, and E. Poulin. 2010. Heterochronic phenotypic plasticity with lack of genetic differentiation in the southeastern Pacific squat lobster *Pleuroncodes monodon*. *Evol. Dev.* 12:628–634.

Hazlett, B. A., and C. McLay. 2000. Contingencies in the behaviour of the crab *Heterozius rotundifron*. *Anim. Behav.* 59:965–974.

Herrmann, M., W. E. Mayer, and R. J. Sommer. 2006. Nematodes of the genus *Pristionchus* are closely associated with scarab beetles and the Colorado potato beetle in Western Europe. *Zoology* 109:96–108.

Herrmann, M., W. E. Mayer, R. L. Hong, S. Kienle, R. Minasaki, and R. J. Sommer. 2007. The nematode *Pristionchus pacificus* (Nematoda: Diplogastridae) is associated with the oriental beetle *Exomala orientalis* (Coleoptera: Scarabaeidae) in Japan. *Zoolog. Sci.* 24:883–889.

Herrmann, S. Kienle, J. Rochat, W. E. Mayer, and R. J. Sommer. 2010. Haplotype diversity of the nematode *Pristionchus pacificus* on Réunion in the Indian Ocean suggests multiple independent invasions. *Biol. J. Linn. Soc.* 100:170–179.

Herrmann, M., N. Kanzaki, C. Weiler, P. Theam, C. Rödelsperger, and R. J. Sommer. 2024. Description of two new *Pristionchus* species from South Korea. *J. Nematol.* 56:20240032.

Hess, C., J. M. Levine, M. M. Turcotte, and S. P. Hart. 2022. Phenotypic plasticity promotes species coexistence. *Nat. Ecol. Evol.* 6:1256–1261.

Hille-Rehfeld, A. 2025. Die Ascaroside. *Chem. Unserer Zeit* 59:20–27.

Hirschmann, H. 1951. Über das Vorkommen zweier Mundhöhlentypen bei *Diplogaster lheritieri* Maupas und *Diplogaster biformis* n. sp. und die Entstehung dieser hermaphroditischen Art aus *Diplogaster lheritieri*. *Zool. Jahrb. Abt. Syst.* 80:132–170.

Hittinger, C. T. 2013. *Saccharomyces* diversity and evolution: a budding model genus. *Trends Genet.* 29:309–317.

Ho, W.-C., D. Li, Q. Zhu, and J. Zhang. 2020. Phenotypic plasticity as a long-term memory easing readaptations to ancestral environments. *Sci. Adv.* 6:eaba3388.

Hobert, O. 2003. Behavioral plasticity in *C. elegans*: paradigms, circuits, genes. *J. Neurobiol.* 54:203–223.

Holloway, G. J., and P. M. Brakefield. 1995. Artificial selection of reaction norms of wing pattern elements in *Bicyclus anynana*. *Heredity* 74:91–99.

Hong, R. L. 2015. *Pristionchus pacificus* olfaction. In R. J. Sommer, ed., Pristionchus pacificus: *A Nematode Model for Comparative and Evolutionary Biology*. Koninklijke Brill NV, Leiden, The Netherlands.

Hsueh, Y.-P., D. H. W. Leighton, and P. W. Sternberg. 2014. Nematode communication. In G. Witzany, ed., *Biocommunication of Animals*. Springer, Dordrecht, The Netherlands.

Hu, P. J. 2007. Dauer. In The *C. elegans* Research Community, ed., WormBook: The Online Review of *C. elegans* Biology. Pasadena, CA.

Hwang, S., N. E. Chavarria, R. K. Hackley, A. K. Schmid, and J. A. Maupin-Furlow. 2019. Gene expression of *Haloferax volcanii* on intermediate and abundant sources of fixed nitrogen. *Int. J. Mol. Sci.* 20:4784.

Igreja, C., and R. J. Sommer. 2022. The role of sulfation in nematode development and phenotypic plasticity. *Front. Mol. Biosci.* 9:838148.

Imre, I., R. L. McLaughlin, and D. L. G. Noakes. 2002. Phenotypic plasticity in brook charr: changes in caudal fin induced by water flow. *J. Fish Biol.* 61:1171–1181.

Ingram, K. K., S. Krummey, and M. LeRoux. 2009. Expression patterns of a circadian clock gene are associated with age-related polyethism in harvester ants, *Pogonomyrmex occidentalis*. *BMC Ecol.* 9:7.

Irion, U., and C. Nusslein-Volhard. 2022. Developmental genetics with model organisms. *Proc. Natl. Acad. Sci. U.S.A.* 119:e2122148119.

Ishita, Y., A. Onodera, T. Ekino, T. Chihara, and M. Okumura. 2023. Co-option of an astacin metalloprotease is associated with an evolutionarily novel feeding morphology in a predatory nematode. *Mol. Biol. Evol.* 40:msad266.

Jain, N., F. Hasan, and B. C. Fries. 2008. Phenotypic switching in fungi. *Curr. Fungal Infect. Rep.* 2:180–188.

Jarrett, B. J. M., P. A. Downing, and E. I. Svensson. 2025. Meta-analysis reveals that phenotypic plasticity and divergent selection promote reproductive isolation during incipient speciation. *Nat. Ecol. Evol.* 9:833–844.

Jeong, P.-Y., M. Jung, Y.-H. Yim, H. Kim, M. Park, E. Hong, W. Lee, Y. H. Kim, K. Kim, and Y.-K. Paik. 2005. Chemical structure and biological activity of the *Caenorhabditis elegans* dauer-inducing pheromone. *Nature* 433:541–545.

Johanson, U., J. West, C. Lister, S. Michaels, R. Amasino, and C. Dean. 2000. Molecular analysis of *FRIGIDA*, a major determinant of natural variation in *Arabidopsis* flowering time. *Science* 290:344–347.

Johnigk, S.-A., and R.-U. Ehlers. 1999. Juvenile development and life cycle of *Heterorhabditis bacteriophora* and *H. indica* (Nematoda: Heterorhabditidae). *Nematology* 1:251–260.

Joly, S., and D. J. Schoen. 2021. Repeated evolution of a reproductive polyphenism in plants is strongly associated with bilateral flower symmetry. *Curr. Biol.* 31:1515–1520.

Kaletta, T., and M. O. Hengartner. 2006. Finding function in novel targets: *C. elegans* as a model organism. *Nat. Rev. Drug Discov.* 5:387–399.

Kalirad, A., and R. J. Sommer. 2024. Spatial and temporal heterogeneity alter the cost of plasticity in *Pristionchus pacificus*. *PLoS Comput. Biol.* 20:e1011823.

Kalirad, A., P. Theam, and R. J. Sommer. 2025. The dynamics of coexistence and succession in a decaying ecosystem. *bioRxiv* 2025.04.28.650976.

Kanzaki, N. 2008. Taxonomy and systematics of the nematode genus *Bursaphelenchus* (Nematoda: Parasitaphelenchidae). In B. G. Zhao, K. Futai, J. R. Sutherland, and Y. Takeuchi, eds., *Pine Wilt Disease*. Springer, Tokyo, Japan.

Kanzaki, N., E. J. Ragsdale, M. Herrmann, and R. J. Sommer. 2012. Two new species of *Pristionchus* (Rhabditida: Diplogastridae): *P. fissidentatus* n. sp. from Nepal and La Réunion island and *P. elegans* n. sp. from Japan. *J. Nematol.* 44:80–91.

Kanzaki, N., E. J. Ragsdale, M. Herrmann, W. Röseler, and R. J. Sommer. 2013. *Pristionchus bucculentus* n. sp. (Rhabditida: Diplogastridae) isolated from a shining mushroom beetle (Coleoptera: Scaphidiidae) in Hokkaido, Japan. *J. Nematol.* 45:78–86.

Kanzaki, N., E. Ekino, and R. M. Giblin-Davis. 2019. Feeding dimorphism in a mycophagous nematode, *Bursaphelenchus sinensis*. *Sci. Rep.* 9:13956.

Kasinathan, B., K. Ahmad, and H. S. Malik. 2017. Waddington redux: *de vovo*

mutations underlie the genetic assimilation of stress-induced phenocopies in *Drosophila melanogaster*. *Genetics* 207:49–51.

Katayama, N, K. Okamura, and K. Tanimura. 2021. Phenotypic plasticity of salamander hatchlings in the pre-feeding stage in response to future prey. *Zoolog. Sci.* 38:397–404.

Katsougia, E., S. J. Connors, and E. J. Ragsdale. 2025. A species-specific nuclear receptor was integrated into a developmental polyphenism pathway. *Genetics* 231:iyaf140.

Kelly, S. A., T. M. Panhuis, and A. M. Stoehr. 2012. Phenotypic plasticity: molecular mechanisms and adaptive significance. *Compr. Physiol.* 2:1417–1439.

Kieninger, M. R., N. A. Ivers, C. Rödelsperger, G. V. Markov, R. J. Sommer, and E. J. Ragsdale. 2016. The nuclear hormone receptor NHR-40 acts downstream of the sulfatase EUD-1 as part of a developmental plasticity switch in *Pristionchus*. *Curr. Biol.* 26:2174–2179.

Kishida, O., Y. Mizuta, and K. Nishimura. 2006. Reciprocal phenotypic plasticity in a predator-prey interaction between larval amphibians. *Ecology* 87:1599–1604.

Kohlmeier, P., Y. Zhang, J. A. Gorter, C.-Y. Su, and J.-C. Billeter. 2021. Mating increases *Drosophila melanogaster* females' choosiness by reducing olfactory sensitivity to a male pheromone. *Nat. Ecol. Evol.* 5:1165–1173.

Koenig, D., and D. Weigel. 2015. Beyond the thale: comparative genomics and genetics of *Arabidopsis* relatives. *Nat. Rev. Genet.* 16:285–298.

Kümmerli, R., N. Jiricny, L. S. Clarke, S. A. West, and A. S. Griffin. 2009. Phenotypic plasticity of a cooperative behaviour in bacteria. *J. Evol. Biol.* 22:589–598.

Lala, K. N., T. Uller, N. Feiner, M. W. Feldman, and S. F. Gilbert. 2024. *Evolution Evolving: The Developmental Origins of Adaptation and Biodiversity*. Princeton University Press, Princeton, NJ.

Latta, R. G. 2010. Natural selection, variation, adaptation, and evolution: a primer of interrelated concepts. *Int. J. Plant Sci.* 171:930–944.

Launay, C., E. Wenger, B. Letcher, and M. Delattre. 2025. Somatic programmed DNA elimination is widespread in free-living Rhabditidae nematodes. *bioRxiv* 2025.08.21.671558.

Le, H. H., C. J. J. Wrobel, S. M. Cohen, J. Yu, H. Park, M. J. Helf, B. J. Curtis, J. C. Kruempel, P. R. Rodrigues, P. J. Hu, P. W. Sternberg, and F. C. Schroeder. 2020. Modular metabolite assembly in *Caenorhabditis elegans* depends on carboxylesterases and formation of lysosome-related organelles. *eLife* 9:e61886.

Lee, R. C., R. L. Feinbaum, and V. Ambros. 1993. The *C. elegans* heterochronic gene

lin-4 encodes small RNAs with antisense complementarity to *lin-4*. *Cell* 75:843–854.

Lee, M. S. Y, and P. Doughty. 1997. The relationship between evolutionary theory and phylogenetic analysis. *Biol. Rev.* 72:471–495.

Lenuzzi, M., H. Witte, M. Riebesell, C. Rödelsperger, R. L. Hong, and R. J. Sommer. 2023. Influence of environmental temperature on mouth-form plasticity in *Pristionchus pacificus* acts through *daf-11*-dependent cGMP signaling. *J. Exp. Zool. B Mol. Dev. Evol.* 340:214–224.

Leonard, A. M., and L. T. Lancaster. 2020. Maladaptive plasticity facilitates evolution of thermal tolerance during an experimental range shift. *BMC Evol. Biol.* 20:47.

Lepais, O., A. Manicki, S. Glise, M. Buoro, and A. Bardonnet. 2017. Genetic architecture of threshold reaction norms for male alternative reproductive tactics in Atlantic salmon (*Salmo salar* L.). *Sci. Rep.* 7:43552.

Levis, N. A. and D. W. Pfennig. 2016. Evaluating 'plasticity-first' evolution in nature: key criteria and empirical approaches. *Trends Ecol. Evol.* 31:563–574.

Levis, N. A., A. J. Isdaner, and D. W. Pfennig. 2018. Morphological novelty emerges from pre-existing phenotypic plasticity. *Nat. Ecol. Evol.* 2:1289–1297.

Levis, N. A., and D. W. Pfennig. 2019. Plasticity-led evolution: evaluating the key prediction of frequency-dependent adaptation. *Proc. R. Soc. B* 286:20182754.

Levis, N. A., and D. W. Pfennig. 2020. Plasticity-led evolution: a survey of developmental mechanisms and empirical tests. *Evol. Dev.* 22:71–87.

Levis, N. A., and D. W. Pfennig. 2021. Innovation and diversification via plasticity-led evolution. In D. W. Pfennig, ed., *Phenotypic Plasticity and Evolution: Causes, Consequences, Controversies*. CRC Press, Boca Raton, FL.

Levis, N. A., and E. J. Ragsdale. 2022. Linking molecular mechanisms and evolutionary consequences of resource polyphenism. *Front. Integr. Neurosci.* 16:805061.

Lewis, S. C., L. A. Dyal, C. A. Hilburn, S. Weitz, W.-S. Liau, C. W. LaMunyon, and D. R. Denver. 2009. Molecular evolution in *Panagrolaimus* nematodes: origins of parthenogenesis, hermaphroditism and the Antarctic species *P. davidi*. *BMC Evol. Biol.* 9:15.

Liu, Z., M. J. Kariya, C. D. Chute, A. K. Pribadi, S. G. Leinwand, A. Tong, K. P. Curran, N. Bose, F. C. Schroeder, J. Srinivasan, and S. H. Chalasani. 2018. Predator-secreted sulfolipids induce defensive responses in *C. elegans*. *Nat. Commun.* 9:1128.

Lorant, A., S. Pedersen, I. Holst, M. B. Hufford, K. Winter, D. Piperno, and J. Ross-Ibarra. 2017. The potential role of genetic assimilation during maize

domestication. *PLoS One* 12:e0184202.

Lu, J., M. Podobnik, J. Huang, B. M. McCluskey, S. A. McCarthy, J. Wood, J. Collins, J. Torrance, Y. Sims, D. Gao, J. Huang, J. Liu, W. Fang, P. Huang, C. Ma, D. Huang, U. Irion, J. Liu, K. Howe, and J. H. Postlethwait. 2025. Genomic and genetic insights into speciation and pigment pattern diversification in *Danio* fishes. *bioRxiv* 2025.10.17.682988.

Ludewig, A. H., and F. C. Schroeder. 2012. Ascaroside signaling in *C. elegans*. In The *C. elegans* Research Community, ed., WormBook: The Online Review of *C. elegans* Biology. Pasadena, CA.

Lundsgaard-Hansen, B., B. Matthews, and O. Seehausen. 2014. Ecological speciation and phenotypic plasticity affect ecosystems. *Ecology* 95:2723–2735.

Machado, R. A. R., and S. H. von Reuss. 2022. Chemical ecology of nematodes. *Chimia* 76:945–953.

MacNeil, L. T., and A. J. M. Walhout. 2011. Gene regulatory networks and the role of robustness and stochasticity in the control of gene expression. *Genome Res.* 21:645–657.

Magalhaes, S. Mwaiko, M. V. Schneider, and O. Seehausen. 2009. Divergent selection and phenotypic plasticity during incipient speciation in Lake Victoria cichlid fish. *J. Evol. Biol.* 22:260–274.

Maher J. M., E. E. Werner, and R. J. Denver. 2013. Stress hormones mediate predator-induced phenotypic plasticity in amphibian tadpoles. *Proc. R. Soc. B* 280:20123075.

Manosalva, P., M. Manohar, S. H. von Reuss, S. Chen, A. Koch, F. Kaplan, A. Choe, R. J. Micikas, X. Wang, K.-H. Kogel, P. W. Sternberg, V. M. Williamson, F. C. Schroeder, and D. F. Klessig. 2015. Conserved nematode signalling molecules elicit plant defenses and pathogen resistance. *Nat. Commun.* 6:7795.

Manríquez, P. H., N. A. Lagos, M. E. Jara, and J. C. Castilla. 2009. Adaptive shell color plasticity during the early ontogeny of an intertidal keystone snail. *Proc. Natl. Acad. Sci. U.S.A.* 106:16298–16303.

Martin, C. H., J. E. Crawford, B. J. Turner, and L. H. Simons. 2016. Diabolical survival in Death Valley: recent pupfish colonization, gene flow and genetic assimilation in the smallest species range on earth. *Proc. R. Soc. B* 283: 20152334.

Mayr, E. 1963. *Animal Species and Evolution*. The Belknap Press of Harvard University Press, Cambridge, MA.

McGaughran, A., and K Morgan. 2015. Population genetics and the La Réunion case study. In R. J. Sommer, ed., Pristionchus pacificus: *A Nematode Model for Comparative and Evolutionary Biology*. Koninklijke Brill NV, Leiden, The

Netherlands.

McGrath, P. T., and I. Ruvinsky. 2019. A primer on pheromone signaling in *Caenorhabditis elegans* for systems biologists. *Curr. Opin. Syst. Biol.* 13:23–30.

Merilä, J., and A. P. Hendry. 2014. Climate change, adaptation, and phenotypic plasticity: the problem and the evidence. *Evol. Appl.* 7:1–14.

Meuthen, D., S. A. Baldauf, T. C. M. Bakker, and T. Thünken. 2018. Neglected patterns of variation in phenotypic plasticity: age- and sex-specific antipredator plasticity in a cichlid fish. *Am. Nat.* 191:475–490.

Michener, C. D. 1961. Social polymorphism in Hymenoptera. *Symp. R. Entomol. Soc. Lond.* 1:43–56.

Mikhailova, A. A., S. Rinke, and M. C. Harrison. 2024. Genomic signatures of eusocial evolution in insects. *Curr. Opin. Insect Sci.* 61:101136.

Miner, B. G., S. E. Sultan, S. G. Morgan, D. K. Padilla, and R. A. Relyea. 2005. Ecological consequences of phenotypic plasticity. *Trends Ecol. Evol.* 20:685–692.

Miranda-Vizuete, A., and E. A. Veal. 2017. *Caenorhabditis elegans* as a model for understanding ROS function in physiology and disease. *Redox Biol.* 11:708–714.

Mitchell-Olds, T., J. H. Willis, and D. B. Goldstein. 2007. Which evolutionary processes influence natural genetic variation for phenotypic traits? *Nat. Rev. Genet.* 8:845–856.

Mochizuki, K. 2024. Programed DNA elimination. *Curr. Biol.* 34:R837–R853.

Moczek, A. P., S. Sultan, S. Foster, C. Ledón-Rettig, I. Dworkin, H. F. Nijhout, E. Abouheif, and D. W. Pfennig. 2011. The role of developmental plasticity in evolutionary innovation. *Proc. R. Soc. B* 278:2705–2713.

Moczek, A. P. 2015. Developmental plasticity and evolution—*quo vadis? Heredity* 115:302–305.

Moens, M., R. N. Perry, and J. L. Starr. 2009. *Meloidogyne* species – a diverse group of novel and important plant parasites. In R. N. Perry, M. Moens, and J. L. Starr, eds., *Root-knot Nematodes*. CAB International, Wallingford, UK.

Moens, M., R. N. Perry, and J. T. Jones. 2018. Cyst nematodes – life cycle and economic importance. In R. N. Perry, M. Moens, and J. T. Jones, eds., *Cyst Nematodes*. CAB International, Wallingford, UK.

Monteiro, A., X. Long, A. Bear, S. F. Liew, S. Bhardwaj, B. R. Wasik, A. Dinwiddie, C. Bastianelli, W. F. Cheong, M. R. Wenk, H. Cao, and K. L. Prudic. 2015. Differential expression of ecdysone receptor leads to variation in phenotypic

plasticity across serial homologs. *PLoS Genet.* 1:e1005529.

Moreno, E., J. W. Lightfoot, M. Lenuzzi, and R. J. Sommer. 2019. Cilia drive developmental plasticity and are essential for efficient prey detection in predatory nematodes. *Proc. R. Soc. B* 286:20191089.

Morris, M. R. J., and S. M. Rogers. 2013. Overcoming maladaptive plasticity through plastic compensation. *Curr. Zool.* 59:526–536.

Morrissey, M. B, and M. Liefting. 2016. Variation in reaction norms: statistical considerations and biological interpretation. *Evolution* 70:1944–1959.

Müller, B., and U. Grossniklaus. 2010. Model organisms — a historical perspective. *J. Proteomics* 73:2054–2063.

Mulot, M., K. Marcisz, L. Grandgirard, E. Lara, A. Kosakyan, B. J. M. Robroek, M. Lamentowicz, R. J. Payne, and E. A. D. Mitchell. 2017. Genetic determinism vs. phenotypic plasticity in protist morphology. *J. Eukaryot. Microbiol.* 64:729–739.

Murren, C. J., J. R. Auld, H. Callahan, C. K. Ghalambor, C. A. Handelsman, M. A. Heskel, J. G. Kingsolver, H. J. Maclean, J. Masel, H. Maughan, D. W. Pfennig, R. A. Relyea, S. Seiter, E. Snell-Rood, U. K. Steiner, and C. D. Schlichting. 2015. Constraints on the evolution of phenotypic plasticity: limits and costs of phenotype and plasticity. *Heredity* 115:293–301.

Namdeo, S., E. Moreno, C. Rödelsperger, P. Baskaran, H. Witte, and R. J. Sommer. 2018. Two independent sulfation processes regulate mouth-form plasticity in the nematode *Pristionchus pacificus*. *Development* 145:dev166272.

Nanjundiah, V. 2003. Phenotypic plasticity and evolution by genetic assimilation. In G. B. Müller, and S. A. Newman, eds., *Origination of Organismal Form: Beyond the Gene in Developmental and Evolutionary Biology*. The MIT Press, Cambridge, MA.

Nechipurenko, I., and P. Sengupta. 2025. *C. elegans*: an elegant experimental system for the study of cilia biology. *Semin. Cell Dev. Biol.* 174:103636.

Nettle, D., and M. Bateson. 2015. Adaptive developmental plasticity: what is it, how can we recognize it and when can it evolve? *Proc. R. Soc. B* 282:20151005.

Neufeld, C. J. 2011. Modular phenotypic plasticity: divergent responses of barnacle penis and feeding leg form to variation in density and wave-exposure. *J. Exp. Zool. B Mol. Dev. Evol.* 316:254–262.

Neylan, I. P., R. V. Vaidya, E. L. Crable, B. C. Faircloth, M. Dassanayake, and M. W. Kelly. 2026. Genetic assimilation and accommodation shape adaptation to heat stress in a splash pool copepod. *Proc. R. Soc. B* 293:20253265.

Ng, E. T. H, and A. R. Kinjo. 2023. Plasticity-led evolution as an intrinsic property of developmental gene regulatory networks. *Sci. Rep.* 13:19830.

Nicoglou, A. 2013. West-Eberhard and the notion of plasticity: implications and consequences for an extended synthesis of evolution. In Proc. CAPE Int. Workshops 2012, CAPE Stud. Appl. Philos. Ethics Ser. 1:26–38. Kyoto University, Kyoto, Japan.

Nigon, V. C, and M.-A. Félix. 2017. History of research on *C. elegans* and other free-living nematodes as model organisms. In The *C. elegans* Research Community, ed., WormBook: The Online Review of *C. elegans* Biology. Pasadena, CA.

Nijhout, H. F. 2025. Genetic assimilation, robustness and plasticity are key processes in the development and evolution of novel traits. *Dev. Biol.* 523:132–138.

Nixon, K. J. A., and H. F. Parzer. 2024. Got milkweed? Genetic assimilation as potential source for the evolution of nonmigratory monarch butterfly wing shape. *Evol. Dev.* 26:e12463.

Nonaka, E., R. Svanbäck, X. Thibert-Plante, G. Englund, and Å. Brännström. 2015. Mechanisms by which phenotypic plasticity affects adaptive divergence and ecological speciation. *Am. Nat.* 186:E126–E143.

Nussey, D. H., T. H. Clutton-Brock, D. A. Elston, S. D. Albon, and L. E. B. Kruuk. 2005. Phenotypic plasticity in a maternal trait in red deer. *J. Anim. Ecol.* 74:387–396.

O'Donnell, M. P., B. W. Fox, P.-H. Chao, F. C. Schroeder, and P. Sengupta. 2020. A neurotransmitter produced by gut bacteria modulates host sensory behaviour. *Nature* 583:415–420.

O'Grady, P. M., and R. DeSalle. 2018. Phylogeny of the genus *Drosophila*. *Genetics* 209:1–25.

Orr, H. A. 1999. An evolutionary dead end? *Science* 285:343–344.

Pál, C., and I. Miklós. 1999. Epigenetic inheritance, genetic assimilation and speciation. *J. Theor. Biol.* 200:19–37.

Palacio-Lopez, K., B. Beckage, S. Scheiner, and J. Molofsky. 2015. The ubiquity of phenotypic plasticity in plants: a synthesis. *Ecol. Evol.* 5:3389–3400.

Pan, J., Y. Wang, C. Li, S. Zhang, Z. Ye, J. Ni, H. Li, Y. Li, H. Yue, C. Ruan, D. Zhao, Y. Jiang, X. Wu, X. Shen, R. A. Zufall, Y. Zhang, W. Li, M. Lynch, and H. Long. 2024. Molecular basis of phenotypic plasticity in a marine ciliate. *ISME J.* 18:wrae136.

Papadopoulou, J., and A. C. Triantaphyllou. 1982. Sex differentiation in *Meloidogyne incognita* and anatomical evidence of sex reversal. *J. Nematol.* 14:549–566.

Pelletier, F., D. Garant, and A. P. Hendry. 2009. Eco-evolutionary dynamics. *Philos. Trans. R. Soc. Lond. B Biol. Sci.* 364:1483–1489.

Peng, M., R. Shahzad, A. Gul, H. Subthain, S. Shen, L. Lei, Z. Zheng, J. Zhou, D. Lu,

S. Wang, E. Nishawy, X. Liu, T. Tohge, A. R. Fernie, and J. Luo. 2017. Differentially evolved glucosyltransferases determine natural variation of rice flavone accumulation and UV-tolerance. *Nat. Commun.* 8:1975.

Pérez-Ramos, I. M., L. Matías, L. Gómez-Aparicio, and Ó. Godoy. 2019. Functional traits and phenotypic plasticity modulate species coexistence across contrasting climatic conditions. *Nat. Commun.* 10:2555.

Pfennig, D. W., A. M. Rice, and R. A. Martin. 2006. Ecological opportunity and phenotypic plasticity interact to promote character displacement and species coexistence. *Ecology* 87:769–779.

Pfennig, D. W., M. A. Wund, E. C. Snell-Rood, T. Cruickshank, C. D. Schlichting, and A. P. Moczek. 2010. Phenotypic plasticity's impacts on diversification and speciation. *Trends Ecol. Evol.* 25:459–467.

Pfennig, D. W. 2021. Key questions about phenotypic plasticity. In D. W. Pfennig, ed., *Phenotypic Plasticity and Evolution: Causes, Consequences, Controversies*. CRC Press, Boca Raton, FL.

Pigliucci, M., J. Whitton, and C. D. Schlichting. 1995. Reaction norms of *Arabidopsis*. I. Plasticity of characters and correlations across water, nutrient and light gradients. *J. Evol. Biol.* 8:421–438.

Pigliucci, M., and C. D. Schlichting. 1996. Reaction norms of *Arabidopsis*. IV. Relationships between plasticity and fitness. *Heredity* 76:427–436.

Pigliucci, M., C. D. Schlichting, C. S. Jones, and K. Schwenk. 1996. Developmental reaction norms: the interactions among allometry, ontogeny and plasticity. *Plant Species Biol.* 11:69–85.

Pigliucci, M. 2001. *Phenotypic Plasticity: Beyond Nature and Nurture*. The Johns Hopkins University Press, Baltimore, MD.

Pigliucci, M., and C. J. Murren. 2003. Perspective: genetic assimilation and a possible evolutionary paradox: can macroevolution sometimes be so fast as to pass us by? *Evolution* 57:1455–1464.

Pigliucci, M. 2005. Evolution of phenotypic plasticity: where are we going now? *Trends Ecol. Evol.* 20:481–486.

Pigliucci, M., C. J. Murren, and C. D. Schlichting. 2006. Phenotypic plasticity and evolution by genetic assimilation. *J. Exp. Biol.* 209:2362–2367.

Piskobulu, V., M. Athanasouli, H. Witte, C. Feldhaus, A. Streit, and R. J. Sommer. 2025. High nutritional conditions influence feeding plasticity in *Pristionchus pacificus* and render worms non-predatory. *J. Exp. Zool. B Mol. Dev. Evol.* 344:94–111.

Platt, S. A., and C. A. Sanislow. 1988. Norm-of-reaction: definition and

misinterpretation of animal research. *J. Comp. Psychol.* 102:254–261.

Poinar, G. O., and R. Hess. 1972. Food uptake by the insect-parasitic nematode, *Sphaerularia bombi* (Tylenchida). *J. Nematol.* 4:270–277.

Poinar, G. O., and P. A. van der Laan. 1972. Morphology and life history of *Sphaerularia bombi*. *Nematologica* 18:239–252.

Price, T. D., A. Qvarnström, and D. E. Irwin. 2003. The role of phenotypic plasticity in driving genetic evolution. *Proc. R. Soc. Lond. B* 270:1433–1440.

Price, T. D. 2006. Phenotypic plasticity, sexual selection and the evolution of colour patterns. *J. Exp. Biol.* 209:2368–2376.

Price, J., M. C. Harrison, R. L. Hammond, S. Adams, J. F. Gutierrez-Marcos, and E. B. Mallon. 2018. Alternative splicing associated with phenotypic plasticity in the bumble bee *Bombus terrestris*. *Mol. Ecol.* 27:1036–1043.

Projecto-Garcia, J., J. F. Biddle, and E. J. Ragsdale. 2017. Decoding the architecture and origins of mechanisms for developmental polyphenism. *Curr. Opin. Genet. Dev.* 47:1–8.

Pungaliya, C., J. Srinivasan, B. W. Fox, R. U. Malik, A. H. Ludewig, P. W. Sternberg, and F. C. Schroeder. 2009. A shortcut to identifying small molecule signals that regulate behavior and development in *Caenorhabditis elegans*. *Proc. Natl. Acad. Sci. U.S.A.* 106:7708–7713.

Qing, X., Y. M. Zhang, S. Sun, M. Ahmed, W.-S. Lo, W. Bert, O. Holovachov, and H. Li. 2025. Phylogenomic insights into the evolution and origin of Nematoda. *Syst. Biol.* 74:349–358.

Quach, K. T., and S. H. Chalasani. 2020. Intraguild predation between *Pristionchus pacificus* and *Caenorhabditis elegans*: a complex interaction with the potential for aggressive behaviour. *J. Neurogenet.* 34:404–419.

Quintana-Murci, L. 2016. Understanding rare and common diseases in the context of human evolution. *Genome Biol.* 17:225.

Ragsdale, E. J., M. Müller, C. Rödelsperger, and R. J. Sommer. 2013a. A developmental switch coupled to the evolution of plasticity acts through a sulfatase. *Cell* 155:922–933.

Ragsdale, E. J., N. Kanzaki, W. Röseler, M. Herrmann, and R. J. Sommer. 2013b. Three new species of *Pristionchus* (Nematoda: Diplogastridae) show morphological divergence through evolutionary intermediates of a novel feeding-structure polymorphism. *Zool. J. Linn. Soc.* 168:671–698.

Ragsdale, E. J. 2015. Mouth dimorphism and the evolution of novelty and diversity. In R. J. Sommer, ed., Pristionchus pacificus: *A Nematode Model for Comparative and Evolutionary Biology*. Koninklijke Brill NV, Leiden, The Netherlands.

Ragsdale, E. J., N. Kanzaki, and M. Herrmann. 2015. Taxonomy and natural history: the genus *Pristionchus*. In R. J. Sommer, ed., Pristionchus pacificus: *A Nematode Model for Comparative and Evolutionary Biology*. Koninklijke Brill NV, Leiden, The Netherlands.

Raju, A., B. Xue, and S. Leibler. 2023. A theoretical perspective on Waddington's genetic assimilation experiments. *Proc. Natl. Acad. Sci. U.S.A.* 120:e2309760120.

Remy, J.-J. 2010. Stable inheritance of an acquired behavior in *Caenorhabditis elegans*. *Curr. Biol.* 20:R877–R878.

Reich, S., T. Loschko, J. Jung, S. Nestel, R. J. Sommer, and Werner, M. S. 2025. Developmental transcriptomics in *Pristionchus* reveals the environmental responsiveness of a plasticity gene-regulatory network. *Genome Res.* 35:1560–1573.

Renahan, T., and R. J. Sommer. 2021. Nematode interactions on beetle hosts indicate a role of mouth-form plasticity in resource competition. *Front. Ecol. Evol.* 9:752695.

Renahan, T., and R. J. Sommer. 2022. Multidimensional competition of nematodes affects plastic traits in a beetle ecosystem. *Front. Cell Dev. Biol.* 10:985831.

Rey, C., C. Launay, E. Wenger, and M. Delattre. 2023. Programmed DNA elimination in *Mesorhabditis* nematodes. *Curr. Biol.* 33:3711–3721.

Riddle, D. L. 1977. A genetic pathway for dauer larva formation in *Canorhabditis elegans*. In Stadler Symp. 9:101–120. University of Missouri, Columbia, MO.

Riddle, D. L., T. Blumenthal, B. J. Meyer, and J. R. Priess. 1997. Introduction to *C. elegans*. In D. L. Riddle, T. Blumenthal, B. J. Meyer, and J. R. Priess, eds., *C. elegans II*. Cold Spring Harbor Laboratory Press, Cold Spring Harbor, NY.

Riek, A., and F. Geriser. 2012. Developmental phenotypic plasticity in a marsupial. *J. Exp. Biol.* 215:1552–1558.

Rockman, M. V., S. C. Tintori, T. H. M. Nguyen, V. M. H. Yomai. 2026. *Caenorhabditis* diversity on Pohnpei, Micronesia, provides evidence that the Elegans Supergroup has its roots in the Americas and diversified in the Pacific *en route* to Asia. *Evolution* 80:1013–1034.

Rödelsperger, C., J. M. Meyer, N. Prabh, C. Lanz, F. Bemm, and R. J. Sommer. 2017. Single-molecule sequencing reveals the chromosome-scale genomic architecture of the nematode model organism *Pristionchus pacificus*. *Cell Rep.* 21:834–844.

Rödelsperger, C. 2024. Comparative genomics of sex, chromosomes, and sex chromosomes in *Caenorhabditis elegans* and other nematodes. In J. C.

Setubal, P. F. Stadler, and J. Stoye, eds., *Comparative Genomics: Methods in Molecular Biology*. Humana, New York, NY.

Rödelsperger, C., W. Röseler, M. Athanasouli, S. Wighard, M. Herrmann, and R. J. Sommer. 2024. Genome assembly of the nematode *Rhabditoides inermis* from a complex microbial community. *Genome Biol. Evol.* 16:evae230.

Roff, D. A. 1997. *Evolutionary Quantitative Genetics*. Springer, Boston, MA.

Roggen, D. R., D. J. Raski, and N. O. Jones. 1966. Cilia in nematode sensory organs. *Science* 152:515–516.

Sabarís, G., B. Schuettengruber, G. L. Papadopoulos, M. Coronado-Zamora, M. H. Fitz-James, J. González, and G. Cavalli. 2025. A mechanistic basis for genetic assimilation in natural fly populations. *Proc. Natl. Acad. Sci. U.S.A.* 11:e2415982122.

Sadiq, F., S. Flint, Y. Li, T. Liu, Y. Lei, H. A. Sakandar, and G. He. 2017. New mechanistic insights into the motile-to-sessile switch in various bacteria with particular emphasis on *Bacillus subtilis* and *Pseudomonas aeruginosa*: a review. *Biofouling* 33:306–326.

Sakamoto, T., and H. Innan. 2024. On the evolutionary origin of discrete phenotypic plasticity. *G3* 14:jkae144.

Sarkar, S. 1999. From the *Reaktionsnorm* to the adaptive norm: the norm of reaction, 1909–1960. *Biol. Philos.* 14:235–252.

Schalkowski, R., K. R. Kasimatis, M. A. Greischar, and A. D. Cutter. 2024. Reproductive interference alters species coexistence in nematodes due to asymmetric sperm-induced harm. *Ecol. Lett.* 28:e70067.

Schiffer, P. H., E. G. J. Danchin, A. M. Burnell, C. J. Creevey, S. Wong, I. Dix, G. O'Mahony, B. A. Culleton, C. Rancurel, G. Stier, E. A. Martínez-Salazar, A. Marconi, U. Trivedi, M. Kroiher, M. A. S. Thorne, E. Schierenberg, T. Wiehe, and M. Blaxter. 2019. Signatures of the evolution of parthenogenesis and cryptobiosis in the genomes of panagrolaimid nematodes. *iScience* 21:587–602.

Schlichting, C. D., and M. Pigliucci. 1998. *Phenotypic Evolution: A Reaction Norm Perspective*. Sinauer Associates, Sunderland, MA.

Schlichting, C. D. 2021. Plasticity and evolutionary theory: where we are and where we should be going. In D. W. Pfennig, ed., *Phenotypic Plasticity and Evolution: Causes, Consequences, Controversies*. CRC Press, Boca Raton, FL.

Schneider, R. F., and A. Meyer. 2017. How plasticity, genetic assimilation and cryptic genetic variation may contribute to adaptive radiations. *Mol. Ecol.* 26:330–350.

Schneider, H. M. 2022. Characterization, costs, cues and future perspectives of

phenotypic plasticity. *Ann. Bot.* 130:131–148.

Schwander, T., and O. Leimar. 2011. Genes as leaders and followers in evolution. *Trends Ecol. Evol.* 26:143–151.

Schwartz, H. T., C.-H. Tan, J. Peraza, K. L. T. Raymundo, and P. W. Sternberg. 2024. Molecular identification of a peroxidase gene controlling body size in the entomopathogenic nematode *Steinernema hermaphroditum*. *Genetics* 226:iyad209.

Schwarz, E. M., A. Baniya, J. K. Heppert, H. T. Schwartz, C.-H. Tan, I. Antoshechkin, P. W. Sternberg, H. Goodrich-Blair, and A. R. Dillman. 2025. Genomes of the entomopathogenic nematode *Steinernema hermaphroditum* and its associated bacteria. *Genetics* 231:iyaf170.

Serobyan, V., E. J. Ragsdale, and R. J. Sommer. 2014. Adaptive value of a predatory mouth-form in a dimorphic nematode. *Proc. R. Soc. B* 281:20141334.

Shannon, A. J., J. A. Browne, J. Boyd, D. A. Fitzpatrick, and A. M. Burnell. 2005. The anhydrobiotic potential and molecular phylogenetics of species and strains of *Panagrolaimus* (Nematoda, Panagrolaimidae). *J. Exp. Biol.* 208:2433–2445.

Shatilovich, A., V. R. Gade, M. Pippel, T. T. Hoffmeyer, A. V. Tchesunov, L. Stevens, S. Winkler, G. M. Hughes, S. Traikov, M. Hiller, E. Rivkina, P. H. Schiffer, E. W. Myers, and T. V. Kurzchalia. 2023. A novel nematode species from the Siberian permafrost shares adaptive mechanisms for cryptobiotic survival with *C. elegans* dauer larva. *PLoS Genet.* 19:e1010798.

Sieriebriennikov, B., and R. J. Sommer. 2018. Developmental plasticity and robustness of a nematode mouth-form polyphenism. *Front. Genet.* 9:382.

Sieriebriennikov, B., N. Prabh, M. Dardiry, H. Witte, W. Röseler, M. R. Kieninger, C. Rödelsperger, and R. J. Sommer. 2018. A developmental switch generating phenotypic plasticity is part of a conserved multi-gene locus. *Cell Rep.* 23:2835–2843.

Sieriebriennikov, B., S. Sun, J. W. Lightfoot, H. Witte, E. Moreno, C. Rödelsperger, and R. J. Sommer. 2020. Conserved nuclear hormone receptors controlling a novel plastic trait target fast-evolving genes expressed in a single cell. *PLoS Genet.* 16:e1008687.

Signore, A. V., and J. F. Storz. 2020. Biochemical pedomorphosis and genetic assimilation in the hypoxia adaptation of Tibetan antelope. *Sci. Adv.* 6:eabb5447.

Sikkink, K. L., R. M. Reynolds, C. M. Ituarte, and W. A. Cresko. 2014. Rapid evolution of phenotypic plasticity and shifting thresholds of genetic assimilation in the nematode *Caenorhabditis remanei*. *G3* 4:1103–1112.

Simm, R., M. Morr, A. Kader, M. Nimtz, and U. Römling. 2004. GGDEF and EAL domains inversely regulate cyclic di-GMP levels and transition from sessility to motility. *Mol. Microbiol.* 53:1123–1134.

Simpson, G. G. 1953. The Baldwin effect. *Evolution* 7:110–117.

Simpson, S. J., G. A. Sword, and N. Lo. 2011. Polyphenism in insects. *Curr. Biol.* 21:R738–R749.

Smith, C. R., A. L. Toth, A. V. Suarez, and G. E. Robinson. 2008. Genetic and genomic analyses of the division of labour in insect societies. *Nat. Rev. Genet.* 9:735–748.

Sommer, R. J. 2012. Evolution of regulatory networks: nematode vulva induction as an example of developmental systems drift. In O. Soyer, ed., *Evolutionary Systems Biology: Advances in Experimental Medicine and Biology*. Springer, New York, NY.

Sommer, R. J., M. Dardiry, M. Lenuzzi, S. Namdeo, T. Renahan, B. Sieriebriennikov, and M. S. Werner. 2017. The genetics of phenotypic plasticity in nematode feeding structures. *Open Biol.* 7:160332.

Sommer, R. J. 2020. Phenotypic plasticity: from theory and genetics to current and future challenges. *Genetics* 215:1–13.

Sommer, R. J., and J. W. Lightfoot. 2022. The genus *Pristionchus*: a model for phenotypic plasticity, predatory behavior, self-recognition and other complex traits. In I. Glazer, D. I. Shapiro-Ilan, and P. W. Sternberg, eds., *Nematodes as Model Organisms*. CAB International, Wallingford, UK.

Sommer, R. J. 2025. *Pristionchus* – beetle associations: towards a new natural history. *J. Invertebr. Pathol.* 209:108243.

Somvanshi, V. S., B. Kaufmann-Daszczuk, K.-s. Kim, S. Mallon, and T. A. Ciche. 2010. *Photorhabdus* phase variants express a novel fimbrial locus, *mad*, essential for symbiosis. *Mol. Microbiol.* 77:1021–1038.

Somvanshi, V. S., R. E. Sloup, J. M. Crawford, A. R. Martin, A. J. Heidt, K.-s. Kim, J. Clardy, and T. A. Ciche. 2012. A single promoter inversion switches *Photorhabdus* between pathogenic and mutualistic states. *Science* 337:88–93.

Sorci, G., J. Clobert, and S. Belichon. 1996. Phenotypic plasticity of growth and survival in the common lizard *Lacerta vivipara*. *J. Anim. Ecol.* 65:781–790.

Stearns, S. C. 1989. The evolutionary significance of phenotypic plasticity: phenotypic sources of variation among organisms can be described by developmental switches and reaction norms. *Bioscience* 39:436–445.

Sternberg, P. W. 2015. Why *Caenorhabditis elegans* is great and *Pristionchus pacificus* might be better. In R. J. Sommer, ed., Pristionchus pacificus: *A*

Nematode Model for Comparative and Evolutionary Biology. Koninklijke Brill NV, Leiden, The Netherlands.

Stevens, L., M.-A. Félix, T. Beltran, C. Braendle, C. Caurcel, S. Fausett, D. Fitch, L. Frézal, C. Gosse, T. Kaur, K. Kiontke, M. D. Newton, L. M. Noble, A. Richaud, M. V. Rockman, W. Sudhaus, and M. Blaxter. 2019. Comparative genomics of 10 new *Caenorhabditis* species. *Evol. Lett.* 3:217–236.

Stevens, L., S. Sun, N. Haruta, L. Xiao, N. Uwatoko, M. Kieninger, K. Sato, A. Yoshida, D. Absolon, J. Collins, A. Sugimoto, T. Kikuchi, and M. Blaxter. 2025. Programmed DNA elimination was present in the last common ancestor of *Caenorhabditis* nematodes. *bioRxiv* 2025.10.23.681605.

Steward, R. A., M. A. de Jong, V. Oostra, and C. W. Wheat. 2022. Alternative splicing in seasonal plasticity and the potential for adaptation to environmental change. *Nat. Commun.* 13:755.

Strange, K. 2007. Revisiting the Krogh Principle in the post-genome era: *Caenorhabditis elegans* as a model system for integrative physiology research. *J. Exp. Biol.* 210:1622–1631.

Strauch, O., S. Stoessel, and R.-U. Ehlers. 1994. Culture conditions define automictic or amphimictic reproduction in entomopathogenic rhabditid nematodes of the genus *Heterorhabditis*. *Fundam. Appl. Nematol.* 17:575–582.

Sultan, S. E. 2003. Phenotypic plasticity in plants: a case study in ecological development. *Evol. Dev.* 5:25–33.

Sultan, S. E. 2021. Phenotypic plasticity as an intrinsic property of organisms. In D. W. Pfennig, ed., *Phenotypic Plasticity and Evolution: Causes, Consequences, Controversies*. CRC Press, Boca Raton, FL.

Sun, S., T. Theska, H. Witte, E. J. Ragsdale, and R. J. Sommer. 2022. The oscillating Mucin-type protein DPY-6 has a conserved role in nematode mouth and cuticle formation. *Genetics* 220:iyab233.

Sun, S., H. Witte, and R. J. Sommer. 2023. Chitin contributes to the formation of a feeding structure in a predatory nematode. *Curr. Biol.* 33:15–27.

Susana, I. P., T. S. Sillett, J. T. Rotenberry, and C. K. Ghalambor. 2008. Adaptive phenotypic plasticity in an island songbird exposed to a novel predation risk. *Behav. Ecol.* 19:830–835.

Susoy, V, E. J. Ragsdale, N. Kanzaki, and R. J. Sommer. 2015. Rapid diversification associated with a macroevolutionary pulse of developmental plasticity. *eLife* 4:e05463.

Suzuki, Y., and H. F. Nijhout. 2006. Evolution of a polyphenism by genetic accommodation. *Science* 311:650–652.

Suzuki, Y., S. Amaya, P. Gonzalez, D. Becerril, S. Aquit, M. Davis, M. Hoesel, E. Chou, H. Khong, K. Zaia, H. S. Park, H. F. Nijhout, and B. Tjaden. 2025. Molecular mechanisms underlying the evolution of a color polyphenism by genetic accommodation in the tobacco hornworm, *Manduca sexta*. *Proc. Natl. Acad. Sci. U.S.A.* 12:e2425004122.

Tian, S., B. Lee, T. D. Banerjee, S. N. Murugesan, and A. Monteiro. 2025. A novel Hox gene promoter fuels the evolution of adaptive phenotypic plasticity in wing eyespots of satyrid butterflies. *Nat. Ecol. Evol.* 9:2391–2403.

The *C. elegans* Sequencing Consortium. 1998. Genome sequence of the nematode *C. elegans*: a platform for investigating biology. *Science* 282:2012–2018.

Theam, P., N. Kanzaki, M. Herrmann, C. Weiler, C. Rödelsperger, and R. J. Sommer. 2025. *Pristionchus kravanhensis* n. sp., the first *Pristionchus* species reported from Cambodia. *Nematology* 27:651–663.

Theam, P., H. Witte, R. Liu, T. Loschko, C. Rödelsperger, C. Igreja, and R. J. Sommer. 2026. Plasticity in nonsense-mediated decay and translation initiation regulate polyphenism. *bioRxiv* 2026.03.27.714762.

Thibert-Plante, X., and A. P. Hendry. 2011. The consequences of phenotypic plasticity for ecological speciation. *J. Evol. Biol.* 24:326–342.

Thompson, J. D. 1991. Phenotypic plasticity as a component of evolutionary change. *Trends Ecol. Evol.* 6:246–249.

Torres-Dowdall, J., S. J. Rometsch, J. R. Velasco, G. Aguilera, A. F. Kautt, G. Goyenola, A. C. Petry, G. C. Deprá, W. J. da Graça, and A. Meyer. 2022. Genetic assimilation and the evolution of direction of genital asymmetry in anablepid fishes. *Proc. R. Soc. B* 289: 20220266.

Toth, A. L., and S. M. Rehan. 2017. Molecular evolution of insect sociality: an eco-evo-devo perspective. *Annu. Rev. Entomol.* 62:419–442.

Trainor, F. R., and P. F. Egan. 1991. Discovering the various ecomorphs of *Scenedesmus*: the end of a taxonomic era. *Arch. Protistenkunde* 139:125–132.

Triantaphyllou, A. C. 1960. Sex determination in *Meloidogyne incognita* Chitwood, 1949, and intersexuality in *M. javanica* (Treub, 1885) Chitwood, 1949. *Ann. Inst. Phytopathol. Benaki, N.S.* 3:12–31.

Triantaphyllou, A. C. 1973. Environmental sex differentiation of nematodes in relation to pest management. *Annu. Rev. Phytopathol.* 11:441–462.

Tucker, P. K. 2007. Systematics of the genus *Mus*. In J. G. Fox, M. T. Davisson, F. W. Quimby, S. W. Barthold, C. E. Newcomer, A. L. Smith, eds., *The Mouse in Biomedical Research: History, Wild Mice, and Genetics*. Academic Press, San Diego, CA.

Uller, T., N. Feiner, R. Radersma, I. S. C. Jackson, and A. Rago. 2020. Developmental plasticity and evolutionary explanations. *Evol. Dev.* 22:47–55.

Uller, T., L. Milocco, J. Isanta-Navarro, C. K. Cornwallis, and N Feiner. 2024. Twenty years on from *Developmental Plasticity and Evolution*: middle-range theories and how to test them. *J. Exp. Biol.* 227:jeb246375.

Van Alstyne, K. L. 1988. Herbivore grazing increases polyphenolic defenses in the intertidal brown alga *Fucus distichus*. *Ecology* 69:655–663.

van den Hoogen, J., S. Geisen, D. Routh, H. Ferris, W. Traunspurger, D. A. Wardle, R. G. M. de Goede, B. J. Adams, W. Ahmad, W. S. Andriuzzi, R. D. Bardgett, M. Bonkowski, R. Campos-Herrera, J. E. Cares, T. Caruso, L. B. Caixeta, X. Chen, S. R. Costa, R. Creamer, J. M. C. Castro, M. Dam, D. Djigal, M. Escuer, B. S. Griffiths, C. Gutiérrez, K. Hohberg, D. Kalinkina, P. Kardol, A. Kergunteuil, G. Korthals, V. Krashevska, A. A. Kudrin, Q. Li, W. Liang, M. Magilton, M. Marais, J. A. R. Martín, E. Matveeva, E. H. Mayad, C. Mulder, P. Mullin, R. Neilson, T. A. D. Nguyen, U. N. Nielsen, H. Okada, J. E. P. Rius, K. Pan, V. Peneva, L. Pellissier, J. C. P. da Silva, C. Pitteloud, T. O. Powers, K. Powers, C. W. Quist, S. Rasmann, S. S. Moreno, S. Scheu, H. Setälä, A. Sushchuk, A. V. Tiunov, J. Trap, W. van der Putten, M. Vestergård, C. Villenave, L. Waeyenberge, D. H. Wall, R. Wilschut, D. G. Wright, J.-i. Yang, T. W. Crowther. 2019. Soil nematode abundance and functional group composition at a global scale. *Nature* 572:194–198.

van der Burg, K. R. L., J. J. Lewis, B. J. Brack, R. A. Fandino, A. Mazo-Vargas, and R. D. Reed. 2020. Genomic architecture of a genetically assimilated seasonal color pattern. *Science* 370:721–725.

van Kleunen, M., and M. Fischer. 2005. Constraints on the evolution of adaptive phenotypic plasticity in plants. *New Phytol.* 166:49–60.

Verstraeten, N., K. Braeken, B. Debkumari, M. Fauvart, J. Fransaer, J. Vermant, and J. Michiels. 2008. Living on a surface: swarming and biofilm formation. *Trends Microbiol.* 16:496–506.

Vigne, P., C. Gimond, C. Ferrari, A. Vielle, J. Hallin, A. Pino-Querido, S. El Mouridi, L. Mignerot, C. Frøkjær-Jensen, T. Boulin, H. Teotónio, and C. Braendle. 2021. A single-nucleotide change underlies the genetic assimilation of a plastic trait. *Sci. Adv.* 7:eabd9941.

Volny, V. P., and D. M. Gordon. 2002. Genetic basis for queen–worker dimorphism in a social insect. *Proc. Natl. Acad. Sci. U.S.A.* 99:6108–6111.

von Reuss, S. H., and F. Schroeder. 2015. Combinatorial chemistry in nematodes: modular assembly of primary metabolism-derived building blocks. *Nat. Prod. Rep.* 32:994.

von Reuss, S. H. 2018. Exploring modular glycolipids involved in nematode chemical communication. *Chimia* 72:297–303.

Waddington, C. H. 1953. Genetic assimilation of an acquired character. *Evolution* 7:118–126.

Waddington, C. H. 1956. Genetic assimilation of the *bithorax* phenotype. *Evolution* 10:1–13.

Walworth, N. G., M. D. Lee, F.-X. Fu, D. A. Hutchins, and E. A. Webb. 2016. Molecular and physiological evidence of genetic assimilation to high CO_2 in the marine nitrogen fixer *Trichodesmium*. *Proc. Natl. Acad. Sci. U.S.A.* 113:E7367–E7374.

Wang, N., S. Ning, M. Pourkheirandish, I. Honda, and T. Komatsuda. 2013. An alternative mechanism for cleistogamy in barley. *Theor. Appl. Genet.* 126:2753–2762.

Warkentin, K. M. 2011. Plasticity of hatching in amphibians: evolution, trade-offs, cues and mechanisms. *Integr. Comp. Biol.* 51:111–127.

Weitekamp, C. A., R. Libbrecht, and L. Keller. 2017. Genetics and evolution of social behavior in insects. *Annu. Rev. Genet.* 51:219–239.

Weller, A. M., W. E. Mayer, R. Rae, and R. J. Sommer. 2010. Quantitative assessment of the nematode fauna present on *Geotrupes* dung beetles reveals species-rich communities with a heterogeneous distribution. *J. Parasitol.* 96:525–531.

Werner, M. S., M. H. Claaßen, T. Renahan, M. Dardiry, and R. J. Sommer. 2018. Adult influence on juvenile phenotypes by stage-specific pheromone production. *iScience* 10:123–134.

Werner, M. S., T. Loschko, T. King, S. Reich, T. Theska, M. Franz-Wachtel, B. Macek, and R. J. Sommer. 2023. Histone 4 lysine 5/12 acetylation enables developmental plasticity of *Pristionchus* mouth form. *Nat. Commun.* 14:2095.

West-Eberhard, M. J. 1989. Phenotypic plasticity and the origins of diversity. *Annu. Rev. Ecol. Evol. Syst.* 20:249–278.

West-Eberhard, M. J. 2003. *Developmental Plasticity and Evolution*. Oxford University Press, New York, NY.

Widmayer, S. J., K. S. Evans, S. Zdraljevic, and E. C. Andersen. 2022. Evaluating the power and limitations of genome-wide association studies in *Caenorhabditis elegans*. *G3* 12:jkac114.

Wighard, S., and R. J. Sommer. 2024. The role of epigenetic switches in polyphenism control: implications from a nematode model for the developmental regulation of alternative phenotypes. *Biology* 13:922.

Williams, G. C. 1966. *Adaptation and Natural Selection*. Princeton University Press, Princeton, NJ.

Witkowski, J. 1988. Fifty years on: molecular biology's hall of fame. *Trends Biotechnol.* 6:234–243.

Woltereck, R. 1909. Weitere experimentelle Untersuchungen über Artänderung, speziell über das Wesen quantitativer Artunterschiede bei Daphniden. *Verh. Deutsch. Zool. Ges.* 19:110–172.

Wood, D. P., J. A. Holmberg, O. G. Osborne, A. J. Helmstetter, L. T. Dunning, A. R. Ellison, R. J. Smith, J. Lighten, and A. S. T. Papadopulos. 2023. Genetic assimilation of ancestral plasticity during parallel adaptation to zinc contamination in *Silene uniflora*. *Nat. Ecol. Evol.* 7:414–423.

Wray, G. A., H. E. Hoekstra, D. J. Futuyma, R. E. Lenski, T. F. C. Mackay, D. Schluter, and J. E. Strassmann. 2014. Does evolutionary theory need a rethink? No, all is well. *Nature* 514:161–164.

Wright, C. J., C. W. J. Smith, and C. D. Jiggins. 2022. Alternative splicing as a source of phenotypic diversity. *Nat. Rev. Genet.* 23:697–710.

Wrobel, C. J. J., and F. C. Schroeder. 2023. Repurposing degradation pathways for modular metabolite biosynthesis in nematodes. *Nat. Chem. Biol.* 19:676–686.

Wund, M. A. 2012. Assessing the impacts of phenotypic plasticity on evolution. *Integr. Comp. Biol.* 52:5–15.

Xu, H.-J., J. Xue, B. Lu, X.-C. Zhang, J.-C. Zhuo, S.-F. He, X.-F. Ma, Y.-Q. Jiang, H.-W. Fan, J.-Y. Xu, Y.-X. Ye, P.-L. Pan, Q. Li, Y.-Y. Bao, H. F. Nijhout, and C.-X. Zhang. 2015. Two insulin receptors determine alternative wing morphs in planthoppers. *Nature* 519:464–467.

Xue, W., Y. Xing, X. Weng, Y. Zhao, W. Tang, L. Wang, H. Zhou, S. Yu, C. Xu, X. Li, and Q. Zhang. 2008. Natural variation in *Ghd7* is an important regulator of heading date and yield potential in rice. *Nat. Genet.* 40:761–767.

Yamashita, T., T. Ekino, N. Kanzaki, and R. Shinya. 2023. The developmental and structural uniqueness of the embryo of the extremophile viviparous nematode, *Tokorhabditis tufae*. *Front. Physiol.* 14:1197477.

Yamashita, T., A. Pires-daSilva, S. Oomura, T. Kusano, N. Haruta, M. Hasumi, T. Kikuchi, S. Adams, A. Sugimoto, and R. Shinya. 2025. Microparticle bombardment as a method for transgenesis in *Auanema* and *Tokorhabditis*. *MicroPubl Biol.* 10.17912/micropub.biology.001585.

Yang, C.-H., and J. A. Pospisilik. 2019. Polyphenism – a window into gene-environment interactions and phenotypic plasticity. *Front. Genet.* 10:132.

Yang, W., T. Zhang, Z. Yao, X. Tang, and Y. Qi. 2021. Transcriptome sequencing

provides evidence of genetic assimilation in a toad-headed lizard at high altitude. *Asian Herpetol. Res.* 12:315–322.

Zhang, F., M. Berg, K. Dierking, M.-A. Félix, M. Shapira, B. S. Samuel, and H. Schulenburg. 2017. *Caenorhabditis elegans* as a model for microbiome research. *Front. Microbiol.* 8:485.

Zhang, C.-X., J. A. Brisson, and H.-J. Xu. 2019. Molecular mechanisms of wing polymorphism in insects. *Annu. Rev. Entomol.* 64:297–314.

Zhang, P., P. Theam, W. Xu, S. Ye, H. Witte, T. Liu, R. J. Sommer, and C. Dong. 2025. Biosynthesis of modular signaling molecules requires functional diversification of carboxylesterases in *Pristionchus pacificus*. *Commun. Biol.* 8:1213.

Zheng, X., K. Zhu, Q. Sun, W. Zhang, X. Wang, H. Cao, M. Tan, Z. Xie, Y. Zeng, J. Ye, L. Chai, Q. Xu, Z. Pan, S. Xiao, P. D. Fraser, and X. Deng. 2019. Natural variation in *CCD4* promoter underpins species-specific evolution of red coloration in citrus peel. *Mol. Plant* 12:1294–1307.

Zhong, W., and P. W. Sternberg. 2006. Genome-wide prediction of *C. elegans* genetic interactions. *Science* 311:1481–1484.

6. Appendix

PLOS GENETICS

RESEARCH ARTICLE

Thousands of *Pristionchus pacificus* orphan genes were integrated into developmental networks that respond to diverse environmental microbiota

Marina Athanasouli, Nermin Akduman¤, Waltraud Röseler, Penghieng Theam, Christian Rödelsperger*

Department for Integrative Evolutionary Biology, Max Planck Institute for Biology, Tübingen, Germany

¤ Current address: Interfaculty Institute of Microbiology and Infection Medicine, University of Tübingen, Tübingen, Germany
* christian.roedelsperger@tuebingen.mpg.de

Check for updates

OPEN ACCESS

Citation: Athanasouli M, Akduman N, Röseler W, Theam P, Rödelsperger C (2023) Thousands of *Pristionchus pacificus* orphan genes were integrated into developmental networks that respond to diverse environmental microbiota. PLoS Genet 19(7): e1010832. https://doi.org/10.1371/journal.pgen.1010832

Editor: Kaveh Ashrafi, University of California San Francisco, UNITED STATES

Received: March 2, 2023

Accepted: June 15, 2023

Published: July 3, 2023

Peer Review History: PLOS recognizes the benefits of transparency in the peer review process; therefore, we enable the publication of all of the content of peer review and author responses alongside final, published articles. The editorial history of this article is available here: https://doi.org/10.1371/journal.pgen.1010832

Copyright: © 2023 Athanasouli et al. This is an open access article distributed under the terms of the Creative Commons Attribution License, which permits unrestricted use, distribution, and reproduction in any medium, provided the original author and source are credited.

Data Availability Statement: Raw reads were deposited at the European Nucleotide archive under the study accession PRJEB60166.

Abstract

Adaptation of organisms to environmental change may be facilitated by the creation of new genes. New genes without homologs in other lineages are known as taxonomically-restricted orphan genes and may result from divergence or *de novo* formation. Previously, we have extensively characterized the evolution and origin of such orphan genes in the nematode model organism *Pristionchus pacificus*. Here, we employ large-scale transcriptomics to establish potential functional associations and to measure the degree of transcriptional plasticity among orphan genes. Specifically, we analyzed 24 RNA-seq samples from adult *P. pacificus* worms raised on 24 different monoxenic bacterial cultures. Based on coexpression analysis, we identified 28 large modules that harbor 3,727 diplogastrid-specific orphan genes and that respond dynamically to different bacteria. These coexpression modules have distinct regulatory architecture and also exhibit differential expression patterns across development suggesting a link between bacterial response networks and development. Phylostratigraphy revealed a considerably high number of family- and even species-specific orphan genes in certain coexpression modules. This suggests that new genes are not attached randomly to existing cellular networks and that integration can happen very fast. Integrative analysis of protein domains, gene expression and ortholog data facilitated the assignments of biological labels for 22 coexpression modules with one of the largest, fast-evolving module being associated with spermatogenesis. In summary, this work presents the first functional annotation for thousands of *P. pacificus* orphan genes and reveals insights into their integration into environmentally responsive gene networks.

Author summary

The inference of biological function for genes in newly sequenced genomes heavily relies on sequence conservation with classical model organisms. Consequently, newly evolved

Funding: This work was funded by the Max Planck Society. The funder had no role in study design, data collection and analysis, decision to publish, or preparation of the manuscript.

Competing interests: The authors have declared that no competing interests exist.

orphan genes that do not have homologs will not be associated with any function. Here, we use coexpression with known genes in order to assign potential functions to orphan genes in the nematode *Pristionchus pacificus*. To this end, we generated transcriptome profiles of *P. pacificus* worms that were grown on 24 different bacteria and clustered the genes into 28 large coexpression modules which contain thousands of orphan genes. Integrative analysis could associate most coexpression modules with biological processes or tissues, which results in the first functional annotation for thousands of orphan genes. Complementary analysis of gene ages shows that modules associated with female reproduction are highly constrained whereas a male-reproductive module is much more likely to integrate new genes, which could possibly be explained by sperm competition. This links sexual conflict with gene network evolution and environmental regulation.

Introduction

The evolution of phenotypic diversity across all domains of life has been accompanied by the formation of new genes. As a result, up to one third of the gene content in extant genomes consists of orphan genes that lack homologs in other taxonomic lineages [1]. Although the definition of these taxonomically-restricted orphan genes is context-dependent and the numbers of identified orphan genes will vary with the phylogenetic resolution and methods for homology detection, orphan genes exist in any given genome [2]. Orphan genes may reflect ancient genes that evolve so fast that homology cannot be detected [3]. Alternatively, orphan genes may arise *de novo* from previously non-coding sequences [4,5]. This has been demonstrated in multiple taxonomic groups including vertebrates [6,7], insects [8,9], nematodes [10,11], yeast [12,13], and plants [14,15]. Horizontal gene transfer can be considered as a third mechanism that would lead to the generation of orphan genes [16,17]. The origin of orphan genes can most conclusively be studied for relatively recent gene births because potentially neutrally evolving ancestral sequences may degenerate very fast in sister taxa rendering homology detection impossible [18]. Thus, to what extent more ancient orphan genes arose from divergence or *de novo* formation is currently not known. Another important question concerns the biological functions of orphan genes. Given that large-scale experimental screens for possible functions are only possible in a limited number of model species [19,20] and that inference of function based on sequence conservation is not possible, most orphan genes have no known function. It has been hypothesized that new genes play a role in adapting to changing environments [21], but this is only supported by limited data [22,23]. In this study, we want to test this hypothesis in the nematode model organism *Pristionchus pacificus* by exploring the transcriptomic changes after exposure to different bacteria. *P. pacificus* is a free-living nematode that was initially established as a model system for comparative studies with the classical model organism *Caenorhabditis elegans* [24]. *C. elegans* and *P. pacificus* were estimated to have shared the last common ancestor around 130–310 million years ago [25]. Numerous studies have revealed conserved and divergent patterns across development [26], neurobiology [27], and behavior [28]. When the genome of *P. pacificus* was sequenced, around one third of its genes were classified as orphan genes that do not have any homolog outside the diplogastrid family [29]. By sequencing nine additional diplogastrid genomes, we established a phylogenomic framework to assign these orphan genes into phylostrata and to study their evolutionary dynamics and origin at the inter- and intra-species level [30,31]. These studies confirmed trends such as little expression evidence of orphan genes, rapid evolution, and high turnover which were also found in genomic studies of other animals and plants [32,33]. In contrast to

the broad understanding of new gene evolution in *Pristionchus* nematodes, only two orphan genes have been experimentally characterized. The first orphan gene, *dauerless*, was identified in a screen to dissect the genetic basis of natural variation in dauer formation [34]. The dauer stage represents an alternative developmental stage in most nematodes that allows the worms to survive unfavorable environmental conditions for extended time periods. Overexpression of *dauerless* results in the suppression of dauer formation and it has been speculated that the ability to regulate *dauerless* dosage might provide individual strains an advantage during intraspecific competition [34]. The second orphan gene, *self-1*, encodes a micropeptide that was identified in a screen for killing behavior. Knockouts or modifications of *self-1* resulted in a loss of self-recognition and led to killing by relatives. These two cases demonstrate that *Pristionchus* orphan genes are involved in important developmental decisions and in the evolution of novel behaviors. To complement this detailed functional knowledge of a very limited number of orphan genes with broader functional data on a genome-wide scale, we employ expression data as a proxy for function. This is under the assumption that in order to carry out a certain function, a gene must be expressed at a given condition. Furthermore, large-scale expression data can be used to group genes into functional modules and to transfer functional annotations based on coexpression [35–37]. Specifically, we aim to investigate the *P. pacificus* transcriptome in response to different microbiota which denote the assemblage of microorganisms present in a defined environment [38]. Environmental bacteria can interact with nematodes in a variety of different ways such as serving as food source [39], constituents of the gut microbiome [40], or pathogens [41]. Here, we focus on the transcriptomic response to 24 different bacteria, most of which were isolated previously from *Pristionchus*-associated environments [42]. These bacteria are non-pathogenic in the sense that worm populations can survive for at least several days [42]. This is in contrast to highly pathogenic strains that can kill complete worm populations within a few hours [41]. Our main goals are to group *P. pacificus* genes into functional modules that respond differently to environmental microbiota, to characterize these modules, and finally to test whether some of these modules are enriched in orphan genes. This will allow us to better understand the plastic response to diverse environmental microbiota and to further elucidate the regulation and evolution of the associated gene networks.

Results

The transcriptomic response of nematodes to various microbiota does not strictly reflect bacterial phylogeny

To investigate the transcriptomic response of *P. pacificus* to different environmental microbiota, we grew worms on monoxenic cultures of 24 bacterial strains that included commonly used food bacteria such as *Escherichicha coli* OP50 and HB101 as well as 22 bacterial strains that were previously isolated from *Pristionchus*-associated environments [42]. The selected bacteria represent Alpha-, Beta-, Gammaproteobacteria as well as Flavobacteriia. A single RNA-seq data was generated per bacterial strain from 50 young adult worms that were manually picked from mixed-stage cultures (see *Methods*). Most transcriptome profiles of worms grown on different bacteria appeared to be highly similar (Pearson $r > 0.9$, Fig 1A). One sample, *Wautersiella* LRB104, showed a quite distinct transcriptome with correlation coefficients around 0.8 (Fig 1A and 1B). However, even this outlier shows much higher correlations than transcriptomes from different developmental stages with correlation coefficients of 0.6 [43,44]. The observed correlation coefficients translate into hundreds to thousands of genes with an absolute fold change > 2 between the most similar and most dissimilar pair of samples (S1 Fig). Next, we wanted to test whether the transcriptome profiles follow a phylogenetic pattern,

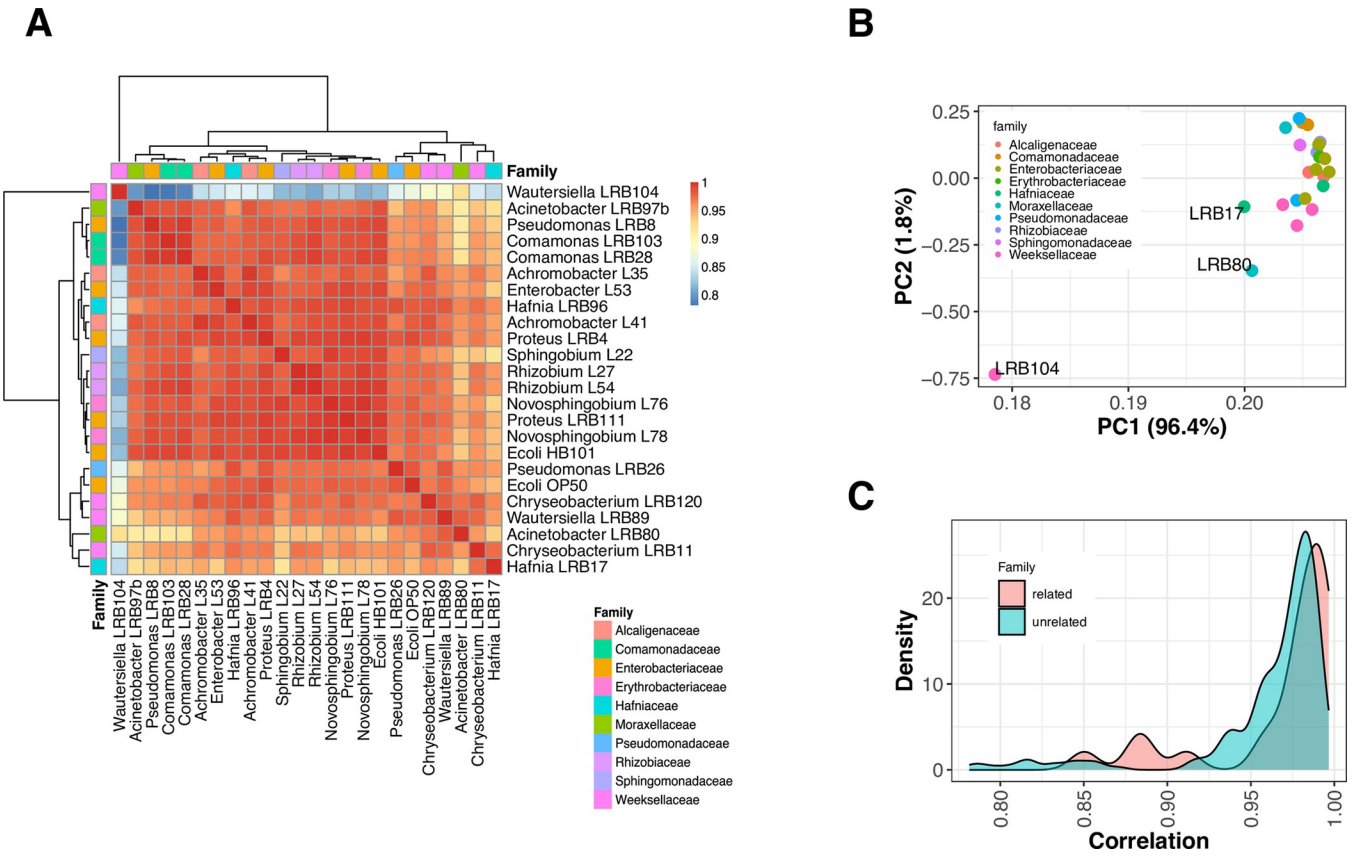


Fig 1. Transcriptional response to 24 bacterial environments. (A) The heatmap shows the correlation between transcriptomes. Apart from *Wautersiella* LRB104 all transcriptomes are highly similar. (B) Complementary analysis using principal component analysis identifies *Wautersiella* LRB104 as the most distinct environment. C) The histograms show the distribution of correlation values for comparisons within and across bacterial families. The expression profiles of *P. pacificus* worms on bacteria of different families can be more similar than the profile on bacteria of the same family. This suggests that the transcriptional response does not strictly reflect bacterial phylogeny.

https://doi.org/10.1371/journal.pgen.1010832.g001

i.e. are transcriptome profiles of worms grown on bacteria of the same family more similar than nematode transcriptomes from more distantly related bacteria (Fig 1C). This did not show significantly higher correlation for transcriptomes from more closely related bacteria (P = 0.35, t-test) suggesting that the transcriptomic response of nematodes to various environmental microbiota do not strictly reflect phylogeny. This observation could indicate that the observed differences are driven by factors that are difficult to control (e.g. bacterial concentration), or alternatively, that strain-specific changes are obscuring family-specific signals. The latter would be the case if critical metabolic pathways are plasmid encoded and could easily be horizontally transferred. In summary, *P. pacificus* nematodes exhibit substantial transcriptomic variation in response to environmental microbiota and these responses do not strictly reflect the bacterial phylogeny.

Almost half of all genes respond to diverse environmental microbiota

Nematodes interact with bacteria in many different ways involving processes like chemical attraction and repulsion [45], digestion [39], and detoxification [46]. Moreover, those processes can trigger secondary effects on worm development and physiology [47]. Thus, the response of worms might involve multiple regulatory and metabolic pathways and might impact many other biological processes. To characterize gene networks that respond to diverse

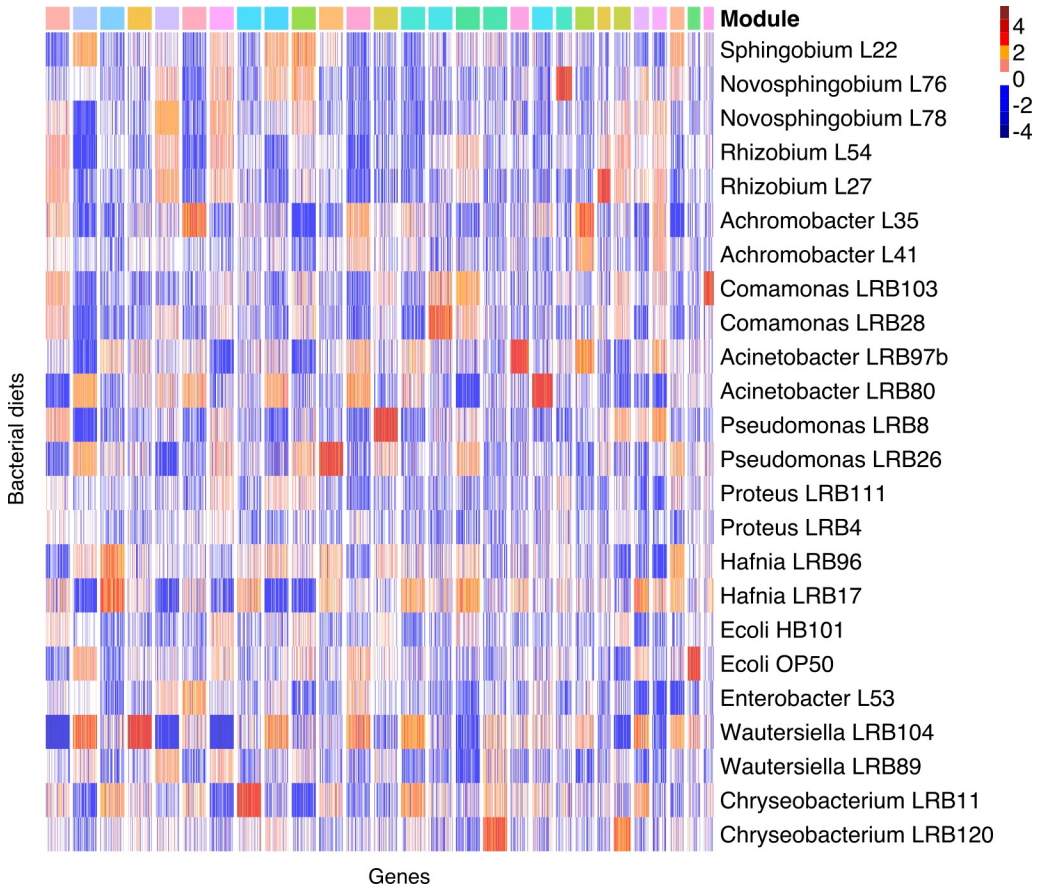


Fig 2. Expression level of environmentally responsive coexpression modules. We visualized the z-score normalized expression levels for the 28 largest modules across the bacterial environments. Modules with more than 100 genes were randomly downsampled to 100 genes. While genes of module 4 are most strongly expressed on *Wautersiella* LRB104, module 3 shows the highest expression in response to the two *Hafnia* strains. This demonstrates that environmental microbiota can modulate specific coexpression modules.

https://doi.org/10.1371/journal.pgen.1010832.g002

environmental microbiota, we computed coexpression modules from the RNA-seq data using a widely used graph clustering approach [48]. Based on correlation coefficient of 0.7 (S2 Fig), we identified 28 large coexpression modules with more than 50 genes (Fig 2 and S1 Table). The largest modules exhibit relatively drastic changes on only one or few bacteria (mostly *Wautersiella* LRB104 and *Hafnia* LRB17), but also more subtle differences on other bacteria. For example, genes of module 1 show strongly reduced expression on *Wautersiella* LRB104, but also mildly lower expression on some other bacteria. These bacteria yield largely opposite trends for genes in module 2. Module 3 shows highest expression on the *Hafnia* strains and the strongest pattern of module 4 results again from high expression on *Wautersiella* LRB104. Also, module 5 shows weak expression on *Wautersiella* LRB104, *Pseudomonas* LRB26, and *Hafnia* LRB17, whereas module 6 stands out by having high expression on *Achromobacter* L35. Given that the most extreme expression differences are frequently observed in the transcriptomic response to *Wautersiella* LRB104, we compared developmental timing between *E. coli* OP50 and both *Wautersiella* strains (LRB89 and LRB104). This demonstrated that worms exhibit a developmental delay on both *Wautersiella* bacteria relative to *E. coli* OP50 (S3 Fig). Given that both *Wautersiella* strains change the developmental timing of *P. pacificus* worms, we cannot fully explain why the transcriptomic response to *Wautersiella LRB104* differs so

starkly from all the other transcriptomes. To test, how strongly this outlier influences the structure of the coexpression network and the subsequent analysis, we recomputed coexpression modules after removing the *Wautersiella* LRB104 data and compared coexpression modules across both data sets (S4 Fig). This showed a clear one-to-one correspondence between most coexpression modules indicating that the structure of the coexpression network is largely robust. In addition, systematic analysis of coexpression networks that were computed from subsampled data revealed that with fewer RNA-seq samples, network modules tend to get larger (S5 Fig). This may be due to two reasons. First, with fewer samples, it is easier to exceed a given correlation threshold just by chance. Second, with higher numbers of RNA-seq samples, expression profiles can only become more complex. This will cause splits of larger modules. Thus, the full data set with all 24 RNA-seq samples yields the most conservative lower estimate of 14,275 for the number of environmentally responsive genes in large coexpression modules. That means that almost half of the 28,896 annotated genes in *P. pacificus* respond to environmental microbiota.

Coexpression modules exhibit developmental signatures

Bacterial diets can alter the developmental rate in *C. elegans* and *P. pacificus* [39,47]. Therefore, we wanted to test whether the coexpression modules also show a developmental signature. To this end, we visualized the normalized expression across *P. pacificus* development [43] for all genes in the largest coexpression modules (Fig 3). This showed that the coexpression modules that were obtained from adult worms on different bacteria also exhibit distinct expression profiles during development. Furthermore, this developmental signature is very consistent between most genes of the same module. For example, genes in module 1 are consistently activated only late in development (>48h, Fig 3). Their expression is preceded by genes in module 2 which consistently increase expression starting from the 40h timepoint (Fig 3). This could mean that the same network modules control development as well as the response to environmental microbiota. Alternatively, this developmental signature could be an indirect effect of altered developmental timing. Even if only adult worms were manually picked for RNA extraction, there might still be differences in the age of these worms. This is because worms may delay or accelerate their development in response to different bacteria [39,47] and consequently, adult worms that were grown on different bacteria may not be of the same chronological age. If the expression of certain modules rather follows the chronological age than the morphological stage, such modules could potentially cause a similar developmental signature. However, no matter if the expression profiles represent immediate response to different bacteria or variation in the chronological age of worms, both scenarios would reflect either direct or indirect consequences of the exposure to different microbial environments.

Coexpression modules have distinct regulatory architecture

The observation of distinct expression profiles among environmentally responsive genes suggests that the coexpression modules might be coregulated by diverse sets of transcription factors. To test this, we searched for overrepresented motifs in the promoter sequences of the largest coexpression modules using a *de novo* motif discovery approach as implemented in the HOMER software [49]. This identified a diverse set of DNA motifs that are highly enriched in specific modules (S6 Fig). While modules 1,5,7, and 23 show enrichments of the same motifs (ZBTB32, CUX1, and LIN54), many other coexpression modules have a unique regulatory architecture with very specific motifs that are only enriched in the given module (e.g. POU5F1 in module 2 and *Foxd3* in module 24, S6 Fig). Unfortunately, it is not straightforward to infer the regulator for a given motif as families of transcription factors might be large and may bind

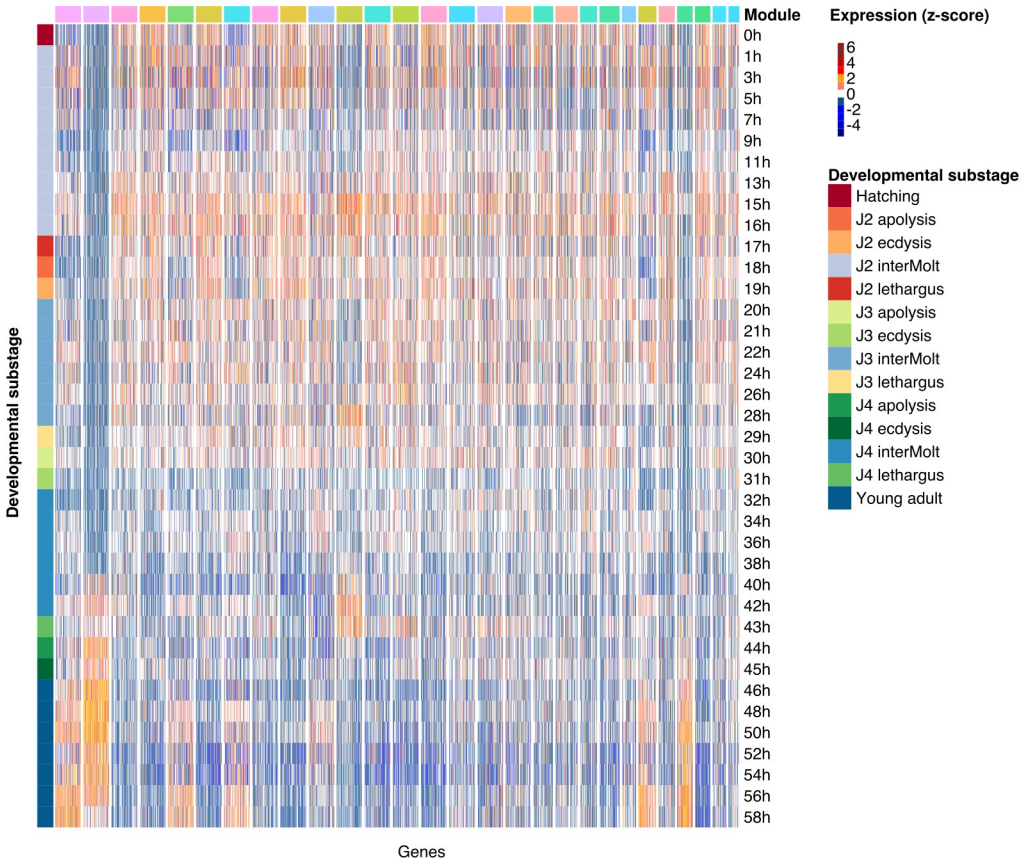


Fig 3. Developmental signature of coexpression modules. We visualized the z-score normalized expression levels of genes in the 28 largest coexpression modules throughout postembryonic development after hatching (0h) on *E. coli* OP50 [43]. Modules with more than 100 genes were randomly downsampled to 100 genes. The coexpression modules show distinct expression profiles suggesting a link between environmental response and developmental regulation.

https://doi.org/10.1371/journal.pgen.1010832.g003

very similar motifs [50]. For example, the human zinc finger and BTB domain containing protein ZBTB32 which binds a motif that is highly enriched in module 1 (S6 Fig) has dozens of orthologs in the genomes of *C. elegans* and *P. pacificus*. However, the most significantly enriched motif of module 2 has the highest similarity with the motif of POU domain homeobox transcription factor POU5F1. This family has only three members (*unc-86*, *ceh-6* and *ceh-18*.) in *C. elegans* [51] and four in *P. pacificus*. Similarly, *C. elegans ces-1* has a one-to-one ortholog in *P. pacificus*. Thus, for individual modules future experimental analysis could be used to dissect the regulatory relationships at a mechanistic level. Nevertheless, already the diversity of motifs that are found across different coexpression modules supports that they have distinct regulatory architecture. In addition, this analysis supports that the genes in a given module are not only coexpressed, but also coregulated.

3,727 *Pristionchus pacificus* orphan genes respond to diverse environmental microbiota

To test to what extent new genes could contribute to the response to diverse environmental microbiota, we performed a phylostratigraphic analysis to determine the distribution of gene ages across coexpression modules. Phylostratigraphy is a commonly used method to map gene birth events to a branch within a species tree by searching for the most distant homolog [52].

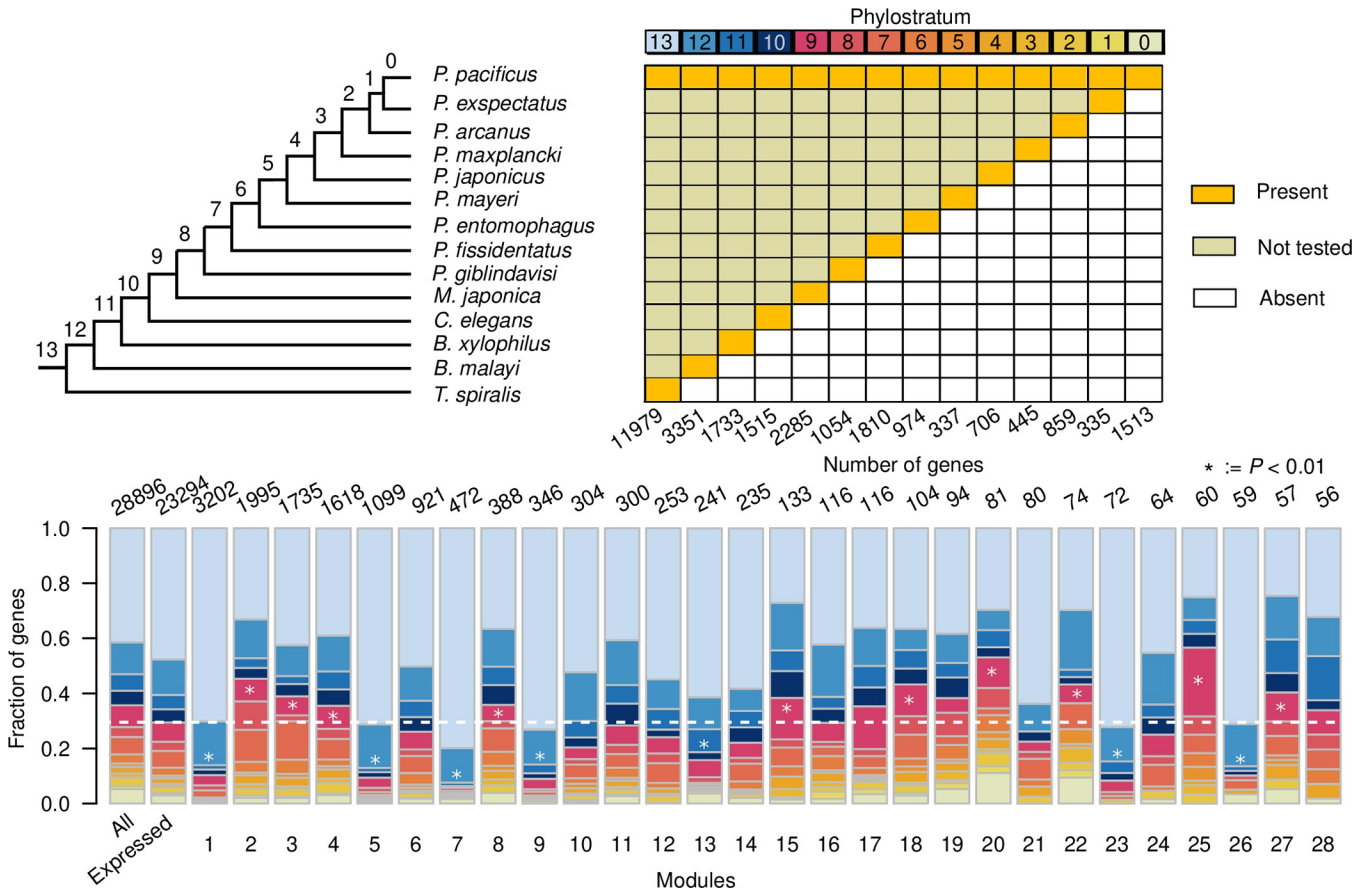


Fig 4. Phylostratigraphic analysis across coexpression modules. Phylostrata were defined based on the presence of homologs for a given gene in the most distantly related species. Each phylostratum defines a branch in the phylogeny where a gene likely originated. The barplot shows the distribution of phylostrata across coexpression modules with the dashed line marking the fraction of diplogastrid-specific orphan genes across all genes. The stars indicate significant enrichment and depletion of orphan genes based on simulating the integration of new genes to existing network modules ($P < 0.01$, S7 Fig).

https://doi.org/10.1371/journal.pgen.1010832.g004

Here, we selected nine additional diplogastrid genomes [30] and the genomes of *C. elegans*, *Bursaphelenchelus xylophilus* [53], *Brugia malayi* [54], and *Trichinella spiralis* [55] to assign genes to phylostrata (S2 Table). Altogether, 10,318 (35.7%) of all genes were defined as diplogastrid family-specific orphan genes (BLASTP e-value $< 10^{-3}$). Visualization of the distribution of phylostrata across the coexpression modules shows that almost half of all the genes in module 2 are diplogastrid-specific orphan genes (Fig 4). Furthermore, among the smaller modules 20 and 22, we observe relatively high ratios of species-specific orphan genes. This finding suggests that the integration of new genes into regulatory networks can happen very rapidly. Alternatively, such genes might represent ancient but rapidly evolving sequences such as antimicrobial peptides where we underestimate the gene age due to the failure to detect homologs [3]. In total, 3,727 diplogastrid-specific orphan genes are found among the 28 largest coexpression modules. As indicated above, this represents a lower estimate for the total number of environmentally-responsive orphan genes as additional orphan genes are found in smaller modules (S4 Fig). Relative to the genome-wide fraction of orphan genes (35.7%), this represents an underrepresentation as only 26.1% of genes in large coexpression modules are orphan genes ($P < 2.2 \times 10^{-16}$, Fisher's exact test). This may be largely explained by the fact that orphan genes are generally lowly expressed [31]. In our data set, only 66.4% of orphan genes are expressed whereas this number increases to 88.5% for non-orphan genes.

Nevertheless, despite their lower level of expression, our study could demonstrate that thousands of orphan genes are indeed embedded into developmental networks that plastically respond to diverse microbiota. Further, it identified which of the orphan genes respond to different environments and it established associations between these orphan genes and specific network modules where they have been embedded.

The major fast-evolving module is associated with spermatogenesis

The distribution of phylostrata across coexpression modules suggests that new genes are not attached randomly into regulatory networks, i.e. not every module is equally likely to acquire a new gene. On the contrary, individual coexpression modules are more likely to integrate new genes than others. To assess the non-randomness in the distribution of diplogastrid-specific orphan genes, we simulated the integration of new genes into existing networks. Specifically, we tested a model where all network modules are equally likely to acquire a new gene and a model where the probability of attachment is proportional to the size of the module (S7 Fig). Basically, the second model predicts much more accurately the number of orphan genes per module and it allows to define fast evolving modules with significant enrichments of orphan genes (Modules 2–4, 8, 15, 18, 20, 22, 25, and 27, $P < 0.01$, S7 Fig and Fig 4). Constrained modules (Modules 1, 5, 7, 9, 13, 23, and 26) were defined analogously as modules that are significantly depleted in orphan genes. To better characterize the biological differences between such fast evolving and more constrained modules, we performed overrepresentation analysis of protein domains (S3 Table), metabolic pathways (S4 Table), and other expression data sets [43,56–58]. The expression data includes 11 sets of regionally expressed genes that were identified from RNA tomography along the anterior-posterior axis of individual worms [58]. These analyses were complemented by tissue enrichment analysis (TEA, S5 Table) using one-to-one orthologs in *C. elegans* [59]. The overrepresentation of germline associated regions P6-P8 and TEA support that the constrained module 1 is associated with oogenesis (Fig 5A and S5 Table). In contrast, the enrichment of Motile sperm proteins, TEA and expression in sperm-related regions (P5, P9) associate the fast evolving module 2 with spermatogenesis (Figs S8 and 5A and S5 Table). Thus, the two largest environmentally responsive coexpression modules represent a constrained module associated with oogenesis and a fast evolving module that is associated with spermatogenesis. In *C. elegans*, the reproductive system is known to plastically respond to changes of environmental microbiota [60,61]. Thus, it is unsurprising to see the corresponding modules to respond dynamically to diverse bacteria in *P. pacificus*. These results also recapitulate previous findings of signatures of rapid evolution in spermatogenesis-associated genes in *C. elegans* and *P. pacificus* [58,62] This out-of-testis trend of new gene formations was also observed in insects and mammals and likely reflects a combination between rapid evolution of spermatogenesis-associated genes and a more permissive chromatin state [63,64].

Thousands of orphan genes can be associated with biological processes or tissues

The strong support for the association of the two largest coexpression modules with oogenesis and spermatogenesis motivated us to test if more coexpression modules could be annotated with biologically meaningful labels. Therefore, we complemented protein domain information (S8 Fig), spatial transcriptomics (Fig 5A), and TEA (S5 Table) with the overrepresentation of Kyoto Encyclopedia of Genes and Genomes (KEGG) pathways (Fig 5B) and other *P. pacificus* expression gene sets (Fig 5C) [43,47,56,57,65–67]. This allowed us to assign labels for 22 of the 28 largest coexpression modules (Table 1). Please note that these labels are not exclusive but rather describe the most strongly enriched biological terms. Notably, nine of the coexpression

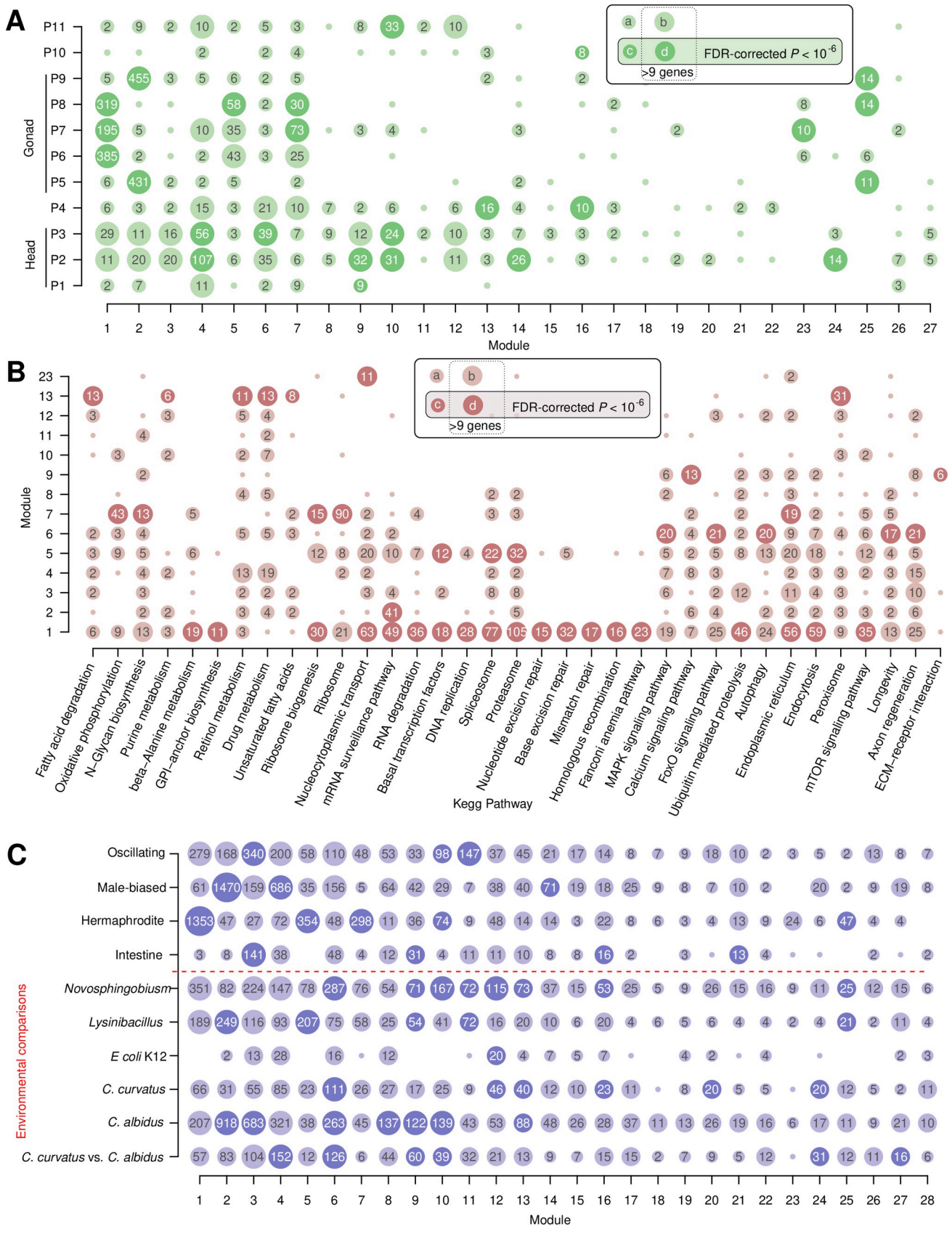

A
Gonad
Head
P11
P10
P9
P8
P7
P6
P5
P4
P3
P2
P1
a
b
c
d
FDR-corrected P < 10-6
>9 genes
Module
B
Module
Kegg Pathway
Fatty acid degradation
Oxidative phosphorylation
N-Glycan biosynthesis
Purine metabolism
beta-Alanine metabolism
GPI-anchor biosynthesis
Retinol metabolism
Drug metabolism
Unsaturated fatty acids
Ribosome biogenesis
Ribosome
Nucleocytoplasmic transport
mRNA surveillance pathway
RNA degradation
Basal transcription factors
DNA replication
Spliceosome
Proteasome
Nucleotide excision repair
Base excision repair
Mismatch repair
Homologous recombination
Fanconi anemia pathway
MAPK signaling pathway
Calcium signaling pathway
FoxO signaling pathway
Ubiquitin mediated proteolysis
Autophagy
Endoplasmic reticulum
Endocytosis
Peroxisome
mTOR signaling pathway
Longevity
Axon regeneration
ECM-receptor interaction
C
Environmental comparisons
Oscillating
Male-biased
Hermaphrodite
Intestine
Novosphingobiusm
Lysinibacillus
E coli K12
C. curvatus
C. albidus
C. curvatus vs. C. albidus
Module

Fig 5. Transcriptomic and metabolic enrichment of coexpression modules. (A) Coexpression modules show distinct overlaps with regional genes (P1-P11) that were identified from spatial transcriptomics. (B) Multiple metabolic pathways are enriched in individual coexpression modules. (C) Coexpression modules were compared with multiple expression gene sets. 16 out of 28 coexpression modules show significant overlap with differentially expressed genes in previous comparisons of environmental microbiota.

https://doi.org/10.1371/journal.pgen.1010832.g005

modules are associated with the nervous system which is also supported by the patterns of G protein coupled receptors (GPCRs), neuropeptides, and nuclear hormone receptors (NHRs) (S9 Fig). All these gene classes are thought to be enriched in neurons [68,69]. In addition, we identified a gland cell related module which captures 17 out of 24 target genes of the regulators of the mouth-form polyphenism in *P. pacificus* [70] (S10 Fig). Altogether, this analysis predicts associations for 13,923 (48%) *P. pacificus* genes with biological processes and anatomical structures. This includes predicted associations for 3,556 (35%) of diplogastrid-specific orphan genes.

Comparisons with previous RNA-seq studies reveal interactions between environmental microbiota and the nervous system

In the current study, we wanted to get a very broad overview of expression changes across a wide range of bacterial environments. Therefore, we decided to sequence only a single

Table 1. Biological annotation for coexpression modules. Most coexpression modules could be labeled with biological processes or tissues based on manual inspection of the results of different overrepresentation analyses.

Module	Number of genes	Name	Evidence
1	3,202	Oogenesis 1	P6-P8, sex-bias, TEA
2	1,995	Spermatogenesis	P5+P9, motile sperm proteins, sex-bias, TEA
3	1,735	Intestine 1	Intestine RNA-seq
4	1,618	Nervous system 1	GPCRs, neuropeptides, NHRs, P1-P3, TEA
5	1,099	Oogenesis 2	P6-P8, sex-bias, TEA
6	921	Nervous system 2	GPCRs, Axon regeneration, P2-P3, TEA
7	472	Oogenesis 3	P6-P8, sex-bias
8	388	Nervous system 3	GPCRs
9	346	Muscle / intestine 2	Intestine RNA-seq, TEA
10	304	Cuticle 1	Collagens, oscillation
11	300	Cuticle 2	Collagens, oscillation, TEA
12	253	Nervous system 4	GPCRs, NHRs
13	241	Intestine 3	Fatty acid degradation, drug metabolism, P4
14	235	Nervous system 5	GPCRs, P2, TEA
15	133	Unknown	
16	116	Intestine 4	Intestine RNA-seq, P4
17	116	Unknown	
18	104	Nervous system 6	TEA
19	94	Nervous system 7	TEA
20	81	Orphan 1	
21	80	Intestine 4	Intestine RNA-seq
22	74	Orphan 2	
23	72	Oogenesis4	P6-P8, TEA
24	64	Gland cell / mouthform	P2, Astacins
25	60	Orphan 3	
26	59	unknown	
27	57	Nervous system 8	TEA
28	56	Nervous system 9	GPCRs

https://doi.org/10.1371/journal.pgen.1010832.t001

transcriptome from many different bacterial environments. This is in contrast to previous studies that focussed on specific interactions between hosts and microbes and defined more robust transcriptomic changes with regard to the standard diet *E. coli* OP50 by sequencing multiple biological replicates [47,65–67]. In order to gain additional support for the environmental regulation of the identified coexpression modules, we quantified how many of the coexpression modules exhibit associations with sets of significantly differentially expressed genes in six transcriptomic comparisons of distinct microbial environments including *Novsphingobium*, *Lysinobacillus*, *E. coli* K12, and two *Cryptococcus* yeast strains [47,65–67]. This showed significant enrichments for 16 modules with differentially expressed genes in at least one of the previous studies (Fig 5C). Moreover, we find the intestinal module 9 and the nervous system related module 6 to be most frequently overrepresented. This further supports the impact of different bacteria on the nematode nervous system with potential consequences on behavior. Such an effect has been experimentally characterized in *P. pacificus* for the case of *Novosphingobium* bacteria. Feeding on these bacteria accelerates development and makes the worms more efficient predators of *C. elegans* [47]. Another example of behavioral modulation constitutes the effect of a neurotransmitter release by bacteria on *C. elegans* perception [45]. Notably, six of the nine nervous system related modules are significantly affected in at least one environmental comparison. This highlights the potential of microbial environments to modulate the nervous system and behavior.

Discussion

Which genes respond to changing environments? Do orphan genes play a role in adapting to diverse microbiota? Can we infer potential functions for orphan genes based on coexpression with known genes? How are new genes integrated into existing biological networks? To study these questions, we characterized the transcriptomic response of *P. pacificus* nematodes to 24 environmental microbiota. This analysis let to the identification of 28 large coexpression modules that contain almost half of all genes in *P. pacificus*. Further integrative analysis associated 22 of these modules with biological processes or tissues. These modules capture previously characterized gene sets such as collagens with oscillating expression [43] or target genes of mouth-form regulators that are expressed in the gland cell [70]. Moreover, these functionally annotated modules contain 3,556 (35%) of diplogastrid-specific orphan genes, of which a large fraction is found in the spermatogenesis associated module 2. While sperm associated genes are known to evolve rapidly [62,71], our study adds evidence that the expression of spermatogenesis-associated genes can be modulated by different microbiota. One major limitation of the current study consists in the fact that we only sequenced a single biological replicate per environment. This strongly limits the usefulness of our data set to dissect the effect of individual bacterial strains on nematode gene expression. However, we would argue that this does not undermine our main findings as coexpression signals can still be inferred from such a data set even if single expression estimates are not robust. In addition, we would like to point out that since the worms have been grown on selected bacteria, the effect of the bacteria likely accumulates in the nematodes throughout development and might be different from an immediate transcriptomic response after short time exposure. Thus, the observed differences could partially represent an indirect consequence of altered developmental rates. Even if only young adults were picked for RNA-seq experiments, we cannot exclude the possibility that the expression of certain gene modules reflects a chronological age rather than a morphological age. Future work could elucidate to what extent the transcriptomic responses represent immediate response to different bacteria or developmental variation. In addition, we currently do not know to what extent different bacteria constitute a diet or could also interact with

nematodes by colonizing their gut [72]. Nevertheless, despite all these uncertainties, we would still argue that most of the observed transcriptomic variation represents either direct or indirect responses to different microbial environments.

One of the main achievements of our work constitutes the association of thousands of *P. pacificus* genes with biological processes and tissues. This includes thousands of diplogastrid-specific orphan genes. Of course, this type of functional annotation represents a completely different level than the knowledge for the two experimentally characterized orphan genes, where knockout and transgenic lines are available that show organism level phenotypes [34,73]. Our functional associations rely on the assumption that coexpression implies cofunctionality. Although this is a frequently employed method for functional assignment [35,36], the example of the out of testis pattern shows that this assumption might not always be true. Specifically, it has been shown that testis-biased expression of many new genes might be an effect of an overall permissive chromatin state leading to higher transcriptional complexity [64]. Thus, our data should rather be considered as a source to generate new hypotheses that have to be tested experimentally. As such, our functional annotations may be helpful to interpret future transcriptomic studies in *P. pacificus*. Some of these modules might also be relevant for studying the polyphenism of the mouth morphology in *P. pacificus*. This phenomenon has developed into one of the best studied animal systems for developmental plasticity [74,75]. Our observation of environmentally dependent expression variation in a gland cell related module that includes many target genes of mouth-form regulators [70] suggests an additional control layer that is independent of the mouth-form. This is because no bacteria are currently known that alter the mouth-form ratio in the highly predatory *P. pacificus* reference strain PS312 [47]. However, it could well be that the same bacteria can induce the predatory morph in a different wild isolate with a low or intermediate frequency of the predatory morph.

Another major finding concerns the integration of new genes into existing gene regulatory networks. Our analysis clearly shows that new genes are not randomly attached to existing modules, but rather specific modules have much higher propensity to acquire new genes. The likelihood to integrate new genes may be associated with the biological function of a given module. For example, while the oogenesis associated modules 1, 5, 7, and 23 are composed of the oldest gene sets, the spermatogenesis-associated module 2 has one of the youngest gene contents. The strong difference in evolvability between these two reproductive processes could be due to strong sperm competition which results from the difference in the number of gametes between both sexes [76]. Another factor could consist in the differential control of transposons between spermatocytes and oocytes resulting in higher potential for molecular innovation during spermatogenesis [77,78]. Another aspect of network evolution concerns the timing of events. The presence of many species-specific orphan genes in some coexpression modules suggests that integration can happen relatively fast. Together with a recent study on the evolution of the polyphenism network [79], our work reveals first insights into the evolution of environmentally responsive networks in *Pristionchus* nematodes and similar studies in other taxonomic groups could be done to test whether these observations reflect general patterns of gene-regulatory network evolution.

Methods

Bacterial Culture Conditions

All bacterial strains were recovered from glycerol stocks [42] and then plated on nematode growth medium (NGM) and incubated overnight at 37˚C. From these plates single colonies were seeded in lysogeny broth (LB) medium and grown overnight at 37˚C in a shaking incubator.

Nematode Culture Conditions

The wild type strain of *P. pacificus* (PS312) was maintained at 20˚C on nematode growth medium (NGM) seeded with *E. coli* OP50 before use in experiments [80]. From every generation, five young adults were transferred to fresh plates with a wormpick.

RNA sequencing

Bleaching was used to synchronize *P. pacificus* nematodes and to remove *E. coli* OP50 before transferring bleached eggs to NGM plates with bacterial strains [80]. These bacterial plates were obtained by spotting 50 μL of overnight bacterial cultures onto each 6 cm NGM plate with an L-spreader followed by incubation for 2 days. The concentration of the overnight bacterial cultures was quantified by measuring the optical density at 600 nm (OD600). To make the OD600 of the initial cultures identical, the OD600 of the overnight cultures were measured and diluted to OD600 = 1 with fresh LB. Worms were grown on these plates at 20˚C and every generation young adult worms were passaged to fresh bacterial plates. This was done for at least two generations. From mixed-stage cultures, 50 young adults with only one egg were manually selected with a wormpick under a binocular microscope into an Eppendorf tube containing 100 μl M9 buffer and immediately frozen at -80˚C. Total RNA was extracted using Direct-Zol RNA Mini prep kit from Zymo Research according to the manufacturer's guidelines. RNA libraries were prepared using the Illumina Truseq RNA library prep kit according to the manufacturer's guidelines. The libraries were quantified using a combination of Qubit and Bioanalyzer (Agilent Technologies) and normalized to 2.5 nM. Samples were sequenced as 150 bp single end reads on multiplexed lanes of an Illumina HiSeq3000 in our inhouse sequencing facility. Raw reads were depositted at the European Nucleotide archive under the study accession PRJEB60166.

Developmental timing

Bacterial strains were grown overnight from a single colony in LB medium. The medium was shaken at 180 rpm and incubated at 30˚C for LRB89 and LRB104 and 37˚C for OP50. These cultures were spotted on 6-cm NGM plates and were grown for 2 days at RT. Synchronized J2 worms were obtained by bleaching and were put on these NGM plates [80]. Nematode cultures were grown at 20˚C. 56h later, the distribution of developmental stages was scored based on the vulval development under a ZEISS SteREO Discovery microscope [47].

Identification of coexpression modules

The raw reads were aligned to the reference *P. pacificus* genome (version El Paco) with STAR (version 2.7.3a) and quantified with featureCounts from the Subread R package (version 2.0.1) using the current gene annotations (El Paco gene annotations version 3) [81–83]. After prefiltering the count matrix by removing genes (rows) that have less than 10 reads total, we retained 23,294 (80.6%) of all *P. pacificus* genes with some evidence of expression. The read counts across the different conditions were normalized with the DESeq2 counts function (with normalized = TRUE option) [84]. The normalized read counts were used to create a coexpression network with MCL [48]. Different correlation and inflation thresholds were assessed for the coexpression network, ranging from 0.6 to 0.8 and from 1.5 to 4 respectively. The network was constructed using a correlation of 0.7 and an inflation threshold of 2. The network modules containing more than 50 genes were selected for further analysis. To assess the robustness of module assignments, we recomputed coexpression networks after either removing the outlier LRB104 or systematically downsampling the data set. Taking the full coexpression network

calculated from 24 RNA-seq samples as reference, we evaluated the classification of 10,000 randomly chosen gene pairs from a subsampled RNA-seq data set. For the full and the subsampled data set, a gene pair was either classified to be part of the same module or not. If a gene pair was classified as being part of the same module in both data sets, such a pair was classified as true positive. If a pair was only part of a module in the subsampled data set, but not in the full data set, this was scored as false positive. True negative and false negative cases were defined analogously. Subsequently, the positive predictive value (PPV) and negative predictive value (NPV) for 10 randomly subsampled data sets of a fixed size (S5 Fig). For comparison, the data set without LRB104 yielded a PPV of 84% and an NPV of 98%.

Motif analysis and phylostratigraphy

To test for overrepresented motifs in the promoter regions, we focused on the 500-bp nucleotide sequence upstream of each annotated gene in a given module. These sequences were taken as input for the findMotif.pl script of the Hypergeometric Optimization of Motif EnRichment (HOMER) suite (version v4.10.1) [49]. As a background set, we used the 500-bp upstream sequences of all the other large coexpression modules. For visualization, we selected among the significant motifs only one representative motif per known motif match and applied a cutoff that a motif needs to be present in at least 20% of the promoter regions of a given module. For analyzing the distribution of phylostrata across coexpression modules, we assigned a gene to a phylostratum based on the presence of the most distant homolog. For this purpose, we performed BLASTP searches (e-value < 0.001) of all 28,896 *P. pacificus* proteins against protein data of nine diplogastrid genomes (version PPCAC) [30], *C. elegans*, *B. xylophilus*, *B. malayi*, and *T. spiralis* (WormBase ParaSite version WBPS14) [85]. This identified 10,318 diplogastrid specific orphan genes. To simulate the integration of new genes into existing network modules, we first defined the ancestral module sizes based on the number of ancient genes (non-orphan genes) for the 28 large modules. We then simulated the integration of new genes by either assigning equal probabilities for attachment to all network modules or by scaling the attachment probability as a linear function of the module size. The second model predicts much more accurately the number of orphan genes per module (Pearson's r = 0.62, S7 Fig). Therefore, we used 100 iterations of the second model to calculate empirical P-values for the overrepresentation of orphan genes ($P < 0.01$, Figs S7 and 4).

Compilation of *P. pacificus* expression gene sets

Sets of 3,502 *P. pacificus* genes with regional expression were extracted from supplementary table S3 in [58]. These genes exhibit enriched expression in at least one out of eleven regions (P1-P11) that were identified by RNA tomography of adult *P. pacificus* animals. A conversion table between assembled transcripts (version trinity 2016) and current gene annotations (El Paco gene annotations V3) were obtained from the supplementary table S10 in [43]. We extracted the set of 2,964 developmentally oscillating genes from the supplementary table S3 in [43]. In addition, we reanalyzed *P. pacificus* RNA-seq data sets to compile candidate genes with intestinal expression [56], sex-biased expression [57], and differentially expressed genes in response to altered microbial environments [47,65–67]. For the intestinal data and exposure to *Lysinibacillus*, we identified candidate genes by aligning RNA-seq reads to the *P. pacificus* reference assembly (version El Paco) with the help of the tophat alignment program (version v2.0.14, default settings) and testing for differential expression using the cuffdiff program (version v2.2.1, $P<0.1$) [86]. This yielded 723 intestine enriched genes, and 1,959 candidate genes with differential expression after one hour exposure to *Lysinibacillus*. For the data sets with multiple biological replicates [47,57,65,67], we realigned RNA-seq data with STAR (version

2.7.1a) [81], generated count matrices with the featureCounts function of the subread package in R (version 3.6.3) [82] and for significant differential expression with the DESeq2 package (FDR-corrected $P<0.05$) [84].

Overrepresentation of gene families, metabolic pathways, and expression sets

To test for overrepresentation of specific gene sets among the coexpression modules, we first generated protein domain annotations by the hmmsearch program (version 3.3, -E 0.001 option) against the Pfam-A.hmm database (version 3.1b2). Similarly, KEGG annotations were obtained by identification of orthologs in the KEGG database using the blastkoala web application (with the 'eukaryotes' and 'family_eukaryotes' values for taxonomic group and database level, respectively) [87]. Genes with orthologs in the KEGG database were then annotated with the corresponding *C. elegans* KEGG accessions. From the protein domain predictions, we identified 1,434 genes with protein domains that were termed as GPCRs and 275 putative NHR genes based on the presence of the Hormone_recep domain (PF00104). Potential neuropeptides were identified by BLASTP search (-evalue 0.001) of 107 *C. elegans* neuropeptides (*flp* and *nlp* genes) against the current *P. pacificus* proteins. For 59 *C. elegans* neuropeptides, we could identify 85 homologs in *P. pacificus* of which we only used 38 single copy candidates as neuropeptide candidates. These annotations were combined with various expression data sets to perform overrepresentation analysis using the Fisher's exact-test with multiple testing correction (FDR corrected $P < 10^6$) in R (version 3.6.3).

Annotation of coexpression modules

In order to associate the coexpression modules with biological processes or tissues, we complemented the results of the overrepresentation analysis in *P. pacificus* with tissue enrichment analysis (TEA) of *C. elegans* orthologs [59]. Specifically, *C. elegans* orthologs of *P. pacificus* genes were extracted from the best reciprocal BLASTP hit data set from Athanasouli *et al.* (2020) [83] and submitted to the WormBase web interface (https://wormbase.org/tools/enrichment/tea/tea.cgi, version WS283) [83]. We manually inspected the results of all different analyses and subjectively assigned biological processes or tissues for a given module. Functional assignments with multiple types of evidence (e.g. Protein domains, spatial transcriptomics, sex-biased expression) should be considered as high confidence associations whereas associations that are supported by only a single analysis are more uncertain.

Supporting information

S1 Fig. Analysis of the most similar and dissimilar RNA-seq data sets. The scatter plots show the normalized expression (TPM) for different pairs of samples. As lowly expressed genes tend to be more variable, we visualized the number of genes with at least two-fold expression difference across multiple mean expression levels.
(PDF)

S2 Fig. Parameter combinations for MCL clustering. We evaluated the total number of modules and singleton modules as a function of the inflation factor (I) and correlation coefficient (r). High r and I values generally increase the number of modules, whereas low r and I parameters generate fewer but larger modules. We decided to use r = 0.7 and I = 2 for the final analysis, because it gave a moderate number of modules with a relatively low number of singletons.
(PDF)

S3 Fig. Developmental timing on different bacteria. The distribution of developmental stages 56h after J2 synchronization is shown for *P. pacificus* worms on *E. coli* OP50 and two *Wautersiella* bacteria (5 biological replicates). Nematodes grow slower on both *Wautersiella* strains. The significance level was computed by a χ^2 -test (mean *P*-value from all pairwise comparisons).
(PDF)

S4 Fig. Comparison of MCL networks constructed with or without LRB104. The heatmap shows fraction genes from modules of the complete coexpression network (including LRB104) that overlap within a given module from the coexpression network without LRB104. For most modules there exists a 1–1 correspondence between both networks, indicating that the network structure is robust with regard to the *Wautersiella* LRB104 data set.
(PDF)

S5 Fig. Comparison of Coexpression networks on subsampled RNA-seq data. Taking the full coexpression network calculated from 24 RNA-seq samples as reference, we evaluated the classification of 10,000 randomly chosen gene pairs using subsampled RNA-seq data. For the full and the subsampled data set, a gene pair was either classified to be part of the same module or not. This allowed us to calculate the positive predictive value (PPV, panel A) and negative predictive value (NPV, panel B) for 10 randomly subsampled data sets of a fixed size. While the NPV is always close to 1, the PPV shows drastic differences between the full and subsampled data. This suggests that with fewer RNA-seq samples, additional gene pairs are assigned to the same coexpression module. However, with additional samples, such modules may be split into smaller components. Consistently, the number of genes in large modules ($N>50$) is much higher for smaller sample sizes (panel C). Panel D shows the number of diplogastrid-specific orphan genes in large modules.
(PDF)

S6 Fig. Regulatory architecture of coexpression modules. Significantly overrepresented motifs were identified for each module by the HOMER software. We arbitrarily selected motifs that occurred in at least 20% of promoters of a given module and visualized their distribution across all modules. Note that the complementary regulation by less frequent motifs and other regulatory mechanisms such as microRNAs are not considered here. Sequence logos for each motif are shown at the right and the labels to the left indicate the best motif match among known motifs.
(PDF)

S7 Fig. Enrichment analysis for simulated network evolution. We simulated the integration of novel genes into existing networks by estimating ancestral module sizes based on the number of ancient genes (non-orphan genes) and then assigning an equivalent number of orphan genes to existing modules with equal probabilities (panel A and C) and with probabilities that were proportional to the module size (panel B and D). The scatterplots show the observed and simulated number of orphan genes per module. The barplots show the median enrichment of the observed relative to the simulated number of orphan genes (error bars indicate the minimal and maximal values from 100 simulations).
(PDF)

S8 Fig. Overrepresented protein domains in coexpression modules. Specific protein domains are strongly overrepresented in twelve coexpression modules. The left barplot shows the number of genes with a given protein domain for each module and the the right bar plot shows the negative logarithm of the FDR corrected P-value (Fisher's exact test). The most

significant association is between Motile sperm proteins (PF00635) and coexpression module 2.
(PDF)

S9 Fig. Distribution of GPCRs, NHRs, and neuropeptides across the coexpression modules.
(PDF)

S10 Fig. Expression of selected module 24 genes. The heatmap shows the expression of genes that are shared between module 24 and the target genes of mouth form regulators and additional module 24 genes with 1–1 orthologs in *C. elegans*. The *C. elegans* ortholog of PPA25527 (D1044.3) is reported to be expressed in the gland cell and reporter lines of multiple candidate genes show expression in the gland of *P. pacificus* (Sieribriennikov et al. 2020) [70].
(PDF)

S1 Table. Coexpression modules.
(XLSX)

S2 Table. Phylostrata.
(XLSX)

S3 Table. Protein domain information.
(XLSX)

S4 Table. *Pristionchus pacificus* KEGG annotation.
(XLSX)

S5 Table. Tissue enrichment analysis (TEA).
(XLSX)

Acknowledgments

We would like to thank all members of the Sommer lab for helpful discussions.

Author Contributions

Conceptualization: Christian Rödelsperger.

Data curation: Marina Athanasouli, Christian Rödelsperger.

Formal analysis: Marina Athanasouli, Christian Rödelsperger.

Investigation: Nermin Akduman, Waltraud Röseler, Penghieng Theam.

Methodology: Marina Athanasouli, Christian Rödelsperger.

Project administration: Marina Athanasouli, Christian Rödelsperger.

Supervision: Christian Rödelsperger.

Visualization: Marina Athanasouli, Christian Rödelsperger.

Writing – original draft: Marina Athanasouli, Christian Rödelsperger.

Writing – review & editing: Christian Rödelsperger.

References

1. Tautz D, Domazet-Lošo T. The evolutionary origin of orphan genes. Nat Rev Genet. 2011; 12: 692–702. https://doi.org/10.1038/nrg3053 PMID: 21878963

2. Arendsee ZW, Li L, Wurtele ES. Coming of age: orphan genes in plants. Trends Plant Sci. 2014; 19: 698–708. https://doi.org/10.1016/j.tplants.2014.07.003 PMID: 25151064
3. Weisman CM, Murray AW, Eddy SR. Many but not all lineage-specific genes can be explained by homology detection failure. PLoS Biol. 2020; 18: e3000862. https://doi.org/10.1371/journal.pbio.3000862 PMID: 33137085
4. Schlötterer C. Genes from scratch—the evolutionary fate of de novo genes. Trends Genet. 2015; 31: 215–219. https://doi.org/10.1016/j.tig.2015.02.007 PMID: 25773713
5. Van Oss SB, Carvunis A-R. De novo gene birth. PLoS Genet. 2019; 15: e1008160. https://doi.org/10.1371/journal.pgen.1008160 PMID: 31120894
6. Knowles DG, McLysaght A. Recent de novo origin of human protein-coding genes. Genome Res. 2009; 19: 1752–1759. https://doi.org/10.1101/gr.095026.109 PMID: 19726446
7. Ruiz-Orera J, Hernandez-Rodriguez J, Chiva C, Sabidó E, Kondova I, Bontrop R, et al. Origins of De Novo Genes in Human and Chimpanzee. PLoS Genet. 2015; 11: e1005721. https://doi.org/10.1371/journal.pgen.1005721 PMID: 26720152
8. Zhao L, Saelao P, Jones CD, Begun DJ. Origin and spread of de novo genes in Drosophila melanogaster populations. Science. 2014; 343: 769–772. https://doi.org/10.1126/science.1248286 PMID: 24457212
9. Gubala AM, Schmitz JF, Kearns MJ, Vinh TT, Bornberg-Bauer E, Wolfner MF, et al. The Goddard and Saturn Genes Are Essential for Drosophila Male Fertility and May Have Arisen De Novo. Mol Biol Evol. 2017; 34: 1066–1082. https://doi.org/10.1093/molbev/msx057 PMID: 28104747
10. Zhang W, Gao Y, Long M, Shen B. Origination and evolution of orphan genes and de novo genes in the genome of Caenorhabditis elegans. Sci China Life Sci. 2019; 62: 579–593. https://doi.org/10.1007/s11427-019-9482-0 PMID: 30919281
11. Prabh N, Rödelsperger C. De Novo, divergence, and Mixed Origin Contribute to the Emergence of Orphan Genes in Pristionchus Nematodes. G3. 2019; 9: 2277–2286. https://doi.org/10.1534/g3.119.400326 PMID: 31088903
12. Carvunis A-R, Rolland T, Wapinski I, Calderwood MA, Yildirim MA, Simonis N, et al. Proto-genes and de novo gene birth. Nature. 2012; 487: 370–374. https://doi.org/10.1038/nature11184 PMID: 22722833
13. Vakirlis N, Hebert AS, Opulente DA, Achaz G, Hittinger CT, Fischer G, et al. A Molecular Portrait of De Novo Genes in Yeasts. Mol Biol Evol. 2018; 35: 631–645. https://doi.org/10.1093/molbev/msx315 PMID: 29220506
14. Zhang L, Ren Y, Yang T, Li G, Chen J, Gschwend AR, et al. Rapid evolution of protein diversity by de novo origination in Oryza. Nature Ecology & Evolution. 2019; 3: 679–690.
15. Yates TB, Feng K, Zhang J, Singan V, Jawdy SS, Ranjan P, et al. The Ancient Salicoid Genome Duplication Event: A Platform for Reconstruction of De Novo Gene Evolution in *Populus trichocarpa*. Genome Biology and Evolution. 2021; 13: evab198.
16. Wissler L, Gadau J, Simola DF, Helmkampf M, Bornberg-Bauer E. Mechanisms and dynamics of orphan gene emergence in insect genomes. Genome Biol Evol. 2013; 5: 439–455. https://doi.org/10.1093/gbe/evt009 PMID: 23348040
17. Athanasouli M, Rödelsperger C. Analysis of repeat elements in the Pristionchus pacificus genome reveals an ancient invasion by horizontally transferred transposons. BMC Genomics. 2022; 23: 523. https://doi.org/10.1186/s12864-022-08731-1 PMID: 35854227
18. Rödelsperger C, Prabh N, Sommer RJ. New Gene Origin and Deep Taxon Phylogenomics: Opportunities and Challenges. Trends Genet. 2019; 35: 914–922. https://doi.org/10.1016/j.tig.2019.08.007 PMID: 31610892
19. Vakirlis N, Acar O, Hsu B, Castilho Coelho N, Van Oss SB, Wacholder A, et al. De novo emergence of adaptive membrane proteins from thymine-rich genomic sequences. Nat Commun. 2020; 11: 781. https://doi.org/10.1038/s41467-020-14500-z PMID: 32034123
20. Chen S, Zhang YE, Long M. New Genes in *Drosophila* Quickly Become Essential. Science. 2010; 330: 1682–1685.
21. Khalturin K, Hemmrich G, Fraune S, Augustin R, Bosch TCG. More than just orphans: are taxonomically-restricted genes important in evolution? Trends Genet. 2009; 25: 404–413. https://doi.org/10.1016/j.tig.2009.07.006 PMID: 19716618
22. Cardoso-Silva CB, Aono AH, Mancini MC, Sforça DA, da Silva CC, Pinto LR, et al. Taxonomically Restricted Genes Are Associated With Responses to Biotic and Abiotic Stresses in Sugarcane (spp.). Front Plant Sci. 2022; 13: 923069.
23. Cheng CH. Evolution of the diverse antifreeze proteins. Curr Opin Genet Dev. 1998; 8: 715–20. https://doi.org/10.1016/s0959-437x(98)80042-7 PMID: 9914209

24. Sommer RJ. Pristionchus pacificus. WormBook. 2006; 1–8.

25. Howard RS, Giacomelli M, Lozano-Fernandez J, Edgecombe GD, Fleming JF, Kristensen RM, et al. The Ediacaran origin of Ecdysozoa: integrating fossil and phylogenomic data. J Geol Soc London. 2022; 179: gs2021–107.

26. Wang X, Sommer RJ. Antagonism of LIN-17/Frizzled and LIN-18/Ryk in nematode vulva induction reveals evolutionary alterations in core developmental pathways. PLoS Biol. 2011; 9: e1001110. https://doi.org/10.1371/journal.pbio.1001110 PMID: 21814488

27. Ishita Y, Chihara T, Okumura M. Serotonergic modulation of feeding behavior in Caenorhabditis elegans and other related nematodes. Neurosci Res. 2020; 154: 9–19. https://doi.org/10.1016/j.neures.2019.04.006 PMID: 31028772

28. Lo W-S, Roca M, Dardiry M, Mackie M, Eberhardt G, Witte H, et al. Evolution and Diversity of TGF-β Pathways are Linked with Novel Developmental and Behavioral Traits. Molecular Biology and Evolution. 2022;39: msac252.

29. Borchert N, Dieterich C, Krug K, Schütz W, Jung S, Nordheim A, et al. Proteogenomics of *Pristionchus pacificus* reveals distinct proteome structure of nematode models. Genome Research. 2010; 20: 837–846.

30. Prabh N, Roeseler W, Witte H, Eberhardt G, Sommer RJ, Rödelsperger C. Deep taxon sampling reveals the evolutionary dynamics of novel gene families in *Pristionchus* nematodes. Genome Research. 2018; 28: 1664–1674.

31. Prabh N, Rödelsperger C. Multiple Pristionchus pacificus genomes reveal distinct evolutionary dynamics between de novo candidates and duplicated genes. Genome Res. 2022; 32: 1315–1327. https://doi.org/10.1101/gr.276431.121 PMID: 35618417

32. Stein JC, Yu Y, Copetti D, Zwickl DJ, Zhang L, Zhang C, et al. Genomes of 13 domesticated and wild rice relatives highlight genetic conservation, turnover and innovation across the genus Oryza. Nat Genet. 2018; 50: 285–296. https://doi.org/10.1038/s41588-018-0040-0 PMID: 29358651

33. Dowling D, Schmitz JF, Bornberg-Bauer E. Stochastic Gain and Loss of Novel Transcribed Open Reading Frames in the Human Lineage. Genome Biol Evol. 2020; 12: 2183–2195. https://doi.org/10.1093/gbe/evaa194 PMID: 33210146

34. Mayer MG, Rödelsperger C, Witte H, Riebesell M, Sommer RJ. The Orphan Gene dauerless Regulates Dauer Development and Intraspecific Competition in Nematodes by Copy Number Variation. PLoS Genet. 2015; 11: e1005146. https://doi.org/10.1371/journal.pgen.1005146 PMID: 26087034

35. Li J, Singh U, Arendsee Z, Wurtele ES. Landscape of the Dark Transcriptome Revealed Through Remining Massive RNA-Seq Data. Front Genet. 2021; 12: 722981. https://doi.org/10.3389/fgene.2021.722981 PMID: 34484307

36. Szklarczyk D, Morris JH, Cook H, Kuhn M, Wyder S, Simonovic M, et al. The STRING database in 2017: quality-controlled protein–protein association networks, made broadly accessible. Nucleic Acids Research. 2017; 45: D362–D368. https://doi.org/10.1093/nar/gkw937 PMID: 27924014

37. Kim SK, Lund J, Kiraly M, Duke K, Jiang M, Stuart JM, et al. A gene expression map for Caenorhabditis elegans. Science. 2001; 293: 2087–2092. https://doi.org/10.1126/science.1061603 PMID: 11557892

38. Marchesi JR, Ravel J. The vocabulary of microbiome research: a proposal. Microbiome. 2015; 3: 31. https://doi.org/10.1186/s40168-015-0094-5 PMID: 26229597

39. Watson E, MacNeil LT, Ritter AD, Safak Yilmaz L, Rosebrock AP, Caudy AA, et al. Interspecies Systems Biology Uncovers Metabolites Affecting C. elegans Gene Expression and Life History Traits. Cell. 2014; 156: 759–770. https://doi.org/10.1016/j.cell.2014.01.047 PMID: 24529378

40. Zhang F, Berg M, Dierking K, Félix M-A, Shapira M, Samuel BS, et al. Caenorhabditis elegans as a Model for Microbiome Research. Frontiers in Microbiology. 2017; 8: 485. https://doi.org/10.3389/fmicb.2017.00485 PMID: 28386252

41. Sinha A, Rae R, Iatsenko I, Sommer RJ. System wide analysis of the evolution of innate immunity in the nematode model species Caenorhabditis elegans and Pristionchus pacificus. PLoS One. 2012; 7: e44255. https://doi.org/10.1371/journal.pone.0044255 PMID: 23028509

42. Akduman N, Rödelsperger C, Sommer RJ. Culture-based analysis of Pristionchus-associated microbiota from beetles and figs for studying nematode-bacterial interactions. PLoS One. 2018; 13: e0198018. https://doi.org/10.1371/journal.pone.0198018 PMID: 29864131

43. Sun S, Rödelsperger C, Sommer RJ. Single worm transcriptomics identifies a developmental core network of oscillating genes with deep conservation across nematodes. Genome Res. 2021; 31: 1590–1601. https://doi.org/10.1101/gr.275303.121 PMID: 34301622

44. Baskaran P, Rödelsperger C, Prabh N, Serobyan V, Markov GV, Hirsekorn A, et al. Ancient gene duplications have shaped developmental stage-specific expression in Pristionchus pacificus. BMC Evol Biol. 2015; 15: 185. https://doi.org/10.1186/s12862-015-0466-2 PMID: 26370559

45. O'Donnell MP, Fox BW, Chao P-H, Schroeder FC, Sengupta P. A neurotransmitter produced by gut bacteria modulates host sensory behaviour. Nature. 2020; 583: 415–420. https://doi.org/10.1038/s41586-020-2395-5 PMID: 32555456

46. Lansdon P, Carlson M, Ackley BD. Wild-type Caenorhabditis elegans isolates exhibit distinct gene expression profiles in response to microbial infection. BMC Genomics. 2022; 23: 229. https://doi.org/10.1186/s12864-022-08455-2 PMID: 35321659

47. Akduman N, Lightfoot JW, Röseler W, Witte H, Lo W-S, et al. Bacterial vitamin B_{12} production enhances predatory behaviors in nematodes. ISME J. 2020; 14:1494–1507.

48. Enright AJ, Van Dongen S, Ouzounis CA. An efficient algorithm for large-scale detection of protein families. Nucleic Acids Res. 2002; 30: 1575–1584. https://doi.org/10.1093/nar/30.7.1575 PMID: 11917018

49. Heinz S, Benner C, Spann N, Bertolino E, Lin YC, Laslo P, et al. Simple combinations of lineage-determining transcription factors prime cis-regulatory elements required for macrophage and B cell identities. Mol Cell. 2010; 38: 576–589. https://doi.org/10.1016/j.molcel.2010.05.004 PMID: 20513432

50. Narasimhan K, Lambert SA, Yang AWH, Riddell J, Mnaimneh S, Zheng H, et al. Mapping and analysis of Caenorhabditis elegans transcription factor sequence specificities. Elife. 2015; 44: e06967. https://doi.org/10.7554/eLife.06967 PMID: 25905672

51. Burglin TR, Ruvkun G. Regulation of ectodermal and excretory function by the C. elegans POU homeobox gene ceh-6. Development. 2001; 128: 779–790. https://doi.org/10.1242/dev.128.5.779 PMID: 11171402

52. Domazet-Lošo T, Brajković J, Tautz D. A phylostratigraphy approach to uncover the genomic history of major adaptations in metazoan lineages. Trends in Genetics. 2007; 23: 533–539. https://doi.org/10.1016/j.tig.2007.08.014 PMID: 18029048

53. Kikuchi T, Cotton JA, Dalzell JJ, Hasegawa K, Kanzaki N, McVeigh P, et al. Genomic insights into the origin of parasitism in the emerging plant pathogen Bursaphelenchus xylophilus. PLoS Pathog. 2011; 7: e1002219. https://doi.org/10.1371/journal.ppat.1002219 PMID: 21909270

54. Foster JM, Grote A, Mattick J, Tracey A, Tsai Y-C, Chung M, et al. Sex chromosome evolution in parasitic nematodes of humans. Nat Commun. 2020; 11: 1964. https://doi.org/10.1038/s41467-020-15654-6 PMID: 32327641

55. Mitreva M, Jasmer DP, Zarlenga DS, Wang Z, Abubucker S, Martin J, et al. The draft genome of the parasitic nematode Trichinella spiralis. Nat Genet. 2011; 43: 228–235. https://doi.org/10.1038/ng.769 PMID: 21336279

56. Lightfoot JW, Chauhan VM, Aylott JW, Rödelsperger C. Comparative transcriptomics of the nematode gut identifies global shifts in feeding mode and pathogen susceptibility. BMC Res Notes. 2016; 9: 142. https://doi.org/10.1186/s13104-016-1886-9 PMID: 26944260

57. Rödelsperger C, Röseler W, Prabh N, Yoshida K, Weiler C, Herrmann M, et al. Phylotranscriptomics of Pristionchus Nematodes Reveals Parallel Gene Loss in Six Hermaphroditic Lineages. Curr Biol. 2018; 28: 3123–3127.e5. https://doi.org/10.1016/j.cub.2018.07.041 PMID: 30245109

58. Rödelsperger C, Ebbing A, Sharma DR, Okumura M, Sommer RJ, Korswagen HC. Spatial Transcriptomics of Nematodes Identifies Sperm Cells as a Source of Genomic Novelty and Rapid Evolution. Mol Biol Evol. 2021; 38: 229–243. https://doi.org/10.1093/molbev/msaa207 PMID: 32785688

59. Angeles-Albores D N Lee RY, Chan J, Sternberg PW. Tissue enrichment analysis for C. elegans genomics. BMC Bioinformatics. 2016; 17: 366.

60. Le TS, Nguyen THG, Ha BH, Huong BTM, Nguyen TTH, Vu KD, et al. Reproductive Span of is Extended by Sp. J Nematol. 2022; 54: 20220010.

61. Kissoyan KAB, Peters L, Giez C, Michels J, Pees B, Hamerich IK, et al. Exploring Effects of Protective Natural Microbiota on Host Physiology. Front Cell Infect Microbiol. 2022; 12: 775728.

62. Cutter AD, Ward S. Sexual and Temporal Dynamics of Molecular Evolution in C. elegans Development. Molecular Biology and Evolution. 2005; 22: 178–188. https://doi.org/10.1093/molbev/msh267 PMID: 15371532

63. Levine MT, Jones CD, Kern AD, Lindfors HA, Begun DJ. Novel genes derived from noncoding DNA in Drosophila melanogaster are frequently X-linked and exhibit testis-biased expression. Proc Natl Acad Sci U S A. 2006; 103: 9935–9939. https://doi.org/10.1073/pnas.0509809103 PMID: 16777968

64. Soumillon M, Necsulea A, Weier M, Brawand D, Zhang X, Gu H, et al. Cellular source and mechanisms of high transcriptome complexity in the mammalian testis. Cell Rep. 2013; 3: 2179–2190. https://doi.org/10.1016/j.celrep.2013.05.031 PMID: 23791531

65. Han Z, Sieriebriennikov B, Susoy V, Lo W-S, Igreja C, Dong C, et al. Horizontally Acquired Cellulases Assist the Expansion of Dietary Range in Pristionchus Nematodes. Mol Biol Evol. 2022;39: msab370. https://doi.org/10.1093/molbev/msab370 PMID: 34978575

66. Lo W-S, Han Z, Witte H, Röseler W, Sommer RJ. Synergistic interaction of gut microbiota enhances the growth of nematode through neuroendocrine signaling. Curr Biol. 2022; 32: 2037–2050.e4. https://doi.org/10.1016/j.cub.2022.03.056 PMID: 35397201

67. Sanghvi GV, Baskaran P, Röseler W, Sieriebriennikov B, Rödelsperger C, Sommer RJ. Life History Responses and Gene Expression Profiles of the Nematode Pristionchus pacificus Cultured on Cryptococcus Yeasts. PLoS One. 2016; 11: e0164881. https://doi.org/10.1371/journal.pone.0164881 PMID: 27741297

68. Sural S, Hobert O. Nematode nuclear receptors as integrators of sensory information. Curr Biol. 2021; 31: 4361–4366.e2. https://doi.org/10.1016/j.cub.2021.07.019 PMID: 34348120

69. Hobert O. The neuronal genome of Caenorhabditis elegans. WormBook. 2013. 1–106. https://doi.org/10.1895/wormbook.1.161.1 PMID: 24081909

70. Sieriebriennikov B, Sun S, Lightfoot JW, Witte H, Moreno E, et al. Conserved nuclear hormone receptors controlling a novel plastic trait target fast-evolving genes expressed in a single cell. PLoS Genet. 2020; 16: e1008687. https://doi.org/10.1371/journal.pgen.1008687 PMID: 32282814

71. Verster AJ, Styles EB, Mateo A, Derry WB, Andrews BJ, Fraser AG. Taxonomically Restricted Genes with Essential Functions Frequently Play Roles in Chromosome Segregation in and. G3. 2017; 7: 3337–3347.

72. Dirksen P, Marsh SA, Braker I, Heitland N, Wagner S, Nakad R, et al. The native microbiome of the nematode Caenorhabditis elegans: gateway to a new host-microbiome model. BMC Biol. 2016; 14: 38. https://doi.org/10.1186/s12915-016-0258-1 PMID: 27160191

73. Lightfoot JW, Wilecki M, Rödelsperger C, Moreno E, Susoy V, Witte H, et al. Small peptide-mediated self-recognition prevents cannibalism in predatory nematodes. Science. 2019; 364: 86–89. https://doi.org/10.1126/science.aav9856 PMID: 30948551

74. Sommer RJ, Dardiry M, Lenuzzi M, Namdeo S, Renahan T, Sieriebriennikov B, et al. The genetics of phenotypic plasticity in nematode feeding structures. Open Biol. 2017;7. https://doi.org/10.1098/rsob.160332 PMID: 28298309

75. Namdeo S, Moreno E, Rödelsperger C, Baskaran P, Witte H, Sommer RJ. Two independent sulfation processes regulate mouth-form plasticity in the nematode. Development. 2018; 145: dev166272.

76. Parker GA. Conceptual developments in sperm competition: a very brief synopsis. Philosophical Transactions of the Royal Society B: Biological Sciences. 2020; 375:20200061.

77. Kurhanewicz NA, Dinwiddie D, Bush ZD, Libuda DE. Elevated Temperatures Cause Transposon-Associated DNA Damage in C. elegans Spermatocytes. Curr Biol. 2020; 30: 5007–5017.e4.

78. Bhalla N. Meiosis: Is Spermatogenesis Stress an Opportunity for Evolutionary Innovation? Current biology: CB. 2020. pp. R1471–R1473. https://doi.org/10.1016/j.cub.2020.10.042 PMID: 33352126

79. Casasa S, Biddle JF, Koutsovoulos GD, Ragsdale EJ. Polyphenism of a Novel Trait Integrated Rapidly Evolving Genes into Ancestrally Plastic Networks. Mol Biol Evol. 2021; 38: 331–343. https://doi.org/10.1093/molbev/msaa235 PMID: 32931588

80. Pires-daSilva A. Pristionchus pacificus protocols. WormBook. 2013; 1–20. https://doi.org/10.1895/wormbook.1.114.2 PMID: 23505072

81. Dobin A, Davis CA, Schlesinger F, Drenkow J, Zaleski C, Jha S, et al. STAR: ultrafast universal RNA-seq aligner. Bioinformatics. 2013; 29: 15–21. https://doi.org/10.1093/bioinformatics/bts635 PMID: 23104886

82. Liao Y, Smyth GK, Shi W. featureCounts: an efficient general purpose program for assigning sequence reads to genomic features. Bioinformatics. 2014; 30: 923–30. https://doi.org/10.1093/bioinformatics/btt656 PMID: 24227677

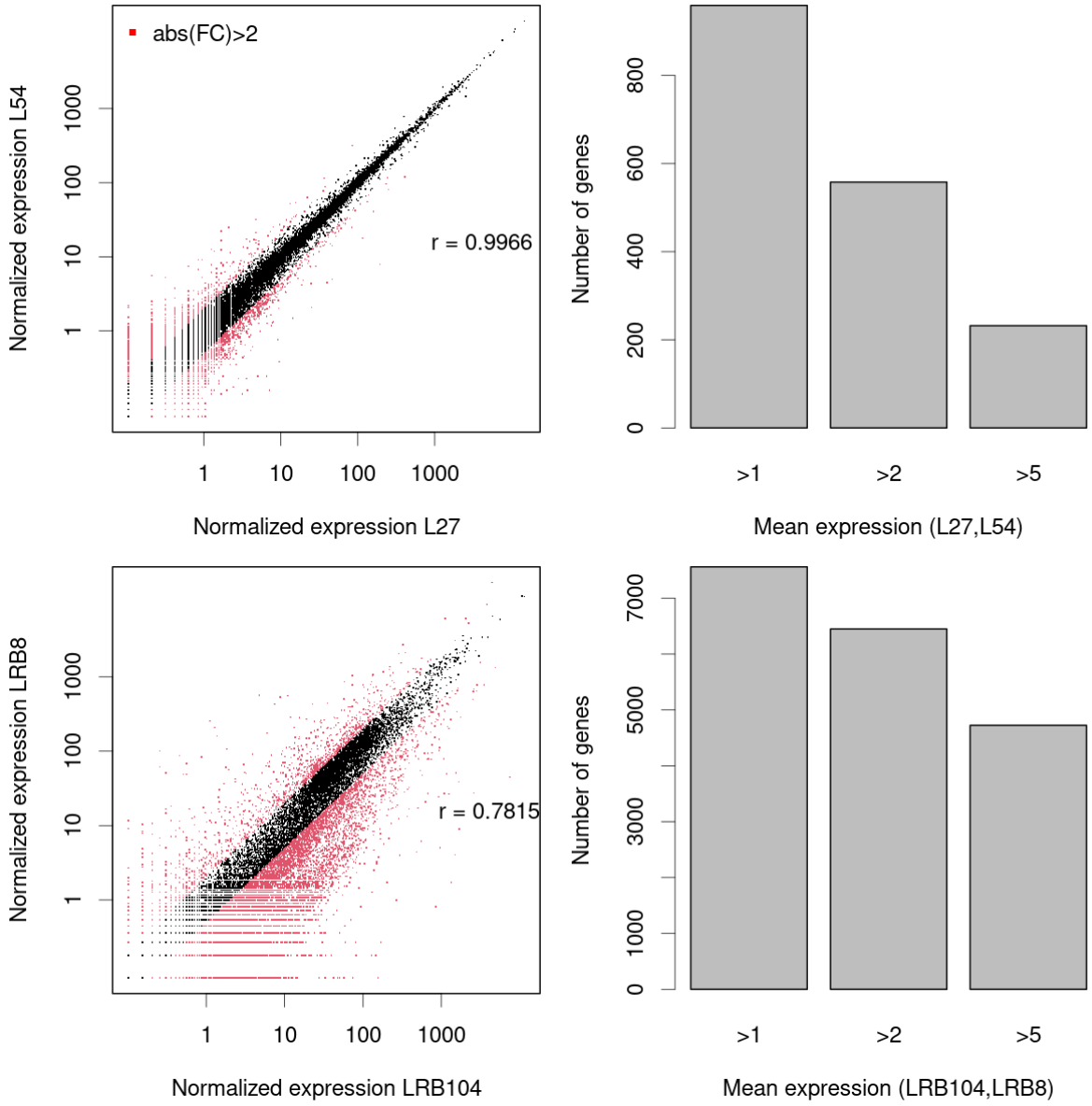
83. Athanasouli M, Witte H, Weiler C, Loschko T, Eberhardt G, Sommer RJ, et al. Comparative genomics and community curation further improve gene annotations in the nematode Pristionchus pacificus. BMC Genomics. 2020; 21: 708. https://doi.org/10.1186/s12864-020-07100-0 PMID: 33045985

84. Love MI, Huber W, Anders S. Moderated estimation of fold change and dispersion for RNA-seq data with DESeq2. Genome Biol. 2014; 15: 550. https://doi.org/10.1186/s13059-014-0550-8 PMID: 25516281

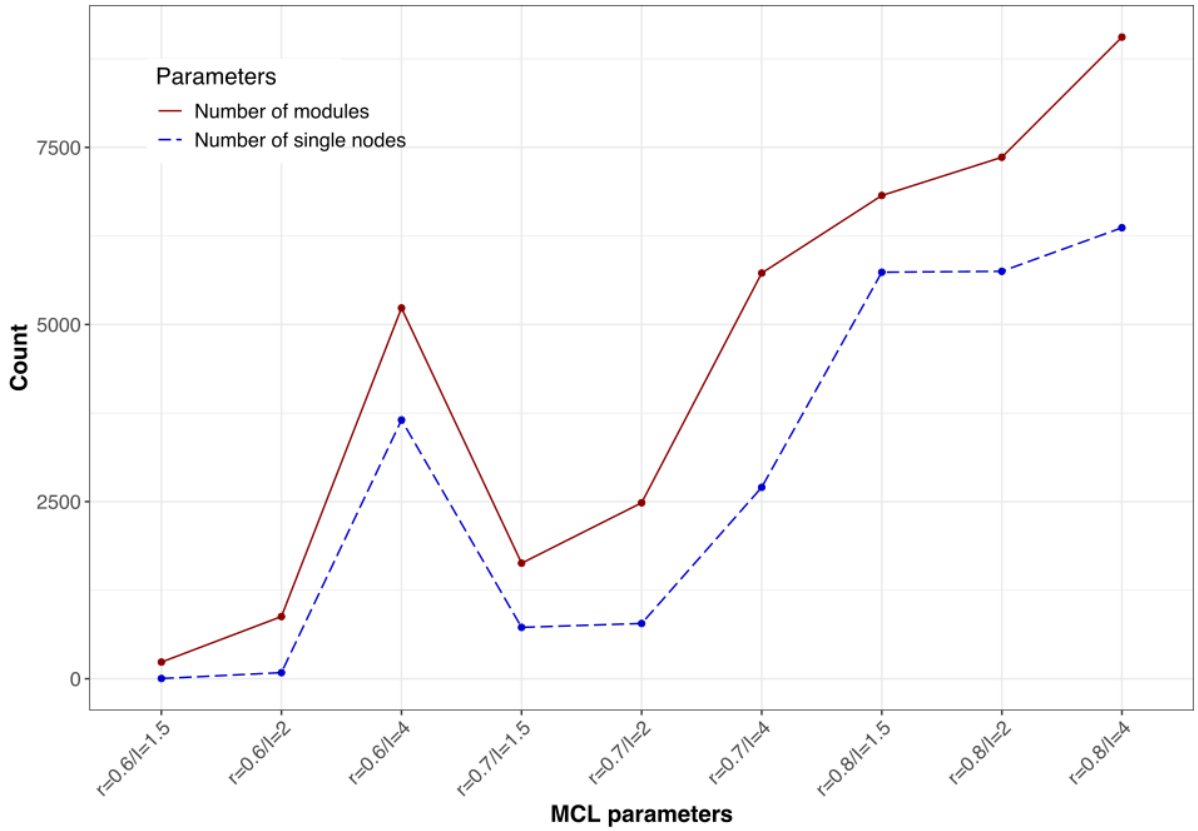
85. Bolt BJ, Rodgers FH, Shafie M, Kersey PJ, Berriman M, Howe KL. Using WormBase ParaSite: An Integrated Platform for Exploring Helminth Genomic Data. Methods Mol Biol. 2018; 1757: 471–491.

86. Trapnell C, Roberts A, Goff L, Pertea G, Kim D, Kelley DR, et al. Differential gene and transcript expression analysis of RNA-seq experiments with TopHat and Cufflinks. Nat Protoc. 2012; 7: 562–578. https://doi.org/10.1038/nprot.2012.016 PMID: 22383036

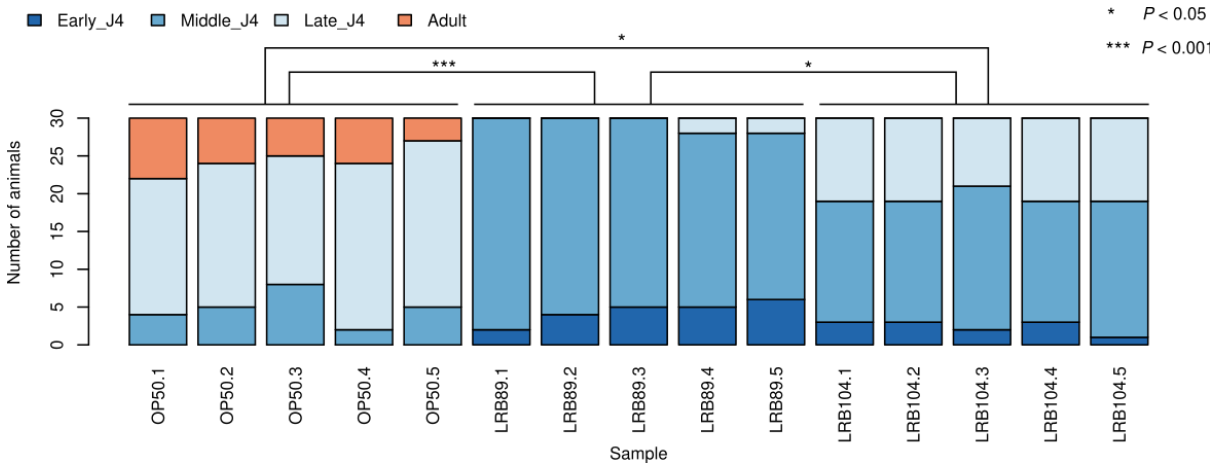
87. Kanehisa M, Sato Y, Morishima K. BlastKOALA and GhostKOALA: KEGG Tools for Functional Characterization of Genome and Metagenome Sequences. J Mol Biol. 2016; 428: 726–731. https://doi.org/10.1016/j.jmb.2015.11.006 PMID: 26585406



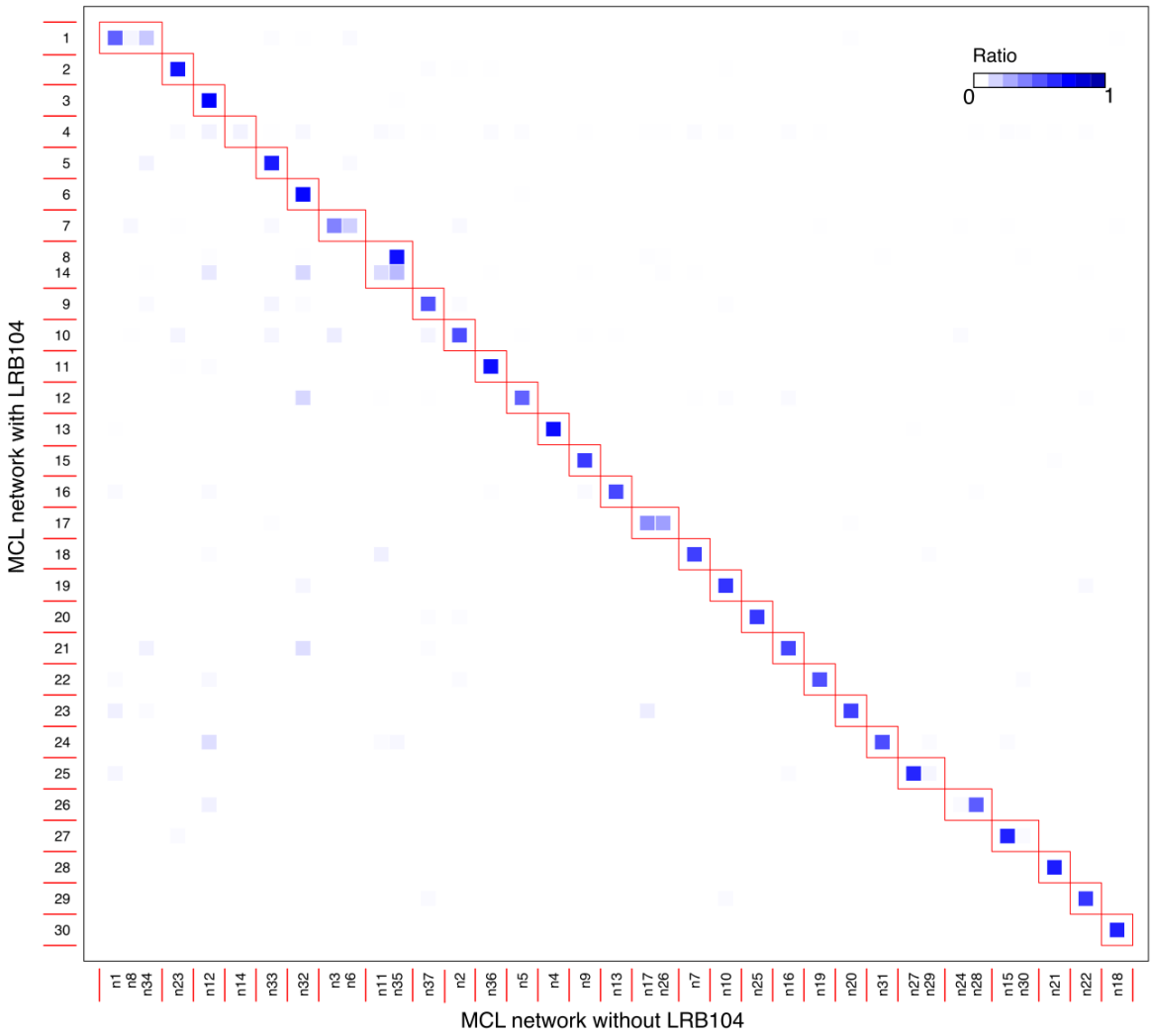
S1 Fig. Analysis of the most similar and dissimilar RNA-seq data sets. The scatter plots show the normalized expression (TPM) for different pairs of samples. As lowly expressed genes tend to be more variable, we visualized the number of genes with at least two-fold expression difference across multiple mean expression levels.



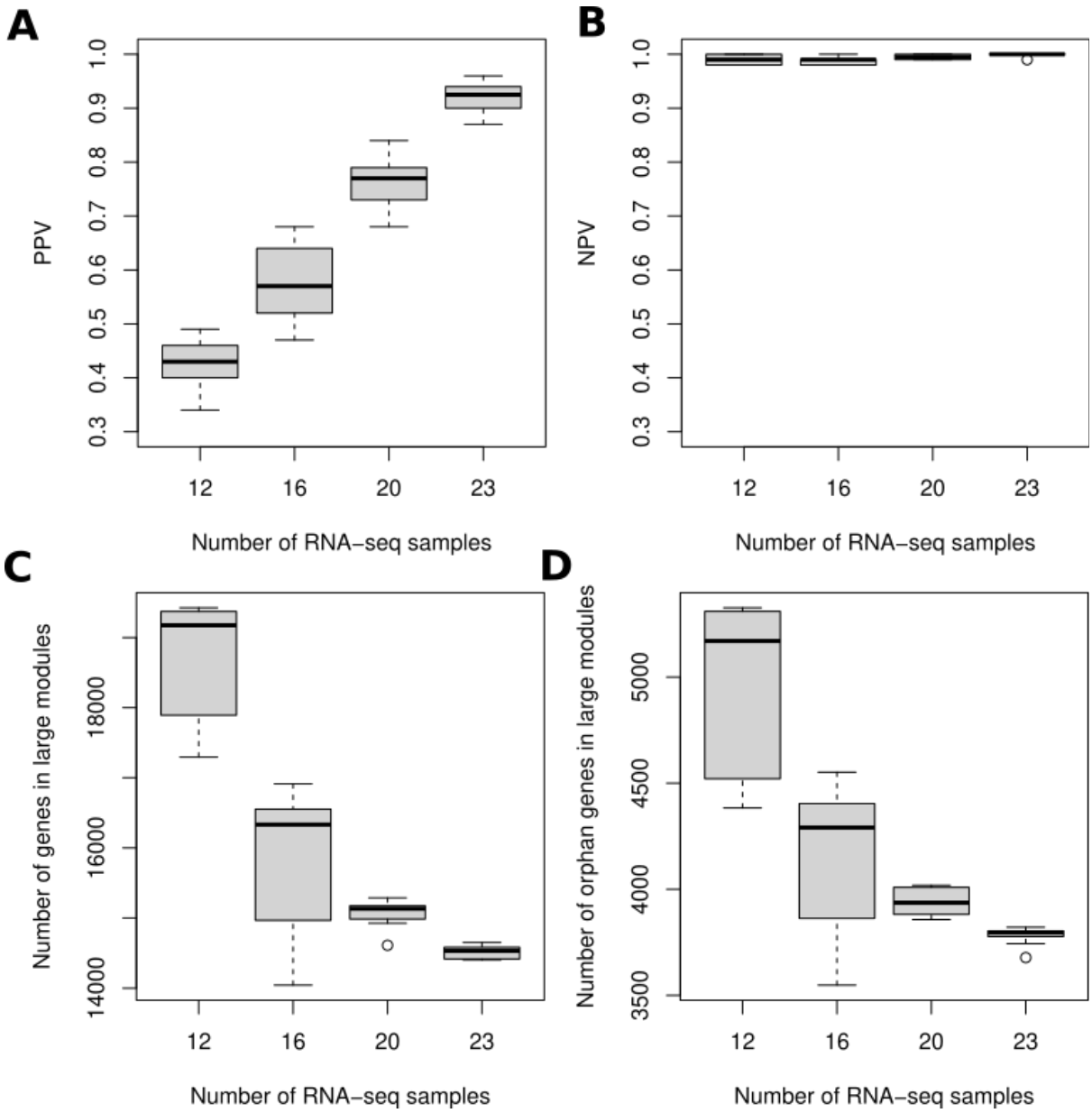
S2 Fig. Parameter combinations for MCL clustering. We evaluated the total number of modules and singleton modules as a function of the inflation factor (I) and correlation coefficient (r). High r and I values generally increase the number of modules, whereas low r and I parameters generate fewer but larger modules. We decided to use r=0.7 and I=2 for the final analysis, because it gave a moderate number of modules with a relatively low number of singletons.



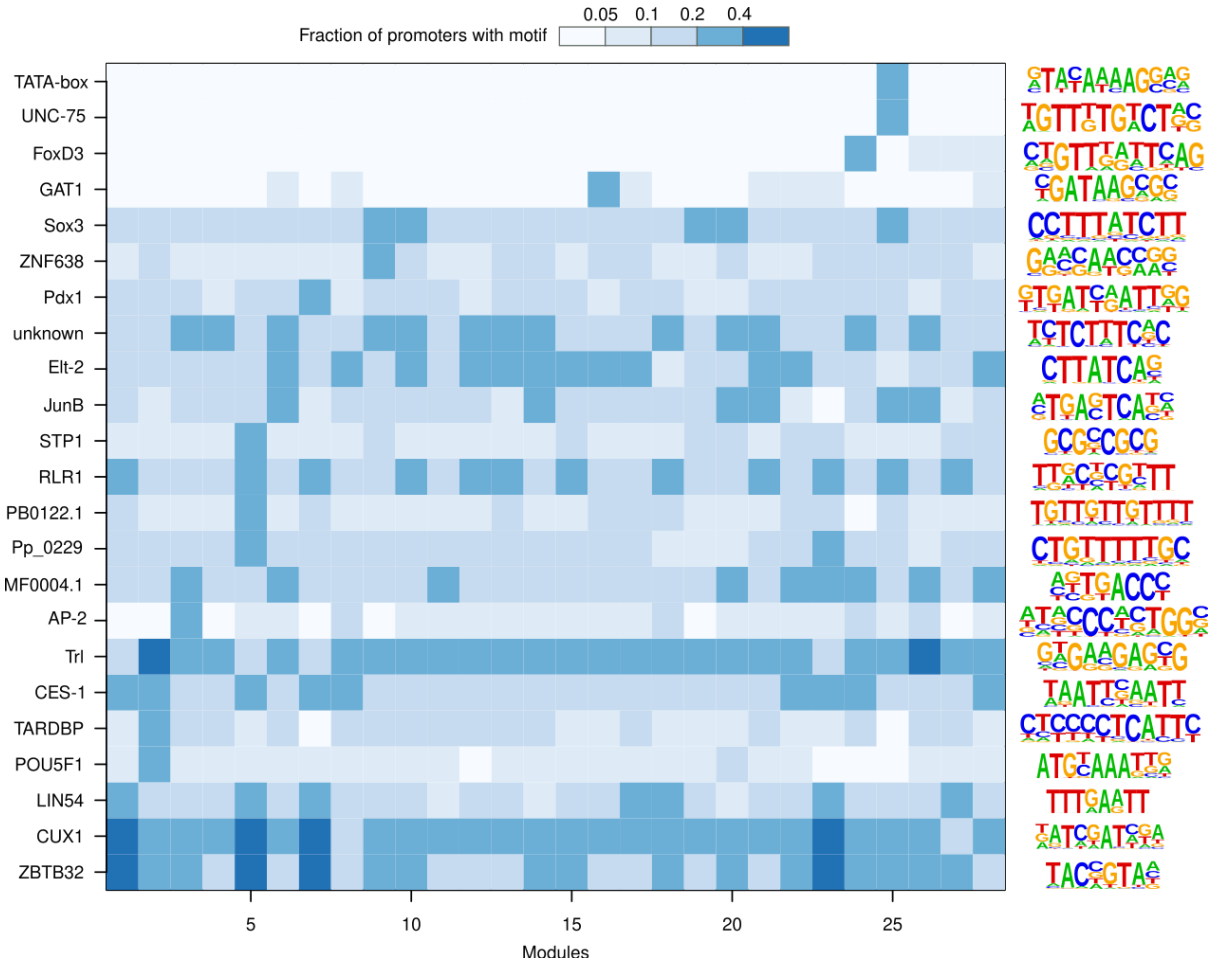
S3 Fig. Developmental timing on different bacteria. The distribution of developmental stages 56h after J2 synchronization is shown for *P. pacificus* worms on *E. coli* OP50 and two *Wautersiella* bacteria (5 biological replicates). Nematodes grow slower on both *Wautersiella* strains. The significance level was computed by a χ^2-test (mean *P*-value from all pairwise comparisons).



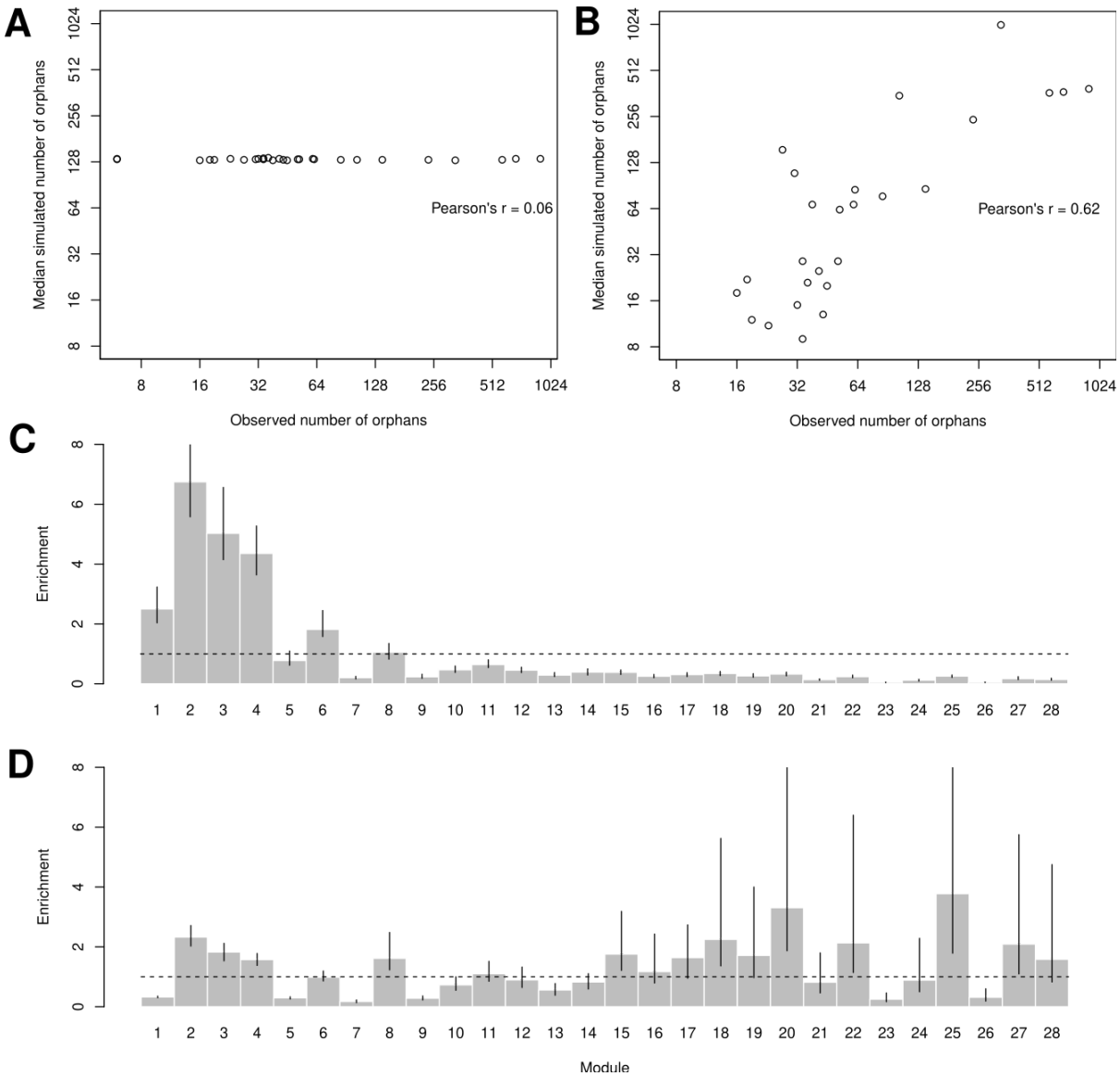
S4 Fig. Comparison of MCL networks constructed with or without LRB104. The heatmap shows fraction genes from modules of the complete coexpression network (including LRB104) that overlap within a given module from the coexpression network without LRB104. For most modules there exists a 1-1 correspondence between both networks, indicating that the network structure is robust with regard to the *Wautersiella* LRB104 data set.



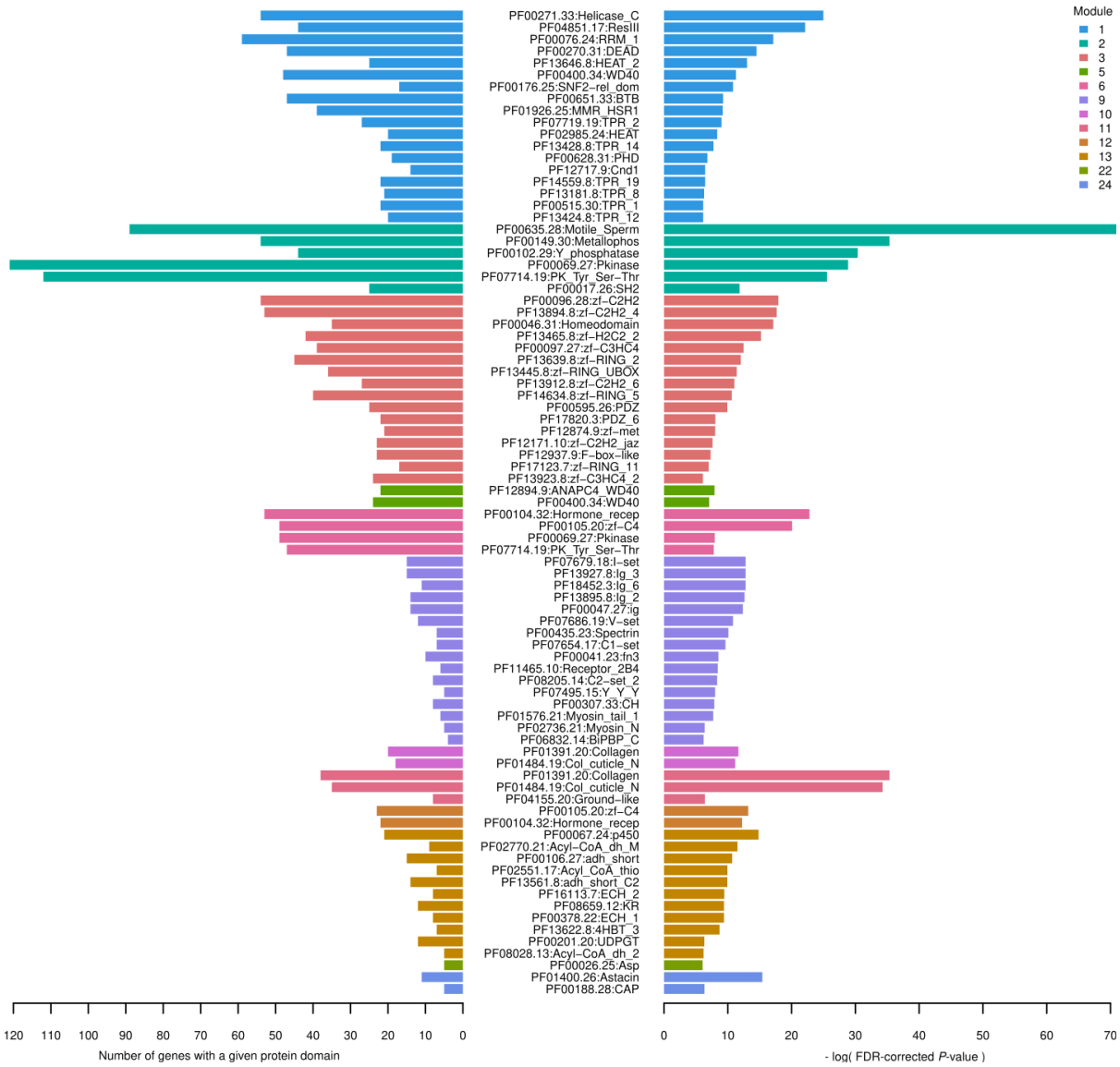
S5 Fig. Comparison of Coexpression networks on subsampled RNA-seq data. Taking the full coexpression network calculated from 24 RNA-seq samples as reference, we evaluated the classification of 10,000 randomly chosen gene pairs using subsampled RNA-seq data. For the full and the subsampled data set, a gene pair was either classified to be part of the same module or not. This allowed us to calculate the positive predictive value (PPV, panel A) and negative predictive value (NPV, panel B) for 10 randomly subsampled data sets of a fixed size. While the NPV is always close to 1, the PPV shows drastic differences between the full and subsampled data. This suggests that with fewer RNA-seq samples, additional gene pairs are assigned to the same coexpression module. However, with additional samples, such modules may be split into smaller components. Consistently, the number of genes in large modules (N>50) is much higher for smaller sample sizes (panel C). Panel D shows the number of diplogastrid-specific orphan genes in large modules.



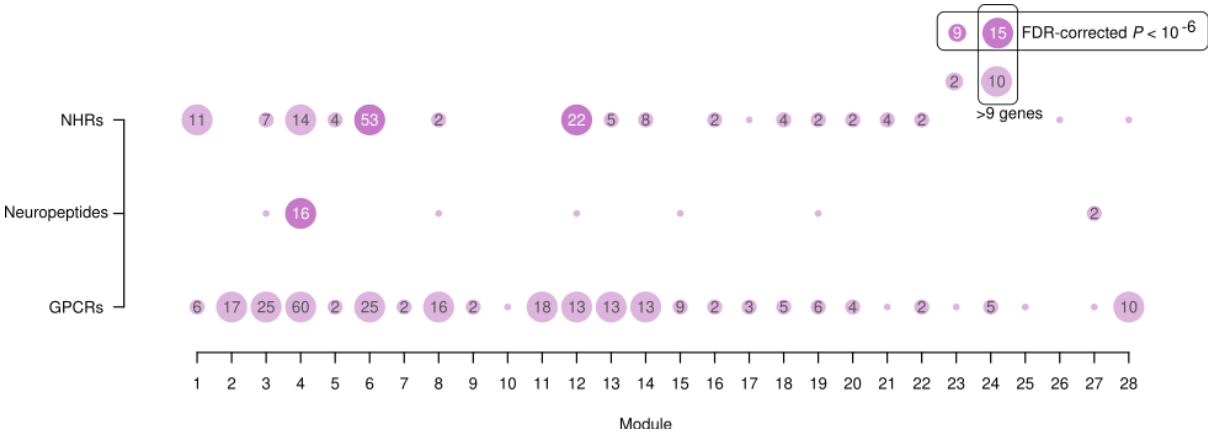
S6 Fig.. Regulatory architecture of coexpression modules. Significantly overrepresented motifs were identified for each module by the HOMER software. We arbitrarily selected motifs that occurred in at least 20% of promoters of a given module and visualized their distribution across all modules. Note that the complementary regulation by less frequent motifs and other regulatory mechanisms such as microRNAs are not considered here. Sequence logos for each motif are shown at the right and the labels to the left indicate the best motif match among known motifs.



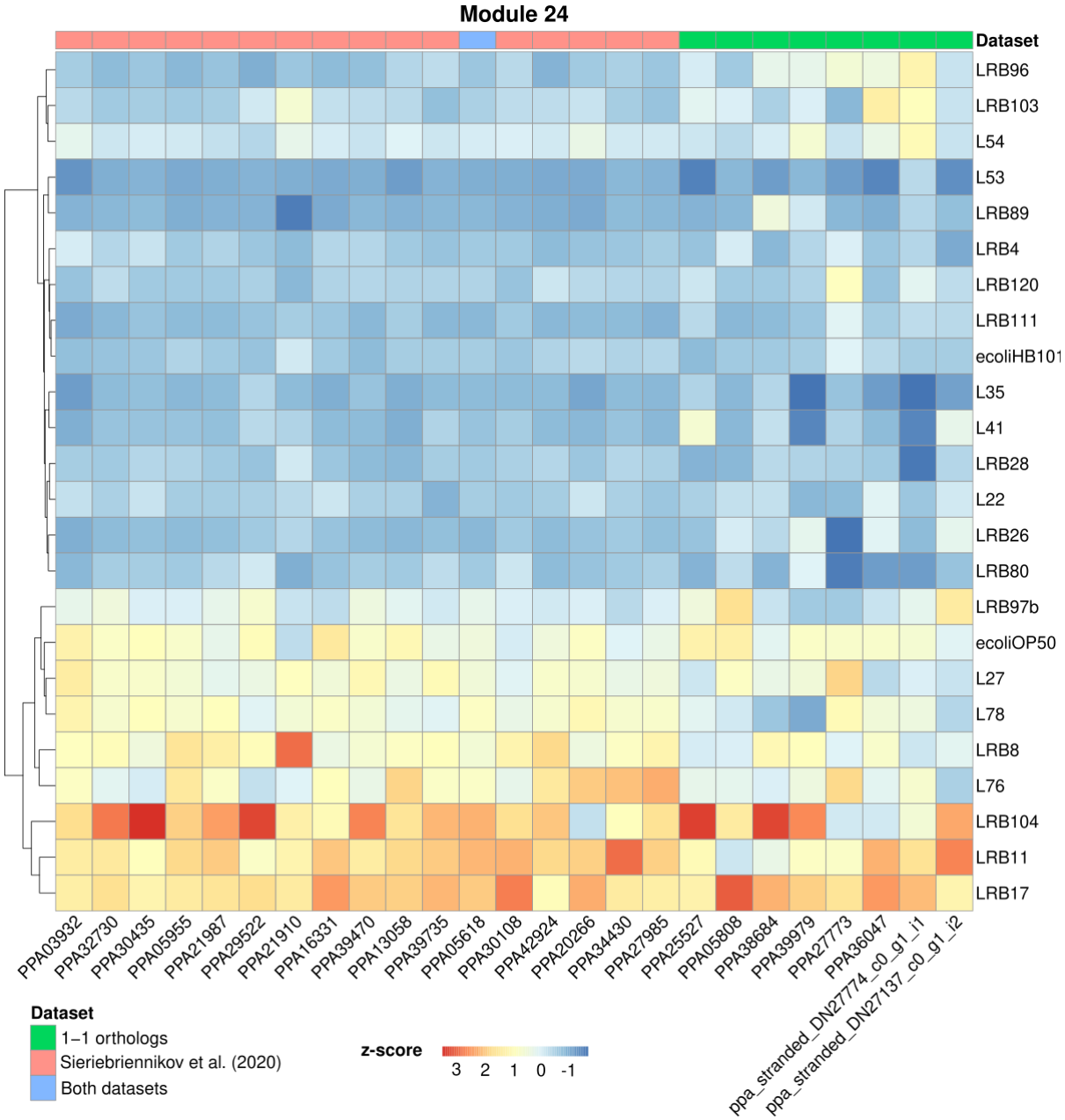
S7 Fig. Enrichment analysis for simulated network evolution. We simulated the integration of novel genes into existing networks by estimating ancestral module sizes based on the number of ancient genes (non-orphan genes) and then assigning an equivalent number of orphan genes to existing modules with equal probabilities (panel A and C) and with probabilities that were proportional to the module size (panel B and D). The scatterplots show the observed and simulated number of orphan genes per module. The barplots show the median enrichment of the observed relative to the simulated number of orphan genes (error bars indicate the minimal and maximal values from 100 simulations).



S8 Fig. Overrepresented protein domains in coexpression modules. Specific protein domains are strongly overrepresented in twelve coexpression modules. The left barplot shows the number of genes with a given protein domain for each module and the the right bar plot shows the negative logarithm of the FDR corrected P-value (Fisher's exact test). The most significant association is between Motile sperm proteins (PF00635) and coexpression module 2.



S9 Fig. Distribution of GPCRs, NHRs, and neuropeptides across the coexpression modules.



S10 Fig. Expression of selected module 24 genes. The heatmap shows the expression of genes that are shared between module 24 and the target genes of mouth form regulators and additional module 24 genes with 1-1 orthologs in *C. elegans*. The *C. elegans* ortholog of PPA25527 (D1044.3) is reported to be expressed in the gland cell and reporter lines of multiple candidate genes show expression in the gland of *P. pacificus* (Sieribriennikov et al. 2020) [1].

References

1. Sieriebriennikov B, Sun S, Lightfoot JW, Witte H, Moreno E, et al. Conserved nuclear hormone receptors controlling a novel plastic trait target fast-evolving genes expressed in a single cell. PLoS Genet. 2020;16: e1008687.

JOURNAL OF NEMATOLOGY
Research Paper | DOI: 10.2478/jofnem-2024-0032
e2024-1 | Vol. 56

Description of two new *Pristionchus* species from South Korea

Matthias Herrmann[1,*], Natsumi Kanzaki[2], Christian Weiler[1], Penghieng Theam[1], Christian Rödelsperger[1] and Ralf Sommer[1]

[1]Max Planck Institute for Biology Tübingen, Department of Integrative Evolutionary Biology, Max-Planck Ring 9, 72076 Tübingen, Germany

[2]Kansai Research Center, Forestry and Forest Products Research Institute (FFPRI), 68 Nagaikyutaroh, Momoyama, Fushimi, Kyoto 612-0855, Japan

*E-mail: matthias.herrmann@tuebingen.mpg.de

LSID code publication: urn:lsid:zoobank.org:act:960C79FF-D1F0-440BB7B4-36539ECA5F86

urn:lsid:zoobank.org:act:79BB22D3-2D25-401B-803B-69594562F3CF

This paper was edited by Zafar Ahmad Handoo.

Received for publication July 03, 2024.

Abstract

Based on molecular markers, mating experiments, morphological observations and ecological data, two *Pristionchus* species (Nematoda: Diplogastridae) new to science are described. Both were collected from different Scarabaeoid beetles in South Korea, have a gonochoristic mode of reproduction and fall into a sub-clade of the *pacificus* clade. *Pristionchus coreanus* n. sp. does not show a eurystomatous morph under laboratory conditions and might therefore be suitable for the study of gain and loss of polymorphism. *Pristionchus hangukensis* n. sp. is phylogenetically close to Chinese and Japanese species and helps to separate an Asian clade from an American clade.

Keywords

Diplogastridae, *Pristionchus*, *hangukensis*, *coreanus*, n. sp., Molecular phylogeny, South Korea

The nematode genus *Pristionchus* Kreis 1932 gained interest in the scientific community due to the importance of the species *Pristionchus pacificus* in (24) as a model organism in eco–evo–devo (22). While original studies focused on comparisons to *Caenorhabditis elegans* (for review see 31), work over the last decade established *P. pacificus* as a genetic, molecular and ecological model organism to study developmental plasticity of its feeding structures (for review see 32). Specifically, most *Pristionchus* species can form two alternative mouth forms, one of which enables predation on other nematodes (19,33). Predation can in principle be cannibalistic and requires sophisticated self-recognition mechanisms to distinguish kin from non-kin at the intra- and interspecies level (34,35). The analysis of such complex organismal traits heavily depends on a rich collection of *Pristionchus* material from nature. To bring more *P. pacificus* strains and additional species of the genus *Pristionchus* into the laboratory, long-term and large-scale efforts were already initiated 20 years ago. Since then, around 40 expeditions to different parts of the world led to the discovery and description of more than 50 species new to science (19,7,12,30,36). Our current understanding suggests that the genus *Pristionchus* has a nearly world-wide distribution with a biodiversity hot spot in Asia (13). While the Nearctic, Neotropic and Afrotropic did not show as many species (4,5), "Asia" is home to 35 *Pristionchus* species, which makes it a treasure chest for nematode biodiversity research. In addition, the genus *Pristionchus* most likely originated in Asia because the sister genus *Parapristionchus* is so far restricted to this region

Open Access. Published by Sciendo. BY-NC-ND
© 2024 Herrmann et al. This is an Open Access article licensed under the Creative Commons CC BY 4.0 license, https://creativecommons.org/licenses/by/4.0/

(37,38). However, our sampling efforts throughout Asia are far from being complete and as a result, all of the last sampling expeditions have resulted in the isolation and characterization of species new to science (13). To increase the number of described species as well as our observation range, we conducted a collecting trip to the South Korean peninsula and the island of Jeju in summer 2022.

Materials and Methods

Nematode isolation

From June 26th to July 11th, 2022, we travelled to South Korea and sampled potentially nematode harboring insects at different locations. Beetles of the Superfamily Scarabaeoidea were collected using light traps (Lepi LED) at several locations in South Korea. Beetles were brought to our laboratory in Germany alive. There, they were dissected and put on individual Petri dishes with NGM agar. Plates were scanned for developing nematodes over two weeks. Single gravid females were transferred to new plates with NGM agar and *E. coli* strain OP50 as food. Initial bacterial contamination was eradicated by bleaching cultures with NaOH&Hydrogenperoxide.

After the establishment of isogenic lines, followed by successful freezing in liquid nitrogen confirmed by thawing tests, these lines got 'RS' numbers and database entries were generated.

Morphological observation

Live adults of *P. hangukensis* n. sp. and *P. coreanus* n. sp. from two 1-2-week-old cultures were used for morphological observations. Because the eurystomatous form was not observed in *P. coreanus* n. sp. using *E. coli* OP50 as food, we attempted to induce this mouth form using *Novosphingobium* sp. as a food source of the species because previous work has shown that this bacterial strain regularly induces the predatory morph (39). Morphological observations and drawings were performed using a microscope (Zeiss Axioskop) equipped with differential interference contrast optics and a drawing tube following the methods of (19)). Light micrographs were taken with a microscope (Zeiss AxioImager Z1) equipped with differential interference contrast optics and a microscopic digital camera (Zeiss Axiocam 506 mono) operated by computer software ZEN (Zeiss). The drawings and micrographs were edited using Photoshop Elements 2020 software (Adobe) to construct figures.

To prepare type material, nematodes were isolated from cultures, rinsed in distilled water to remove bacteria, heat killed at 65°C, fixed in 5% formalin and processed through a glycerol and ethanol series using Seinhorst's method (9). Then, single specimens were mounted on microscopic slides in glycerol, surrounded by a wax ring and labeled.

Remark concerning morphometric measurements

We use a multi-dimensional approach for modern description of nematodes, combining molecular, morphological, biological and ecological information to characterize new material as broadly as possible. This is based on our repeated findings that measurements of certain nematode dimensions can change over time as a result to different culture conditions (3,7,10,11,20).

Molecular characterization, phylogeny and reproductive isolation

A species phylogeny of the complete *Pristionchus* genus was reconstructed as described in (18). In brief, transcriptome libraries were generated from mixed-stage worm cultures and sequenced on an Illumina HiSeq 3000. Raw reads were assembled *de novo* and clustered into orthologous gene families. Protein sequences of more than 2,000 orthologous gene clusters without duplications were further aligned and a maximum likelihood tree was reconstructed based on the concatenated alignment (please see (18) for full details).

Mating experiments

To examine reproductive isolation of the isolated strains, we always performed crosses with the most closely related strains from our collection. Mating experiments were performed as previously described with some modifications (5). Three virgin females of a strain were tested with 6 males of another strain on a mating plate that contained a small amount of *E. coli* OP50 bacteria. All crosses were performed reciprocally and in quadruplicate. To test for the production of viable F1 hybrids, crosses were set up between all possible pairs and F1 hybrids were tested for their ability to produce F2 progeny. We considered strains to belong to the same species if they produced viable and fertile offspring.

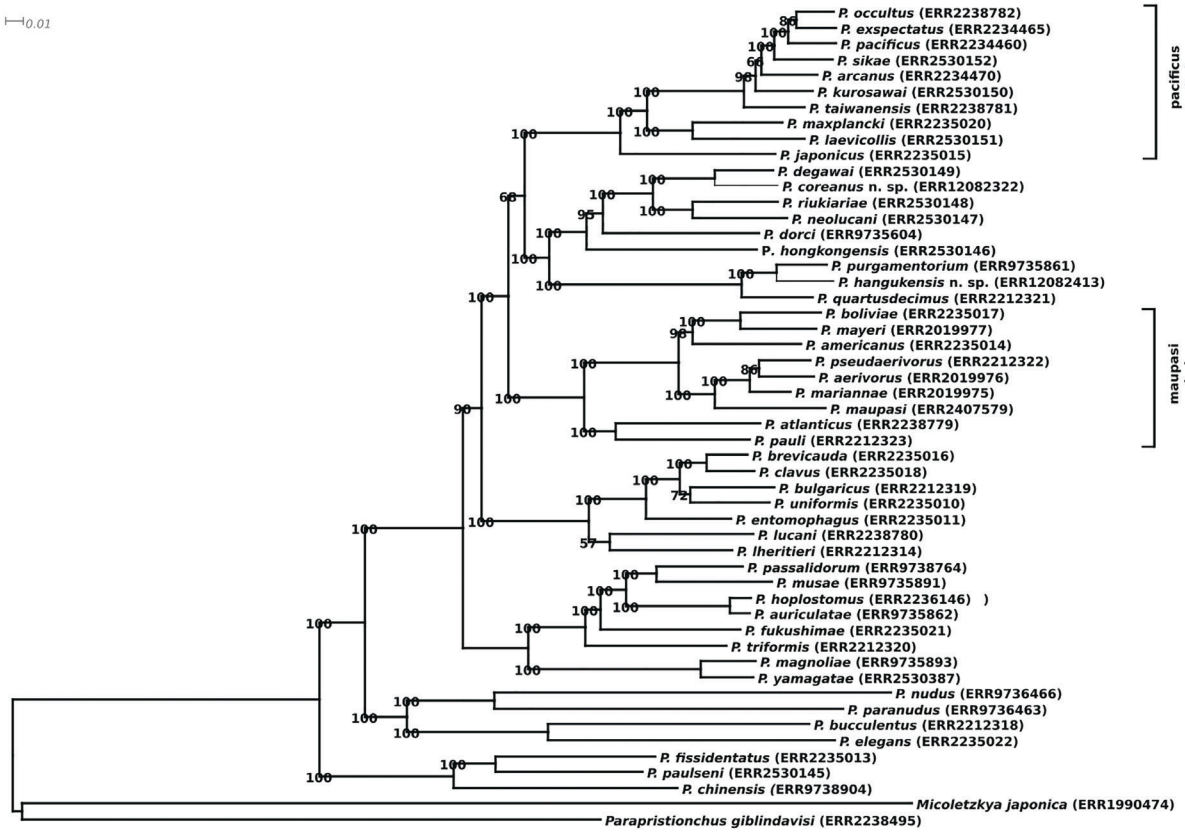


Figure 1: Molecular phylogeny of *Pristionchus* species. The phylogeny shows a maximum likelihood tree that was inferred from a concatenated alignments of more than 1200 orthologous gene clusters. Branch lengths reflect the estimated number of amino acid substitutions per site and branch labels show bootstrap support values (100 pseudoreplicates). The accession numbers next to the species names denote the Run accession in the European nucleotide Archive, where the raw RNA-seq reads were deposited.

Results

Molecular profiles and phylogeny

(Fig. 1).

Description

Description of common characters

Most *Pristionchus* species, except for some basal clades and fig-associates, are typologically similar to each other and generally distinguished based on stomatal and male tail characters. Therefore, the general morphology is described first as common characters for the two new species, and subsequently the distinctive characters are described for each species.

Adult

The body was cylindrical, stout, and the cuticle was thick, with fine annulation and clear longitudinal striations. Lateral field consisted of two lines, only weakly distinguishable from body striation with the presence of deirid. Head was without apparent lips, and with six short and papilliform labial sensillae; four small, papilliform cephalic papillae were present in males. Amphidial apertures located on the lateral sector, slightly dorsally shifted, at the level of margin of cheilo- and gymnostom. Detailed stomatal morphology is described below for each species. The dorsal pharyngeal gland was clearly observed, penetrating dorsal tooth to gland opening. Anterior part of pharynx (=pro and metacorpus) was 1.5 times as long as posterior part (=isthmus and basal bulb); the procorpus very muscular and

stout, occupying half to two-thirds of corresponding body diameter; the metacorpus was very muscular, forming a well-developed median bulb; isthmus was narrow, not muscular; basal bulb was glandular. Pharyngo-intestinal junction was clearly observed and well developed. Nerve ring usually surrounded middle region of isthmus; excretory pore was not conspicuous and ventrally located at level of isthmus to pharyngo-intestinal junction, the excretory duct extended anteriad and reflexed back to position of the pore. Deirid was observed laterally, located from the slightly anterior to pharyngo-intestinal junction to a half body diameter posterior to the junction. Hemizonid was not observed. Lateral glands, small pores connected to secretory cell, were present and observed on the lateral body surface, with positions inconsistent among individuals, numbering 5 to 8 for males and 9 to 13 for females. Postdeirid was at anterior part of *vas deferens* in male and the posterior part of posterior gonad in female, on the second dorsally neighboring striation to the lateral field.

Male

Body was ventrally arcuate, strongly ventrally curved at tail region when killed by heat. Testis single, ventrally located and anterior part reflexed to right side. Spermatogonia arranged in three to five rows in reflexed part, then well-developed spermatocytes arranged as three to four rows in anterior two-thirds of the main branch, then mature amoeboid spermatids arranged in multiple rows in remaining, proximal part of gonad; *vas deferens* not clearly separated from other parts of gonad. Three (two subventral and one dorsal) cloacal gland cells were observed at distal end of testis and intestine. Spicules paired, separate; spicules smoothly curved in ventral view, adjacent to each other for the distal third of their length, each smoothly tapering to pointed distal end; spicule in lateral view was smoothly ventrally arcuate, giving spicule about 100° curvature, oval manubrium was present at anterior end, lamina/calomus complex (blade) was clearly expanded slightly posterior to manubrium (*ca* 1/4 of blade length from anterior) and was then smoothly tapering to the pointed distal end. Gubernaculum conspicuous, about one-third of the spicule length, was broad anteriorly such that the dorsal wall was slightly recurved with dorsal and ventral walls separate at a 50 to 60° angle at the posterior end; the dorsal side of the gubernaculum possessing a single, membranous, anteriorly directed process and lateral pair of more sclerotized, anteriorly and obliquely ventrally directed processes. In the lateral view, the anterior half of gubernaculum was with two serial curves separated by an anteriorly and obliquely ventrally directed process, with anterior terminal curvature highly concave and almost closed, and with deep posterior curvature being one-third of the gubernaculum length; the posterior half was forming a tube-like process enveloping spicules. There was a thick cuticle around the tail region, falsely appearing as a narrow leptoderan bursa in the ventral view. Cloacal opening (co) was slit-like in the ventral view; one small, ventral, single genital papilla (vs) was on the anterior cloacal lip; nine pairs of genital papillae (v1-v7, ad, pd) and a pair of phasmids (ph) were present, and three precloacal and six postcloacal pairs. Within those pairs, three distal ventral pairs (v5, v6, and v7) and a dorsal pair (pd) were close to each other around the posterior end of tail (just anterior to the root of the spike). Anterior five pairs of papillae (v1-4 and ad) were almost equal in size and rather large and conspicuous, v7 and pd papillae were obviously smaller than the anterior five pairs, v5 and v6 were very small and sometimes difficult to observe with a light microscope. There were anterior two pairs of the ventral triplet papillae (v5 and v6) papilliform and they were borne from the socket-like base and were v7 simple or typical thorn-like in shape. The tip of v6 papillae split into two small papilla-like projections. Detailed arrangement of papillae and phasmid will be described for each species below. Tail conical, with a long spike, was about two to three cloacal body diameters (CDB) long; the bursa or bursal flap was absent.

Female

The body was relaxed or slightly ventrally arcuate when killed by heat. Gonad didelphic, amphidelphic; each gonadal system arranged from vulva/vagina as uterus, oviduct, and ovary. Anterior gonads right of intestine with uterus and oviduct extending ventrally and anteriorly on right of intestine and with a totally reflexed (=antidromous reflexion) ovary extending dorsally on left of intestine; oocytes mostly arranged in three to four rows in distal two-thirds of ovary and in double or single rows in rest of the ovary, with the distal tips of each ovary reaching the oviduct of the opposite gonad branch; the anterior end of the oviduct (=junction tissue between ovary and oviduct) consisted of rounded cells; anterior part of oviduct consisted of rounded cells, forming a simple tube; middle part of the oviduct served as spermatheca, consisting of roundish and relatively large cells. Eggs in single to multiple-cell stage or even further developed at the posterior part of the oviduct (=uterus) in young females were being composed of squared or angular

cells long enough to contain one well developed oocyte. *Receptaculum seminis* was not observed, i.e., the organ is not independent, and a part of oviduct/uterus works as the organ; vaginal glands were present but obscure; vagina was perpendicular to the body's surface, surrounded by sclerotized tissue; vulva was slightly protuberant in lateral view, pore-like in ventral view; rectum about one anal body diameter long, the intestine/rectum junction was surrounded by a well-developed sphincter muscle; three anal glands (two subventral and one dorsal) were present but not obvious; anus in the form of dome-shaped slit, posterior anal lip slightly protuberant; phasmid about one to two anal body diameters posterior to anus; tail was long, smoothly tapered, with the distal end variable from filiform to long and conical.

*Pristionchus hangukensis** n. sp. (Figs. 2–5)

**Etymology*

So far, the species has only been found in South Korea. Hanguk is the traditional and informal name for South Korea.

Measurements

See Table 1.

Stenostomatous form

Cheilostom consisted of six per- and interradial plates. Incision between plates was not always easily distinguished. Anterior end of each plate was rounded and elongated to project from the stomal opening forming a small flap. Gymnostom was short, cuticular ring-like anterior end overlapping the cheilostom internally. Stegostom separated into three subsections: pro-meso, meta and telostegostom. Pro-mesostegostom formed a weakly cuticularized indistinctive ring internally overlapping with gymnostom to connect the gymnostom and metastegostom. Metastegostom bore the conspicuous and movable triangular or flint-shaped dorsal tooth with a strongly sclerotized surface giving an appearance of an inverted V-shape in light microscopy in lateral view; the left subventral ridge was with three, minute adventitious blunt denticles on a plate, most ventral denticles were often masked by the remaining two in lateral view; pointed or blunt right subventral ridges were often with a distinct distal adventitious denticle. Because of the size difference between male and females, i.e., females generally have a larger stoma than males, tooth and denticles are larger (wider) in females than males. Telostegostom weakly sclerotized cup-like cavity connecting the stoma and pharynx.

Eurystomatous form

Cheilostom was divided into six well-distinguished per- and interradial plates. Anterior end of each plate was rounded and elongated to protrude from stomal opening and form a small flap. Gymnostom was with a thick cuticle, forming a short, ring-like tube being thicker posteriorly; and the anterior end of the gymnostom internally overlapped the posterior end of the cheilostomatal plates. Stegostom separated into three subsections: pro-meso, meta and telostegostom. Pro-mesostegostom formed a weakly cuticularized indistinctive ring internally overlapping with the gymnostom to connect the gymnostom and metastegostom. Metastegostom bore a large claw-like dorsal tooth, and large, claw-like right subventral tooth sometimes with a small indistinct extra peak on its ventral side. Left subventral sector of metastegostom bore three triangular ridges; the tip of each ridge sometimes split into two or more fine tips, and the shape varied among individuals. As in stenostomatous form, the teeth and denticles are generally larger in females than in males. The dorsal tooth and right subventral tooth were movable. Movement was not observed in the left subventral denticles. Telostegostom weakly sclerotized a cup-like cavity connecting the stoma and pharynx.

Male

Nine pairs of genital papillae and a pair of phasmid were present with an arrangement <v1, v2, v3d / v4, ad, ph, (v5, v6, v7, pd)>, where v1 located about 1-1.5 cloacal body diam. (CBD) anterior to co; v2 about 0.5 CBD anterior to co; v3d slightly (less than 1/4 CBD) posterior to v2; v4 about 1/4 CBD posterior to co, i.e., v2, v3d, co and v4 were close to each other; ad about 1 CBD posterior to co; ph immediately anterior to v5; v5–v7 forming triplet, immediately anterior to the root of tail spike; and pd around the level of or slightly posterior to v7. The distance between v1 and v2 is generally shorter than that between v2 and v4. The papillae v1, v2, v4 and ph subventral, v3d and ad lateral, v5–7 ventral, pd subdorsal in the male tail. Within nine paired papillae, v1-v4 and ad were the same size, v7 and pd were smaller than former four pairs, and v5 and v6 were smaller than v7 and ad. All nine paired genital papillae papilliform, but v5 and v6 are baring from a socket-like base, and the tip of v6 laterally split into two small tips. Tail conoid with a long spike which occupies more than 60% of the whole tail length. Bursa or bursal flap was absent.

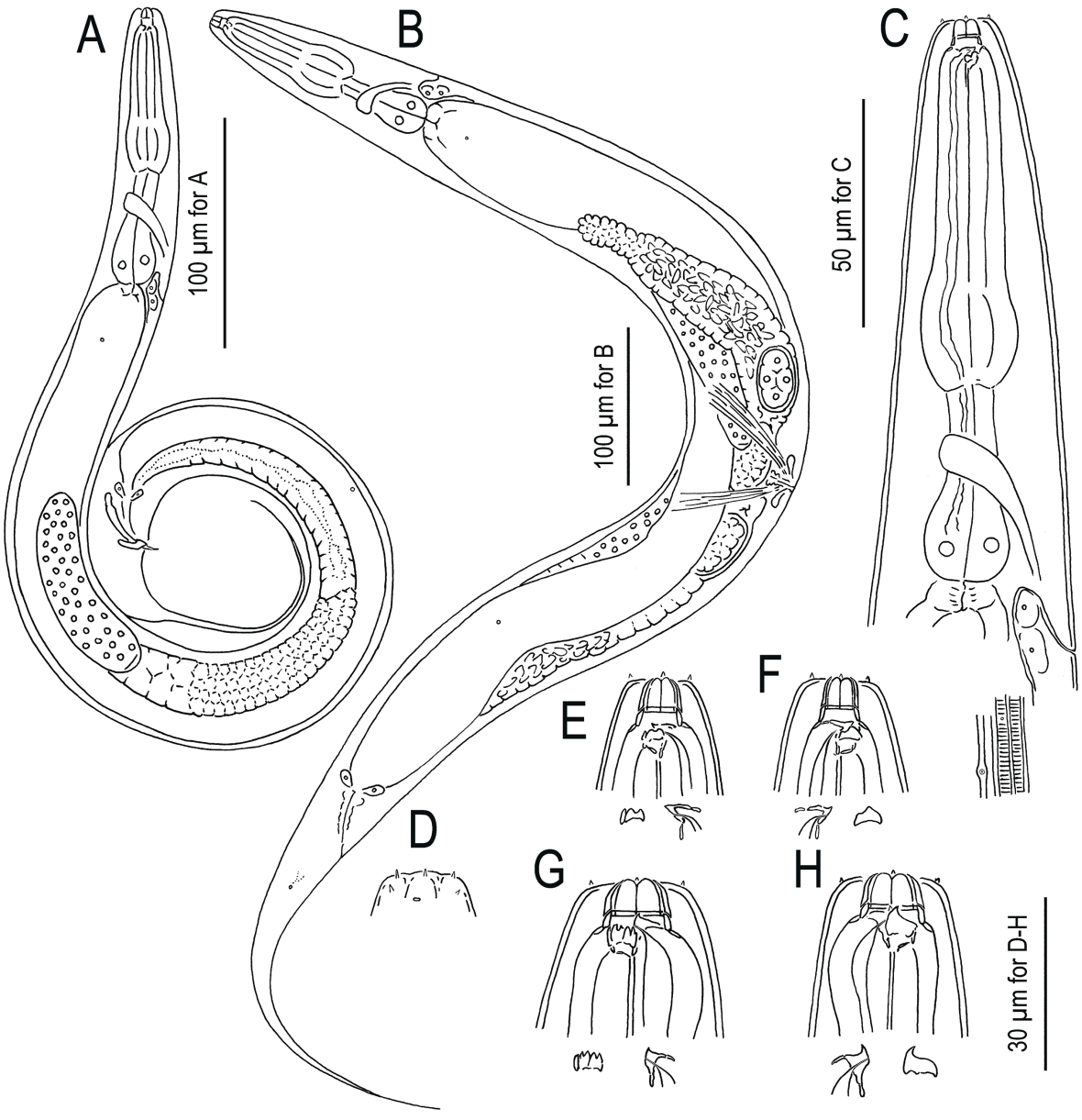


Figure 2: *Pristionchus hangukensis* n. sp. A: Male; B: Female; C: Anterior region; D: Relative position of secretory-excretory pore, deirid and one of lateral glands; E: Surface of anterior end of adult male in right lateral view showing the relative position of labial sensilla, cephalic sensilla and amphid; E, F: Male stenostomatous form in left (E) and right (F) lateral views; G, H: Male eurystomatous form in left (G) and right (H) lateral views. Tooth and denticules are separately drawn under whole head region in E-H.

Female

As described for common character.

Type host and locality

Pristionchus hangukensis RS6291 was collected from a specimen of *Dorcus titanus castanicolor* Motschulski 1861 (Coleoptera: Lucanidae) caught at a light trap at N33°15.498´E126°21.456´ on July 3rd, 2022, while eating a picknick style dinner with our Korean colleagues near "the road to contemplation" (Chusa or Kim Jeong-Hui). RS6271, another strain of this species was collected at the same location from an *Anomala* sp. (Coleoptera: Rutelidae).

Type designation and deposition

The type material was obtained from a 2-week-old culture. The samples included a holotype male (collection ID), four paratype males (collection ID) and five paratype females (collection ID) deposited at the Natural History Museum Karlsruhe, Germany, and five paratype males (collection ID) and five paratype females (collection ID) deposited at the Swedish Museum of Natural History, Stockholm, Sweden. In

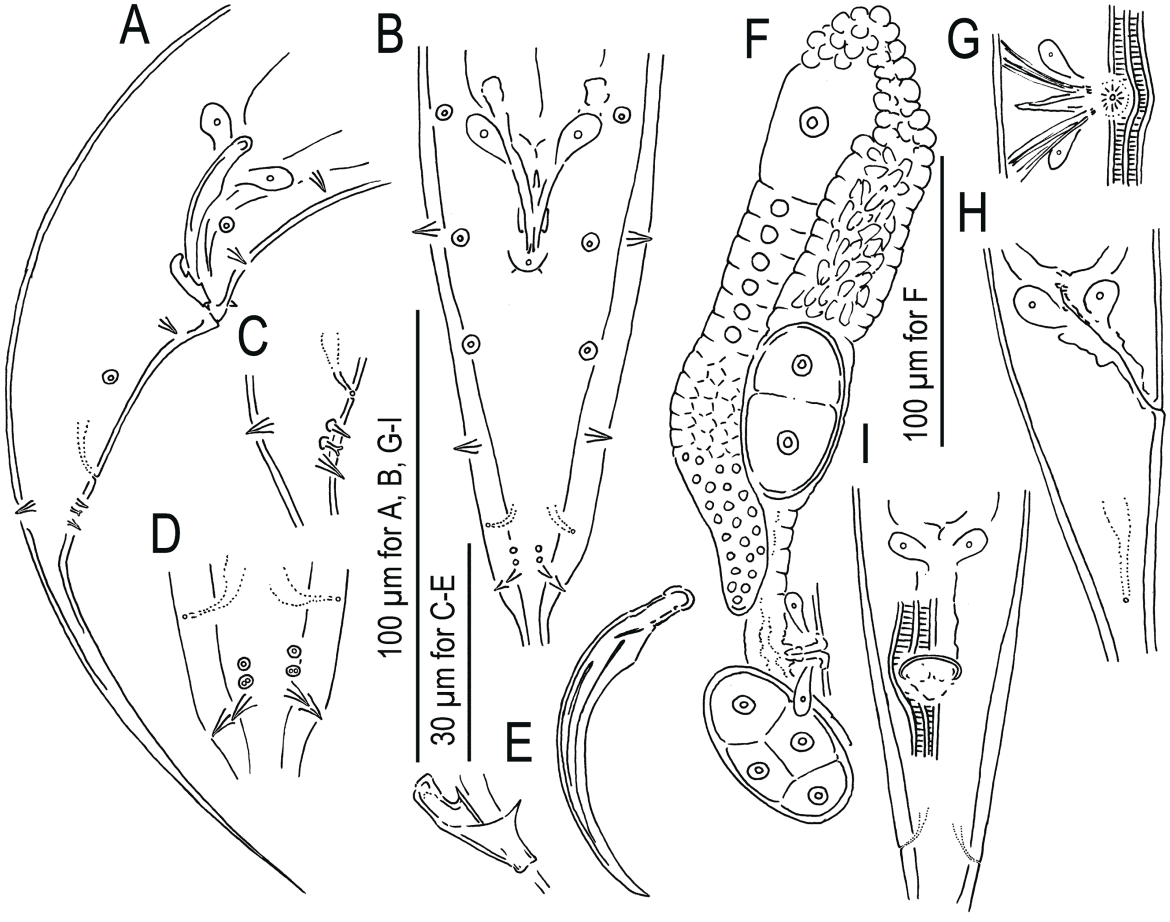


Figure 3: *Pristionchus hangukensis* n. sp. A, B: Whole male tail in right lateral (A) and ventral (B) views; C, D: Close-up of posterior four pairs of genital papillae and phasmid in right lateral (C) and ventral (D) views; E, F: Spicule and gubernaculum of two different individuals in right lateral view; G: Ventral view of female vulval region; H, I: Anal region of female in left lateral (H) and ventral (I) views.

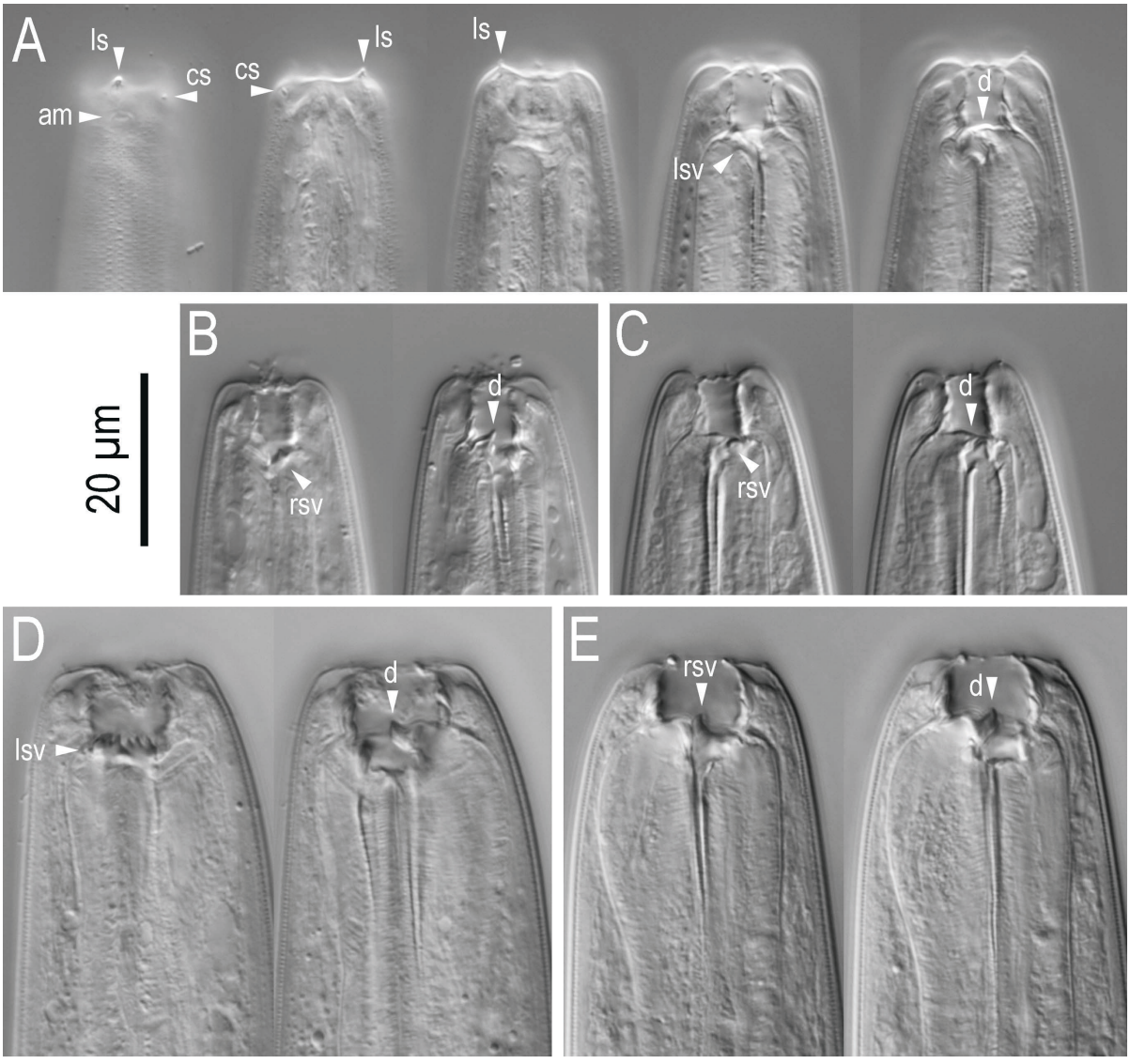


Figure 4: Stomatal region of *Pristionchus hangukensis* n. sp. showing variation among individuals. A: Surface and stoma of male in left lateral view in five different focal planes showing the relative position of labial sensilla, cephalic sensilla, amphid, left subventral ridge and dorsal tooth; B, C: Male (B) and female (C) stenostomatous form in right lateral views in two different focal planes; D, E: Female eurystomatous form in left (D) and right (E) lateral views in two different focal planes. Abbreviations are as follows: am = amphid; cs = cephalic sensilla; d = dorsal tooth; ls = labial sensilla; lsv = left subventral ridge; rsv = right subventral ridge or tooth.

addition to the type material, mass-fixed materials (fixed in TAF or processed in dehydrated glycerin) were deposited at the Max Planck Institute for BiologyTübingen, Germany.

As the strain RS6291 is also frozen in liquid nitrogen at the MPI for Biology Tübingen, it can be provided upon request as a living culture. urn:lsid:zoobank.org:act:960C79FF-D1F0-440B-B7B4-36539ECA5F86.

Differential diagnosis

Pristionchus hangukensis n. sp. is characterized by its stomatal morphology, i.e., flint-shaped dorsal tooth with or without the anteriorly directed curvature at the tip, the left subventral ridge with three blunt denticles and right subventral ridge with a small pointed or blunt denticle of the stenostomatous form; claw-like right subventral

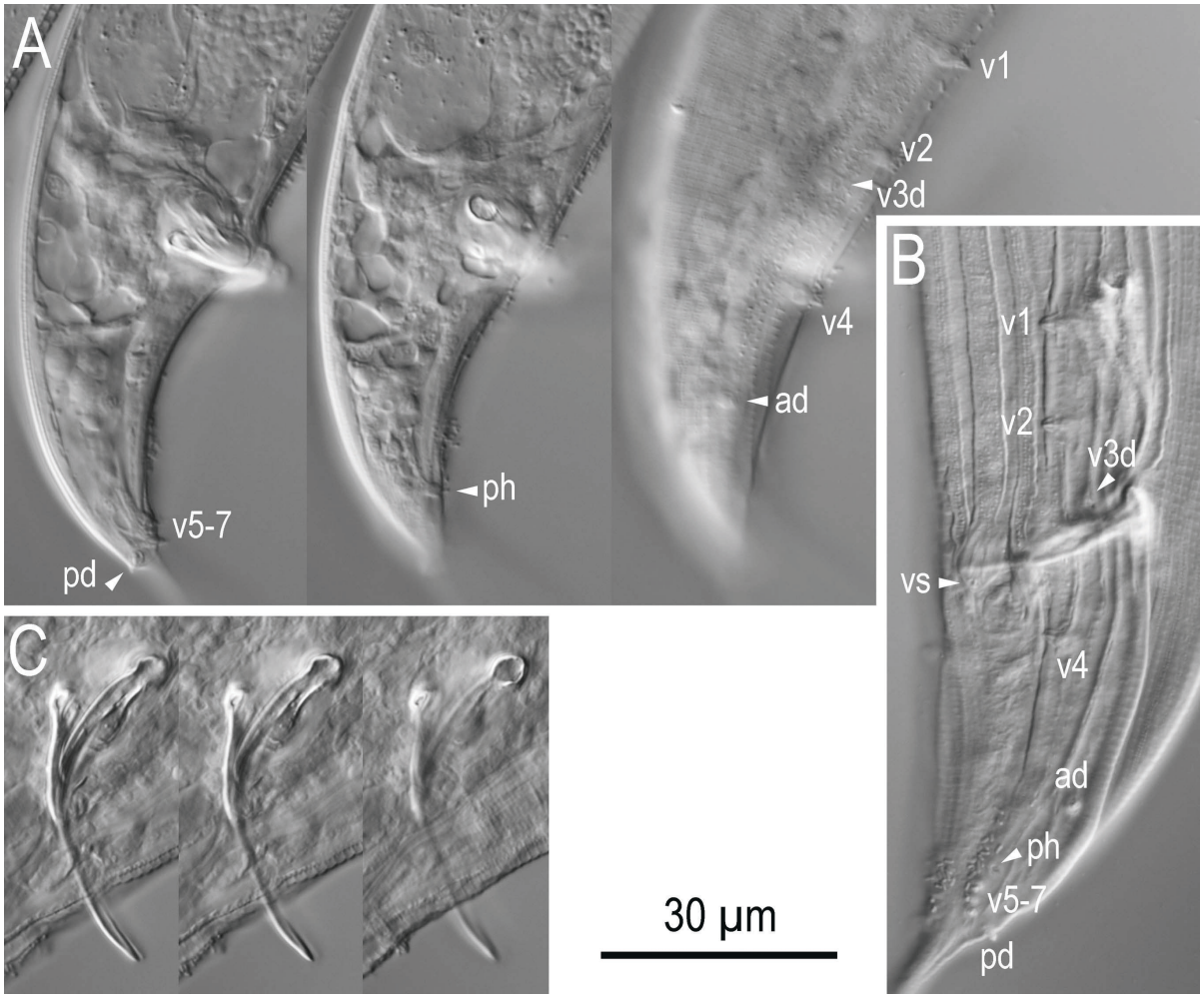


Figure 5: Male tail characters of *Pristionchus hangukensis* n. sp. A: Right lateral view of whole tail in three different focal planes; B: Left subventral view of whole tail; C: Spicule and gubernaculum in right lateral view in three focal planes. Abbreviations are as follows: ad, pd and v + number = genital papillae, where ending with 'd' suggests that the papillae are directed laterally or subdorsally; ph = phasmid; vs = ventral single papilla.

stegostomal tooth sometimes with an indistinctive extra peak, and three left subventral ridges each with two or more pointed tips in eurystomatous form, the arrangement of male genital papillae, <v1, v2, v3d / v4, ad, ph, (v5, v6, v7, pd)> where v2, v3d, co and v4 were close to each other, and ph and posterior four paired papillae formed a cluster, and distinctive and long male tail spike. *Pristionchus hangukensis* n. sp. belongs to a clade intermediate between *maupasi* and *pacificus* groups (Fig. 1), which was previously treated as a part of the *maupasi* group (13). Within the clade, *P. hangukensis* n. sp. shares its laterally directed third paired papillae with *P. hongkongensis* Kanzaki, Herrmann, Yoshida, Weiler, Rödelsperger & Sommer, 2018, *P. dorci* (13), *P. purgamentorium* (13) and *P. quartusdecimus* (11). *Pristionchus hangukensis* n. sp. is readily distinguished from *P. hongkongensis* by its whole stomatal shape of the eurystomatous form, regular *pacificus* group-like barrel-shaped stoma *vs* extremely well-developed wide barrel-shaped stoma similar to that of the *triformis* group (12). *Pristionchus hangukensis* n. sp. is distinguished from *P. dorci* by the stomatal elements in the eurystomatous form, i.e., each of the three left subventral ridges with two or more tips *vs* one or two tips, and right subventral tooth with *vs* without indistinctive peak on the ventral side (13). *Pristionchus hangukensis* n. sp. is phylogenetically close to *P. purgamentorium* and *P.*

Table 1: Morphological measurements of the two new species.

Character	*Pristionchus coreanus* n.sp. RS6268		*Pristionchus hangukensis* n.sp. RS6291	
	stenostomatous male	stenostomatous female	stenostomatous male	stenostomatous female
n	10	10	10	10
L	1002 ± 94.3 (872 - 1158)	1448 ± 126.0 (1312 - 1661)	928 ± 54.8 (858 - 1001)	1336 ± 90.2 (1248 - 1542)
L'	851 ± 93.3 (721 - 1025)	1211 ± 120.4 (1067 - 1442)	764 ± 41.0 (685 - 820)	1078 ± 76.5 (993 - 1249)
a	13 ± 2.2 (9.1 - 16)	12 ± 1.5 (11 - 16)	13 ± 1.3 (11 - 16)	13 ± 0.7 (11 - 14)
b	6.0 ± 0.4 (5.5 - 6.7)	7.6 ± 0.5 (6.8 - 8.4)	7.0 ± 0.4 (6.5 - 7.6)	9.0 ± 0.7 (8.0 - 10.0)
c	6.7 ± 0.9 (5.7 - 8.5)	6.1 ± 0.5 (5.4 - 7.1)	5.8 ± 0.4 (5.3 - 6.6)	5.3 ± 0.5 (4.9 - 6.3)
c'	3.4 ± 0.5 (2.5 - 4.0)	4.4 ± 0.6 (3.8 - 5.5)	4.4 ± 0.5 (3.9 - 5.3)	6.4 ± 0.6 (5.5 - 7.7)
Ant. stoma length (cheilo- + gymnostom)	5.1 ± 0.8 (4.0 - 6.7)	5.7 ± 1.4 (4.0 - 7.8)	6.9 ± 1.1 (5.0 - 9.3)	7.7 ± 0.7 (6.7 - 9.1)
Total stoma length	11 ± 1.0 (9.3 - 12)	12 ± 1.1 (11 - 14)	10 ± 1.1 (8.3 - 11.6)	13 ± 1.0 (11 - 14)
Stoma width	5.8 ± 0.4 (5.3 - 6.5)	7.5 ± 0.9 (6.0 - 8.7)	4.9 ± 0.9 (3.6 - 6.5)	5.4 ± 0.9 (4.3 - 7.5)
Ant. pharynx (pro + metacorpus)	95 ± 7.6 (83 - 111)	109 ± 8.2 (99 - 130)	69 ± 5.6 (63 - 82)	79 ± 6.0 (72 - 89)
Post. pharynx (isthmus + basal bulb)	67 ± 7.0 (56 - 78)	77 ± 5.1 (69 - 87)	57 ± 2.9 (54 - 61)	61 ± 3.6 (55 - 66)
Total pharynx length	162 ± 13.6 (142 - 183)	186 ± 12.1 (176 - 217)	126 ± 7.6 (120 - 143)	140 ± 7.4 (131 - 152)
Ant./total pharynx %	59 ± 1.7 (57 - 62)	58 ± 1.5 (56 - 62)	55 ± 1.6 (52 - 57)	57 ± 2.2 (54 - 60)
Median bulb diameter	27 ± 2.5 (24 - 32)	35 ± 2.9 (31 - 40)	23 ± 1.2 (21 - 24)	27 ± 2.0 (25 - 31)
Terminal bulb diameter	28 ± 3.9 (22 - 36)	36 ± 4.9 (31 - 46)	22 ± 1.1 (20 - 23)	27 ± 2.3 (24 - 33)
Ant. end to cardia	167 ± 13.2 (151 - 191)	192 ± 8.8 (185 - 212)	132 ± 8.4 (123 - 148)	148 ± 7.5 (139 - 160)
Ant. end to S-E pore	149 ± 15.5 (125 - 170)	195 ± 15.5 (171 - 214)	114 ± 11.3 (99 - 139)	153 ± 12.0 (137 - 172)
Ant. end to nerve ring	118 ± 9.2 (109 - 133)	136 ± 8.9 (124 - 155)	97 ± 6.2 (90 - 108)	111 ± 6.5 (104 - 124)
Testis length	703 ± 83.8 (571 - 827)	-	630 ± 59.4 (529 - 718)	-
Ant. end to vulva distance	-	691 ± 66.1 (600 - 821)	-	608 ± 40.2 (563 - 703)
Vulva to anus distance	-	525 ± 60.0 (454 - 628)	-	473 ± 37.3 (420 - 543)
T or V	70 ± 4.3 (66 - 80)	48 ± 1.5 (46 - 50)	68 ± 6.7 (53 - 77)	46 ± 1.1 (43 - 47)
Max. body diameter	78 ± 19.1 (63 - 127)	121 ± 16.4 (91 - 141)	71 ± 5.1 (64 - 81)	105 ± 8.1 (93 - 115)
Cloacal or anal body diameter	45 ± 5.3 (40 - 54)	54 ± 5.3 (43 - 63)	36 ± 2.2 (33 - 39)	39 ± 3.5 (33 - 45)
Tail length	149 ± 10.8 (129 - 161)	237 ± 23.7 (208 - 296)	159 ± 13.9 (132 - 178)	252 ± 27.0 (204 - 297)
Spicule curve	50 ± 4.3 (40 - 54)	-	46 ± 2.3 (43 - 50)	-
Spicule chord	42 ± 2.9 (36 - 47)	-	38 ± 2.6 (35 - 43)	-
Gubernaculum length	18 ± 2.4 (13 - 21)	-	18 ± 1.6 (16-22)	-

quartusdecimus. However, the new species can be distinguished from *P. purgamentorium* by the right subventral ridge of stenostomatous form with single *vs* multiple peak(s), and from *P. quartusdecimus* by the left subventral ridges of the eurystomatous form, each split into two or more vs one or two small denticles (11,13).

In mating tests, *P. hangukensis* RS6291 was crossed with the *P. purgamentorium* strain RS6138 and also with strain RS6271. Crosses with *P. purgamentorium* RS6138 did not result in offspring while crosses between the strains RS6271 and RS6291 resulted in fertile offspring. Therefore, we consider both RS6291 and RS6271 to be members of one species, described here as *P. hangukensis* n. sp.

The 1616bp fragment of the 18S-SSU (GenBank accession) matches to 99% (1608/1614) with *Pristionchus quartusdecimus* and to 99% (1586/1589) with *P. purgamentorium*.

Remarks

Phylogenetically, *P. hangukensis* n. sp. belongs to either an intermediate clade between the *maupasi* and *pacificus* groups, or an independent small clade consisting of *P. hangukensis* n. sp., *P. purgamentorium* and *P. quartusdecimus* (Fig. 1). Further sampling may yield additional phylogenetically close relatives to expand this clade. These three species share a characteristic arrangement of male genital papillae, where the third pair is directed laterally (v3d). As previously noted, the character is found at the basal position of several subclades in the genus, and seemingly the same transition from v3d to v2d occurred independently several times. Further biological examination of these species may reveal the evolutionary and ecological significance of the arrangement of the genital papillae.

*Pristionchus coreanus** n. sp. (Figs. 6–10)

* *Etymology*

The species is named after the country of origin.

Measurements

See Table 1.

Stenostomatous form

Cheilostom consisted of six per- and interradial plates. Incision between plates was not always easily distinguished. The anterior end of each plate was rounded and elongated to project from stomal opening and form a small flap. Gymnostom was short, with a cuticular ring-like anterior end overlapping the cheilostom internally. Stegostom was separated into three subsections: pro-meso, meta and telostegostom. Pro-mesostegostom formed a weakly cuticularized indistinctive ring internally overlapping with the gymnostom to connect the gymnostom and metastegostom. Metastegostom bore the conspicuous and movable triangular dorsal tooth with strongly a sclerotized surface giving an appearance of an inverted V-shape in light microscopy in lateral view, the anterior end of the tooth anteriorly curved to form a somewhat claw-like shape; the left subventral ridge was with three adventitious blunt denticles on a plate, most ventral denticles were often masked by the remaining two in lateral view; the pointed or blunt right subventral ridge was often with a distinct distal adventitious denticle. Because of the size difference between males and females, i.e., females generally have a larger stoma than males, tooth and denticles are larger (wider) in females than in males. Whole length-width ratio of the stoma varies among individuals, and relatively small individuals from starved culture tend to have wider stoma. Telostegostom weakly sclerotized a cup-like cavity connecting stoma and pharynx.

Eurystomatous form

Not found in regular and induced cultures.

Male

Nine pairs of genital papillae and a pair of phasmid were present with an arrangement <v1, (v2d, v3) / v4, ad, ph, (v5, v6, v7, pd)>, where v1 located about 1-1.5 cloacal body diam. (CBD) anterior to co; v2d less than 1/2 CBD anterior to co; v3 slightly (less than 1/4 CBD) posterior to v2; v4 1/4-1/2 CBD posterior to co, i.e., v2, v3d, co and v4 were close to each other; ad about 1 CBD posterior to co; ph immediately anterior to v5; v5–v7 forming triplet, immediately anterior to the root of tail spike; and pd was around the level of triplet, i.e., the v5-v7 and pd were overlapping each other. The distance between v1 and v2 is generally longer than that between v2 and v4. The papillae v1, v2, v4 and ph subventral, v3d and ad lateral, v5–7 ventral, pd subdorsal in the male tail. Within nine paired papillae, v1-v4 and ad were the same size, v7 and pd were smaller than former four pairs, and v5 and v6 were smaller than v7 and ad. All nine paired genital papillae papilliform, but v5 and v6 are baring from the socket-like base, and the tip of v6 laterally split into two small tips. Tail conoid was with a long

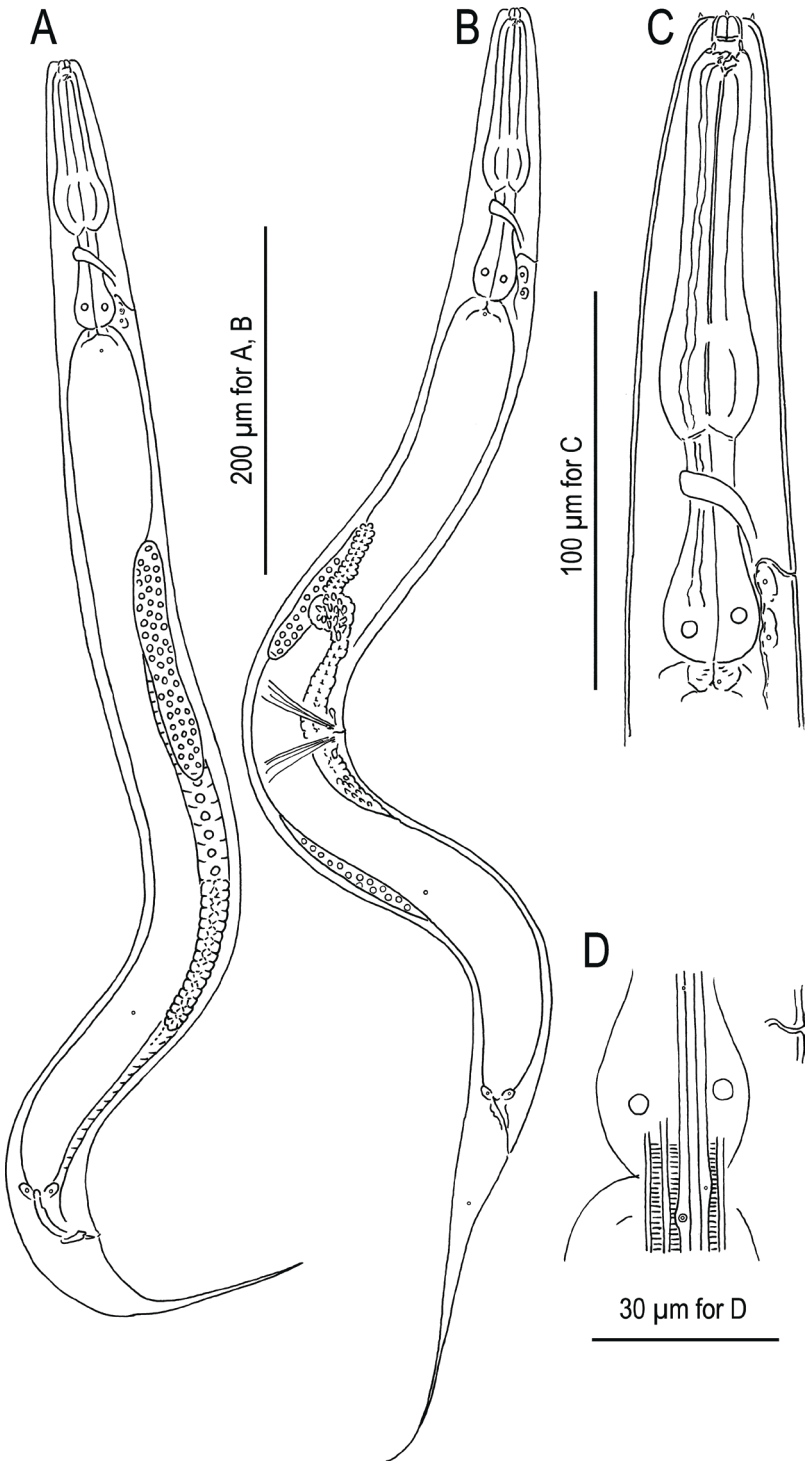


Figure 6: *Pristionchus coreanus* n. sp. A: Male; B: Female; C: Anterior region; D: Relative position of secretory-excretory pore, deirid, and two lateral glands on the lateral field.

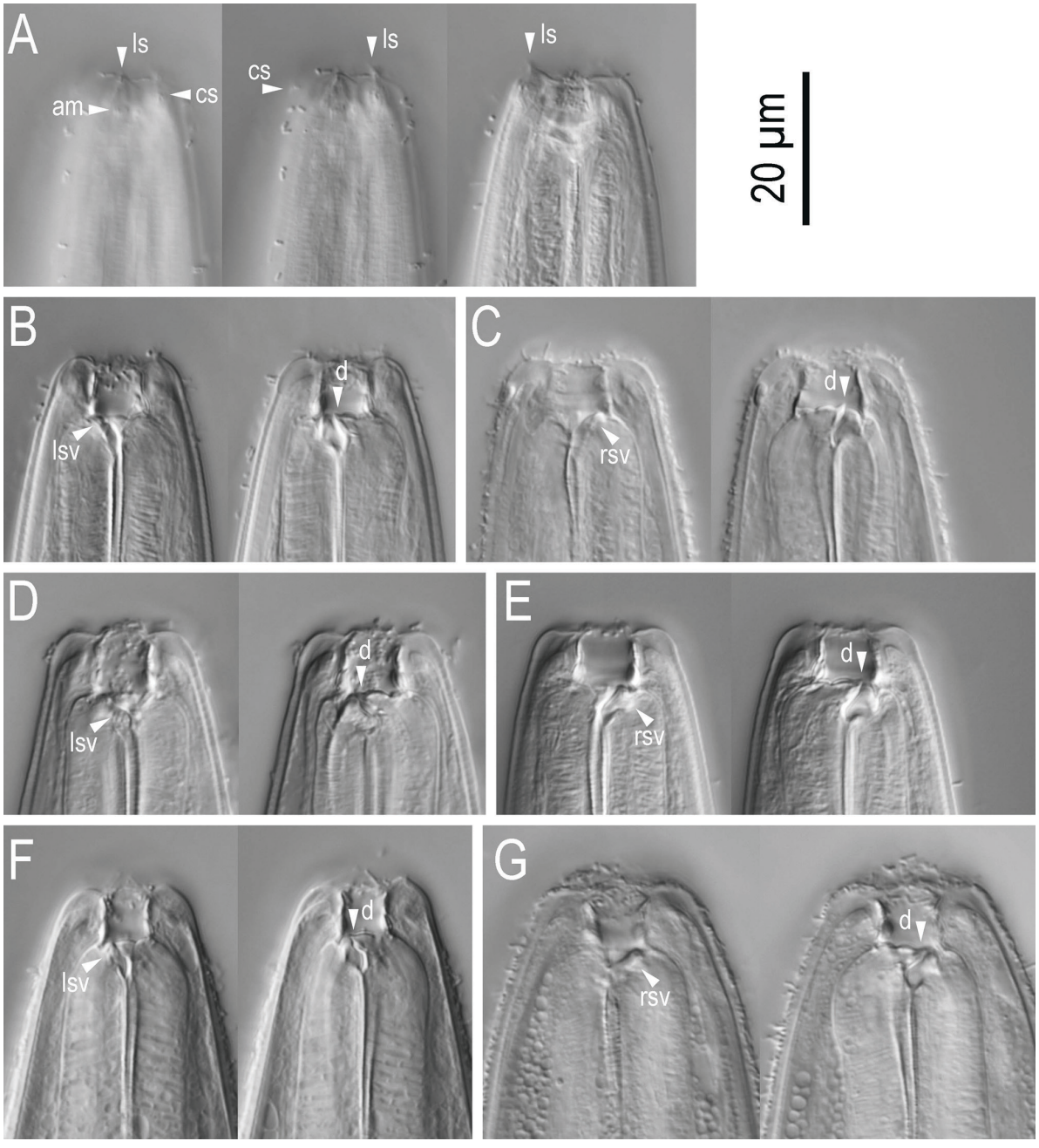


Figure 7: Stomatal region of *Pristionchus coreanus* n. sp. showing variation among individuals. A: Surface of anterior end of adult male in right lateral view showing the relative position of labial sensilla, cephalic sensilla and amphid; B, C: Male stenostomatous form starved culture in left (B) and right (C) lateral views; D, E: Female stenostomatous form from starved culture in left (D) and right (E) lateral views; F, G: Female stenostomatous form from well-fed culture in left (F) and right (G) lateral views. Tooth and denticules are separately drawn under whole head region in B-G.

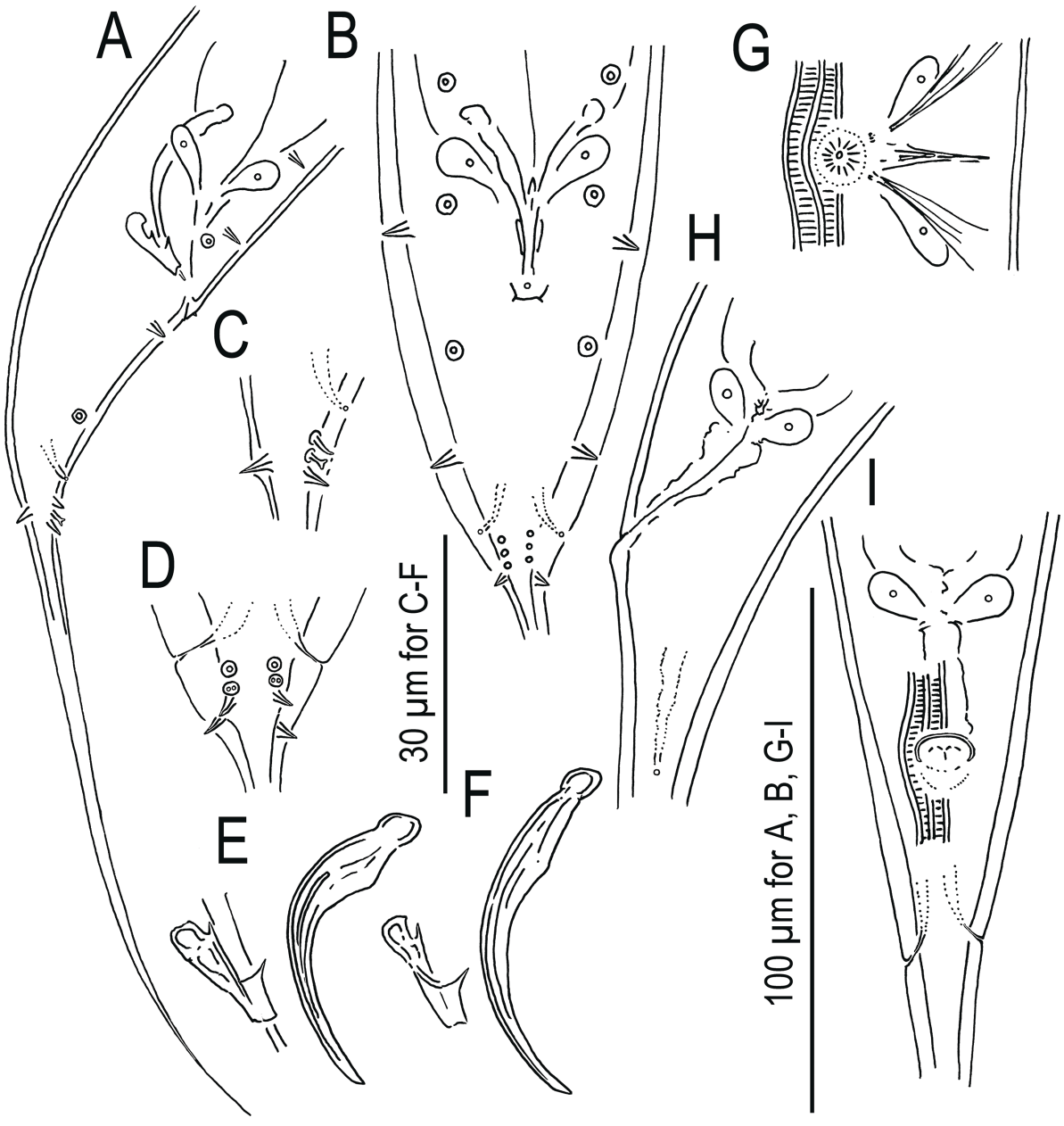


Figure 8: *Pristionchus coreanus* n. sp. A, B: Whole male tail in right lateral (A) and ventral (B) views; C, D: Close-up of posterior four pairs of genital papillae and phasmid in right lateral (C) and ventral (D) views; E: Spicule and gubernaculum in right lateral view; F: Anterior gonad of mature female in right lateral view; G: Ventral view of female vulval region; H, I: Anal region of female in right lateral (H) and ventral (I) views.

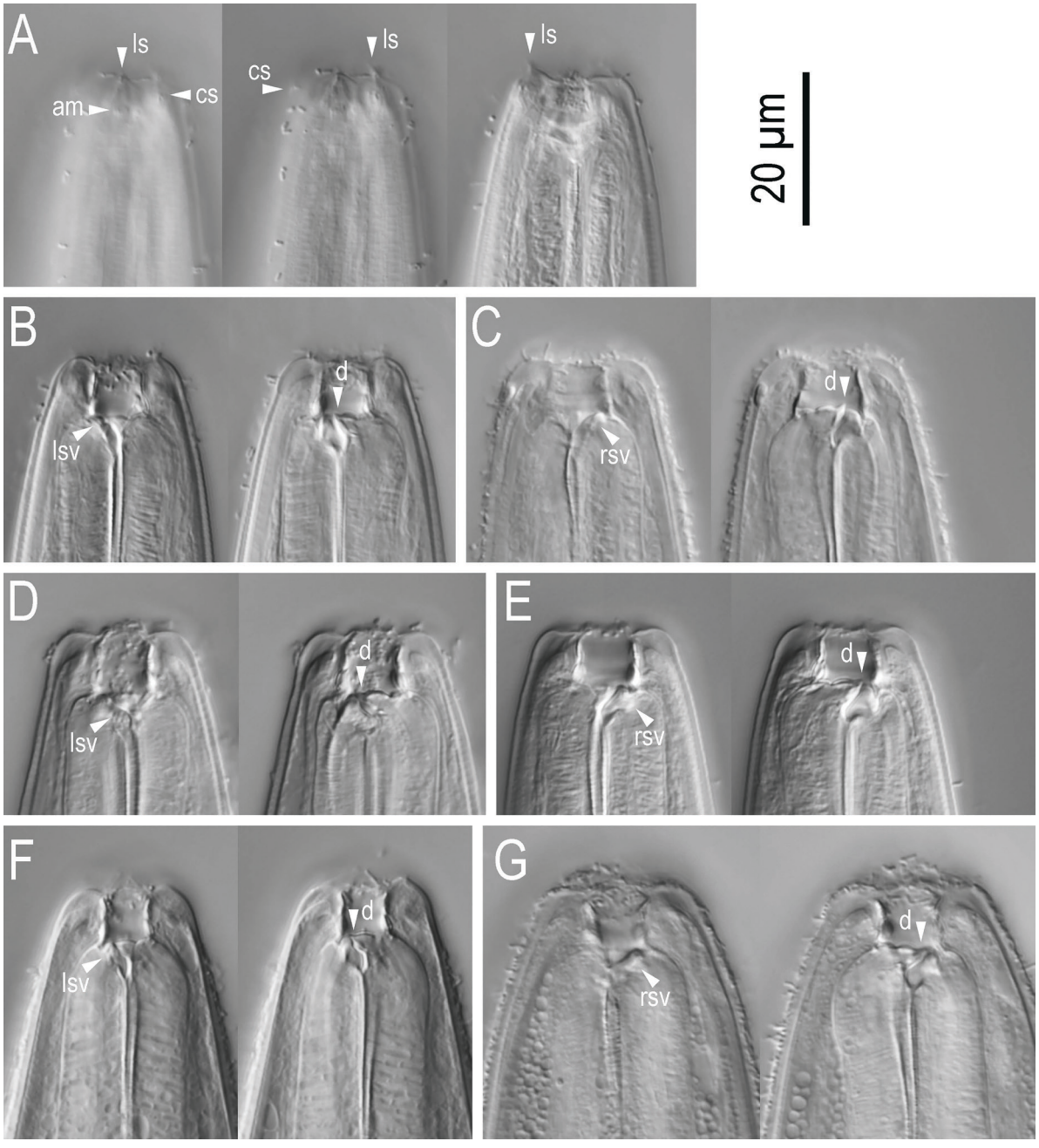


Figure 9: Stomatal region of stenostomatous form of *Pristionchus coreanus* n. sp. showing variation among individuals. A: Surface and stoma of male in left lateral view in three different focal planes showing the relative position of labial sensilla, cephalic sensilla and amphid; B: Left lateral view of male from well-fed culture in two different focal planes; C: Right lateral view of male from starved culture in two different focal planes; D: Left lateral view of female from starved culture in two different focal planes; E: Right lateral view of female from starved culture in two different focal planes; F: Left lateral view of female from well-fed culture in two different focal planes; G: Right lateral view of female from well-fed culture in two different focal planes. Abbreviations are as follows: am = amphid; cs = cephalic sensilla; d = dorsal tooth; ls = labial sensilla; lsv = left subventral ridge; rsv = right subventral ridge or tooth.

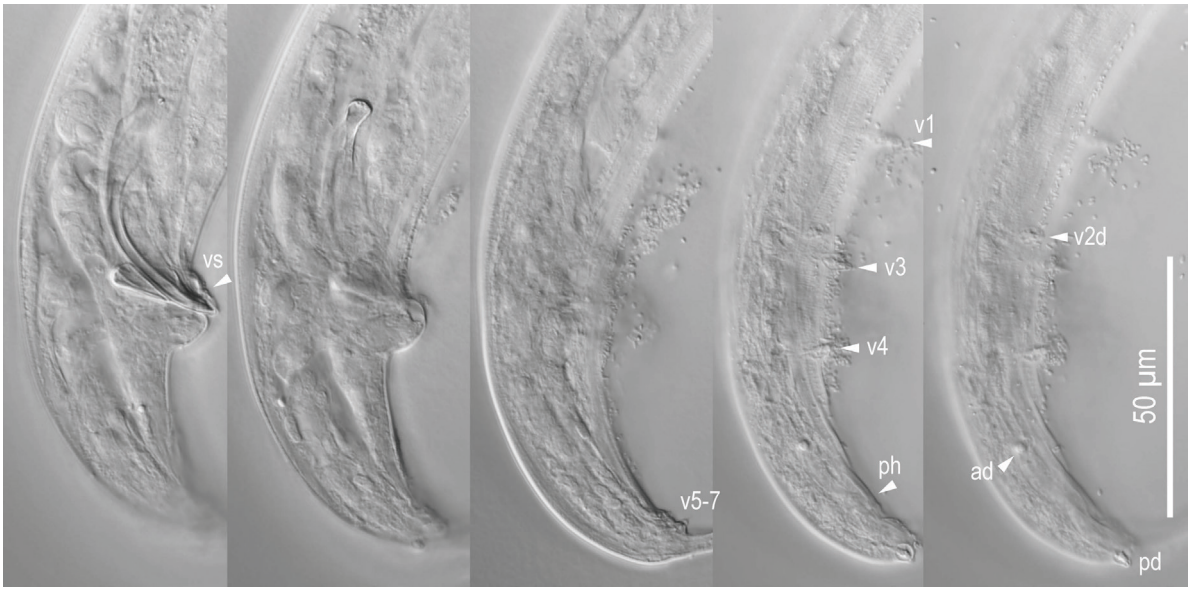


Figure 10: Male tail characters of *Pristionchus coreanus* n. sp. Right lateral view of whole male tail in five different focal planes. Abbreviations are as follows: ad, pd and v + number = genital papillae where ending with 'd' suggests that the papillae are directed laterally or subdorsally; ph = phasmid; vs = ventral single papilla.

spike which occupied more than half of the whole tail length. Bursa or bursal flap was absent.

Female

As described for common character.

Type host and locality

Pristionchus coreanus n. sp., type strain RS6268 was isolated from *Lasiopsis sahlbergi* (16), (Coleoptera: Melolonthidae) collected close to the Georin Saseum Observatory bus stop (N33°18.446´E126°27.284´) on July 2nd, 2022. The strain RS6267 originated from the same beetle specimen.

Type designation and deposition

The type material was obtained from a 2-week-old culture. The samples included a holotype male (collection ID), four paratype males (collection ID) and five paratype females (collection ID) were deposited at the Natural History Museum Karlsruhe, Germany, and five paratype males (collection ID) and five paratype females (collection ID) were deposited at the Swedish Museum of Natural History, Stockholm, Sweden. In addition to the type material, mass-fixed materials (fixed in TAF or processed in dehydrated glycerin) were deposited at the Max Planck Institute for Biology Tübingen, Germany.

As the strain RS6268 is also frozen in liquid nitrogen at the MPI for Biology Tübingen, it can be provided upon request as a living culture. urn:lsid:zoobank.org:act:79BB22D3-2D25-401B-803B-69594562F3CF.

Differential diagnosis

Pristionchus coreanus n. sp. is characterized by its stomatal morphology of the stenostomatous form, i.e., the left subventral ridge composed by three bump-like denticles, right subventral ridge with a single or blunt peak, and a flint-shaped dorsal tooth with conspicuous anterior curvature, and the arrangement of male genital papillae, <v1, (v2d, v3) / v4, ad, ph, (v5, v6, v7, pd)>. In addition, rather high intraspecific variation of stomatal morphology and the absence of the eurystomatous form can be noted as its diagnostic characters. *Pristionchus coreanus* n. sp. belongs to a clade intermediate between *maupasi* and *pacificus* groups (Fig. 1), which was previously treated as a part of the *maupasi* group (13). Within the clade, *P. coreanus* n. sp. shares the arrangement of male genital papillae, where the second pair is directed laterally (v2d), with *P. degawai* (12) *P. riukiariae* (12) and *P. neolucani* (12).

However, *P. coreanus* n. sp. is distinguished from *P. degawai* by the arrangement of genital papillae, v2d and v3 were close to each other by clearly separate vs very close to each other and sometimes overlapping; from *P. riukiariae* by the right subventral ridge of the stenostomatous form possessed a single pointed or blunt peak *vs* two peaks; and from *P. neolucani* by the arrangement of male genital papillae, where v2d and v3 were close to each other in both species, but these two pairs were closer in *P. neolucani*, i.e., these two pairs were always separable in *P. coreanus* n. sp., but sometimes very close and overlapping in *P. neolucani* (12). In addition to these characters, the absence (or difficulty in occurrence) of the eurystomatous form and high intraspecific variation in the width-depth ratio of stoma in the stenostomatous form can differentiate new species from these three close relatives.

To examine reproductive isolation of *P. coreanus* with related species, we crossed the type strain RS6268 with *Pristionchus degawai* strain RS5999, which is the closest relative. As a control, we crossed RS6268 with RS6267. No viable offspring was observed in the crosses with *P. degawai* RS5999. In contrast, RS6268 mates with RS6267 in both ways and crosses always resulted in fertile offspring.

The 1619bp fragment of the 18S-SSU (GenBank accession) matches to 99% (1601/1610) with *Pristionchus neolucani* and to 99% (1596/1602) with *P. degawai*.

Discussion

This study adds two new species to the genus *Pristionchus* and indicates further variation in the number of mouth forms. While the majority of *Pristionchus* species and many other diplogastrid nematodes have two alternative mouth forms, several independent evolutionary transitions have been observed in this family. The evolution of a third morph is well documented in *Pristionchus* (i.e., *P. triformis*, 11) and was recently also described in the distant relative *Allodiplogaster sudhausi* (28). Fig-associated *Pristionchus* species were also shown to form three or even five distinct mouth morphs (26). However, the dimorphism can also be lost during evolution, a process often referred to as 'canalization' (25). In this study, we describe a new example of a *Pristionchus* species with only one mouth form. Regardless of the intensive observation of the stomatal morphology using more than 2000 individuals of *P. coreanus* n. sp. from various conditions of cultures, e.g., different food bacteria and different age (population density), the eurystomatous form was not found during the observation. However, the stomatal shape, mostly width, varied among individuals, and individuals collected from starved culture (high population density) tended to have a relatively wide stoma with a clearly curved dorsal tooth, which is somewhat intermediate between the stenostomatous and eurystomatous forms, although their carnivorous behavior was not observed. These observations suggest that the eurystomatous form of *P. coreanus* n. sp. was lost or required a special condition for induction. Similar stomatal shape can be found in *P. uniformis* (2) and *P. seladoniae* (14). The eurystomatous form is rare in *P. uniformis*, and tentatively absent in *P. seladoniae*, and their stenostomatous form has clearly curved, large and an anteriorly directed dorsal tooth (2,14, Kanzaki, unpubl. obs.). Considering their apartness in the *Pristionchus* phylogeny (14) (Fig. 1), this character is likely to have occurred independently possibly according to their biological characters, e.g., preference of food and/or specified environment. In fact, *P. seladoniae* is hypothesized to inhabit a less competitive habitat, a subterranean bee nest where the necessity of the eurystomatous form is lower than in other habitats (14). Nevertheless, it might still be possible to induce the eurystomatous form of *P. coreanus* n. sp., and further culturing experiments are necessary to understand the feeding strategy of the species.

Regarding the molecular phylogeny, both new species fall into a subclade of the *pacificus* clade *sensu* (20). In 2015, this subclade included *P. pacificus*, *P. exspectatus*, *P. arcanus*, *P. maxplancki*, *P. japonicus* and *P. quartusdecimus*. Since then, nine new species were described, from Taiwan and China which expanded the *pacificus* clade *sensu stricto* and also formed a second clade around *P. quartusdecimus*. While the crown clade (*occultus* until *japonicus*) seems to be of Japanese/Taiwanese origin, the remainder has a Japanese/Chinese/Korean distribution. This fits well with the notion that the whole phylogeny of *Pristionchus* has a biogeographical pattern. The sister clade to this new *pacificus* clade *sensu lato* is a group of species that were collected in North and South America. The discovery of new *Pristionchus* species is still ongoing and seems far from saturation. With the systematic screen for new species, this project sets *Pristionchus* as an example for nematode biodiversity and we will see in the years to come how many more species this genus might include.

Acknowledgements

We would like to express our deep gratitude to our Korean colleagues from the International Parasite Resource Bank, in particular to Prof. Keesom S. Eom

and Dr. Dongmin Lee. During fieldwork and after, Prof. Tilak Chandra Nath, Dr. Hansol Park and Dr. Mohammed Mebarek Bia. Our work was supported by permits from the South Korean Government. This study was supported in part by the Grant-in-Aid for Scientific Research (B), No. 23K23953 from the Japan Society for the Promotion of Science.

Literature Cited

[1] Dieterich C, Clifton SW, Schuster L, Chinwalla A, Delehaunty K, Dinkelacker I, et al. The *Pristionchus pacificus* genome provides a unique perspective on nematode lifestyle and parasitism. Nature Genetics 2008;40:1193–1198. doi: 10.1038/ng.227

[2] Fedorko A, Stanuszek S. *Pristionchus uniformis* sp. n. (Nematoda, Rhabditida, Diplogastridae) a facultative parasite of *Leptinotarsa decemlineata* Say and *Melolontha melolontha* L. in Poland. Morphology and biology, Acta Parasitologica Polanica. 1971;19:95–112.

[3] Fonderie P, Steel H, Moens T, Bert W. Experimental induction of intraspecific morphometric variability in a single population of *Halicephalobus* cf. *gingivalis* may surpass total interspecific variability. Nematology. 2013;15:529–544. doi: 10.1163/15685411-00002699

[4] Herrmann M, Mayer WE, Sommer RJ. Nematodes of the genus *Pristionchus* are closely associated with scarab beetles and the Colorado potato beetle in Western Europe. Zoology. 2006;109:96–108. doi: 10.1016/j.zool.2006.03.001

[5] Herrmann M, Mayer WE, Sommer RJ. Sex, bugs and Haldane's rule: The nematode genus *Pristionchus* in the United States. Frontiers in Zoology. 2006;3:14. doi: 10.1186/1742-9994-3-14

[6] Herrmann M, Mayer WE, Hong RL, Kienle S, Minasaki R, Sommer RJ. The nematode *Pristionchus pacificus* (Nematoda: Diplogastridae) is associated with the Oriental beetle *Exomala orientalis* (Coleoptera: Scarabaeidae) in Japan. Zoological Science. 2007;24:883–889. doi: 10.2108/zsj.24.883

[7] Herrmann M, Weiler C, Rödelsperger C, Kanzaki N, Sommer RJ. Two new *Pristionchus* species (Nematoda: Diplogastridae) from Taiwan are part of a species-cluster representing the closest known relatives of the model organism *P. pacificus*. Zoological Studies. 2016;55:48. doi: 10.6620/ZS.2016.55-48

[8] Herrmann M, Kanzaki N, Weiler C, Yoshia K, Rödelsperger C, Sommer RJ. Two new Species of *Pristionchus* (Nematoda: Diplogastridae) include the Gonochoristic Sister Species of *P. fissidentatus*. Journal of Nematology. 2009;51:1–14.

[9] Hooper DJ. Handling, fixing, staining and mounting nematodes. In: Southey JF, editor. Methods for work with plant and soil nematodes. London: Her Majesty's Stationary Office; 1986. p. 59–80.

[10] Kanzaki N, Ragsdale EJ, Herrmann M, Mayer WE, Sommer RJ. Description of three *Pristionchus* species (Nematoda: Diplogastridae) from Japan that form a cryptic species complex with the model organism *P. pacificus*. Zoological Science. 2012;29:403–417. doi: 10.2108/zsj.29.403

[11] Kanzaki N, Ragsdale EJ, Herrmann M, Röseler W, Sommer RJ. Two new species of *Pristionchus* (Nematoda: Diplogastridae) support the biogeographic importance of Japan for the evolution of the genus *Pristionchus* and the model system *P. pacificus*. Zoological Science. 2013;30:680–692. doi: 10.2108/zsj.30.680

[12] Kanzaki N, Herrmann M, Yoshida K, Weiler C, Rödelsperger C, Sommer RJ. Samplings of millipedes in Japan and scarab beetles in Hong Kong result in five new Species of *Pristionchus* (Nematoda: Diplogastridae). Journal of Nematology. 2018;50:517–610. doi: 10.21307/jofnem-2018-044

[13] Kanzaki N, Herrmann M, Weiler C, Röseler W, Theska T, Berger J, et al. Nine new *Pristionchus* (Nematoda: Diplogastridae) species from China. Zootaxa. 2021;4943:1–66. doi: 10.11646/zootaxa.4943.1

[14] Kanzaki N, Fujimori Y, Ekino T, Degawa Y. *Pristionchus seladoniae* n. sp. (Diplogastridae) isolated from a eusocial soil-dwelling bee, *Halictus (Seladonia) aerarius*, in Nagano, Japan. Nematology. 2024 ;26:in press. doi: 10.1163/15685411-bja10326

[15] Kreis HA. Beiträge zur Kenntnis pflanzenparasitischer Nematoden. Zeitschrift für Parasitenkunde. 1932;5:184–194.

[16] Mannerheim CG. Insectes coléopteres de la Sibérie orientale, nouveaux ou peu connus. Bulletin de la Société impériale des naturalistes de Moscou. 1849;22:220–249.

[17] Motschulski V. Insectes du Japon. Études Entomologiques. 1861;10:3–24.

[18] Rödelsperger C, Röseler W, Prabh N, Yoshida K, Weiler C, Herrmann M, et al. Phylotransciptomics of *Pristionchus* nematodes reveals parallel gene loss in six hermaphroditic lineages. Current Biology. 2018;28:3123–3127. doi: 10.1016/j.cub.2018.07.041

[19] Ragsdale E, Kanzaki N, Roeseler W, Herrmann M, Sommer RJ. Three new species of *Pristionchus* (Nematoda: Diplogastridae) show morphological divergence through evolutionary intermediates of a novel feeding polymorphism. Zoological Journal of the Linnean Society. 2013;168:671–698. doi: 10.1111/zoj.12041

[20] Ragsdale EJ, Kanzaki N, Herrmann M. 2015Taxonomy and natural history: the genus *Pristionchus*. In: Sommer RJ, Hunt DJ, Perry RN, editors. *Pristionchus pacificus* - a nematode model for comparative and evolutionary biology. Nematology Monographs and Perspectives vol. 11. Leiden: Brill; 2015. p. 77–120. doi: 10.1163/9789004260306_005

[21] Schlager B, Wang X, Braach G, Sommer RJ. Molecular cloning of a dominant Roller mutant and establishment of DNA-mediated transformation in the nematode model *Pristionchus pacificus*. Genesis. 2009;47:300–304. doi: 10.1002/dvg.20499

[22] Sommer RJ, Lightfoot JW. The genus *Pristionchus*: a model for phenotypic plasticity, predatory behavior, self-recognition and other complex traits. In: Glazer I, Shapiro-Ilan D, Sternberg PW, editors. Nematodes as biological models. Wallingford: CABI Publishing; 2022. p.1–23. doi: 10.1079/9781789248814.00

[23] Sommer R J. Integrative evolutionary biology and mechanistic approaches in comparative biology. In: Sommer RJ, Hunt DJ, Perry RN, editors. *Pristionchus pacificus* - a nematode model for comparative and evolutionary biology. Nematology Monographs and Perspectives vol. 11. Leiden: Brill; 2015. p. 19–41. doi: 10.1163/9789004260306_003

[24] Sommer RJ, Carta LK, Kim SY, Sternberg PW. Morphological, genetic and molecular description of *Pristionchus pacificus* n. sp. (Nematoda: Neodiplogastridae). Fundamental and Applied Nematology. 1996;19:511–521.

[25] Susoy V, Ragsdale EJ, Kanzaki N, Sommer RJ. Rapid diversification associated with a macroevolutionary pulse of developmental plasticity. eLIFE. 2015;4:e05463.

[26] Susoy V, Herrmann M, Kanzaki N, Kruger M, Nguyen CN, Rödelsperger C, et al. Large-scale diversification without genetic isolation in nematode symbionts of figs. Science Advance. 2016;2:e1501031.

[27] Tian H, Schlager B, Xiao H, Sommer RJ. Wnt signaling by differentially expressed Wnt ligands induces vulva development in *Pristionchus pacificus*. Current Biology. 2008;18:142–146. doi: 10.1016/j.cub.2007.12.048.

[28] Wighard S, Witte H, Sommer R. Conserved switch genes that arose via whole-genome duplication regulate a cannibalistic nematode morph. Science Advances. 2024;10(15).

[29] Witte H, Moreno E, Rödelsperger C, Kim J, Kim J-S, Streit A, et al. 2015. Gene inactivation using the CRISPR/Cas9 system in the nematode *Pristionchus pacificus*. Development Genes & Evolution. 2015;225:55–62. doi: 10.1007/s00427-014-0486-8

[30] Yoshida K, Herrmann M, Kanzaki N, Weiler C, Rödelsperger C, Sommer RJ. Two new species of *Pristionchus* (Nematoda: Diplogastridae) from Taiwan and the definition of the *pacificus* species-complex *sensu stricto*. Journal of Nematology. 2018;50:355–368. doi: 10.21307/jofnem-2018-019

[31] Sommer RJ, McGaughran A. The nematode Pristionchus pacificus as a model system for integrative studies in evolutionary biology. Molecular Ecology. 2013; 22, 2380-2393.

[32] Sommer RJ. Phenotypic Plasticity: from theory and genetics to current and future challenges. Genetics. 2020; 215, 1-13.

[33] Bento G, Ogawa A, Sommer RJ. Co-option of the hormone-signalling module dafachronic acid–DAF-12 in nematode evolution. Nature. 2010; 466, 494-497.

[34] Lightfoot JW, Wilecki M, Roedelsperger C, Moreno E, Susoy V, Witte H, Sommer, RJ. Small peptide mediated self-recognition prevents cannibalism in predatory nematodes. Science. 2019; 364, 86-89. doi:10.1126/science.aav9856

[35] Lightfoot JW, Dardiry M, Kalirad A, Giaimo S, Eberhardt G, Witte H, Wilecki M, Roedelsperger C, Traulsen A, Sommer RJ. Sex or cannibalism: polyphenism and kin recognition control social action startegies in nematodes. Science Advances. 2021; 7, eabg8042.

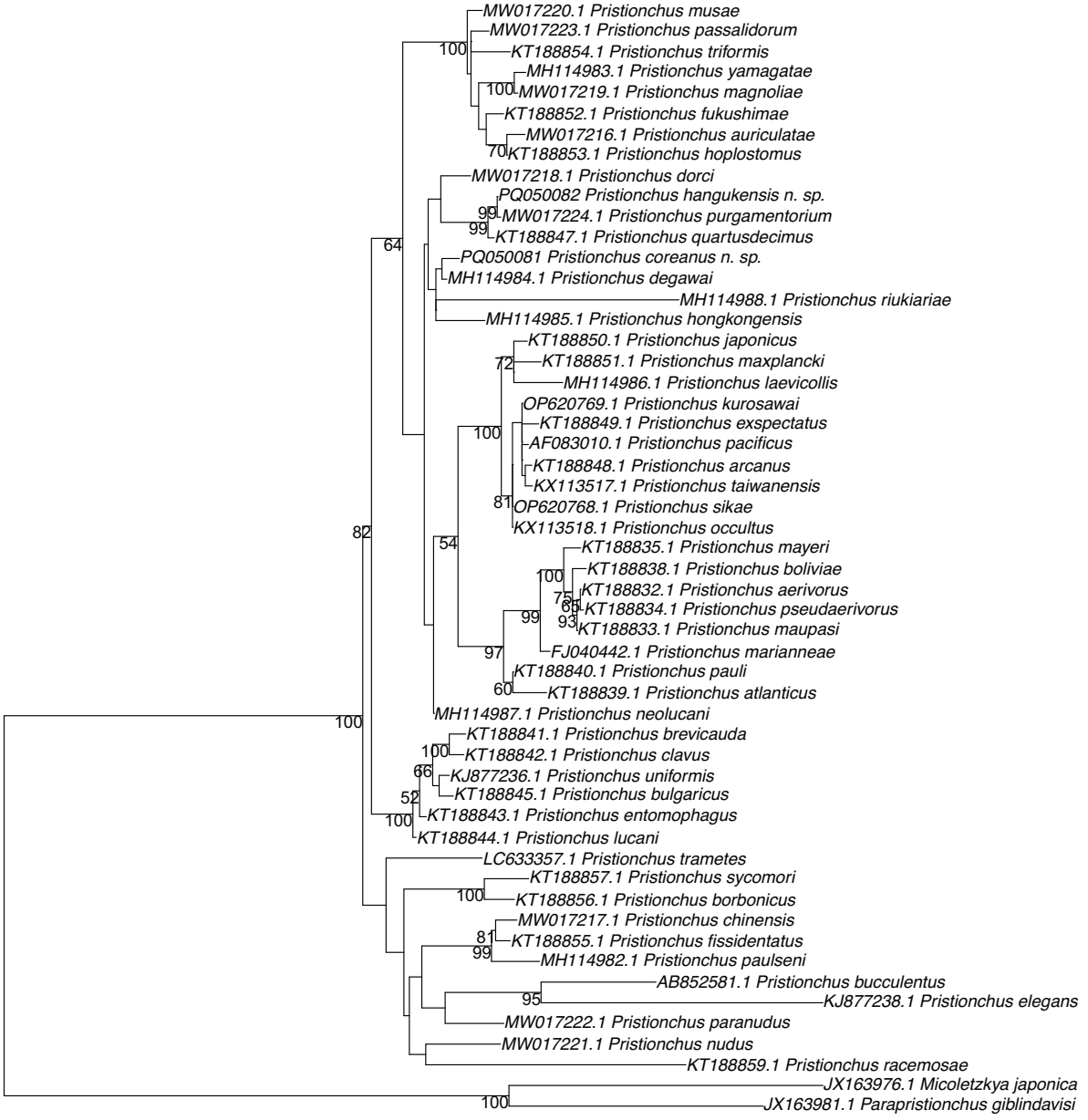
[36] Herrmann M, Kanzaki N, Weiler C, Yoshida K, Rödelsperger C, Sommer RJ. Two new Species of Pristionchus (Nematoda: Diplogastridae) include the Gonochoristic Sister Species of P. fissidentatus. J. of Nematology. 2019; 51, 1-14.

[37] Kanzaki N, Ragsdale EJ, Herrmann M, Mayer WE, Tanaka R, Sommer RJ. Parapristionchus giblindavisi n. gen., n. sp. (Rhabditida: Diplogastridae) isolated from stag beetles (Coleoptera: Lucanidae) in Japan. Nematology. 2012; 14(8), 933-947.

[38] Röseler W, Collenberg M, Yoshida K, Lanz C, Sommer RJ, Rödelsperger C. The improved genome of the nematode Parapristionchus giblindavisi provides insights into lineage-specific gene family evolution. G3 Volume 12, Issue 10, October 2022, jkac215, https://doi.org/10.1093/g3journal/jkac215

[39] Dardiry M, Piskobulu V, Kalirad A, Sommer RJ. Experimental and theoretical support for costs of plasticity and phenotype in a nematode cannibalistic trait. Evolution Letters. 2023; 7, 48-57.

Supplementary Material



Supplemental Figure 1: 18S tree for different Pristionchus species. The 18S rRNA sequences for the two new species were aligned together with their best hits from the NCBI database and a maximum likelihood tree was calculated using the phangorn package in R.

BRILL

Nematology 27 (2025) 651-663

Nematology
brill.com/nemy

Pristionchus kravanhensis n. sp., the first *Pristionchus* species reported from Cambodia

Penghieng THEAM [1], Natsumi KANZAKI [2], Matthias HERRMANN [1,*], Christian WEILER [1], Christian RÖDELSPERGER [1] and Ralf J. SOMMER [1]

[1] *Department for Evolutionary Biology, Max Planck Institute for Biology Tübingen, Max Planck Ring 9, 72076 Tübingen, Germany*

[2] *Kansai Research Center, Forestry and Forest Products Research Institute, Kyoto 612-0855, Japan*

ORCID iDs: Theam: 0000-0001-8232-6538; Kanzaki: 0000-0001-8752-1674; Herrmann: 0000-0002-4801-2524; Weiler: 0000-0002-0875-6633; Rödelsperger: 0000-0002-7905-9675; Sommer: 0000-0003-1503-7749

Received: 27 March 2025; revised: 15 May 2025
Accepted for publication: 23 May 2025; published online: 24 June 2025

Summary – A new *Pristionchus* species, *P. kravanhensis* n. sp. (Nematoda: Diplogastridae), from Cambodia is described. It was isolated from a melolonthine beetle in the Cardamom Mountains, has a gonochoristic mode of reproduction, and falls into the *triformis* group of *Pristionchus* species using a phylogeny based on orthologous proteins. *Pristionchus kravanhensis* n. sp. is sister to all other species in its group and most closely related to *P. yamagatae* and *P. magnoliae*. The new species is characterised by the arrangement of male genital papillae, ⟨v1, v2, v3d/v4, ad, ph, (v5, v6, v7, pd)⟩, where v2, v3d, co and v4 and v5, v6, v7, pd are close to each other, the distance v1-v2 is generally shorter than v2-v4, and v5-7 and pd overlap. The stomatal morphology is also used to distinguish *P. kravanhensis* n. sp. from other species in the *triformis* group. It has anteriorly split cheilostomatal plates, which rarely occur in eurystomatous form, and has only two alternative mouth forms (stenostomatous and one type of eurystomatous forms), while others have three (stenostomatous and two types of eurystomatous forms). Hence, this new species represents an interesting biological entity to study the molecular basis underlying the transition from dimorphism to triformism.

Keywords – Cardamom Mountains, Diplogastridae, molecular phylogeny, scarab beetles, Southeast Asia, *triformis* group.

The nematode genus *Pristionchus* Kreis 1932 has received detailed attention due to the establishment of *Pristionchus pacificus* Sommer, Carta, Kim and Sternberg 1996 as a model system in evolutionary developmental biology (evo-devo) and for studying developmental plasticity and related traits (Sommer *et al*., 1996; Sommer, 2015; Sommer & Lightfoot, 2022). To place *P. pacificus* in a larger phylogenetic context, we set out to collect additional *Pristionchus* species through long-term and large-scale efforts. Early studies already revealed that *Pristionchus* nematodes could be readily discovered from beetles of the superfamily Scarabaeoidea in Europe, North America and Japan (Herrmann *et al*., 2006a, b, 2007). They largely sit as dauer larvae on the beetle cuticle, waiting for the natural death of the insect to then resume development on the carcass, where they feed on microorganisms and other nematodes. This results in a complicated boom-and-bust life cycle that was also experimentally investigated (Renahan & Sommer, 2021; Renahan *et al*., 2021). Collecting beetles all over the world has resulted by now in more than 50 species of *Pristionchus*. In addition, broader beetle and insect samplings provided a higher-level phylogenetic understanding of the family Diplogastridae to which the genus *Pristionchus* belongs (Susoy *et al*., 2015). Biogeographically, Asia seems to be a hotspot for *Pristionchus* diversity as well as the origin of the genus (Kanzaki *et al*., 2021) and is also home to the sister genus *Parapristionchus* (Kanzaki *et al*., 2012a,b; Röseler *et al*., 2022). Therefore, we have focused our sampling efforts on Asian countries in the past years. Here we describe a new *Pristionchus* species from a collection trip to Cambodia.

* Corresponding author, e-mail: matthias.herrmann@tuebingen.mpg.de

Published with license by Koninklijke Brill BV | DOI: 10.1163/15685411-bja10413
© PENGHIENG THEAM ET AL., 2025 | ISSN: 1388-5545 (print) 1568-5411 (online)



Fig. 1. Host and collection site of *Pristionchus kravanhensis* n. sp. A: Phoretic host beetle, *Lepidiota discedens* Sharp, 1876; B: Collection site, *locus typicus*.

Materials and methods

Nematode collection

On an expedition to Cambodia from April 20-28, 2023, 546 beetles of the superfamily Scarabaeoidea were collected at two different locations (Thma Bang district and Kirirom National Park). These beetles were brought to our laboratory in Tübingen, Germany, alive for identification, dissection and isolation of nematodes.

Nematode isolation

All beetles were dissected and individually placed on Petri dishes with NGM agar. These plates were screened for emerging nematodes for up to 14 days. When nematodes started developing, single gravid females were transferred to new 6 cm NGM Petri dishes. Cultures arising from such single females are called isogenic female lines. A new *Pristionchus* species was isolated from one specimen of *Lepidiota discedens* Sharp, 1876 (Coleoptera: Melolonthinae) collected in Kravanh La Vallée Eco Resort, Cambodia, on 21 April, 2023 (Fig. 1). The strain RS6323 was designated as the reference strain for the new species. Another strain of the new species, originating from the same beetle specimen, is kept in our nematode collection as RS6325.

Morphological observation

Live adults of the new species from 1- to 2-week-old cultures were used for morphological observations. Morphological observations and drawings were performed using a microscope (Zeiss Axioskop) equipped with differential interference contrast optics and a drawing tube following the methods of Kanzaki *et al*. (2013). Light micrographs were taken with a microscope (Zeiss AxioImager Z1) equipped with differential interference contrast optics and a microscopic digital camera (Zeiss Axiocam 506 mono) operated by the computer software ZEN (Zeiss). The drawings and micrographs were edited to construct figures using Photoshop Elements 2020 software (Adobe).

To prepare type material, nematodes were isolated from cultures, rinsed in distilled water to remove bacteria, heat-killed at 65°C, fixed in 5% formalin, and processed through a glycerol and ethanol series using Seinhorst's

method (Hooper, 1986). Then, single specimens were mounted on microscopic slides in glycerol, surrounded by a wax ring and labelled.

Molecular characterisation and phylogenetic reconstruction

A species phylogeny of the complete *Pristionchus* genus was reconstructed as described in Rödelsperger *et al*. (2018). In brief, transcriptome libraries were generated from mixed-stage worm cultures and sequenced on an Illumina HiSeq 3000. Raw reads were assembled *de novo* and clustered into orthologous gene families. Protein sequences of gene clusters without duplications were further aligned by the MUSCLE software (version 3.8.31 with default options) (Edgar, 2004) and a maximum likelihood tree was reconstructed from the concatenated alignment with the help of the RAxML program (version 8.2.12 with -m PROTGAMMAILG -f a -N 100 options) (Stamatakis, 2014).

Mating experiments

To examine reproductive isolation of the new species with related species, we crossed the type strain RS6323 with *Pristionchus magnoliae* RS5999 and *Pristionchus yamagatae* RS5964, which are the closest relatives. Mating experiments were performed as previously described with some modifications (Herrmann *et al*., 2006b). Three virgin females of a strain were tested with six males of another strain on a mating plate that contained a small amount of *Escherichia coli* OP50 bacteria. All crosses were performed reciprocally and in quadruplicate. To test for the production of viable F1 hybrids, crosses were set up between all possible pairs and F1 hybrids were tested for their ability to produce F2 progeny. We considered strains to belong to the same species if they produced viable and fertile offspring.

Results

Molecular profiles, phylogeny and reproductive isolation

The new species is sister to all other known species of the *triformis* group of *Pristionchus*, with *P. magnoliae* and *P. yamagatae* being the closest relatives (Fig. 2).

The strains RS6323 and RS6325 belong to the new species and formed fertile offspring when mated. By contrast, no offspring was observed when RS6323 were mated with *P. magnoliae* or *P. yamagatae*.

Pristionchus kravanhensis **n. sp.**

(Figs 3-8)

Measurements

See Table 1.

Morphological description

Adults

Body cylindrical, stout, *i.e.*, body length-maximum body diam. ratio (a value) ranges from 10 to 15, depending on culture conditions; cuticle with fine annulation, clear longitudinal striations and indistinct lateral field consisting of two lines, weakly separated from the body striations by presence of deirid, and absence of clear annulations. Lip region without apparent lips, six mound-like anteriorly directed expansions, one on each sector. Six labial sensilla one on each lip sector, papilliform, and four male cephalic papillae papilliform, on each of right and left subventral and right and left dorsal lip sectors, smaller than labial sensilla. Stomatal dimorphism present; its details are described below. Dorsal pharyngeal gland clearly observed, penetrating dorsal tooth to gland opening. Anterior pharynx 1.3 times as long as posterior pharynx, muscular, composed of tube-shaped procorpus and well-developed oval-shaped metacorpus (median bulb); posterior pharynx glandular with nerve ring at mid-isthmus length. Pharyngo-intestinal junction (cardia) clearly observed, well-developed. Intestine simple tube, not forming pre-rectum, extending posteriorly from cardia to rectum; three (two subventral and one dorsal) rectal gland cells observed at distal end of intestine (margin between intestine and rectum). Secretory-excretory pore not conspicuous, ventrally located at level of isthmus to pharyngo-intestinal junction, excretory duct extending anteriad and reflexed back to position of pore; two large secretory-excretory cells around the excretory duct. Deirid observed laterally on lateral field, located at the level around the posterior end of basal bulb to pharyngo-intestinal junction to a half body diam. posterior to the junction, *ca* 0.5-1.0 body diam. posterior to secretory-excretory pore. Hemizonid not observed. Lateral glands (small pores connected to secretory cell) on lateral body surface, with positions inconsistent among individuals, numbering 5-8 for males and 9-13 for females. Postdeirid

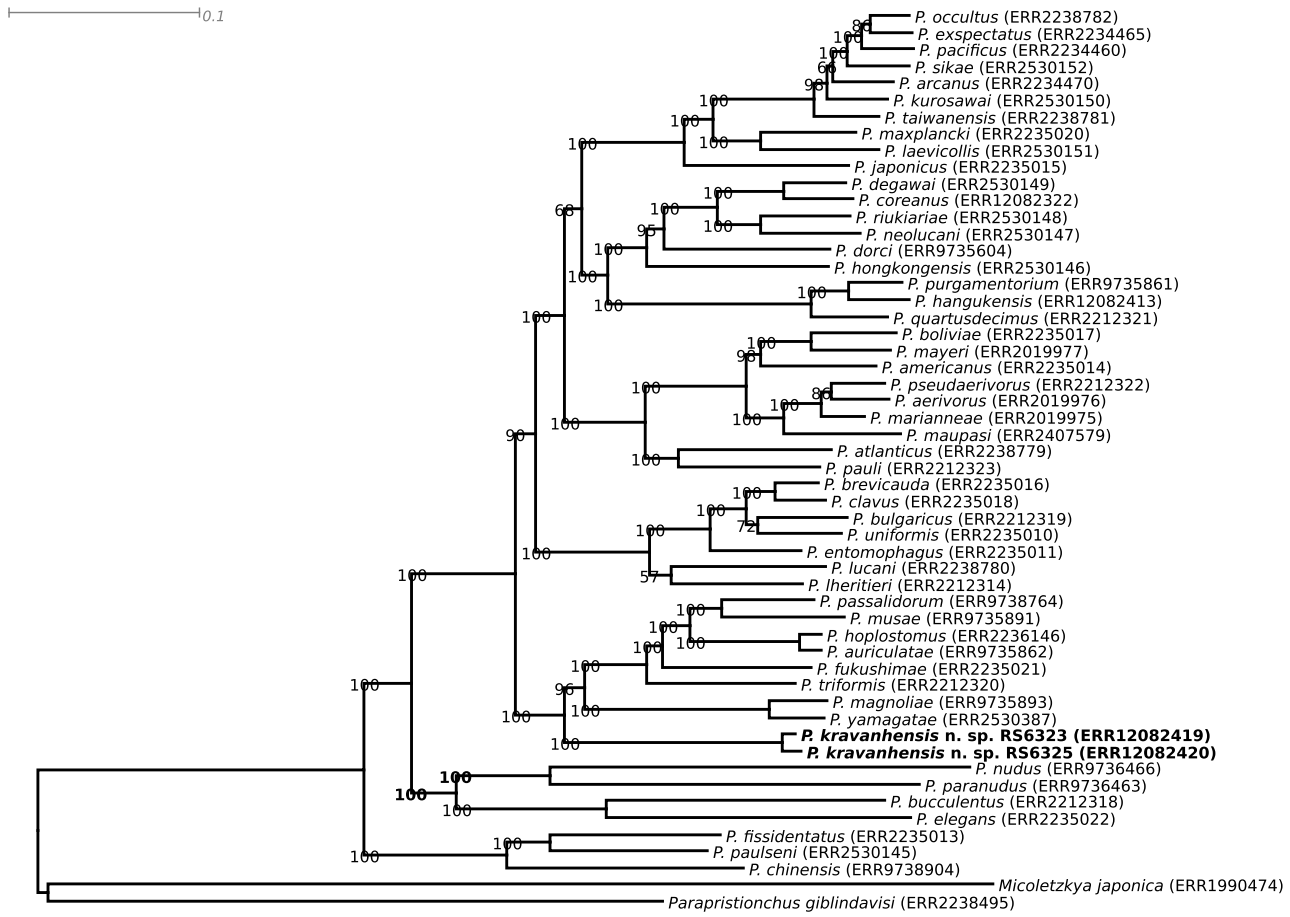


Fig. 2. Molecular phylogeny of the genus *Pristionchus* as inferred from a maximum likelihood tree reconstructed from a concatenated protein alignment, with *Micoletzkya japonica* and *Parapristionchus giblindavisi* as outgroups.

at anterior part of *vas deferens* in males and the posterior part of posterior gonad in females on the second dorsally neighbouring striation to lateral field.

Stenostomatous form

Cheilostom consisting of six per- and interradial plates. Incision between plates not always easily distinguished. Anterior end of each plate rounded and elongated to project from stomatal opening, forming small flap. Gymnostom short, cuticular ring-like anterior end overlapping cheilostom internally. Stegostom separated into three subsections: pro-meso, meta, and telostegostom. Promesostegostom forming a weakly cuticularised indistinctive ring internally overlapping with gymnostom to connect gymnostom and metastegostom. Metastegostom bearing conspicuous and movable triangular or flint-shaped dorsal tooth with strongly sclerotised surface giving an appearance of an inverted V-shape in light microscopy in lateral view, anterior end (tip) of dorsal tooth sometimes slightly curved anteriorly; left subventral ridge with three minute adventitious pointed or blunt denticles on a plate, most ventral denticle often masked by remaining two in lateral view; pointed right subventral ridge, often with distinct distal adventitious denticle(s). Because of the size difference between males and females, *i.e.*, females generally have larger stoma than males, tooth and denticles are larger (wider) in females than males. Telostegostom weakly sclerotised cup-like cavity connecting stoma and pharynx.

Eurystomatous form

Cheilostom divided into six well-distinguished per- and interradial plates. Anterior end of each plate rounded and elongated to protrude from stomatal opening, for-

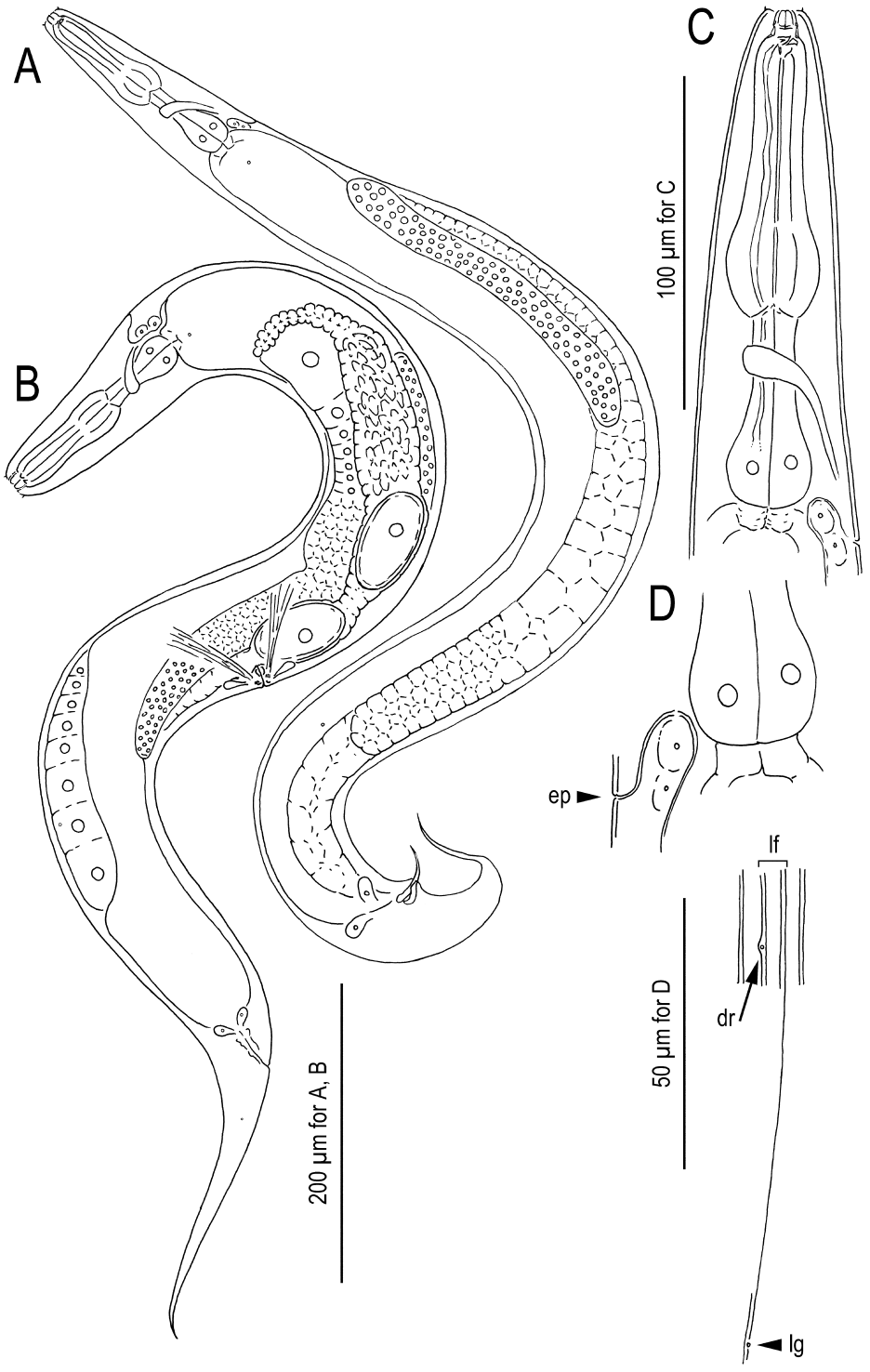


Fig. 3. *Pristionchus kravanhensis* n. sp. A: Male whole body; B: Female whole body; C: Anterior region; D: Relative position of secretory-excretory pore (ep), deirid (dr) and one of lateral glands (lg) which are on the lateral field (lf).

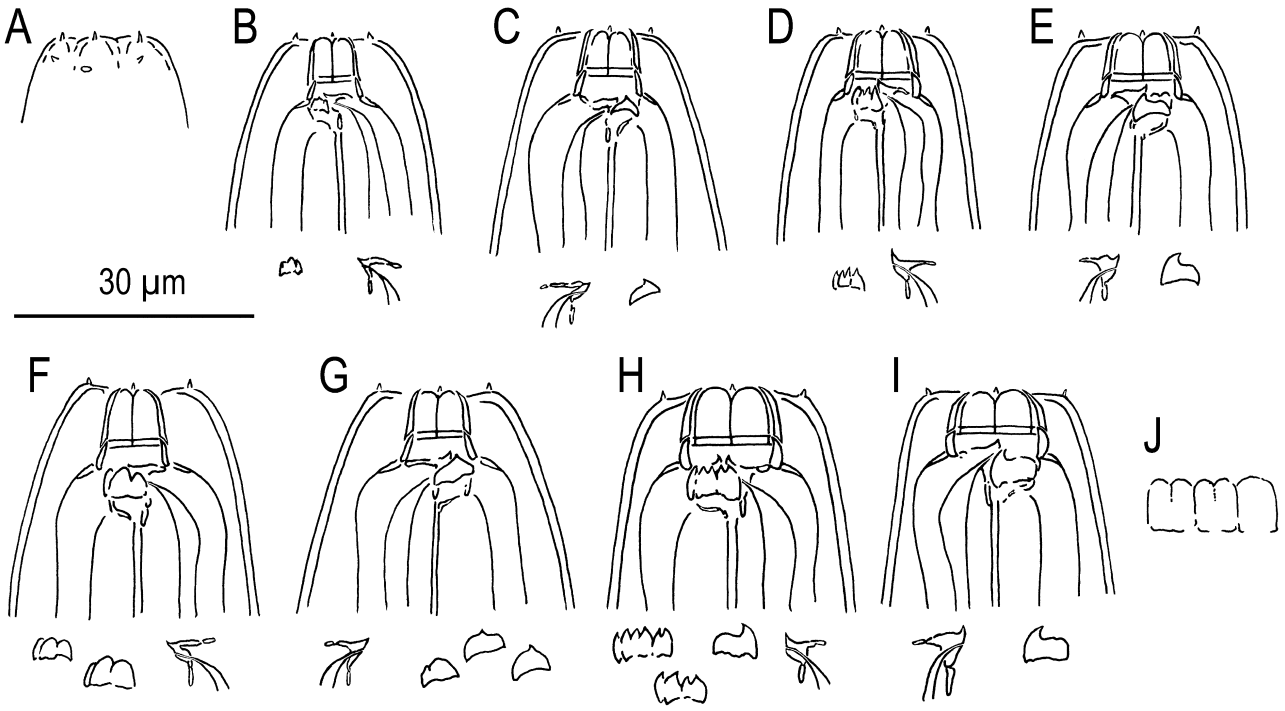


Fig. 4. Stomatal region of *Pristionchus kravanhensis* n. sp. showing variation among individuals. A: Surface of anterior end in right lateral view showing the relative position of labial sensilla, cephalic sensilla and amphid; B, C: Male stenostomatous form in left (B), and right (C) lateral views; D, E: Male eurystomatous form in left (D), and right (E) lateral views; F, G: Female stenostomatous form in left (F), and right (G) lateral views; H, I: Female eurystomatous form in left (H), and right (I) lateral views; J: Cheilostomatal plates of an eurystomatal female where two of six plates have split anterior tip. Tooth and denticules are separately drawn under whole lip region in B-I.

ming a small flap. In only a few individuals, one or two out of six plates with split tip; 6-8 cheilostomatal flaps derived from six plates. Gymnostom with thick cuticle forming short, ring-like tube being thicker posteriorly; anterior end of gymnostom internally overlapping posterior end of cheilostomatal plates. Stegostom separated into three subsections: pro-meso, meta, and telostegostom. Pro-mesostegostom forming a weakly cuticularised indistinctive ring internally overlapping with gymnostom to connect gymnostom and metastegostom. Metastegostom bearing large claw-like dorsal tooth, and large, claw-like right subventral tooth. Left subventral sector of metastegostom bearing three triangular ridges; tip of each ridge sometimes split into two or more fine tips, shapes varying among individuals. As in the stenostomatous form, the teeth and denticles are generally larger in females than males. Dorsal tooth and right subventral tooth movable. Movement not observed in left subventral denticles. Telostegostom weakly sclerotised cup-like cavity connecting stoma and pharynx.

Male

Whole body ventrally arcuate, strongly ventrally curved at tail region when killed by heat. Testis single, left subventrally located, anterior part reflexed to right side; spermatogonia arranged in 3-5 rows in reflexed part, well-developed spermatocytes arranged as 3-4 rows in anterior two-thirds of main branch, mature amoeboid spermatids arranged in multiple rows in proximal part of gonad. *Vas deferens* not clearly separated from other parts of gonad. Posterior end of *vas deferens* and rectum fused to form a cloacal tube. Spicules paired, separate; spicules smoothly curved in ventral view, adjacent to each other for distal third of their length, each smoothly tapering to pointed distal end; spicule in lateral view smoothly ventrally arcuate, giving spicule about 100° curvature, oval manubrium at anterior end, lamina/calomus complex smoothly tapering to pointed distal end. Gubernaculum conspicuous, *ca* one-third of spicule length, broad anteriorly such that dorsal wall slightly recurved with dorsal and ventral walls separate at 50-60° angle at posterior end; dorsal side of

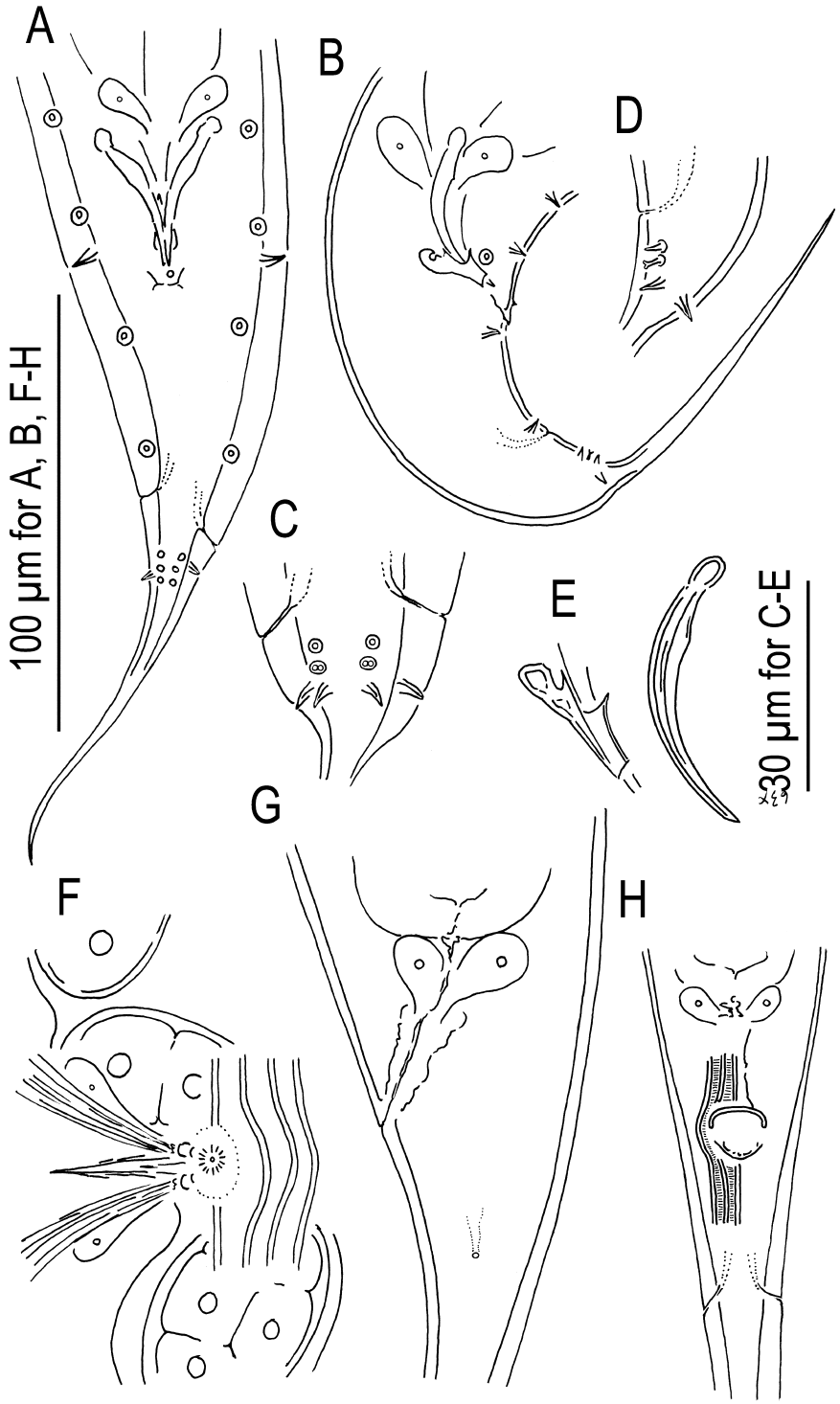


Fig. 5. *Pristionchus kravanhensis* n. sp. A, B: Whole male tail in ventral (A) and right lateral (B) views; C, D: Close-up of posterior four pairs of genital papillae and phasmid in ventral (C) and left lateral (D) views; E: Spicule and gubernaculum in right lateral view; F: Ventral view of female vulval region; G, H: Anal region of female in left lateral (G) and ventral (H) views.

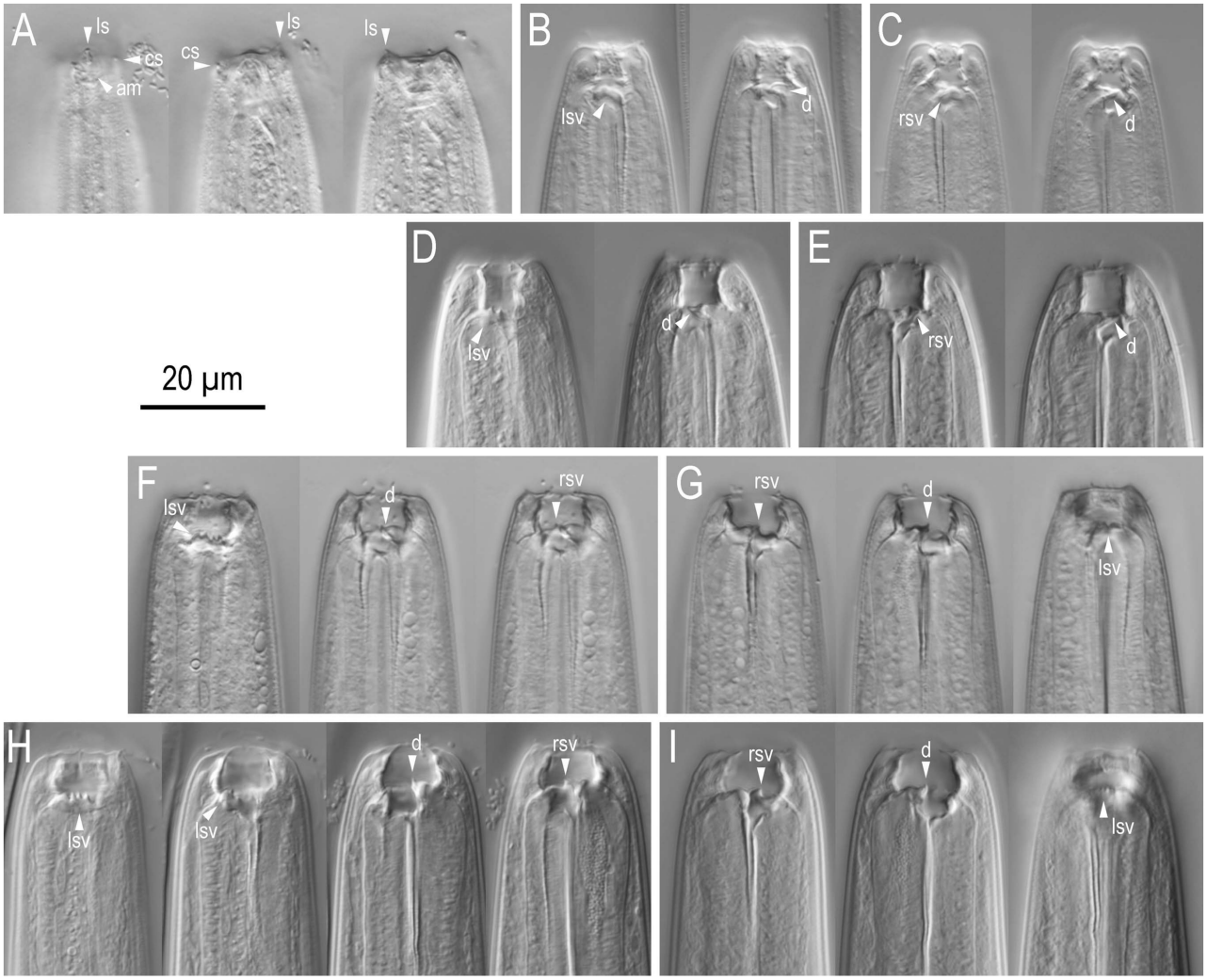


Fig. 6. Stomatal region of *Pristionchus kravanhensis* n. sp. showing variation among individuals. A: Surface of anterior end of male in left lateral view in three different focal planes showing the relative position of labial sensilla, cephalic sensilla and amphid; B, C: Male stenostomatous form in left (B), and right (C) lateral views in two different focal planes; D, E: Female stenostomatous form in left (D), and right (E) lateral views in two different focal planes; F, G: Male eurystomatous form in left (F), and right (G) lateral views in three different focal planes; H, I: Female eurystomatous form in left (H), and right (I) lateral views in four different focal planes. Abbreviations: am = amphid; cs = cephalic sensilla; d = dorsal tooth; ls = labial sensilla; lsv = left subventral ridge; rsv = right subventral ridge or tooth.

gubernaculum possessing single, membranous, anteriorly directed process and lateral pair of more sclerotised, anteriorly and obliquely ventrally directed processes. In lateral view, anterior half of gubernaculum with two successive curves separated by anteriorly and obliquely ventrally directed process, with anterior terminal curvature highly concave and almost closed, with deep posterior curvature being one-third of gubernaculum length; posterior half forming tube-like process enveloping spicules. Cloacal opening (co) slit-like in ventral view; one small, ventral, single genital papilla (vs) on anterior cloacal lip. Nine pairs of genital papillae and a pair of phasmid present with an arrangement ⟨v1, v2, v3d/v4, ad, ph, (v5, v6, v7, pd)⟩, where v1 is located about 1 cloacal body diam. (CBD) anterior to co; v2 less than 1/3 CBD anterior to co; v3d slightly (less than 1/4 CBD) posterior to v2; v4 less than

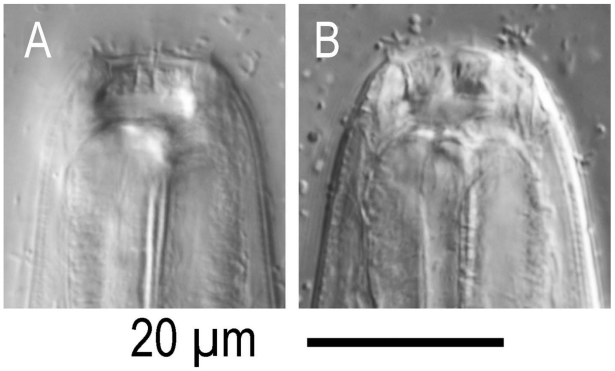


Fig. 7. Cheilostomatal plates of two different eurystomatous females of *Pristionchus kravanhensis* n. sp. A: Partially split plates; B: Regular plates without split tip.

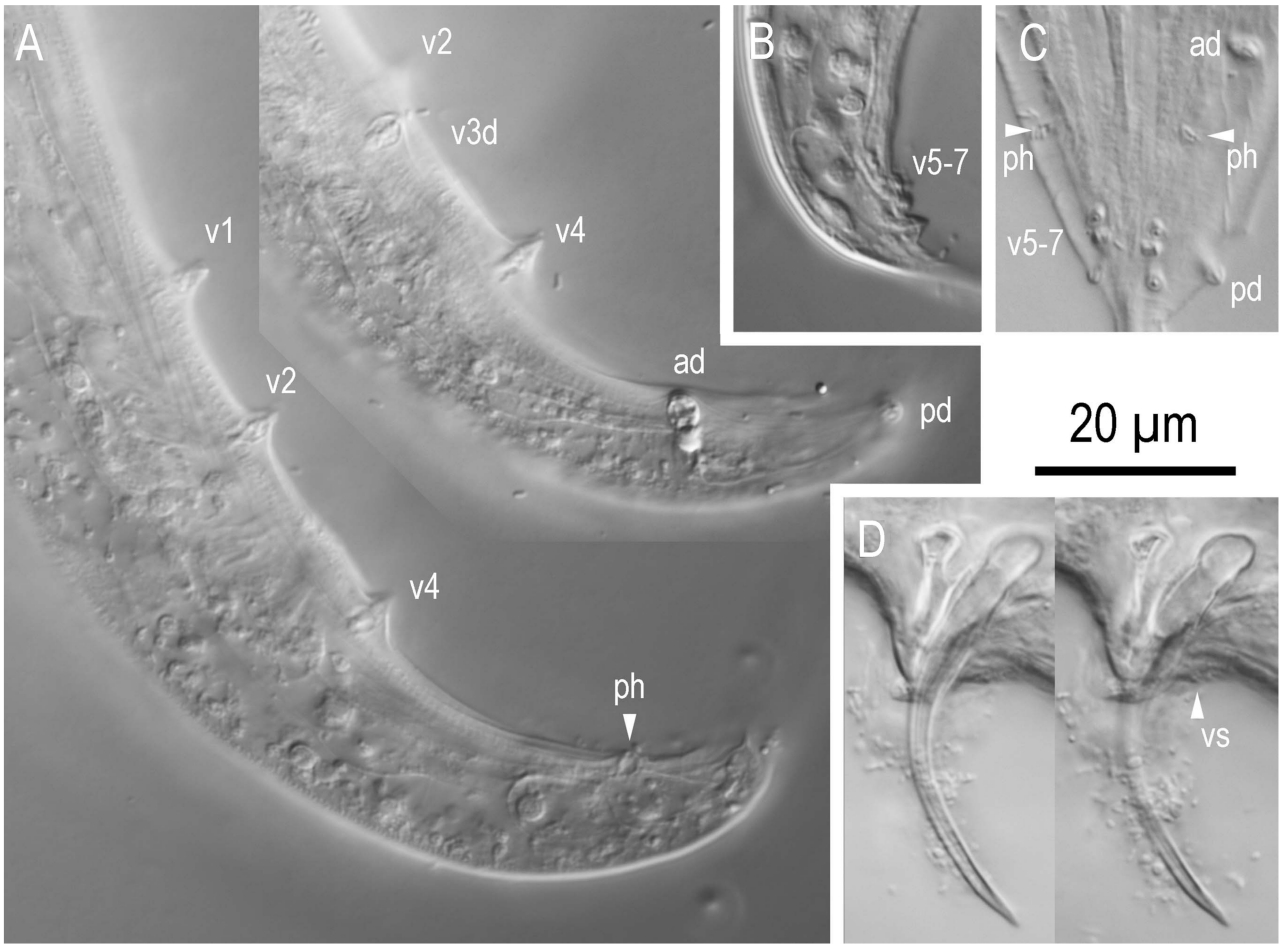


Fig. 8. Male tail characters of *Pristionchus kravanhensis* n. sp. A: Right lateral view of whole tail in two different focal planes; B: Posterior part of tail in right lateral view; C: Ventral view of the posterior part of tail; D: Spicule and gubernaculum in right lateral view. Abbreviations: ad, pd and v + number = genital papillae where ending with 'd' suggests that the papillae are directed laterally or subdorsally; ph = phasmid; vs = ventral single papilla.

Table 1. Morphometrics of *Pristionchus kravanhensis* n. sp. All measurements are in μm and in the form: mean ± s.d. (range).

	Male		Female
	Holotype	Temporal water mount	Temporal water mount
n	–	10	10
L	1099	905 ± 74.5 (831-1029)	1160 ± 84.2 (1040-1283)
L′	976	778 ± 70.8 (695-900)	986 ± 79.5 (869-1111)
a	13	13 ± 1.2 (10-15)	12 ± 0.8 (10-13)
b	7.6	6.7 ± 0.3 (6.1-7.1)	7.7 ± 0.4 (7.1-8.4)
c	9.2	7.0 ± 0.2 (6.6-7.2)	6.9 ± 0.6 (5.9-7.7)
c′	3.0	3.2 ± 0.3 (2.9-3.8)	4.4 ± 0.3 (3.9-5.0)
Ant. stoma length (cheilo- + gymnostom)	7.5	6.2 ± 0.4 (5.3-6.7)	6.3 ± 0.6 (5.2-7.2)
Total stoma length	12	11 ± 0.7 (9.9-11.9)	11 ± 0.9 (10-12)
Stoma width	5.4	5.1 ± 0.7 (4.2-6.4)	5.0 ± 0.6 (4.3-6.2)
Ant. pharynx (pro + metacorpus)	74	72 ± 4.8 (64-81)	81 ± 3.9 (75-88)
Post. pharynx (isthmus + basal bulb)	63	57 ± 3.4 (51-62)	63 ± 3.8 (58-69)
Total pharynx length	137	129 ± 7.6 (119-144)	144 ± 7.4 (133-158)
Ant./total pharynx %	–	56 ± 1.3 (53-57)	56 ± 0.8 (55-58)
Median bulb diam.	24	23 ± 1.3 (21-26)	27 ± 1.7 (25-30)
Terminal bulb diam.	24	23 ± 1.6 (20-25)	27 ± 1.9 (25-30)
Ant. end to cardia	144	136 ± 7.4 (125-148)	150 ± 7.0 (142-164)
Ant. end to S-E pore	170	132 ± 9.2 (123-148)	138 ± 14.5 (100-156)
Ant. end to nerve ring	109	96 ± 8.7 (84-107)	103 ± 5.3 (92-111)
Testis length	861	668 ± 72.5 (580-782)	–
Ant. end to vulva distance	–	–	558 ± 49.4 (475-633)
Vulva to anus distance	–	–	429 ± 34.8 (396-493)
T or V	78	74 ± 4.7 (68-85)	48 ± 1.4 (46-49)
Max. body diam.	87	71 ± 8.7 (57-83)	98 ± 8.6 (83-111)
Cloacal or anal body diam.	40	40 ± 2.5 (35-45)	39 ± 2.2 (36-43)
Tail length	120	130 ± 12.2 (115-149)	170 ± 18.6 (146-215)
Spicule curve	48	44 ± 3.0 (38-48)	–
Spicule chord	41	37 ± 2.4 (33-41)	–
Gubernaculum length	18	16 ± 2.5 (11-20)	–

1/3 CBD posterior to co, *i.e.*, v2, v3d, co and v4 are close to each other; ad about 1 CBD posterior to co; ph slightly (less than 1/4 CBD) posterior to ad; v5-v7 forming triplet, immediately anterior to the root of tail spike; and pd around level of triplet, *i.e.*, triplet papillae and pd overlap each other. The distance between v1 and v2 generally shorter than that between v2 and v4. The papillae v1, v2, v4 and ph subventral, v3d and ad lateral, v5-7 ventral, pd subdorsal in male tail. Within nine paired papillae, v1-v4 and ad in same size, v7 and pd are smaller than former five pairs, and v5 and v6 are smaller than v7 and ad. All nine paired genital papillae papilliform, but v5 and v6 originating from socket-like base, and the tip of v6 laterally split into two small tips. Tail conoid with a long spike occupying more than half of whole tail length. Bursa or bursal flap absent.

Female

Body relaxed or weakly ventrally arcuate when killed by heat. Gonad didelphic, amphidelphic; each gonadal system arranged from vulva/vagina as uterus, oviduct, and ovary; anterior gonad right of intestine, with uterus and oviduct extending ventrally and anteriorly on right of intestine and with totally reflexed (= antidromous reflexion) ovary extending dorsally on left of intestine; oocytes mostly arranged in 3-4 or more rows in distal two-thirds of ovary and in double or single row in rest of ovary, distal tips of each ovary reaching oviduct of opposite gonad branch; anterior end of oviduct (= junction tissue between ovary and oviduct) consisting of rounded cells; anterior part of oviduct consisting of rounded cells, forming a simple tube; middle part of oviduct serving as spermatheca, consisting of roundish and relatively large

cells. Eggs in single to multiple-cell stage or even further developed at posterior part of oviduct (= uterus), in young females being composed of squared or angular cells, long enough to contain one well-developed oocyte. *Receptaculum seminis* not observed, *i.e.*, the organ is not independent, and a part of oviduct/uterus works as the organ; vaginal glands present but obscure; vagina perpendicular to body surface, surrounded by sclerotised tissue; vulva slightly protuberant in lateral view, pore-like in ventral view; rectum about one anal body diam. (ABD) long, intestine/rectum junction surrounded by well-developed sphincter muscle. Anus in form of dome-shaped slit, posterior anal lip slightly protuberant. Tail elongate conoid with filiform terminus. Phasmid ventrolaterally located at about 1.5 (1-2) ABD posterior to anal opening.

Type material

The type material was obtained from a 2-week-old culture. The samples included a holotype male, four paratype males and five paratype females deposited at the Natural History Museum Karlsruhe, Germany, and five paratype males and five paratype females deposited at the Swedish Museum of Natural History, Stockholm, Sweden. In addition to the type material, mass-fixed materials (fixed in TAF or processed in dehydrated glycerin) were deposited at the Max Planck Institute for Biology, Tübingen, Germany.

Type host and locality

Cambodia, Kravanh La Vallee Eco Resort (11°39.746′N, 103°24.192′E, 380 m a.s.l.) on *Lepidiota discedens* Sharp, 1876, a large maybeetle (Coleoptera: Scarabaeoidea: Scarabaeidae: Melolonthinae) collected on April 21, 2023 on a light trap.

Etymology

Kravanh is the Khmer word for cardamom (*Elettaria cardamomum*), and the *locus typicus* of the species lies in the Cardamom Mountains, Cambodia. The new specific epithet has been registered in ZooBank under LSID: urn:lsid:zoobank.org:pub:A1217D3D-1763-48D4-A48E-18D907555B98

Diagnosis and relationships

Pristionchus kravanhensis n. sp. is characterised by its stomatal morphology, *i.e.*, anteriorly split cheilostomatal plate(s) that rarely occur in eurystomatous form; triangular dorsal tooth with or without anteriorly curved tip, and the right and left subventral ridges with denticles of stenostomatous form, claw-like right subventral stegostomal tooth, claw-like to diamond-shaped dorsal tooth and left subventral plate with multiple pointed denticles in eurystomatous form. The new species is also diagnosed by the arrangement of male genital papillae, ⟨v1, v2, v3d/v4, ad, ph, (v5, v6, v7, pd)⟩, where v2, v3d, co and v4 and v5, v6, v7, pd are close to each other, respectively, the distance v1-v2 is generally shorter than v2-v4, and v5-7 and pd are overlapping. Based on the arrangement of male genital papillae, *P. kravanhensis* n. sp. is typologically similar to that of *P. dorci* Kanzaki, Herrmann, Weiler, Röseler, Theska, Berger, Rödelsperger & Sommer, 2021, *P. hongkongensis* Kanzaki, Herrmann, Yoshida, Weiler, Rödelsperger & Sommer, 2018, *P. maupasi* (Potts, 1910) Paramonov, 1952 and *P. linstowi* (Potts, 1910) Paramonov, 1952 (Ragsdale *et al*., 2015; Kanzaki *et al*., 2018, 2021). Within these four species, *P. kravanhensis* n. sp. is readily distinguished from the latter two by the positions of v2 and v3d papillae; these two papillae are close in the new species, but somewhat apart in *P. maupasi* and *P. linstowi* (Ragsdale *et al*., 2015). *Pristionchus kravanhensis* n. sp. is distinguished from *P. dorci* by the stomatal characters of eurystomatous females, *i.e.*, presence *vs.* absence of partially split cheilostomatal plate(s) and left subventral ridges with 3-6 tips *vs.* 6-9 tips (Kanzaki *et al*., 2021). *Pristionchus kravanhensis* n. sp. and *P. hongkongensis* share the most typological characters employed for species identification, *i.e.*, the arrangement of male genital papillae. However, the new species can be distinguished from *P. hongkongensis* by the presence *vs.* absence of partially split cheilostomatal plate(s) in eurystomatous females (Kanzaki *et al*., 2018). Further, the new species is distinguished from all other species by its phylogenetic status as a sister to all other species in the *triformis* group, and a *ca.* 1600 bp fragment of the SSU rRNA gene (GenBank accession number PQ050080) is 20 bp and 35 bp distinct from that of the closest relatives *P. magnoliae* (MW017219) and *P. yamagatae* (MH114983), respectively.

Discussion

Despite its phylogenetic position as sister to all other known species in the *triformis* group (Fig. 2), *P. kravanhnesis* n. sp. has, in some diagnostic characters (*i.e.*, genital papillae), more typological similarity to species

outside the *triformis* group than those within it (Kanzaki *et al*., 2018). On the other hand, *P. kravanhensis* n. sp. is clearly distinguished from other *triformis* group species, which commonly have trimorphic stoma with a stenostomatous form and two types of eurystomatous forms where the cheilostomatal plates are partially or totally split into two narrow plates and the anterior edge of gymnostomatal ring is serrated, and the laterally directed second pair of genital papillae (v2d) (Kanzaki *et al*., 2021). The stoma of *P. kravanhensis* n. sp., however, is dimorphic, where only few eurystomatous females have one or two partially split cheilostomatous plate(s) and the anterior edge of gymnostomatal ring does not have serratae, and males having laterally directed third paired papillae (v3d). In addition, it should be noted that this laterally directed third papillae is found in five phylogenetic clades in the genus, namely *P. fissidentatus* Kanzaki, Ragsdale, Mayer, Herrmann & Sommer, 2012 and *P. paulseni* Herrmann, Kanzaki, Weiler, Yoshida, Rödelsperger & Sommer, 2019 in *fissidentatus* group; *P. kravanhensis* n. sp. in *triformis* group; *P. purgamentorium* Kanzaki, Herrmann, Weiler, Röseler, Theska, Berger, Rödelsperger & Sommer, 2021, *P. quartusdecimus* Kanzaki, Ragsdale, Herrmann, Röseler & Sommer, 2013, *P. dorci*, and *P. hongkongensis* in the middle clade between *pacificus* and *maupasi* groups; *P. japonicus* Kanzaki, Ragsdale, Herrmann, Mayer & Sommer, 2012, *P. maxplancki* Kanzaki, Ragsdale, Herrmann, Röseler & Sommer, 2013 and *P. laevicollis* Kanzaki, Herrmann, Yoshida, Weiler, Rödelsperger & Sommer, 2018 in *pacificus* group; and *P. maupasi*, *P. aerivorus* (Cobb in Merrill & Ford, 1916) Chitwood, 1937, *P. pseudaerivorus* Herrmann, Kanzaki, Ragsdale & Sommer, 2017 in *maupasi* group (Ragsdale *et al*., 2015; Kanzaki *et al*., 2018, 2021). Thus, the transition from v3d to v2d has occurred independently five times.

In conclusion, the *triformis* group presents an interesting experimental model for the examination of the development of stomatal polymorphism. The new species described here basically has a dimorphism, but partially split cheilostomatal plate(s) occur in a few individuals, *i.e.*, there is an intermediate or transitional form between dimorphism and trimorphism. Therefore, the species could be important for future comparisons of the *triformis* group to analyse the genetic mechanisms of the development of trimorphism.

Acknowledgements

We would like to thank the Cambodian colleagues Sareach Chea, Penghaing Ly and Dr Kim Eang Tho for supporting our project, the Cambodian government for permits, and Heike Haussmann for freezing the strains.

References

Edgar, R.C. (2004). MUSCLE: multiple sequence alignment with high accuracy and high throughput. *Nucleic Acids Research* 32, 1792-1897. DOI: 10.1093/nar/gkh340

Fonderie, P., Steel, H., Moens, T. & Bert, W. (2013). Experimental induction of intraspecific morphometric variability in a single population of *Halicephalobus* cf. *gingivalis* may surpass total interspecific variability. *Nematology* 15, 529-544. DOI: 10.1163/15685411-00002699

Herrmann, M., Mayer, W.E. & Sommer, R.J. (2006a). Nematodes of the genus *Pristionchus* are closely associated with scarab beetles and the Colorado potato beetle in Western Europe. *Zoology* 109, 96-108. DOI: 10.1016/j.zool.2006.03.001

Herrmann, M., Mayer, W.E. & Sommer, R.J. (2006b). Sex, bugs and Haldane's rule: the nematode genus *Pristionchus* in the United States. *Frontiers in Zoology* 3, 14. DOI: 10.1186/1742-9994-3-14

Herrmann, M., Mayer, W.E., Hong, R.L., Kienle, S., Minasaki, R. & Sommer, R.J. (2007). The nematode *Pristionchus pacificus* (Nematoda: Diplogastridae) is associated with the oriental beetle *Exomala orientalis* (Coleoptera: Scarabaeidae) in Japan. *Zoological Science* 24, 883-889. DOI: 10.2108/zsj.24.883

Herrmann, M., Weiler, C., Rödelsperger, C., Kanzaki, N. & Sommer, R.J. (2016). Two new *Pristionchus* species (Nematoda: Diplogastridae) from Taiwan are part of a species-cluster representing the closest known relatives of the model organism *P. pacificus*. *Zoological Studies* 55, 48. https://zoolstud.sinica.edu.tw/Journals/55/55-48.html

Herrmann, M., Kanzaki, N., Ragsdale, E.J. & Sommer, R.J. (2017). Redescription of four species of the genus *Pristionchus* (Nematoda: Diplogastridae) from the United States of America. *Dumerilia* 7, 97-103.

Herrmann, M., Kanzaki, N., Weiler, C., Yoshia, K., Rödelsperger, C. & Sommer, R.J. (2019). Two new species of *Pristionchus* (Nematoda: Diplogastridae) include the gonochoristic sister species of *P. fissidentatus*. *Journal of Nematology* 51, 1-14. DOI: 10.21307/jofnem-2019-024

Hooper, D.J. (1986). Handling, fixing, staining and mounting nematodes. In: Southey, J.F. (Ed.). *Laboratory methods for work with plant and soil nematodes*. London, Her Majesty's Stationary Office, MAFF, pp. 59-80.

Kanzaki, N., Ragsdale, E.J., Herrmann, M., Mayer, W.E., Tanaka, R. & Sommer, R.J. (2012a). *Parapristionchus gib-*

lindavisi n. gen., n. sp. (Rhabditida: Diplogastridae) isolated from stag beetles (Coleoptera: Lucanidae) in Japan. *Nematology* 14, 933-947. DOI: 10.1163/156854112X635878

Kanzaki, N., Ragsdale, E.J., Herrmann, M., Mayer, W.E. & Sommer, R.J. (2012b). Description of three *Pristionchus* species (Nematoda: Diplogastridae) from Japan that form a cryptic species complex with the model organism *P. pacificus*. *Zoological Science* 29, 403-417. DOI: 10.2108/zsj.29.403

Kanzaki, N., Ragsdale, E.J., Herrmann, M., Röseler, W. & Sommer, R.J. (2013). Two new species of *Pristionchus* (Nematoda: Diplogastridae) support the biogeographic importance of Japan for the evolution of the genus *Pristionchus* and the model system *P. pacificus*. *Zoological Science* 30, 680-692. DOI: 10.2108/zsj.30.680

Kanzaki, N., Herrmann, M., Yoshida, K., Weiler, C., Rödelsperger, C. & Sommer, R.J. (2018). Samplings of millipedes in Japan and scarab beetles in Hong Kong result in five new species of *Pristionchus* (Nematoda: Diplogastridae). *Journal of Nematology* 50, 587-610. DOI: 10.21307/jofnem-2018-044

Kanzaki, N., Herrmann, M., Weiler, C., Röseler, W., Theska, T., Berger, J., Rödelsperger, C. & Sommer, R.J. (2021). Nine new *Pristionchus* (Nematoda: Diplogastridae) species from China. *Zootaxa* 4943, 1-66. DOI: 10.11646/zootaxa.4943.1.1

Kreis, H.A. (1932). Beiträge zur Kenntnis pflanzenparasitischer Nematoden. *Zeitschrift für Parasitenkunde* 5, 184-194.

Merrill, J.H. & Ford, A.L. (1916). Life history and habits of two new nematodes parasitic in insects. *Journal of Agricultural Research* 6, 115-127.

Paramonov, A.A. (1952). Ecological classification of plant nematodes. *Trudy Gelmintologicheskoi Laboratorii, Akademia Nauk SSSR* 6, 338-369.

Potts, F.A. (1910). Notes on the free-living nematodes. *Quarterly Journal of Microscopical Science* 55, 433-484.

Ragsdale, E.J., Kanzaki, N. & Herrmann, M. (2015). Taxonomy and natural history: the genus *Pristionchus*. In: Sommer, R.J. (Ed.). Pristionchus pacificus – *a nematode model for comparative and evolutionary biology*. *Nematology Monographs and Perspectives 11* (Series Editors: Hunt, D.J. & Perry, R.N.). Leiden, The Netherlands, Brill, pp. 77-120. DOI: 10.1163/9789004260306_005

Renahan, T. & Sommer, R.J. (2021). Nematode interactions on beetle hosts indicate a role of mouth-form plasticity in resource competition. *Frontiers in Ecology and Evolution* 9, 752695. DOI: 10.3389/fevo.2021.752695

Renahan, T., Lo, W.-S., Werner, M.S., Rochat, J., Herrmann, M. & Sommer, R.J. (2021). Nematode biphasic 'boom and bust' dynamics are dependent on host bacterial load while linking dauer and mouth-form polyphenisms. *Environmental Microbiology* 23, 5102-5113. DOI: 10.1111/1462-2920.15438

Rödelsperger, C., Röseler, W., Prabh, N., Yoshida, K., Weiler, C., Herrmann, M. & Sommer, R.J. (2018). Phylotranscriptomics of *Pristionchus* nematodes reveals parallel gene loss in six hermaphroditic lineages. *Current Biology* 28, 3123-3127. DOI: 10.1016/j.cub.2018.07.041

Röseler, W., Collenberg, M., Yoshida, K., Lanz, C., Sommer, R.J. & Rödelsperger, C. (2022). The improved genome of the nematode *Parapristionchus giblindavisi* provides insights into lineage-specific gene family evolution. *G3* 12, jkac215. DOI: 10.1093/g3journal/jkac215

Sharp, D. (1876). III. Descriptions of some new species of Scarabaeidae from tropical Asia and Malasia. *Coleopterologische Hefte XV. 1876* 15, 65-90.

Sommer, R.J. (2009). The future of evo-devo: model systems and evolutionary theory. *Nature Reviews Genetics* 10, 416-422. DOI: 10.1038/nrg2567

Sommer, R.J. (2015). Integrative evolutionary biology and mechanistic approaches in comparative biology. In: Sommer, R.J. (Ed.). Pristionchus pacificus – *a nematode model for comparative and evolutionary biology*. *Nematology Monographs and Perspective 11* (Series Editors: Hunt, D.J. & Perry, R.N.). Leiden, The Netherlands, Brill, pp. 19-41. DOI: 10.1163/9789004260306_003

Sommer, R.J. & Lightfoot, J.W. (2022). The genus *Pristionchus*: a model for phenotypic plasticity, predatory behavior, self-recognition and other complex traits. In: Glazer, I., Shapiro-Ilan, D. & Sternberg, P.W. (Eds). *Nematodes as model organisms*. Wallingford, UK, CAB International, pp. 1-23. DOI: 10.1079/9781789248814.0001

Sommer, R.J., Carta, L.K., Kim, S.Y. & Sternberg, P.W. (1996). Morphological, genetic and molecular description of *Pristionchus pacificus* n. sp. (Nematoda: Neodiplogastridae). *Fundamental and Applied Nematology* 19, 511-521.

Stamatakis, A. (2014). RAxML version 8: a tool for phylogenetic analysis and post-analysis of large phylogenies. *Phylogenetics* 30, 1312-1313. DOI: 10.1093/bioinformatics/btu033

Susoy, V., Ragsdale, E.J., Kanzaki, N. & Sommer, R.J. (2015). Rapid diversification associated with a macroevolutionary pulse of developmental plasticity. *eLife* 4, e05463. DOI: 10.7554/eLife.05463

Yoshida, K., Herrmann, M., Kanzaki, N., Weiler, C., Rödelsperger, C. & Sommer, R.J. (2018). Two new species of *Pristionchus* (Nematoda: Diplogastridae) from Taiwan and the definition of the *pacificus* species-complex *sensu stricto*. *Journal of Nematology* 50, 355-368. DOI: 10.21307/jofnem-2018-019

communications biology

A Nature Portfolio journal

Article

https://doi.org/10.1038/s42003-025-08641-4

Biosynthesis of modular signaling molecules requires functional diversification of carboxylesterases in *Pristionchus pacificus*

Check for updates

Pei Zhang[1,2,8], Penghieng Theam[3,8], Wenya Xu[1,2,8], Shudan Ye[1,4,5,6,7], Hanh Witte[3], Tingwei Liu[1,2], Ralf J. Sommer[3] ✉ & Chuanfu Dong[1,2,3,4,5] ✉

The entomophilic roundworm *Pristionchus pacificus* produces a group of complex ascaroside pheromones (e.g., ubas#1), which are built with various intermediates originating from primary metabolic pathways. However, the exact biosynthetic pathways resulting in the production of these modular pheromones remain enigmatic. Here, the application of a workflow combing bioinformatic tools, CRISPR engineering and chemical analysis supports the discovery of three new carboxylesterases *Ppa*-UAR-5, *Ppa*-UAR-6 and *Ppa*-UAR-12 from *P. pacificus*. *Ppa*-UAR-5 links two simple ascarosides oscr#9 and ascr#12 to the 2'-position of ubas#3 to furnish the biosynthesis of ubas#1 and ubas#2, whereas *Ppa*-UAR-12 links two ascr#1 at the 4'-position to synthesize dasc#1. Finally, *Ppa*-UAR-6 is essential for the biosynthesis of npar#1-3 and part#9. The expression patterns of *Ppa-uar-6* and *Ppa-uar-12* in intestinal and epidermal cells further suggest pheromone biosynthesis is tissue-specific. These findings support the notion that the expansion and subsequent diversification of carboxylesterases in *P. pacificus* generates complex modular signaling pheromones.

The entomophilic roundworm *Pristionchus pacificus* is a model nematode for evolutionary developmental biology[1,2]. Most *Pristionchus* species are found to be ecologically associated with scarab beetles[3–5], normally arresting as dauer larvae (a developmentally stress-resistant larval stage) on living beetles. These nematodes resume development when bacteria proliferate on beetle carcasses and become available as food source. Like other nematodes of the family Diplogastridae, *P. pacificus* exhibits a mouth-form dimorphism with the so-called stenostomatous (St) or eurystomatous (Eu) form, a striking example of phenotypic plasticity of feeding structures[6]. Specifically, St animals have a single tooth and feed on bacteria, whereas Eu animals are equipped with two sharp teeth enabling them to predate on other nematodes[7–12]. As genome editing by CRISPR/Cas9 engineering is reliably established in *P. pacificus*[13–16], this technique allows the in-depth investigation of the regulatory mechanism of mouth-form development and its associated predatory behavior. For example, the combination of forward and reverse genetic tools resulted in the identification of the major regulator of mouth-form plasticity *eud-1*[17], and the self-recognition locus *self-1* that prevents cannibalism against genetically identical kin[12]. In addition, *P. pacificus* excretes signaling molecules referred to as "nematode-derived modular metabolites", a group of ascaroside pheromones initially characterized from *Caenorhabditis elegans*[18–32], which are also found to influence the development of the mouth form and dauer formation[33–35].

Similar to *C. elegans*, *P. pacificus* produces a wide variety of signaling ascarosides[33,36,37]. However, unlike *C. elegans* only three simple ascarosides—ascr#9 (asc-C5), ascr#12 (asc-C6) and ascr#1 (asc-C7)—have so far been identified (Fig. 1a). These simple ascarosides harbor an ascarylose sugar

[1]Department of Biology, Faculty of Arts and Sciences, Beijing Normal University, 519087 Zhuhai, China. [2]The Key Laboratory of Cell Proliferation and Regulation Biology, Ministry of Education, Department of Biology, College of Life Sciences, Beijing Normal University, 100875 Beijing, China. [3]Department for Integrative Evolutionary Biology, Max Planck Institute for Biology Tübingen, Max Planck Ring 9, 72076 Tübingen, Germany. [4]Center for Biological Science and Technology, Advanced Institute of Natural Sciences, Beijing Normal University, 519087 Zhuhai, China. [5]Zhuhai-Macao Biotechnology Joint Laboratory, Beijing Normal University, 519087 Zhuhai, China. [6]Present address: Key Laboratory of Biomacromolecules (CAS), National Laboratory of Biomacromolecules, CAS Center for Excellence in Biomacromolecules, Institute of Biophysics, Chinese Academy of Sciences, 100101 Beijing, China. [7]Present address: College of Life Sciences, University of Chinese Academy of Sciences, 100049 Beijing, China. [8]These authors contributed equally: Pei Zhang, Penghieng Theam, Wenya Xu.
✉e-mail: ralf.sommer@tuebingen.mpg.de; cdong@bnu.edu.cn

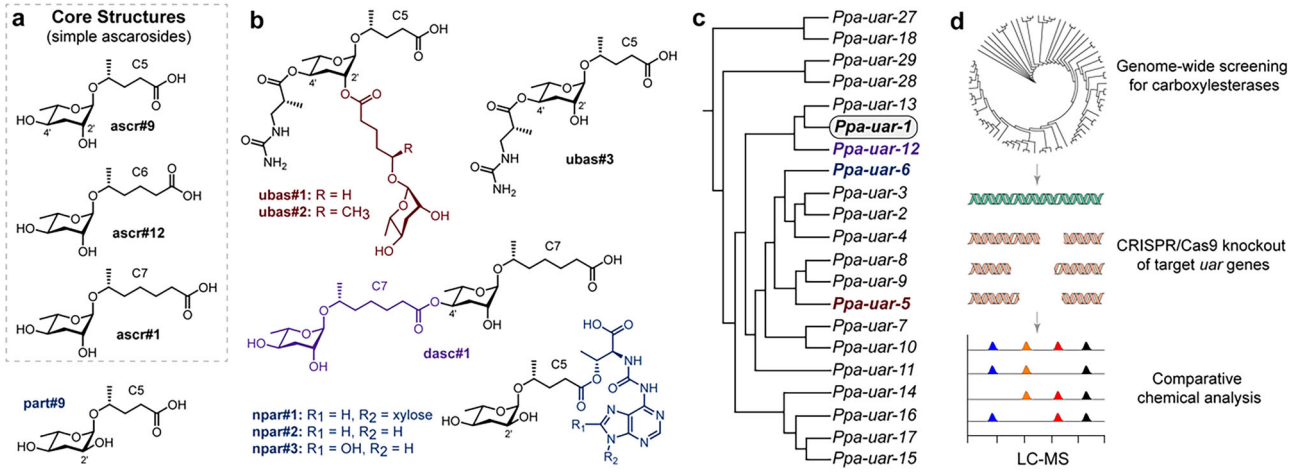


Fig. 1 | Pheromonal components and their biosynthetic genes from *P. pacificus*. **a** Chemical structures of simple ascarosides including ascr#9, ascr#12, and ascr#1. **b** Structures of chemically modified modular signaling molecules (e.g., UBAS, DASC, and NPAR pheromones). **c** 20 out of 76 candidate genes (Supplementary Tables 1 and 2) with homology to *Ppa-uar-1*[49] were knocked out by CRISPR/Cas9, from which *Ppa-uar-5*, *Ppa-uar-12*, and *Ppa-uar-6* genes were shown to regulate the biosynthesis of UBAS, DASC and NPAR pheromones, respectively. **d** A workflow for screening carboxylesterase genes that are responsible for the biosynthesis of modular pheromones from *P. pacificus*.

linked to the aglycone of a short fatty acid side chain, which are derived from the long chain ascarosides via several cycles of peroxisomal β-oxidation[38–44]. In addition, simple ascarosides can act as core structures (Fig. 1a) that are further decorated with additional building blocks to generate three types of complex modular ascarosides (Fig. 1b), including UBAS (3-ureidoisobutyrate ascarosides), DASC (dimeric ascaroside) and PASC (phenylethanolamide ascaroside)[33]. *P. pacificus*-produced ascarosides or paratosides are named using four-letter codes "SMIDs" (Small Molecule Identifiers, see the SMID database, www.smid-db.org), for example, ubas#1 and dasc#1[33]. Indeed, each type of modular ascaroside incorporates different kinds of intermediates originating from various primary metabolic pathways. For example, UBAS ascarosides carry a common unit of pyrimidine metabolic pathway-derived ureidoisobutyric acid at the 4'-position, with some complex UBAS ascarosides, like ubas#1 and ubas#2, even separately containing an additional building block of oscr#9 (asc-ωC5) and ascr#12 (asc-C6) at the 2'-position. In contrast, DASC ascarosides are normally comprised of two units of simple ascarosides, which are linked at the 2'- or 4'-position. Finally, *P. pacificus* produces a group of unique NPAR paratosides including part#9 (paratoside) and npar#1-3 (nucleoside-based paratoside). Based on the structural skeleton of part#9 that is an epimer of ascr#9, npar#1-3 are integrated with additional groups of adenosine-based threonine at their C5 fatty acid side chains (Fig. 1b). So far, only *P. pacificus* and its closely related species from the genus *Pristionchus* have been reported to produce these specialized metabolites[33,37].

These decorated signaling molecules play critical roles in the regulation of various developmental processes in *P. pacificus*. For example, the dimeric ascaroside dasc#1 is able to trigger the formation of the Eu mouth form[33], while UBAS and NPAR pheromones are capable of inducing dauer formation[7,33,34,36,45–48]. Given this complex biochemistry that is in part linked to the developmental decisions which respond to changing environmental influences, we seek to investigate the biosynthetic origins of these modular signaling molecules. While little is known about these biosynthetic pathways, Falcke and co-workers[49] previously discovered a key gene *Ppa-uar-1* in the genome of *P. pacificus* by analyzing both metabolomes and transcriptomes of 264 *P. pacificus* wild isolates. Differences in the metabolome of independent wild isolates were linked to the *Ppa-uar-1* gene through a genome-wide association study (GWAS) mapping. *Ppa-uar-1* mutants, analyzed by LC-MS (Liquid Chromatography Mass Spectrometry) of both worm culture medium (*exo*-metabolomes) and worm pellets (*endo*-metabolomes), showed the absence of UBAS ascarosides, which are characteristic of the attachment of a ureidoisobutyric acid unit at the 4'-position (Fig. 1b). These results indicate for the first time, that the carboxylesterase *Ppa*-UAR-1 is capable of linking ureidoisobutyric acid to the 4'-position of simple ascarosides to further produce a group of modular UBAS ascarosides (Fig. 1b)[49]. However, up to date, the downstream factors of the biosynthetic pathway of ubas#1 and ubas#2 have still been elusive, i.e., the exact mechanism of how additional units of oscr#9 and ascr#12 are incorporated into the 2'-position of ubas#3 remains unknown. In addition, the biosynthetic origins of the remaining types of modular signaling molecules are completely uninvestigated. Therefore, it will be important to explore the mechanisms of how different building blocks are integrated into the core structures of simple ascarosides for the biosynthesis of these structurally complex pheromones.

Here, we report the discovery of three new carboxylesterase proteins *Ppa*-UAR-5, *Ppa*-UAR-12 and *Ppa*-UAR-6 in *P. pacificus*, which are required for the biosynthesis of UBAS, DASC and NPAR pheromones, respectively (Fig. 1c). Knockout mutants of *Ppa-uar-5*, *Ppa-uar-12* and *Ppa-uar-6* led to the loss of specific sets of pheromones in both *exo*-metabolomes and *endo*-metabolomes. *Ppa-uar-6* and *Ppa-uar-12* were further observed to be specifically expressed in the intestine of *P. pacificus*, which highlights the importance of this tissue for pheromone biosynthesis. The discovery of these biosynthetic proteins provides new opportunities for uncovering the evolution and biological functions of signaling molecules in nematodes.

Results

Knockout of 20 homologs of *Ppa-uar-1* by CRISPR/Cas9

To explore the biosynthetic origins of structurally complex pheromones in *P. pacificus* (Fig. 1b), we hypothesized that homologs of the carboxylesterase *Ppa*-UAR-1[49] might play important roles in the formation of these signaling molecules. Bioinformatic analysis of the *P. pacificus* genome revealed 75 homologs of *Ppa-uar-1*[49] and they were renamed as *Ppa-uar-x* (*x* marked from 2 to 76) (Supplementary Tables 1 and 2). The amino acid sequences of the homologous UAR proteins were properly aligned and 20 of them were found to be most closely related to *Ppa*-UAR-1 in the phylogenetic tree (Fig. 1c, Supplementary Fig. 1 and Supplementary Data). Thus, we were motivated to concentrate on these 20 *uar* genes, all of which were targeted for the creation of knockout mutants through CRISPR/Cas9 engineering (Fig. 1c, Supplementary Tables 1 and 3). We indeed succeeded in generating presumptive null mutants with a total of 57 mutant alleles in these 20 genes (Supplementary Table 1). To study these mutants further, we cultured all the

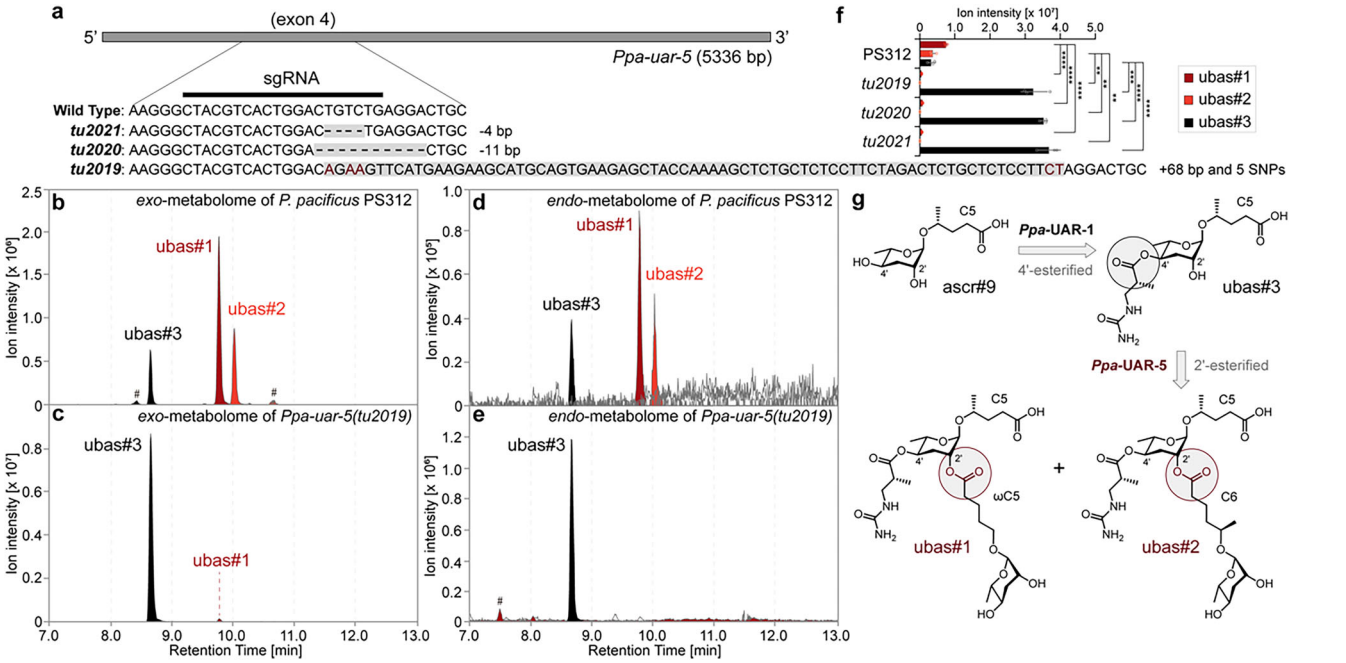


Fig. 2 | Biosynthetic investigation of UBAS pheromones. a Three mutant alleles of *Ppa-uar-5* were generated by CRISPR/Cas9 engineering. **b**–**e** The production of UBAS pheromones including ubas#1, ubas#2, and ubas#3 in the *exo*-metabolomes (**b**, **c**) and *endo*-metabolomes (**d**, **e**) of both wild type *P. pacificus* PS312 and mutants were examined by LC-MS. The pound signs (#) denote non-ascarosides. **f** Ion abundances of UBAS pheromones in the *exo*-metabolomes of wild type *P. pacificus* PS312 and three mutants were quantitatively analysed ($n = 3$ per group) (Supplementary Data). Error bars represent standard deviation (± SD). Statistical analysis was performed using a two-tailed unpaired Student's *t*-test, $^{****}p < 0.0001$; $^{***}p < 0.001$; $^{**}p < 0.01$; $^{*}p < 0.05$; ns not significant. **g** Biosynthetic pathway of UBAS pheromones. *Ppa*-UAR-1 introduced one unit of ureidoisobutyric acid to the 4'-position of simple ascaroside ascr#9 to produce an intermediate ubas#3[49]. *Ppa*-UAR-5 was responsible for attaching another building block of oscr#9 (asc-ωC5) or ascr#12 to the 2'-position of ubas#3 to finally yield ubas#1 and ubas#2, respectively.

mutant worms in S-medium for the collection of *exo*-metabolomes and *endo*-metabolomes (see Methods), followed by LC-MS examination of their pheromonal compositions, which were compared with those of wild type *P. pacificus* worms (Fig. 1d). This workflow supported the discovery of three new genes encoding for biosynthetic enzymes, i.e., *Ppa-uar-5*, *Ppa-uar-6*, and *Ppa-uar-12* (Fig. 1c, d). Similar to *Ppa-uar-1* in *P. pacificus*[49] and the *cest* genes in *C. elegans*[32,50,51], these three genes also encode carboxylesterase proteins (esterase or hydrolase) belonging to the α/β-hydrolase-fold enzyme superfamily with a predicted C-terminal transmembrane domain[32,50,51]. The conserved GXSXG motif containing the catalytic Serine together with the other two catalytic residues Glu and His were also found in *Ppa*-UAR-5, *Ppa*-UAR-6 and *Ppa*-UAR-12 (Supplementary Fig. 2), which suggests a conserved Glu-His-Ser catalytic triad in UAR proteins. Four conserved Cys residues that are responsible for forming the disulfide bonds of protein structures were also observed (Supplementary Fig. 2). Here, we found that *Ppa*-UAR-5, *Ppa*-UAR-12, and *Ppa*-UAR-6 separately regulated the biosynthesis of UBAS, DASC, and NPAR pheromones (Fig. 1c). In the following paragraphs, the biosynthetic capacities for each newly identified carboxylesterase are described in detail.

Ppa-UAR-5 functions downstream of *Ppa*-UAR-1 to furnish the biosynthesis of dauer pheromones ubas#1 and ubas#2

First, we generated three new alleles of *Ppa-uar-1* mutants by CRISPR/Cas9 (Supplementary Table 1) to add to the previously reported *Ppa-uar-1* mutants[49]. Indeed, these new mutants did not produce any trace of UBAS ascarosides. Given that both ubas#1 and ubas#2 carry a common building block of ubas#3, these results suggested that ubas#3 might be a biosynthetic precursor of ubas#1 and ubas#2[49]. However, how the remaining two building blocks oscr#9 (asc-ωC5)[39] and ascr#12 (asc-C6) (Fig. 1a) are incorporated into the 2'-position of ubas#3 for the biosynthesis of ubas#1 and ubas#2 was still elusive.

To elucidate the biosynthetic pathways of ubas#1 and ubas#2, all of the above-mentioned 57 mutants were maintained in 50 ml liquid culture, and the resulting *exo*-metabolomes and *endo*-metabolomes were freeze-dried, extracted by methanol, concentrated and aliquoted for LC-MS analysis (see Methods). Out of these mutants, CRISPR/Cas9 targeting exon 4 of *Ppa-uar-5* produced three mutant alleles, including *tu2019* that carried an insertion of 68 bp along with 5 single nucleotide polymorphisms (SNPs). Additionally, the *Ppa-uar-5* alleles *tu2020* and *tu2021* carried deletions of 11 bp and 4 bp, respectively (Fig. 2a). We found that all three alleles of *Ppa-uar-5* did not produce ubas#2 anymore, while only trace amounts of ubas#1 remained detectable in the *exo*-metabolomes (Fig. 2b, c, Supplementary Fig. 3 and Supplementary Data). Previously, tiny amounts of ubas#1 were also detected in *Ppa-uar-1* mutants[49]. However, in contrast to the complete absence of ubas#3 in *Ppa-uar-1* mutants[49], ubas#3 was abundantly produced in *Ppa-uar-5* mutants (Fig. 2b, c). Quantitative analysis of the three major UBAS ascarosides in the *exo*-metabolomes clearly showed that *Ppa-uar-5* mutants markedly produced much larger amounts of ubas#3 than wild type worms (Fig. 2f and Supplementary Data), indicating that ubas#3-should act as the biosynthetic precursor of ubas#1 and ubas#2. Furthermore, LC-MS examination of the *endo*-metabolomes of *Ppa-uar-5* mutants also showed that very large amounts of ubas#3 were produced, whereas ubas#1 and ubas#2 completely disappeared (Fig. 2d, e). Together, these experiments suggest that the absence of ubas#1 and ubas#2 was a result of blocking their biosynthetic pathway instead of the excretory process. Thus, *Ppa*-UAR-5 likely acts on the intermediate precursor ubas#3 and is involved in the biosynthesis of ubas#1 and ubas#2. Therefore, we have identified a new enzyme, *Ppa*-UAR-5, that acts downstream of *Ppa*-UAR-1 and is involved in linking oscr#9 and ascr#12 to the 2'-position of ubas#3 to finally furnish the biosynthesis of ubas#1 and ubas#2 (Fig. 2g). Lastly, microinjection experiments were performed to explore the expression patterns of *Ppa-uar-1* and *Ppa-uar-5*. However, we did not succeed in generating fluorescent worms, which might be due to several potential reasons, such as associated toxicity or extremely low level of expression.

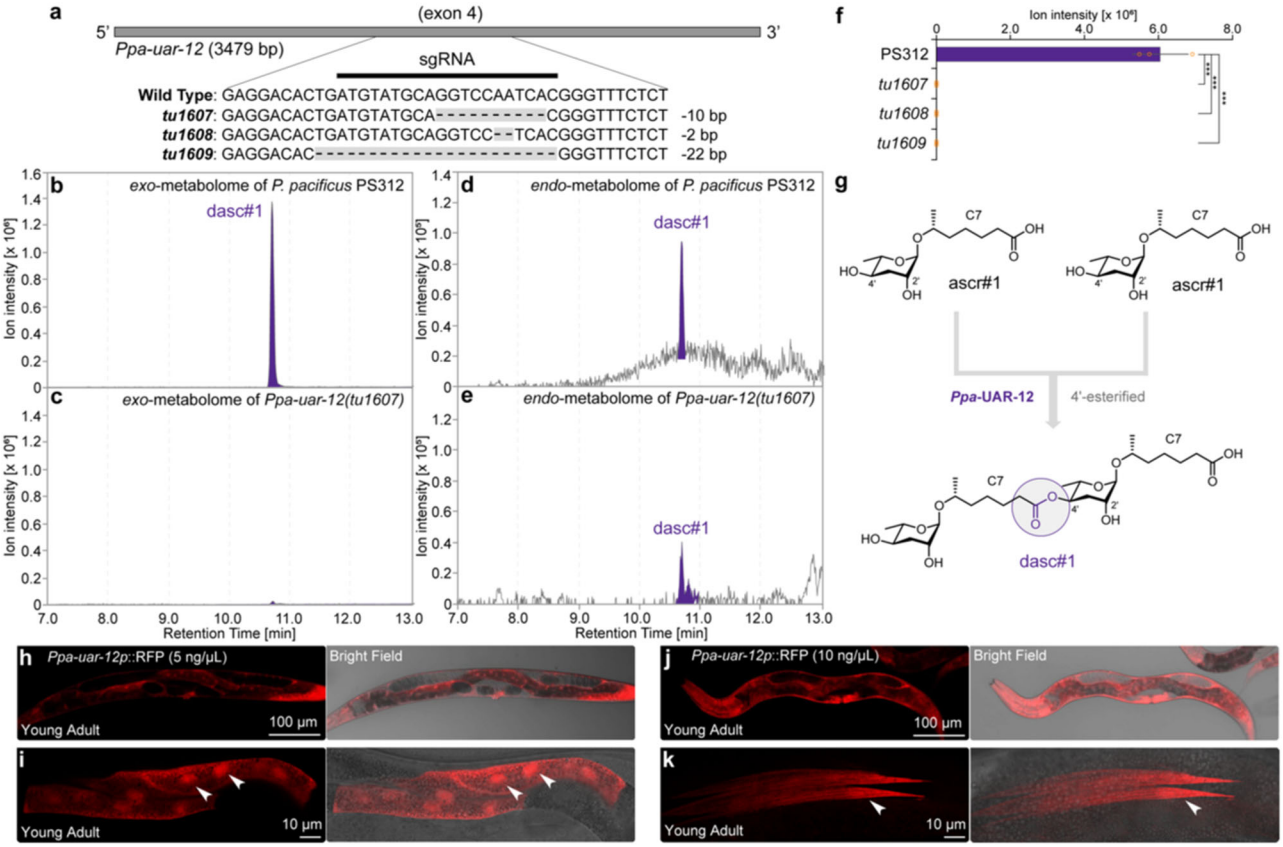


Fig. 3 | *Ppa*-UAR-12 regulates the biosynthesis of dimeric ascaroside dasc#1. **a** Three mutant alleles of *Ppa-uar-12* were generated by CRISPR/Cas9. **b**–**e** The production of dasc#1 in the *exo*-metabolomes (**b, c**) and *endo*-metabolomes (**d**, **e**) of both wild type *P. pacificus* PS312 and mutants were examined by LC-MS. **f** Ion abundances of dasc#1 in the *exo*-metabolomes of wild type *P. pacificus* PS312 and three mutants were quantitatively analysed ($n = 3$ per group) (Supplementary Data). Error bars represent standard deviation (± SD). Statistical analysis was performed using a two-tailed unpaired Student's *t*-test, $^{****}p < 0.0001$; $^{***}p < 0.001$; $^{**}p < 0.01$; $^{*}p < 0.05$; ns not significant. **g** Biosynthetic pathway of ascaroside dimer dasc#1. *Ppa*-UAR-12 specifically linked two units of ascr#1 at the 4'-position to biosynthesize dimeric ascaroside dasc#1. **h**, **i** Confocal sections and overlaid Nomarski images of the reporter line expressing *Ppa-uar-12p*::RFP at 5 ng/µL in the intestine. Scale bar of (**h**) is 100 µm. Scale bar of (**i**) is 10 µm. White arrows highlighted the nuclear localization of *Ppa-uar-12p*::RFP. **j**, **k** Confocal sections and overlaid Nomarski images of the reporter line expressing *Ppa-uar-12p*::RFP at 10 ng/µL in the epidermal cells. Scale bar of (**j**) is 100 µm. Scale bar of (**k**) is 10 µm. White arrows highlighted the expression of *Ppa-uar-12p*::RFP in an individual epidermal cell.

Ppa-UAR-12 regulates the biosynthesis of dimeric ascaroside dasc#1

Utilizing two monomeric building blocks of simple ascarosides, many nematodes including *C. elegans*[52] and its relatives[53] are able to produce specific pheromonal content of dimeric ascarosides, each of which harbors an exclusive homo- or heterodimeric structure isomerized through a 2'- or 4'-ester linkage. Extensive chemical investigation of the *P. pacificus exo*-metabolomes also supports the identification of four dimeric ascarosides dasc#1, dasc#4, dasc#6, and dasc#9 (Fig. 1b, Supplementary Figs. 4 and 5), from which dasc#1 [4'-(asc-C7)-asc-C7] and dasc#4 [2'-(asc-C5)-asc-C5] represent the two most abundant components[33,37]. The homodimeric dasc#1 is constructed by connecting two identical monomeric building blocks of ascr#1 (asc-C7) via a 4'-ester linkage (Fig. 1b), whereas another ascaroside dimer, dasc#4, carries two units of ascr#9 (asc-C5), which are instead linked at the 2'-position (Supplementary Fig. 4). However, how two simple ascarosides like ascr#1 and ascr#9 (Fig. 1a) are biochemically processed to yield diverse dimeric ascarosides with different structures and activities is still mysterious. Here, we report a new gene, *Ppa-uar-12*, encoding the *Ppa*-UAR-12 enzyme which is capable of establishing a unique 4'-ester linkage for the biosynthesis of dasc#1.

When analyzing the pheromone production in *Ppa-uar-12* mutants, we found that all three alleles of *Ppa-uar-12* mutants (*tu1607*, *tu1608* and *tu1609*), carrying deletions of 10 bp, 2 bp and 22 bp in exon 4, respectively (Fig. 3a), did not produce any trace of dasc#1 in their *exo*-metabolomes (Fig. 3b, c, f and Supplementary Data). In addition, only trace amounts of dasc#1 could be detected in the corresponding *endo*-metabolome samples (Fig. 3d, e), indicating that the biosynthesis of dasc#1 was abolished in *Ppa-uar-12* mutants. However, *Ppa-uar-12* mutants were still able to produce other types of pheromones (Supplementary Fig. 6 and Supplementary Data), suggesting that *Ppa*-UAR-12 regulates the biosynthesis of dasc#1 and has substrate-specificity on the biosynthetic precursor ascr#1. When we examined dasc#4, a previously identified 2'-linked homodimeric ascaroside[37], we found that dasc#4 was present in both the *exo*- and *endo*-metabolomes of *Ppa-uar-12* mutants (Supplementary Fig. 4a-e and Supplementary Data). These observations suggest that *Ppa*-UAR-12 is only involved in the biosynthesis of the 4'-linked but not the 2'-linked ascaroside dimer (Fig. 3g and Supplementary Fig. 4f). This was further supported by the detection of the other two 2'-linked minor dimeric ascarosides dasc#6 and dasc#9 in *Ppa-uar-12* mutants (Supplementary Fig. 5). Taken together, these results should demonstrate that *Ppa*-UAR-12 enables the connection of two monomeric building blocks of ascr#1 and regulates the biosynthesis of dasc#1 via the formation of a specific 4'-ester linkage (Fig. 3g). However, in vitro enzymatic assays will be required in the future to test the promiscuity of *Ppa*-UAR-12.

P. pacificus-produced dasc#1 has previously been reported to modulate its mouth-form dimorphism by inducing the Eu mouth morph[33]. We found that all three *Ppa-uar-12* mutants defective in dasc#1 production were still

capable of forming the Eu mouth form with ratios similar to the *P. pacificus* wild type animals (Supplementary Fig. 7). Thus, the abolishment of dasc#1 did not influence the mouth-form dimorphism of *P. pacificus*, indicating that pheromone signaling and dasc#1 alone cannot override other aspects of mouth-form regulation which resulted in the predominance of the Eu phenotype under the standard laboratory growth conditions.

Dissecting the expression patterns of biosynthetic genes may provide crucial insights into the cellular localization and the identification of the specific tissues responsible for synthesizing target pheromones. To investigate the expression pattern of *Ppa-uar-12*, a plasmid carrying the coding region of RFP codon-optimized for *P. pacificus*, under the control of the *Ppa-uar-12* promoter was generated[14], and stable transgenic reporter lines were obtained after microinjection. Confocal imaging revealed that the biosynthetic gene *Ppa-uar-12* was mainly expressed in the intestine of the worms (Fig. 3h). Besides the nuclei of intestinal cells (Fig. 3i), some weak RFP fluorescence was also observed in the epidermal cells (Fig. 3h). When we subsequently generated transgenic lines by injecting higher concentrations of the target DNA with a concentration of 10 ng/µL after linearization, we could further confirm that *Ppa-uar-12* was indeed expressed in the epidermal cells of *P. pacificus* (Fig. 3j, k). Together, we identified a new biosynthetic enzyme *Ppa*-UAR-12 from *P. pacificus* and revealed its cellular localization in the intestinal and epidermal cells for the biosynthesis of the dimeric ascaroside dasc#1.

Ppa-UAR-6 is essential for the biosynthesis of dauer pheromones part#9 and npar#1-3

In 2012, a group of NPAR pheromones including part#9 and npar#1-3 (Fig. 1b) was identified in *P. pacificus*[33]. All of these paratosides harbor an unusual core structure of paratose probably derived from the common ascarylose sugar via 2'-epimerization[33,54], and exhibit the ability to induce dauer formation[33,36]. So far, only some closely related species of *P. pacificus* from the *pacificus*-clade were found to produce NPAR pheromones[37]. Also, we have not found any clues about the biosynthetic origins of these signaling molecules over the last decade. Here, we identify a new gene *Ppa-uar-6* in *P. pacificus*, which encodes the *Ppa*-UAR-6 enzyme that is essential for the biosynthesis of both part#9 and npar#1-3.

Three *Ppa-uar-6* mutant alleles were generated by CRISPR/Cas9 engineering. While the first allele *tu2011* carried a 5 bp deletion in exon 3, the other two alleles *tu2012* and *tu2013* displayed insertions of 11 bp and 7 bp, respectively (Fig. 4a). LC-MS profiling of the NPAR pheromones from *Ppa-uar-6* mutant-derived *exo*-metabolomes showed that part#9 and npar#1-3 were all lost (Fig. 4b, c, f and Supplementary Data). Similarly, part#9 and npar#1-3 were also fully abolished in the corresponding *endo*-metabolome samples (Fig. 4d, e). These results represent the first evidence demonstrating that the biosynthesis of NPAR-type pheromones was completely blocked by mutating a specific gene, in this case *Ppa-uar-6*. In contrast, the other types of pheromones could still be detected from the *Ppa-uar-6* mutant worms (Supplementary Fig. 8 and Supplementary Data). Accumulating amounts of ascr#9 in mutant worms were observed when analyzing the production of three simple ascarosides (ascr#9, ascr#12 and ascr#1) (Supplementary Fig. 9 and Supplementary Data). These observations suggest that ascr#9 should play a role as the biosynthetic precursor of part#9 and npar#1-3, i.e., we hypothesize that *Ppa*-UAR-6 creates an ester link on ascr#9, resulting in the production of npar#1-3, by connecting tRNA metabolism-derived intermediate[33,55,56] to the C5 fatty acid side chain (Fig. 4g). Our findings also suggest that part#9 is derived from ascr#9 via hydrolysis of npar#1-3 (Fig. 4g), which happens downstream of the peroxisomal β-oxidation pathway that converts long-chain ascarosides into short-chain ascarosides (e.g., ascr#9) (Fig. 5a)[39,41]. This was further corroborated by our prior discovery that *Ppa-daf-22* mutant animals defective in the peroxisomal β-oxidation pathway, did not produce part#9 and npar#1-3 (Fig. 5)[41], which should result from blocking the production of their biosynthetic precursor ascr#9. Furthermore, recent studies showed that none of the long-chain paratosides could be detected from *Ppa-daf-22* mutants[54], which confirmed the short-chain paratoside part#9 should not originate from long-chain paratosides through cycles of the peroxisomal β-oxidation pathway. Collectively, these results demonstrate that the biosynthetic mechanism of the short-chain paratoside part#9 is very distinguishable from that of short-chain ascarosides (Figs. 4g and 5).

We generated *Ppa-uar-6p*::RFP transgenic lines through microinjection. We found the expression of *Ppa-uar-6* in the intestine of young adult hermaphrodites (Fig. 4h, i). Notably, earlier developmental stages from J1 to J4 worms (Fig. 4j-n) together with males (Fig. 4o) were also shown to have an identical intestinal expression pattern. Thus, the intestine of *P. pacificus* serves as the primary site for the biosynthesis of NPAR pheromones. Taken together, our work indicates that the complex *P. pacificus* pheromones discussed above are synthesized and pooled in the intestinal or epidermal cells.

Future applications of our workflow—genome-wide bioinformatics of genes encoding certain enzyme classes, followed by the systematic generation of gene knockouts, and subsequent LC-MS analysis of mutants—will possibly involve bioinformatic analysis from other *Pristionchus* and more distantly related nematode species given the many genome sequences are currently available (Fig. 1d). As a proof of principle, we have finally screened the orthologs of *Ppa*-UAR-6 across 31 *Pristionchus* species. We found single 1:1 ortholog of the *Ppa*-UAR-6 enzyme from each of the five *Pristionchus* species that are most closely related to *P. pacificus*, i.e. *P. taiwanensis*, *P. kurosawai*, *P. sikae*, *P. occultus* and *P. exspectatus* (Supplementary Fig. 10). In contrast, more distantly related *Pristionchus* species do not contain such 1:1 orthologs of *Ppa*-UAR-6. This result indicates the recent and ongoing evolutionary diversification of enzymes involved in the production of NPAR pheromones and is in line with our previous findings that NPAR pheromones are only produced by species of the *pacificus*-clade[37].

Discussion

The biosynthesis of plant and microbe-derived secondary metabolites has been intensively studied using many different bacteria and plant species[57–65]. In contrast, the biosynthesis of nematode pheromones is still challenging and has thus far only been investigated in *C. elegans* and *C. briggsae*, together with some preliminary studies in *P. pacificus*[32,49–51,66,67]. Here, we seek to investigate the biosynthetic origins of modular signaling molecules in *P. pacificus*, each of which exhibits considerable complex chemical structures (Fig. 1b). Previously, only one gene, *Ppa-uar-1*, had been discovered to be involved in the biosynthesis of UBAS ascarosides from *P. pacificus*[49]. In this study, LC-MS analysis of CRISPR/Cas9-generated mutants of 20 homologs of *Ppa-uar-1* facilitated the discovery of three carboxylesterase proteins *Ppa*-UAR-5, *Ppa*-UAR-12 and *Ppa*-UAR-6, which function downstream of the peroxisomal β-oxidation pathway (Fig. 5a) to regulate the biosynthesis of UBAS, DASC and NPAR pheromones, respectively (Fig. 5b). These continuous efforts provide a step forward in uncovering the intricate biosynthetic regulatory mechanisms for each type of modular signaling molecules in *P. pacificus*.

In the future, the application of such a workflow—genome-wide bioinformatics of genes encoding certain enzyme classes, followed by the systematic generation of gene knockouts, and subsequent LC-MS analysis of mutants—will possibly accelerate the discovery of biosynthetic genes for modular signaling molecules from other *Pristionchus* and more distantly related nematode species (Fig. 1d). Given that the CRISPR/Cas9 technique is widely applicable to knock out genes in *Pristionchus* species (e.g., *P. mayeri*)[68], it is increasingly feasible to investigate the detailed biosynthetic mechanisms of modular ascarosides in other nematodes. For example, it is very likely that *Ppa*-UAR-5 is also involved in the biosynthesis of the recently identified UPAS pheromones (Supplementary Fig. 11), given that UPAS pheromones share very similar structures with UBAS[37]. Similarly, the recent discovery of novel ascarosides from other *Caenorhabditis* species like *C. briggsae*[53,54,69–71], also offers great opportunities to explore their detailed biosynthetic mechanisms[32,51,67]. Therefore, the workflow described in this study highlights a promising strategy to identify enzymes involved in the regulation of other complex pheromones in nematodes and potentially beyond (Fig. 1d).

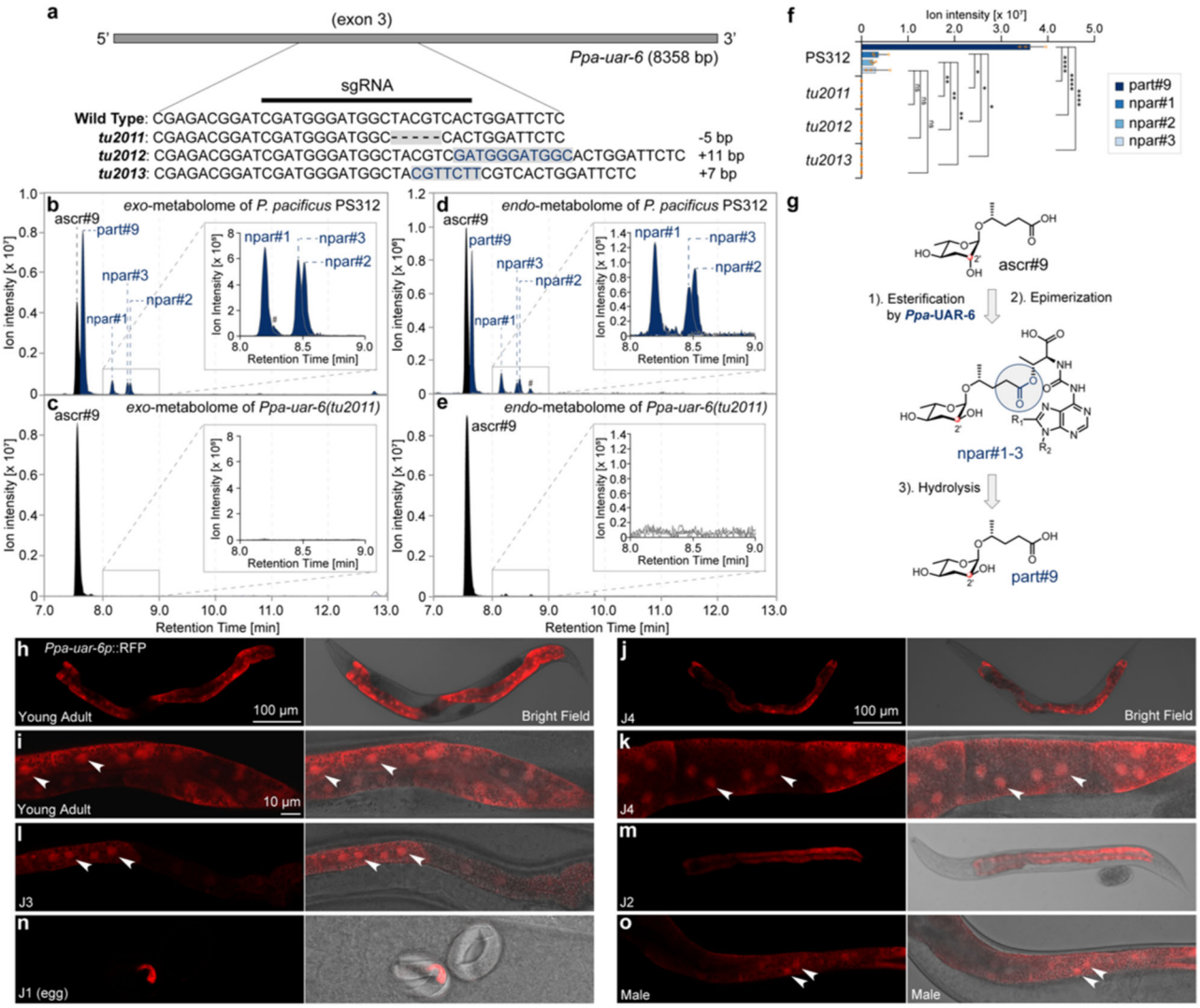


Fig. 4 | Biosynthetic investigation of NPAR pheromones. a Three mutant alleles of *Ppa-uar-6* were generated by CRISPR/Cas9. **b**—**e** The production of NPAR pheromones in the *exo*-metabolomes (**b**, **c**) and *endo*-metabolomes (**d**, **e**) of both wild type *P. pacificus* PS312 and mutants were examined by LC-MS. The pound sign (#) denotes non-ascarosides. Inserted ion chromatograms of npar#1-3 were magnified 10 times. **f** Ion abundances of NPAR pheromones in the *exo*-metabolomes of wild type *P. pacificus* PS312 and mutants were quantitatively analysed ($n = 3$ per group) (Supplementary Data). Error bars represent standard deviation (± SD). Statistical analysis was performed using a two-tailed unpaired Student's *t*-test, $^{****}p < 0.0001$; $^{***}p < 0.001$; $^{**}p < 0.01$; $^{*}p < 0.05$; ns not significant. **g** Proposed biosynthetic pathway of NPAR pheromones. 1). *Ppa*-UAR-6 linked tRNA metabolism-derived intermediate to the C5 fatty acid side chain of ascr#9; 2). npar#1-3 were then biosynthesized following an epimerization step; 3). part#9 should be a hydrolysis product of npar#1-3. **h**—**n** Section and Nomarski images of a transgenic worm in all developmental stages ((**h**, **i**) Young adult; (**j**, **k**) J4 larval stage; (**l**) J3 larval stage; (**m**) J2 larval stage; (**n**) J1 larval stage) expressing *Ppa-uar-6p*::RFP. Scale bar of (**h**) and (**j**) is 100 µm. Scale bar of (**i**) and (**k**—**n**) is 10 µm. White arrows highlighted the nuclear localization of *Ppa-uar-6p*::RFP. **o** Section and Nomarski images of a male worm expressing *Ppa-uar-6p*::RFP in the nucleus of intestinal cells. Scale bar is 10 µm. White arrows highlighted the nuclear localization of *Ppa-uar-6p*::RFP.

Similar to the discovery of the *uar* genes in *P. pacificus*, more than 40 homologs of *Ppa-uar-1* were identified in the genome of *C. elegans*, which are referred to as *Cel-cest* genes. Indeed, five important candidate genes were ascertained to regulate the biosynthesis of different types of modular ascarosides, through the formation of an ester or amide bond[32,50,51]. For example, the *C. elegans* sex pheromone ascr#8[72] is formed by CEST-2.2 through the introduction of a folate metabolic pathway-derived intermediate to the terminal carboxyl group of ascr#7 (asc-ΔC7)[51]. Thus, it will be highly interesting to study the biosynthetic mechanisms and capacities of UAR and CEST proteins in a broader evolutionary context.

Along with the CEST enzymes from *C. elegans*[50,51], all the newly identified proteins *Ppa*-UAR-5, *Ppa*-UAR-6, and *Ppa*-UAR-12, as well as *Ppa*-UAR-1, share high similarities of their predicted protein structures (Supplementary Fig. 12) and exhibit high specificity for their substrates. For example, the esterase proteins *Ppa*-UAR-1 and *Ppa*-UAR-5 exhibit substrate-specificity on ascr#9 and ubas#3, respectively, by selectively targeting their 4'- and 2'-position for the biochemical reactions (Fig. 2g). Similarly, *Ppa*-UAR-12 establishes a 4'- but not a 2'-linkage for the biosynthesis of dimeric ascarosides (Fig. 3g). However, to test the selectivity and specificity of these enzymes in more detail will require additional efforts to purify UAR proteins from heterogeneous system to reconstitute the biosynthesis of pheromones in vitro. Currently, we can not completely rule out the promiscuity of some of the studied enzymes.

Based on our experiments and other studies from different laboratories[44,50,51,73], the confirmed expressions of the carboxylesterase genes in the intestine and in several epidermal cells further support the notion that these excretory tissues serve as the primary sites for the biosynthesis of nematode signaling molecules. In summary, using a workflow including (i) bioinformatic tools for genome-wide carboxylesterase identification, (ii) CRISPR/Cas9 gene knockouts and (iii) chemical analysis of multiple mutant

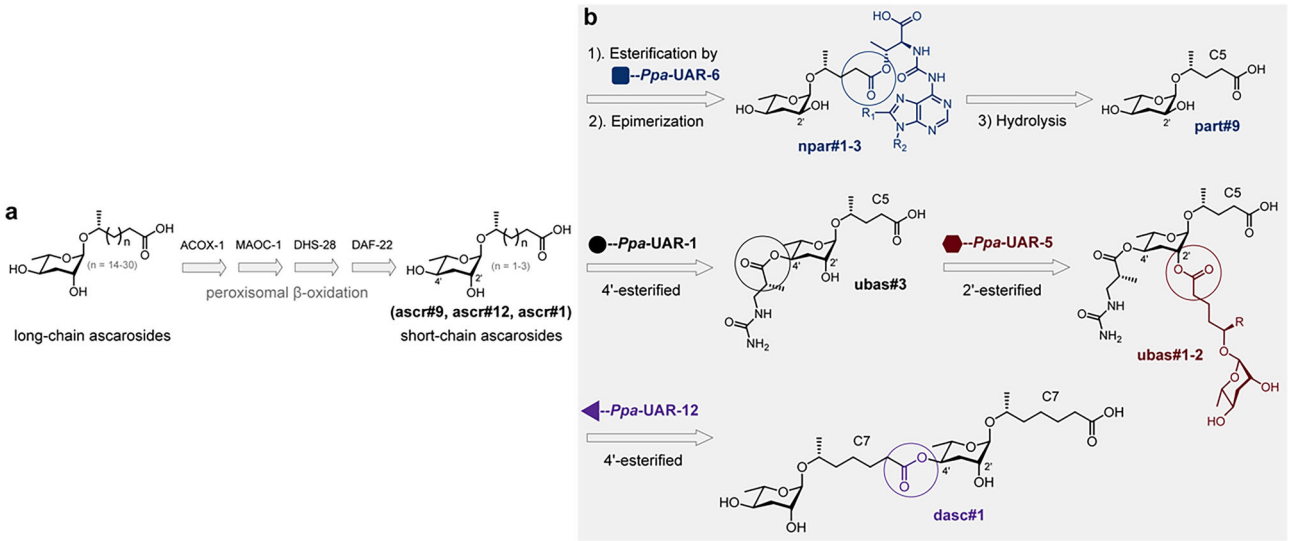


Fig. 5 | Biosynthetic mechanisms of modular pheromones from *P. pacificus*. **a** Long-chain ascarosides went through several cycles of peroxisomal β-oxidation pathway[41] to yield short-chain ascarosides as the core structures, which could be further chemically modified by divergent carboxylesterases to produce complex modular pheromones. *Ppa-daf-22* mutants did not produce any short-chain ascarosides or modular pheromones[41]. **b** In this study, *Ppa*-UAR-5, *Ppa*-UAR-12 and *Ppa*-UAR-6 were discovered to be involved in the biosynthesis of ubas#1-2, dasc#1, and the group of npar#1-3 and part#9 pheromones, respectively. *Ppa*-UAR-1 was previously found to specifically link ureidoisobutyric acid to the 4'-position of ascr#9 for the biosynthesis of ubas#3[49].

lines, three new biosynthetic genes *Ppa-uar-5*, *Ppa-uar-12*, and *Ppa-uar-6* were discovered from *P. pacificus*. The identified carboxylesterases specifically function in the intestinal and epidermal cells to regulate the biosynthesis of modular pheromones. All of these biosynthetic enzymes exhibit substrate-specificity. This systematic study largely illuminates the intricate biosynthetic mechanisms by which diversification of carboxylesterases in *P. pacificus* generates complex modular signaling pheromones.

Methods

Nomenclature of ascarosides from *P. pacificus*

In additional to the four-letter codes "SMID" nomenclature rules (www.smid-db.org), structure-based abbreviations "(head group-)asc-(ω)(Δ)C#(terminal group)" were also used to describe common ascarosides, UBAS ascarosides and NPAR. For those DASC ascarosides consisting of two simple ascaroside units, the first ascaroside was placed in parentheses to differentiate it from the second ascaroside. For example, 4'-linked dimeric ascaroside dasc#1 was named as dasc#1 [4'-(asc-C7)-asc-C7]; 2'-linked dimeric ascaroside dasc#4 was named as dasc#4 [2'-(asc-C5)-asc-C5].

Nematode strains and maintenance

All the mutant nematodes used in this study were listed in the Supplementary Table 1. A mixture of 3 g NaCl, 16 g Agar (Kobe I pulv. 1100 g/cm^2), 2.5 g peptone, 1 ml 1 M $CaCl_2$, 1 ml 1 M $MgSO_4$, 25 ml 1 M KPO_6 (KH_2PO_4 and K_2HPO_4) was dissolved in 1 l distilled water, which was mixed well and autoclaved. Nematode Growth Medium (NGM) agar was prepared by further adding 1 ml 5 mg/ml Cholesterol (in Ethanol) into the sterilized solution. The NGM agar could be poured or pumped into petri plates. Medium size plates (60 mm diameter) were used for general strain maintenance, and larger plates (90 mm diameter) were used for growing large quantities of worms, such as for liquid culture. All the strains of wild type and mutants were maintained at 20 °C on NGM agar plates seeded with *E. coli* OP50 lawn.

Chemicals and reagents

All the pheromones from *P. pacificus* PS312 wild type animals have already been elucidated before[33,36,37], these known pheromones were applied as standard control for chemical analysis while investigating their biosynthetic pathways. For the target pheromones from CRISPR/Cas9 generated mutants, their retention times, molecular weights and MS/MS fragmentation patterns were carefully and extensively examined by LC-ESI-qTOF-HR-MS, all of which were highly consistent with those from wild type worms (Figs. 2, 3 and 4, Supplementary Data). New biosynthetic intermediates, by-products or end products were not described or discovered from any mutants in this study.

Protein sequence alignment and phylogenetic reconstruction

The amino acid sequence of *Ppa*-UAR-1 annotated by Falcke et al.[49] was used for BLASTP search (*e*-value < 0.00001) against *P. pacificus* protein annotations (version 3) on www.pristionchus.org. Seventy-five protein sequences were obtained as the top BLASTP hits. These sequences were aligned using the MUSCLE program (version 3.8.31)[74]. The resulting multiple sequence alignment was used for a maximum likelihood tree reconstruction using the phangorn package in R (version 4.3.1, model = "WAG + G(4) + I", optNni = TRUE)[75]. The best tree model was determined using the pml_bb function. 100 bootstrap replicates were calculated for the midpoint rooted tree and nodes with the standard support values above 50 were visualized on the generated tree in Supplementary Fig. 1.

To examine the conserved Glu-His-Ser catalytic triad, the alignments of amino acid sequences from four functional proteins (i.e., *Ppa*-UAR-1, *Ppa*-UAR-5, *Ppa*-UAR-12 and *Ppa*-UAR-6) were visualized on Clustal Omega webpage[76]. The conserved motif and catalytic residues were characterized in Supplementary Fig. 2.

Previously, we have screened all the pheromone compositions from 31 *Pristionchus* species across the genus of *Pristionchus*, and only few nematodes from the *pacificus*-clade were restrictively found to produce NPAR pheromones[37]. In this study, *Ppa*-UAR-6 enzyme was discovered to be essential for the biosynthesis of NPAR pheromones. To test the evolutionary consistency, a phylogenetic tree of 1531 homologous proteins of *Ppa*-UAR-6 across 31 *Pristionchus* species was constructed in Supplementary Fig. 10. In brief, BLASTP search using default settings (*e*-value = 10) on the internal BLAST server was applied to screen the protein sequences, which were aligned using the MUSCLE program (version 3.8.31)[74,77]. The aligned sequences were used to generate a phylogenetic tree on raxmlGUI (version 2.0.10) with an application of the default settings (Model: BLOSUM62; Run mode: ML tree search + bootstrapping (Transfer Bootstrap); Bootstrap replicates: 100)[78]. The resultant tree was then visualized and annotated on the Interactive Tree of Life (iTOL) platform (version 7.2.1)[79].

CRISPR/Cas9-mediated knockout of twenty esterase genes

CRISPR/Cas9 knockouts were generated using previously published protocols in *P. pacificus*[13,14]. CRISPR RNAs (crRNAs) were designed to target the first, second, third or fourth exon of the gene. crRNAs and tracrRNA (Cat. No. 1072534) were synthesized by Integrated DNA Technologies (IDT). crRNAs were fused to tracrRNA (IDT) at 95 °C for 5 min, after which the Cas9 endonuclease (Cat. No. 1081058) purchased from IDT was further added. The CRISPR/Cas9 complex was prepared by mixing 0.5 mg/ml Cas9 nuclease, 0.1 mg/ml tracrRNA, and 0.056 mg/ml crRNA in the TE buffer followed by a 10 min incubation at 37 °C. The *Ppa-eft-3p*::RFP plasmid (20 ng/μl) was added as co-injection marker[14]. Specific crRNA and primers applied for knocking out each candidate gene were listed in Supplementary Table 3. Microinjections were performed following standard practice using an Eppendorf microinjection system. Injected P0s were removed ca. 16 h post injection. Eggs from each injected P0 animal were allowed to hatch and further transferred onto single NGM agar plates. These F1 animals were genotyped via Sanger sequencing to establish heterozygous null mutant worms. A similar protocol was used to screen homozygous worms in the subsequent F2 generation.

Reporter line of *Ppa-uar-12*

To construct the transcriptional reporter line for *Ppa-uar-12*, a 3.0 kb *Ppa-uar-12* promoter fragment was amplified from *P. pacificus* genomic DNA using 2 × Phanta Flash Master Mix (Vazyme, P520). This fragment was cloned into the *Ppa-eft-3p*::RFP plasmid vector (a gift from Ziduan Han, Northwest A&F University, China) upstream of RFP to substitute the *Ppa-eft-3* promoter using ClonExpress Ultra One Step Cloning Kit (Vazyme, C115) through homologous recombination. DNAs were prepared from multiple independent isolates, then verified by restriction digestion and sequencing. Plasmid DNA and genomic DNA were cut by PstI and injected as two fragments into the gonads of young adult *P. pacificus* worms at concentrations of 5 ng/μL and 30 ng/μL, respectively, to establish intergenerationally inherited worms that could consistently express RFP fluorescence. Constructs were normally injected at 5 ng/μL or 10 ng/μL. The expression pattern was confirmed in more than three independent lines. Single worms were imaged using a Zeiss LSM 980 confocal microscope. Stable lines of *Ppa-uar-12* were imaged and properly frozen at -80 °C for further usage. Worms recovered from -80 °C were confirmed to consistently express RFP fluorescence.

Reporter line of *Ppa-uar-6*

Reporter lines of *Ppa-uar-6* were constructed using the identical method as described for *Ppa-uar-12*. Constructs were injected at 10 ng/μL. The expression pattern was confirmed in more than three independent lines. Single worms were imaged using a Zeiss LSM 980 confocal microscope. Stable lines of *Ppa-uar-6* were also imaged and frozen at -80 °C for further usage. Worms recovered from -80 °C were confirmed to consistently express RFP fluorescence.

Preparation of bacterial food source for growing nematodes in liquid culture

LB medium (4 l) inoculated with a single colony of *E. coli* OP50 was incubated in a shaker at 37 °C with 170 rpm. After one night, *E. coli* OP50 pellets were collected by centrifugation (Beckman Coulter, Avanti JE 369003, JA10 rotor, 5000 rpm, 10 min, 4 °C). The supernatants were removed and resulted *E. coli* OP50 pellets were transferred into 50 ml falcon tubes for further centrifugation (Cence, H2050R, Swing rotor 0302891036, 4000 rpm, 10 min, 4 °C). *E. coli* OP50 pellets were equally split into six sterilized plastic tubes (50 ml) and stored in the refrigerator at 4 °C for further usage. All the experiments were performed in a clean bench to avoid any potential contamination. Each tube of *E. coli* OP50 pellet was diluted by adding 10 ml M9 buffer. On the first day, 2.5 ml *E. coli* OP50 pellets were added into the nematode liquid cultures (50 ml) as their bacterial food source.

Collection of *exo*-metabolome (culture medium) and *endo*-metabolome (worm pellets) from mutant worms grown in 50 ml liquid culture

Bleached worms were initially cultured on five NGM plates (9 cm diameter) that were coated with 700 μl *E. coli* OP50. Using 6 ml M9 buffer to wash worms into a sterilized glass flask containing 50 ml S-medium. On the first day, prepared *E. coli* OP50 was diluted in 10 ml M9 buffer, and 2.5 ml of diluted *E. coli* OP50 pellets were added into each flask as bacterial food source. Worm cultures were incubated at 22 °C and 140 rpm for 1 week. Worms were harvested through centrifugation (Eppendorf, Centrifuge 5810 R, FA-45-6-30 rotor, 8000 rpm, 10 min, 4 °C) to collect the culture medium (*exo*-metabolome) as well as the worm pellets (*endo*-metabolome). The resulting *exo*-metabolome samples were frozen at -80°C for one night and further dried into solid powder by lyophilizer. The solid powder was then extracted three times with 100 ml methanol each. Crude extracts were combined, filtered and dried at 40 °C under reduced pressure to remove organic solvents. Samples were finally dissolved in 1 ml methanol and 100 μl aliquots were applied for LC-MS analysis. The *endo*-metabolome samples were also frozen at -80 °C for one night and further dried by lyophilization into a solid powder. The dried powder was extracted three times by adding 5 ml methanol each time. Crude extracts were combined, filtered and dried at 40 °C under reduced pressure to remove methanol. Samples were finally dissolved in 0.5 ml methanol and 100 μl aliquots were applied for LC-MS analysis. All the 57 mutant strains were successfully grown in S-medium for chemical analysis. *Exo*-metabolome and *endo*-metabolome samples of wild type *P. pacificus* PS312 were prepared as standard controls. Three biological replicates were performed for each strain.

Chemical analysis of pheromones in *exo*-metabolomes and *endo*-metabolomes

Exo-metabolome and *endo*-metabolome samples were separately dissolved in 1 ml and 0.5 ml methanol. Samples were further filtered and 100 μl aliquots were applied for LC-MS analysis. LC-HR(ESI^-)-MS analysis was performed using an Agilent 1290 Infinity II Series HPLC system connected to an Agilent 6546 high resolution qTOF spectrometer equipped with an electrospray ionization operating in negative ion mode. The HPLC instrument was equipped with an Agilent Eclipse XDB-C18 column (250 × 3 mm, 5 μm particle diameter). A mixture of water (H_2O + 0.1% Formic acid) and acetonitrile (ACN + 0.1% Formic acid) was used to elute the LC-MS system with a flow rate of 0.4 ml/min (an injection volume of 2 μl). The LC-MS system was equilibrated with 3% acetonitrile for 3 min, followed by gradient elution (3%-100% acetonitrile) over 15 min, and finally washed with 100% acetonitrile for 2 min, after which the acetonitrile content of the solvent was decreased to 3% within the next 2 min. After every third sample, a blank MeOH run was performed using the same method. The *exo*- and *endo*-metabolomes of mutants were analyzed by LC-MS under the condition of Electrospray ionization (ESI) with Agilent 6546 high resolution qTOF system operating with capillary voltage 3500 V, dry gas flow of 12.0 l/min and dry temperature 275 °C. LC-MS analysis was conducted using the single MS mode by scanning from m/z 50 to 1700. Area (relative ion abundances) of the EIC (Extracted Ion Chromatograms) ion peaks for each individual pheromone in both wild type and mutants were calculated for quantitative analysis (Figs. 2, 3, 4). Agilent Qualitative Analysis 10.0 software was used to calibrate, process and analyze the mass data of mutants and wild type *P. pacificus* PS312.

Mouth-form phenotyping

The mouth-form dimorphism of *tu1607*, *tu1608* and *tu1609* mutants were screened by a Zeiss LSM 980 microscope using standard protocols[33]. Wild type *P. pacificus* PS312 was used as control. All the nematodes grown on NGM agar plates were kept in non-starved conditions and crowding of populations was properly avoided. Fresh *E. coli* OP50 culture was applied as food source. Young adult worms were picked for mouth-form screening (Supplementary Fig. 7). At least ten individual worms for each mutant strain and wild type were selected for mouth-form screening. All the tested worms

were equipped with the Eu mouth form. Intermediate or St mouth form was not observed for any strains in this study.

Statistics and reproducibility

Statistical analyses were conducted to determine significance of pairwise differences of pheromone production between mutants and wild type worms by using GraphPad Prism 10.5.0. At least three biological replicates for all the experiments were performed. Data were analyzed using a two-tailed unpaired Student's *t*-test. Significance levels were indicated as $^{****}p < 0.0001$; $^{***}p < 0.001$; $^{**}p < 0.01$; $^{*}p < 0.05$; ns not significant. Data were expressed as mean ± SD. R version 4.3.1 (www.R-project.org) was used to analyze the phylogenetic relationship of 76 UAR proteins.

Reporting summary

Further information on research design is available in the Nature Portfolio Reporting Summary linked to this article.

Data availability

The data that support the findings of this study are available within the main text and the Supplementary information. Supplementary Data are provided as source data with this paper. Raw LC-MS data that support the findings of this study are available in the Figshare repository with the identifier https://doi.org/10.6084/m9.figshare.29648123. Chemical identities of each individual pheromone such as molecular weights and retention times are described in Supplementary Data.

Received: 13 April 2025; Accepted: 31 July 2025;
Published online: 13 August 2025

References

1. Sommer, R. J. *Pristionchus Pacificus-a Nematode Model For Comparative And Evolutionary Biology*. Vol. 420 (Brill Academic Pubulisher, Nertherlands, 2015).
2. Schroeder, N. E. Introduction to *Pristionchus pacificus* anatomy. *J. Nematol.* **53**, e2021-91 (2021).
3. Herrmann, M., Mayer, W. E. & Sommer, R. J. Nematodes of the genus *Pristionchus* are closely associated with scarab beetles and the Colorado potato beetle in Western Europe. *Zool. (Jena.)* **109**, 96–108 (2006).
4. Herrmann, M. et al. The nematode *Pristionchus pacificus* (Nematoda: Diplogastridae) is associated with the oriental beetle *Exomala orientalis* (Coleoptera: Scarabaeidae) in Japan. *Zool. Sci.* **24**, 883–889 (2007).
5. Kanzaki, N. et al. Nine new *Pristionchus* (Nematoda: Diplogastridae) species from China. *Zootaxa* **4943**, zootaxa.49431 (2021).
6. Susoy, V., Ragsdale, E. J., Kanzaki, N. & Sommer, R. J. Rapid diversification associated with a macroevolutionary pulse of developmental plasticity. *eLife* **4**, e05463 (2015).
7. Bento, G., Ogawa, A. & Sommer, R. J. Co-option of the hormone-signalling module dafachronic acid-DAF-12 in nematode evolution. *Nature* **466**, 494–497 (2010).
8. Bumbarger, D. J., Riebesell, M., Rödelsperger, C. & Sommer, R. J. System-wide rewiring underlies behavioral differences in predatory and bacterial-feeding nematodes. *Cell* **152**, 109–119 (2013).
9. Wilecki, M., Lightfoot, J. W., Susoy, V. & Sommer, R. J. Predatory feeding behaviour in *Pristionchus* nematodes is dependent on phenotypic plasticity and induced by serotonin. *J. Exp. Biol.* **218**, 1306–1313 (2015).
10. Sieriebriennikov, B., Markov, G. V., Witte, H. & Sommer, R. J. The role of DAF-21/Hsp90 in mouth-form plasticity in *Pristionchus pacificus*. *Mol. Biol. Evol.* **34**, 1644–1653 (2017).
11. Sieriebriennikov, B. & Sommer, R. J. Developmental plasticity and robustness of a nematode mouth-form polyphenism. *Front. Genet.* **9**, 382 (2018).
12. Lightfoot, J. W. et al. Small peptide–mediated self-recognition prevents cannibalism in predatory nematodes. *Science* **364**, 86–89 (2019).
13. Witte, H. et al. Gene inactivation using the CRISPR/Cas9 system in the nematode *Pristionchus pacificus*. *Dev. Genes Evol.* **225**, 55–62 (2015).
14. Han, Z. et al. Improving trangenesis efficiency and CRISPR-associated tools through codon optimization and native intron addition in *Pristionchus* nematodes. *Genetics* **216**, 947–956 (2020).
15. Nakayama, K. I., Ishita, Y., Chihara, T. & Okumura, M. Screening for CRISPR/Cas9-induced mutations using a co-injection marker in the nematode *Pristionchus pacificus*. *Dev. Genes Evol.* **230**, 257–264 (2020).
16. Hiraga, H., Ishita, Y., Chihara, T. & Okumura, M. Efficient visual screening of CRISPR/Cas9 genome editing in the nematode *Pristionchus pacificus*. *Dev. Growth Differ.* **63**, 488–500 (2021).
17. Ragsdale, E. J., Müller, M. R., Rödelsperger, C. & Sommer, R. J. A developmental switch coupled to the evolution of plasticity acts through a sulfatase. *Cell* **155**, 922–933 (2013).
18. Golden, J. W. & Riddle, D. L. A pheromone influences larval development in the nematode *Caenorhabditis elegans*. *Science* **218**, 578–580 (1982).
19. Bartley, J. P. Structure of the ascarosides from *Ascaris suum*. *J. Nat. Prod.* **59**, 921–926 (1996).
20. Jeong, P. Y. et al. Chemical structure and biological activity of the *Caenorhabditis elegans* dauer-inducing pheromone. *Nature* **433**, 541–545 (2005).
21. Butcher, R. A., Fujita, M., Schroeder, F. C. & Clardy, J. Small-molecule pheromones that control dauer development in *Caenorhabditis elegans*. *Nat. Chem. Biol.* **3**, 420–422 (2007).
22. Choe, A. et al. Ascaroside signaling is widely conserved among nematodes. *Curr. Biol.* **22**, 772–780 (2012).
23. Srinivasan, J. et al. A modular library of small molecule signals regulates social behaviors in *Caenorhabditis elegans*. *PLoS Biol.* **10**, e1001237 (2012).
24. Ludewig, A. H. & Schroeder, F. C. Ascaroside signaling in *C. elegans*. *WormBook* **18**, 1–22 (2013).
25. Schroeder, F. C. Modular assembly of primary metabolic building blocks: a chemical language in *C. elegans*. *Chem. Biol.* **22**, 7–16 (2015).
26. von Reuss, S. H. & Schroeder, F. C. Combinatorial chemistry in nematodes: modular assembly of primary metabolism-derived building blocks. *Nat. Prod. Rep.* **32**, 994–1006 (2015).
27. Leighton, D. H. & Sternberg, P. W. Mating pheromones of Nematoda: olfactory signaling with physiological consequences. *Curr. Opin. Neurobiol.* **38**, 119–124 (2016).
28. Butcher, R. A. Decoding chemical communication in nematodes. *Nat. Prod. Rep.* **34**, 472–477 (2017a).
29. Butcher, R. A. Small-molecule pheromones and hormones controlling nematode development. *Nat. Chem. Biol.* **13**, 577–586 (2017b).
30. von Reuss, S. H. Exploring modular glycolipids involved in nematode chemical communication. *Chimia* **72**, 297–303 (2018).
31. Butcher, R. A. Natural products as chemical tools to dissect complex biology in *C. elegans*. *Curr. Opin. Chem. Biol.* **50**, 138–144 (2019).
32. Wrobel, C. J. J. & Schroeder, F. C. Repurposing degradation pathways for modular metabolite biosynthesis in nematodes. *Nat. Chem. Biol.* **19**, 676–686 (2023).
33. Bose, N. et al. Complex small-molecule architectures regulate phenotypic plasticity in a nematode. *Angew. Chem. Int. Ed.* **52**, 12438–12443 (2012).
34. Bose, N. et al. Natural variation in dauer pheromone production and sensing supports intraspecific competition in nematodes. *Curr. Biol.* **24**, 1536–1541 (2014).
35. Sommer, R. J. *Pristionchus*-beetle association: towards a new natural history. *J. Invertebr. Pathol.* **209**, 108243 (2025).

36. Yim, J. J., Bose, N., Meyer, J. M., Sommer, R. J. & Schroeder, F. C. Nematode signaling molecules derived from multimodular assembly of primary metabolic building blocks. *Org. Lett.* **17**, 1648–1651 (2015).
37. Dong, C., Weadick, C. J., Truffault, V. & Sommer, R. J. Convergent evolution of small molecule pheromones in *Pristionchus* nematodes. *eLife* **9**, e55687 (2020).
38. Butcher, R. A. et al. Biosynthesis of the *Caenorhabditis elegans* dauer pheromone. *Proc. Natl. Acad. Sci. USA.* **106**, 1875–1879 (2009).
39. von Reuss, S. H. et al. Comparative metabolomics reveals biogenesis of ascarosides, a modular library of small-molecule signals in *C. elegans*. *J. Am. Chem. Soc.* **134**, 1817–1824 (2012).
40. Zhang, X. et al. Acyl-CoA oxidase complexes control the chemical message produced by *Caenorhabditis elegans*. *Proc. Natl. Acad. Sci. USA.* **112**, 3955–3960 (2015).
41. Markov, G. V. et al. Functional conservation and divergence of *daf-22* paralogs in *Pristionchus pacificus* dauer development. *Mol. Biol. Evol.* **33**, 2506–2514 (2016).
42. Zhang, X., Li, K., Jones, R. A., Bruner, S. D. & Butcher, R. A. Structural characterization of acyl-CoA oxidases reveals a direct link between pheromone biosynthesis and metabolic state in *Caenorhabditis elegans*. *Proc. Natl. Acad. Sci. USA.* **113**, 10055–10060 (2016).
43. Zhang, X., Wang, Y., Perez, D. H., Jones Lipinski, R. A. & Butcher, R. A. Acyl-CoA oxidases fine-tune the production of ascaroside pheromones with specific side chain lengths. *ACS Chem. Biol.* **13**, 1048–1056 (2018).
44. Zhou, Y. et al. Biosynthetic tailoring of existing ascaroside pheromones alters their biological function in *C. elegans*. *eLife* **7**, e33286 (2018).
45. Ogawa, A., Streit, A., Antebi, A. & Sommer, R. J. A conserved endocrine mechanism controls the formation of dauer and infective larvae in nematodes. *Curr. Biol.* **19**, 67–71 (2009).
46. Mayer, M. G. & Sommer, R. J. Natural variation in *Pristionchus pacificus* dauer formation reveals cross-preference rather than self-preference of nematode dauer pheromones. *Proc. Biol. Sci.* **278**, 2784–2790 (2011).
47. Mayer, M. G., Rödelsperger, C., Witte, H., Riebesell, M. & Sommer, R. J. The orphan gene dauerless regulates dauer development and intraspecific competition in nematodes by copy number variation. *PLoS Genet.* **11**, e1005146 (2015).
48. Werner, M. S., Claaßen, M. H., Renahan, T., Dardiry, M. & Sommer, R. J. Adult influence on juvenile phenotypes by stage-specific pheromone production. *iScience* **10**, 123–134 (2018).
49. Falcke, J. M. et al. Linking genomic and metabolomic natural variation uncovers nematode pheromone biosynthesis. *Cell Chem. Biol.* **25**, 787–796.e12 (2018).
50. Faghih, N. et al. A large family of enzymes responsible for the modular architecture of nematode pheromones. *J. Am. Chem. Soc.* **142**, 13645–13650 (2020).
51. Le, H. H. et al. Modular metabolite assembly in *C. elegans* depends on carboxylesterases and formation of lysosome-related organelles. *eLife* **9**, e61886 (2020).
52. Bhar, S. et al. An acyl-CoA thioesterase is essential for the biosynthesis of a key dauer pheromone in *C. elegans*. *Cell Chem. Biol.* **31**, 1011–1022 (2024).
53. Dong, C., Dolke, F., Bandi, S., Paetz, C. & von Reuss, S. H. Dimerization of conserved ascaroside building blocks generates species-specific male attractants in *Caenorhabditis* nematodes. *Org. Biomol. Chem.* **18**, 5253–5263 (2020).
54. Bergame, C. P., Dong, C., Sutour, S. & von Reuss, S. H. Epimerization of an ascaroside-type glycolipid downstream of the canonical β-oxidation cycle in the nematode *Caenorhabditis nigoni*. *Org. Lett.* **21**, 9889–9892 (2019).
55. Machnicka, M. A. et al. MODOMICS: a database of RNA modification pathways-2013 update. *Nucleic Acids Res.* **41**, D262–D267 (2012).
56. Thiaville, P. C., Iwata-Reuyl, D. & de Crécy-Lagard, V. Diversity of the biosynthesis pathway for threonylcarbamoyladenosine (t^6A), a universal modification of tRNA. *RNA Biol.* **11**, 1529–1539 (2014).
57. Wink, M. *Annual Plant Reviews: Biochemistry Of Plant Secondary Metabolism* 40th edn (Wiley-Blackwell Publishing Ltd, 2010).
58. Crawford, J. M. & Clardy, J. Bacterial symbionts and natural products. *Chem. Commun.* **47**, 7559–7566 (2011).
59. Donia, M. S. et al. A systematic analysis of biosynthetic gene clusters in the human microbiome reveals a common family of antibiotics. *Cell* **158**, 1402–1414 (2014).
60. Walsh, C. T. Insights into the chemical logic and enzymatic machinery of NRPS assembly lines. *Nat. Prod. Rep.* **33**, 127–135 (2016).
61. Caputi, L. et al. Missing enzymes in the biosynthesis of the anticancer drug vinblastine in Madagascar periwinkle. *Science* **360**, 1235–1239 (2018).
62. Crits-Christoph, A., Diamond, S., Butterfield, C. N., Thomas, B. C. & Banfield, J. F. Novel soil bacteria possess diverse genes for secondary metabolite biosynthesis. *Nature* **558**, 440–444 (2018).
63. Tong, Y., Weber, T. & Lee, S. Y. CRISPR/Cas-based genome engineering in natural product discovery. *Nat. Prod. Rep.* **36**, 1262–1280 (2019).
64. Nett, R. S., Lau, W. & Sattely, E. S. Discovery and engineering of colchicine alkaloid biosynthesis. *Nature* **584**, 148–153 (2020).
65. Addington, E., Sandalli, S. & Roe, A. J. Current understandings of colibactin regulation. *Microbiology* **170**, 001427 (2024).
66. Wyatt, T. D. *Pheromones And Animal Behavior: Communication By Smell And Taste* 1st edn, Vol. 408 (Cambridge Univ. Press, 2003).
67. Cohen, S. M., Wrobel, C. J. J., Prakash, S. J., Schroeder, F. C. & Sternberg, P. W. Formation and function of dauer ascarosides in the nematodes *Caenorhabditis briggsae and Caenorhabditis elegans*. *G3 (Bethesda)* **12**, jkac014 (2022).
68. Yoshida, K. et al. Rapid chromosome evolution and acquisition of thermosensitive stochastic sex determination in nematode androdioecious hermaphrodites. *Nat. Commun.* **15**, 9649 (2024).
69. Dong, C., Dolke, F. & von Reuss, S. H. Selective MS screening reveals a sex pheromone in *Caenorhabditis briggsae* and species-specificity in indole ascaroside signalling. *Org. Biomol. Chem.* **14**, 7217–7225 (2016).
70. Dong, C. et al. Comparative ascaroside profiling of *Caenorhabditis* exometabolomes reveals species-specific (ω) and (ω-2)-hydroxylation downstream of peroxisomal β-oxidation. *J. Org. Chem.* **83**, 7109–7120 (2018).
71. Dolke, F. et al. Ascaroside signaling in the bacterivorous nematode *Caenorhabditis remanei* encodes the growth phase of its bacterial food source. *Org. Lett.* **21**, 5832–5837 (2019).
72. Pungaliya, C. et al. A shortcut to identifying small molecule signals that regulate behavior and development in *Caenorhabditis elegans*. *Proc. Natl. Acad. Sci. USA.* **106**, 7708–7713 (2009).
73. Artyukhin, A. B. et al. Metabolomic "dark matter" dependent on peroxisomal β-oxidation in *Caenorhabditis elegans*. *J. Am. Chem. Soc.* **140**, 2841–2852 (2018).
74. Edgar, R. C. MUSCLE: multiple sequence alignment with high accuracy and high throughput. *Nucleic Acids Res.* **32**, 1792–1797 (2004).
75. Schliep, K. P. Phangorn: phylogenetic analysis in R. *Bioinformatics* **27**, 592–593 (2011).
76. Madeira, F. et al. The EMBL-EBI job dispatcher sequence analysis tools framework in 2024. *Nucleic Acids Res.* **52**, W521–W525 (2024).
77. Rödelsperger, C. et al. Phylotranscriptomics of *Pristionchus* nematodes reveals parallel gene loss in six hermaphroditic lineages. *Curr. Biol.* **28**, 3123–3127 (2018).
78. Edler, D., Klein, J., Antonelli, A. & Silvestro, D. raxmlGUI 2.0: A graphical interface and toolkit for phylogenetic analyses using RAxML. *Methods Ecol. Evol.* **12**, 373–377 (2021).

79. Letunic, I. & Bork, P. Interactive Tree of Life (iTOL) v6: recent updates to the phylogenetic tree display and annotation tool. *Nucleic Acids Res.* **52**, W78–W82 (2024).

Acknowledgements

We thank Dr. Frank C. Schroeder for valuable discussions about the biosynthetic pathway of NPAR pheromones. We also thank Dr. Ziduan Han and Dr. Shuai Sun for their assistance with microinjection. LC-MS data and confocal microscopic images were collected by using Waters LCMS, Agilent LC-HR(ESI)-qTOF-MS and Zeiss LSM 980. Mutants were generated by using the CRISPR/Cas9 genome editing microinjection system. All the instruments were accessed from the Instrumentation and Service Center for Science and Technology (ISCST), Beijing Normal University, Zhuhai. We are grateful to Dr. Wu Wen, Dr. Yuan Gao, Dr. Xianxin Dong and Dr. Pingzhou Du at ISCST for technical supports and data acquisition. This work was funded by the Max Planck Society, National Natural Science Foundation of China (Grants NO. 22107011, 22407016 & 22477010) and Department of Education of Guangdong Province (Grant NO. 2021KQNCX269).

Author contributions

P.Z., P.T. and W.X. performed experiments and conducted data analysis. S.Y., H.W. and T.L. assisted with microinjection and worm culturing. R.J.S. and C.D. supervised the project. P.Z., P.T., W.X., R.J.S. and C.D. wrote the manuscript. All the authors read and approved the final version of the manuscript. P.Z., R.J.S. and C.D. provided the funding.

Competing interests

The authors declare no competing interests.

Additional information

Supplementary information The online version contains supplementary material available at https://doi.org/10.1038/s42003-025-08641-4.

Correspondence and requests for materials should be addressed to Ralf J. Sommer or Chuanfu Dong.

Peer review information *Communications Biology* thanks the anonymous reviewers for their contribution to the peer review of this work. Primary Handling Editors: Tuan Anh Nguyen and Laura Rodríguez Pérez. A peer review file is available.

Reprints and permissions information is available at http://www.nature.com/reprints

Publisher's note Springer Nature remains neutral with regard to jurisdictional claims in published maps and institutional affiliations.

Open Access This article is licensed under a Creative Commons Attribution-NonCommercial-NoDerivatives 4.0 International License, which permits any non-commercial use, sharing, distribution and reproduction in any medium or format, as long as you give appropriate credit to the original author(s) and the source, provide a link to the Creative Commons licence, and indicate if you modified the licensed material. You do not have permission under this licence to share adapted material derived from this article or parts of it. The images or other third party material in this article are included in the article's Creative Commons licence, unless indicated otherwise in a credit line to the material. If material is not included in the article's Creative Commons licence and your intended use is not permitted by statutory regulation or exceeds the permitted use, you will need to obtain permission directly from the copyright holder. To view a copy of this licence, visit http://creativecommons.org/licenses/by-nc-nd/4.0/.

© The Author(s) 2025

Description of Additional Supplementary Files

File name: Supplementary Data

Description: The source data behind the graphs of Fig. 2f, Fig. 3f, Fig. 4f, SFig. 1, SFig. 3, SFig. 4, SFig. 5e, SFig.8 and SFig.9 are consolidated as different tabs in the Supplementary Data file.

Biosynthesis of modular signaling molecules requires functional diversification of carboxylesterases in *Pristionchus pacificus*

Pei Zhang[1,2,8], Penghieng Theam[3,8], Wenya Xu[1,2,8], Shudan Ye[1,4,5,6,7], Hanh Witte[3], Tingwei Liu[1,2], Ralf J. Sommer[3] & Chuanfu Dong[1,2,3,4,5]

[1]Department of Biology, Faculty of Arts and Sciences, Beijing Normal University, 519087 Zhuhai, China

[2]The Key Laboratory of Cell Proliferation and Regulation Biology, Ministry of Education, Department of Biology, College of Life Sciences, Beijing Normal University, 100875 Beijing, China

[3]Department for Integrative Evolutionary Biology, Max Planck Institute for Biology Tübingen, Max Planck Ring 9, 72076 Tübingen, Germany

[4]Center for Biological Science and Technology, Advanced Institute of Natural Sciences, Beijing Normal University, 519087 Zhuhai, China

[5]Zhuhai-Macao Biotechnology Joint Laboratory, Beijing Normal University, 519087 Zhuhai, China

[6]Present address: Key Laboratory of Biomacromolecules (CAS), National Laboratory of Biomacromolecules, CAS Center for Excellence in Biomacromolecules, Institute of Biophysics, Chinese Academy of Sciences, 100101 Beijing, China

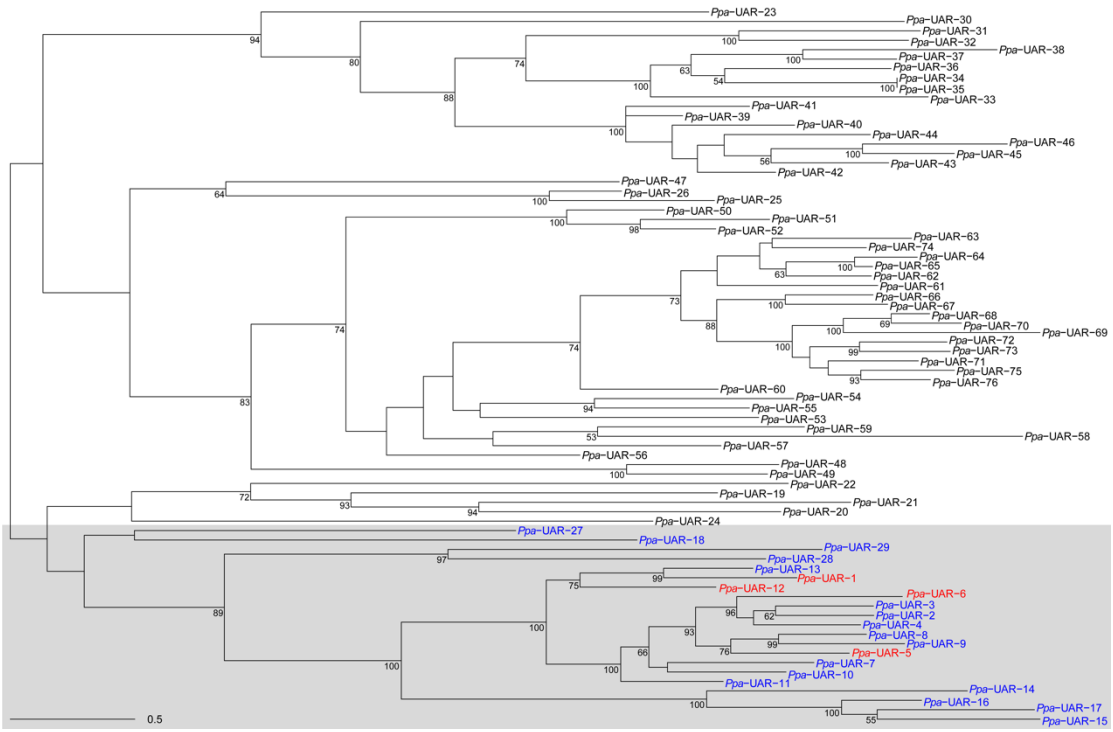
[7]Present address: College of Life Sciences, University of Chinese Academy of Sciences, 100049 Beijing, China

[8]These authors contributed equally: Pei Zhang, Penghieng Theam, Wenya Xu.

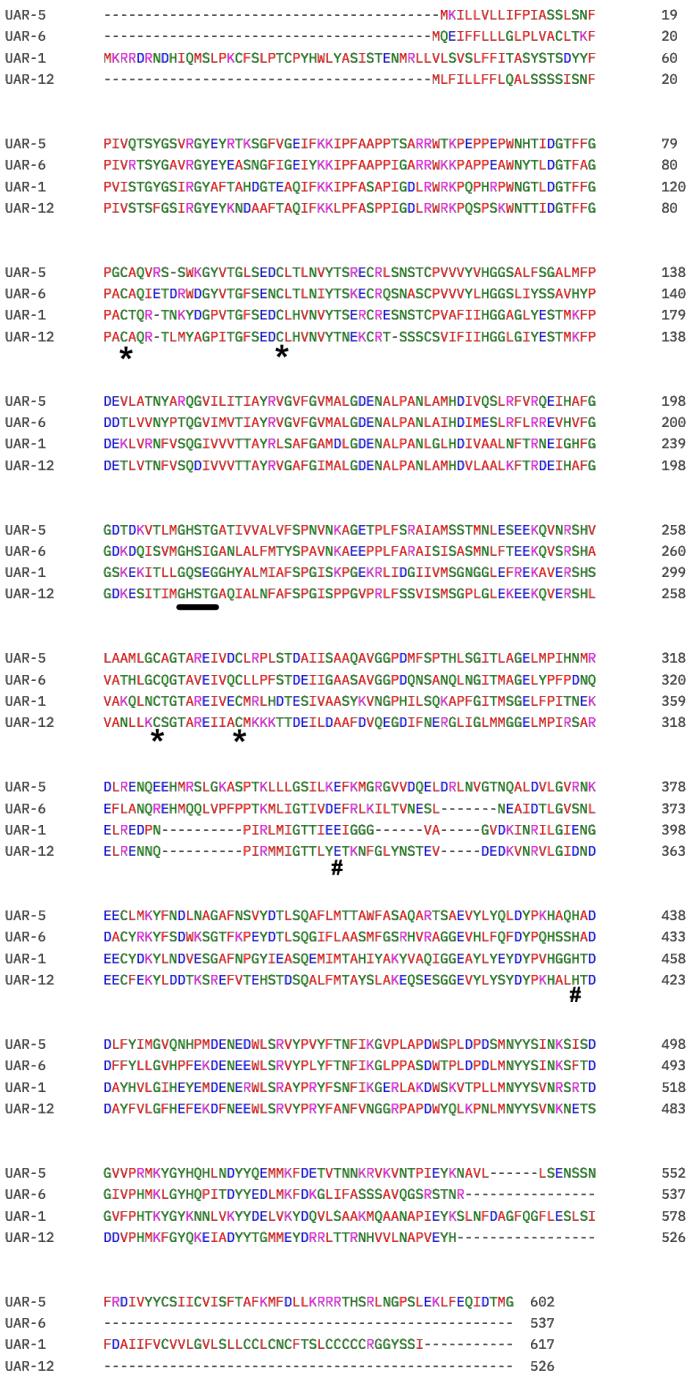
Correspondence: ralf.sommer@tuebingen.mpg.de; cdong@bnu.edu.cn

Content		page
Supplementary Figures		
Supplementary Fig. 1	Phylogenetic relationship of UAR enzymes from *P. pacificus*.	3
Supplementary Fig. 2	Amino acid sequence alignments of *Ppa*-UAR-1, *Ppa*-UAR-5, *Ppa*-UAR-6 and *Ppa*-UAR-12.	4
Supplementary Fig. 3	The production of all the pheromones in *Ppa-uar-5* mutant.	5
Supplementary Fig. 4	The production of dimeric ascaroside dasc#4 in *Ppa-uar-12* mutants.	6
Supplementary Fig. 5	The production of minor dimeric ascarosides dasc#6 and dasc#9 in *Ppa-uar-12* mutants.	7
Supplementary Fig. 6	The production of all the pheromones in *Ppa-uar-12* mutant.	8
Supplementary Fig. 7	Confocal images of mouth-form of both wild type and *Ppa-uar-12* mutants.	9
Supplementary Fig. 8	The production of all the pheromones in *Ppa-uar-6* mutant.	10
Supplementary Fig. 9	Quantitative analysis of the production of ascr#9 in both wild type and *Ppa-uar-6* mutants.	11
Supplementary Fig. 10	Orthologous enzymes of *Ppa*-UAR-6 are evolutionarily restricted to five *Pristionchus* species from the *pacificus*-clade.	12
Supplementary Fig. 11	Proposed biosynthetic pathways of UBAS and UPAS pheromones.	13
Supplementary Fig. 12	Predicted protein structures of *Ppa*-UAR-1, *Ppa*-UAR-5, *Ppa*-UAR-12 and *Ppa*-UAR-6.	14
Supplementary Tables		
Supplementary Table 1	List of carboxylesterase genes were knocked out by CRISPR/Cas9 for biosynthetic investigation.	15
Supplementary Table 2	List of the remaining carboxylesterase genes were not mutated for biosynthetic investigation.	16
Supplementary Table 3	Primers and sgRNA were used for knocking out carboxylesterase genes.	17
Supplementary References		

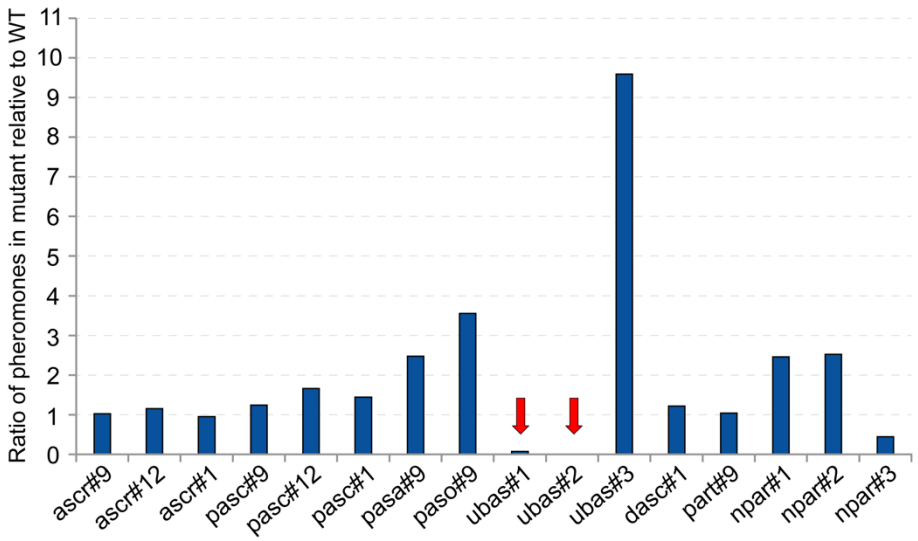
Supplementary Figures



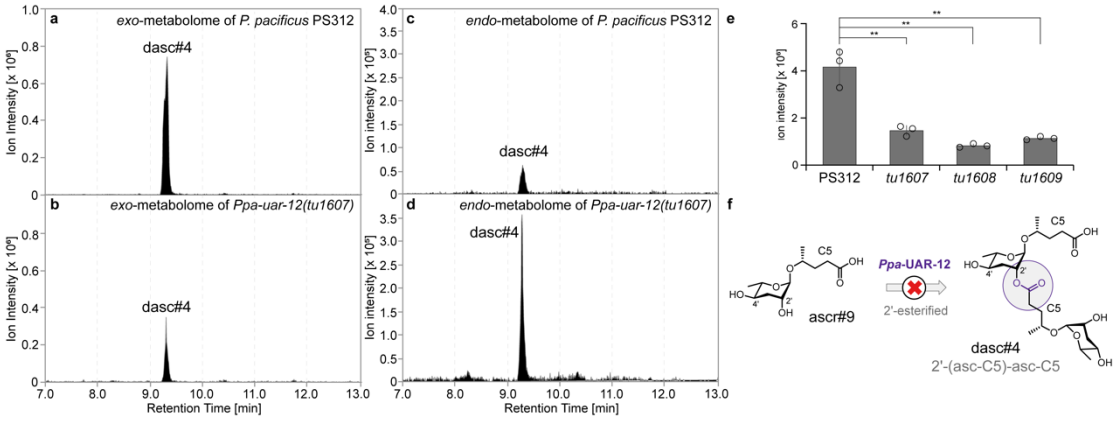
Supplementary Fig. 1. Phylogenetic relationship of UAR enzymes from *P. pacificus*. 75 homologous proteins of *Ppa*-UAR-1 were discovered from *P. pacificus* (Supplementary Data). Their amino acid sequences were aligned with *Ppa*-UAR-1, from which twenty proteins (marked in blue) share high similarities with *Ppa*-UAR-1 in the phylogenetic tree (four functional biosynthetic enzymes were marked in red). These 20 encoding genes were selectively knocked out by CRISPR/Cas9.



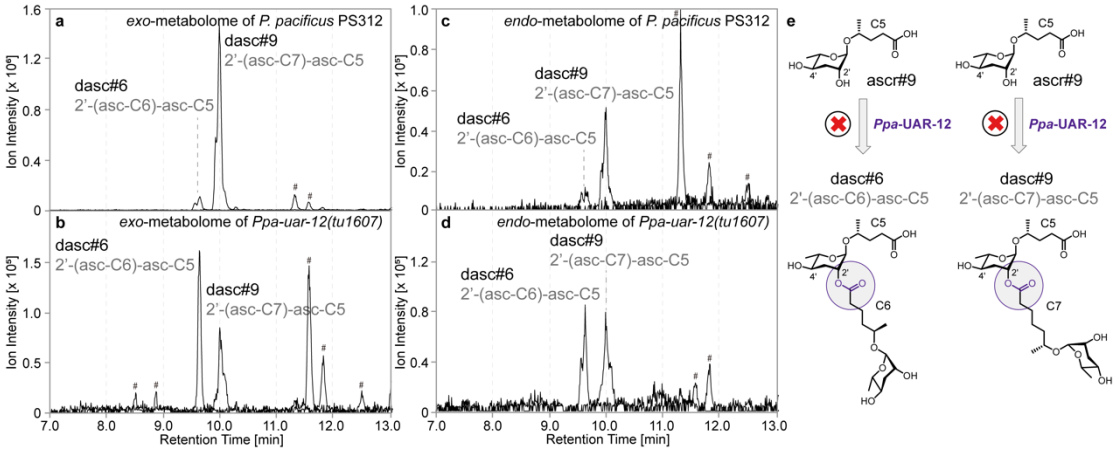
Supplementary Fig. 2. Amino acid sequence alignments of *Ppa*-UAR-1, *Ppa*-UAR-5, *Ppa*-UAR-6 and *Ppa*-UAR-12. The conserved catalytic triad of Glu-His-Ser was characterized among *Ppa*-UAR-1, *Ppa*-UAR-5, *Ppa*-UAR-6 and *Ppa*-UAR-12. The conserved GXSXG motif containing the catalytic Ser was marked with a bar, the other two catalytic residues Glu and His were marked with the pound signs. Four conserved Cys residues that are responsible for the formation of disulfide bonds of the protein structures were marked with asterisks.



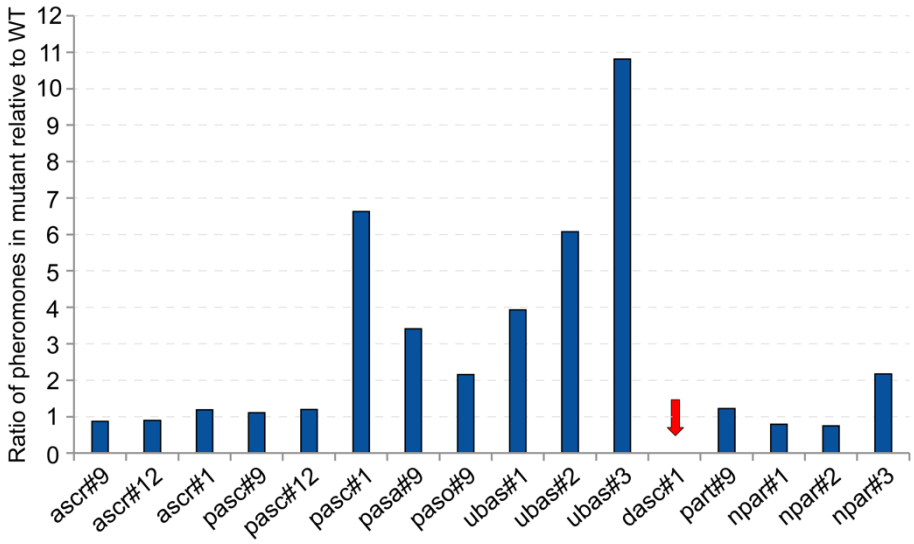
Supplementary Fig. 3. The production of all the pheromones in *Ppa-uar-5* mutant. The whole set of pheromones from *Ppa-uar-5(tu2019)* mutant worms and wild type was quantitatively analyzed (Supplementary Data). The ratio of ion abundances of pheromones produced by *Ppa-uar-5(tu2019)* mutant relative to wild type was determined by LC-(ESI-)-qTOF-HR-MS. The loss of the production of ubas#1 and ubas#2 in mutant worms was highlighted by red arrows. Three biological replicates were performed for *Ppa-uar-5(tu2019)* mutant and wild type.



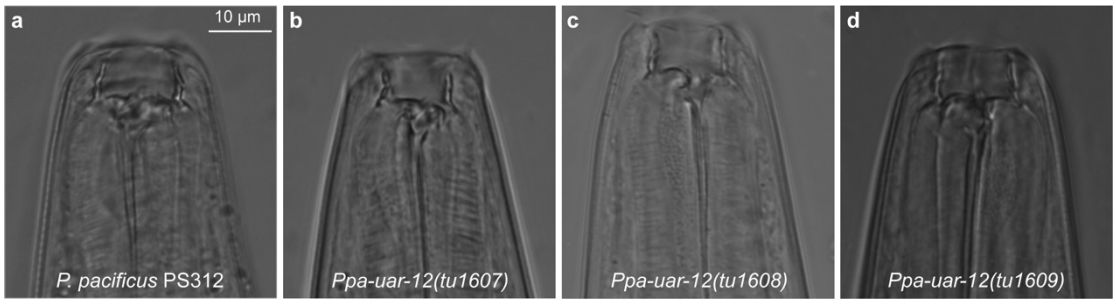
Supplementary Fig. 4. The production of dimeric ascaroside dasc#4 in *Ppa-uar-12* mutants. a-d, The production of dasc#4 [2'-(asc-C5)-asc-C5] in the *exo*-metabolomes (**a**, **b**) and *endo*-metabolomes (**c**, **d**) of both wild type *P. pacificus* PS312 and mutants were examined by LC-MS. **e**, Ion abundances of dasc#4 in the *exo*-metabolomes of wild type *P. pacificus* PS312 and three mutants were quantitatively analysed (n = 3 per group) (Supplementary Data). Error bars represent standard deviation (± SD). Statistical analysis was performed using a two-tailed unpaired Student's *t* test, $^{****}p < 0.0001$; $^{***}p < 0.001$; $^{**}p < 0.01$; $^{*}p < 0.05$; ns not significant. **f**, Carboxylesterase *Ppa*-UAR-12 is not involved in the biosynthesis of the 2'-linked dimeric ascaroside dasc#4.



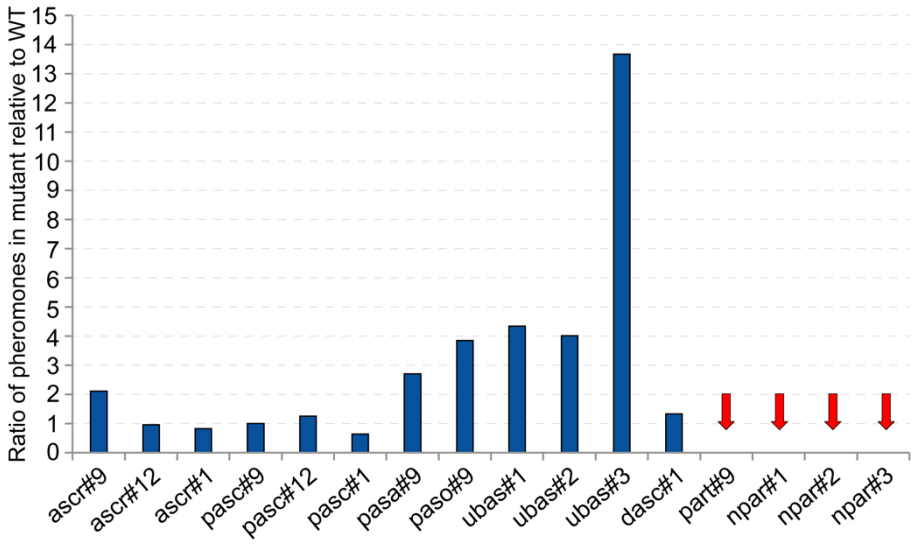
Supplementary Fig. 5. The production of minor dimeric ascarosides dasc#6 [2'-(asc-C6)-asc-C5] and dasc#9 [2'-(asc-C7)-asc-C5] in *Ppa-uar-12* mutants. a-d, The production of the 2'-linked dimeric ascarosides dasc#6 and dasc#9 in the *exo*-metabolomes (**a**, **b**) and *endo*-metabolomes (**c**, **d**) of both wild type *P. pacificus* PS312 and mutants were examined by LC-MS. The pound signs (#) denote non-ascarosides. **e**, Carboxylesterase *Ppa*-UAR-12 is not involved in the biosynthesis of the 2'-linked dimeric ascarosides dasc#6 and dasc#9.



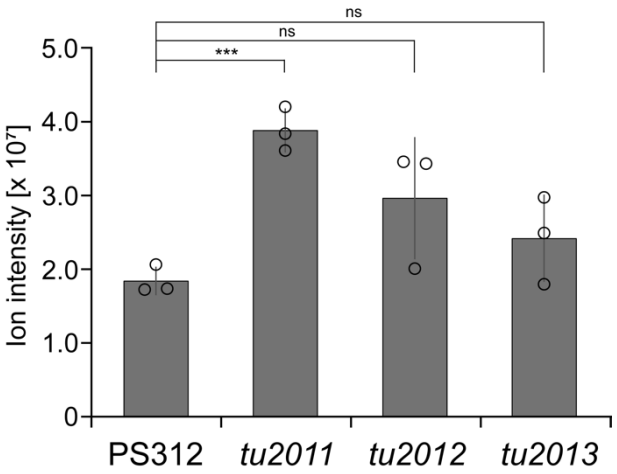
Supplementary Fig. 6. The production of all the pheromones in *Ppa-uar-12* mutant. All the pheromones from *Ppa-uar-12(tu1607)* mutant worms and wild type were quantitatively analyzed (Supplementary Data). The ratio of ion abundances of pheromones produced by *Ppa-uar-12(tu1607)* mutant relative to wild type was determined by LC-(ESI-)-qTOF-HR-MS. The complete loss of the production of dasc#1 in mutant worms was highlighted by a red arrow. Three biological replicates were performed for *Ppa-uar-12(tu1607)* mutant and wild type.



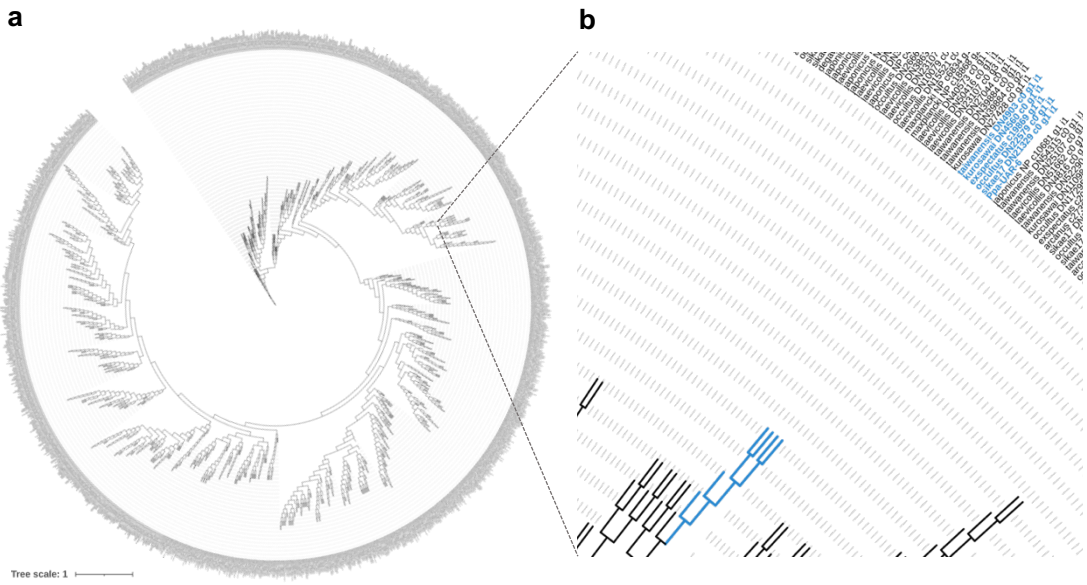
Supplementary Fig. 7. Confocal images of mouth-form of both wild type and *Ppa-uar-12* mutants. a-d, The mouth-form of wild type *P. pacificus* PS312 (**a**) and *Ppa-uar-12* mutant animals (**b**, *tu1607*; **c**, *tu1608*; **d**, *tu1069*) was Eu under normal culture conditions. Ten individual worms for each mutant strain and wild type were selected for mouth-form screening, all the tested worms were equipped with Eu mouth form. Scale bar is 10 μm.



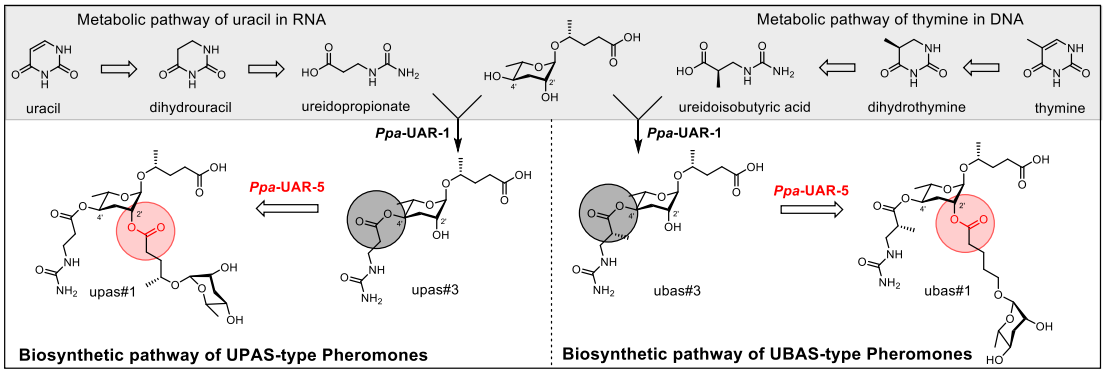
Supplementary Fig. 8. The production of all the pheromones in *Ppa-uar-6* mutant. All the pheromones from *Ppa-uar-6(tu2011)* mutant worms and wild type were quantitatively analyzed (Supplementary Data). The ratio of ion abundances of pheromones produced by *Ppa-uar-6(tu2011)* mutant relative to wild type was determined by LC-(ESI-)-qTOF-HR-MS. The complete loss of the production of NPAR pheromones (part#9 and npar#1-3) in mutant worms was highlighted by red arrows. Three biological replicates were performed for *Ppa-uar-6(tu2011)* mutant and wild type.



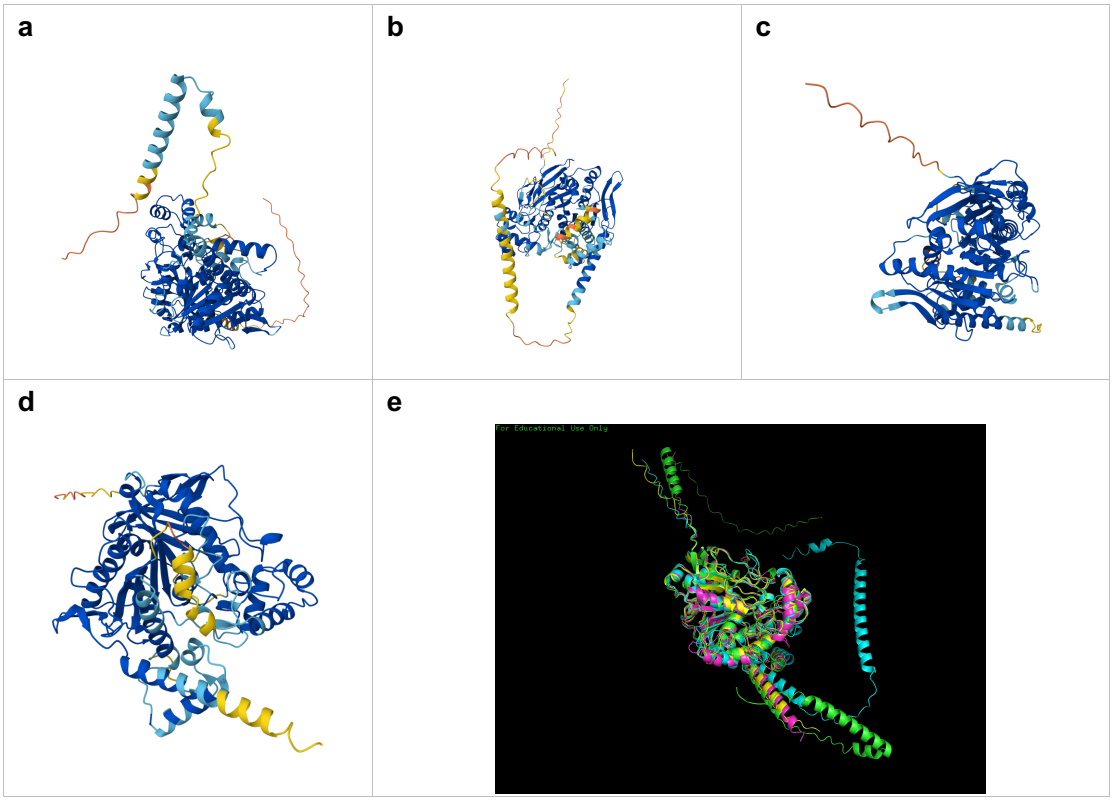
Supplementary Fig. 9. Quantitative analysis of the production of ascr#9 in both wild type and *Ppa-uar-6* mutants. Three biological replicates were performed for both wild type *P. pacificus* PS312 and *Ppa-uar-6* mutants (n = 3 per group) (Supplementary Data). Error bars represent standard deviation (± SD). Statistical analysis was performed using a two-tailed unpaired Student's *t* test, $^{****}p < 0.0001$; $^{***}p < 0.001$; $^{**}p < 0.01$; $^{*}p < 0.05$; ns not significant.



Supplementary Fig. 10. Orthologous enzymes of *Ppa*-UAR-6 are evolutionarily restricted to five *Pristionchus* species from the *pacificus*-clade. a, Phylogenetic tree of 1531 *Ppa*-UAR-6 homologous proteins across 31 *Pristionchus* species. **b**, 1:1 ortholog of *Ppa*-UAR-6 was discovered from each of five *Pristionchus* species, including *P. taiwanensis*, *P. kurosawai*, *P. sikae*, *P. occultus*, and *P. exspectatus*, which were previously confirmed to produce NPAR pheromones. The nodes and labels of these orthologous proteins were highlighted in blue.



Supplementary Fig. 11. Proposed biosynthetic pathways of UBAS and UPAS pheromones. *Ppa*-UAR-1 functions upstream of *Ppa*-UAR-5 to synthesize intermediate precursor upas#3 or ubas#3, by linking pyrimidine (uracil and thymine) metabolism-derived intermediates (ureidopropionate and ureidoisobutyric acid) to the 4'-position of ascr#9. *Ppa*-UAR-5 further integrates another building block of ascr#9 or oscr#9 to the 2'-position of upas#3 or ubas#3 to finally synthesize upas#1 or ubas#1.



Supplementary Fig. 12. Predicted protein structures of *Ppa*-UAR-1, *Ppa*-UAR-5, *Ppa*-UAR-12 and *Ppa*-UAR-6. a-d, Structures of *Ppa*-UAR-1 (**a**), *Ppa*-UAR-5 (**b**), *Ppa*-UAR-12 (**c**) and *Ppa*-UAR-6 (**d**) were predicted by AlphaFold3[1]. **e**, Analysis of overlapped structures of *Ppa*-UAR-1, *Ppa*-UAR-5, *Ppa*-UAR-12 and *Ppa*-UAR-6 showed that they shared high similarities (Green: *Ppa*-UAR-1, Blue: *Ppa*-UAR-5, Yellow: *Ppa*-UAR-12, Pink: *Ppa*-UAR-6).

Supplementary Tables

Supplementary Table 1. List of carboxylesterase genes were knocked out by CRISPR/Cas9 for biosynthetic investigation.

Name	Esterase or hydrolase genes	Allele 1	Allele 2	Allele 3
Ppa-uar-1	Iso_D.223.8	*tu1948* (8 bp deletion, exon 2)	*tu1949* (7 bp insertion and 4 SNPs, exon 2)	*tu1950* (29 bp insertion and 1 SNP, exon 2)
Ppa-uar-2	ppa_stranded_DN9008_c0_g1_i1	*tu2022* (10 bp deletion and 1 SNP, exon 4)	*tu2023* (19 bp insertion, exon 4)	*tu2024* (8 bp deletion, exon 4)
Ppa-uar-3	ppa_stranded_DN30926_c0_g3_i15	*tu2014* (1 bp insertion and 4 SNPs, exon 4)	*tu2015* (4 bp insertion, exon 4)	*tu2016* (5 bp deletion, exon 4)
Ppa-uar-4	Iso_D.224.1	*tu2068* (4 bp deletion, exon 4)	*tu2069* (11 bp deletion, exon 4)	*tu2070* (20 bp deletion, exon 4)
Ppa-uar-5	ppa_stranded_DN26633_c0_g2_i1	*tu2019* (68 bp insertion and 5 SNPs, exon 4)	*tu2020* (11 bp deletion, exon 4)	*tu2021* (4 bp deletion, exon 4)
Ppa-uar-6	ppa_stranded_DN30149_c0_g1_i2	*tu2011* (5 bp deletion, exon 3)	*tu2012* (11 bp insertion, exon 3)	*tu2013* (7 bp insertion, exon 3)
Ppa-uar-7	ppa_stranded_DN20512_c0_g1_i2	*tu1993* (14 bp deletion, exon 3)	*tu1994* (4 bp deletion, exon 3, “variant#1”)	*tu1995* (4 bp deletion, exon 3, “variant#2”)
Ppa-uar-8	ppa_stranded_DN28083_c0_g1_i4	*tu1934* (1 bp deletion, exon 3)	*tu1935* (11 bp deletion and 2 SNPs, exon 3)	*tu1936* (41 bp insertion and 5 SNPs, exon 3)
Ppa-uar-9	PPA42050	*tu2017* (20 bp deletion and 1 SNP, exon 7)	*tu2018* (4 bp deletion and 1 SNP, exon 7)	
Ppa-uar-10	Iso_D.1590.1	*tu1919* (2 bp deletion, exon 3)	*tu1920* (26 bp insertion and 2 SNPs, exon 3)	*tu1921* (5 bp deletion, exon 3)
Ppa-uar-11	PPA17279	*tu1991* (5 bp insertion, exon 5)	*tu1992* (1 bp deletion, exon 5)	
Ppa-uar-12	ppa_stranded_DN30542_c0_g1_i2	*tu1607* (10 bp deletion, exon 4)	*tu1608* (2 bp deletion, exon 4)	*tu1609* (22 bp deletion, exon 4)
Ppa-uar-13	PPA21991	*tu1563* (5 bp deletion, exon 3)	*tu1564* (55 bp deletion, exon 3)	
Ppa-uar-14	PPA39247	*tu1937* (11 bp insertion and 6 SNPs, exon 4)	*tu1938* (4 bp deletion, exon 4)	*tu1939* (11 bp deletion and 8 SNPs, exon 4)
Ppa-uar-15	ppa_stranded_DN31291_c3_ g5_ i5	*tu1930* (8 bp deletion, exon 3)	*tu1931* (1 bp deletion and 1 SNP, exon 3)	*tu1932* (1 bp insertion, exon 3)
Ppa-uar-16	ppa_stranded_DN29519_c1_g1_i1	*tu1975* (11 bp deletion and 3 SNPs, exon 5)	*tu1976* (2 bp insertion and 9 SNPs, exon 5)	*tu1977* (14 bp deletion and 2 SNPs, exon 5)
Ppa-uar-17	PPA23744	*tu1911* (31 bp insertion and 1 SNP, exon 1)	*tu1912* (10 bp deletion, exon 1)	*tu1913* (4 bp deletion, exon 1)
Ppa-uar-18	PPA23795	Embryonic lethality (exon 1)		
Ppa-uar-22	PPA23754	In-frame mutation (exon 3)		
Ppa-uar-24	PPA23779	Embryonic lethality (exon 3)		
Ppa-uar-27	ppa_stranded_DN23720_c0_g1_i2	*tu2071* (28 bp deletion, exon 4)	*tu2072* (10 bp insertion and 5 SNPs, exon 4)	*tu2073* (7 bp deletion, exon 4)
Ppa-uar-28	ppa_stranded_DN25492_c0_g3_i2	*tu1972* (5 bp deletion, exon 4)	*tu1973* (37 bp insertion and 5 SNPs, exon 4)	*tu1974* (8 bp deletion, exon 4)
Ppa-uar-29	Contig35-snapTAU.30	*tu1924* (1 bp insertion and 1 SNP, exon 2)	*tu1925* (4 bp deletion, exon 2)	*tu1926* (39 bp deletion, exon 2)

Supplementary Table 2. List of the remaining carboxylesterase genes were not mutated for biosynthetic investigation.

Name	Esterase or hydrolase genes	Name	Esterase or hydrolase genes	Name	Esterase or hydrolase genes
Ppa-uar-19	PPA15738	***Ppa-uar-41***	ppa_stranded_DN16831_c0_g1_i1	***Ppa-uar-60***	ppa_stranded_DN30573_c0_g1_i2
Ppa-uar-20	ppa_stranded_DN26620_c0_g1_i2	***Ppa-uar-42***	ppa_stranded_DN27477_c0_g1_i1	***Ppa-uar-61***	PPA04333
Ppa-uar-21	PPA25312	***Ppa-uar-43***	ppa_stranded_DN18687_c0_g1_i1	***Ppa-uar-62***	PPA37960
Ppa-uar-22	PPA23754	***Ppa-uar-44***	Contig58-snapTAU.64	***Ppa-uar-63***	PPA39767
Ppa-uar-23	ppa_stranded_DN25900_c0_g1_i1	***Ppa-uar-45***	ppa_stranded_DN29180_c0_g1_i2	***Ppa-uar-64***	PPA41660
Ppa-uar-24	PPA23779	***Ppa-uar-46***	PPA36339	***Ppa-uar-65***	PPA10010
Ppa-uar-25	Iso_D.2531.1	***Ppa-uar-47***	ppa_stranded_DN28328_c1_g1_i1	***Ppa-uar-66***	ppa_stranded_DN25758_c0_g1_i1
Ppa-uar-26	ppa_stranded_DN13491_c0_g1_i1	***Ppa-uar-48***	PPA35183	***Ppa-uar-67***	ppa_stranded_DN9111_c0_g2_i1
Ppa-uar-30	PPA39427	***Ppa-uar-49***	PPA10555	***Ppa-uar-68***	ppa_stranded_DN31013_c0_g1_i1
Ppa-uar-31	Contig58-snapTAU.108	***Ppa-uar-50***	PPA03821	***Ppa-uar-69***	PPA03767
Ppa-uar-32	PPA02785	***Ppa-uar-51***	PPA13063	***Ppa-uar-70***	PPA41108
Ppa-uar-33	PPA07019	***Ppa-uar-52***	PPA22191	***Ppa-uar-71***	PPA36944
Ppa-uar-34	PPA40913	***Ppa-uar-53***	PPA28522	***Ppa-uar-72***	PPA34289
Ppa-uar-35	PPA40915	***Ppa-uar-54***	PPA00898	***Ppa-uar-73***	ppa_stranded_DN30123_c0_g1_i5
Ppa-uar-36	Iso_D.10131.1	***Ppa-uar-55***	Contig34-snap.12	***Ppa-uar-74***	PPA40739
Ppa-uar-37	ppa_stranded_DN18279_c0_g1_i1	***Ppa-uar-56***	PPA22060	***Ppa-uar-75***	PPA42366
Ppa-uar-38	PPA10777	***Ppa-uar-57***	PPA30526	***Ppa-uar-76***	PPA26246
Ppa-uar-39	Contig58-snapTAU.63	***Ppa-uar-58***	PPA22915		
Ppa-uar-40	Iso_D.6227.1	***Ppa-uar-59***	ppa_stranded_DN26305_c0_g1_i1		

Supplementary Table 3. Primers and sgRNA were used for knocking out carboxylesterase genes listed in Supplementary Table 1.

Name	Esterase or hydrolase genes	Sequence of gRNA	Forward primer	Reverse primer
Ppa-uar-1	Iso_D.223.8	CCATGGAATGGGACGCTAGA	GTGATCAGCACTGGATATGGTTCG	CGATTACCTCTCGACATCTCTCGC
Ppa-uar-2	ppa_stranded_DN9008_c0_g1_i1	GTCTATATCCATGGAGGCTC	GTGCTCAAGTCGACTCATCATGGG	GAACGAAGCGCAGACTCTCCACG
Ppa-uar-3	ppa_stranded_DN30926_c0_g3_i15	CCTGGGTCGGATACGTAACT	CATCGAGTACCAAGCAGGGAATGG	CTTTGTGCACATCACCTTGTCTCGG
Ppa-uar-4	Iso_D.224.1	CCAGTGGTAGTGTACATCCA	TCAGAAGACTGCCTAACACTGAACG	AGGCAATACGTGCTCGTCACC
Ppa-uar-5	ppa_stranded_DN26633_c0_g2_i1	CTACGTCACTGGACTGTCTG	CCAATCGTCCAAACGTCATACGGC	CTTGCCTCGCGTAGTTTGTCGC
Ppa-uar-6	ppa_stranded_DN30149_c0_g1_i2	CGATGGGATGGCTACGTCAC	GAAGCGAGTAATGGATTCATCGG	GATAATTCACAACAAGCGTATCATCGG
Ppa-uar-7	ppa_stranded_DN20512_c0_g1_i2	GGGCCATTCAGAGGACTGCC	GATAGTGAGGAGAATCTAGTCGAGG	GACGATAGTCCATTGTGACCAGG
Ppa-uar-8	ppa_stranded_DN28083_c0_g1_i4	CAGGTTCCCTCACACTGGGA	CCTCATCAGCCCTGGAATCAC	CTGTCTGCACTCTGTTGACGTG
Ppa-uar-9	PPA42050	GAACAAATCGCACGTAGTCG	AGCTACAATCGTGCTGGCTCTCG	CTGAGGCTGCATTGATGATCTCACTG
Ppa-uar-10	Iso_D.1590.1	CCATTCTACTGGCGCGACGA	CTCGAATCTGTTCTTGCATGGTAC	GGAGATGCACTCATAGCAATGG
Ppa-uar-11	PPA17279	CGCAAGGAGATTCACAATTT	GCCAATATTGCTATTCACGGTAAGC	CGATCCACTCATGGCTATCGC
Ppa-uar-12	ppa_stranded_DN30542_c0_g1_i2	ATGTATGCAGGTCCAATCAC	CGGATCAATTCGTGGGTATGAATACAAGAAC	CGATAGGCTGTAGTGACCACGACG
Ppa-uar-13	PPA21991	GCCTATCGCCTTGCAGCGTT	GGCATTTTCGAAGCTACGATGAAG	CCACTCGTTGACTCCTCTCTACTGTC
Ppa-uar-14	PPA39247	GACTTCATTCCCACCAATTT	TACGTGAGCGCTGAATGCAGG	GACCCATTAGAGTGAGGGCATCTG
Ppa-uar-15	ppa_stranded_DN31291_c3_ g5_ i5	TGCGATGGAAACTGCCTGAG	GGATGACTGGATAGCGAAGACC	TGCGAAGACGTTGATGTAGAGG
Ppa-uar-16	ppa_stranded_DN29519_c1_g1_i1	CAACGGACGGTACAAGAGTT	CACTCGCCGATAAGAATGCTCC	GTTGAGTTGCTCATACAAGCTGCTG
Ppa-uar-17	PPA23744	TTGATAGTTAACACCAGCTA	CTTATCTCGAGACTGGTTATCAAC	GTGGAGTTACTCATACAAGCTGC
Ppa-uar-18	PPA23795	AAGCAACTTCAAATCTTCCG	CCTTCCTCTTTCCTCATCTC	CCAATTCTTGATGCCATCGAG
Ppa-uar-27	ppa_stranded_DN23720_c0_g1_i2	GTCGCATCCAGAGAGAAGTC	GCAACGATTATGCAATCTTCAAGG	GATGCTCCACCGTACTGGAAC
Ppa-uar-28	ppa_stranded_DN25492_c0_g3_i2	CGGACGGGCTACGGATTTCT	GGGACTGTGAGTCTCAAGATCAGG	GTTGCCACAGTACAGCGATGC
Ppa-uar-29	Contig35-snapTAU.30	AAATCACGAGTAACTCTATT	TTGCATCCAGGTCAGTTACGAC	CATGAAGCTGCGATGTTCACATC
Ppa-uar-22	PPA23754	ATGCATTCAAACTGGACTAC	CATTATGGAAGTGCTGTCTCATCC	GGACGAATATGTTCATGTAGAGGC
Ppa-uar-24	PPA23779	CCCTGGTACGAATCCGTATT	GAACAACAACGACTCCGAGACC	CACCATGGAAGAATACTATCACTGG

Supplementary References

1. Abramson, J. et al. Accurate structure prediction of biomolecular interactions with AlphaFold 3. *Nature* **630**, 493-500 (2024).

nature portfolio

Corresponding author(s): Chuanfu Dong; Ralf J. Sommer

Last updated by author(s): July 27, 2025

Reporting Summary

Nature Portfolio wishes to improve the reproducibility of the work that we publish. This form provides structure for consistency and transparency in reporting. For further information on Nature Portfolio policies, see our Editorial Policies and the Editorial Policy Checklist.

Please do not complete any field with "not applicable" or n/a. Refer to the help text for what text to use if an item is not relevant to your study.
For final submission: please carefully check your responses for accuracy; you will not be able to make changes later.

Statistics

For all statistical analyses, confirm that the following items are present in the figure legend, table legend, main text, or Methods section.

n/a	Confirmed	
☐	☒	The exact sample size (*n*) for each experimental group/condition, given as a discrete number and unit of measurement
☐	☒	A statement on whether measurements were taken from distinct samples or whether the same sample was measured repeatedly
☐	☒	The statistical test(s) used AND whether they are one- or two-sided *Only common tests should be described solely by name; describe more complex techniques in the Methods section.*
☐	☒	A description of all covariates tested
☐	☒	A description of any assumptions or corrections, such as tests of normality and adjustment for multiple comparisons
☐	☒	A full description of the statistical parameters including central tendency (e.g. means) or other basic estimates (e.g. regression coefficient) AND variation (e.g. standard deviation) or associated estimates of uncertainty (e.g. confidence intervals)
☐	☒	For null hypothesis testing, the test statistic (e.g. *F*, *t*, *r*) with confidence intervals, effect sizes, degrees of freedom and *P* value noted *Give P values as exact values whenever suitable.*
☐	☒	For Bayesian analysis, information on the choice of priors and Markov chain Monte Carlo settings
☐	☒	For hierarchical and complex designs, identification of the appropriate level for tests and full reporting of outcomes
☐	☒	Estimates of effect sizes (e.g. Cohen's *d*, Pearson's *r*), indicating how they were calculated

Our web collection on statistics for biologists contains articles on many of the points above.

Software and code

Policy information about availability of computer code

Data collection	The methods of collecting data were properly stated within the main text and the supplementary information.
Data analysis	The methods of data analysis was properly stated within the main text and the supplementary information.

For manuscripts utilizing custom algorithms or software that are central to the research but not yet described in published literature, software must be made available to editors and reviewers. We strongly encourage code deposition in a community repository (e.g. GitHub). See the Nature Portfolio guidelines for submitting code & software for further information.

Data

Policy information about availability of data

All manuscripts must include a data availability statement. This statement should provide the following information, where applicable:

- Accession codes, unique identifiers, or web links for publicly available datasets
- A description of any restrictions on data availability
- For clinical datasets or third party data, please ensure that the statement adheres to our policy

The data that supports the findings of this study are available within the main text and the supplementary information.

Research involving human participants, their data, or biological material

Policy information about studies with human participants or human data. See also policy information about sex, gender (identity/presentation), and sexual orientation and race, ethnicity and racism.

Reporting on sex and gender	n/a
Reporting on race, ethnicity, or other socially relevant groupings	n/a
Population characteristics	n/a
Recruitment	n/a
Ethics oversight	n/a

Note that full information on the approval of the study protocol must also be provided in the manuscript.

Field-specific reporting

Please select the one below that is the best fit for your research. If you are not sure, read the appropriate sections before making your selection.

☒ Life sciences ☐ Behavioural & social sciences ☐ Ecological, evolutionary & environmental sciences

For a reference copy of the document with all sections, see nature.com/documents/nr-reporting-summary-flat.pdf

Life sciences study design

All studies must disclose on these points even when the disclosure is negative.

Sample size	Sample sizes were chosen according to the previous relative studies and the methods were properly stated within the main text and the supplementary information.
Data exclusions	No data or data points were excluded when analyzing all the data in this study.
Replication	At least three or more biological replicates were performed in this study.
Randomization	Control groups or data were strictly arranged or anlyzed, all the data or experiments were not randomly assigned.
Blinding	Investigators were not blinded to all assays or experimental processes.

Reporting for specific materials, systems and methods

We require information from authors about some types of materials, experimental systems and methods used in many studies. Here, indicate whether each material, system or method listed is relevant to your study. If you are not sure if a list item applies to your research, read the appropriate section before selecting a response.

Materials & experimental systems

n/a	Involved in the study
☒	☐ Antibodies
☒	☐ Eukaryotic cell lines
☒	☐ Palaeontology and archaeology
☐	☒ Animals and other organisms
☒	☐ Clinical data
☒	☐ Dual use research of concern
☒	☐ Plants

Methods

n/a	Involved in the study
☒	☐ ChIP-seq
☒	☐ Flow cytometry
☒	☐ MRI-based neuroimaging

Animals and other research organisms

Policy information about studies involving animals; ARRIVE guidelines recommended for reporting animal research, and Sex and Gender in Research

Laboratory animals	The model nematode of Pristionchus pacificus PS312 and its mutants were applied in this study.
Wild animals	Wild animals were not involved in this study.
Reporting on sex	Sex-based analysis were not reported in this study.
Field-collected samples	This study did not involve sample collection from any wild fields.
Ethics oversight	No ethnic approval was required because this nematode is a free-living worm, it is non-pathogenic to humans, any other animals or plants.

Note that full information on the approval of the study protocol must also be provided in the manuscript.

Plants

Seed stocks	n/a
Novel plant genotypes	n/a
Authentication	n/a

This checklist template is licensed under a Creative Commons Attribution 4.0 International License, which permits use, sharing, adaptation, distribution and reproduction in any medium or format, as long as you give appropriate credit to the original author(s) and the source, provide a link to the Creative Commons license, and indicate if changes were made. The images or other third party material in this article are included in the article's Creative Commons license, unless indicated otherwise in a credit line to the material. If material is not included in the article's Creative Commons license and your intended use is not permitted by statutory regulation or exceeds the permitted use, you will need to obtain permission directly from the copyright holder. To view a copy of this license, visit http://creativecommons.org/licenses/by/4.0/

G3, 2026, 16(4), jkag038
https://doi.org/10.1093/g3journal/jkag038
Advance Access Publication Date: 13 February 2026
Investigation

Bacterial diet influences mutation rate in *Pristionchus pacificus*

Yinan Wang,† Penghieng Theam ,† Shiela Pearl Quiobe,† Waltraud Röseler, Hanh Witte, Christian Rödelsperger , Ralf J. Sommer *

Department for Integrative Evolutionary Biology, Max Planck Institute for Biology Tübingen, Max-Planck Ring 9, Tübingen 72076, Baden-Württemberg, Germany

*Corresponding author: Department for Integrative Evolutionary Biology, Max Planck Institute for Biology Tübingen, Max-Planck Ring 9, Tübingen 72076, Baden-Württemberg, Germany.
Email: ralf.sommer@tuebingen.mpg.de
†Contributed equally.

Mutation is a major force of evolution and its accumulation is suggested to be influenced by environmental and genetic factors in both unicellular and multicellular species. While ample of evidence showed an effect of temperature on mutation rate, the influence of diet is less well characterized, especially in multicellular organisms. Here, we present mutation accumulation (MA) rate differences for the same nematode species comparing a variety of bacterial diets. MA rates were estimated from whole-genome sequencing data of MA lines of different natural isolates of the free-living nematode *Pristionchus pacificus* on various bacterial diets isolated from *Pristionchus*-associated environments. Average single-nucleotide mutation rates varied between 1.69×10^{-9} and 2.23×10^{-9} nucleotide site^{-1} × generation^{-1}, whereas the average insertion rates varied between 1.53×10^{-10} and 2.90×10^{-10} nucleotide site^{-1} × generation^{-1} and the average deletion accumulation rates varied between 3.01×10^{-10} nucleotide site^{-1} × generation^{-1} and 4.51×10^{-10} nucleotide site^{-1} × generation^{-1}. We observed around a 1.4-fold mutation rate difference among groups on bacterial diets. Despite mutation-rate differences, the mutation spectra are largely unchanged. These results suggest that bacterial diet influences MA rate without drastically changing other mutational features.

Keywords: *Pristionchus pacificus*; *Caenorhabditis elegans*; mutation accumulation; mutation rate; nematodes; dietary influence

Introduction

Mutations are one of the major evolutionary forces and they are influenced by environmental and genetic factors in both unicellular and multicellular organisms (Matsuba et al. 2013; Lynch et al. 2023). Mutation accumulation (MA) experiments represent a powerful approach to study the influence of various factors on mutation rate and mutation spectra with many case studies in various organisms (Denver et al. 2012; Matsuba et al. 2013; Weller et al. 2014; Ness et al. 2015; Liu and Zhang 2019; Waldvogel and Pfenninger 2021; Lynch et al. 2023). For example, genetic factors were shown to influence mutation rate up to seven-fold in the green alga *Chlamydomonas reinhardtii* (Ness et al. 2015).

Among environmental factors potentially influencing MA, temperature has been studied in multiple animal species (Matsuba et al. 2013; Waldvogel and Pfenninger 2021). The influence of high temperature is suggested to be achieved through the increased level of stress on the organism in the nematode model organism *Caenorhabditis elegans* (Matsuba et al. 2013). In contrast to temperature, the influence of dietary conditions on MA is less studied, in particular in animals. Previous studies in *Drosophila melanogaster* suggest that poor nutritional conditions can contribute to the accumulation of deleterious mutations (Agrawal and Wang 2008). However, it is currently unclear whether diet has an influence on MA in nematodes.

In multicellular organisms, MA experiments are performed by propagating organisms for a certain number of generations, with only one or two individuals picked for establishing the next generation (Denver et al. 2012; Matsuba et al. 2013; Weller et al. 2014; Waldvogel and Pfenninger 2021). Experiments are often performed in the laboratory under highly controlled environmental conditions and with ample resources to reduce competition (Denver et al. 2012; Matsuba et al. 2013; Weller et al. 2014; Waldvogel and Pfenninger 2021). Usually, MA experiments are performed in species with a short generation time and simple maintenance. Meeting those criteria, MA experiments can be performed in the nematode *Pristionchus pacificus*, a free-living species with a generation time of around four days. This species has recently been established as a model organism for studying developmental plasticity of two alternative mouth forms, potential predation on other nematodes and self-recognition largely by using the laboratory strain *P. pacificus* PS312 (Sommer et al. 1996; Lightfoot et al. 2019; Schroeder 2021; Sommer 2025). As *P. pacificus* is often found in association with scarab beetles, a multitude of wild isolates is available for this species (McGaughran et al. 2016). In recent times, several of these wild isolates were started to be used in natural variation studies (Dardiry et al. 2023).

Received on 11 November 2025; accepted on 05 February 2026
© The Author(s) 2026. Published by Oxford University Press on behalf of The Genetics Society of America.
This is an Open Access article distributed under the terms of the Creative Commons Attribution License (https://creativecommons.org/licenses/by/4.0/), which permits unrestricted reuse, distribution, and reproduction in any medium, provided the original work is properly cited.

Downloaded from https://academic.oup.com/g3journal/article/16/4/jkag038/8482277 by Max-Planck Society user on 08 April 2026

To investigate how diverse dietary sources contribute to MA, we used *P. pacificus* strains of different genetic backgrounds and exposed worms of one of these strains to distinct bacterial diets. In this study, we performed MA experiments of the *P. pacificus* wild isolate RSC019 on different bacteria isolated from *Pristionchus*-associated environment. Specifically, MA data were newly generated for *P. pacificus* RSC019 on 3 bacterial diets, *E. coli* OP50, *Hafnia alvei* LRB17 (*H. alvei* LRB17), and *Agrobacterium tumefaciens* L27 (*A. tumefaciens* L27). *H. alvei* LRB17 is also known to reduce predation and life span compared to *E. coli* OP50 in *P. pacificus* P312, while *A. tumefaciens* L27 increased the predation but did not show any influence on life span (Akduman et al. 2018, 2020). We also obtained MA data of *P. pacificus* RSC011, a wild isolate that was subject to a recent long-term environmental induction experiment, which used a similar experimental setup as MA experiments (Quiobe et al. 2025). In this experiment, *P. pacificus* RSC011 were raised on an alternative diet *Novosphingobium* sp. L76 (referred to as "*N.* sp. L76' for the rest of the manuscript) for 100 generations. *N.* sp. L76 is known to have multiple influences on the laboratory strain *P. pacificus* PS312 including increased predatory behavior and reduced adult lifespan (Akduman et al. 2018, 2020). *N.* sp. L76 can also increase brood size, developmental speed and the probability of producing the predatory mouth form in *P. pacificus* RSC011 (Dardiry et al. 2023; Quiobe et al. 2025; Quiobe and Sommer 2025). Comparing MA properties in those newly generated data together with the MA data generated previously in *P. pacificus* PS312 on *E. coli* OP50 (Weller et al. 2014), we compared MA properties in *P. pacificus* from three different genetic backgrounds and raised on four bacterial diets. In total, we observed a 1.4-fold change in accumulation rate of all three types under different dietary conditions. However, between the 2 different genetic backgrounds we observed no difference in single-nucleotide variation (SNV) accumulation rate, a two-fold change in insertions accumulation and 1.4-fold in deletion accumulation.

Materials and methods

Generation of MA lines

All *P. pacificus* and bacterial strains were from the Sommer lab collection (McGaughran et al. 2016; Akduman et al. 2018). Except for the standard *E. coli* OP50, bacterial strains used in this study were isolated from *Pristionchus*-associated environments (Akduman et al. 2018). Note that the original taxonomic assignments of L27 and LRB17 in Akduman et al. (2018) were revised to *A. tumefaciens* L27 and *H. alvei* LRB17 after whole genome sequencing (Akduman et al. 2018; Athanasouli et al. 2025).

To generate MA lines of *P. pacificus* RSC019, J4 progenies of a single hermaphrodite of RSC019 were grown on the standard lab food source *E. coli* OP50 following a protocol similar to Molnar et al. (2011). For *P. pacificus* RSC019 MA lines propagated on non-*E. coli* OP50 diets, the F1 worms were moved as J4 progenies of the same single hermaphrodite to the new diets. To remove remnants of *E. coli* OP50 cells F1 worms were transferred to new plates five times. In each transfer, worms were let to feed on the new bacteria for at least 15 min. From F2 to F100, all MA lines were raised at 20 °C and only one hermaphroditic J4-stage individual was transferred every generation in each line. Two previous generations of each line were kept and used to rescue when necessary (due to contamination of plates or the reduction of brood size). In *P. pacificus* RSC019, 20 lines each were grown on *E. coli* OP50, *A. tumefaciens L27*, and *H. alvei* LRB17. All lines were frozen in liquid nitrogen every 10 generations. At the start of the experiments, the parental line was also frozen.

The MA experiment in RSC011 was done as described previously (Quiobe et al. 2025). In short, to initiate the experiment, 110 clonal lines were established by isolating individual J4 larvae onto *N.* sp. L76 and 10 lines onto *E. coli* OP50 from the complete brood of a single hermaphrodite. Each line was transferred every 4 days by a single J4 animal with fresh *N.* sp. L76 or *E. coli* OP50, resulting in a continuous propagation for 1 year (101 generations). Populations were cryopreserved in liquid nitrogen every 10 generations (up to F100). For this study, we randomly selected 20 lines on *N.* sp. L76 and eight lines (out of the 10 original lines) on *E. coli* OP50 after 100 generations.

Whole-genomic sequencing (WGS) library preparation

To gain enough material for WGS for the frozen ancestral line and MA lines of *P. pacificus* RSC019, five hermaphroditic J4 individuals were picked from each line transferred to five 6-cm nematode growth medium (NGM) plates. Progenies were collected for DNA extraction after the bacteria were depleted. DNA extraction and genomic sequencing were done at the same time for all the lines of *P. pacificus* RSC019 including the ancestral line to avoid potential batch effects. WGS library preparation was done using the Monarch Genomic DNA Purification Kit. The manufacturer's protocol was followed with some adjustments for nematode tissues. Briefly, each sample was lysed with 250 µl of tissue lysis buffer and 15 µl of proteinase K at 56 °C and kept agitated at 400 rpm for 1–1.5 h. It was then centrifuged for 3 min at maximum speed and supernatant was transferred to a new Eppendorf tube. Five microliters of RNase was added to the lysate that was then lightly and thoroughly mixed and kept agitated at 400 rpm for 10 min at 56 °C. Afterward, 400 µl of gDNA binding buffer was added to the sample. After mixing thoroughly, the sample was loaded onto the gDNA purification column. This was followed by a 3-min centrifugation to bind to the purification column at 100×*g*. Then, the same was centrifuged for 1 min more at maximum speed to remove the supernatant. The washing step was repeated twice with 500 µl of gDNA wash buffer and 1-min centrifugation at maximum each time. Finally, 32 µl of pre-heated elution buffer at 60 °C was added to the sample, which was allowed to stand for 1 min at room temperature. The elution was done by centrifuging the sample at maximum speed. WGS libraries of *P. pacificus* RSC011 MA lines were also generated with Monarch® Genomic DNA Purification Kit and in a separate single batch, following the manufacturer's instructions. All sequencing of lines of *P. pacificus* RSC019 and RSC011 were conducted by Novogene. Raw WGS data for *P. pacificus* PS312 on *E. coli* OP50 and *P. pacificus* RSC011 on *N.* sp. L76 were obtained from a previous publication (Weller et al. 2014; Quiobe et al. 2025).

Generation of a reference genome for RSC019

To reduce the influence of the divergence of genetic background on mutation detection, all resequencing data were mapped to the PacBio genomes of the corresponding genetic backgrounds. Specifically, the El Paco genome was used for *P. pacificus* PS312, and the PacBio genome generated previously was used for RSC011 (Rödelsperger et al. 2017; Quiobe et al. 2025). To generate a genome assembly of the *P. pacificus* RSC019, we followed previously established protocols (Röseler et al. 2024). In short, sequencing of a PacBio library yielded 15 Gb HiFi reads that were assembled into a raw assembly by the software Canu (version 1.4) (Korean et al. 2017). This assembly was scaffolded by the software RagTag (version 2.1.0), which used the chromosome-scale *P. pacificus* assembly for the strain PS312 (version El Paco) as reference (Rödelsperger et al. 2017, Alonge et al. 2022). Evidence-based gene

Downloaded from https://academic.oup.com/g3journal/article/16/4/jkag038/8482277 by Max-Planck Society user on 08 April 2026

annotations were generated by the software PPCAC based on strain-specific RNA-seq data and the community curated *P. pacificus* gene annotations (version El Paco annotations 3) (Athanasouli et al. 2020; Rödelsperger 2021). The transcriptomic data for the RSC019 strain were generated as described previously (Sun et al. 2021). The final assembly spans 152.6Mb with an N50 value of 23.3Mb. The resulting 27,588 gene models showed a BUSCO completeness of 94.9% (version 3 with the nematode odb9 data set) (Simão et al. 2015).

Raw data analysis

Mutation detection was performed following the GATK pipeline (version 4.2.5.0) for germline short variant discovery (SNPs + indels) (Poplin et al. 2018). Specifically, alignment of raw sequencing data to the corresponding reference genome was done with bwa mem (version 0.7.17) (Li 2013). HaplotypeCaller, GenomicsDBImport, and GenotypeGVCFs in the GATK pipeline were used separately for variant calling for each sample, further consolidate GVCFs, and the final VCFs (Poplin et al. 2018).

Mutation sharing detection

To detect if there were oversharing among lines in the same group, we compared the number of shared alternative homozygotes loci among pairs of line in the three genetic background separately. To have a fair comparison among pairs and remove the influence of potential background heterozygosity, we only counted loci with all lines covered by more than five reads less than 30% alternative homozygotes. Results are shown in Supplementary Figs. 1–3.

Mutation detection

Line-specific mutations following similar criteria to those previously described, including SNPs and indels, were identified as accumulated mutations (Weller et al. 2014). Specifically, accumulated mutations were defined if one meets the following criteria: (i) only one type of homozygotes genotype exists with more than one line on the focal site; (ii) the alternative homozygotes only occurred in one line with no less than five reads in total supporting the genotype (DP in the vcf file); (iii) no alternative heterozygotes were inferred in any other line in the same group; (iv) at least 10 lines of the group had the reference homozygotes with support from more than five good quality reads; (v) genotype quality of the accumulated homozygotes was larger than 20 (GQ in the vcf file); and (vi) no other linking accumulated SNVs or indels in the same line. To reduce the influence of group size on mutation detection, lines were grouped into *P. pacificus* PS312 on *E. coli* OP50, RSC011 on *N.* sp. L76, RSC019 on *E. coli* OP50, RSC019 on *H. alvei* LRB17, and RSC019 on *A. tumefaciens* L27, allowing each group having animals within 19 to 22 lines. Potential cross contamination occurred among lines would reduce the number of detected accumulated mutations. Therefore, we removed PT34 in RSC019 on *A. tumefaciens* L27, PT7 in RSC019 on *E. coli* OP50, MAN_44 in RSC011 on *N.* sp. L76, and all eight lines in the whole group of RSC011 on *E. coli* OP50. Mutations were filtered in each group separately.

To compare the MA rate between RSC011 on the two bacterial diets, we separately grouped the eight lines from RSC011 on *E. coli* OP50 with 19 lines of RSC011 on *N.* sp. L76 to avoid the influence the potential cross contamination among lines. The estimated mutations of the 19 lines of RSC011 on *N.* sp. L76 showed no difference indicating comparable estimated mutation rates among analysis. The estimated SNV accumulation rates were higher and deletion accumulation rate were lower in RSC011 on *E. coli* OP50 (Supplementary Fig. 4, Supplementary Table 5).

Calculation of mutation rate

To reduce the influence of sequencing depth on MA rate calculation, the MA rate in each line was calculated as the total number of mutations divided by the generations and length of genomic regions with more than half lines in the group having more than five reads mapped to the loci. The influences of mutations were annotated with the bcftools (version 1.15) csq function (Danecek and McCarthy 2017). Mutations were defined as coding ones if their annotation contained one of the following consequences: missense, synonymous, or stop_gained.

Statistical test

A Wilcoxon rank sum test was applied to test if MA rates were different among groups with wilcox.test function in R, an *F*-test was applied to test if variants of MA rates were different with var.test function in R, and a fisher's exact test was applied for testing if the mutation spectra were different among groups with fisher.test function in R.

Estimation of false positive and false negative mutation rates

To estimate the false-positive (FP) and false-negative (FN) rate for mutation detection, we employed both experimental and computational methods. Experimentally, we tested the detection of 16 randomly picked accumulated mutations from PT9 and PT10 in the group of *P. pacificus* RSC019 on *E. coli* OP50 with Sanger sequencing. Two of those mutations were in a distance of 2 bp, so the sequenced region was largely overlapping and covered both mutations. In total, 15 regions on the genome from the two lines were tested. Information about the primers and mutation detection in those two lines can be found in Supplementary Table 7. Sanger sequencing results were transformed to fasta format using the Bio.SeqIO package in python with the first and last 50 bp sequence with potentially low quality being removed. The generated sequences in fasta format were then used as query to blast to the reference genome of *P. pacificus* RSC019 for testing the mutation detection. Both FP and FN rates in those two lines could be estimated from Sanger sequencing of those regions in both lines. The only case with a discrepancy between the Sanger sequencing result and GATK reported mutations was found in the tested region with two mutations within a 2 bp distance (mutation set number 12 in Supplementary Table 7).

To estimate FP rates computationally, we used the WGS data of the ancestral line of *P. pacificus* RSC019 (PT1) on *E. coli* OP50. The FP rate of the ancestral line was calculated as the proportion of alternative homozygotes that were only detected in the ancestral line among all (3 out of 5,101 alternative homozygotes in the region with the potential to call mutations in the group of *P. pacificus* RSC019 on *E. coli* OP50).

To estimate FN rates computationally, we introduced random mutations into the reference genome of all three *P. pacificus* genetic backgrounds. We calculated the FN rate of insertions and false recall rates of deletions as the proportion of inserted mutations that were not detected after applying the same mutation detection pipeline among all inserted ones in the region with enough coverage for each sample. We randomly inserted SNVs, insertions and deletions to the chromosomes of all three reference genomes, and rerun the GATK pipeline with the edited reference genome and WGS of *P. pacificus* PS312, RSC011, and RSC019 on *E. coli*. To simplify mutation detection, we only inserted mutations in the region where there was no mutation detected within 200 bp in the flanking region. Inserted SNVs were considered as detected if

Downloaded from https://academic.oup.com/g3journal/article/16/4/jkag038/8482277 by Max-Planck Society user on 08 April 2026

Table 1. Statistics of the number of mutations and properties of accumulated mutations in each mutation accumulation groups.

Strain	Bacteria	SNV	Insertion	Deletion	ts/tv	Coding/Noncoding	Genic/Intergenic	ATBias	uSNV ($\times10^{-9}$)	uInsertion ($\times10^{-10}$)	uDeletion ($\times10^{-10}$)
PS312	*E. coli* OP50	944	243	253	0.79	0.43	2.59	5.60	2.35 ± 1.14	5.95 ± 0.92	6.18 ± 5.73
RSC011	N. sp. L76	484	66	123	1.03	0.34	2.72	3.30	1.88 ± 0.65	2.57 ± 2.43	4.78 ± 4.42
RSC019	*A. tumefaciens* L27	431	56	77	1.30	0.41	1.99	4.66	1.69 ± 0.55	2.19 ± 2.09	3.01 ± 3.01
RSC019	*E. coli* OP50	569	74	115	1.21	0.41	2.16	5.24	2.23 ± 0.70	2.90 ± 2.70	4.51 ± 3.66
RSC019	*H. alvei* LRB17	466	41	89	0.96	0.39	1.93	5.24	1.74 ± 0.69	1.53 ± 1.87	3.32 ± 2.86

Note: The unit of mutation rates are per-site, per-generation. 95% confidence of mutation rates are shown in the table.

the alternative homozygotes with the same changes were detected in the same loci as they were inserted. Inserted indels were considered to be detected if alternative homozygotes of mutations as the same type were detected within 5 bp upstream, since assigning indels uniquely is not always possible.

Results

Mutation accumulation experiments in different *P. pacificus* isolates

Diet is an important environmental factor for all animals. In this study, we investigated MA in *P. pacificus* under different bacterial diets and genetic backgrounds. Specifically, MA data were generated for *P. pacificus* RSC019 on three bacterial diets and for RSC011 on two bacterial diets, propagating worms for 100 generations via single-worm descend under laboratory conditions. The *P. pacificus* RSC019 data is described here for the first time, whereas the *P. pacificus* RSC011 lines on *E. coli* OP50 and *N.* sp. L76 were previously generated in a long-term environmental induction experiment in the context of developmental plasticity. The whole-genome sequencing data for the RSC011 lines on *N.* sp. L76 had been characterized previously (Quiobe et al. 2025), whereas the corresponding data on *E. coli* OP50 is described here for the first time. In total, 20 lines of *P. pacificus* RSC011 on *N.* sp. L76, 8 on *E. coli* OP50, and 60 lines of RSC019 separately on *E. coli* OP50, *H. alvei* LRB17, and *A. tumefaciens* L27 and the ancestral line of RSC019 were sequenced. Those data were combined with previously published MA data of the standard laboratory strain *P. pacificus* PS312 on *E. coli* OP50 propagated for 142 generations (Weller et al. 2014). To reduce the influence of difference in genetic backgrounds on mutation detection, raw sequencing data were mapped to the reference genome for the corresponding *P. pacificus* strains. Published reference genomes were used for *P. pacificus* PS312 and RSC011 (Rödelsperger et al. 2017; Quiobe et al. 2025), while the PacBio genome assembly for RSC019 was newly generated for this study using previously established protocols (Röseler et al. 2024). Detection of mutations followed the GATK pipeline (Poplin et al. 2018). While analyzing the data, we observed pairs of samples with higher number of shared mutations, indicating potential sample swap/cross contamination during the experiment (Supplementary Figs. 1–3). Therefore, one RSC019 sample on *E. coli* OP50, one on *A. tumefaciens* L27, one RSC011 sample on *N.* sp., and eight in RSC011 on *E. coli* OP50 were removed from the main analyses of our study. SNVs and indels which were only detected in one line in each group were identified as accumulated mutations and used for the following analysis. In total, 2,894 SNPs and 1,138 indels were detected for 99 samples in total (Supplementary Tables 1 and 2).

Mutation rates are largely consistent between two genetic backgrounds

To study the influence of genetic background on the MA, we compared the accumulation rates of SNVs and indels of groups of *P. pacificus* PS312 and RSC019 on *E. coli* OP50. For *P. pacificus* strain PS312, the average MA rate of SNVs is $2.35 \pm 1.14 \times 10^{-9}$ nucleotide site^{-1} × generation^{-1} with an average insertion rate of $5.95 \pm 5.92 \times 10^{-10}$ nucleotide site^{-1} × generation^{-1} and a deletion rate of $6.18 \pm 5.73 \times 10^{-10}$ nucleotide site^{-1} × generation^{-1} (Table 1). For RSC019, the MA rate of SNVs is $2.23 \pm 0.70 \times 10^{-9}$ nucleotide site^{-1} × generation^{-1} with an insertions rate of $2.90 \pm 2.70 \times 10^{-10}$ nucleotide site^{-1} × generation^{-1} and a deletion rate of $4.51 \pm 3.66 \times 10^{-10}$ nucleotide site^{-1} × generation^{-1} (Table 1). Thus, we observed differences in MA rates for insertions and deletions but not for SNVs between these two groups (Fig. 1a, Wilcoxon rank sum tests, Supplementary Table 4). The variance of mutation rates of *P. pacificus* PS312 raised on *E. coli* OP50 is higher than RSC019 on the same bacteria for insertions as well as SNVs but not deletions (Supplementary Table 4, two-sided *F*-test).

We further tested differences in other properties of those three types of mutations. We found a significant difference in mutation spectrum between *P. pacificus* PS312 and RSC019 (P-value = 0.015, Fisher's exact test, Fig. 2, Supplementary Table 4). The ratios of transitions and transversions were also significantly different between *P. pacificus* PS312 and RSC019 (P-value = 5×10^{-5}, Fisher's exact test, Supplementary Table 4), whereas the distribution of mutations across coding and noncoding regions and genic and intergenic regions were not (P-value > 0.05, Fisher's exact test, Supplementary Table 4). Length distribution of deletions but not insertions in *P. pacificus* PS312 was different from that in *P. pacificus* RSC019 (P-value < 0.05 with Fisher's exact test, 5.1 bp for PS312 and 8.1 bp for RSC019, Supplementary Tables 3 and 4). These results show that the indel properties also had subtle changes.

Mutation accumulation rate changed with bacterial diet

To study the effect of bacterial diet on the mutation rate, we compared the MA rates of *P. pacificus* RSC019 on different bacteria (average MA rates on *E. coli* OP50: SNV: $2.23 \pm 0.70 \times 10^{-9}$ nucleotide site^{-1} × generation^{-1}, insertion: $2.90 \pm 2.70 \times 10^{-10}$ nucleotide site^{-1} × generation^{-1}, deletion: $4.51 \pm 3.66 \times 10^{-10}$ nucleotide site^{-1} × generation^{-1}, on *A. tumefaciens* L27: SNV: $1.69 \pm 0.55 \times 10^{-9}$ nucleotide site^{-1} × generation^{-1}, insertion: $2.19 \pm 2.09 \times 10^{-10}$ nucleotide site^{-1} × generation^{-1}, deletion: $3.01 \pm 3.01 \times 10^{-10}$ nucleotide site^{-1} × generation^{-1}, and on *H. alvei* LRB17: SNV: $1.74 \pm 0.70 \times 10^{-9}$ nucleotide site^{-1} × generation^{-1}, insertion: $1.53 \pm 1.87 \times 10^{-10}$ nucleotide site^{-1} × generation^{-1}, deletion: $3.32 \pm 2.86 \times 10^{-10}$ nucleotide site^{-1} × generation^{-1}, Table 1). In *P. pacificus* RSC019, the SNV accumulation rate of worms grown on *E. coli* OP50 was detected to be higher than those on the other two bacterial diets (Fig. 1a, Table 1, P-value < 0.05 compared to RSC019 on *A. tumefaciens* L27 and *H. alvei* LRB17, Wilcoxon rank sum test, Supplementary Table 4). The insertion accumulation rates of *P. pacificus* RSC019 on *E. coli* OP50 showed significantly higher accumulation rates of insertions compared to those on *H. alvei* LRB17, and higher deletion

Downloaded from https://academic.oup.com/g3journal/article/16/4/jkag038/8482277 by Max-Planck Society user on 08 April 2026

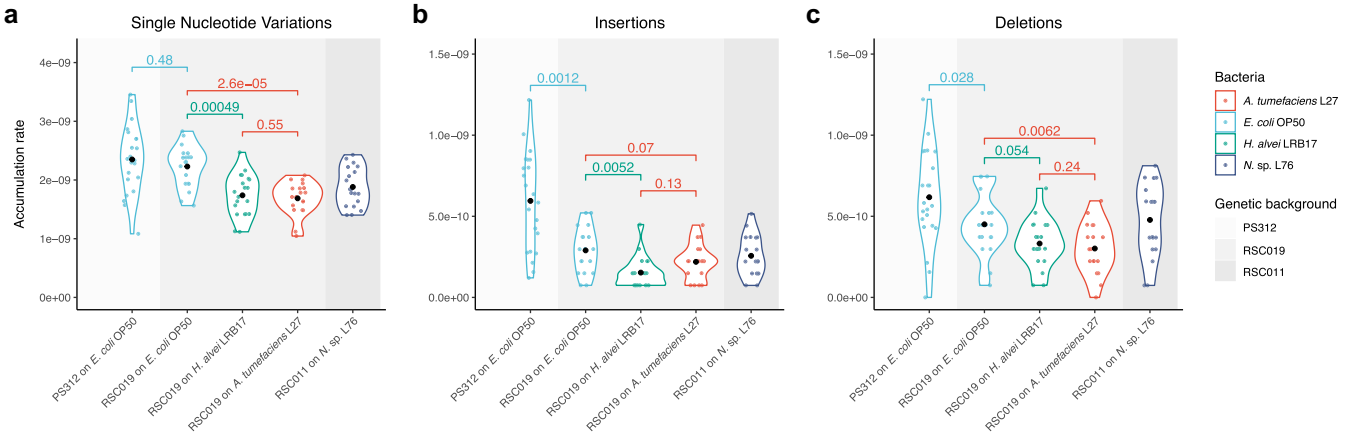


Fig. 1. Summary of mutation accumulation rates across different conditions. Accumulation rates of a) single-nucleotide variations (SNVs), b) insertions, and c) deletions. The color in the background indicates the genetic background of each group, and the color indicates the bacterial diet. Unit of y-axis is nucleotide site^{-1} × generation^{-1}. *P*-values are shown for each pair of comparisons, and statistical tests were done with the Wilcoxon's rank sum test.

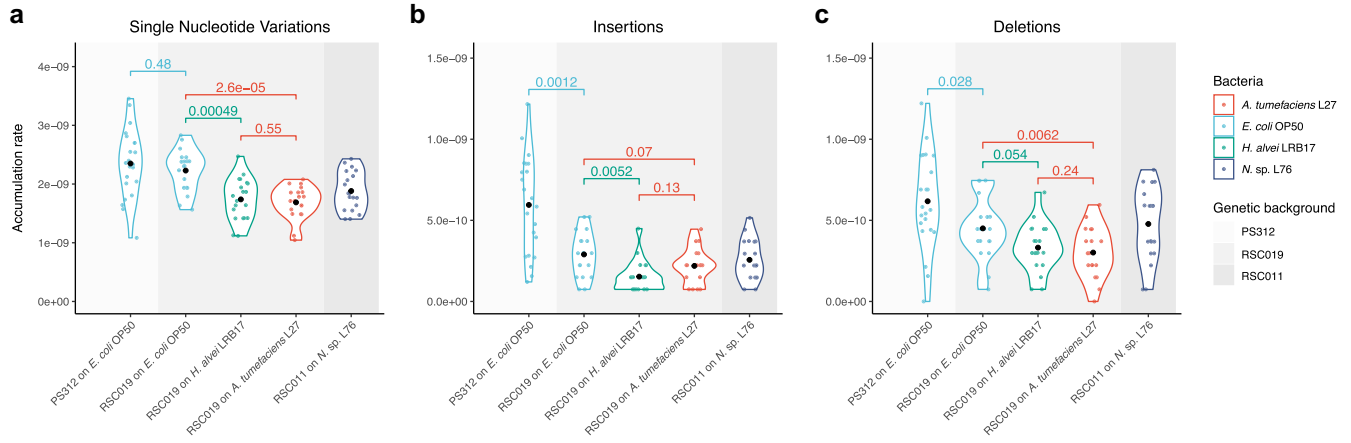


Fig. 2. Summary of the mutation spectra across different conditions. a) Spectra of SNV and length distribution of b) insertion and c) deletions of each group. Color in the background indicates the genetic background, and color corresponds to the types of mutations.

accumulation rates compared to *A. tumefaciens* L27 (Fig. 1, b and c, Table 1). The length distributions of insertions and deletions were detected to be different between *P. pacificus* RSC019 on *E. coli* OP50 and those on *H. alvei* LRB17 (P-value < 0.05, Fisher's exact test, 2.8 and 8.1 bp for *E. coli* OP50 group and 4.4 and 10.8 bp for *H. alvei* LRB17 group, Supplementary Table 4), but not between the other two groups. The difference in mutation rate between diets is also supported by a separate comparison of our RSC011 data on *N. sp.* L76 and *E. coli* OP50 (Supplementary Fig. 4, Supplementary Table 5). Thus, while the SNV mutation rates are largely consistent across genetic backgrounds, we observe an up to 1.3-fold increase in mutation rates between bacterial diets.

Estimation of false positive and false negative mutation detection with GATK

Finally, we wanted to validate the quality of our mutation detection by performing false-positive (FP) and false-negative (FN) analyses. For estimating the FP and FN rates, we employed both experimental and computational strategies. Experimentally, we estimated FP and FN rates within two lines (PT9 and PT10) in the group of *P. pacificus* RSC019 on *E. coli* OP50 as described in more details in Materials and Methods. We investigated mutation detection in both lines in 15 regions covering six SNVs, six insertions and four deletions Sanger sequencing (Supplementary Table 6). All mutations were detected as originally reported except for two closely located indels where the discrepancy in results could be attributed to the ambiguity in indel annotation. Therefore, we did not consider that specific case as FN. Given that this experimental validation did not identify any FP or FN, we would estimate the associated FP and FN rates to be close to 0%.

In addition, we computationally estimated the FP and FN rates in all three *P. pacificus* genetic backgrounds. We randomly inserted around 400 SNVs, around 3,000 insertions and deletions into the reference genome of those three genetic backgrounds and tested the detection of this set of mutations with those edited reference genome in around 20 lines from each genetic background (Supplementary Table 7). The FN rates were defined as the ratio of simulated mutations that could not be detected in the regions covered by sufficient reads in each line. We observed FN rates varied within 0–5.8% for SNVs, and false recall rates of 3.9–17.2% for insertions and 2.7–9.1% for deletions among lines (Supplementary Table 7), and estimated lower number of FN rates for insertions and deletions. To estimate the FP rates, we incorporated WGS data of the ancestral line of RSC019 (PT1), the only sequenced ancestral line among all three groups. The FP rate of the ancestral line was 0.06% and was calculated as the proportion of alternative

Downloaded from https://academic.oup.com/g3journal/article/16/4/jkag038/8482277 by Max-Planck Society user on 08 April 2026

homozygotes that were only detected in the ancestral line among all when comparing to the group of *P. pacificus* RSC019 (Supplementary Table 7). Thus, the experimental validation and computational evaluation points toward low error rates of our mutation detection procedure.

Discussion

In this study, we compared SNV and indel accumulation rates of *P. pacificus* nematodes between genetic backgrounds and various bacterial diets. The average SNV accumulation rates observed in this study ($1.08–3.34 \times 10^{-9}$ nucleotide site^{-1} × generation^{-1}) span a similar range with previously reported rates in two free-living nematodes of the genus *Caenorhabditis* ($0.78–2.14 \times 10^{-9}$ nucleotide site^{-1} × generation^{-1}) (Denver et al. 2012). When further split SNVs based on their mutation and sequence context, we observed similar trends of an excess of mutations between T and A under the sequence context of TTA or TAA between *P. pacificus* groups and *C. elegans* N2 (Supplementary Fig. 5, Konrad et al. 2019). Thus, our results suggest that the magnitude of mutation rates and fold changes appears to be conserved across the two nematode genera *Caenorhabditis* and *Pristionchus*, which were recently estimated to have diverged roughly 300 MYA (Qing et al. 2025). This indicates that mutation rates and spectra can overall be stable during nematode evolution, and we therefore speculate that these values can serve as a first estimate of mutation rate even for more distantly related free-living nematodes.

While we could not detect significant differences in the average SNV accumulation rates between genetic backgrounds, we observed significant differences in the mean and variance of indel frequencies between PS312 and RSC019. However, we would like to point out that our data sets for PS312 and RSC019 on *E. coli* are not completely comparable, as both experiments have not been carried out for the same number of generations (142 generations in the case of PS312 vs 100 generations for RSC019) and previous comparisons of first-order and second-order MA lines have identified significant differences in indel frequencies between both regimes of MA lines pointing toward the evolvability of the mutational process (Saxena et al. 2019). Thus, we cannot completely rule out an effect of such a process on the mean and variance of the observed results.

Previous studies have indicated that organisms under stressful conditions such as high temperature or poor diet quality resulting in lower fecundity or body mass can experience increased mutation rate (Agrawal and Wang 2008; Sharp and Agrawal 2012; Matsuba et al. 2013; Waldvogel and Pfenninger 2021). In our study, we showed, to the best of our knowledge for the first time, that diet can influence the MA in nematodes. One potential explanation for the difference in MA rate is the physiological stress caused by diet. Among all tested bacteria, *N.* sp. L76 and *H. alvei* LRB17 could potentially cause stress responses in *P. pacificus* PS312, since they induced reduced adult survival compared to the other tested bacteria (Akduman et al. 2018). In contrast, *P. pacificus* RSC019 on *H. alvei* LRB17 had a slightly lower mutation rate compared to that on *E. coli* OP50. Thus, the biological processes that affect mutation rates across different microbiota remain to be elucidated.

Data availability

The Pacbio genome assembly of *P. pacificus* RSC019 and WGS data for *P. pacificus* RSC011 on *E. coli* OP50 and all *P. pacificus* RSC019 are newly generated for this study and available on European Nucleotide Archive under the study accession PRJEB94012. The RSC019 genome assembly and gene annotations are available at http://www.pristionchus.org. All strains used in this study area available upon request from the corresponding author.

Supplemental material available at G3 online.

Acknowledgments

We thank all members of the Sommer lab for fruitful discussions throughout these studies. We would also like to thank the *Caenorhabditis* Genetics Center for providing us with a strain of *E. coli* OP50.

Funding

This work was fully funded by the Max-Planck Society.

Conflicts of interest

None declared.

Literature cited

Agrawal AF, Wang AD. 2008. Increased transmission of tutations by low-condition females: evidence for condition-dependent DNA repair. PLoS Biol. 6:e30. https://doi.org/10.1371/journal.pbio.0060030.

Akduman N *et al.* 2020. Bacterial vitamin B12 production enhances nematode predatory behavior. ISME J. 14:1494–1507. https://doi.org/10.1038/s41396-020-0626-2.

Akduman N, Rödelsperger C, Sommer RJ. 2018. Culture-based analysis of *Pristionchus*-associated microbiota from beetles and figs for studying nematode-bacterial interactions. PLoS One. 13: e0198018. https://doi.org/10.1371/journal.pone.0198018.

Alonge M, *et al.* 2022. Automated assembly scaffolding using RagTag elevates a new tomato system for high-throughput genome editing. Genome Biol. 23:258. https://doi.org/10.1186/s13059-022-02823-7.

Athanasouli M *et al.* 2020. Comparative genomics and community curation further improve gene annotations in the nematode *Pristionchus pacificus*. BMC Genomics. 21:708. https://doi.org/10.1186/s12864-020-07100-0.

Athanasouli M, Loschko T, Rödelsperger C. 2025. Interspecies systems biology links bacterial metabolic pathways to nematode gene expression, chemotaxis behavior, and survival. Genome Res. 35:2363–2374. https://doi.org/10.1101/gr.280848.125.

Danecek P, McCarthy SA. 2017. BCFtools/csq: haplotype-aware variant consequences. Bioinformatics. 33:2037–2039. https://doi.org/10.1093/bioinformatics/btx100.

Dardiry M, Piskobulu V, Kalirad A, Sommer RJ. 2023. Experimental and theoretical support for costs of plasticity and phenotype in a nematode cannibalistic trait. Evol Lett. 7:48–57. https://doi.org/10.1093/evlett/qrac001.

Denver DR *et al.* 2012. Variation in base-substitution mutation in experimental and natural lineages of *Caenorhabditis* Nematodes. Genome Biol Evol. 4:513–522. https://doi.org/10.1093/gbe/evs028.

Konrad A, Brady MJ, Bergthorsson U, Katju V. 2019. Mutational landscape of spontaneous base substitutions and small indels in experimental *Caenorhabditis elegans* populations of differing size. Genetics. 212:837–854. https://doi.org/10.1534/genetics.119.302054.

Koren S, *et al.*. 2017. Canu: scalable and accurate long-read assembly via adaptive k-mer weighting and repeat separation. Genome Res. 27:722–736. https://doi.org/10.1101/gr.215087.116.

Downloaded from https://academic.oup.com/g3journal/article/16/4/jkag038/8482277 by Max-Planck Society user on 08 April 2026

Li H. 2013. Aligning sequence reads, clone sequences and assembly contigs with BWA-MEM [preprint]. arXiv 3997. [accessed 2025 Jul 15]. http://arxiv.org/abs/1303.3997. https://doi.org/10.48550/arXiv.1303.3997

Lightfoot JW *et al.* 2019. Small peptide–mediated self-recognition prevents cannibalism in predatory nematodes. Science. 364:86–89. https://doi.org/10.1126/science.aav9856.

Liu H, Zhang J. 2019. Yeast spontaneous mutation rate and spectrum vary with environment. Curr Biol. 29:1584–1591.e3. https://doi.org/10.1016/j.cub.2019.03.054.

Lynch M *et al.* 2023. The divergence of mutation rates and spectra across the Tree of Life. EMBO Rep. 24:e57561. https://doi.org/10.15252/embr.202357561.

Matsuba C, Ostrow DG, Salomon MP, Tolani A, Baer CF. 2013. Temperature, stress and spontaneous mutation in *Caenorhabditis briggsae* and *Caenorhabditis elegans*. Biol Lett. 9:20120334. https://doi.org/10.1098/rsbl.2012.0334.

McGaughran A *et al.* 2016. Genomic profiles of diversification and enotype-phenotype association in island nematode lineages. Mol Biol Evol. 33:2257–2272. https://doi.org/10.1093/molbev/msw093.

Molnar RI, Bartelmes G, Dinkelacker I, Witte H, Sommer RJ. 2011. Mutation rates and intraspecific divergence of the mitochondrial genome of Pristionchus pacificus. Mol Biol Evol. 28:2317–2326. https://doi.org/10.1093/molbev/msr057.

Ness RW *et al.* 2015. Extensive de novo mutation rate variation between individuals and across the genome of *Chlamydomonas reinhardtii*. Genome Res. 25:1739–1749. https://doi.org/10.1101/gr.191494.115.

Poplin R *et al.* 2018. Scaling accurate genetic variant discovery to tens of thousands of samples [preprint]. bioRxiv 201178. [accessed 2024 Apr 3]. https://www.biorxiv.org/content/10.1101/201178v3. https://doi.org/10.1101/201178

Qing X *et al.* 2025. Phylogenomic insights into the evolution and origin of *Nematoda*. Syst Biol. 74:349–358. https://doi.org/10.1093/sysbio/syae073.

Quiobe SP *et al.* 2025. EBAX-1/ZSWIM8 destabilizes miRNAs, resulting in transgenerational inheritance of a predatory trait. Sci Adv. 11:eadu0875. https://doi.org/10.1126/sciadv.adu0875.

Quiobe SP, Sommer RJ. 2025. Adaptive consequences of transgenerational inheritance of a predatory mouth-form trait in nematodes [preprint]. bioRxiv 680509. [accessed 2025 Nov 2]. https://www.biorxiv.org/content/10.1101/2025.10.05.680509v1. https://doi.org/10.1101/2025.10.05.680509

Rödelsperger C *et al.* 2017. Single-molecule sequencing reveals the chromosome-scale genomic architecture of the nematode model organism *Pristionchus pacificus*. Cell Rep. 21:834–844. https://doi.org/10.1016/j.celrep.2017.09.077.

Rödelsperger C. 2021. The community-curated *Pristionchus pacificus* genome facilitates automated gene annotation improvement in related nematodes. BMC Genomics. 22:216. https://doi.org/10.1186/s12864-021-07529-x.

Röseler W, Sommer RJ, Rödelsperger C. 2024. Nematode genome announcement: a chromosome-scale genome assembly for the *Pristionchus pacificus* reference mapping strain PS1843. J Nematol. 56:20240063. https://doi.org/10.2478/jofnem-2024-0063.

Saxena AS, Salomon MP, Matsuba C, Yeh S-D, Baer CF. 2019. Evolution of the mutational process under relaxed selection in *Caenorhabditis elegans*. Mol Biol Evol. 36:239–251. https://doi.org/10.1093/molbev/msy213.

Schroeder NE. 2021. Introduction to *Pristionchus pacificus* anatomy. J Nematol. 53:e2021–e2091. https://doi.org/10.21307/jofnem-2021-091.

Sharp NP, Agrawal AF. 2012. Evidence for elevated mutation rates in low-quality genotypes. Proc Natl Acad Sci U S A. 109:6142–6146. https://doi.org/10.1073/pnas.1118918109.

Simão FA, Waterhouse RM, Ioannidis P, Kriventseva EV, Zdobnov EM. 2015. BUSCO: assessing genome assembly and annotation completeness with single-copy orthologs. Bioinformatics. 31:3210–3212. https://doi.org/10.1093/bioinformatics/btv35.

Sommer RJ. 2025. *Pristionchus*—beetle associations: towards a new natural history. J Invertebr Pathol. 209:108243. https://doi.org/10.1016/j.jip.2024.108243.

Sommer RJ, Carta L, Kim S-Y, Sternberg PW. 1996. Morphological, genetic and molecular description of *Pristionchus pacificus* sp. n. (Nematoda: *Neodiplogastridae*). Fundament Appl Nematol. 19:511–521.

Sun S, Rödelsperger C, Sommer RJ. 2021. Single worm transcriptomics identifies a developmental core network of oscillating genes with deep conservation across nematodes. Genome Res. 31:1590–1601. https://doi.org/10.1101/gr.275303.121.

Waldvogel A-M, Pfenninger M. 2021. Temperature dependence of spontaneous mutation rates. Genome Res. 31:1582–1589. https://doi.org/10.1101/gr.275168.120.

Weller AM, Rödelsperger C, Eberhardt G, Molnar RI, Sommer RJ. 2014. Opposing forces of A/T-biased mutations and G/C-biased gene conversions shape the genome of the nematode *Pristionchus pacificus*. Genetics. 196:1145–1152. https://doi.org/10.1534/genetics.113.159863.

Editor: E. Haag

Downloaded from https://academic.oup.com/g3journal/article/16/4/jkag038/8482277 by Max-Planck Society user on 08 April 2026

Supplementary Material

Supplementary Figure 1: Number of shared alternative homozygotes in pairs in PS312 on *E. coli* OP50. Results indicate little mutation sharing among lines.

Supplementary Figure 2: Number of shared alternative homozygotes in pairs in RSC019. Results indicate large proportion of mutation sharing between PT33 and PT34, and mild mutation sharing between PT6 and PT7.

Supplementary Figure 3: Number of shared alternative homozygotes in pairs in RSC011. Results indicate mild mutation sharing between MAN_35 and MAN_44, and large proportion of mutation sharing among MAE lines (RSC011 on *E. coli* OP50).

Supplementary Figure 4: Mutation rate comparison between RSC011 on *E. coli* OP50 and *N.* sp. L76. Each line of RSC011 on *E. coli* OP50 were group with the group on *N.* sp. L76 separately for accumulated mutation detection and mutation rates calculation. Mutation rates of RSC011 on *N.* sp. L76 were also estimated in these eight groups and shown.

Supplementary Figure 5: Mutational spectra across 96 SNV types in *P. pacificus* and *C. elegans* N2. SNVs are divided into 96 types based on the mutation and the nucleotide 1 bp up and down stream of it. a-f) mutation spectra of *P. pacificus* groups and g) mutation spectra of *C. elegans* N2.

Supplementary Table 1: Summary information of all mutations.

Supplementary Table 2: Summary information of all lines.

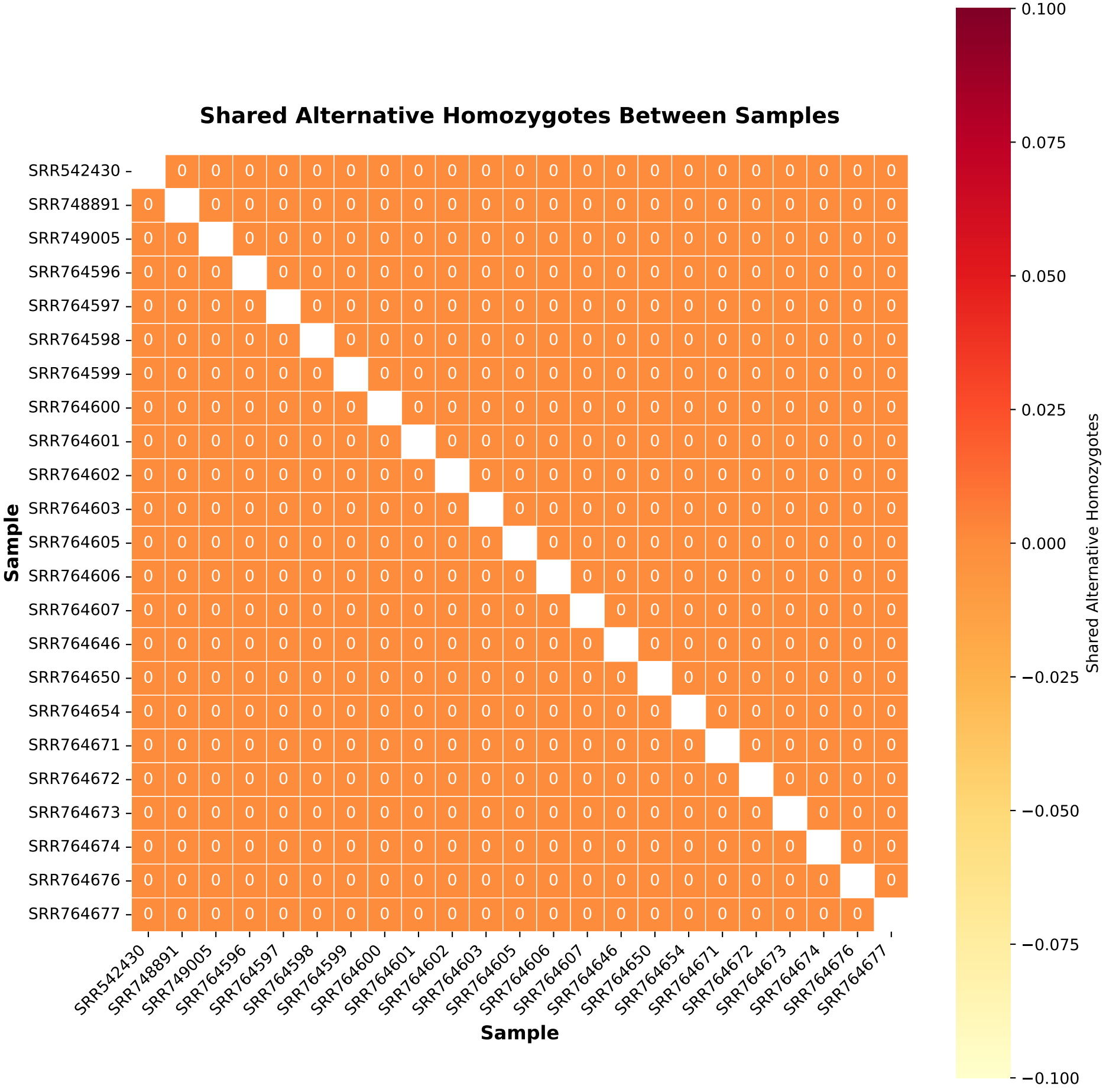
Supplementary Table 3: Full list of statistics of mutations in all five groups.

Supplementary Table 4: *p*-values of comparisons of mutation properties among groups.

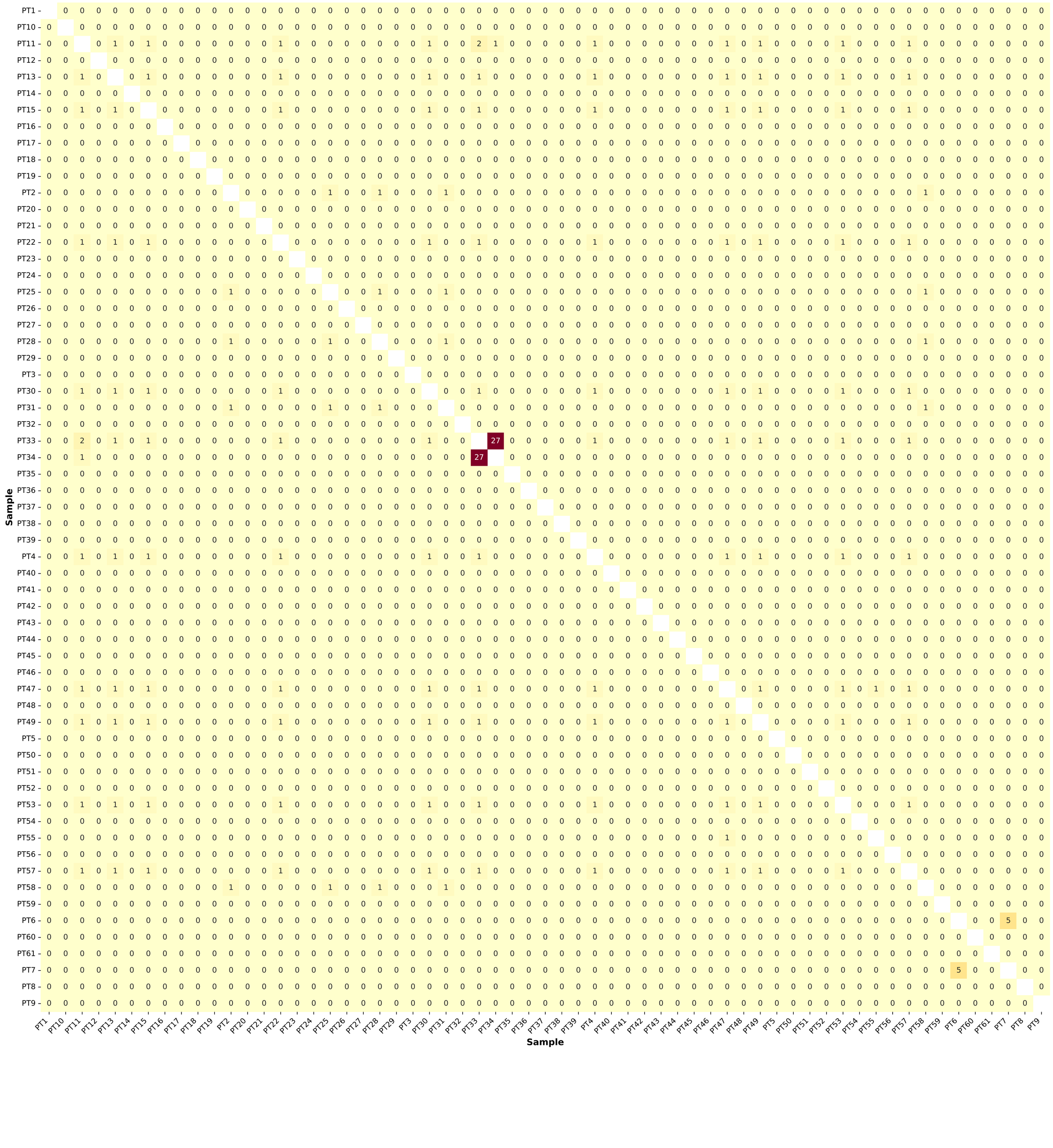
Supplementary Table 5: Mutation rates estimated for RSC011 on *E. coli* OP50 and on *N.* sp. L76.

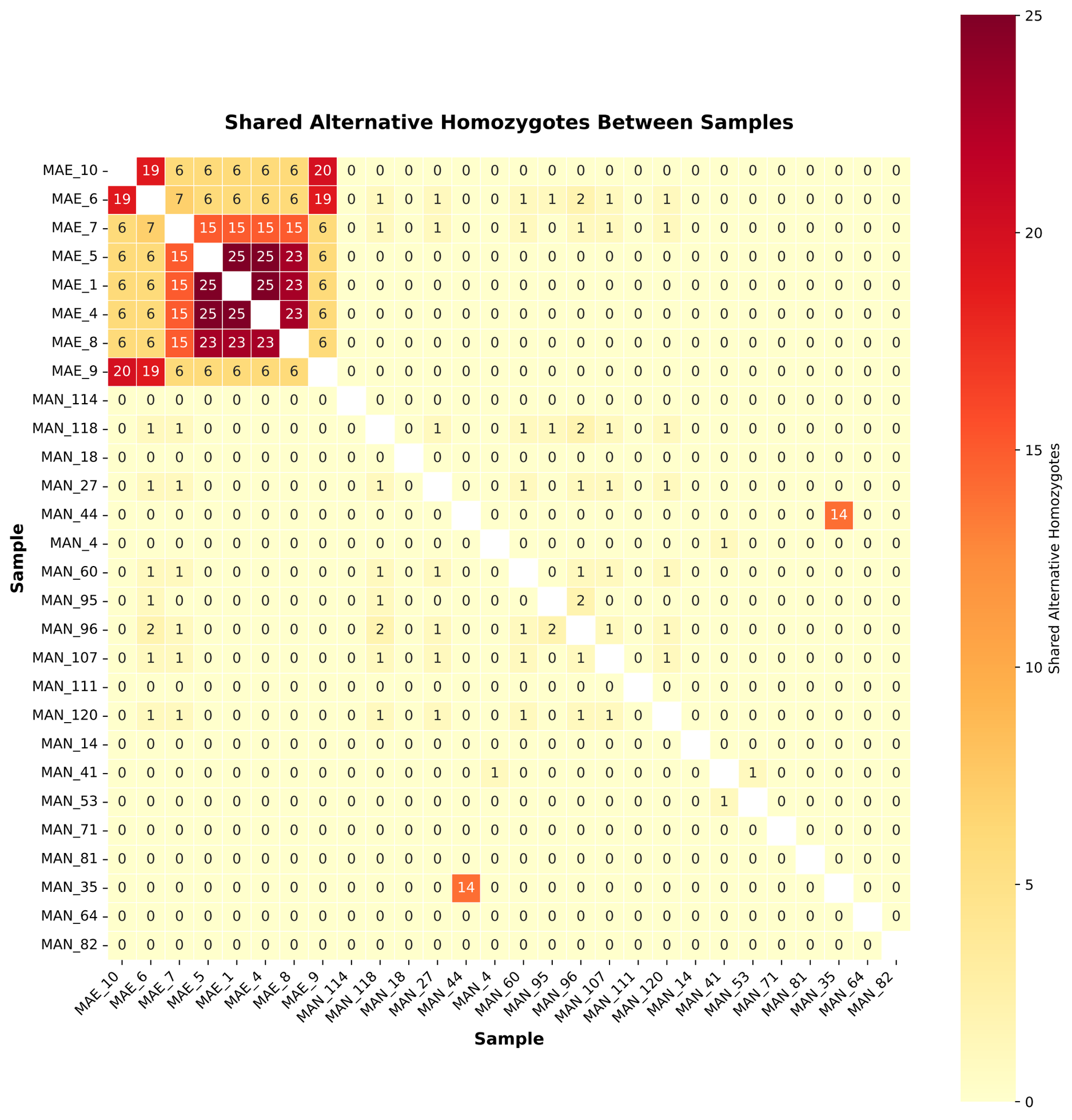
Supplementary Table 6: Primers used for sanger sequencing.

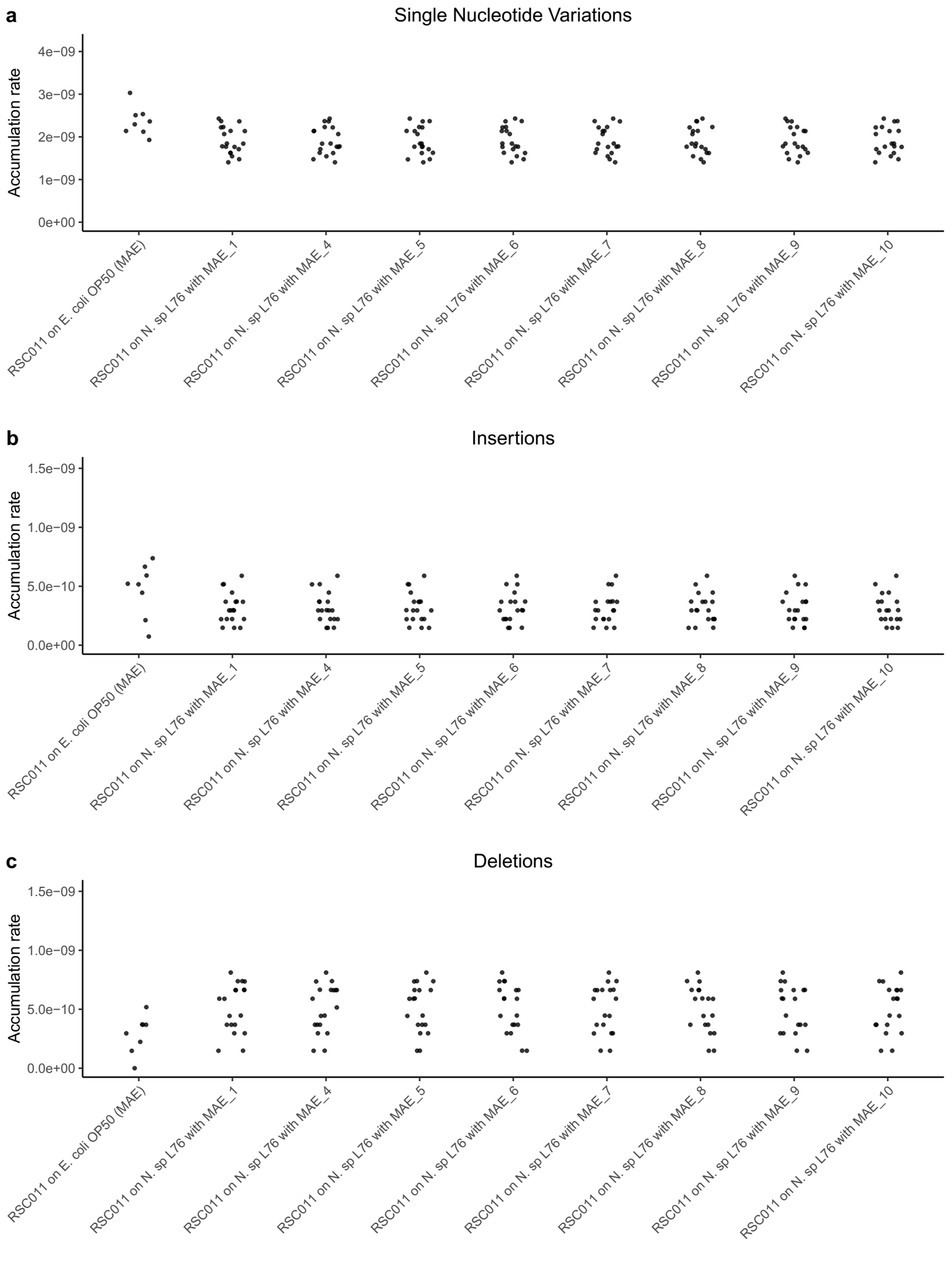
Supplementary Table 7: Computational estimation of FN rates.


Shared Alternative Homozygotes Between Samples
Sample
SRR542430
SRR748891
SRR749005
SRR764596
SRR764597
SRR764598
SRR764599
SRR764600
SRR764601
SRR764602
SRR764603
SRR764605
SRR764606
SRR764607
SRR764646
SRR764650
SRR764654
SRR764671
SRR764672
SRR764673
SRR764674
SRR764676
SRR764677
Sample
Shared Alternative Homozygotes
0.100
0.075
0.050
0.025
0.000
−0.025
−0.050
−0.075
−0.100

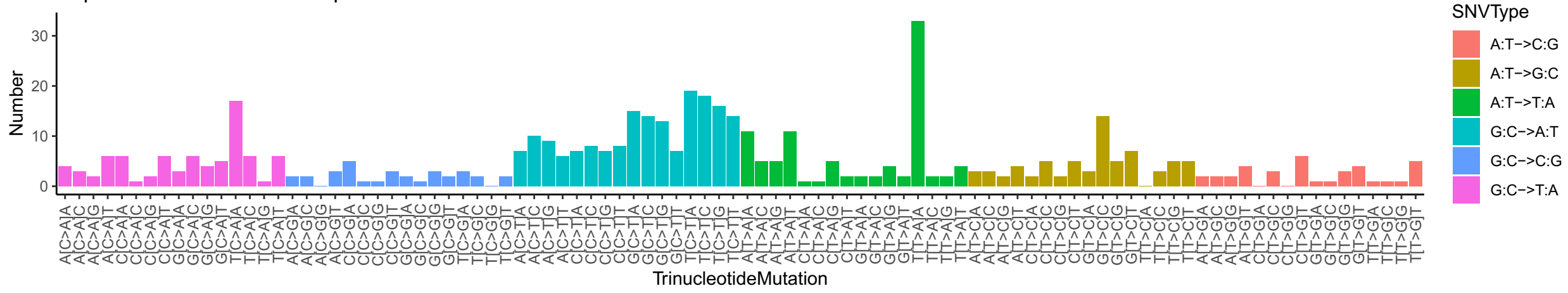
Shared Alternative Homozygotes Between Samples



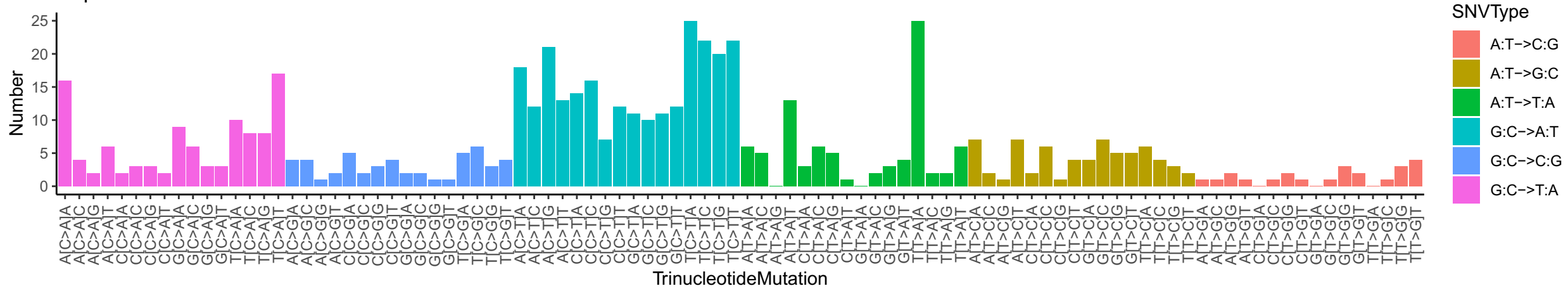

Shared Alternative Homozygotes Between Samples
Sample
MAE_10 19 6 6 6 6 6 20 0 0 0 0 0 0 0 0 0 0 0 0 0 0 0 0 0 0 0 0
MAE_6 19 7 6 6 6 6 19 0 1 0 1 0 0 1 1 2 1 0 1 0 0 0 0 0 0 0 0
MAE_7 6 7 15 15 15 15 6 0 1 0 1 0 0 1 0 1 1 0 1 0 0 0 0 0 0 0 0
MAE_5 6 6 15 25 25 23 6 0 0 0 0 0 0 0 0 0 0 0 0 0 0 0 0 0 0 0 0
MAE_1 6 6 15 25 25 23 6 0 0 0 0 0 0 0 0 0 0 0 0 0 0 0 0 0 0 0 0
MAE_4 6 6 15 25 25 23 6 0 0 0 0 0 0 0 0 0 0 0 0 0 0 0 0 0 0 0 0
MAE_8 6 6 15 23 23 23 6 0 0 0 0 0 0 0 0 0 0 0 0 0 0 0 0 0 0 0 0
MAE_9 20 19 6 6 6 6 6 0 0 0 0 0 0 0 0 0 0 0 0 0 0 0 0 0 0 0 0
MAN_114 0 0 0 0 0 0 0 0 0 0 0 0 0 0 0 0 0 0 0 0 0 0 0 0 0 0 0
MAN_118 0 1 1 0 0 0 0 0 0 0 1 0 0 1 1 2 1 0 1 0 0 0 0 0 0 0 0
MAN_18 0 0 0 0 0 0 0 0 0 0 0 0 0 0 0 0 0 0 0 0 0 0 0 0 0 0 0
MAN_27 0 1 1 0 0 0 0 0 0 1 0 0 0 1 0 1 1 0 1 0 0 0 0 0 0 0 0
MAN_44 0 0 0 0 0 0 0 0 0 0 0 0 0 0 0 0 0 0 0 0 0 0 0 0 0 14 0 0
MAN_4 0 0 0 0 0 0 0 0 0 0 0 0 0 0 0 0 0 0 0 0 0 1 0 0 0 0 0 0
MAN_60 0 1 1 0 0 0 0 0 0 1 0 1 0 0 0 1 1 0 1 0 0 0 0 0 0 0 0 0
MAN_95 0 1 0 0 0 0 0 0 0 1 0 0 0 0 0 0 2 0 0 0 0 0 0 0 0 0 0 0
MAN_96 0 2 1 0 0 0 0 0 0 2 0 1 0 0 1 2 0 1 0 1 0 0 0 0 0 0 0 0
MAN_107 0 1 1 0 0 0 0 0 0 1 0 1 0 0 1 0 1 0 1 0 0 0 0 0 0 0 0 0
MAN_111 0 0 0 0 0 0 0 0 0 0 0 0 0 0 0 0 0 0 0 0 0 0 0 0 0 0 0 0
MAN_120 0 1 1 0 0 0 0 0 0 1 0 1 0 0 1 0 1 1 0 0 0 0 0 0 0 0 0 0
MAN_14 0 0 0 0 0 0 0 0 0 0 0 0 0 0 0 0 0 0 0 0 0 0 0 0 0 0 0 0
MAN_41 0 0 0 0 0 0 0 0 0 0 0 0 0 1 0 0 0 0 0 0 0 0 1 0 0 0 0 0
MAN_53 0 0 0 0 0 0 0 0 0 0 0 0 0 0 0 0 0 0 0 0 0 1 0 0 0 0 0 0
MAN_71 0 0 0 0 0 0 0 0 0 0 0 0 0 0 0 0 0 0 0 0 0 0 0 0 0 0 0 0
MAN_81 0 0 0 0 0 0 0 0 0 0 0 0 0 0 0 0 0 0 0 0 0 0 0 0 0 0 0 0
MAN_35 0 0 0 0 0 0 0 0 0 0 0 0 14 0 0 0 0 0 0 0 0 0 0 0 0 0 0 0
MAN_64 0 0 0 0 0 0 0 0 0 0 0 0 0 0 0 0 0 0 0 0 0 0 0 0 0 0 0 0
MAN_82 0 0 0 0 0 0 0 0 0 0 0 0 0 0 0 0 0 0 0 0 0 0 0 0 0 0 0 0
MAE_10 MAE_6 MAE_7 MAE_5 MAE_1 MAE_4 MAE_8 MAE_9 MAN_114 MAN_118 MAN_18 MAN_27 MAN_44 MAN_4 MAN_60 MAN_95 MAN_96 MAN_107 MAN_111 MAN_120 MAN_14 MAN_41 MAN_53 MAN_71 MAN_81 MAN_35 MAN_64 MAN_82
Sample
Shared Alternative Homozygotes
25
20
15
10
5
0


a
Single Nucleotide Variations
Accumulation rate
4e−09
3e−09
2e−09
1e−09
0e+00
b
Insertions
Accumulation rate
1.5e−09
1.0e−09
5.0e−10
0.0e+00
c
Deletions
Accumulation rate
1.5e−09
1.0e−09
5.0e−10
0.0e+00
RSC011 on E. coli OP50 (MAE)
RSC011 on N. sp L76 with MAE_1
RSC011 on N. sp L76 with MAE_4
RSC011 on N. sp L76 with MAE_5
RSC011 on N. sp L76 with MAE_6
RSC011 on N. sp L76 with MAE_7
RSC011 on N. sp L76 with MAE_8
RSC011 on N. sp L76 with MAE_9
RSC011 on N. sp L76 with MAE_10

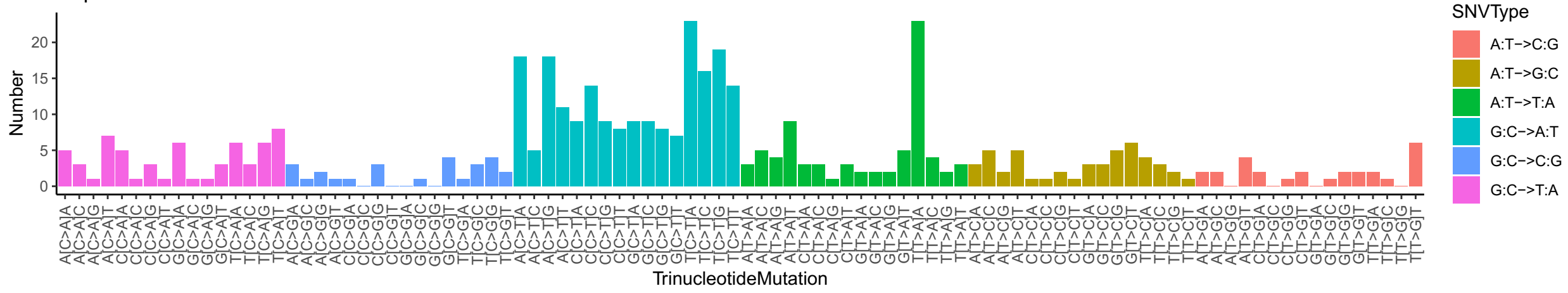
a P. pacificus RSC011 on N. sp L76



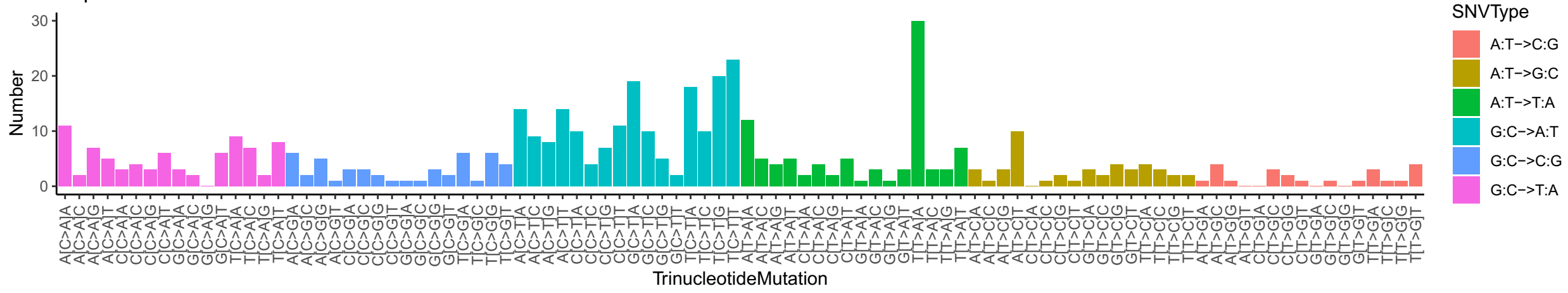
b P. pacificus RSC019 on E. coli OP50



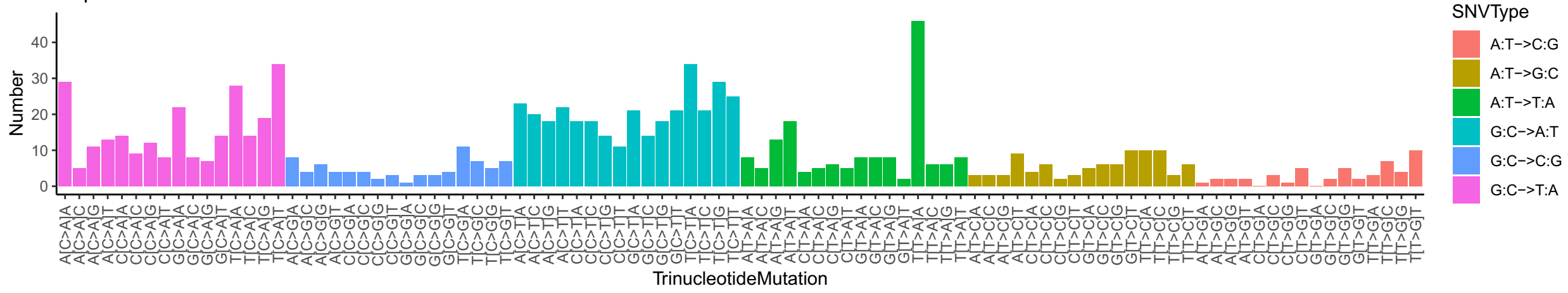
c P. pacificus RSC019 on A. tumefaciens L27



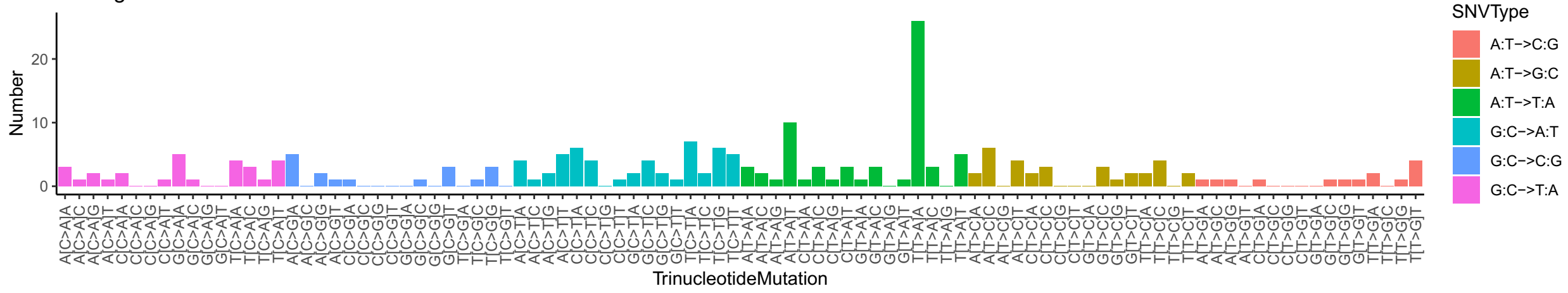
d P. pacificus RSC019 on H. alvei LRB17



e P. pacificus PS312 on E. coli OP50



f C. elegans N2 mutation accumulation



The dynamics of coexistence and succession in a decaying ecosystem

Ata Kalirad,[1] Penghieng Theam[1] Ralf J. Sommer,[1*]

[1]Department for Integrative Evolutionary Biology,
Max Planck Institute for Biology Tübingen, Tübingen, 72076, Germany

[*]To whom correspondence should be addressed; E-mail: ralf.sommer@tuebingen.mpg.de

Elucidating the rules that govern community assembly and enable the coexistence of species is central to ecology. Much of the current understanding revolves around the composition of communities at equilibrium. In contrast, transient ecological dynamics, in particular the succession of species following an environmental disturbance, remain largely unexplored. We present *Gymnogaster buphthalma* beetle carcasses as a model to study species coexistence in disequilibrium. In this community, nematodes appear in succession – with multiple feeding and reproductive strategies, transience, and associated dispersal – creating a perfect model for metacommunity ecology. We computationally reconstructed decaying *G. buphthalma* beetles sampled from the wild using experimentally-derived life history data, i.e. emergence times, sex ratios, and fecundity measurements. Through agent-based modeling, we show that nematode coexistence is possible over a wide range of scenarios. This work provides a unique experimental and computational framework to synthesize various approaches to metacommunity and species succession theories.

Introduction

The importance of transient dynamics in shaping short-lived ecosystems is increasingly being recognized (*1–6*). Particularly, the rapid transformation of habitats due to global climate change (*7, 8*) necessitates experimental and theoretical work to better understand the ecological dynamics in transient ecosystems. Filling this knowledge gap would also relate the paradox of coexistence in ecological communities to the long-standing problem of species succession, which plays a major role in shaping the composition of short-lived communities (*9, 10*). This paradox – the observation that, instead of competitive exclusion, species can coexist in a community – remains a central problem in ecology (*11, 12*). Mechanistic solutions postulate long-term coexistence as an asymptotic state resulting from various forms of competitions due to limited resources, predation, and other ecological interactions (*13*). In contrast, the neutral approach interprets the observed coexistence as a short-lived state, shaped by chance, before an inevitable monodominance (*14, 15*).

Deterministic models predict long-term coexistence over time scales approaching infinity in communities where species densities can vary in a continuous fashion (*16*). By their very design, such models exclude the consequences of discrete individuals in a population, e.g., demographic stochasticity (*17, 18*). Therefore, the patterns of coexistence in ecosystems with rapid turn-over, specifically those that follow a boom-and-bust dynamic, remain largely unexplored. Despite extensive studies of plant communities, little is known about transient coexistence during succession. In invertebrates, one notable study system is decaying insect carcasses frequently found in the soil, which are characterized by their organismal diversity and rapid decomposition. As such, decaying insects are a perfect model to study succession and coexistence over short periods of time (*19, 20*).

Here we take advantage of *Gymnogaster buphthalma* beetles of the Scarabaeidae family as a

model to study succession and coexistence in a decaying ecosystem. Various free-living nematodes are found in association with these and other scarab beetles (*21*). We integrate laboratory data of nematode species that emerged from *G. buphthalma* beetles sampled on Réunion island with an agent-based modeling approach to understand the dynamics of species coexistence and succession.

Results

The community composition emerging on *G. buphthalma* beetle carcasses

For this study, *G. buphthalma* beetles sampled from Réunion island were sacrificed in the laboratory on nematode growth medium (NGM) plates (Fig. 1A). As long as beetles are alive, nematodes stay in the arrested dauer stage. Following the beetle´s death, microbes decompose the carcass, providing food for nematodes, which in response exit the dauer stage and develop into adults. Following the sacrifice, plates were regularly observed to accurately infer nematode emergence time on the carcasses (Fig. 1B). All 24 *G. buphthalma* beetles harbored nematodes with three distinct patterns. Interestingly, all beetles contained isolates of a previously unknown *Acrostichus* species, which will be described elsewhere. On 13 carcasses, the presence of this species were accompanied by isolates of *Pristionchus pacificus* – an established model organism (*22*) – or *Pristionchus mayeri* (*23*). Importantly, isolates of *P. pacificus*, *P. mayeri*, and *Acrostichus* sp. emerged together on 6 beetles (Fig. 1B). In addition to observing the nematode composition patterns, we were able to accurately estimate the timing of emergence of each nematode on a given beetle. This allowed us to incorporate differences in the emergence strategies in addition to life history measurements into an integrative modeling framework to reconstruct the dynamics on a decaying beetle.

The communities containing three nematode species provide a rare opportunity to investigate community dynamics of a transient ecosystem with three unique characteristics, i) a diver-

sity of feeding structures, ii) different reproductive strategies, and iii) a boom-and-bust life cycle (Fig. 1C) (*24*). *P. pacificus* isolated from the beetles developed the wide-mouthed (eurystomatous) form with two teeth, which enables them to kill juveniles of other nematodes in addition to consuming bacteria (Fig. 1D) (*25, 26*). In contrast, *P. mayeri* and *Acrostichus* sp. developed bacteriovorus feeding structures under the same condition (Fig. 1D). Thus, the beetle carcass is inhabited by nematodes with different feeding strategies including life history intraguild predation by *P. pacificus* (*27*). However, given the amount of surplus killing observed in the lab, this interaction can also be described as interference competition (*28*).

Intriguingly, these nematodes also reflect a plethora of reproductive strategies (Fig. 1C). Both *Pristionchus* species encountered on these *G. buphthalma* cadavers are androdioecious hermaphrodites that can only reproduce by selfing because males were not found among the emerging nematodes. In contrast, *Acrostichus* sp. is a gonochoristic species with distinct males and females, indicating that beetle carcasses are populated by free-living nematodes with vastly different reproductive strategies. Therefore, with respect to reproductive strategies, the presence of these three species raises a fascinating question: Given the well-known cost of males, which has been hypothesized to handicap gonochorist species in competition with hermaphrodites (*29, 30*), how could *Acrostichus* sp. compete with its two rivals? Additionally, the cost of males in these competitions will be confounded with intraguild predation by *P. pacificus*.

We attempted to reconstruct the dynamics of coexistence and succession using an approach that combines laboratory measurements of nematode life history traits with an agent-based modeling framework (Fig. 2). Firstly, we measured the sex ratio of the *Acrostichus* sp. RSO013 under laboratory conditions, which indicated an equal proportion of males to females over lifetime fecundity (Fig. 1E). Secondly, we measured the fecundity of the three nematode species (Fig. 1F–I). For that, we quantified the number of progenies produced by a single mother during a 24-hour time period for a total of 7 days. The fecundities were consistent amongst the isolates

of *P. pacificus* and *P. mayeri*, with the isolates of the latter species having consistently higher fecundities relative to the former (Fig. 1F–G, Fig. S1). For the gonochorist *Acrostichus* sp., we followed mating pairs over 17 days. Total progeny number is much higher for *Acrostichus* relative to the hermaphroditic *Pristionchus* species (Fig. S1). This observation reflects the role of sperm availability as the limiting factor in nematode life-time fecundity. Taken together, these measurements provide a treasure trove of data, enabling a computationally-thorough reconstruction of the dynamics in these communities.

Communotron: an agent-based reconstruction of a decaying beetle

To computationally reconstruct the dynamics of competition between nematodes on decaying *G. buphthalma* beetles, we constructed an agent-based model, referred to as *Communotron* (Figs. 2A–2B). This model is inspired by a model previously introduced to illustrate the role of phenotypic plasticity in competition among nematodes (*31*). In *Communotron*, individual worms follow a realistic life cycle, which includes environmentally-dependent transitions to alternative developmental paths – i.e., arrested juvenile and dauer stages – and include life-history intraguild predation by *P. pacificus* adults (Fig. 2A). In short, *Communotron* enables an agent-based framework that combines the ability to include experimental data, resource dynamics, and simulation on the scale of hours (For more detail, see Materials and Methods).

The cost of males in *Acrostichus* sp. is mitigated by its dauer-exit strategy

To illustrate the workflow of *Communotron*, we reconstructed the community observed on one of the beetles, which contained *Acrostichus* sp. RSO013, *P. pacificus* RSO011, and *P. mayeri* RSO012 (Fig. 2C). In this community, adult *Acrostichus* sp. emerged 24 hours after the beetle was sacrificed, whereas *P. pacificus* and *P. mayeri* emerged after 48 and 72 hours, respectively (Fig. 2C). The reconstructed communities indicate that the early emergence of *Acrostichus*

sp. mitigates much of its shortcomings as a competitor, resulting in communities where this species composes most of the biomass at every developmental stage. In addition, given that dauer larvae can exit the local community, this strategy results in much higher migrant dauer larvae belonging to *Acrostichus* sp. compared to its competitors (Fig. 2D).

It is notable that on all 24 observed communities, the *Acrostichus* sp. isolates emerged early out of their dauer stage, even in the absence of any other nematode on the decaying beetle (Fig. 1B). Thus, we hypothesized that the dauer-exist strategy in *Acrostichus* sp. – which ensures a head start relative to hermaphroditic and potentially predatory competitors at the expense of having access to higher levels of resource during these initial decomposition phase – can offset both the cost of having males in this species and its non-predatory feeding structure. The results of *Communotron* are in line with this hypothesis.

The observed dynamics is strongly affected by the number of dauer larvae of each species present at the start of the formation of the community. To illustrate this point, we simulated the same community under the counterfactual condition in which all of the three species emerged on the beetle carcass in equal numbers. Under this condition, *Acrostichus* sp. performs worse than its competitors. However, none of the species are competitively excluded from the community and dauer larvae of all three species can be found in the surrounding environment (Fig. 2E). Taken together, these findings illustrate how the theoretical cost of males can be mitigated in nature.

Species coexist during pairwise competition on the beetle carcass

The three-way interaction between these nematode species was observed in 25% of the analyzed beetles, whereas more than 50% carry *Acrostichus* sp. together with one of the *Pristionchus* species. These two-way interactions differ from each other because *Acrostichus* sp. competes with a potential predator only when it co-occurs with *P. pacificus*. To investigate how coexis-

tence is possible in these two-way interactions, we simulated communities on decaying beetles that contain a pair of species (Fig. 3).

Pairwise competition between *P. pacificus* and *Acrostichus* sp. should be both affected by the cost of males in *Acrostichus* sp. and the effect of intraguild predation exerted by *P. pacificus*. It is possible *a priori* that the combined effect would result in the competitive exclusion of the gonochorist population on the carcass. However, we found that these species can coexist as long as resources are available (Fig. 3A). In comparison, pairwise competition between *P. mayeri* and *Acrostichus* sp. is intriguing since it is directly a result of cost of males in *Acrostichus* sp. versus a hermaphroditic competitor, who is bacteriovorus and does not engage in predation. Interestingly, these two species can also coexist in a community (Fig. 3B). It should be noted that the realized cost of males is both affected by the dauer-exit strategy of *Acrostichus* sp. and the initial number of dauer larvae of each species on the beetle (Fig. S2). Thus, similarly as in the three-species communities explored before, multiple factors can overcome the cost of males at the community level.

Finally, our modeling approach also allows us to investigate the interaction of the two *Pristionchus* species in isolation even though this is not observed in nature (Fig. 3C). Hypothetically, the pairwise competition between *P. pacificus* and *P. mayeri* should be the net outcome of the effect of intraguild predation by *P. pacificus* and the higher fecundities of *P. mayeri*. Does the interplay between factors prevent coexistence as long as resource is available? The results of our simulations indicate that, while intraguild predation reduces the proportion of *P. mayeri* in the community, both species still coexist (Fig. 3C). Thus, coexistence is observed across a wide range of conditions.

Longer resource availability does not hinder coexistence

The outcome of competition on a decaying beetle differs from a stochastic model of population dynamics without resource dynamics, which predicts all-or-nothing outcomes (*31*). One could imagine that the transient coexistence in our model is purely a function of the single phase of resource availability, and would vanish if bacterial load was periodically replenished on the carcass. Given that a decaying beetle carcass in the soil is an open system, and other microbes can enter it, it is not unrealistic to imagine multiple phases of resource availability. To test this notion, we first simulated communities of three species with two phases of bacterial growth (Fig. 4A). Interestingly, the addition of a second resource availability phase resulted in communities in which all three species still coexist. But even more surprisingly, under the same conditions, a counterfactual scenario in which the dauer larvae of all three species emerge from the carcass in equal quantities promotes coexistence (Fig. 4B). This result differs from similar simulations with only a single resource availability phase. Thus, the periodic availability of resource promotes coexistence, instead of hindering it. This point can be made even more explicit if we simulate an extreme scenario, in which bacterial population is perpetually replenished. Here, the coexistence of all three species is still observed, with *Acrostichus* sp. RSO013 accounting for the majority of dauer larvae produced on a carcass (Fig. 4C).

Taken together, the communities reconstructed using *Communotron* with single or multiple resource availability phases illustrate how a boom-and-bust dynamic results in competitive outcomes that are different from a model without explicit resource availability dynamic. While the latter predicts competitive exclusion, the former indicate conditions under which species can coexist, in spite of *a priori* disadvantages attributed to each competitor in isolation.

Discussion

Much of our understanding of community ecology revolves around the composition of communities at equilibrium and their stability following perturbations (*32–34*). However, the importance of disequilibrium in shaping ecological dynamics has been noted since the inception of spatial ecology, further highlighted by the introduction of patch dynamics, which in turn led to the establishment of metacommunity ecology (*35–37*). Much of the theoretical contributions in ecology remains rooted in classical models designed to explore ecosystems at equilibrium. Furthermore, incommensurable predictions derived from various metacommunity theories — the patch dynamics model, the neutral theory model, the species sorting model, and the mass effect model, each emphasizing distinct processes — have prompted an ongoing research program to provide an integrative "Übermodel" that could integrate all these processes (*37*).

The importance of the combined effects of various ecological processes at disequilibrium is probably nowhere as prominent as when multiple species occupy an emergent ecosystem following an environmental disturbance. This phenomenon of species succession (*38, 39*) has been extensively documented, albeit almost exclusively in plants (*40*). In this context, the decaying *G. buphthalma* beetle provides a comprehensive model for metacommunity ecology, since it incorporates various processes relevant to metacommunity theories, e.g., dispersal, predation, demographic heterogeneity, and reproductive modes (Fig. 5). These processes are intertwined during the formation of a habitat following a disturbance, i.e., the natural death of the beetle. The community on the dacaying carcass is established with a limited number of dauer larvae. During the initial colonization phase, stochastic events can lead to ecological drift, which has long been suggested to play a crucial role in shaping community composition when the initial community size is small (*41–44*). This ecosystem lasts as long as microbial resources remain available, a case of species succession in disequilibrium. Our computational reconstruction

of the decaying beetle indicates, contrary to many deterministic models, the breath of scenarios that promote transient coexistence in such a model. This framework can be used to study the competition-colonization trade-off models to better understand the relative importance of factors such as local competitiveness and dispersal in a natural system (*45, 46*).

Despite the insights gained from our integrative study, crucial aspects remain unexplored. For example, the diversity of feeding structures in various *Pristionchus* species is a case of developmental (phenotypic) plasticity, where the population-level proportion of predatory to bacteriovorus nematodes is determined by various environmental factors (*47–50*). Most notably, the microbial diet strongly influences mouth-form development and can even result in transgenerational epigenetic inheritance (*51, 52*). We have previously explored how phenotypic plasticity can affect ecological competition (*31, 53*). However, it remains to be seen how the composition of the microbial community sampled from the decaying beetle – instead of the standard laboratory diet – would affect life-history traits. More importantly, the extent to which these natural diets would result in diet-induced plasticity in feeding structures is currently unknown and awaits future analysis that will profit from strong modeling contributions. In conclusion, the experimental and theoretical study of the decaying *G. buphthalma* beetle can be used to address various metacommunity and succession questions, resulting in a better understanding of long-term as well short-term coexistence in such systems – by combining empirical manipulations with agent-based modeling.

References

1. R. E. Snyder, *Theoretical Population Biology* **77**, 243 (2010).

2. A. Hastings, *et al.*, *Science* **361**, eaat6412 (2018).

3. L. G. Shoemaker, *et al.*, *Ecology* **101**, e02922 (2020).

4. A. Swain, L. Fussell, W. F. Fagan, *Proceedings of the National Academy of Sciences* **119**, e2020956119 (2022).

5. Y. Yang, K. Z. Coyte, K. R. Foster, A. Li, *Nat Commun* **14**, 7204 (2023).

6. I. Hayashi, H. Fujita, H. Toju, *ISME Communications* **4**, ycae007 (2024).

7. J. E. Williams, J. L. Blois, *Journal of Biogeography* **45**, 2175 (2018).

8. P. Amarasekare, *Journal of Animal Ecology* **93**, 428 (2024).

9. E. P. Odum, *Science* **164**, 262 (1969).

10. J. H. Connell, R. O. Slatyer, *The American Naturalist* **111**, 1119 (1977).

11. G. E. Hutchinson, *The American Naturalist* **95**, 137 (1961).

12. P. Chesson, *Annual Review of Ecology, Evolution, and Systematics* **31**, 343 (2000).

13. M. A. McPeek, *Coexistence in Ecology: A Mechanistic Perspective*, Monographs in Population Biology (Princeton University Press, 2022).

14. S. P. Hubbell, *Science* **203**, 1299 (1979).

15. J. Rosindell, S. P. Hubbell, R. S. Etienne, *Trends in Ecology & Evolution* **26**, 340 (2011).

16. S. J. Schreiber, J. M. Levine, O. Godoy, N. J. B. Kraft, S. P. Hart, *Ecology* **104**, e3838 (2023).

17. S. P. Hart, S. J. Schreiber, J. M. Levine, *Ecology Letters* **19**, 825 (2016).

18. J. Pande, T. Fung, R. Chisholm, N. M. Shnerb, *Ecology Letters* **23**, 274 (2020).

19. M. Salimi, *et al.*, *Journal of Medical Entomology* **55**, 1410 (2018).

20. A. Cruise, D. W. Watson, C. Schal, *PLoS One* **13**, e0195785 (2018).

21. N. Kanzaki, *et al.*, *Zootaxa* **4943**, zootaxa.4943.1.1 (2021).

22. R. J. Sommer, A. a. Mcgaughran, *Molecular Ecology* **22**, 2380 (2013).

23. N. Kanzaki, E. J. Ragsdale, M. Herrmann, V. Susoy, R. J. Sommer, *J Nematol* **45**, 172 (2013).

24. T. Renahan, *et al.*, *Environmental Microbiology* **23**, 5102 (2021).

25. J. W. Lightfoot, *et al.*, *Science* **364**, 86 (2019).

26. J. W. Lightfoot, *et al.*, *Science Advances* **7**, eabg8042 (2021).

27. G. A. Polis, C. A. Myers, R. D. a. Holt, *Annual Review of Ecology and Systematics* **20**, 297 (1989).

28. T. J. Case, M. E. Gilpin, *Proc Natl Acad Sci U S A* **71**, 3073 (1974).

29. J. Maynard Smith, *Journal of Theoretical Biology* **30**, 319 (1971).

30. C. M. Lively, *J Evol Biol* **22**, 2086 (2009).

31. A. Kalirad, R. J. Sommer, *Ecology Letters* **27**, e14370 (2024).

32. R. M. May, *Nature* **238**, 413 (1972).

33. D. Gravel, F. Massol, M. A. Leibold, *Nature Communications* **7**, 12457 (2016).

34. J. J. Qian, E. Akçay, *Nature Ecology & Evolution* **4**, 356 (2020).

35. D. Tilman, P. Kareiva, eds., *Spatial Ecology* (Princeton University Press, 1997).

36. M. Vellend, *The Theory of Ecological Communities (MPB-57)* (Princeton University Press, 2016).

37. M. A. Leibold, J. M. Chase, *Metacommunity Ecology, Volume 59* (Princeton University Press, 2018).

38. J. M. Chase, *Proceedings of the National Academy of Sciences* **104**, 17430 (2007).

39. L. Jiang, S. N. Patel, *Ecology* **89**, 1931 (2008).

40. L. Poorter, *et al.*, *Biological Reviews* **98**, 2049 (2023).

41. T. Fukami, *Ecology* **85**, 3234 (2004).

42. J. L. Orrock, R. J. Fletcher Jr., *The American Naturalist* **166**, 107 (2005). PMID: 15937793.

43. J. L. Orrock, J. I. Watling, *Proceedings: Biological Sciences* **277**, 2185 (2010).

44. M. Vellend, A. Agrawal, *The Quarterly Review of Biology* **85**, 183 (2010).

45. J. G. Skellam, *Biometrika* **38**, 196 (1951).

46. V. Calcagno, N. Mouquet, P. Jarne, P. David, *Ecology Letters* **9**, 897 (2006).

47. N. Akduman, *et al.*, *The ISME Journal* **14**, 1494 (2020).

48. M. Lenuzzi, *et al.*, *Journal of Experimental Zoology Part B: Molecular and Developmental Evolution* pp. 1–11 (2021).

49. M. S. Werner, *et al.*, *Scientific Reports* **7**, (2017).

50. M. S. Werner, M. H. Claaßen, T. Renahan, M. Dardiry, R. J. a. Sommer, *iScience* **10**, 123 (2018).

51. M. Dardiry, V. Piskobulu, A. Kalirad, R. J. Sommer, *Evolution Letters* **7**, 48 (2023).

52. S. P. Quiobe, *et al.*, *Science Advances* **11**, eadu0875.

53. A. Kalirad, R. J. Sommer, *PLOS Computational Biology* **20**, e1011823 (2024).

54. C. R. Harris, *et al.*, *Nature* **585**, 357 (2020).

55. J. Salvatier, T. V. Wiecki, C. Fonnesbeck, *PeerJ Computer Science* **2**, e55 (2016).

Acknowledgments

We used the Opuntia cluster from the Hewlett Packard Enterprise Data Science Institute at the University of Houston. We thank the support from the Research Computing Data Core at the University of Houston.

Supplementary Materials

Materials and Methods

Figs. S1 and S2

Table S1

Funding

This work was funded by the Max Planck Society. The funders had no role in study design, data collection and analysis, decision to publish, or preparation of the manuscript.

Authors contributions

RJS and AK conceived the project. PT observed the succession on beetle carcasses. PT and AK measured the life-history traits. AK wrote the code and visualized the results. RJS and AK wrote the manuscript.

Competing interests

The authors declare that they have no competing financial interests.

Data and materials availability

The software used to run all simulations and conduct all the data analysis was written in Python 3.11.7 with NumPy 1.26.4 (*54*). The Bayesian statistical analyses were done using PyMC 5.21.1 (*55*). The code and the raw experimental data are available at https://github.com/Kalirad/Communotron.

Figure captions

Figure 1

Emergence dynamics and composition of nematode communities on beetle carcasses. (A) *G. buphthalma* beetles sampled from Réunion island were used to construct "community on a plate" (Photo of *G. buphthalma* courtesy of Zeeshan Mirza). (B) Two or more nematode species emerged from the majority of *G. buphthalma* carcasses (19 out of 24), with six containing various isolates belonging to three different nematode species. (C) The three-species communities represent diverse feeding structures: the *P. pacificus* isolates develop the wide-mouth eurystomatous mouth form, which enables killing of competing nematodes, while the *P. mayeri* and *Acrostichus* sp. isolates develop feeding structures suited to bacterivory. Additionally, both *Pristionchus* species are androdioecious hermaphrodites, in contrast to *Acrostichus* sp., which is a gonochoristic species. (D) The proportion of predatory adults in the isolates of *P. pacificus* and *P. mayeri*. (E) *Acrostichus* sp. RSO013 progeny over the entire egg-laying period showed a 1:1 sex ratio. Vertical bars represent the 95% the highest density interval (HDI) for the sex ratio based on a binomial model. (F) Fecundity of the *P. pacificus* isolates. (G) Fecundity of the *P. mayeri* isolates. The number of viable male (H) and female (I) progenies of *Acrostichus* RSO013. Horizontal lines in (F) to (I) represent the mean values.

Figure 2

Computational reconstruction of nematode communities using *Communotron*. (A) Nematodes in *Communotron* follow a realistic life cycle, which includes alternative developmental states, namely, arrested juvenile and the dauer state. Transitions I to IV represent alternative developmental paths which are determined by local population density and/or resource availability. *P. pacificus* adults can kill juvenile, dauer, and arrested juvenile stages of *P. mayeri* and *Acrostichus* sp., resulting in life-history intraguild predation. (B) Worms in *Communotron*

occupy points on a two-dimensional lattice. Bacterial growth is simulated as a dynamic component of the model, generating a time-dependent gradient that affects the bias of the movement of the motile stages in the community and the probabilities of transitioning to alternative developmental states. (C) The pattern of succession on a *G. buphthalma* beetle as observed on a plate. We used *Communotron* to computationally reconstruct the dynamics of this community based on laboratory measurements and the succession timeline. (D) The community dynamics based on 100 simulations of *Communotron* (C). The species diversity is calculated using the Gini–Simpson index, with the dotted gray line indicating the maximum expected value, $1 - \frac{1}{z}$, where z is the number of species. (E) Simulation of the community under the counterfactual condition of equal starting population sizes for the three species. Parameters used in these simulations: initial number of dauers: 200 *Acrostichus* sp., 10 *P. mayeri*, 10 *P. pacificus*; $m = 100 \times 100$, $\eta = 0.005$, $L = 10$; in the counterfactual scenario, all the parameters are the same, except for starting population sizes: 200 *Acrostichus* sp., 200 *P. mayeri*, 200 *P. pacificus*.

Figure 3

Coexistence during pairwise competition. (A) Pairwise competition between *P. pacificus* and *Acrostichus* sp., (B) pairwise competition between *P. mayeri* and *Acrostichus* sp., and (C) pairwise competition between *P. mayeri* and *P. pacificus*. Parameters used in these simulations: initial number of dauers: 200 *Acrostichus* sp., 10 *P. mayeri*, 10 *P. pacificus*; $m = 100 \times 100$, $\eta = 0.005$, $L = 10$.

Figure 4 caption

Counterfactual scenarios of resource availability and coexistence. (A) Three-way competition between *P. pacificus*, *P. mayeri*, and *Acrostichus* sp. with two phases of resource availability. (B) Another counterfactual scenario in which all three species exit the dauer stage on

a decaying carcass in equal numbers with conditions identical to (A). (C) Three-way competition between *P. pacificus*, *P. mayeri*, and *Acrostichus* sp. with multiple phases of resource availability. Parameters used in these simulations: initial number of dauers in (A) and (C): 200 *Acrostichus* sp., 10 *P. mayeri*, 10 *P. pacificus*; $m = 100 \times 100$, $\eta = 0.005$, $L = 10$.

Figure 5 caption

The role of succession and dispersal in coexistence on a decaying beetle as a model for metacommunity ecology. The decaying beetle can be envisioned as a transient patch, in which processes such as predation and strategies including dauer-exit timing and reproductive mode result in a specific pattern of succession. The dispersal at the metacommunity level can result in coexistence, given the constant dispersal and succession events at the metacommunity level. Additionally, selection could shape various traits of nematodes at the eco-evolutionary time scale to maximize their long-term fitness.

Figures

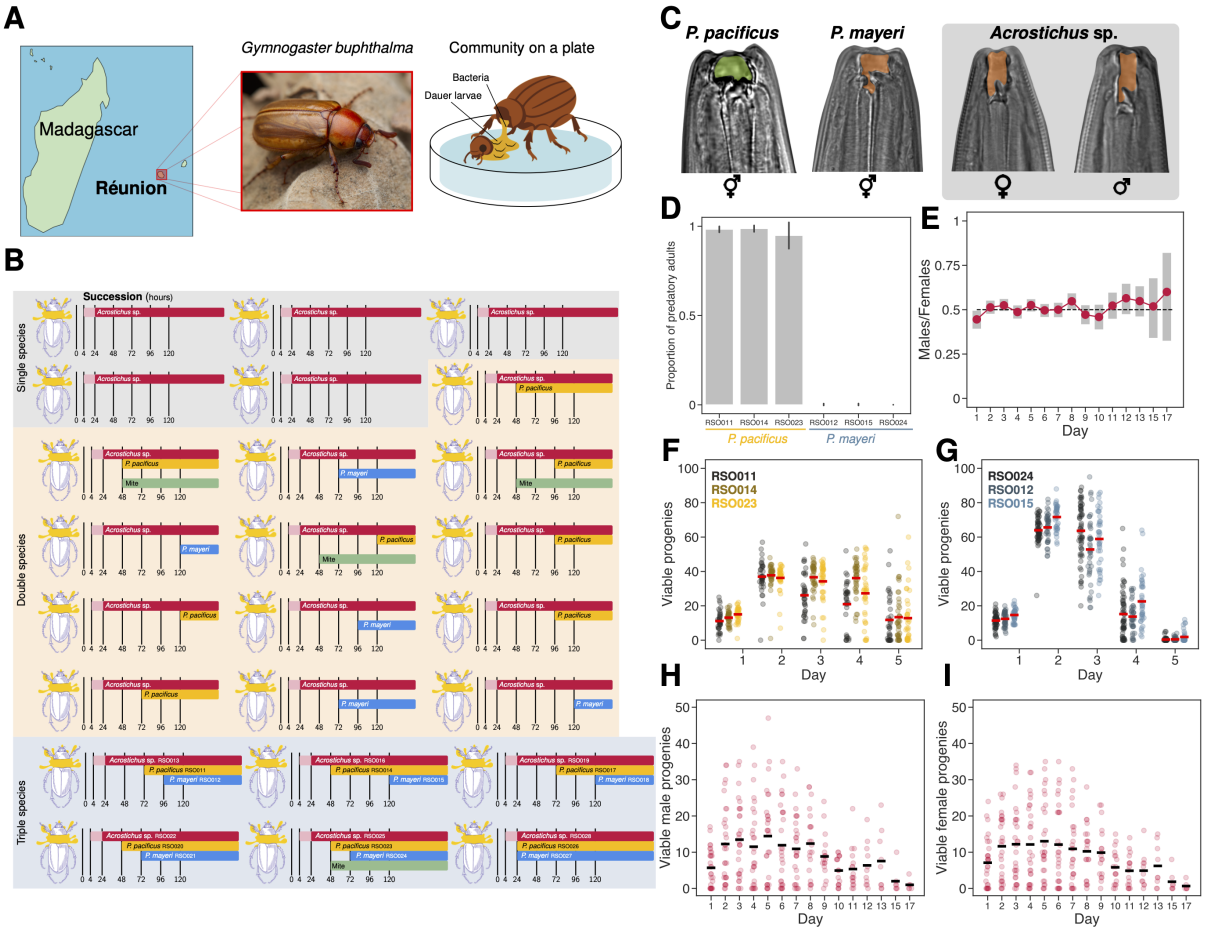


Figure 1

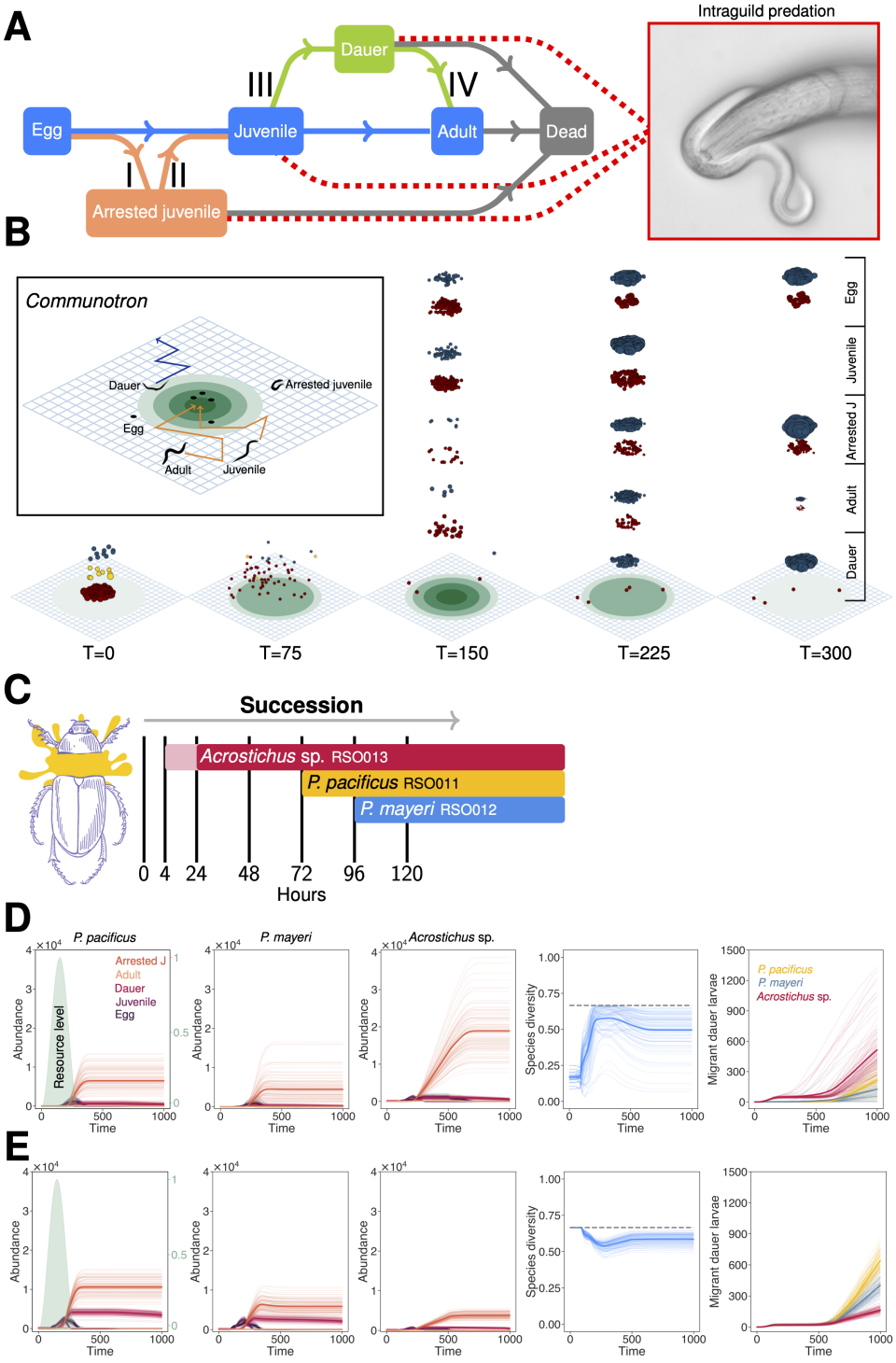

A
Intraguild predation
Dauer
III
IV
Egg
Juvenile
Adult
Dead
I
II
Arrested juvenile
B
Communotron
Dauer
Arrested juvenile
Egg
Adult
Juvenile
Egg
Juvenile
Arrested J
Adult
Dauer
T=0
T=75
T=150
T=225
T=300
C
Succession
Acrostichus sp. RSO013
P. pacificus RSO011
P. mayeri RSO012
0 4 24 48 72 96 120
Hours
D
P. pacificus
P. mayeri
Acrostichus sp.
Arrested J
Adult
Dauer
Juvenile
Egg
Resource level
Abundance
Species diversity
Migrant dauer larvae
Time
E

Figure 2

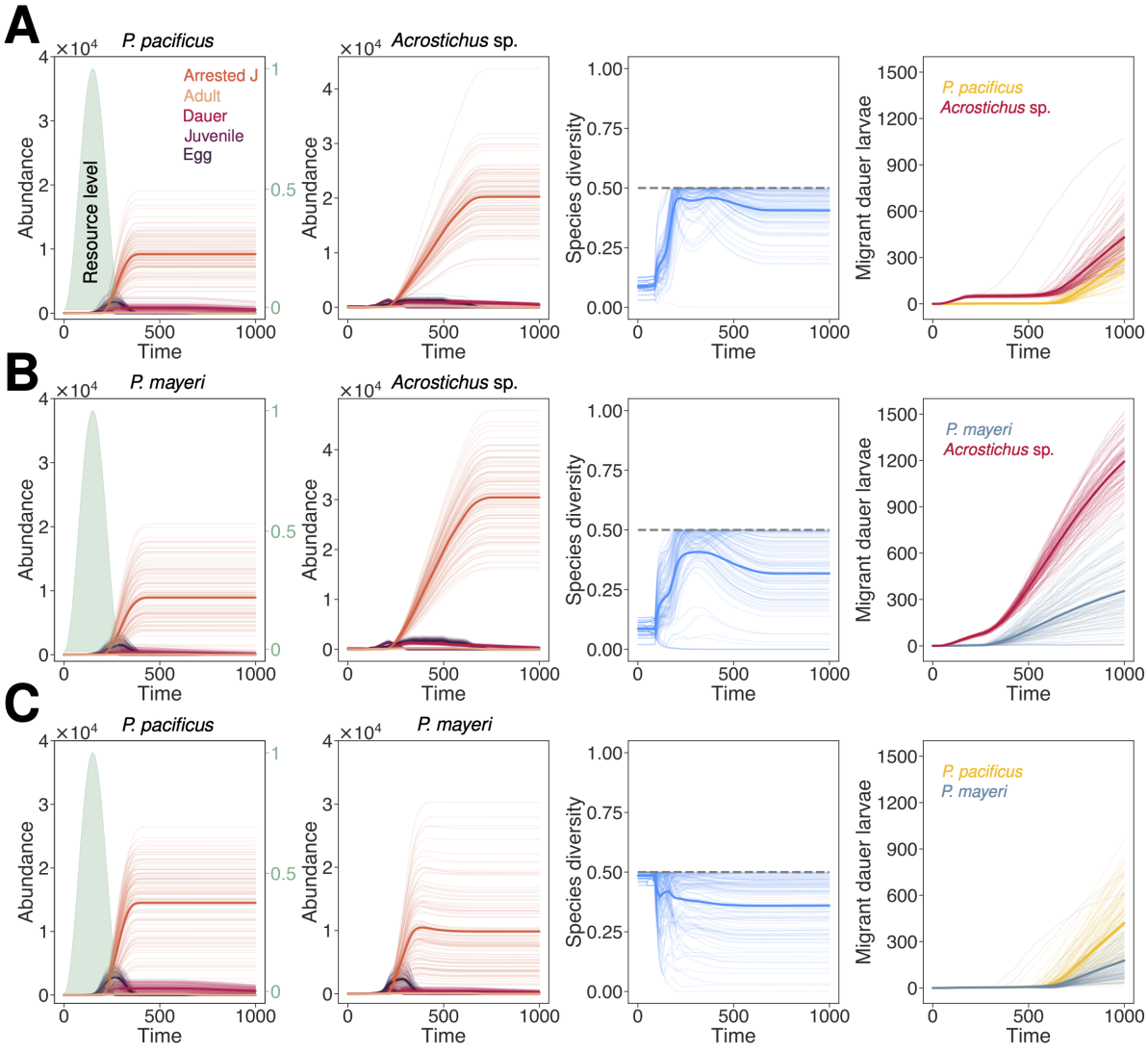

A
B
C
P. pacificus
Acrostichus sp.
P. mayeri
Arrested J
Adult
Dauer
Juvenile
Egg
Resource level
Abundance
Species diversity
Migrant dauer larvae
Time
×10⁴

Figure 3

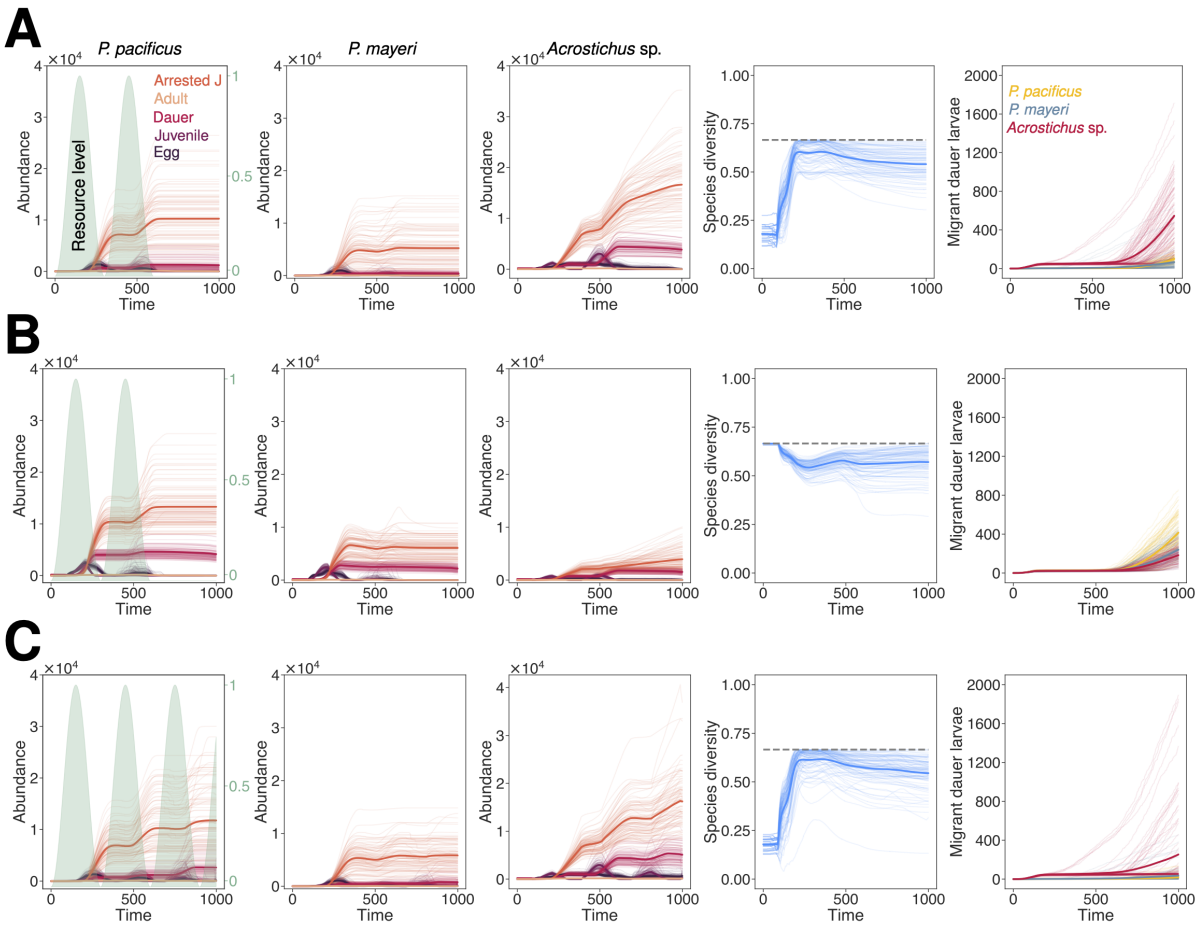

A
B
C
P. pacificus
P. mayeri
Acrostichus sp.
Arrested J
Adult
Dauer
Juvenile
Egg
Resource level
Abundance
Species diversity
Migrant dauer larvae
Time
P. pacificus
P. mayeri
Acrostichus sp.

Figure 4

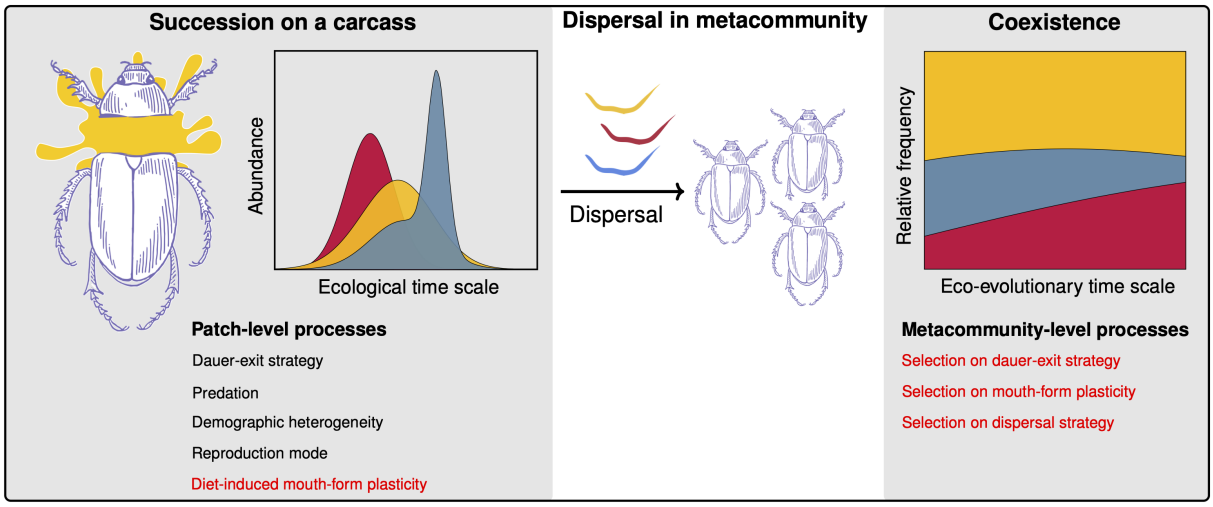

Succession on a carcass
Abundance
Ecological time scale
Patch-level processes
Dauer-exit strategy
Predation
Demographic heterogeneity
Reproduction mode
Diet-induced mouth-form plasticity
Dispersal in metacommunity
Dispersal
Coexistence
Relative frequency
Eco-evolutionary time scale
Metacommunity-level processes
Selection on dauer-exit strategy
Selection on mouth-form plasticity
Selection on dispersal strategy

Figure 5

Supplementary Materials

Materials and Methods

The structure of *Communotron*

Below, we describe our agent-based model using the Overview, Design concepts and Details (ODD) protocol [*1*].

Purpose

Communotron is designed to enable a quasi-realistic simulation of individual worms, as autonomous entities, that follow a life cycle, can interact with other entities in the environment and whose characteristics are influenced by the environment. These entities move on a 2-dimensional grid, a simulacrum of a decaying beetle and its immediate surrounding. Specifically, *Communotron* was designed to enable formation and decline of a community in order to study the boom-and-bust cycle observed in free-living nematodes that are found in association with scarab beetles. The model aims to capture the dynamics of these interactions and their ecological implications, providing insights into the community assembly processes.

Entities, state variables, and scales

In *Communotron*, each worm is simulated as an independent entity which, depending on its developmental stage, can move on a 2-dimensional grid. Each worm has a designated universally unique identifier. The probability of transition from developmental state i to state j is

$$P_{i \to j} = \frac{1}{1 + e^{-k(\tau - \tau_0)}} \quad , \tag{S1}$$

where τ is the current age of the worm and τ_0 is the expected age at which the transition occurs. The temporal unit of the model is hour. During the life-cycle of a worm, alternative developmental stages are reached as a function of the environment. For egg i at (x_i, y_i), normal development results in a juvenile. However, if at (x_i, y_i) the amount of resource available $< R_{\mathrm{lim}}$, egg i develops into an arrested juvenile. For juvenile i at (x_i, y_i), if all the positions within a Moore neighborhood with range $r = 1$ around (x_i, y_i) are occupied, juvenile i develops into a dauer instead of an adult. Both an arrested juvenile and a dauer larvae can re-enter the normal life cycle if resource availability in their location is $\geq R_{\mathrm{lim}}$ and a Moore neighborhood with range $r = 1$ around their current position is not fully occupied (Note: eggs or dead worms are not counted when calculating occupancy in a Moore neighborhood).

Within radius r around the center of the lattice, resource is available at $R_{\max}(t)$, which changes during a simulation following

$$R_{\max}(t) = \frac{1 + \mathrm{Sin}(\omega \Delta t)}{2} \quad , \tag{S2}$$

where t is the current time of simulation, $\Delta t = t - t0$, where $t0$ determines how long from the start of the simulation bacterial growth would start, and $\omega = 2\pi n_{\mathrm{cycle}}$, enabling modification of the number of growth phases of the bacterial resource during the simulation. Parameter n_{cycle} specifies the number of resource availability phases during the simulation.

The resource level at any position outside radius r around the center– reflecting the growth and decline of bacterial load on the decaying carcass at the given point in time and space – follows

$$R_(x_i, y_i) = e^{-\delta(d-r)} \times R_{\max}(t) \quad , \tag{S3}$$

where δ is the decline rate, d is the Euclidean distance between the center and (x_i,y_i), and r is the radius.

The gradient of bacterial resource in the environment affects the movement of worms. Juvenile and adult worms move in a biased random walk in the direction of the gradient. In contrast, dauer larvae move randomly, but biased against the gradient. Table S1 provides a summary of the parameters used in *Communotron*.

Process overview and scheduling

During each step of a simulation, the following steps are taken:

1. Motile stages – juvenile, adult, and dauer – move in a biased random walk on the grid. Predation occurs during this step, where *P. pacificus* adult i can kill juveniles, arrested juveniles, or dauer larvae of the other species with probability ψ. The probability is a function of the age of the predatory adult:

$$\psi(\tau_i) = \eta e^{-\theta \tau_i} \quad , \tag{S4}$$

   resulting in a decline in the ability to engage in surplus killing due to aging.

2. The adults lay their eggs in a Moore neighborhood with range $r = 1$ around their current position. The number of eggs laid per hour is based on the mean number of viable progeny per day for each nematode species. To use these values, the daily mean values are uniformly distributed for each worm over 24 hours.

3. The decision to develop to the next developmental stage is taken by comparing a random number sampled from a uniform distribution with $P_{i \to j}$ (Eq. S1). The alternative developmental paths are taken as specified above. The feeding structures are also updated in cases where an adult is developed from a juvenile or dauer larva.

4. Survival of adults, arrested juveniles, and dauer larvae are calculated based on a sigmoidal transition function identical to Eq. S1.

5. The simulation clock moves an hour forward.

Design concepts

Basic principles: The purpose of *Communotron* was to enable an agent-based framework with quasi-realistic life-cycles, the ability to include experimental data, resource dynamics, and simulation on the scale of hours. Specifically, *Communotron* addresses a number of the limitations of our previous agent-based framework [*2*], namely the absence of resource dynamics and restricted spatial components. Additionally, the emigration of dauer larvae in *Communotron* is tied to the biased random walk of worms in this stage.

Emergence: The probabilistic nature of interactions between the worms compounded by the effect of the explicit spatial aspect of the model results in emergent dynamics that deviate from a deterministic model.

Learning: The model does not include any learning.

Prediction: Communotron is designed to predict how the emergence of nematodes on a decaying beetle, coupled with their feeding structure, their modes of reproduction, and their fecundities, shapes the community composition during the decomposition of the beetle carcass.

Interaction: In *Communotron*, predation of juveniles, arrested juveniles, and dauer larvae of competing species by *P. pacificus* adults is the direct interaction between the agents. By affecting the local densities, species indirectly affect each other by influencing the likelihood of transitioning to alternative developmental stages.

Observation: Each worm in *Communotron* has a designated universally unique identifier, enabling tracking the worms during the simulations. The age, developmental stage, location, migration status of worms are recorded during the simulation, as well as killing events.

Initialization

The parameters used to start a simulation are specified in Table S1. Additional information concerning the initial parameters can be found in figure legends. The initial number of each nematode species is drawn from a Poisson distribution based on the specified expected numbers provided by the user.

Laboratory Assays

Community on a plate

G. buphthalma beetles sampled from Réunion island during a sampling trip in January 2024 were used to construct "community on a plate", where each sacrificed beetle is placed on a nematode growth medium (NGM) plate. Following the outgrowth of bacteria and fungi from the carcass, nematodes in their dauer state emerge from the carcass and develop into adults. The plates were observed in regular intervals for 120 hours following the sacrifice of the beetle in order to record the timing and the identity of the nematodes emerging from the carcass. The nematode species were identified morphologically based on the published descriptions of *P. pacificus*, *P. mayeri*, and *Acrostichus* [*3–5*]. Subsequently, the identity of the nematodes were confirmed genetically using the following 18S primers: SSU988F (5'-CTCAAAGATTAAGCCATGC-3') and SSU2646R (5'-GCTACCTTGTTACGACTTTT-3').

Fecundity

To measure the fecundity of the isolates of *P. pacificus* and *P. mayeri*, both self-fertilizing hermaphrodites, we transferred single worms to fresh plates – seeded with 20 μL *Escherichia coli* OP50 – every 24 hours for 7 days. For each day, viable juveniles observed on plates after 48 hours were recorded. For each isolate of *P. pacificus*, 40 hermaphrodites were transferred daily (120 mothers in total). In the case of *P. mayeri*, 60 hermaphrodites of each strain (180 mothers in total) during a 7 day period. For both species, given the low number of viable progeny in the last three days of the assay, the progeny for days $5-7$ were grouped together. For the gonochorist *Acrostichus* sp. RSO013, a pair of male and female – both at J4 larval stage – were transferred every 24 hours to a freshly-seeded plate with *E. coli* OP50 for 17 days. We transferred 30 pairs daily. During the course of the experiment unhealthy or dead males was replaced. Given the missing information on fecundities on days 14 and 16, we used the mean fecundities of day $i+1$ and day $i-1$ for these two days, where $i \in \{14, 16\}$.

Sex ratio

The sex ratio of *Acrostichus* sp. RSO013 was estimated by counting the number of male and female progenies during the fecundity assay of this isolate.

Feeding structures

Three isolates of *P. pacificus* and three isolates of *P. mayeri* were grown on *E. coli* OP50 under standard laboratory conditions and 750 adult worms from each isolate (4500 worms in total) were examined morphologically – based on the mouth width and the shape of the dorsal tooth.

Statistical analyses

Fecundity parameter

To estimate difference in the total number of progeny between species of *Pristionchus* and *Acrostichus*, we constructed a bayesian model:

$$\begin{aligned} y_i &\sim \text{Poisson}(\lambda_j) \quad , \\ \lambda_j &\sim \text{Gamma}(\alpha, \beta) \quad , \end{aligned} \tag{S5}$$

where y_i is the number of viable progenies of individual i of isolate j. For the gamma prior, $\alpha = 2$ and $\beta = 1$. The model was fitted to the laboratory measurements using PyMC [*6*] to estimate λ for each isolate. We ensured that the estimated λ values were stable using common convergence diagnostics with effective sample sizes $\geq 10,000$ [*7*].

References

1. V. Grimm, *et al.*, *Journal of Artificial Societies and Social Simulation* **23**, 7 (2020).
2. A. Kalirad, R. J. Sommer, *Ecology Letters* **27**, e14370 (2024).
3. R. J. Sommer, L. K. Carta, S.-Y. Kim, P. W. Sternberg, *Fundamental and applied Nematology* **19**, 511 (1996).
4. N. Kanzaki, E. J. Ragsdale, M. Herrmann, V. Susoy, R. J. Sommer, *J Nematol* **45**, 172 (2013).
5. N. Kanzaki, W.-R. Liang, C.-I. Chiu, H.-F. Li, *Zoologischer Anzeiger* **286**, 20 (2020).
6. O. Abril-Pla, *et al.*, *PeerJ Computer Science* **9**, e1516 (2023).
7. J. K. Kruschke, *Nature human behaviour* **5**, 1282 (2021).

Supplementary Tables

Parameter	Description	Value
$m \times m$	Determines the size of the grid	100×100
r	The radius of the resource	20
δ	The decline rate of the resource using in Eq. S3	0.3
k	Determines the shape of Eq. S1	0.1
R_{lim}	The lower limit of resource level used for alternative developmental paths	0.4
η	Predation parameter used in Eq. S4	0.005
θ	Predation parameter used in Eq. S4	0.01
L	Number of steps taken during random walk by each agent at each step	10
τ_0 (Egg)	The parameter used in Eq. S1 to calculate transition probability form egg to juvenile or arrested juvenile	48
τ_0 (Juvenile)	The parameter used in Eq. S1 to calculate transition probability form juvenile or adult or dauer	72★, 96☆, 120†
τ_0 (Dauer)	The parameter used in Eq. S1 to calculate dauer exit into adult	72★, 96☆, 24†
σ_0	The parameter used to calculate survival probability	500 (A), 1000 (D, AJ)

Table S1: **The main parameters used in *Communotron*.** ★: *P. pacificus*; ☆: *P. mayeri*; †: *Acrostichus* sp.; A: adult; D: dauer; AJ: arrested juvenile.

Supplementary Figures

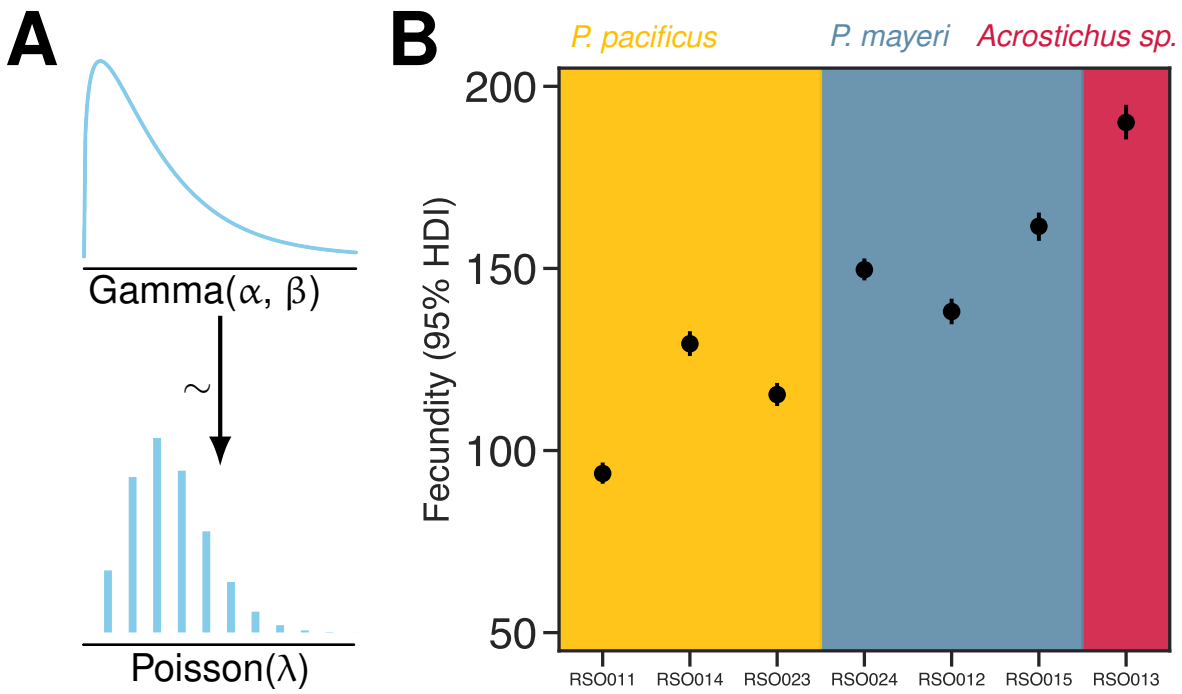


Figure S1: **(A)** A Kruschke-style model diagram, showing the structure of the bayeisan model used to estimate the life-time fecundity of the nematodes based on our experimental measurements. The model assumed that for each isolate, the total number of viable progenies can be explained as a Poisson process with an isolate-specific fecundity parameter (λ). (B) The estimated 95% highest density interval (HDI) for the fecundity of isolates of three nematode species.

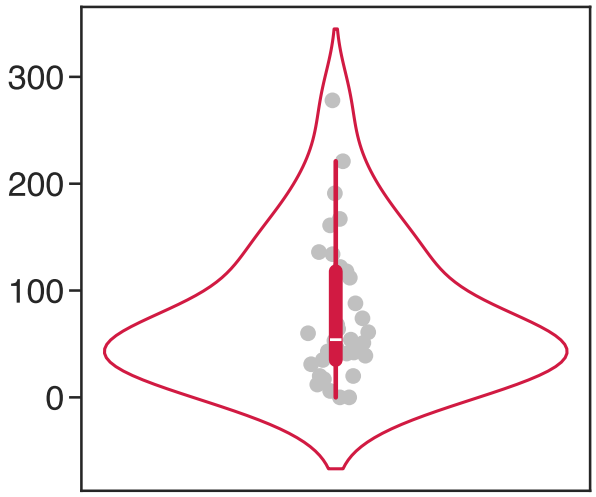


Figure S2: The observed number of nematodes on the beetle carcasses 24 hours following the sacrifice of the beetle. All the nematodes emerged at this point belonged to *Acrostichus* sp.

Evidence of a predator-prey co-evolutionary arms race within a nematode microhabitat

Desiree L. Goetting[1], Kamal Kaur Sarai[1], Penghieng Theam[2], Ralf J. Sommer[2] and James W. Lightfoot[1*]

Affiliations:

1. Max Planck Research Group Genetics of Behavior, Max Planck Institute for Neurobiology of Behavior – caesar, Ludwig-Erhard-Allee 2, 53175 Bonn, Germany.
2. Department for Integrative Evolutionary Biology, Max Planck Institute for Biology Tübingen, Max-Planck-Ring 9, 72076 Tübingen, Germany.

* Corresponding author: james.lightfoot@mpinb.mpg.de

Abstract

Predator-prey interactions are key drivers of behavioural and life-history evolution. Yet, understanding the mechanisms underlying these processes remains challenging due to the inherent complexities of investigating these events within natural ecological contexts. The nematode *Pristionchus pacificus* is a well-established model for studying predatory behaviour, but most experimental work has relied on *Caenorhabditis elegans* as prey, a species that it likely only rarely encounters in nature. Here, we investigate predation in a natural framework by focusing on nematode communities associated with beetles, the native necromenic (carrion-associated) habitat of *P. pacificus*. We identify *Oscheius myriophilus* as a species that cohabits this niche and likely represents a natural prey. Using established predatory assays combined with automated behavioural tracking and machine-learning-based state analysis, we show that *P. pacificus* actively kills and consumes this co-occurring species. Strikingly, predation rates are lower than observed for *C. elegans*, suggesting the evolution of partial resistance or reciprocal adaptation in natural prey. Consistent with this, we uncover distinct life-history strategies in the prey species, including a mixed reproductive mode characterized by early oviposition followed by ovoviviparity and matricide. As later developmental stages of *O. myriophilus* exhibit increased resistance to predatory attack, embryo retention and hatching within the maternal body may protect offspring from predation while allowing them to use maternal resources to develop within a sheltered environment. Thus, our work establishes these nematodes as a tractable model

system for dissecting predator-prey interactions and their evolutionary consequences, offering insight into how behavioural interactions and life-history traits co-evolve in natural communities.

Significance statement

Predator–prey interactions are major drivers of behaviour and life-history evolution, yet studying them in natural contexts is difficult. Here, we establish a natural predator–prey model system using the nematodes *Pristionchus pacificus* and *Oscheius myriophilus*, which co-occur in beetle-associated microhabitats. *P. pacificus* preys on *O. myriophilus* at lower rates than on *Caenorhabditis elegans*, suggesting that natural prey may have evolved resistance through reciprocal adaptation. Strikingly, *O. myriophilus* uses a mixed reproductive strategy: some offspring are laid early and disperse, while others hatch internally and are protected from predation during vulnerable early development. By balancing dispersal and offspring protection, this species hedges against environmental uncertainty. More broadly, this system provides a tractable platform for studying how predation drives co-evolutionary adaptations.

Introduction

Organisms evolve in response to the ecological contexts they inhabit, with interactions between species serving as some of the strongest drivers of adaptation and diversification. Among these, predator-prey dynamics are particularly potent, shaping not only short-term population fluctuations but also long-term evolutionary trajectories. Such interactions can influence a wide range of organismal traits including their life history strategies, behavioural repertoires, morphology, and physiology [1]. Surprisingly, despite their global abundance, ecological diversity, and experimental tractability, nematodes remain an underexplored system for studying predator-prey interactions [2–4]. This is striking given that multiple nematode species often coexist within the same shared habitat and employ diverse social and trophic strategies [5]. These can range from microbial grazing to obligate predation, and can give rise to complex interspecific interactions that are capable of shaping both community structure and broader evolutionary changes.

Of the nematode species capable of predatory feeding, *Pristionchus pacificus* is the most well-characterised [6]. It is an omnivorous species that feeds on bacteria but also acts as a predator of other nematodes [7]. Predation is dependent on teeth-like structures that occur in two different forms within a population. The stenostomatous (St) morph has a narrow mouth with a

single tooth and feeds only on bacteria, while the eurystomatous (Eu) morph has a wider mouth that contains two teeth and is capable of both bacterial feeding as well as predatory behaviours [8]. In the predatory morph, contact with another nematode can trigger an attack. This action can be driven by nutritional demands but may also be an aggressive response to remove potential competitors [9]. The attack decision is modulated by the nematode noradrenergic system that switches the organism's behavioural states between aggressive and docile modalities [10] . Prey contact during aggressive bouts is sensed through both mechanosensory and chemosensory receptors, and results in the puncturing of the outer cuticle layer that is usually fatal for the victim [11,12]. The coordinated actions of the teeth and pharyngeal musculature are required for this activity and this is regulated through the neuromodulator serotonin [13,14] . Moreover, predatory aggression is not indiscriminate as *P. pacificus* has evolved a kin-recognition system that allows close relatives to be identified and kin contact does not result in attacks [15–17]. Importantly, the dissection of the molecular pathways involved in predation has mostly been achieved through investigating interactions between *P. pacificus* isolates with the distantly related model nematode species, *Caenorhabditis elegans,* although these species often do not share the same ecological niche [18] .

While much still remains unknown regarding the ecology of *P. pacificus*, ongoing worldwide sampling efforts continue to identify new *P. pacificus* isolates as well as uncover previously unknown *Pristionchus* species [19–21]. As such, more of the complex ecology of these organisms is being revealed. *Pristionchus* species are reliably found in close association with scarab beetles with which they share a necromenic association [22–24]. This is a specific lifestyle whereby these nematodes reside on a beetle host as non-feeding, stress-resistant individuals called dauer larvae, the evolutionarily conserved dispersal stage of free-living nematodes [23]. Many of these nematodes stay associated with their beetle host until insect death occurs via natural causes. This event results in the establishment of a stable microbiome on the decaying beetle carcass and *Pristionchus* species exploit this habitat in order to develop and propagate [25]. Within this ecosystem, they display a biphasic boom-and-bust growth and dispersal strategy that, alongside a robust ability to sense insect pheromones, likely facilitates their capacity to locate and colonise new hosts [26–28]. Moreover, beetle hosts harbour not only *Pristionchus* but also other nematode species and additionally, other soil-dwelling nematodes are likely attracted to the microbial bloom on the decaying insect carcass [29,30] . Therefore, the resultant microhabitat is a species-rich environment consisting of many bacterial, fungal, and

nematode species interacting and competing [25]. Importantly, most wild *P. pacificus* isolates exhibit the predatory Eu mouth form [8], and this morphology can be rapidly induced by specific environmental cues [31–34]. These features suggest that predatory aggression likely forms a central component of their behavioural interactions on the beetle carcass, although kin-recognition mechanisms ensure that such aggression is directed toward non-relatives and other species within this ecological niche [15–17].

Here, we characterize a predator–prey system among beetle-associated nematodes that share an intricate microhabitat. By dissecting their ecological interactions and their life-history traits, we outline the selective forces shaping their coexistence. Strikingly, our investigations into the natural prey of *P. pacificus* reveal unexpected adaptations that bear the hallmarks of an evolutionary arms race. Thus, we offer new insight into how complex nematode communities persist and diversify.

Results

Identification and isolation of nematode predator-prey systems

To better understand the behavioural interactions between *P. pacificus* and its natural prey species, we set out to identify and isolate nematodes that naturally co-occur with these facultative predators. Given that *P. pacificus* is reliably, although not exclusively, found on beetle hosts [35], we conducted field experiments on La Réunion Island to capture beetles of the family Scarabaeidae that may harbour *P. pacificus* nematodes and their prey (**Fig. 1A**). On La Réunion Island, beetles have been previously demonstrated to have a *P. pacificus* infestation rate of over 90% [36]. At the Parc du Colorado sampling site on La Réunion Island (covering area around latitude: 20°54'43.6"S, longitude: 55°25'12.4"E), we captured numerous beetles belonging to the genus *Adoretus* that were infested with several nematode species (**Fig. 1A, B; Supp Table 1**). Initial morphological analysis indicated these nematode species primarily belonged to the family Rhabditidae due to the presence of a pharyngeal grinder, and the family Diplogastridae, identified by their characteristic pharyngeal shape and structure [37] . We focused on five *Adoretus* isolates that each harboured both a single diplogastrid and a single rhabditid specimen. As these are not gonochoristic species, we used the individual nematodes to initiate an isogenic master culture of each that was then maintained as an independent line and frozen stock (**Fig. 1B**). To precisely determine the species composition harboured on these five beetles, we

performed molecular genotyping using whole genome sequencing and universal nematode molecular markers and also constructed phylogenetic trees based on these results. All diplogastrid isolates were *P. pacificus* and belong to clade C1 with other *P. pacificus* specimens isolated from La Réunion Island [38] (**Supp Fig. 1**). Alongside these, the rhabditids were all identified as specimens of *Oscheius myriophilus* based on the near full-length small subunit (SSU) and the D2-D3 region of large subunit (LSU) sequences [39] (**Fig. 1C**). The monophyletic genus *Oscheius* comprises two groups (clades), *Insectivorus*- and *Dolichura*-groups [40] , and consists of many free-living members including the well-established satellite model species *Oscheius tipulae* [41–44]. Members of this genus, including *O. myriophilus*, are frequently associated with insects, and this species has previously been recovered from a broad range of insect hosts. [39,45,46]. Thus, from five *Adoretus* beetle hosts we identified distinct *P. pacificus* isolates, each co-occurring with an associated *O. myriophilus* strain. Together, these represent ecologically relevant species pairs with which to explore their interactions and traits.

P. pacificus **are predators of** ***O. myriophilus***

Having established the ecological association between these nematodes, we next examined whether these pairs constitute bona fide predator–prey relationships. We first assessed the mouth morphology ratios in these newly acquired wild *P. pacificus* strains to determine their predatory capability. In *P. pacificus*, only the Eu morph exhibits aggressive predatory behaviour and this behaviour is entirely absent in the St morph (**Fig. 2A, B**) [7]. As most wild isolates characterised to date show a strong bias toward the Eu fate [8], we assessed all five of our beetle-associated *P. pacificus* strains for the presence of the Eu mouth type. In all strains we identified a similar Eu bias indicating a natural predisposition towards the predatory-capable morphotype in these isolates (**Fig. 2C**). This is consistent with previous findings in other wild *P. pacificus* lineages [8].

With the predominance of the predatory morph confirmed under laboratory conditions, we next investigated predatory interactions between *P. pacificus* and their co-occurring *O. myriophilus* isolate. Additionally, we also compared these to predatory interactions with *C. elegans*, as well as their own kin. We conducted predatory "corpse assays" whereby we placed several *P. pacificus* predators on an assay plate with an abundance of the selected larval prey. After two hours, the number of corpses generated by predatory events are counted indicating the amount of predatory activity [7,47]. We found that all of the wild *P. pacificus* isolates do indeed

predate upon their naturally co-occurring *O. myriophilus* isolate, confirming the occurrence of a predator-prey dynamic between the species. Interestingly, we noted that for the majority of the *P. pacificus* isolates, there tended to be lower levels of predation observed on *O. myriophilus* than on *C. elegans* prey. As expected, all *P. pacificus* isolates robustly avoid killing their own offspring, consistent with the existence of a kin-recognition system in this species (**Fig. 2D-H**) [16,17]. These patterns of predation are reinforced when all the data are pooled to look for species-level trends (**Fig. 2I**).

To investigate the predatory interactions further, we exploited a recently developed automated behavioural tracking and machine learning model to identify behavioural states associated with feeding and predatory activity [10,48]. These methods depend on tracking the activity of the pharynx, a neuromuscular pump required for feeding. This is achieved using an integrated *myo-2p*::RFP fluorescent marker [49]. Using this approach, we previously detected six distinct behavioural states that together capture the *P. pacificus* behavioural repertoire. Three of these correspond to behaviours known from *C. elegans* including a "dwelling" state and two distinct forms of "roaming" [50], whereas the remaining three are associated with predatory contexts and comprise "predatory search", "predatory biting", and "predatory feeding" (**Fig. 3A**). Velocity and pharyngeal pumping rate are the strongest indicators distinguishing predatory from non-predatory behaviours, with biting and feeding both occurring when movement nearly ceases. Visualising the joint distribution of these two features reveals the relative abundance of predatory vs. exploratory-focused behaviours (**Fig. 3A**). Furthermore, by applying a machine-learning model previously trained on behavioural data using a combination of unsupervised and supervised learning, we can estimate state occupancy while animals are exposed to potential prey (**Fig. 3A**). To apply these methods to our ecologically relevant predator-prey system we crossed the *myo-2p*::RFP fluorescent indicator into the *P. pacificus* RSO005 line and backcrossed this 6 times with the RSO005 wild type to generate a near-isogenic line (NIL). Accordingly, this strain contained mostly RSO005 DNA as well as the *myo-2p*::RFP marker facilitating the tracking of predatory activity. We tracked the interactions of the *P. pacificus* RSO005 NIL with its kin, *C. elegans*, and the *O. myriophilus* strain, RSO006, that was found co-infesting the same beetle host. As expected, behavioural states associated with predatory aggression were absent on kin, again confirming robust kin recognition in these recently collected wild isolates. However, behavioural states associated with predation were observed on both *C. elegans* and the co-occurring *O. myriophilus.* Intriguingly, we found that the level of predatory biting is significantly

greater when predators were exposed to *C. elegans* prey compared to *O. myriophilus* prey, but that this increase in biting occured without a concomitant increase in predatory feeding (**Fig. 3B, C**). This, taken together with an increased tendency to transition into predatory states when exposed to *C. elegans* prey (**Fig 3D)**, may be suggestive of lower levels of aggression toward familiar species with which *P. pacificus* frequently cohabitates. Thus, *P. pacificus* successfully identifies both *C. elegans* and *O. myriophilus* as prey but seems to engage in predatory aggression more frequently toward *C. elegans* than the naturally co-occurring *O. myriophilus* specimens.

Distinct life history traits are evident in co-occurring predator-prey species

After verifying the ecological and behavioural association between these nematodes, we next examined their life-history traits for evidence of any potential adaptations linked to their respective trophic strategies and reciprocal interactions. These traits included their development, fertility, and longevity.

To assess the development and longevity of our co-occurring predator-prey species, we followed individual animals from young adults (one day post J4) until their death. The lifespan of *P. pacificus* varied between isolates with the shortest lifespan of 12.6 ± 2.9 days observed in RSO009 and the longest lifespan of 33.0 ± 8.8 days observed in RSO005 (mean ± SD) (**Fig. 4A-E, S2A**). The mean lifespan of all the wild isolates combined was 23.0 ± 10.7 days (**Fig 4K),** slightly shorter than previous reports investigating *P. pacificus* longevity [51]. We noted that there was less variability in longevity among the *O. myriophilus* isolates, which had lifespans ranging from 7.8 ± 3.0 days in RSO006 to 9.8 ± 3.4 days in RSO004 **(Fig 4F-J, S2A).** Strikingly, the combined mean lifespan of all the *O. myriophilus* isolates, at 8.7 ± 4.3 days, was significantly shortened compared to that of *P. pacificus* (**Fig. 4K)**. While the majority of *P. pacificus* individuals produced offspring through oviposition, in all the *O. myriophilus* specimens we instead observed a mixed reproductive mode. This began with the oviposition of a few eggs followed by consistent ovoviviparous reproduction and death of the hermaphrodite soon after (**Fig. 4L-M, S2B, Supp video 1)**, suggesting an evolved retention of embryos that is correlated with a shortened lifespan resulting from matricide (**Fig. 4F-J**). Furthermore, embryo retention and matricide were also observed when *O. myriophilus* isolates were grown on native beetle-associated bacteria [52–54], demonstrating that this phenotype is not specific to standard laboratory culture conditions. (**supp fig 3**). To investigate the origins of the mixed reproductive

mode further, we also assessed two more strains of *O. myriophilus*, EM435 and DF5020, which were deposited at the *Caenorhabditis* Genetics Center (CGC). *O. myriophilus* EM435 was isolated from a compost pile in Brooklyn, New York and *O. myriophilus* DF5020 was isolated from the millipede *Oxidus gracilis* in Azusa, California [39]. In both strains, we again observed ovoviviparous reproduction, although this phenotype was not fully penetrant in strain EM435 (**Supp Fig. 4**). Notably, many EM435 individuals were sterile and alongside this they exhibited extended lifespans, further supporting a link between ovoviviparity and matricide in this species. Together, these findings suggest that natural variation of this reproductive mechanism exists within the species. Importantly, this reproductive strategy resulted in many *O. myriophilus* larvae breaking free of their mother's carcass at a much later developmental stage in all strains examined, sometimes even as fertile adults (**Fig 4M, Supp Video 2**).

Given the consistent mixed reproductive mode and matricide observed in *O. myriophilus*, we next assessed the fertility of both *P. pacificus* and their co-occurring *O. myriophilus* by quantifying the number of live offspring produced. In two predator-prey pairs, *P. pacificus* had significantly more progeny than their cohabiting *O. myriophilus,* while the remaining three pairs had similar progeny numbers across both species (**Fig S2C**). In addition, we found a large variation of within species fertility with *P. pacificus* RSO005 averaging the most offspring (127.7 ± 18.9 larvae) compared to RSO009 with the least (28.6 ± 20.8 larvae) (mean ± SD). A similar phenomenon was observed within *O. myriophilus* with the greatest difference observed between RSO004 and RSO010 strains (92.1 ± 45.8 and 31.46 ± 11.8 larvae, respectively). When the data from the isolates are combined to look for species-level trends, we find that *P. pacificus* has significantly more offspring than *O. myriophilus* (**Fig 4N**). Taken together, we speculate that the higher numbers of progeny and lengthened lifespan of *P. pacificus* may contribute to an ecological advantage within the beetle carcass environment.

As the observed ovoviviparous reproduction resulted in some progeny reaching later developmental stages before breaking free of their mother's cuticle, effectively delaying exposure to the predatory environment, we lastly assessed the impact of this for avoiding fatal predatory interactions. We directly observed the effectiveness of *P. pacificus* predatory bites on distinct *O. myriophilus* developmental stages by comparing bite effectiveness on early-stage larvae (J1 or J2) to bite effectiveness on the last larval stage (J4) or young adults. We found *P. pacificus* bites were much less effective against later developmental stages of *O. myriophilus,* with bites on J1 or J2 larvae resulting in a kill 69% of the time, whereas only 4% of bites on J4

or adults were fatal (**Fig. 4O**). Thus, we hypothesize that the thicker cuticle of the later developmental stages of *O. myriophilus* likely offers a significant challenge for the *P. pacificus* predators to penetrate, and greatly enhances their chance of surviving a predatory attack.

Discussion

P. pacificus represents the best-characterised predatory nematode species, yet interactions with its natural prey have remained largely unexplored. Such antagonistic interactions exert strong reciprocal selection, potentially generating an evolutionary arms race that influences both behavioural and developmental traits. Here, we identify *O. myriophilus* as a natural prey for *P. pacificus* and establish this species pairing as a tractable system to study ecologically significant predator-prey dynamics.

Using our well-established corpse assays to explore predation behaviour between co-occurring *P. pacificus* and *O. myriophilus,* we observed evidence of abundant predator-prey interactions. Unexpectedly, we found *P. pacificus* is less aggressive and predatory towards its natural co-occurring prey species, *O. myriophilus,* than it is towards *C. elegans*, which it likely encounters far less often. It has previously been shown that different nematode species acquire distinct surface properties, which likely reflect species-specific ecological pressures and environmental adaptations [55–57] . Therefore, the surface of *O. myriophilus* may have acquired specific adaptations that help to mask it from the predatory *P. pacificus*. These surface modifications may represent an evolutionary countermeasure to the aggression of *P. pacificus* and would likely require continual refinement to maintain their effectiveness.

In addition to reduced predation, all *O. myriophilus* isolates exhibited a specific reproductive strategy characterized by early oviposition followed by ovoviviparity and death soon after. In *C. elegans,* reproduction occurs via egg laying, and matricidal hatching, or bagging, is a rare event mostly observed in response to adverse environmental conditions including starvation [58], aging [59] or exposure to pathogenic bacteria [60]. These conditions are thought to cause alterations or defects in the mechanisms that modulate the egg-laying machinery itself [59]. Similarly, in *O. tipulae*, the model species of the genus *Oscheius*, matricidal hatching is a rare event [41]. However, in many nematode species ovoviviparity and matricide is a well-documented reproductive strategy. This includes entomopathogenic species such as those belonging to the families Steinernematidae and Heterorhabditidae [61]. In these species, matricide is thought to facilitate transmission of their insect-pathogenic bacterial

symbionts and is essential for their specific life cycle [61,62]. In *O. myriophilus*, internally hatched progeny are sheltered from environmental hazards and potential predation during their early development. This corresponds to when their cuticle is relatively thin and has not yet developed the thicker, more protective properties characteristic of later stages [63]. Importantly, given the penetrance and ubiquity of this phenotype in the *O. myriophilus* isolates described in this study, we hypothesize ovoviviparity and matricide is likely the primary mechanism of reproduction and represents an evolved strategy to maximize offspring survival.

Intriguingly, an early period of oviposition at the onset of fertility is retained by *O. myriophilus*. As a result, early progeny hatch directly into the environment while later progeny are more likely to hatch and develop within the mother. We posit that this reproductive strategy, and its inherent trade-off with the parent's longevity, likely represents a bet-hedging strategy resulting in dual offspring phenotypes that maximize fitness across unpredictable environments [64,65]. Here, externally hatched larvae, though vulnerable to predation, could enter dauer diapause or disperse to locate new hosts and environments [27]. Conversely, internally hatched progeny are sheltered from environmental hazards and predation. By partitioning offspring between dispersal and protection strategies, *O. myriophilus* hedges against the inherent temporal variations caused by the boom-and-bust resource availability observed on its beetle carcass habitat [28], as well as spatial heterogeneity linked to predator presence. Thus, this reproductive bet-hedging strategy maximises the possibility that at least some offspring survive regardless of external conditions.

The potential evolutionary arms race we have uncovered between *P. pacificus* and *O. myriophilus* reflects a phenomenon observed across diverse predator-prey systems. For example, aphids and their ladybird (lady bug) predators engage in a chemical arms race whereby the aphid alarm pheromone acts as both a prey defense signal as well as a predator foraging cue with both species adapting to exploit this information [66]. Similarly, rough-skinned newts produce the potent neurotoxin, tetrodotoxin (TTX), that binds to voltage-gated sodium channels in nerves and muscles and blocks action potential propagation. To counteract this, the newt's natural predator, the garter snake, has evolved TTX-resistant sodium channels, resulting in escalating toxicity in prey and resistance in predators [67–69]. Finally, bats have evolved echolocation to hunt flying insects at night, while their moth prey have evolved sensitive ultrasonic hearing, evasive flight behaviors, and in the case of tiger moths, ultrasonic clicks that can interfere with bat abilities [70,71]. Within the confined microhabitat of an insect cadaver, *P. pacificus* and *O. myriophilus*

compete directly for limited resources, creating strong selective pressure for improved predatory efficiency in *P. pacificus* and the evolution of defensive counterstrategies in *O. myriophilus*. Crucially, unlike the systems described above, this nematode species pair offers exceptional genetic and experimental tractability, enabling direct dissection of the molecular and developmental mechanisms that drive predator-prey conflict and evolutionary arms races.

Figure Legends

Figure 1. *Pristionchus pacificus* and *Oscheius myriophilus* consistently cohabitate on *Adoretus* beetles

(A) Map of La Réunion Island showing the approximate location of the Parc du Colorado sampling site where beetles from the genus *Adoretus* were collected. (B) Corresponding *P. pacificus* and *O. myriophilus* isolates collected from each *Adoretus* beetle, along with representative images of each species. Scale bars indicate 100 μm. (C) Maximum likelihood tree showing relatedness among the wild *O. myriophilus* isolates collected in this study to the previous *O. myriophilus* strains EM435 and DF5020, as well as other nematodes within the family Rhabditidae, and *P. pacificus* within the family Diplogastridae. Scale bar indicates 0.1 nucleotide substitutions per site.

Figure 2. Naturally co-occurring *P. pacificus* and *O. myriophilus* demonstrate a predator-prey dynamic

(A) Representative image of an animal with the predatory eurystomatous mouth form. Scale bar indicates 5μm. (B) Representative image of the nonpredatory stenostomatous mouth form. Scale bar indicates 5μm. (C) Percent occurrence of the eurystomatous and stenostomatous mouth forms in the wild *P. pacificus* isolates collected in this study. N = a minimum of 99 animals per isolate (D-H) Number of corpses present after five *P. pacificus* adult predators are exposed to larval prey that is either self-progeny, *C. elegans,* or the naturally co-occurring *O. myriophilus* isolate for two hours. (I) Combined data from D-H depicting species-level trend of decreased predation on *O. myriophilus* compared to *C. elegans* prey. (D-I) Data points are individual trials with mean and ± SEM shown. * $p<0.05$, ** $p<0.01$, *** $p< 0.001$, **** $p<0.0001$, Kruskal-Wallis followed by Dunn's test with Bonferroni correction.

Figure 3. *P. pacificus* demonstrates higher levels of aggression towards *C. elegans* than its cohabitating species, *O. myriophilus*

(A) Schematic depicting workflow for data analysis with custom Python packages, PharaGlow and PpaPred. PharaGlow is used to analyse high throughput tracking data of fluorescently-tagged predators, extracting over 30 behavioural features, which are utilized by PpaPred to perform behavioural state predictions. (B) Probability density plots of pumping rate and velocity for RSO005 NIL predators demonstrating that exploratory behavioural clusters predominate when predators are exposed to kin, and predatory behavioural clusters emerge when exposed to interspecific prey. (C) Mean fraction of time RSO005 NIL predators spend in each behavioural state when exposed to either conspecific, *C. elegans,* or *O. myriophilus* prey. RSO005 NIL predators spend significantly more time in predatory biting, but not feeding, on *C. elegans* prey than on the co-occurring *O. myriophilus* strain isolated from the same beetle. Box plots shown with the first to third quartiles indicated by the box, the median by the center line, and 1.5x interquartile range by the whiskers. ns = not significant, ** $p < 0.01$, *** $p < 0.001$, **** $p < 0.0001$, Mann–Whitney *U* test with Bonferroni correction for multiple comparisons. (D) Average transition rates between behavioural states for RSO005 NIL predators exposed to different types of larval prey. Numbers in circles indicate mean state duration as in (C) and arrow size indicates the transition rate normalized to outgoing transitions from each respective state. Arrows indicating transitions < 20% are transparent to aid in clarity.

Figure 4. Ovoviviparity is a fixed trait in *O. myriophilus* isolates

(A-J) Adult lifespan plotted against the onset of hatching of internal progeny for *P. pacificus* isolates (A-E), and *O. myriophilus* isolates (F-J). Death typically occurs within days after the onset of ovoviviparity in *O. myriophilus.* Day 0 is when animals are picked as early J4 larvae. N = a minimum of 10 animals per isolate (K) Combined data from all wild isolates showing that *P. pacificus* has a significantly extended lifespan compared to *O. myriophilus.* Data points indicate the lifespan of one individual animal. (L) Nearly 100% of *O. myriophilus* individuals show internal hatching of progeny. Data points indicate the mean number of animals showing ovoviviparity per isolate with mean and ± SEM shown. (M) Representative images of internally hatched progeny at various developmental stages in *O. myriophilus,* spanning from early-stage larvae (top) to gravid adults (bottom). Scale bars indicate 100 μm. (N) Combined data from all isolates demonstrating that *P. pacificus* has significantly more offspring than *O. myriophilus.*

Data points indicate the number of progeny from one individual animal. (O) Percent of *O. myriophilus* (RSO006) individuals, either early-stage larvae (J1 or J2) or animals J4 or older, that survived following a bite from an adult *P. pacificus* (RSO005) predator. Older animals are significantly more likely to survive a predatory attack. N = 100 worms per age group (K-L, N-O) ** p <0.01, **** p<0.0001, Mann–Whitney *U* test (K-L, N), or Fisher's exact (O) test. (K, N) Box plots shown with the first to third quartiles indicated by the box, the median by the center line, and min to max by the whiskers.

Supplemental Figure 1. Newly isolated *P. pacificus* strains belong to Clade C1

Neighbour-joining tree generated by whole genome sequencing showing the alignment of the *P. pacificus* isolates collected in this study (indicated by red diamonds) with other *P. pacificus* strains collected worldwide. Letters and numbers around the edge of the phylogeny indicate *P. pacificus* clades following Rödelsperger et al [38]. Scale bar indicates 0.01 nucleotide substitutions per site.

Supplemental Figure 2. Lifespan, reproductive mode, and fertility vary between individual isolates

(A) *P. pacificus* has a longer lifespan than *O. myriophilus* in three out of five cohabitating strain pairs. Data points indicate the lifespan of one individual animal with mean and ± SEM shown. (B) Ovoviviparity consistently occurs in each of the *O. myriophilus* isolates but is rare for *P. pacificus* isolates. (C) *P. pacificus* has higher levels of fertility than *O. myriophilus* in two out of five cohabitating strain pairs. Data points indicate the number of offspring from one individual with mean and ± SEM shown. (A, C) ns = not significant, ** p < 0.01, *** p < 0.001, **** p < 0.0001, Kruskal-Wallis followed by Dunn's test with Bonferroni correction.

Supplemental Figure 3. *O. myriophilus* is ovoviviparous when grown on beetle-associated bacteria

Representative images of dead *O. myriophilus* (RSO006) adults with internally hatched progeny (white arrows) when grown on a selection of beetle-associated bacterial species, including (A) *Pseudomonas fluorescens* (LRB26), (B) *Kurthia gibsonii* (LRB56), (C) *Comamonas thiooxydan* (LRB28), and (D) *Providencia rettgeri* (LRB44). Scale bars indicate 200 μm.

Supplemental Figure 4. Reference *O. myriophilus* strains also show ovoviviparity

(A-B) Adult lifespan plotted against the onset of hatching of internal progeny for *O. myriophilus* reference strains, EM435 (A), and DF5020 (B). Day 0 is when animals were picked as early J4 larvae. N = a minimum of 11 animals per isolate (C) Lifespan of *O. myriophilus* reference strains. Data points indicate the lifespan of one individual animal with mean and ± SEM shown. (D) Ovoviviparity occurs at varying frequencies in the two *O. myriophilus* reference strains. (E) Fertility of EM435 and DF5020. Data points indicate the number of offspring from a single animal with mean and ± SEM shown.

Movie S1. Ovoviviparity and matricide is the primary mechanism of reproduction of in *O. myriophilus*.

Movie S2. *O. myriophilus* can complete their development within the corpse of the mother.

Materials and Methods

Specimen collection

Live beetle specimens belonging to the genus *Adoretus* (Dejean, 1833) were collected by hand from Parc du Colorado, La Réunion (covering area around latitude: 20°54'43.6"S, longitude: 55°25'12.4"E) (Fig. 1A, B). They were later sacrificed on nematode growth medium (NGM) plates seeded with *Escherichia coli* OP50 at the Max Planck Institute for Biology Tübingen. A mixture of *E. coli* and native beetle carcass microbes served as a food signal for nematode dauer emergence [24].

General body and pharyngeal morphology was used to identify the emerging *P. pacificus* and *Oscheius* nematodes [36,37] followed by molecular identification (see below). Each isogenic nematode strain was established from a single gravid hermaphrodite, and frozen for long-term storage as soon as possible to avoid domestication.

Nematode husbandry

All nematodes were maintained on standard NGM plates on a diet of *E. coli* OP50.

Strains

Strain	Description	Origin
RSO001	Pristionchus pacificus	This study
RSO003	*Pristionchus pacificus*	This study
RSO005	*Pristionchus pacificus*	This study
RSO007	*Pristionchus pacificus*	This study
RSO009	*Pristionchus pacificus*	This study
RSO002	*Oscheius myriophilus*	This study
RSO004	*Oscheius myriophilus*	This study
RSO006	*Oscheius myriophilus*	This study
RSO008	*Oscheius myriophilus*	This study
RSO0010	*Oscheius myriophilus*	This study
N2	*C. elegans* wild type	CGC
JWL27	*Pristionchus pacificus, bnnls1 [myo-2p::RFP;egl20p::GFP]*	Eren & Böger et al., 2026
JWL296	*Pristionchus pacificus, RSO005 Near-isogenic line (back crossed six times) bnnls1 [myo-2p::RFP;egl20p::GFP]*	This study
DF5020	*Oscheius myriophilus*	CGC
EM435	*Oscheius myriophilus*	CGC

O. myriophilus molecular identification and phylogenetic reconstruction

Two rDNA regions of *Oscheius* natural isolates originating from La Réunion Island and the isolates deposited at the *Caenorhabditis* Genetics Center (CGC) were sequenced including the near full-length small subunit (SSU) and the D2-D3 region of large subunit (LSU). The primer pairs used were SSU988F (5'-CTCAAAGATTAAGCCATGC-3') and SSU2646R (5'-GCTACCTTGTTACGACTTTT-3') and D2A (5'-ACAAGTACCGTGAGGGAAAGT-3') and D3B (5'-TCGGAAGGAACCAGCTACTA-3') for the SSU and LSU regions, respectively [72] . The sequences were used for BLASTN search in the NCBI database with *O. myriophilus* being the top hits (>99% identical).

To reconstruct the *O. myriophilus* phylogenetic relationships, the SSU and D2-D3 region of LSU sequences of *Oscheius*, *Caenorhabditis*, *Pristionchus*, *Parapristionchus* and *Bunonema* genera available on the NCBI database were concatenated and aligned using the MUSCLE program (version 3.8.31) (Table S2) [73] . The resultant multiple sequence alignment was then used to reconstruct a maximum likelihood tree using the phangorn package in R (version 4.3.1; model = "GTR+G(4)", optNni = TRUE) [74] . The best tree model was determined using the pml_bb function. *Bunonema* sp. was used for tree rooting. 100 bootstrap replicates were set for this rooted tree and nodes with the support values more than 50 were visualized on the generated tree (Figure 1C).

P. pacificus whole genome sequencing and phylogenetic reconstruction

Genomic DNA of *P. pacificus* natural isolates co-existing with *O. myriophilus* was extracted using the Monarch® Genomic DNA Purification Kit. The whole genome sequencing (WGS) was done by Novogene. The phylogenetic reconstruction was carried out following the protocol in Rödelsperger *et al.* [38] . Briefly, the new WGS data were aligned against the reference *P. pacificus* PS312 genome (version El Paco 3) with the software BWA (version 0.7.17-r1188, with option mem) [75] . The resulting alignments were then genotyped by the SAMtools mpileup (version 0.1.18 r982:295) and BCFtools (version 0.1.17-dec r973:277) at a set of candidate positions that were shown to be variable across different *P. pacificus* natural isolates Rödelsperger, C. *et al.* [20,38,76,77]. Variable positions that could be genotyped in all strains with a minimum quality score of 20 were concatenated into an artificial multiple sequence alignment. This variant information was used to calculate a neighbour-joining tree based on Hamming distances between strains with the phangorn package in R (version 4.3.1) (Fig. S1) [74] .

La Réunion Map

The La Réunion Island map was generated using the software GeoMapApp [78] .

Mouthform assays

Mouthform analysis of *P. pacificus* isolates was performed by picking worms into 20mM sodium azide mixed with M9 on a 24 x 24 mm glass slide. Sodium azide was used to immobilize worms. Following the addition of a cover glass, the mouth form of each animal was examined at 60x/oil immersion on an inverted microscope (Zeiss Axiovert 200). Animals were characterized as stenostomatous or eurystomatous based on their mouth width and the presence of either one or two teeth (Figure 2A, B). Two replicates, containing approximately 50 worms each, were performed on separate days for every isolate.

Lifespan and fertility assays

Lifespan and fertility were assessed in tandem. On day 0, early J4 hermaphrodites were selected based on their vulval morphology and picked onto individual NGM 6 cm plates seeded with OP50. The following day was counted as day one of adulthood, and every day or every other day

thereafter, hermaphrodites were transferred to fresh plates while still fertile to separate the parent from progeny. Before transferring, hermaphrodites were examined for internal hatching of progeny and, if present, the initial date of occurrence was recorded. Eggs on progeny plates were allowed to hatch and then the number of live offspring were quantified. Each parent was then followed until the date of their death was determined.

Predatory corpse assay

Corpse assays were performed as in Wilecki et al [7] . Briefly, large quantities of prey were cultivated, and freshly starved plates containing primarily adults and freshly hatched larvae were gently rinsed with M9. The solution was then filtered through two 20 μm filters to separate adults from larvae. The adults were discarded and the solution containing the larvae was spun at 2000 rpm for one minute. The supernatant was discarded and two more wash and spin cycles were performed with M9. Subsequently, 2 μl of the larval prey pellet was then pipetted to an unseeded 6 cm NGM plate and animals were allowed to disperse for approximately two hours. For *P. pacificus* or *C. elegans* prey, pipetting a single volume of prey to the center of the plate is sufficient to allow for adequate dispersal. However, we noted that *O. myriophilus* prey does not disperse as readily. Thus, *O. myriophilus* prey were pipetted to two offset regions of the plate to aid in dispersal. Young adult predators were picked and left off food for one hour prior to the assay to remove residual bacteria. Finally, five adult predators were placed on each prey-saturated plate for a period of two hours, after which, the predators were removed and the number of corpses were counted manually using a stereo microscope (Zeiss Stemi 508).

Automated behavioural tracking and machine learning

To generate transgenic animals, RSO005 hermaphrodites were crossed with JWL27 males containing an integrated *myo-2p*::RFP transgene on the X chromosome that expresses RFP in pharyngeal muscle. Progeny were then back crossed six times to RSO005 to create a near-isogenic line (NIL) with a fluorescently labelled pharynx that can be used for tracking predatory activity. Tracking and behavioural state prediction were then performed on the RSO005 NIL as described in [10] . Briefly, plates were prepared as for corpse assays with 4 μl of the larval prey. Predators were picked and left off of food for two hours prior to the start of the assay. After this period of food restriction, approximately 40 predators were placed inside a copper arena on the plate with prey to help retain the predators within the field of recording. After a ten-minute

acclimation period, animals were recorded at 30 fps for ten minutes with a Basler camera (acA3088-57μm) on an epi-fluorescence microscope (Zeiss Axio Zoom V16). Recordings were then analysed with the custom Python analysis package, PharaGlow, which extracts/calculates a number of behavioural features, such as pumping and velocity [10,48] . Finally, the features extracted with PharaGlow were utilized by a second custom Python analysis package, PpaPred, to perform behavioural state predictions.

Killing efficiency assay

To assess the effectiveness of *P. pacificus* predatory bites on *O. myriophilus* we selected a predator-prey pairing of these species (*P. pacificus* strain RSO005 and *O. myriophilus* strain RSO006). Subsequently, we isolated two different developmental stages of *O. myriophilus* to be used as prey, J1/J2 larvae and J4/young adult animals. For *O. myriophilus* J1/J2 early- stage larvae, we collected larvae from 5 plates depleted of OP50 food by washing with M9 and passing the larval wash through two 20 μm filters to remove older developmental stages. A larval pellet was formed by centrifugation (2000 rpm, 1 min) and 1 μl of larval pellet was pipetted onto a 6 cm unseeded plate. The larvae were left to disperse for 2 hours and then >10 young adult *P. pacificus* predators placed onto the *O. myriophilus* larval plate. Individual *P. pacificus* predators were observed using a Zeiss Stemi 508 and the number of 'bites' and 'kills' assessed. Interactions were scored as 'bites' if the predator successful grasped the larval prey. 'Kills' were scored if a bite resulted in the penetration of the cuticle and subsequent death of the larvae. To assess *P. pacificus* predator killing efficiency against *O. myriophilus* J4/young adults, we picked ~300 *O. myriophilus* J4/young adults to a 6 cm unseeded plate. The J4/young adult stage was determined by the presence of the classic vulva morphology during this developmental period. >10 young adult *P. pacificus* predators were subsequently placed onto the *O. myriophilus* J4/young adult plate and the number of 'bites' and 'kills' assessed as described above.

O. myriophilus matricide on natural beetle associated bacteria

The influence of bacterial diet on *O. myriophilus* matricide was assessed by growing *O. myriophilus* on four bacterial species that have previously been found naturally co-occurring on the beetle carcass [52] . These were *Pseudomonas fluorescens* (LRB26), *Kurthia gibsonii* (LRB56), *Comamonas thiooxydan* (LRB28), and *Providencia rettgeri* (LRB44) [54] . A starter culture of each of these bacteria was grown overnight at 25 ºC and 200 μl was then seeded onto

standard NGM plates. These were grown for 24 h at room temperature before freshly bleached *O. myriophilus* RSO006 were added to each. *O. myriophilus* were grown for 4-5 days on the bacterial plates and then imaged for evidence of matricide using an epi-fluorescence microscope (Zeiss Axio Zoom V16).

Statistics

With the exception of Figure 3, all statistical analysis was performed by GraphPad Prism. Data in figure 3 was analysed using the custom Python package PpaPred.

Funding

This work was funded by the Max Planck Society (MPG).

Acknowledgements

We thank Nurit Zorn for strain maintenance, Dr Christian Rödelsperger for bioinformatic discussions, Heike Haussmann for freezing and thawing of natural nematode isolates and relevant La Réunion Island authorities for specimen collection permits. *Oscheius* strains EM435 and DF5020 were provided by the CGC, which is funded by NIH Office of Research Infrastructure Programs (P40 OD010440).

References

1. Abrams PA. 2000 The Evolution of Predator-Prey Interactions: Theory and Evidence. *Annu. Rev. Ecol. Syst.* **31**, 79–105. (doi:10.1146/annurev.ecolsys.31.1.79)

2. Ettema CH. 1998 Soil nematode diversity: species coexistence and ecosystem function. *J. Nematol.* **30**, 159–69.

3. Hoogen J van den *et al.* 2019 Soil nematode abundance and functional group composition at a global scale. *Nature* **572**, 194–198. (doi:10.1038/s41586-019-1418-6)

4. Bardgett RD, Putten WH van der. 2014 Belowground biodiversity and ecosystem functioning. *Nature* **515**, 505–511. (doi:10.1038/nature13855)

5. Yeates GW, Bongers T, Goede RGD, Freckman DW, Georgieva SS. 1993 Feeding habits in soil nematode families and genera-an outline for soil ecologists. *J. Nematol.* **25**, 315–31.

6. Sommer RJ, Lightfoot JW. 2022 Nematodes as Model Organisms. , 1–23. (doi:10.1079/9781789248814.0001)

7. Wilecki M, Lightfoot JW, Susoy V, Sommer RJ. 2015 Predatory feeding behaviour in Pristionchus nematodes is dependent on phenotypic plasticity and induced by serotonin. *J Exp Biol* **218**, 1306–1313. (doi:10.1242/jeb.118620)

8. Ragsdale EJ, Müller MR, Rödelsperger C, Sommer RJ. 2013 A Developmental Switch Coupled to the Evolution of Plasticity Acts through a Sulfatase. *Cell* **155**, 922–933. (doi:10.1016/j.cell.2013.09.054)

9. Quach KT, Chalasani SH. 2022 Flexible reprogramming of Pristionchus pacificus motivation for attacking Caenorhabditis elegans in predator-prey competition. *Curr Biol* (doi:10.1016/j.cub.2022.02.033)

10. Eren GG *et al.* 2026 Predatory aggression evolved through adaptations to noradrenergic circuits. *Nature* , 1–10. (doi:10.1038/s41586-025-10009-x)

11. Moreno E, Lightfoot JW, Lenuzzi M, Sommer RJ. 2019 Cilia drive developmental plasticity and are essential for efficient prey detection in predatory nematodes. *Proc Royal Soc B* **286**, 20191089. (doi:10.1098/rspb.2019.1089)

12. Roca M, Eren GG, Böger L, Didenko O, Lo W-S, Scholz M, Lightfoot JW. 2026 Evolution of sensory systems underlies the emergence of predatory feeding behaviors in nematodes. *Proc. Natl. Acad. Sci. United States Am.* **123**, e2514172123. (doi:10.1073/pnas.2514172123)

13. Ishita Y, Chihara T, Okumura M. 2021 Different combinations of serotonin receptors regulate predatory and bacterial feeding behaviors in the nematode Pristionchus pacificus. *G3 Genes Genomes Genetics* **11**, jkab011-. (doi:10.1093/g3journal/jkab011)

14. Okumura M, Wilecki M, Sommer RJ. 2017 Serotonin Drives Predatory Feeding Behavior via Synchronous Feeding Rhythms in the Nematode Pristionchus pacificus. *G3 Genes Genomes Genetics* **7**, 3745–3755. (doi:10.1534/g3.117.300263)

15. Hiramatsu F, Lightfoot JW. 2023 Kin-recognition and predation shape collective behaviors in the cannibalistic nematode Pristionchus pacificus. *PLOS Genet.* **19**, e1011056. (doi:10.1371/journal.pgen.1011056)

16. Lightfoot JW *et al.* 2021 Sex or cannibalism: Polyphenism and kin recognition control social action strategies in nematodes. *Sci Adv* **7**, eabg8042. (doi:10.1126/sciadv.abg8042)

17. Lightfoot JW, Wilecki M, Rödelsperger C, Moreno E, Susoy V, Witte H, Sommer RJ. 2019 Small peptide–mediated self-recognition prevents cannibalism in predatory nematodes. *Science* **364**, 86–89. (doi:10.1126/science.aav9856)

18. Félix M-A, Duveau F. 2012 Population dynamics and habitat sharing of natural populations of Caenorhabditis elegans and C. briggsae. *Bmc Biol* **10**, 59. (doi:10.1186/1741-7007-10-59)

19. Mayer WE, Herrmann M, Sommer RJ. 2007 Phylogeny of the nematode genus Pristionchus and implications for biodiversity, biogeography and the evolution of hermaphroditism. *BMC Evol. Biol.* **7**, 104. (doi:10.1186/1471-2148-7-104)

20. Rödelsperger C, Neher RA, Weller AM, Eberhardt G, Witte H, Mayer WE, Dieterich C, Sommer RJ. 2014 Characterization of Genetic Diversity in the Nematode Pristionchus pacificus from Population-Scale Resequencing Data. *Genetics* **196**, 1153–1165. (doi:10.1534/genetics.113.159855)

21. Rödelsperger C, Röseler W, Prabh N, Yoshida K, Weiler C, Herrmann M, Sommer RJ. 2018 Phylotranscriptomics of Pristionchus Nematodes Reveals Parallel Gene Loss in Six Hermaphroditic Lineages. *Curr Biol* **28**, 3123-3127.e5. (doi:10.1016/j.cub.2018.07.041)

22. Herrmann M, Mayer WE, Hong RL, Kienle S, Minasaki R, Sommer RJ. 2007 The Nematode Pristionchus pacificus (Nematoda: Diplogastridae) Is Associated with the Oriental Beetle Exomala orientalis (Coleoptera: Scarabaeidae) in Japan. *Zool Sci* **24**, 883–889. (doi:10.2108/zsj.24.883)

23. Sommer RJ. 2025 Pristionchus – Beetle associations: Towards a new natural history. *J. Invertebr. Pathol.* **209**, 108243. (doi:10.1016/j.jip.2024.108243)

24. KANZAKI N, HERRMANN M, WEILER C, RÖSELER W, THESKA T, BERGER J, RÖDELSPERGER C, SOMMER RJ. 2021 Nine new Pristionchus (Nematoda: Diplogastridae) species from China. *Zootaxa* **4943**, 1–66. (doi:10.11646/zootaxa.4943.1.1)

25. Meyer JM, Baskaran P, Quast C, Susoy V, Rödelsperger C, Glöckner FO, Sommer RJ. 1476 Succession and dynamics of Pristionchus nematodes and their microbiome during decomposition of Oryctes borbonicus on La Réunion Island. *Environ Microbiol* **19**, 1476–1489. (doi:10.1111/1462-2920.13697)

26. Hong RL, Witte H, Sommer RJ. 2008 Natural variation in Pristionchus pacificus insect pheromone attraction involves the protein kinase EGL-4. *Proc National Acad Sci* **105**, 7779–7784. (doi:10.1073/pnas.0708406105)

27. Hong RL, Sommer RJ. 2006 Chemoattraction in Pristionchus Nematodes and Implications for Insect Recognition. *Curr. Biol.* **16**, 2359–2365. (doi:10.1016/j.cub.2006.10.031)

28. Renahan T, Lo W, Werner MS, Rochat J, Herrmann M, Sommer RJ. 2021 Nematode biphasic 'boom and bust' dynamics are dependent on host bacterial load while linking dauer and mouth-form polyphenisms. *Environ Microbiol* (doi:10.1111/1462-2920.15438)

29. Koneru SL, Salinas H, Flores GE, Hong RL. 2016 The bacterial community of entomophilic nematodes and host beetles. *Mol. Ecol.* **25**, 2312–2324. (doi:10.1111/mec.13614)

30. Giblin-Davis RM, Kanzaki N, Davies KA. 2013 Nematodes that Ride Insects: Unforeseen Consequences of Arriving Species. *Fla. Èntomol.* **96**, 770–780. (doi:10.1653/024.096.0310)

669 31. Bento G, Ogawa A, Sommer RJ. 2010 Co-option of the hormone-signalling module
670 dafachronic acid–DAF-12 in nematode evolution. *Nature* **466**, 494–497.
671 (doi:10.1038/nature09164)

672 32. Levis NA, Ragsdale EJ. 2025 Genomic parallelism defines repeated evolution of an inducible
673 offense. *Sci. Adv.* **11**, eadw9964. (doi:10.1126/sciadv.adw9964)

674 33. Bose N, Ogawa A, von Reuss SH, Yim JJ, Ragsdale EJ, Sommer RJ, Schroeder FC. 2012
675 Complex Small-Molecule Architectures Regulate Phenotypic Plasticity in a Nematode . *Angew*
676 *Chem-ger Edit* **124**, 12606–12611. (doi:10.1002/ange.201206797)

677 34. Werner MS, Sieriebriennikov B, Loschko T, Namdeo S, Lenuzzi M, Dardiry M, Renahan T,
678 Sharma DR, Sommer RJ. 2017 Environmental influence on Pristionchus pacificus mouth form
679 through different culture methods. *Sci Rep-uk* **7**, 7207. (doi:10.1038/s41598-017-07455-7)

680 35. Félix M-A, Ailion M, Hsu J-C, Richaud A, Wang J. 2018 Pristionchus nematodes occur
681 frequently in diverse rotting vegetal substrates and are not exclusively necromenic, while
682 Panagrellus redivivoides is found specifically in rotting fruits. *Plos One* **13**, e0200851.
683 (doi:10.1371/journal.pone.0200851)

684 36. HERRMANN M, KIENLE S, ROCHAT J, MAYER WE, SOMMER RJ. 2010 Haplotype
685 diversity of the nematode Pristionchus pacificus on Réunion in the Indian Ocean suggests
686 multiple independent invasions. *Biol. J. Linn. Soc.* **100**, 170–179. (doi:10.1111/j.1095-
687 8312.2010.01410.x)

688 37. Harry CJ, Messar SM, Ragsdale EJ. 2022 Comparative reconstruction of the predatory
689 feeding structures of the polyphenic nematode Pristionchus pacificus. *Evol. Dev.* **24**, 16–36.
690 (doi:10.1111/ede.12397)

691 38. Rödelsperger C, Meyer JM, Prabh N, Lanz C, Bemm F, Sommer RJ. 2017 Single-Molecule
692 Sequencing Reveals the Chromosome-Scale Genomic Architecture of the Nematode Model
693 Organism Pristionchus pacificus. *Cell Reports* **21**, 834–844. (doi:10.1016/j.celrep.2017.09.077)

694 39. Poinar Jr. 1986 Rhabditis myriophila sp.n. (Rhabditidae: Rhabditida), associated with the
695 millipede, Oxidis gracilis (Polydesmida: Diplopoda). *Proceedings of the Helminthological*
696 *Society of Washington,* **Vol. 53,**, 232–236 ref. 5.

697 40. Sudhaus W, Hooper DJ. 1994 Rhabditis (Oscheius) Guentheri1 Sp.N., an Unusual Species
698 With Reduced Posterior Ovary, With Observations On the Dolichura and Insectivora Groups
699 (Nematoda: Rhabditidae). *Nematologica* **40**, 508–533. (doi:10.1163/003525994x00391)

700 41. Felix M-A. 2006 Oscheius tipulae. *WormBook* , 1–8. (doi:10.1895/wormbook.1.119.1)

701 42. Ahn I-Y, Winter CE. 2006 The genome of Oscheius tipulae : determination of size,
702 complexity, and structure by DNA reassociation using fluorescent dye. *Genome* **49**, 1007–1015.
703 (doi:10.1139/g06-045)

704 43. Rosa PMG de la, Thomson M, Trivedi U, Tracey A, Tandonnet S, Blaxter M. 2020 A
705 telomere-to-telomere assembly of Oscheius tipulae and the evolution of rhabditid nematode
706 chromosomes. *G3: GenesGenomesGenet.* **11**, jkaa020. (doi:10.1093/g3journal/jkaa020)

707 44. Dockendorff TC *et al.* 2022 The nematode Oscheius tipulae as a genetic model for
708 programmed DNA elimination. *Curr. Biol.* **32**, 5083-5098.e6. (doi:10.1016/j.cub.2022.10.043)

709 45. Demir İ, Demirbağ Z, Erbaş Z. 2017 Isolation and Characterization of a Parasitic Nematode,
710 Oscheius myriophila (Nematoda: Rhabditida), Associated with European Mole Cricket,
711 Gryllotalpa gryllotalpa (Orthoptera: Gryllotalpidae). *Hacet. J. Biol. Chem.* **2**, 197–203.
712 (doi:10.15671/hjbc.2017.152)

713 46. Ghavamabad RG, Talebi AA, Mehrabadi M, Farashiani ME, Pedram M. 2021 First record of
714 Oscheius myriophilus (Poinar, 1986) (Rhabditida: Rhabditidae) from Iran; and its efficacy
715 against two economic forest trees pests, Cydalima perspectalis (Walker, 1859) (Lepidoptera:
716 Crambidae) and Hyphantria cunea (Drury, 1773) (Lepidoptera: Erebidae) in laboratory
717 condition. *J. Nematol.* **53**, 1–16. (doi:10.21307/jofnem-2021-035)

718 47. Lightfoot JW, Wilecki M, Okumura M, Sommer RJ. 2016 Assaying Predatory Feeding
719 Behaviors in Pristionchus and Other Nematodes. *J Vis Exp* (doi:10.3791/54404)

720 48. Bonnard E, Liu J, Zjacic N, Alvarez L, Scholz M. 2022 Automatically tracking feeding
721 behavior in populations of foraging C. elegans. *Elife* **11**, e77252. (doi:10.7554/elife.77252)

722 49. Eren GG, Roca M, Han Z, Lightfoot JW. 2022 Genomic integration of transgenes using UV
723 irradiation in Pristionchus pacificus. *Micropublication Biology* **2022**,
724 10.17912/micropub.biology.000576. (doi:10.17912/micropub.biology.000576)

725 50. Flavell SW, Pokala N, Macosko EZ, Albrecht DR, Larsch J, Bargmann CI. 2013 Serotonin
726 and the Neuropeptide PDF Initiate and Extend Opposing Behavioral States in C. elegans. *Cell*
727 **154**, 1023–1035. (doi:10.1016/j.cell.2013.08.001)

728 51. Weadick CJ, Sommer RJ. 2016 Mating System Transitions Drive Life Span Evolution in
729 Pristionchus Nematodes. *Am Nat* **187**, 517–531. (doi:10.1086/685283)

730 52. Akduman N, Rödelsperger C, Sommer RJ. 2018 Culture-based analysis of Pristionchus-
731 associated microbiota from beetles and figs for studying nematode-bacterial interactions. *Plos*
732 *One* **13**, e0198018. (doi:10.1371/journal.pone.0198018)

733 53. Akduman N, Lightfoot JW, Röseler W, Witte H, Lo W-S, Rödelsperger C, Sommer RJ. 2020
734 Bacterial vitamin B12 production enhances nematode predatory behavior. *Isme J* **14**, 1494–1507.
735 (doi:10.1038/s41396-020-0626-2)

736 54. Athanasouli M, Loschko T, Rödelsperger C. 2025 Interspecies systems biology links
737 bacterial metabolic pathways to nematode gene expression, chemotaxis behavior, and survival.
738 *Genome Res.* **35**, 2363–2374. (doi:10.1101/gr.280848.125)

739 55. Hiramatsu F, Goetting DL, Kotowska AM, Zorn N, Chauhan VM, Lightfoot JW. 2026
740 Contact-based kin discrimination is associated with specific surface lipids in the cannibalistic
741 nematode Pristionchus pacificus. (doi:10.64898/2026.01.13.699210)

742 56. Kotowska AM, Hiramatsu F, Alexander MR, Scurr DJ, Lightfoot JW, Chauhan VM. 2025
743 Surface Lipids in Nematodes are Influenced by Development and Species-specific Adaptations.
744 *J. Am. Chem. Soc.* **147**, 6439–6449. (doi:10.1021/jacs.4c12519)

745 57. Chauhan VM, Scurr DJ, Christie T, Telford G, Aylott JW, Pritchard DI. 2017 The
746 physicochemical fingerprint of Necator americanus. *Plos Neglect Trop D* **11**, e0005971.
747 (doi:10.1371/journal.pntd.0005971)

748 58. Chen J, Caswell-Chen EP. 2004 Facultative Vivipary is a Life-History Trait in
749 Caenorhabditis elegans. *J. Nematol.* **36**, 107–13.

750 59. Pickett CL, Kornfeld K. 2013 Age-related degeneration of the egg-laying system promotes
751 matricidal hatching in Caenorhabditis elegans. *Aging Cell* **12**, 544–553. (doi:10.1111/acel.12079)

752 60. Mosser T, Matic I, Leroy M. 2011 Bacterium-Induced Internal Egg Hatching Frequency Is
753 Predictive of Life Span in Caenorhabditis elegans Populations. *Appl. Environ. Microbiol.* **77**,
754 8189–8192. (doi:10.1128/aem.06357-11)

755 61. BALIADV Y, YOSHIGA T, KONDO E. 2011 Development of Endotokia Matricida and
756 Emergence of Originating Infective Juveniles of Steinernematid and Heterorhabditid Nematodes.
757 *Nematol. Res. (Jpn. J. Nematol.)* **31**, 26. (doi:10.3725/jjn1993.31.1-2_26)

758 62. Ciche TA, Kim K, Kaufmann-Daszczuk B, Nguyen KCQ, Hall DH. 2008 Cell Invasion and
759 Matricide during Photorhabdus luminescens Transmission by Heterorhabditis bacteriophora
760 Nematodes. *Appl. Environ. Microbiol.* **74**, 2275–2287. (doi:10.1128/aem.02646-07)

761 63. Ichiishi K, Ekino T, Kanzaki N, Shinya R. 2021 Thick cuticles as an anti-predator defence in
762 nematodes. *Nematology* **24**, 11–20. (doi:10.1163/15685411-bja10107)

763 64. Crean AJ, Marshall DJ. 2009 Coping with environmental uncertainty: dynamic bet hedging
764 as a maternal effect. *Philos. Trans. R. Soc. B: Biol. Sci.* **364**, 1087–1096.
765 (doi:10.1098/rstb.2008.0237)

766 65. Philippi T, Seger J. 1989 Hedging one's evolutionary bets, revisited. *Trends Ecol. Evol.* **4**,
767 41–44. (doi:10.1016/0169-5347(89)90138-9)

768 66. Kunert G, Otto S, Röse USR, Gershenzon J, Weisser WW. 2005 Alarm pheromone mediates
769 production of winged dispersal morphs in aphids. *Ecol. Lett.* **8**, 596–603. (doi:10.1111/j.1461-
770 0248.2005.00754.x)

771 67. Brodie ED, Brodie ED. 1990 TETRODOTOXIN RESISTANCE IN GARTER SNAKES:
772 AN EVOLUTIONARY RESPONSE OF PREDATORS TO DANGEROUS PREY. *Evolution*
773 **44**, 651–659. (doi:10.1111/j.1558-5646.1990.tb05945.x)

68. Brodie ED, Feldman CR, Hanifin CT, Motychak JE, Mulcahy DG, Williams BL, Brodie ED. 2005 Parallel Arms Races between Garter Snakes and Newts Involving Tetrodotoxin as the Phenotypic Interface of Coevolution. *J. Chem. Ecol.* **31**, 343–356. (doi:10.1007/s10886-005-1345-x)

69. Feldman CR, Brodie ED, Brodie ED, Pfrender ME. 2009 The evolutionary origins of beneficial alleles during the repeated adaptation of garter snakes to deadly prey. *Proc. Natl. Acad. Sci.* **106**, 13415–13420. (doi:10.1073/pnas.0901224106)

70. Barber JR, Leavell BC, Keener AL, Breinholt JW, Chadwell BA, McClure CJW, Hill GM, Kawahara AY. 2015 Moth tails divert bat attack: Evolution of acoustic deflection. *Proc. Natl. Acad. Sci.* **112**, 2812–2816. (doi:10.1073/pnas.1421926112)

71. Corcoran AJ, Barber JR, Conner WE. 2009 Tiger moth jams bat sonar. *Sci. (N. York, NY)* **325**, 325–7. (doi:10.1126/science.1174096)

72. Kanzaki N, Giblin-Davis RM. 2025 Practical Plant Nematology. , 125–163. (doi:10.1079/9781836990413.0007)

73. Edgar RC. 2004 MUSCLE: multiple sequence alignment with high accuracy and high throughput. *Nucleic Acids Res.* **32**, 1792–1797. (doi:10.1093/nar/gkh340)

74. Schliep KP. 2010 phangorn: phylogenetic analysis in R. *Bioinformatics* **27**, 592–593. (doi:10.1093/bioinformatics/btq706)

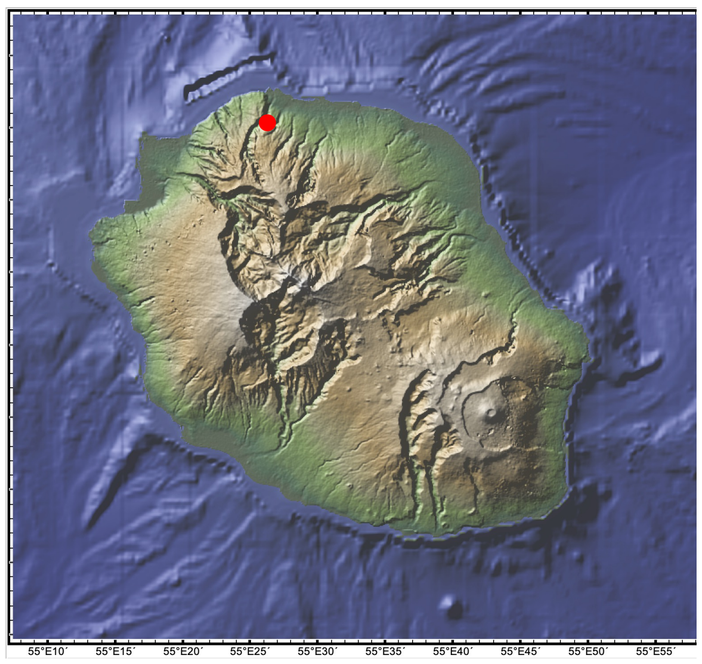
75. Li H, Durbin R. 2010 Fast and accurate long-read alignment with Burrows–Wheeler transform. *Bioinformatics* **26**, 589–595. (doi:10.1093/bioinformatics/btp698)

76. McGaughran A *et al.* 2016 Genomic Profiles of Diversification and Genotype–Phenotype Association in Island Nematode Lineages. *Mol Biol Evol* **33**, 2257–2272. (doi:10.1093/molbev/msw093)

77. Danecek P *et al.* 2021 Twelve years of SAMtools and BCFtools. *GigaScience* **10**, giab008. (doi:10.1093/gigascience/giab008)

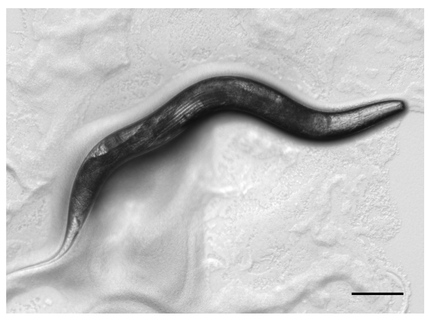
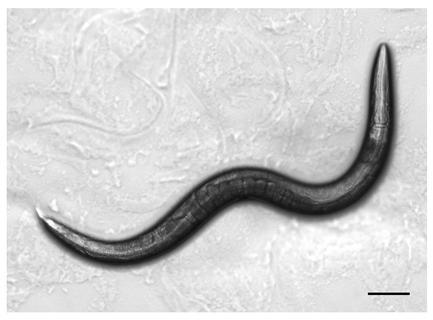
78. Ryan WBF *et al.* 2009 Global Multi-Resolution Topography synthesis: GLOBAL MULTI-RESOLUTION TOPOGRAPHY SYNTHESIS. *Geochem., Geophys., Geosystems* **10**, n/a-n/a. (doi:10.1029/2008gc002332)

A

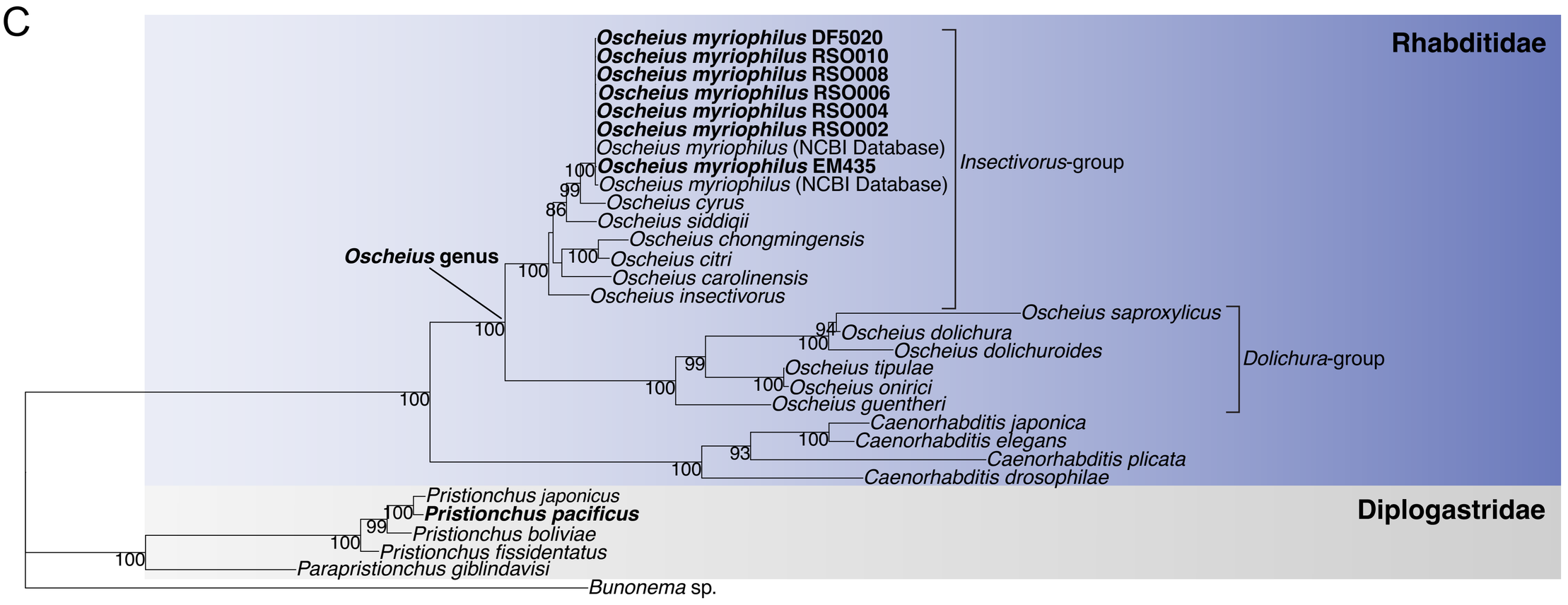


● **Parc du Colorado sampling site**

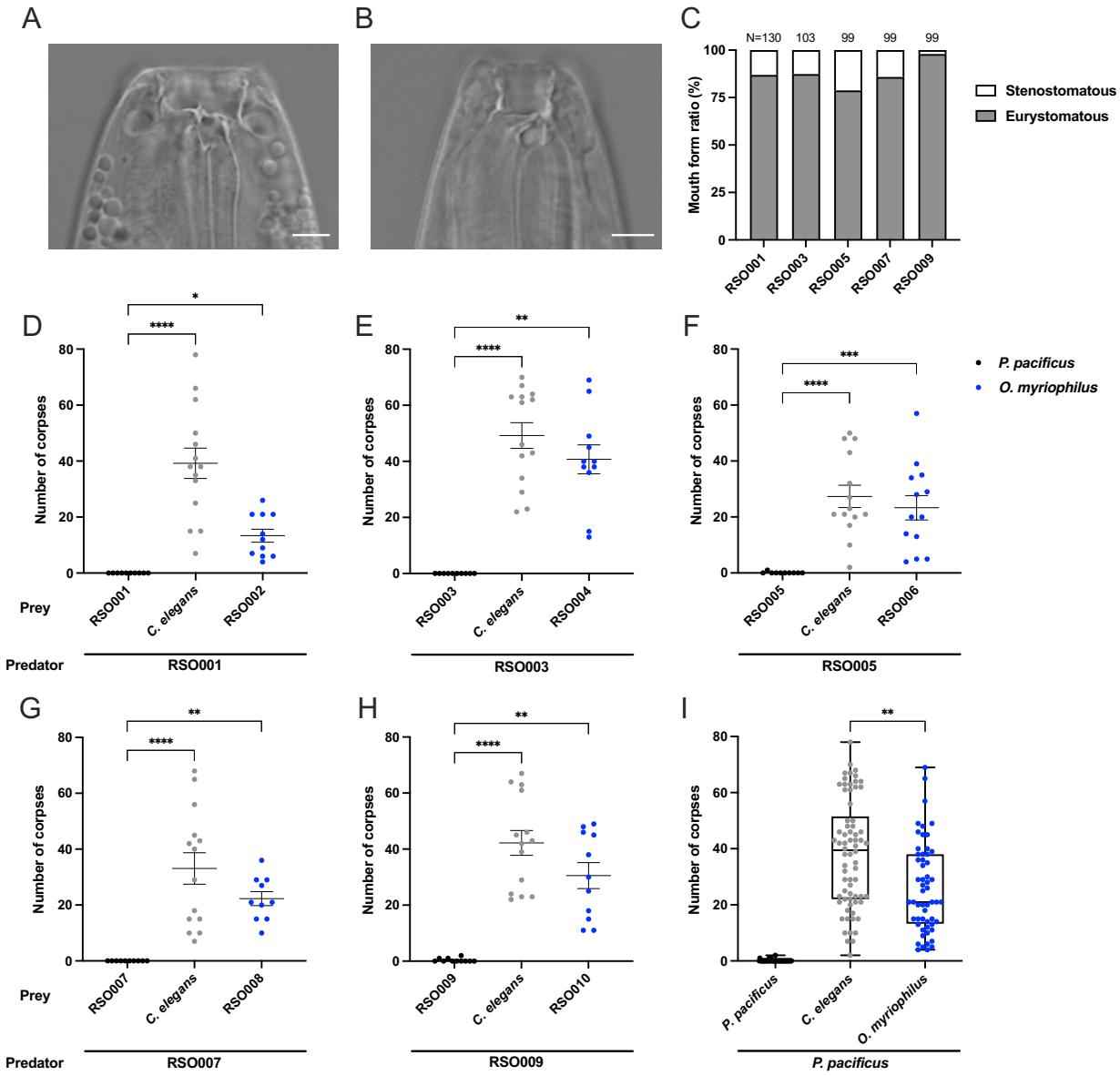
B

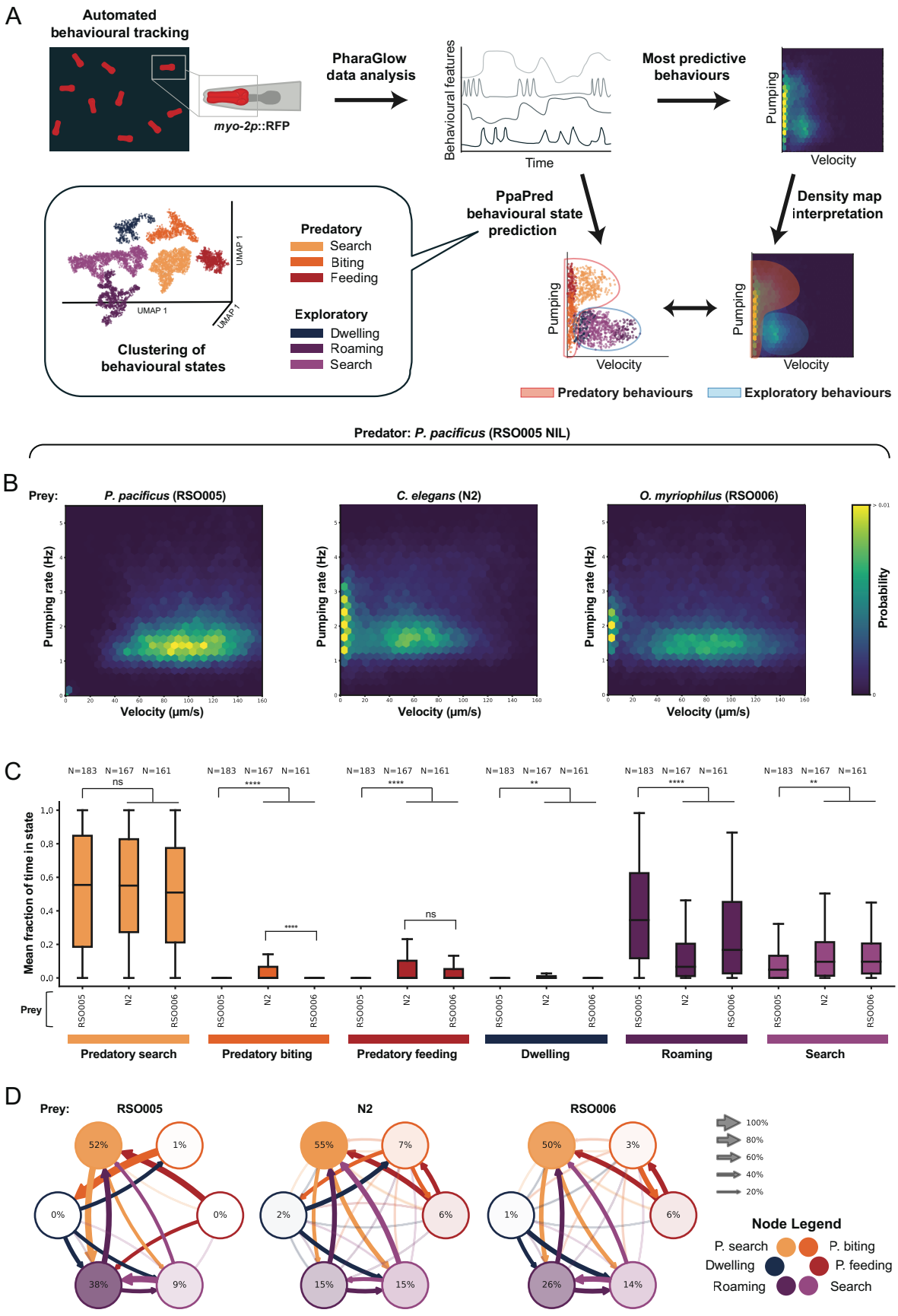
		
***Adoretus* beetle**	***Pristionchus pacificus***	***Oscheius myriophilus***
1	RSO001	RSO002
2	RSO003	RSO004
3	RSO005	RSO006
4	RSO007	RSO008
5	RSO009	RSO010

C



0.1 nucleotide substitutions per site


A
B
C
N=130
103
99
99
99
Mouth form ratio (%)
Stenostomatous
Eurystomatous
RSO001
RSO003
RSO005
RSO007
RSO009
D
E
F
Number of corpses
P. pacificus
O. myriophilus
Prey
Predator
RSO001
C. elegans
RSO002
RSO003
RSO004
RSO005
RSO006
G
H
I
RSO007
RSO008
RSO009
RSO010
P. pacificus


A
Automated behavioural tracking
myo-2p::RFP
PharaGlow data analysis
Behavioural features
Time
Most predictive behaviours
Pumping
Velocity
Density map interpretation
PpaPred behavioural state prediction
UMAP 1
UMAP 1
Clustering of behavioural states
Predatory
Search
Biting
Feeding
Exploratory
Dwelling
Roaming
Search
Predatory behaviours
Exploratory behaviours
Predator: P. pacificus (RSO005 NIL)
B
Prey:
P. pacificus (RSO005)
C. elegans (N2)
O. myriophilus (RSO006)
Pumping rate (Hz)
Velocity (µm/s)
Probability
C
N=183 N=167 N=161
ns
****
**
Mean fraction of time in state
Prey
RSO005
N2
RSO006
Predatory search
Predatory biting
Predatory feeding
Dwelling
Roaming
Search
D
Prey:
RSO005
N2
RSO006
52%
1%
0%
0%
38%
9%
55%
7%
2%
6%
15%
15%
50%
3%
1%
6%
26%
14%
100%
80%
60%
40%
20%
Node Legend
P. search
P. biting
Dwelling
P. feeding
Roaming
Search

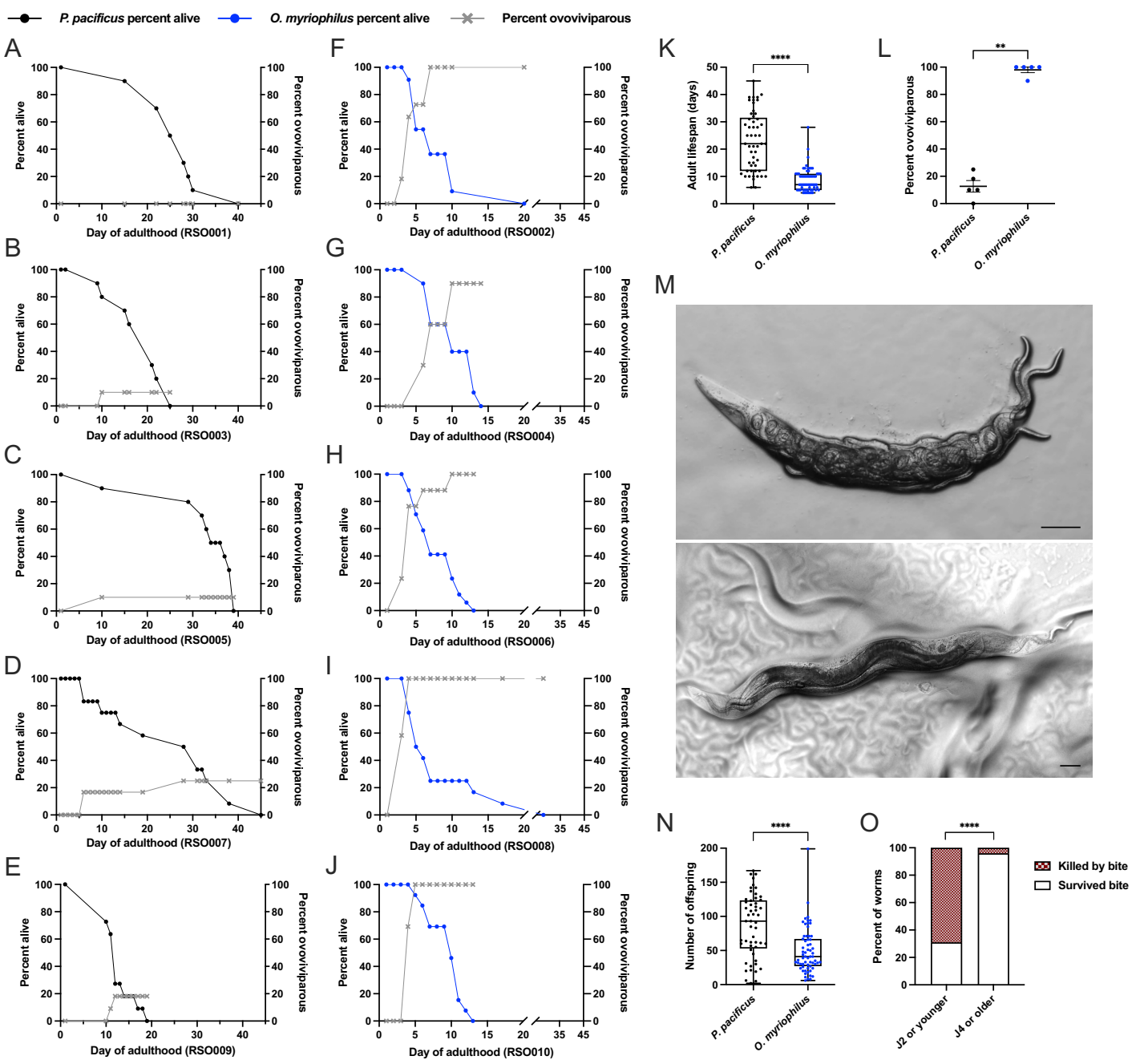
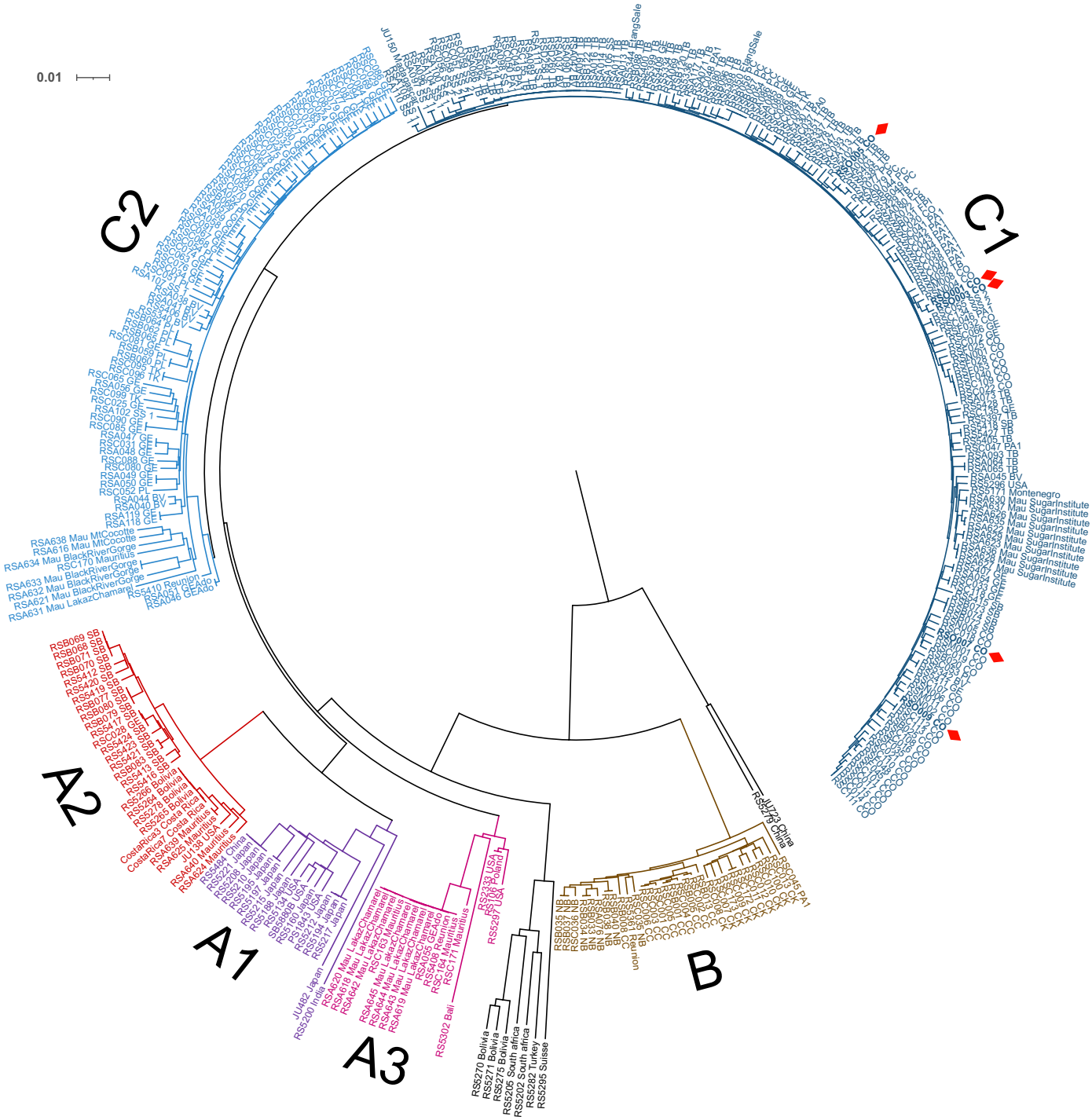
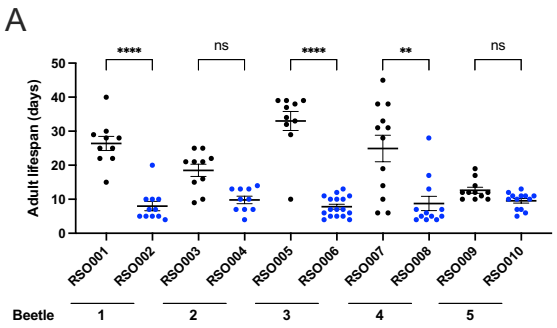
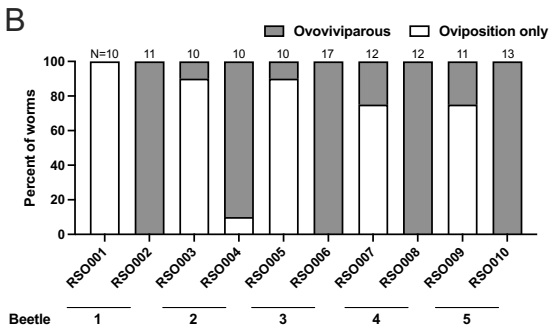

P. pacificus percent alive
O. myriophilus percent alive
Percent ovoviviparous
A
B
C
D
E
F
G
H
I
J
Percent alive
Percent ovoviviparous
Day of adulthood (RSO001)
Day of adulthood (RSO002)
Day of adulthood (RSO003)
Day of adulthood (RSO004)
Day of adulthood (RSO005)
Day of adulthood (RSO006)
Day of adulthood (RSO007)
Day of adulthood (RSO008)
Day of adulthood (RSO009)
Day of adulthood (RSO010)
K
Adult lifespan (days)
****
P. pacificus
O. myriophilus
L
Percent ovoviviparous
**
M
N
Number of offspring
****
O
Percent of worms
****
Killed by bite
Survived bite
J2 or younger
J4 or older

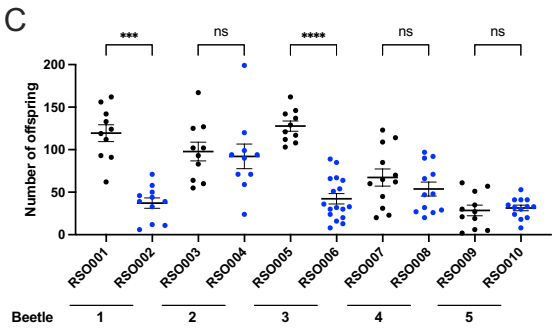
Figure 4

Figure S1

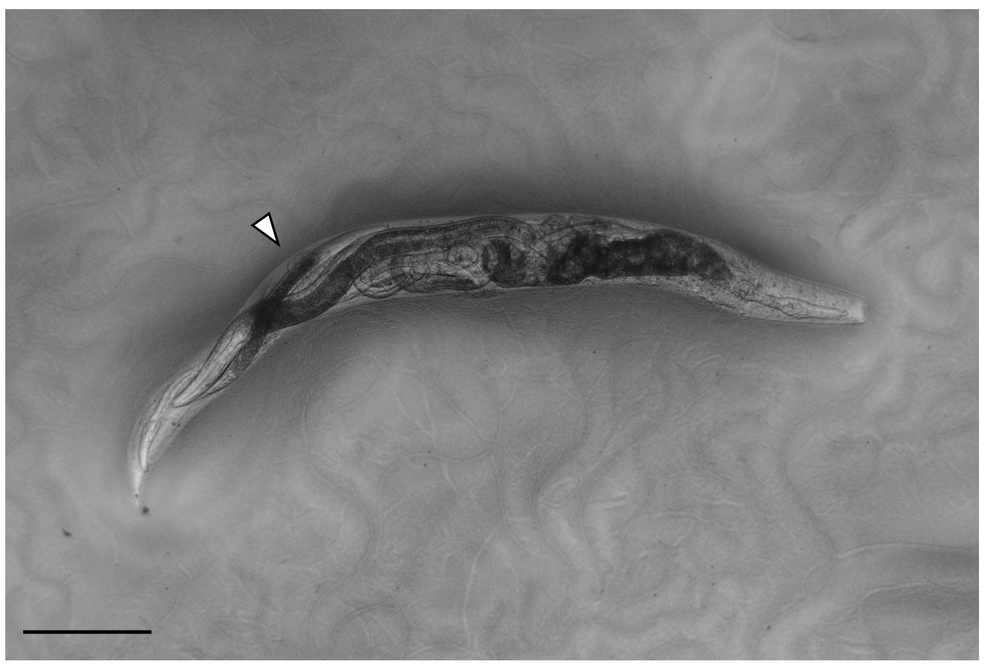



A
Adult lifespan (days)
****
ns
****
**
ns
RSO001
RSO002
RSO003
RSO004
RSO005
RSO006
RSO007
RSO008
RSO009
RSO010
Beetle
1
2
3
4
5

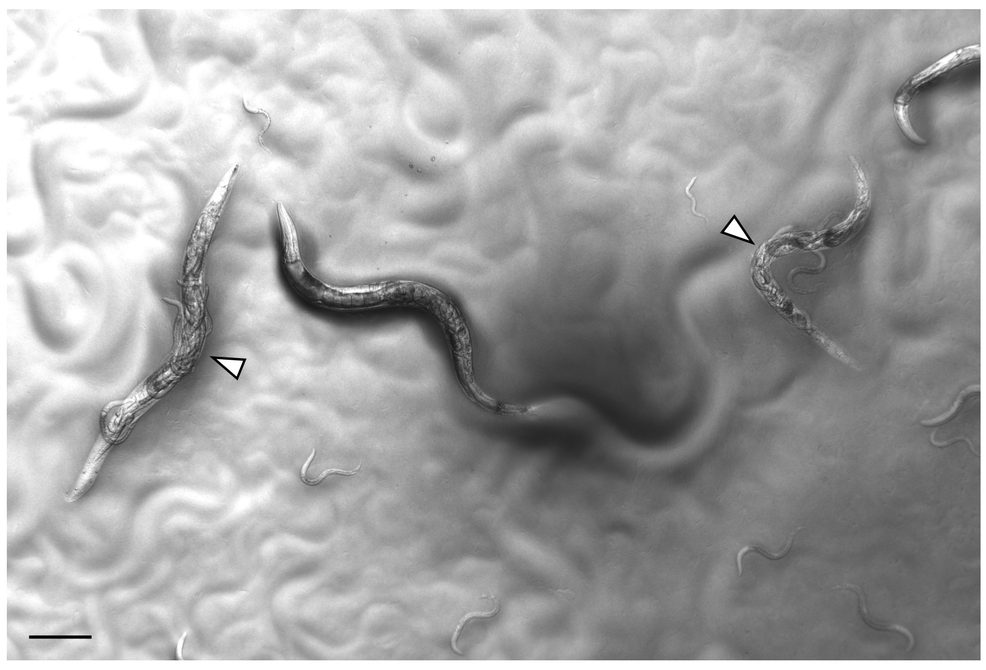

B
Ovoviviparous
Oviposition only
Percent of worms
N=10
11
10
10
10
17
12
12
11
13
RSO001
RSO002
RSO003
RSO004
RSO005
RSO006
RSO007
RSO008
RSO009
RSO010
Beetle
1
2
3
4
5


C
Number of offspring
***
ns
****
ns
ns
RSO001
RSO002
RSO003
RSO004
RSO005
RSO006
RSO007
RSO008
RSO009
RSO010
Beetle
1
2
3
4
5

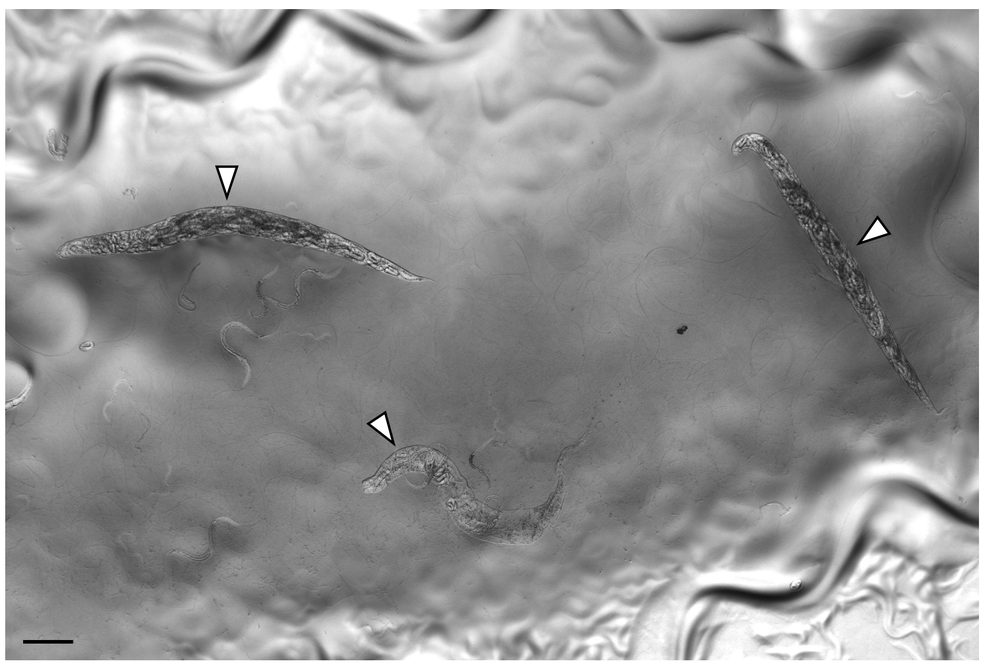
A



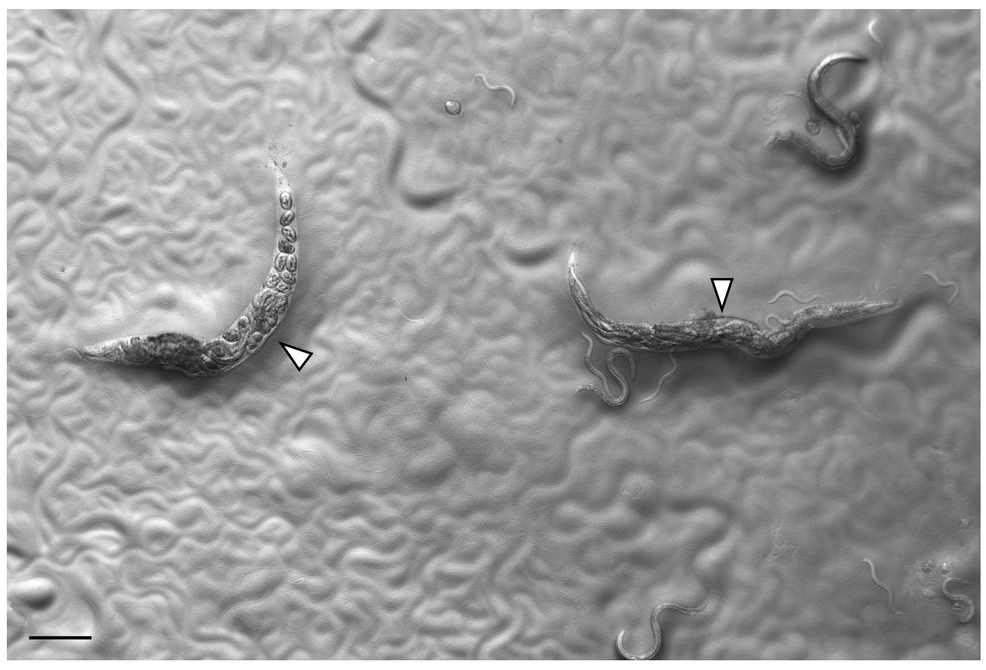
B

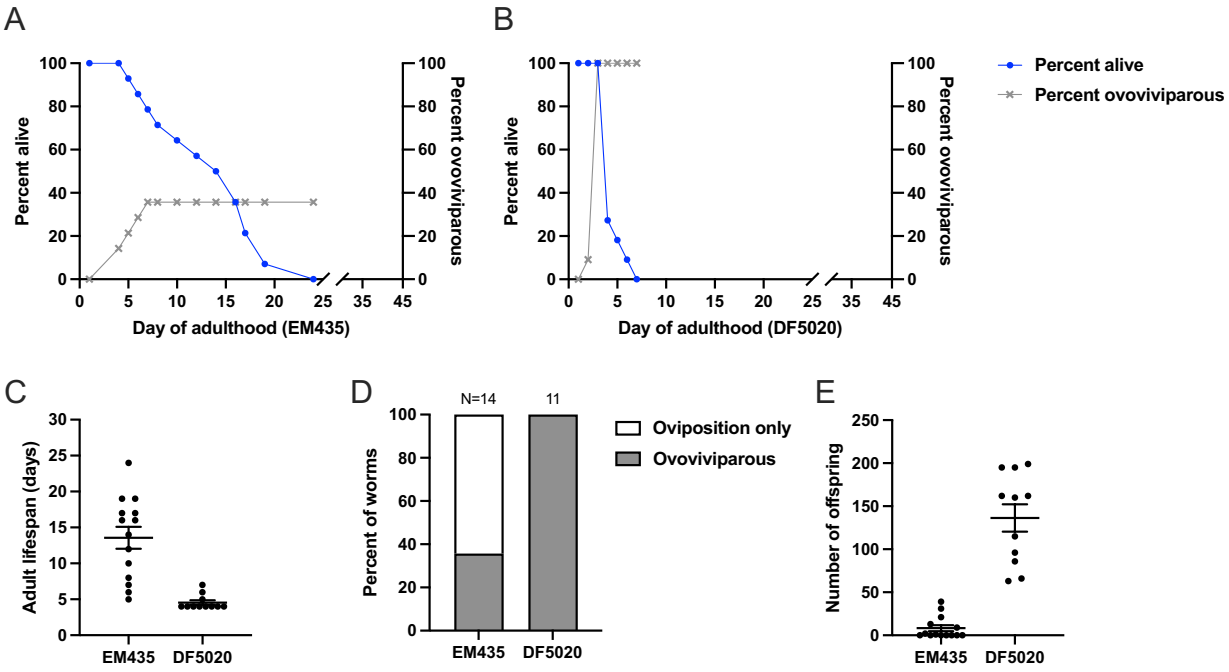


C



D




A
B
Percent alive
Percent ovoviviparous
Day of adulthood (EM435)
Day of adulthood (DF5020)
C
Adult lifespan (days)
EM435
DF5020
D
N=14
11
Percent of worms
Oviposition only
Ovoviviparous
E
Number of offspring

Supplementary table 1

No. of *Adoretus* beetle specimens sampled	**No. of beetles positive for single *P. pacificus* isolate**	**No. of beetles positive for single *O. myriophilus* isolate**	**Number of beetles positive for both *P. pacificus* and *O. myriophilus***
293	101	34	18

Supplementary table 2

Nematode taxon	**SSU accession number**	**LSU accession number**
Oscheius carolinensis	FJ547240.1	FJ547239.1
Oscheius chongmingensis	EU273597.1	EU273599.1
Oscheius citri	MK932670.2	MK932087.2
Oscheius cyrus	PV400801.1	PV400786.1
Oscheius dolichura	EU196010.1	EU195971.1
Oscheius dolichuroides	AF082998.1	EU195970.1
Oscheius guentheri	EU196022.1	EU195996.1
Oscheius insectivorus	AF083019.1	EU195968.1
Oscheius myriophilus	KP756941.1	AY602176.1
	U81588.1	
Oscheius onirici	LN613261.1	LN613263.1
Oscheius saproxylicus	MK959600.1	MK959602.1
Oscheius siddiqii	MT835468.1	MH819729.1
Oscheius tipulae	MF196095.1	MF196098.1
Caenorhabditis elegans	AY284652.1	EF417141.1
Caenorhabditis japonica	AY602182.1	AY602173.1
Caenorhabditis plicata	AY602178.1	AY602167.1
Caenorhabditis drosophilae	AF083025.1	AY602172.1
Pristionchus pacificus	AF083010.1	MK541659.1
Pristionchus boliviae	KT188838.1	KT188868.1
Pristionchus fissidentatus	KT188855.1	KJ877273.1
Pristionchus japonicus	KT188850.1	KT188880.1
Parapristionchus giblindavisi	JX163981.1	JX163972.1
Bunonema sp.	MF470206.1	MG051225.1

bioRxiv preprint doi: https://doi.org/10.64898/2026.03.27.714762; this version posted March 27, 2026. The copyright holder for this preprint (which was not certified by peer review) is the author/funder, who has granted bioRxiv a license to display the preprint in perpetuity. It is made available under aCC-BY-NC 4.0 International license.

Plasticity in nonsense-mediated decay and translation initiation regulate polyphenism

Penghieng Theam[1], Hanh Witte[1], Rebecca Liu[1], Tobias Loschko[1], Christian Rödelsperger[1], Cátia Igreja[1] & Ralf J. Sommer[1,*]

[1] **Department for Integrative Evolutionary Biology, Max Planck Institute for Biology Tübingen, Max Planck Ring 9, 72076 Tübingen, Germany**

*** Corresponding author**

bioRxiv preprint doi: https://doi.org/10.64898/2026.03.27.714762; this version posted March 27, 2026. The copyright holder for this preprint (which was not certified by peer review) is the author/funder, who has granted bioRxiv a license to display the preprint in perpetuity. It is made available under aCC-BY-NC 4.0 International license.

Abstract

Developmental plasticity is increasingly recognised as facilitator of evolutionary novelty. However, how plasticity itself evolves and how variation in plastic trait expression is structured in populations remain unknown[1,2]. The predatory nematode *Pristionchus pacificus* exhibits mouth-form plasticity with underlying molecular mechanisms being increasingly identified[3]. We investigate the temporal scale of natural variation of mouth-form plasticity. An 11-year survey characterised *Adoretus* beetle-derived isolates from Colorado, La Réunion Island and revealed a gradual shift in mouth-form preference. Quantitative trait locus mapping of mouth-form preferences identified a single peak harbouring the developmental switch gene *eud-1*. Through CRISPR-engineering and biochemical assays, we show that plasticity in nonsense-mediated decay coupled with alternative start codon selection resulting in different N-terminal proteoforms of EUD-1 are associated with natural variation of mouth-form preference. This work provides molecular explanations for variation in plastic trait expression and links nonsense variants in the major developmental switch locus to ecological and evolutionary processes.

Keywords: *Pristionchus pacificus*, developmental plasticity, developmental switches, *eud-1*/sulfatase, nonsense-mediated decay, alternative start codon selection

bioRxiv preprint doi: https://doi.org/10.64898/2026.03.27.714762; this version posted March 27, 2026. The copyright holder for this preprint (which was not certified by peer review) is the author/funder, who has granted bioRxiv a license to display the preprint in perpetuity. It is made available under aCC-BY-NC 4.0 International license.

Resource polyphenisms are some of the most extreme examples of developmental plasticity and are known to facilitate the utilisation of distinct food sources in many animals[1]. In general, developmental (phenotypic) plasticity, the ability of a genotype to produce different phenotypes in response to environmental variation, is increasingly recognised as a major facilitator of evolutionary novelty and organismal diversification[2]. Recent case studies are beginning to identify gene regulatory networks (GRNs) in vertebrates, insects, nematodes and other organisms exhibiting polyphenisms and other plastic traits[3]. Such molecular understanding on how plastic systems work is crucial for an overall acceptance of developmental plasticity as a significant factor for evolution. However, scepticism remains and important research questions about the relationship between developmental plasticity and evolution are still unanswered. For example, little is known about how plasticity itself evolves and how variation in plastic trait expression is structured in natural populations.

One animal that has been intensively studied in the last decade is the facultative predatory nematode *Pristionchus pacificus,* which exhibits two alternative mouth forms resulting in different feeding strategies[4,5]. During postembryonic development, individual *P. pacificus* worms execute one of two alternative morphs in an irreversible manner[6]. Stenostomatous (St) animals have a single tooth and a narrow mouth (called the buccal cavity in nematodes) and are strict bacterial feeders (Fig. 1a). In contrast, eurystomatous (Eu) animals have two teeth with a broad buccal cavity and can supplement their bacterial diet by predation on other nematodes (Fig. 1a). This mouth-form dimorphism is a bistable developmental switch with various environmental stimuli being able to influence the mouth-form ratio, making it an attractive system to manipulate plastic trait formation[7-12]. The GRN controlling mouth-form development has been studied in detail and the sulfatase-encoding gene *eud-1* has been identified as the key developmental switch locus[13-19] (Fig. 1b). EUD-1 acts as a dosage-dependent switch and mutations in *eud-1* result in the absence of the Eu mouth form[13]. However, the characterisation of a GRN on its own does not provide evidence for the ecological and evolutionary significance of a plastic trait or developmental plasticity in general[20]. Such claims, and further arguments for the potential adaptive value of developmental plasticity require specific ecological and evolutionary investigations[21]. Here, we study the temporal scale of natural variation of mouth-form plasticity and made the surprising finding that plasticity in nonsense-mediated decay (NMD) and translational control of the key developmental switch gene *eud-1* regulate natural variation in mouth-form bias.

Adoretus beetle-derived *P. pacificus* strains are a hotspot for stenostomatous-biased genotypes

The overwhelming majority of *P. pacificus* natural isolates from around the world preferentially express the Eu mouth form under standard laboratory growth conditions[13,22]. We performed large-scale surveys using the Sommer Lab strain collection with more than 2,000 *P. pacificus* natural isolates in search for genotypes that would be biased towards the St morph instead[23-27]. Ideally, we aimed for pairs of *P. pacificus* strains from the same locality and even the same beetle host species with opposite mouth-form preferences. Indeed, we found that in material isolated in 2012 from beetles of the genus *Adoretus* at Colorado on La Réunion Island most strains are St-biased (Fig. 1c,d). Colorado is in the northern part of the

bioRxiv preprint doi: https://doi.org/10.64898/2026.03.27.714762; this version posted March 27, 2026. The copyright holder for this preprint (which was not certified by peer review) is the author/funder, who has granted bioRxiv a license to display the preprint in perpetuity. It is made available under aCC-BY-NC 4.0 International license.

Island close to the capital St. Denis at an altitude of around 600 m with mixed, endemic and invasive vegetation (Fig. 1c). Of 15 *P. pacificus* strains isolated in 2012, 11 strains were preferentially St: four strains were below or around 10% Eu, whereas the other strains were 10-40% Eu. The remaining four strains were Eu-biased (Fig. 1d). Thus, the majority of strains isolated from *Adoretus* beetles at Colorado are St-biased under laboratory conditions.

We performed additional surveys at Colorado in 2015 and in 2022 and 2023. From a smaller survey in 2015, seven of nine isolates were Eu-biased and only two strains were preferentially St (Fig. 1d). In two more recent samplings in 2022 and 2023, all eight newly isolated strains were highly Eu (Fig. 1d). Note that 2022 and 2023 were extremely dry years, which resulted in low *P. pacificus* yields although the number of *Adoretus* beetle samples were quite large. Taken together, *Adoretus*-derived *P. pacificus* sampling at one particular locality on La Réunion Island identified a shift in mouth-form preferences from St-biased towards Eu-biased strains over an 11-year period and resulted in the isolation of a total of 13 wild isolates with a mouth-form ratio biased towards the St form, which is otherwise rare throughout the world. Note that we have initiated ongoing studies on an annual basis to better understand the dynamics and fluctuations of *Adoretus*-derived *P. pacificus* strains from Colorado.

Recombinant inbred line analysis identifies a single QTL at the *eud-1* locus

Genome-wide single nucleotide polymorphism (SNP) analysis indicated that the *Adoretus*-derived strains from Colorado are indeed very closely related to each other (Suppl. Fig. 1). To study the molecular composition associated with the natural variation in mouth-form preference of strains from Colorado, we selected *P. pacificus* RSC017 (a St strain isolated in 2012) and RSN001 (a Eu strain isolated in 2023) to perform a recombinant inbred line (RIL) experiment. We followed the protocol previously established in *P. pacificus*[28-30] (Fig. 1d and 2a). In short, after reciprocal crosses between RSC017 and RSN001, we inbred 141 lines until the F12 generation and performed genotyping and phenotyping between generations 13-15 (Suppl. Fig. 2) (see Methods for details). Quantitative trait locus (QTL) analysis revealed a single locus on the X chromosome in the region of *eud-1* (Fig. 2b,c). Strikingly, a previous study of *P. pacificus* strains from a different clade and a different locality on Réunion Island had also identified a single QTL at the *eud-1* locus[28] (Fig. 1c and Suppl. Fig. 1). Thus, RIL analysis of *Adoretus*-derived strains RSC017 and RSN001 identified a single QTL at the *eud-1* locus indicating this gene to be repeatedly associated with natural variation in mouth-form preference.

Sequencing of St-biased strains identified molecular lesions in *eud-1* coding sequences

We performed whole genome sequencing of RSC017 and RSN001 and all other St-biased strains to identify potential molecular lesions in *eud-1* and its flanking genes. The *eud-1* locus was previously shown to form a supergene with two other genes regulating mouth-form plasticity[15] (Fig. 2c). We found two different variants at the *eud-1* locus in these St-biased wild isolates, both of which are different from those previously identified[28]. First, we found a variant in the promoter region of *eud-1* with the St-biased strain RSC017 having a

bioRxiv preprint doi: https://doi.org/10.64898/2026.03.27.714762; this version posted March 27, 2026. The copyright holder for this preprint (which was not certified by peer review) is the author/funder, who has granted bioRxiv a license to display the preprint in perpetuity. It is made available under aCC-BY-NC 4.0 International license.

235 bp deletion in the promoter, located 701 bp upstream of exon 1 (Fig. 2d). Interestingly, this deletion was found in 18 additional strains and was present in the meta-population between 2012 and 2023 (Supplementary Table 1). Second, RSC017 harbours a nonsense *eud-1* variant with a 19 bp deletion in the coding sequence (CDS) of exon 1, which encodes part of the signal peptide of EUD-1 (Fig. 2c,d). This 19 bp deletion results in a frameshift (Fig. 2d,e). Note that this deletion is close to the boundary of exon 1 and intron 1 and creates a new *cga* codon (Arg) with the final '*a*' nucleotide coming from exon 2, which normally starts with an *aug* (Met) codon (Fig. 2d,e). This 19 bp deletion was found in seven more independent strains isolated between 2012 and 2015 (predominantly St), but it was not found in any strains isolated in 2022 and 2023 (Supplementary Table 1). We also searched for natural variants in the neighbouring genes that have been implicated in mouth-form regulation, but did not find any natural variants that would be considered as candidates. Thus, a novel RIL experiment and whole genome sequencing of the 13 St-biased strains identified two new molecular variants at the *eud-1* locus indicating that mutations in this gene are over-represented in nature.

The *eud-1* promoter variant is not involved in mouth-form regulation

In *P. pacificus*, CRISPR-associated engineering has been well-established and used in various large-scale studies[31,32]. We used CRISPR engineering to test for the functional significance of natural variants observed between RSC017 and RSN001 (Fig. 3a–c and Supplementary Tables 2 and 3). In principle, RSC017-specific deletions can be eliminated in the RSN001 background, or in a reverse way, RSN001-specific sequences can be reintroduced into the RSC017 background (Fig. 3a–c). First, we investigated a potential role of the 235 bp deletion in the RSC017 *eud-1* promoter region. Specifically, we deleted the 235 bp fragment that is absent in RSC017 in the Eu-biased strain RSN001 using a repair template (Supplementary Table 3). We found that two independent lines with a 235 bp deletion in the RSN001 genetic background had a high Eu mouth-form ratio similar to wild type RSN001 animals (Fig. 3a). We conclude that this natural variant in the *eud-1* promoter does not on its own control mouth-form expression.

Nonsense *eud-1* variants confer mouth-form plasticity

Next, we studied the potential role of the natural nonsense variant in exon 1 of *eud-1* (Fig. 3b,c). We had expected that the 19 bp deletion frameshift variant in RSC017 induces an all-St mouth-form phenotype similar to *eud-1* mutants isolated in forward genetic screens[13], as it elicits premature translation termination in exon 2 (Fig. 2e). However, while RSC017 has a St-biased mouth-form ratio, around 10% of RSC017 worms still have the Eu morph (Fig. 1d). When we created CRISPR-engineered variants of this 19 bp fragment in the RSC017 and RSN001 backgrounds, we observed major shifts in mouth-form preferences. Specifically, a RSN001 worm population with the exact CRISPR-engineered 19 bp deletion (RSN001$^{eud\text{-}1\ \Delta 19bp}$) had less than 50% Eu mouth-form ratio (Fig. 3b). Similarly, the reintroduction of the 19 bp fragment into RSC017 (RSC017$^{eud\text{-}1\ +19\ bp}$), thereby recreating the reading frame of exon 1, increased the Eu mouth form from 10% to 50-60% in the population

bioRxiv preprint doi: https://doi.org/10.64898/2026.03.27.714762; this version posted March 27, 2026. The copyright holder for this preprint (which was not certified by peer review) is the author/funder, who has granted bioRxiv a license to display the preprint in perpetuity. It is made available under aCC-BY-NC 4.0 International license.

(Fig. 3c). These results indicate that the 19 bp deletion has a key role in the regulation of the mouth-form ratios in *P. pacificus* natural isolates. However, these shifts were not complete, which suggest that additional variants at the *eud-1* locus or other genetic loci contribute to the differential mouth-form preference between the two strains. RSN001 animals with both the 235 bp promoter deletion and the 19 bp deletion in exon 1 were still less than 50% Eu (Fig. 3b), confirming that the *eud-1* promoter deletion does not account for the effects observed in the mouth dimorphism.

One potential explanation for the absence of a 'complete *eud-1* mutant phenotype' would be that the formation of the Eu morph might be partially independent of EUD-1/sulfatase activity in these natural isolates. To test this hypothesis, we performed experiments with the steroid sulfatase inhibitor STX64[33,34] that is known to prevent the development of the Eu morph in the *P. pacificus* PS312 reference strain[11]. We found that *P. pacificus* RSC017, RSN001 and the CRISPR-engineered mutant lines RSC017$^{eud\text{-}1\ +19\ bp}$ and RSN001$^{eud\text{-}1\ \Delta 19bp}$ were all-St when grown in the presence of STX64 (Suppl. Fig. 3). These findings suggest that all Eu animals seen in these cultures rely on EUD-1/sulfatase activity, and that the 19 bp deletion nonsense variant does not completely interfere with EUD-1 protein production.

Variation in NMD strength accounts for changes in mouth-form phenotype

Nonsense-mediated mRNA decay (NMD) is an mRNA surveillance pathway that precludes translation of potentially harmful protein variants by affecting the stability of transcripts harbouring premature termination codons (PTCs)[35]. However, some nonsense transcripts escape NMD surveillance and undergo translation[36]. In particular, NMD is inefficient in detecting and targeting start-proximal PTCs[37-42], such as the one observed in the *eud-1* nonsense variant (Fig. 2e). To shed light into the mechanism underlying the synthesis of EUD-1, we tested the possibility that strain-specific differences in *eud-1* nonsense mRNA levels result in the observed partial phenotypes. To determine the impact of the 19 bp deletion in *eud-1* expression, we measured *eud-1* mRNA levels in RSC017 and RSN001 animals with reintroduction (RSC017$^{eud\text{-}1\ +19\ bp}$) or deletion (RSN001$^{eud\text{-}1\ \Delta 19bp}$) of the 19 bp fragment, respectively. *eud-1* mRNA levels in RSC017 animals were approximately 6-fold increased following the correction of *eud-1* exon 1 sequence (Fig. 3d), suggesting that *eud-1* mRNA tends to be degraded by the NMD pathway following premature translation termination[43] in the St-biased strain. This 6-fold increase in *eud-1* mRNA levels is accompanied by a 5-fold increase in the numbers of Eu animals in these lines (Fig. 3c). In contrast, in the Eu-biased RSN001 strain, *eud-1* mRNA levels were not altered upon deletion of the same 19 bp sequence (Fig. 3e). This finding suggests that in this strain, NMD is unable to induce the degradation of *eud-1* nonsense mRNAs. These findings are in agreement with other studies indicating that NMD activity is context-dependent[44] and provide first evidence that NMD efficiency towards nonsense mRNAs with start-proximal PTCs differs among closely related wild isolates of *P. pacificus*.

bioRxiv preprint doi: https://doi.org/10.64898/2026.03.27.714762; this version posted March 27, 2026. The copyright holder for this preprint (which was not certified by peer review) is the author/funder, who has granted bioRxiv a license to display the preprint in perpetuity. It is made available under aCC-BY-NC 4.0 International license.

Alternative initiation of translation allows the synthesis of a functional EUD-1 sulfatase

Knowing that NMD is a translation-dependent process, we investigated possible mechanisms leading to the synthesis of a functional EUD-1 enzyme that results in the development of Eu animals in strains carrying the nonsense transcript variant in exon 1 (Suppl. Fig. 3). First, we considered whether inefficient termination of translation at the PTC via stop codon readthrough allows the ribosome to produce the EUD-1 sulfatase[40,41]. In this scenario, the ribosome continues translating and incorporates a non-cognate amino acid in the PTC codon[42]. The 19 bp deletion in *eud-1* exon 1 changes the frame of the ribosome; thus, stop codon readthrough would lead to the production of a protein with a distinct amino acid sequence unable to have the sulfatase activity required for the determination of the Eu morph (Fig. 2e). Therefore, our observations contradict the stop codon readthrough hypothesis, as Eu animals requiring EUD-1 activity are frequently observed in the different strains expressing the nonsense transcript (Fig. 3b,c and Suppl. Fig. 3).

We then evaluated the possibility that alternative translation initiation allows the synthesis of a functional EUD-1 enzyme. One striking feature of the *eud-1* mRNA is that it contains two potential alternative start *aug* in exon 1 (M1) and exon 2 (M14), respectively (Fig. 4a). Note that the second Met (M14) is still part of the predicted signal peptide of EUD-1 (Fig. 2c and 6b). One potential explanation for the absence of a 'complete *eud-1* mutant phenotype' (all-St) in RSC017 or RSN001$^{eud\text{-}1\ \Delta 19bp}$ would be that synthesis of EUD-1 utilises the *aug* at exon 2. The shortened signal peptide resulting from translational initiation in exon 2 would, according to SignalP 6.0 prediction[45,46], not hinder effective translocation of the protein into the endoplasmic reticulum (ER) (Fig. 6b).

To provide evidence for this hypothesis, we generated additional CRISPR-engineered *eud-1* variants. In the RSN001$^{eud\text{-}1\ \Delta 19bp}$ background, the 19 bp deletion shortens the nucleotide sequence between the second bases of the *cgg* (Arg 7) and *agg* (Arg 13) codons of exon 1, just before the Met 14 *aug* codon (Fig. 3f and 4a). The resulting reading frame is altered and an early *uga* stop codon that overlaps with, but does not destroy the coding potential of the alternative translation initiation site in exon 2, occurs in the potentially translated protein after amino acid position 8 (Arg 7 Stop 8, *cg**a ug**a*, Fig. 3f). We added an *a>c* or *a>g* nonsynonymous mutation in the third base of the *cg<u>a</u>* (Arg 7) codon. These nucleotide substitutions affect the start *aug* of exon 2 (resulting in *<u>c</u>ug* (M14L) or *gug* (M14V)) but do not remove the PTC (Fig. 3f). We found that CRISPR-engineered lines with either M14L or M14V substitution did not produce Eu animals and were all-St (Fig. 3f). Thus, when a nucleotide substitution modifies the alternative start codon in exon 2 (Fig. 3f), synthesis of a functional EUD-1/sulfatase in the nonsense *eud-1* mRNA is impaired, and animals are all-St. Mechanisms underlying the alternative use of start codons in mRNAs with start-proximal PTCs include leaky scanning, an event in which the ribosome scanning the mRNA misses the 5' proximal *aug* triplet and proceeds until it recognises the next *aug*[47], and/or reinitiation of translation following stop codon recognition[37-39]. As the efficiency of leaky scanning and reinitiation of translation is not 100%, but conditioned by multiple factors, both processes can explain the partial phenotype (50% Eu) of RSN001$^{eud\text{-}1\ \Delta 19bp}$ (Fig. 3b,f). Thus, variation in NMD efficiency together with regulation of translation initiation modulate the mouth dimorphism in *P. pacificus*.

Mouth dimorphism is controlled by N-terminal EUD-1 proteoforms

bioRxiv preprint doi: https://doi.org/10.64898/2026.03.27.714762; this version posted March 27, 2026. The copyright holder for this preprint (which was not certified by peer review) is the author/funder, who has granted bioRxiv a license to display the preprint in perpetuity. It is made available under aCC-BY-NC 4.0 International license.

Our results so far indicate that a EUD-1 protein with a shorter signal peptide is functionally relevant for the expression of the Eu phenotype in natural worm populations. To further explore the presence of alternative N-terminal proteoforms in the EUD-1 enzyme, we modified the *aug* codons in exons 1 and 2 to introduce M1A and M14A substitutions in the RSN001 background (lacking the PTC), respectively (Supplementary Tables 2 and 3). We generated two worm lines for each variant. None of the lines with RSN001$^{eud\text{-}1\ M1A}$ and RSN001$^{eud\text{-}1\ M14A}$ showed changes in the mouth-form ratio and animals remained largely Eu (Fig. 4a). One explanation for these findings is that translation can start at M1 or M14 and that both versions of the protein are functional. To support this notion, we measured the association of *eud-1* mRNA with ribosomes in the different RSN001 strains (wild type, M1A and M14A) using polysome profiling, following sucrose density gradient separation, and coupled with RT-qPCR (Fig. 4b–e). Similar to the RSN001 wild type version (66.4±5.5%), the majority of RSN001$^{eud\text{-}1\ M1A}$ (52.8±8.2%) and RSN001$^{eud\text{-}1\ M14A}$ (57.1±4.5%) *eud-1* mRNAs remained associated with polysomes indicating active translation (Fig. 4d). In agreement with the Eu phenotype in the RSN001 strains, translation from both start sites produces active N-terminal EUD-1 proteoforms. As the association of the single mutant *eud-1* mRNAs with ribosomes slightly decreases compared to the wild type version (Fig. 4d), our results also suggest that alternative translation initiation (as a result of leaky scanning) can modulate *eud-1* expression and the synthesis of N-terminal EUD-1 proteoforms.

Next, we created a double mutant with both *aug* codons being mutated (RSN001$^{eud\text{-}1\ M1A,\ M14A}$). Strikingly, the RSN001$^{eud\text{-}1\ M1A,\ M14A}$ mutant strains have a fully penetrant mouth-form phenotype and result in all-St animals (Fig. 4a). This phenotype is similar to *eud-1* mutants originally isolated in the *P. pacificus* reference strain PS312[13,15]. These findings support the notion that M1 and M14 can both serve to initiate translation of N-terminal proteoforms of EUD-1. The all-St phenotype in the RSN001$^{eud\text{-}1\ M1A,\ M14A}$ animals was not caused by a reduction in *eud-1* mRNA levels, as the presence of single or double substitutions in the start *aug* codons increased *eud-1* mRNA abundance (Fig. 4e). We also measured the association of the RSN001$^{eud\text{-}1\ M1A,\ M14A}$ double mutant to ribosomes by polysome profiling. Curiously, the majority (68.3±3,5%) of mutant mRNAs were still associated with ribosomes (Fig. 4d). In the absence of M1 and M14, the most proximal *aug* codon is located after the signal peptide and at position 53 of the amino sequence of EUD-1 (Suppl. Fig. 4a). In the eventuality that the double mutant mRNA is still used for the translation of additional N-terminal variants of EUD-1, the lack of a signal peptide will result in the synthesis of an inactive enzyme as ER import is required for sulfatase maturation and activity[48] (Suppl. Fig. 4b). In the presence of an inactive sulfatase, *P. pacificus* animals are exclusively St (Suppl. Fig. 3).

Finally, we used the RSN001$^{eud\text{-}1\ M1A,\ M14A}$ double mutant line and created a novel start *aug* at amino acid position 15 (Fig. 4f). We found that these RSN001$^{eud\text{-}1\ M1A,\ M14A,\ T15M}$ lines restored the high Eu ratio of the RSN001 wild type background (Fig. 4f). Similarly, a mutation resulting in an amino acid substitution G2M at position 2 in the M1A, M14A background (RSN001$^{eud\text{-}1\ M1A,\ M14A,\ G2M}$), restored the preferential Eu mouth-form phenotype

bioRxiv preprint doi: https://doi.org/10.64898/2026.03.27.714762; this version posted March 27, 2026. The copyright holder for this preprint (which was not certified by peer review) is the author/funder, who has granted bioRxiv a license to display the preprint in perpetuity. It is made available under aCC-BY-NC 4.0 International license.

(Fig. 4f). Taken together, these experiments indicate that alternative N-terminal EUD-1 proteoforms are produced in different *P. pacificus* wild isolates.

Alternative N-terminal EUD-1 proteoforms are widespread among *P. pacificus* strains

We then analysed how conserved the *eud-1* two alternative *aug* start codons are in *P. pacificus* and the genus *Pristionchus*. We found that M1 and M14 are conserved among *P. pacificus* strains and closely related species, such as *P. exspectatus* and *P. arcanus,* also have the M1 and M14 arrangement (Suppl. Fig. 5a,b). To study if the observed alternative translation initiation of EUD-1 in RSN001 is functionally conserved, we generated similar mutants in the highly Eu PS312 strain. These mutant lines also contained a C-terminal ALFA tagged version of EUD-1 (Supplementary Table 2). We found that PS312$^{eud\text{-}1\ M1A}$ and PS312$^{eud\text{-}1\ M14A}$ animals maintain the Eu-biased mouth-form ratio, whereas PS312$^{eud\text{-}1\ M1A,\ M14A}$ worms are all-St (Fig. 5a). In agreement with mouth morphology, using anti-ALFA immunostaining we observed that EUD-1 was produced in the pharyngeal (head) sensory neurons of PS312 wild type, PS312$^{eud\text{-}1\ M1A}$ and PS312$^{eud\text{-}1\ M14A}$ animals, but not in the same corresponding cells of PS312$^{eud\text{-}1\ M1A,\ M14A}$ worms (Fig. 5b). These results indicate that also in the *P. pacificus* PS312 strain, the M1 and M14 *aug* codons can be alternatively used in the translation of *eud-1* mRNA that produces a functional enzyme. Together, these findings suggest that alternative N-terminal proteoforms are widespread and conserved in different *P. pacificus* clades.

Alternative N-terminal proteoforms are common in eukaryotic sulfatases

Finally, we wanted to know if alternative N-terminal proteoforms are specific to EUD-1 or if such forms are also found in sulfatases of other nematodes or even more distantly related animals and humans. The *eud-1* gene arose from a recent duplication of *sul-2* in the genus *Pristionchus* and is one of three *sul-2* paralogs (*eud-1*, *PPA06135* and *PPA21290*) in *P. pacificus*[13]. Curiously, the signal peptide (SP) sequence of PPA21290 also contains multiple Met residues (M1, M4, M12, M13 and M19) (Fig. 6a,c). *In silico* analysis of PPA21290 N-terminal proteoforms at these different residues indicates that with the exception of the M19, initiation of translation at the different Met residues allows the synthesis of this SUL-2 enzyme with functional SP sequences (Fig. 6c). Although unknown to date, this observation suggests that alternative N-terminal proteoforms of PPA21290 might also occur in *P. pacificus*.

Nematode SUL-2 sulfatases belong to the arylsulfatase enzyme family with activity towards steroid hormones[49]. Interestingly, in human cells, the expression of the steroid sulfatase (STS) is modulated by different promoters mediating the synthesis of transcripts with alternative first exons. The resulting STS enzymes display functional variations of the SP sequence (Fig. 6a, 7a) and are expressed in a cell-type/tissue-specific manner[50-52]. Human STS is not the only eukaryotic sulfatase with reported or putative N-terminal variants. Indeed, a survey at the SP sequences of human sulfatases for the presence of multiple Met residues also identified the arylsulfatases ARSJ (Q5FYB0), GALNS (P34059), ARSF (P54793) and short and long isoforms of ARSL (A0A5F9ZHZ5 and F5GYY5) (Fig. 6a, 7b–f). Such as in

bioRxiv preprint doi: https://doi.org/10.64898/2026.03.27.714762; this version posted March 27, 2026. The copyright holder for this preprint (which was not certified by peer review) is the author/funder, who has granted bioRxiv a license to display the preprint in perpetuity. It is made available under aCC-BY-NC 4.0 International license.

the case of human STS or EUD-1, usage of alternative *aug* codons will produce variants of the ARSJ and ARSL enzymes with functional SPs (Fig. 7b,e,f). Taken together, these observations suggest that alternative N-terminal proteoforms are common in eukaryotic sulfatases. However, despite the roles of sulfatases in development and diseases, the detection, roles and mechanisms underlying the expression of N-terminal variants of these enzymes remain understudied.

Discussion

This work provides a molecular explanation for variation in mouth-form bias in natural isolates of the nematode plasticity model *P. pacificus* carrying nonsense variants of the *eud-1* developmental switch locus, thereby linking evolutionary and ecological aspects of developmental plasticity to molecular mechanisms. Our findings are derived from large scale population surveys, organismal-specific genetic manipulations and multiple biochemical assays. We provide evidence for variability of NMD in natural populations and distinct translational control mechanisms regulating the synthesis of variants of a sulfatase with a key role in plasticity.

We observed that NMD strength differs among *P. pacificus* natural populations, as the abundance of the *eud-1* Δ19 bp nonsense mRNA differed from its wild type counterpart in RSC017 animals, but not in the RSN001 animals. Variability in NMD efficiency is observed in animals, plants and fungi across environmental and developmental conditions, genetic background, cell type and individuals[53-55].This variation in NMD efficiency results in phenotypic variability and different degrees of expressivity of a nonsense *eud-1* variant. Our study supports the role of NMD in facilitating adaptive evolution by modulating the expression of cryptic genetic variation in response to environmental stimuli[44]. Therefore, we speculate that mechanisms that turn on and off the expression of plastic traits will facilitate evolutionary capacitance by increasing the potential of an organism to adapt and evolve when faced with novel environmental or genetic constraints. Although the mechanisms linked to variations in NMD robustness in *P. pacificus* wild isolates require further investigation, this collection of strains isolated over several years can provide valuable information on the molecular complexities of the NMD pathway and holds promise for the identification of novel therapeutic strategies to counter genetic disorders caused by nonsense mutations. In addition, our results provide a molecular explanation for the synthesis of a functional sulfatase from the nonsense *eud-1* transcript. CRISPR-targeted disruption of in-frame start codons and biochemical assays indicate that the presence of alternative *aug* in *eud-1* transcript mediates the synthesis of functional N-terminal proteoforms of the sulfatase by leaky scanning and/or translation reinitiation.

The N-terminal region of sulfatases performs a crucial function in enzyme activity. It contains the signal peptide that directs sulfatases to the ER where they undergo a co-translation modification essential for activity[48]. Despite the restricted number of studies addressing N-terminal proteoforms in sulfatases, alternative promoter usage has been proposed to elicit the synthesis of STS enzymes with functional variations of the signal peptide in a tissue-dependent fashion[50-52,56]. Our analysis of nematode and human sulfatases N-terminal sequences highlights the presence of in-frame methionines in multiple enzymes

bioRxiv preprint doi: https://doi.org/10.64898/2026.03.27.714762; this version posted March 27, 2026. The copyright holder for this preprint (which was not certified by peer review) is the author/funder, who has granted bioRxiv a license to display the preprint in perpetuity. It is made available under aCC-BY-NC 4.0 International license.

and the possibility of alternative translation start sites to modulate signal peptide structure or function, adding a new and previously unrecognisable layer to the regulation of enzymes with crucial role in hormone regulation, modulation of signal pathways, and cellular degradation[57].

In conclusion, using a survey englobing ecological, genetic and biochemical studies on a nematode phenotypic polyphenism, we uncover molecular mechanisms with vast implications in animal biology and evolution.

bioRxiv preprint doi: https://doi.org/10.64898/2026.03.27.714762; this version posted March 27, 2026. The copyright holder for this preprint (which was not certified by peer review) is the author/funder, who has granted bioRxiv a license to display the preprint in perpetuity. It is made available under aCC-BY-NC 4.0 International license.

Methods

Beetle collection and nematode isolation

Beetles of the genus *Adoretus* Dejean, 1833 were hand collected from Parc du Colorado, La Réunion[58] (Fig. 1c). They were brought alive to the Max Planck Institute for Biology Tübingen to be sacrificed on nematode growth medium (NGM) plates seeded with *Escherichia coli* OP50. A cocktail of *E. coli* and proliferating native beetle carcass bacteria induce the emergence of nematode dauers. *P. pacificus* isolates were established as a single gravid isogenic hermaphrodite using morphological identification[59].

P. pacificus population genomics

A genome-wide phylogeny of diverse *P. pacificus* strains was generated by sequencing the genomes of newly isolated strains and integrating them into the previously published population genomic data sets for *P. pacificus*[23,26,27] (Suppl. Fig. 1). To this end, the whole genome sequencing datasets were aligned against the genome assembly of the *P. pacificus* reference strain PS312 (version El Paco) with the software BWA (version 0.7.17-r1188, with option mem)[27,60]. The resulting alignment files were then genotyped by the samtools mpileup (version 0.1.18 r982:295) and bcftools (version 0.1.17-dec r973:277) at a set of candidate positions that were previously found to be variable across different *P. pacificus* natural isolates[23,26,27,61]. Variable positions that could be genotyped in all strains with a quality score of at least 20 were concatenated into an artificial multiple sequence alignment that was taken as an input by the phylogenetic R package phangorn in order to calculate a neighbour-joining tree based on Hamming distances between strains[62].

P. pacificus mouth-form phenotype assays

The modular stereomicroscope ZEISS SteREO Discovery.V12 was used to determine the mouth form of adult *P. pacificus* hermaphrodites. Overall stomatal differences were used to determine the mouth-form phenotype. The Eu individuals have a wider and more sclerotised stoma than St animals[13] (Fig. 1a).

All mouth-form assays were performed in standard laboratory conditions with *E. coli* OP50 as food source and nematode cultures grown at 20°C. For each genotype, an individual J4 was picked onto an NGM plate seeded with 300 µl of *E. coli*. The mouth-form phenotyping was done for their progeny six days later. For *P. pacificus* natural isolates, phenotyping was conducted on five technical replicates (plates) over three independent experiments (n = 15). Depending on the genotype's fecundity, thirty to fifty animals were phenotyped per plate to determine the Eu mouth-form ratio (Fig. 1d). For the rest of the genotypes, mouth-form assays were carried out with three biological replicates (10 plates per biological; n = 30). The proportion of Eu phenotype was determined from fifty animals per plate.

bioRxiv preprint doi: https://doi.org/10.64898/2026.03.27.714762; this version posted March 27, 2026. The copyright holder for this preprint (which was not certified by peer review) is the author/funder, who has granted bioRxiv a license to display the preprint in perpetuity. It is made available under aCC-BY-NC 4.0 International license.

Recombinant inbred line (RIL) analysis

Self-sperm-depleted hermaphrodites and males were needed to generate RILs. Late J4 hermaphrodites were picked and transferred daily to a new plate for four days at which point self-sperm ran out. To induce males for crosses, two spontaneous males of each strain were crossed with five self-sperm depleted hermaphrodites of the corresponding genotype on a 100-µl *E. coli* OP50 lawn.

To generate a panel of RILs, P0 males of *P. pacificus* RSC017 and self-sperm-depleted hermaphrodites of *P. pacificus* RSN001 were crossed at a ratio of 2:5. A reciprocal cross was also set up to balance the panel[63]. Parents were removed after ~16 h. A day later, F1 J4-stage hermaphrodites were singled out and left to lay F2 eggs before worm lysis. Sanger sequencing was used to confirm the heterozygosity using a single nucleotide polymorphism (SNP) (*g* in RSN001 > *a* in RSC017) at ChrI:3434406. The primer pair is provided in Supplementary Table 3. All tested F1 animals were heterozygous and 80 F2 individual J4 hermaphrodites were isolated per cross. A total of 160 RILs was transferred as individual J4 hermaphrodites until near homozygosity was reached at F12 (Fig. 2a). These lines were subsequently subjected to mouth-form phenotyping as described above. Eu mouth-form ratio was determined from thirty individuals per plate. Three replicates per RIL were assayed (n = 3) (Suppl. Fig. 2).

RILs were genotyped using in-house Tn5-transposase-based single worm whole genome sequencing protocol as previously described[64]. Briefly, a single RIL individual was lysed in 20 µl of worm lysis buffer. One fifth of the lysate was used for DNA cleanup by Sera-Mag Speedbead carboxylate-modified [E3] magnetic particles (Cytiva Cat. No. 65152105050250) at a ratio of 1:9. The purified DNA sample was then subject to tagmentation by in-house-produced Tn5 transposase (a gift from the Weichenrieder lab, MPI for Biology, Tübingen). This step was followed by a specific i5-and-i7-barcoded 14-cycle PCR. The resultant PCR product was size-selected for fragments between 300 and 600 bp. Afterwards, DNA concentration and size were determined using Qubit (Thermo Fisher) and Bioanalyzer (Agilent), respectively. Finally, a total of 141 RILs' DNA samples were pooled and sequenced at Novogene.

Genome assembly and gene annotation of the RSC017 strain

To establish genomic resources for the *P. pacificus* strain RSC017, we sequenced and assembled its genome following recently established protocols[65]. In short, a PacBio library was generated, sequenced and subsequently assembled into a raw assembly by the software Canu (version 1.4)[66]. This assembly was scaffolded by the software RagTag (version 2.1.0) with the help of the chromosome-scale *P. pacificus* assembly for the strain PS312 (version El Paco)[27,67]. Protein-coding genes were annotated by the software PPCAC which incorporates strain-specific RNA-seq data and the community-curated *P. pacificus* gene annotations (version El Paco annotations 3)[68,69].

bioRxiv preprint doi: https://doi.org/10.64898/2026.03.27.714762; this version posted March 27, 2026. The copyright holder for this preprint (which was not certified by peer review) is the author/funder, who has granted bioRxiv a license to display the preprint in perpetuity. It is made available under aCC-BY-NC 4.0 International license.

QTL mapping

To find associations between genotype and phenotype of the RILs, we followed a similar protocol as described previously[28]. In summary, whole genome sequencing data of the RILs were aligned against the RSC017 reference genome using BWA mem and genotyped at variable positions by samtools mpileup bcftools[27,61]. Subsequently, the logarithm of the odds (LOD) scores for the association between genotype and phenotype (high or low mouth-form ratio; Suppl. Fig. 2) were calculated at 50,000 randomly selected variant positions as the negative $\log_{10}$ of the *p*-value of a Fisher's exact-test. A LOD score above six was considered as a significant association (Bonferroni correction).

Analysis of QTL gene candidate sequence variants

The software Integrative Genomics Viewer (IGV; version 2.16.2) was used to visually analyse the *eud-1* locus sequence variants between the RIL parental strains, RSN001 and RSC017, and the rest of strains tested for mouth-form in this study[70] (Fig. 1d and 2d and Supplementary Table 1). *P. pacificus* PS312 genome and gene annotations were used as the reference to which bam files of natural isolates were aligned. The observed sequence variants in the *eud-1* promoter and exon 1 between RSN001 and RSC017 were confirmed by Sanger sequencing using primers provided in Supplementary Table 3.

CRISPR/Cas9 mutagenesis

The Eppendorf microinjection system was used for gonadal delivery of CRISPR/Cas9-sgRNA mix into well-fed late-J4 hermaphrodites following a well-established protocol in *P. pacificus*[71]. An sgRNA (single guide RNA) was prepared by forming a duplex between a target-specific CRISPR RNA (crRNA) and a trans-activating crRNA (tracrRNA) at an amount of 5 µl each. This mix was incubated at 95°C for 5 min followed by another 5-min incubation at room temperature (RT). crRNAs (Supplementary Table 3) and tracrRNA (Cat. No. 1072534) were synthesised by Integrated DNA Technologies (IDT). Target-specific crRNAs are 20-nucleotide long and were designed to be immediately upstream of protospacer adjacent motifs (PAMs). A CRISPR/Cas9-sgRNA mix was prepared by mixing 5 µl of sgRNA with 1 µl of Cas9 endonuclease (IDT Cat. No. 1081058). This solution was incubated for 5 min at RT and 2 µl of a specific repair template synthesised by IDT (Supplementary Table 3) were added. A final concentration of approximately 25 ng/µl of *Ppa-eft-3p*::RFP was added to the mix as a coinjection marker before 1xTE (Promega Cat. No V6231) was added to bring the total volume to 20 µl. Finally, this solution was centrifuged at maximum speed at 4°C for 10 min to remove any precipitates before injection. The final concentration of specific sgRNA, Cas9, *Ppa-eft-3p*::RFP and repair template is 12.5 µM, 0.5 µg/µl, 25 ng/µl and 10 µM, respectively.

Injected P0 were individually recovered and let lay eggs on a 50-µl *E. coli* OP50 lawn for ~16 h before getting sacrificed. F1 progeny were screened for red fluorescence, an indication of successful gonadal injection. From a positive plate, 16 hermaphrodites were randomly singled out, let lay F2 eggs and Sanger sequenced. F1 heterozygotes with the

bioRxiv preprint doi: https://doi.org/10.64898/2026.03.27.714762; this version posted March 27, 2026. The copyright holder for this preprint (which was not certified by peer review) is the author/funder, who has granted bioRxiv a license to display the preprint in perpetuity. It is made available under aCC-BY-NC 4.0 International license.

correct DNA editing (Supplementary Table 3) as shown by sequence alignment to the wild type sequence using the MAFFT online service[72] were further singled out at F2 to reach homozygosity. Two independent alleles were used for further assays and frozen in liquid nitrogen for long-term storage (Supplementary Table 2).

Steroid sulfatase inhibitor STX64 experiments

To assay the activity of *P. pacificus* sulfatase EUD-1, the steroid sulfatase inhibitor STX64 (Sigma-Aldrich Cat. No. S1950) was used following a previous study[11]. Ten hermaphrodites of each *P. pacificus* genotype (Suppl. Fig. 3) were picked onto an NGM plate seeded with a 300-µl-*E. coli*-lawn. Five plates were prepared per genotype. After five days, population synchronisation was done from the egg stage using the routine bleaching protocol in nematodes[73]. These eggs were plated onto freshly prepared STX64 or the control DMSO (Sigma-Aldrich Cat. No. D8418) plates. These plates were prepared by seeding with 200 µl of OP50 + 10 µl of STX64 (1mg/ml in DMSO) or 10 µl of DMSO for a final concentration of ~1 µg/ml and left to dry in the dark before the assay. After 72 h at 20°C, the mouth-form phenotype of 50 bleach-synchronised adult hermaphrodites was scored. The assays were performed in three biological replicates with 10 plates per replicate (n = 30).

RNA extraction, reverse transcription (RT) and quantitative PCR (qPCR)

P. pacificus mutants and corresponding wild type animals (Supplementary Table 2) were harvested from three 6 cm Petri dishes of mixed stage cultures with M9 medium. Total RNA was isolated from pelleted animals using 1 ml of TRIzol Reagent (Invitrogen Cat. No. 15596018), according to the manufacturer's instructions, with minor changes. Before phase separation, three cycles of flash freezing in liquid nitrogen and thawing at 37°C with vigorous shaking were conducted on the TRIzol resuspended animals to achieve complete worm lysis. DNase treatment and RNA purification were performed with the RNA Clean and Concentrator Kit-25 (Zymo Research Cat. No. R1018). 1 µg of RNA was reverse transcribed using the manufacturer protocol of SuperScript III Reverse Transcriptase (Invitrogen Cat. No. 18080044) in a reaction containing additional 2.5 µM of oligo $(dT)_{20}$ (Jena Bioscience Cat. No. PM-304), 0.5 mM dNTPs, 40 U RNaseOUT recombinant ribonuclease inhibitor (Invitrogen Cat. No. 10777019), and 200 U of the reverse transcriptase. The qPCR reactions were performed with Luna Universal qPCR Master Mix (New England Biolabs Cat. No. M3003), with 0.25 µM of each primer and 1 and 2 µl of the cDNA for *sult-8* and *eud-1* reactions, respectively. Transcript-specific qPCR primers are listed in Supplementary Table 3. Normalised transcript expression ratios from three independent experiments (n = 3) were determined using the Livak-Schmittgen method[74].

Polysome profiling

To obtain the amount of worm material required for polysome profiling assays in triplicate, seven young hermaphroditic animals of each worm strain (Supplementary Table 2) were picked onto 40 plates 6-cm diameter NGM plates with *E. coli* OP50 as food source.

bioRxiv preprint doi: https://doi.org/10.64898/2026.03.27.714762; this version posted March 27, 2026. The copyright holder for this preprint (which was not certified by peer review) is the author/funder, who has granted bioRxiv a license to display the preprint in perpetuity. It is made available under aCC-BY-NC 4.0 International license.

Four to five days later and before the worms run out of food, plates were chunked into small agar cubes with worms, and each cube was transferred onto 100-150 10-cm plates with *E. coli* OP50. Three to four days later, non-starved animals from the mixed stage cultures were collected with M9 buffer into Falcon tubes. Following three gentle washes in M9 and filtration on a 5 µm Nylon net filter (Millipore Cat. No. NY0504700) to remove remaining bacteria, and one wash in hypotonic buffer (10 mM Tris-HCl pH 7.9, 2.5 mM $MgCl_2$), worms were flash frozen in liquid nitrogen and stored at -80°C. In total, 1-2 g of frozen worm popcorns were collected per strain. Worm popcorns were crushed with a pestle to fine powder on a mortar pre-cooled with liquid nitrogen. Worm powder was distributed between different microfuge tubes. Per polysome profiling assay, 400-500 µl (w/v) of worm powder was thawed and lysed in 1x vol of hypotonic lysis buffer containing 0.1 mM of cycloheximide (Carl ROTH Cat. No. 8682), 1 mM DTT, 0.5% Nonidet P40 (MP Biomedicals Cat. No. RIST1315), 1% sodium deoxycholate monohydrate (DOC) (Sigma Aldrich Cat. No. D6750) and 2% polyoxyethylene-10-tridecylether (PET) (Sigma Aldrich Cat. No. P2393) on ice. Following 40 strokes with an Eppendorf micropestle, worm lysates were kept on ice for 10 min. Worm debris was removed by a 10 min centrifugation at 12 000 *g* at 4°C. The soluble lysate was transferred to a fresh tube and absorbance was measured at 260 nm. 70 U A260 of worm lysate were layered on a linear 10-50% (w/v) sucrose gradient, prepared using Gradient Master 107ip (Biocomp) in gradient buffer (10 mM Tris-HCl pH 7.9, 2.5 mM MgCl2, 80 U units RNase OUT (Invitrogen Cat. No. 10777019)/RiboLock RNase inhibitor (Thermo Scientific Cat. No. EO0382), 0.1 mM cycloheximide. Centrifugation was carried in a Beckman ultracentrifuge using a SW55Ti at 45 000 rpm, for 45 min at 4°C. Polysome fractions were collected using the TRIAX Gradient Fractionation System Model FC-2 (Biocomp) and polysomes profiles were monitored by absorbance of light at 254 nm.

Samples for RNA isolation were first digested with proteinase K (Sigma Aldrich Cat. No. 1.24568, 1% of the sample volume; 100 mg/ml in 50 mM Tris-HCl pH=8.1, 10 mM $CaCl_2$ buffer) at 37°C for 45 min and shaking at 400 rpm. The digested sucrose fractions were mixed with 1 volume of Phenol:Chloroform:Isoamyl alcohol (PanReac AppliChem, 25:24:1, v/v), vortexed and spun down 5 min at 20,000 *g* at 4°C. Supernatants were transferred into 3 volumes of 100% ethanol, 0.1 volumes of 3M NaOAc pH=5.2 and 1 µl of GlycoBlue (Ambion Cat. No. AM9515), and precipitated at -20°C. Samples were pelleted for 30 min at 20,000 *g* and 4°C, washed once with 100% ethanol and another time with 70% ethanol, dried and resuspended in 15 µl H_2O. Fractions were reverse transcribed and analysed by RT-qPCR.

Statistical tests

Statistical tests were performed using R language-based packages (R version 4.3.1)[75]. Homogeneity of variances and normal distribution were tested using Levene's and Shapiro–Wilk tests, respectively. *eud-1* mRNA and polysome profiling data met the assumptions for parametric tests, i.e. the data are normally distributed and variances are homogenous. The unpaired two-samples *t*-test was used to analyse *eud-1* mRNA levels in wild type and 19 bp deletion or insertion mutants (Fig. 3d,e). The one-way analysis of variance (ANOVA) and the post-hoc Dunnett's test were used for statistical tests of *eud-1* and *sult-8* mRNA levels in the polysome fractions (Fig. 4d,e). Mouth-form ratio data did not meet the parametric test

bioRxiv preprint doi: https://doi.org/10.64898/2026.03.27.714762; this version posted March 27, 2026. The copyright holder for this preprint (which was not certified by peer review) is the author/funder, who has granted bioRxiv a license to display the preprint in perpetuity. It is made available under aCC-BY-NC 4.0 International license.

assumptions, thus the non-parametric Kruskal–Wallis test and the post-hoc Dunn's test with a Holm–Bonferroni method were used to test each pair (Fig. 3a–c,f, 4a,f and 5a). Significance levels were indicated as ****$p < 0.0001$; ***$p < 0.001$; **$p < 0.01$; * $p < 0.05$; ns (not significant) $p > 0.05$.

Immunofluorescence

ALFA-tagged EUD-1 protein immunofluorescent staining was performed according to the protocol previously described[76]. Briefly, *P. pacificus* PS312 wild type and EUD-1 M-to-A mutants from mixed stage cultures were collected from ten 6-cm NGM plates, filtered on a 5-µm Nylon net filter (Millipore Cat. No. NY0504700) to remove remaining bacteria, and fixed with a 4% para-formaldehyde, 1x PBS solution overnight at room temperature on a tube rotator. Fixed animals were washed thrice with 0.5% Triton X-100, 1x PBS (washing solution), and incubated in 5% β-mercaptoethanol, 1% Triton X-100, 0.1M Tris-HCl pH 7.4 solution overnight at 37°C and shaking (300 rpm). Worm cuticle digestion was performed at 37°C for 1-2 h in buffer containing 500 units of collagenase type IV (Gibco Cat. No. 17104-019) after two consecutive washes with 1% Triton X-100, 0.1M Tris-HCl pH 7.4 buffer and one wash with collagenase buffer (1mM CaCl2, 1% Triton X-100, 0.1M Tris pH 7.4). Following three washes in washing solution, and one hour incubation at room temperature with blocking solution (1% BSA, 0.5% Triton X-100, 1x PBS), the digested animals were stained overnight at 4°C with anti-ALFA primary antibody coupled with the AZDye568 fluorophore (FluoTag-X2 anti-ALFA AZDye568, NanoTag Biotechnologies Cat. No: N1502-AF568-L; dilution 1:100) and diluted in blocking solution. Stained animals were washed thrice with washing solution and then mounted on 5% Noble agar pads in VECTASHIELD antifade mounting medium (Vector Laboratories Cat. No. H-1000) containing 4',6-diamidino-2-phenylindole (DAPI, 1 mg/ml, Molecular Probes Cat. No. 15451244). Images were acquired on a Leica TCS SP8 microscope and assembled on Fiji version 2.16.0/1.54p (Image J)[77].

Alignment of sulfatases and *in silico* signal peptide predictions

For *P. pacificus* and human sulfatases, sequences were accessed from the UniProt platform[78] and aligned using ESPript 3.0[79]. Sequences of *P. exspectatus* and *P. arcanus* EUD-1 orthologs were retrieved from BLASTp searches on the *Pristionchus* research community public server (http://www.pristionchus.org). The resultant sequences were aligned with *P. pacificus* EUD-1 on Clustal Omega and visualised on Jalview (version 2.11.5.1)[80,81].

In silico signal peptide predictions were carried out on the SignalP 6.0 server[45,46]. The resultant predicted structure and likelihood values were used for data interpretation.

bioRxiv preprint doi: https://doi.org/10.64898/2026.03.27.714762; this version posted March 27, 2026. The copyright holder for this preprint (which was not certified by peer review) is the author/funder, who has granted bioRxiv a license to display the preprint in perpetuity. It is made available under aCC-BY-NC 4.0 International license.

Data availability

All nematode strains used in this study are available from the corresponding author Ralf J. Sommer (ralf.sommer@tuebingen.mpg.de). The genome assembly for the *P. pacificus* strain RSC017 and the newly generated whole genome sequencing data of natural isolates have been deposited at the European Nucleotide Archive under the project accession PRJEB108083. All microscopy images are available upon request. Source data are provided with this paper.

Acknowledgments

We would like to thank relevant La Réunion Island authorities for specimen collection permits and Dr. Matthias Herrmann for the photo of *Amneidus godefroyi*. Dr. Herrmann, Christian Weiler, and former Sommer lab members involved in La Réunion projects are also thanked for help with beetle and nematode collections. We thank Heike Haussmann for freezing of *P. pacificus* materials and Radhika Sharma for discussions. The Weichenrieder lab (Max Planck Institute for Biology, Tübingen) is thanked for providing the Tn5 protein used for tagmentation. This work was supported by the Max Planck Society. P.T. is part of the International Max Planck Research School (IMPRS) 'From Molecules to Organisms'.

Author contributions

Conceptualisation: P.T. and R.S.J. Methodology: P.T., H.W., C.R. and C.I. Investigation: P.T., H.W. R.L., T.L., C.R. and C.I. Visualisation: P.T and C.I. Funding acquisition: R.S.J. Project administration: R.S.J. Supervision: R.S.J. Writing—original draft: R.S.J. and C.I. Writing—review and editing: P.T., C.R., C.I. and R.S.J.

Funding

This work was funded by institutional funds from the Max-Planck Society.

Competing interests

The authors declare no competing interests.

bioRxiv preprint doi: https://doi.org/10.64898/2026.03.27.714762; this version posted March 27, 2026. The copyright holder for this preprint (which was not certified by peer review) is the author/funder, who has granted bioRxiv a license to display the preprint in perpetuity. It is made available under aCC-BY-NC 4.0 International license.

References

1 Pfennig, D. W. Key questions about phenotypic plasticity. in *Phenotypic Plasticity & Evolution: Causes, Consequences, Controversies*. 55-88 (CRC Press, 2021).

2 West-Eberhard, M. J. *Developmental Plasticity and Evolution*. (Oxford University Press, 2003).

3 Sommer, R. J. Phenotypic Plasticity: from theory and genetics to current and future challenges. *Genetics* **215**, 1-13 (2020).

4 Schroeder, N. E. Introduction to *Pristionchus pacificus* anatomy. *J. Nematol.* **53** (2021).

5 Quach, K. T. & Chalasani, S. H. Flexible reprogramming of *Pristionchus pacificus* motivation for attacking *Caenorhabditis elegans* in predator-prey competition. *Curr. Biol.* **32**, 1675-1688 (2022).

6 Bento, G., Ogawa, A. & Sommer, R. J. Co-option of the hormone-signalling module dafachronic acid-DAF-12 in nematode evolution. *Nature* **466**, 494-497 (2010).

7 Kalirad, A. & Sommer, R. J. Spatial and temporal heterogeneity alter the cost of plasticity in *Pristionchus pacificus*. *PLoS Comput. Biol.* **20**, e1011823 (2024).

8 Werner, M. S. *et al.* Environmental influence on *Pristionchus pacificus* mouth form through different culture methods. *Sci. Rep.* **7**, 7207 (2017).

9 Lenuzzi, M. *et al.* Influence of environmental temperature on mouth-form plasticity in *Pristionchus pacificus* acts through *daf-11*-dependent cGMP signaling. *J. Exp. Zool. B Mol. Dev. Evol.* **340**, 214-224 (2023).

10 Dardiry, M., Piskobulu, V., Kalirad, A. & Sommer, R. J. Experimental and theoretical support for costs of plasticity and phenotype in a nematode cannibalistic trait. *Evol. Lett.* **7**, 48-57 (2023).

11 Werner, M. S. *et al.* Histone 4 lysine 5/12 acetylation enables developmental plasticity of *Pristionchus* mouth form. *Nat. Commun.* **14**, 2095 (2023).

12 Piskobulu, V. *et al.* High nutritional conditions influence feeding plasticity in *Pristionchus pacificus* and render worms non-predatory. *J. Exp. Zool. B Mol. Dev. Evol.* **344**, 94-111 (2025).

13 Ragsdale, E. J., Muller, M. R., Rödelsperger, C. & Sommer, R. J. A developmental switch coupled to the evolution of plasticity acts through a sulfatase. *Cell* **155**, 922-933 (2013).

14 Bui, L. T., Ivers, N. A. & Ragsdale, E. J. A sulfotransferase dosage-dependently regulates mouthpart polyphenism in the nematode *Pristionchus pacificus*. *Nat. Commun.* **9**, 4119 (2018).

15 Sieriebriennikov, B. *et al.* A developmental switch generating phenotypic plasticity is part of a conserved multi-gene locus. *Cell Rep.* **23**, 2835-2843 (2018).

16 Sieriebriennikov, B. *et al.* Conserved nuclear hormone receptors controlling a novel plastic trait target fast-evolving genes expressed in a single cell. *PLoS Genet.* **16**, e1008687 (2020).

17 Casasa, S., Katsougia, E. & Ragsdale, E. J. A Mediator subunit imparts robustness to a polyphenism decision. *Proc. Natl. Acad. Sci. USA* **120**, e2308816120 (2023).

18 Levis, N. A. & Ragsdale, E. J. A histone demethylase links the loss of plasticity to nongenetic inheritance and morphological change. *Nat. Commun.* **14**, 8439 (2023).

19 Katsougia, E., Connors, S. J. & Ragsdale, E. J. A species-specific nuclear receptor was integrated into a developmental polyphenism pathway. *Genetics* **231** (2025).

20 Wighard, S. & Sommer, R. J. The role of epigenetic switches in polyphenism control: implications from a nematode model for the developmental regulation of alternative phenotypes. *Biology* **13** (2024).

bioRxiv preprint doi: https://doi.org/10.64898/2026.03.27.714762; this version posted March 27, 2026. The copyright holder for this preprint (which was not certified by peer review) is the author/funder, who has granted bioRxiv a license to display the preprint in perpetuity. It is made available under aCC-BY-NC 4.0 International license.

21 Baugh, L. R. & Day, T. Nongenetic inheritance and multigenerational plasticity in the nematode *C. elegans*. *eLife* **9** (2020).
22 Lightfoot, J. W. *et al.* Sex or cannibalism: polyphenism and kin recognition control social action strategies in nematodes. *Sci. Adv.* **7** (2021).
23 McGaughran, A. *et al.* Genomic profiles of diversification and genotype-phenotype association in island nematode lineages. *Mol. Biol. Evol.* **33**, 2257-2272 (2016).
24 Herrmann, M., Kienle, S., Rochat, J., Mayer, W. E. & Sommer, R. J. Haplotype diversity of the nematode on Réunion in the Indian Ocean suggests multiple independent invasions. *Biol. J. Linn. Soc.* **100**, 170-179 (2010).
25 Morgan, K. *et al.* Multi locus analysis of *Pristionchus pacificus* on La Réunion Island reveals an evolutionary history shaped by multiple introductions, constrained dispersal events and rare out-crossing. *Mol. Ecol.* **21**, 250-266 (2012).
26 Rödelsperger, C. *et al.* Characterization of genetic diversity in the nematode *Pristionchus pacificus* from population-scale resequencing data. *Genetics* **196**, 1153-1165 (2014).
27 Rödelsperger, C. *et al.* Single-molecule sequencing reveals the chromosome-scale genomic architecture of the nematode model organism *Pristionchus pacificus*. *Cell Rep.* **21**, 834-844 (2017).
28 Dardiry, M. *et al.* Divergent combinations of *cis*-regulatory elements control the evolution of phenotypic plasticity. *PLoS Biol.* **21**, e3002270 (2023).
29 Mayer, M. G., Rödelsperger, C., Witte, H., Riebesell, M. & Sommer, R. J. The orphan gene *dauerless* regulates dauer development and intraspecific competition in nematodes by copy number variation. *PLoS Genet.* **11**, e1005146 (2015).
30 Moreno, E., McGaughran, A., Rödelsperger, C., Zimmer, M. & Sommer, R. J. Oxygen-induced social behaviours in *Pristionchus pacificus* have a distinct evolutionary history and genetic regulation from *Caenorhabditis elegans*. *Proc. Biol. Sci.* **283**, 20152263 (2016).
31 Han, Z. *et al.* Improving transgenesis efficiency and CRISPR-associated tools through codon optimization and native intron addition in *Pristionchus* nematodes. *Genetics* **216**, 947-956 (2020).
32 Lo, W. S. *et al.* Evolution and diversity of TGF-beta pathways are linked with novel developmental and behavioral traits. *Mol. Biol. Evol.* **39** (2022).
33 Woo, L. L., Purohit, A., Malini, B., Reed, M. J. & Potter, B. V. Potent active site-directed inhibition of steroid sulphatase by tricyclic coumarin-based sulphamates. *Chem. Biol.* **7**, 773-791 (2000).
34 Malini, B. *et al.* Inhibition of steroid sulphatase activity by tricyclic coumarin sulphamates. *J. Steroid Biochem. Mol. Biol.* **75**, 253-258 (2000).
35 Tan, K. & Wilkinson, M. F. Biological roles of nonsense-mediated RNA decay: insights from the nervous system. *Curr. Opin. Genet. Dev.* **93**, 102356 (2025).
36 Dyle, M. C., Kolakada, D., Cortazar, M. A. & Jagannathan, S. How to get away with nonsense: mechanisms and consequences of escape from nonsense-mediated RNA decay. *Wiley Interdiscip. Rev. RNA* **11**, e1560 (2020).
37 Inácio, A. *et al.* Nonsense mutations in close proximity to the initiation codon fail to trigger full nonsense-mediated mRNA decay. *J. Biol. Chem.* **279**, 32170-32180 (2004).
38 Pereira, F. J. *et al.* Resistance of mRNAs with AUG-proximal nonsense mutations to nonsense-mediated decay reflects variables of mRNA structure and translational activity. *Nucleic Acids Res.* **43**, 6528-6544 (2015).
39 Zhang, J. & Maquat, L. E. Evidence that translation reinitiation abrogates nonsense-mediated mRNA decay in mammalian cells. *EMBO J.* **16**, 826-833 (1997).

bioRxiv preprint doi: https://doi.org/10.64898/2026.03.27.714762; this version posted March 27, 2026. The copyright holder for this preprint (which was not certified by peer review) is the author/funder, who has granted bioRxiv a license to display the preprint in perpetuity. It is made available under aCC-BY-NC 4.0 International license.

40 Hogg, J. R. & Goff, S. P. Upf1 senses 3'UTR length to potentiate mRNA decay. *Cell* **143**, 379-389 (2010).
41 Keeling, K. M. *et al.* Leaky termination at premature stop codons antagonizes nonsense-mediated mRNA decay in *S. cerevisiae*. *RNA* **10**, 691-703 (2004).
42 Celik, A., Kervestin, S. & Jacobson, A. NMD: At the crossroads between translation termination and ribosome recycling. *Biochimie* **114**, 2-9 (2015).
43 Tan, K., Stupack, D. G. & Wilkinson, M. F. Nonsense-mediated RNA decay: an emerging modulator of malignancy. *Nat. Rev. Cancer* **22**, 437-451 (2022).
44 Raxwal, V. K. & Riha, K. Nonsense mediated RNA decay and evolutionary capacitance. *Biochim. Biophys. Acta* **1859**, 1538-1543 (2016).
45 Nielsen, H., Teufel, F., Brunak, S. & von Heijne, G. SignalP: the evolution of a web server. *Methods Mol. Biol.* **2836**, 331-367 (2024).
46 Teufel, F. *et al.* SignalP 6.0 predicts all five types of signal peptides using protein language models. *Nat. Biotechnol.* **40**, 1023-1025 (2022).
47 Kozak, M. An analysis of vertebrate mRNA sequences: intimations of translational control. *J. Cell Biol.* **115**, 887-903 (1991).
48 Appel, M. J. & Bertozzi, C. R. Formylglycine, a post-translationally generated residue with unique catalytic capabilities and biotechnology applications. *ACS Chem. Biol.* **10**, 72-84 (2015).
49 Perez-Jimenez, M. M. *et al.* Steroid hormones sulfatase inactivation extends lifespan and ameliorates age-related diseases. *Nat. Commun.* **12**, 49 (2021).
50 Dalla Valle, L. *et al.* Tissue-specific transcriptional initiation and activity of steroid sulfatase complementing dehydroepiandrosterone sulfate uptake and intracrine steroid activations in human adipose tissue. *J. Endocrinol.* **190**, 129-139 (2006).
51 Dalla Valle, L. *et al.* The expression of the human steroid sulfatase-encoding gene is driven by alternative first exons. *J. Steroid Biochem. Mol. Biol.* **107**, 22-29 (2007).
52 Zaichuk, T., Ivancic, D., Scholtens, D., Schiller, C. & Khan, S. A. Tissue-specific transcripts of human steroid sulfatase are under control of estrogen signaling pathways in breast carcinoma. *J. Steroid Biochem. Mol. Biol.* **105**, 76-84 (2007).
53 Palou-Marquez, G. & Supek, F. Variable efficiency of nonsense-mediated mRNA decay across human tissues, tumors and individuals. *Genome Biol.* **26**, 316 (2025).
54 Sato, H. & Singer, R. H. Cellular variability of nonsense-mediated mRNA decay. *Nat. Commun.* **12**, 7203 (2021).
55 Lindeboom, R. G., Supek, F. & Lehner, B. The rules and impact of nonsense-mediated mRNA decay in human cancers. *Nat. Genet.* **48**, 1112-1118 (2016).
56 Nardi, A. *et al.* Transcriptional control of human steroid sulfatase. *J. Steroid Biochem. Mol. Biol.* **115**, 68-74 (2009).
57 Hanson, S. R., Best, M. D. & Wong, C. H. Sulfatases: structure, mechanism, biological activity, inhibition, and synthetic utility. *Angew. Chem. Int. Ed. Engl.* **43**, 5736-5763 (2004).
58 Lacroix, M., Poussereau J. *Les Scarabéides de l'Île de La Réunion*. (Editions Orphie, 2019).
59 Herrmann, M., Mayer, W. E. & Sommer, R. J. Nematodes of the genus *Pristionchus* are closely associated with scarab beetles and the Colorado potato beetle in Western Europe. *Zoology* **109**, 96-108 (2006).
60 Li, H. & Durbin, R. Fast and accurate long-read alignment with Burrows-Wheeler transform. *Bioinformatics* **26**, 589-595 (2010).
61 Danecek, P. *et al.* Twelve years of SAMtools and BCFtools. *Gigascience* **10** (2021).
62 Schliep, K. P. phangorn: phylogenetic analysis in R. *Bioinformatics* **27**, 592-593 (2011).

bioRxiv preprint doi: https://doi.org/10.64898/2026.03.27.714762; this version posted March 27, 2026. The copyright holder for this preprint (which was not certified by peer review) is the author/funder, who has granted bioRxiv a license to display the preprint in perpetuity. It is made available under aCC-BY-NC 4.0 International license.

63 Andersen, E. C. & Rockman, M. V. Natural genetic variation as a tool for discovery in *Caenorhabditis* nematodes. *Genetics* **220** (2022).

64 Yoshida, K. *et al.* Chromosome fusions repatterned recombination rate and facilitated reproductive isolation during *Pristionchus* nematode speciation. *Nat. Ecol. Evol.* **7**, 424-439 (2023).

65 Röseler, W., Sommer, R. J. & Rödelsperger, C. Nematode genome announcement: a chromosome-scale genome assembly for the *Pristionchus pacificus* reference mapping strain PS1843. *J. Nematol.* **56**, 20240063 (2024).

66 Koren, S. *et al.* Canu: scalable and accurate long-read assembly via adaptive *k*-mer weighting and repeat separation. *Genome Res.* **27**, 722-736 (2017).

67 Alonge, M. *et al.* Automated assembly scaffolding using RagTag elevates a new tomato system for high-throughput genome editing. *Genome Biol.* **23**, 258 (2022).

68 Rödelsperger, C. The community-curated *Pristionchus pacificus* genome facilitates automated gene annotation improvement in related nematodes. *BMC Genomics* **22**, 216 (2021).

69 Athanasouli, M. *et al.* Comparative genomics and community curation further improve gene annotations in the nematode *Pristionchus pacificus*. *BMC Genomics* **21**, 708 (2020).

70 Robinson, J. T., Thorvaldsdottir, H., Wenger, A. M., Zehir, A. & Mesirov, J. P. Variant review with the Integrative Genomics Viewer. *Cancer Res.* **77**, e31-e34 (2017).

71 Witte, H. *et al.* Gene inactivation using the CRISPR/Cas9 system in the nematode *Pristionchus pacificus*. *Dev. Genes Evol.* **225**, 55-62 (2015).

72 Katoh, K., Rozewicki, J. & Yamada, K. D. MAFFT online service: multiple sequence alignment, interactive sequence choice and visualization. *Brief Bioinform.* **20**, 1160-1166 (2019).

73 Stiernagle, T. Maintenance of *C. elegans*. in *WormBook*. https://doi.org/10.1895/wormbook.1.101.1 (2006).

74 Livak, K. J. & Schmittgen, T. D. Analysis of relative gene expression data using real-time quantitative PCR and the 2(-Delta Delta C(T)) Method. *Methods* **25**, 402-408 (2001).

75 R Core Team. *A language and environment for statistical computing. R Foundation for Statistical Computing*. https://www.R-project.org/ (2023).

76 Igreja, C. *et al.* Application of ALFA-tagging in the nematode model organisms *Caenorhabditis elegans* and *Pristionchus pacificus*. *Cells* **11** (2022).

77 Schindelin, J. *et al.* Fiji: an open-source platform for biological-image analysis. *Nat. Methods* **9**, 676-682 (2012).

78 UniProt Consortium. UniProt: the universal protein knowledgebase in 2025. *Nucleic Acids Res.* **53**, D609-D617 (2025).

79 Gouet, P., Courcelle, E., Stuart, D. I. & Metoz, F. ESPript: analysis of multiple sequence alignments in PostScript. *Bioinformatics* **15**, 305-308 (1999).

80 Madeira, F. *et al.* The EMBL-EBI Job Dispatcher sequence analysis tools framework in 2024. *Nucleic Acids Res.* **52**, W521-W525 (2024).

81 Troshin, P. V., Procter, J. B. & Barton, G. J. Java bioinformatics analysis web services for multiple sequence alignment—JABAWS:MSA. *Bioinformatics* **27**, 2001-2002 (2011).

bioRxiv preprint doi: https://doi.org/10.64898/2026.03.27.714762; this version posted March 27, 2026. The copyright holder for this preprint (which was not certified by peer review) is the author/funder, who has granted bioRxiv a license to display the preprint in perpetuity. It is made available under aCC-BY-NC 4.0 International license.

Figure legends

Fig. 1 *Adoretus* beetle-derived *P. pacificus* strains provide St-biased material for mouth-form natural variation studies. a, Nematode life cycle (right) and Nomarski micrographs of adult head structures (left). Adult hermaphroditic *P. pacificus* individuals have an irreversible feeding polyphenism. They can either possess just one dorsal (d) tooth and feed strictly on bacteria (St morph) or decorate their right subventral (rsv) sector of the buccal cavity with another tooth enabling them to kill other nematodes and become omnivorous feeders (Eu morph). **b,** The mouth-form decision is controlled by a complex gene regulatory network with various gene modules, including a 'phenotypic switch module' and a more downstream 'switch transcription module'. Central to the 'phenotypic switch module' is the sulfation pathway comprising the sulfatase-encoding gene *eud-1* and the sulfotransferase-encoding gene *sult-1*/*seud-1*. *eud-1* is the main mouth-form switch gene and *P. pacificus* adults become St when *eud-1* is mutated. Genes shown in blue and orange result in all-Eu and all-St phenotypes, respectively. **c,** Map of La Réunion Island with scarab beetle sample localities indicated. Among other scarab beetles, *P. pacificus* can be isolated from the endemic stag beetle *Amneidus godefroyi* collected from Nez de Bœuf (violet dot) and Coteau Kerveguen (green dot) and species of the genus *Adoretus* collected from Colorado (magenta dot). **d,** Natural variation of mouth-form preference of *Adoretus*-derived *P. pacificus* strains collected from Colorado in different years including 2012 (light blue and blue), 2015 (purple) and 2022 and 2023 (light yellow and orange). Boxplots show the median (centre line), interquartile range (IQR; box), and whiskers extending to 1.5×IQR of mouth-form ratio (n = 15 replicates). Closely-related strains RSC017 (St-biased; blue) and RSN001 (Eu-biased; orange) were selected for further studies (Suppl. Fig. 1). Source data are provided as a Source Data file. Scale bars: 20 µm for embryo and J1 stages, 100 µm for the rest of the stages (right), and 5 µm for mouth-form micrographs (left) (**a**) and 20 km for map of La Réunion (**c**). Map of La Réunion. © Conseil Régional de La Réunion (2006) at Wikimedia Commons, CC BY-SA 2.5. *A. godefroyi* photo. © Dr. Matthias Herrmann (**c**).

Fig. 2 Recombinant inbred line (RIL) analysis revealed a single quantitative trait locus (QTL) at the *eud-1* gene. a, Schematic of RIL generation. Reciprocal cross between self-sperm-depleted hermaphrodites of one strain with males of the other strain and vice versa. This panel of RILs was inbred until generation F12 in which near homozygosity is achieved. Mouth-form phenotyping and sequencing were carried out between generations F13-F15. The mouth-form phenotype of RILs is shown in Suppl. Fig. 2. **b,** QTL mapping revealed a single significant peak on chromosome X. A logarithm of the odds (LOD) score above six indicates a significant association. The most significant region spanned ~0.4 Mb on the left arm of chromosome X and corresponded to the mouth-form supergene locus. **c,** The supergene locus contains four genes, three of which (*nag-1*, *nag-2* and *eud-1*) contribute to the mouth-form decision. *eud-1* is epistatic over the two *nag*-genes. Below the gene organization, an enhanced representation of the exon-intron structure of *eud-1* and a simplified protein structure are shown. The first two exons of *eud-1* encode a signal peptide (SP) important for the proper subcellular localisation of EUD-1 protein (Fig. 6b). **d,** *eud-1* locus 5' vicinity and exon 1 of RSN001 and RSC017 genomes compared to the reference *P. pacificus* genome (version El Paco) viewed on the software IGV. Genomic position is shown on the top. In the RSN001 and RSC017 genome panels, arrow blocks represent strand-oriented reads aligned to the reference genome. Read coverage profiles are represented by histogram-like tracks above each genome. Polymorphisms between RSN001 and RSC017 genomes and the reference genome including SNPs and deletions are indicated by coloured lines and gaps on the read coverage tracks, respectively. Two deletions in the *eud-1* locus were observed in the St-

bioRxiv preprint doi: https://doi.org/10.64898/2026.03.27.714762; this version posted March 27, 2026. The copyright holder for this preprint (which was not certified by peer review) is the author/funder, who has granted bioRxiv a license to display the preprint in perpetuity. It is made available under aCC-BY-NC 4.0 International license.

biased RSC017 strain. One deletion spans 235 bp in the promoter region and is located 701 bp upstream of the coding sequence. The other deletion removes 19 bp in the first exon (underlined). **e,** Representation of the first and second exons of *eud-1* and alternative coding potentials. The 19 bp deletion in exon 1 of the RSC017 strain leads to a frameshift mutation and a premature stop codon (red asterisk). A second in-frame open reading frame (ORF) can start from the second exon in both strains. Scale bars: 1 kb and 50 AA for *eud-1* gene and EUD-1 protein structures, respectively (**c**).

Fig. 3 Elimination and reintroduction of the exonic 19 bp fragment partially alters mouth-form ratios. a–c, Percentage of Eu animals in RSN001 and RSC017 strains with genetic changes in the *eud-1* locus: (**a**) 235 bp deletion in the promoter region (*eud-1p* Δ235 bp) introduced into RSN001 by CRISPR engineering, (**b**) exonic 19 bp deletion (*eud-1* Δ19 bp) in RSN001, and (**c**) reintroduction of the exonic 19 bp (*eud-1* +19 bp) into the St-biased RSC017 strain. (n = 30 replicates). **d,e,** Determination of *eud-1* and *sult-8* mRNA levels by quantitative PCR (qPCR) following reverse transcription of RNA extracted from the different *P. pacificus* strains. *eud-1* mRNA levels were normalized to *sult-8* mRNA levels. Bars represent the mean value and error bars represent standard deviation (SD) (n = 3 biological replicates) **f,** Left, Gene scheme depicting *eud-1* exon 1 and exon 2 nucleotide and amino acid sequences with two in-frame methionines: M1 and M14 and the consequences of CRISPR-engineered genetic changes in nucleotide and amino acid sequences. Deletion of the 19 bp generates a premature termination codon (asterisk) at the beginning of exon 2, overlapping with the exon 2 *aug*. Point mutations resulting in the M14L and M14V amino acid substitutions remove the translation initiation site in exon 2 without disrupting the PTC. Right, quantification of Eu animals in these genetically altered RSN001 mutants (n = 30 replicates). **a**–**c,f,** Boxplots show the median (centre line), interquartile range (IQR; box), and whiskers extending to 1.5×IQR of mouth-form ratio. **a**–**f** Additional mutant information is shown in Supplementary Table 2. Statistical significance in **a**–**c,f** and **d,e** was assessed by Kruskal–Wallis test and the post-hoc Dunn's test with a Holm–Bonferroni method and unpaired two-samples t-test, respectively. Significance levels are indicated as ****$p <$ 0.0001; ***$p < 0.001$; **$p < 0.01$; * $p < 0.05$; ns (not significant) $p > 0.05$. Source data are provided as a Source Data file.

Fig. 4 Alternative N-terminal EUD-1 proteoforms contribute to the Eu phenotype in RSN001. a, Schematic representation of *eud-1* exons 1 and 2 with nucleotide and amino acid sequences being depicted. The *eud-1* mRNA has two in-frame start sites: M1 or M14. The graph shows the percentage of Eu animals in wild type RSN001 animals and carrying single and double nucleotide substitutions disrupting the alternative translation start sites: M1A, M14A, and M1A M14A. Boxplots show the median (centre line), interquartile range (IQR; box), and whiskers extending to 1.5×IQR of mouth-form ratio (n = 30 replicates). **b,** UV absorbance profile at 254 nm of RSN001 wild type (orange) and mutants of *eud-1* alternative start codons (M1A, pink; M14A, purple; M1A, M14A, green) worm extracts following polysome sedimentation in a 10-50% sucrose gradient. Absorbance peaks at 254 nm representing free 40S and 60S subunits, 80S monosomes and polysomes are indicated. The polysome profiles from the different strains were similar without obvious changes in the translation status. **c,** Ethidium bromide staining of total RNA extracted from the sucrose fractions obtained with RSN001 wild type cell lysate. 18S and 28S rRNA bands are highlighted. **d,** Abundance profiles for *eud-1* (blue) and *sult-8* (orange) mRNAs across the density gradient in RSN001 wild type and mutants of *eud-1* alternative start codons (M1A, M14A and M1A, M14A) assessed using qPCR (top four panels). Estimation of the abundance of *eud-1* (blue) and *sult-8* (orange) mRNAs in polysomes (% RNA in fractions 8-

bioRxiv preprint doi: https://doi.org/10.64898/2026.03.27.714762; this version posted March 27, 2026. The copyright holder for this preprint (which was not certified by peer review) is the author/funder, who has granted bioRxiv a license to display the preprint in perpetuity. It is made available under aCC-BY-NC 4.0 International license.

13 of the density gradient) in the *P. pacificus* strains with different variants of *eud-1* alternative start codons (lower left panel). Bars represent the mean value and error bars represent SD ($n = 3$ biological replicates). **e,** Quantification of *eud-1* mRNA abundance in RSN001 wild type (WT) and in-frame methionine mutants using qPCR. *eud-1* mRNA levels were normalized to *sult-8* mRNA levels. Bars represent the mean value and error bars represent standard deviation (SD) ($n = 3$ biological replicates). **f,** Scoring of Eu animals in RSN001 following artificial reintroduction of a Met in the background of EUD-1 M1A, M14A mutants (**a**) at the second or fifteenth amino acid (M1A, M14A, G2M or M1A, M14A, T15M). Boxplots show the median (centre line), interquartile range (IQR; box), and whiskers extending to 1.5×IQR of mouth-form ratio ($n = 30$ replicates). **a,b,d–f** Additional mutant information is shown in Supplementary Table 2. Statistical significance in **a**,**f** and **d,e** was assessed by Kruskal–Wallis test and the post-hoc Dunn's test with a Holm–Bonferroni method and one-way analysis of variance (ANOVA) and the post-hoc Dunnett's test, respectively. Significance levels are indicated as ****$p < 0.0001$; ***$p < 0.001$; **$p < 0.01$; * $p < 0.05$; ns (not significant) $p > 0.05$. Source data are provided as a Source Data file.

Fig. 5 N-terminal EUD-1 proteoforms are synthesised in pharyngeal (head) sensory neurons of *P. pacificus* animals. a, Graph depicts the percentage of Eu animals in wild type and *eud-1* CRISPR-engineered (M1A, M14A, M1A M14A) *P. pacificus* PS312 strain. Boxplots show the median (centre line), interquartile range (IQR; box), and whiskers extending to 1.5×IQR of mouth-form ratio ($n = 30$ replicates). Statistical significance was assessed by Kruskal–Wallis test and the post-hoc Dunn's test with a Holm–Bonferroni method. Significance levels are indicated as ****$p < 0.0001$; ***$p < 0.001$; **$p < 0.01$; * $p < 0.05$; ns (not significant) $p > 0.05$. Source data are provided as a Source Data file. **b,** Representative fluorescent confocal images of the pharyngeal head region of fixed adult *P. pacificus* PS312 wild type (WT), and both alleles (#1 and #2) of EUD-1 M1A and M14A mutant animals. These strains have a C-terminal ALFA tagged version of EUD-1. All animals were stained with anti-ALFA nanobody coupled with AZDye568 fluorophore. Merged pictures depict the anti-ALFA signal in green and the nuclei (DAPI) in purple. Arrows indicate the anterior end of the animals. Scale bars: 10 µm. Additional mutant information is shown in Supplementary Table 2.

Fig. 6 Alternative N-terminal EUD-1 proteoforms are common in *P. pacificus* sulfatases. a, Sequence alignment of the N-terminal regions of the human arylsulfatases ARSJ (Q5FYB0), GALNS (P34059, N-acetylgalactosamine-6-sulfatase), ARSF (P54793), STS (P08842, steroid sulfatase), and ARSL long (F5GYY5) and short (A0A5F9ZHZ5) isoforms, and *P. pacificus* (PRIPA) SUL-2 sulfatases EUD-1 (A0A2ABJD3) and PPA21290 (SUL-2, A0A2A6B6N0) performed with ESPript 3.0. Identical residues are identified in red columns and printed in white whereas similar residues are shown in red. The signal peptide (SP) amino acid sequence for each sulfatase is highlighted by a purple box. Methionine (M) residues are indicated in purple squares. The active site of the enzymes is also indicated. **b,c,** Prediction of signal peptides (n-, h- and c- regions) and cleavage sites (CS) using SignalP 6.0 in the N-terminal proteoforms of EUD-1 (**b**) and PPA21290 (**c**) SUL-2 nematode sulfatases. Δx denotes the predicted proteoform starting from Mx+1. Likelihood values for each prediction are denoted below each graph.

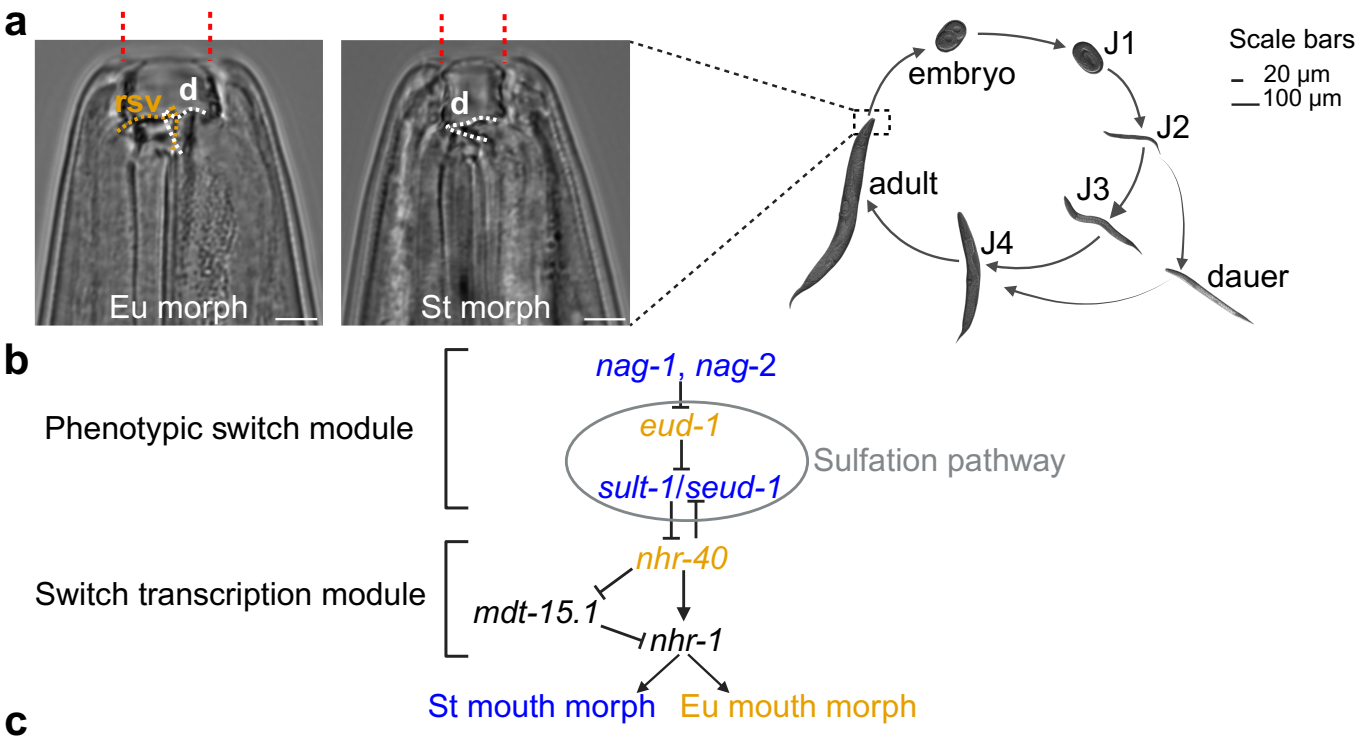
Fig. 7 Alternative N-terminal EUD-1 proteoforms are common in eukaryotic sulfatases. a-f, Analysis of SP and cleavage sites following alternative start site usage in human sulfatases using SignalP 6.0. Proteins are as follow: (**a**) steroid sulfatase (STS, P08842, A0A590UJL0), (**b**) ARSJ (Q5FYB0), (**c**) GALNS (P34059, N-acetylgalactosamine-6-

bioRxiv preprint doi: https://doi.org/10.64898/2026.03.27.714762; this version posted March 27, 2026. The copyright holder for this preprint (which was not certified by peer review) is the author/funder, who has granted bioRxiv a license to display the preprint in perpetuity. It is made available under aCC-BY-NC 4.0 International license.

sulfatase), (**d**) ARSF (P54793), (**e**) ARSL short isoform (A0A5F9ZHZ5) and (**f**) ARSL long isoform (F5GYY5). Δx denotes the predicted proteoform starting from Mx+1. Likelihood values for each prediction are denoted below each graph.

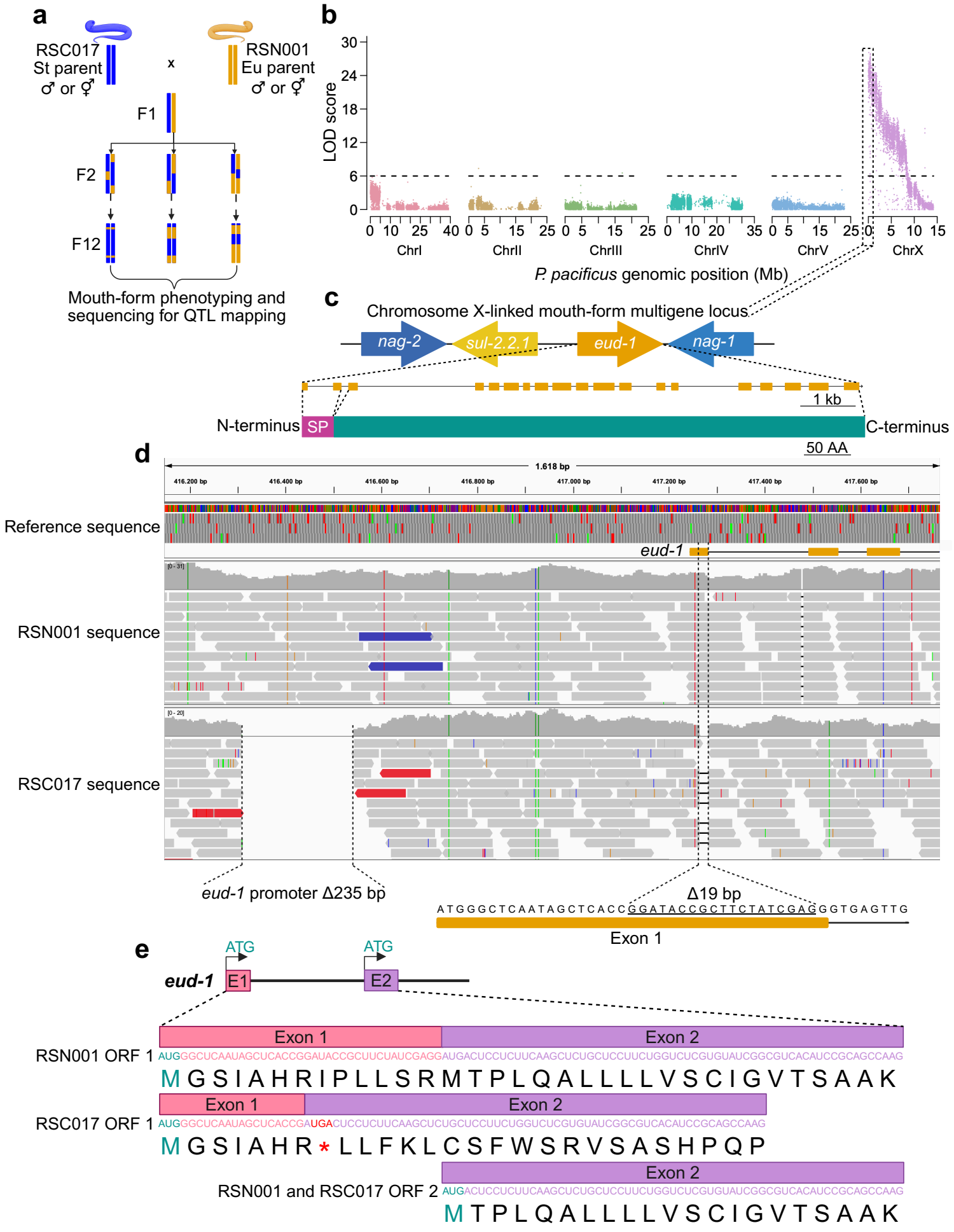
bioRxiv preprint doi: https://doi.org/10.64898/2026.03.27.714762; this version posted March 27, 2026. The copyright holder for this preprint (which was not certified by peer review) is the author/funder, who has granted bioRxiv a license to display the preprint in perpetuity. It is made available under aCC-BY-NC 4.0 International license.

Fig. 1



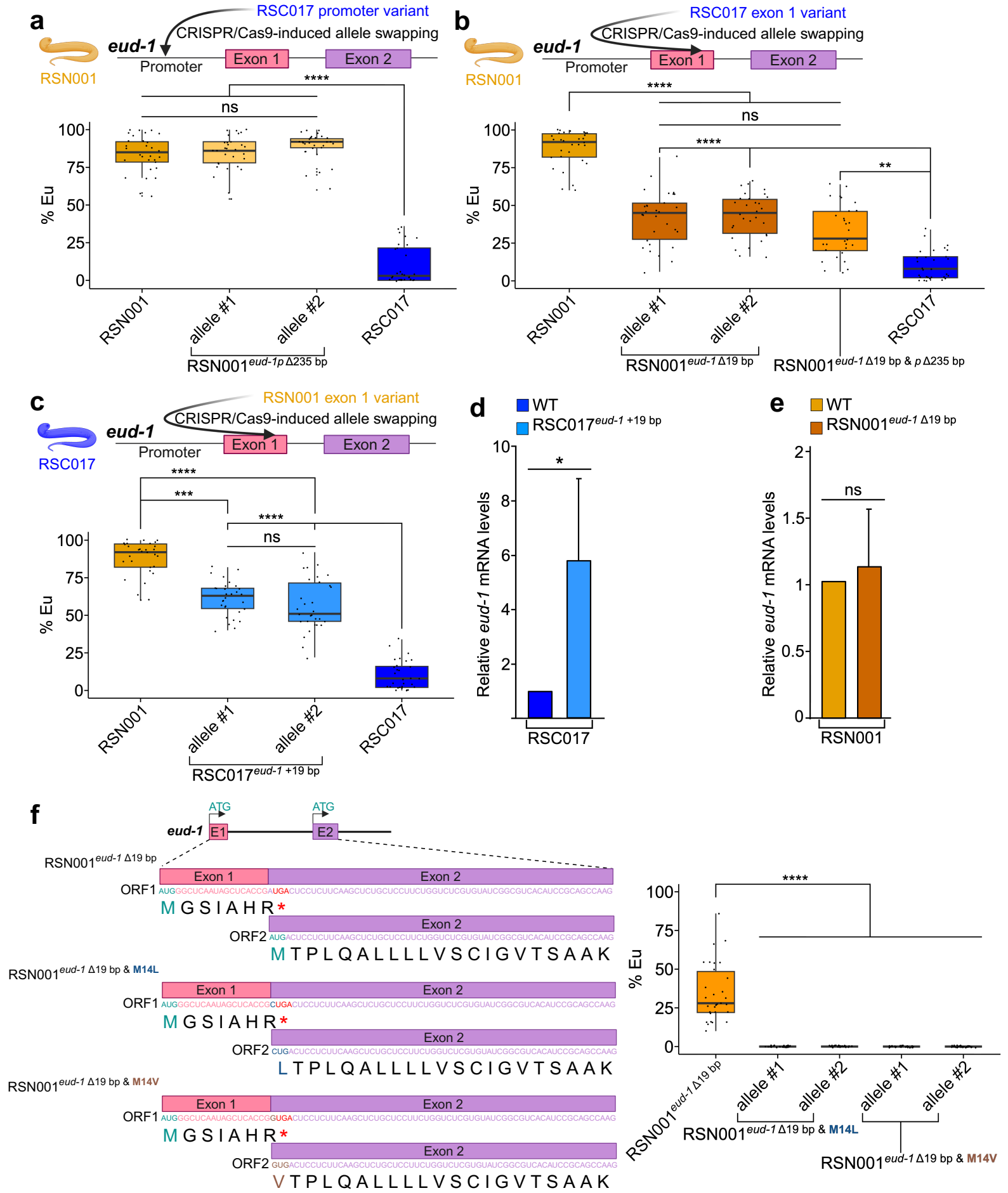
bioRxiv preprint doi: https://doi.org/10.64898/2026.03.27.714762; this version posted March 27, 2026. The copyright holder for this preprint (which was not certified by peer review) is the author/funder, who has granted bioRxiv a license to display the preprint in perpetuity. It is made available under aCC-BY-NC 4.0 International license.

Fig. 2



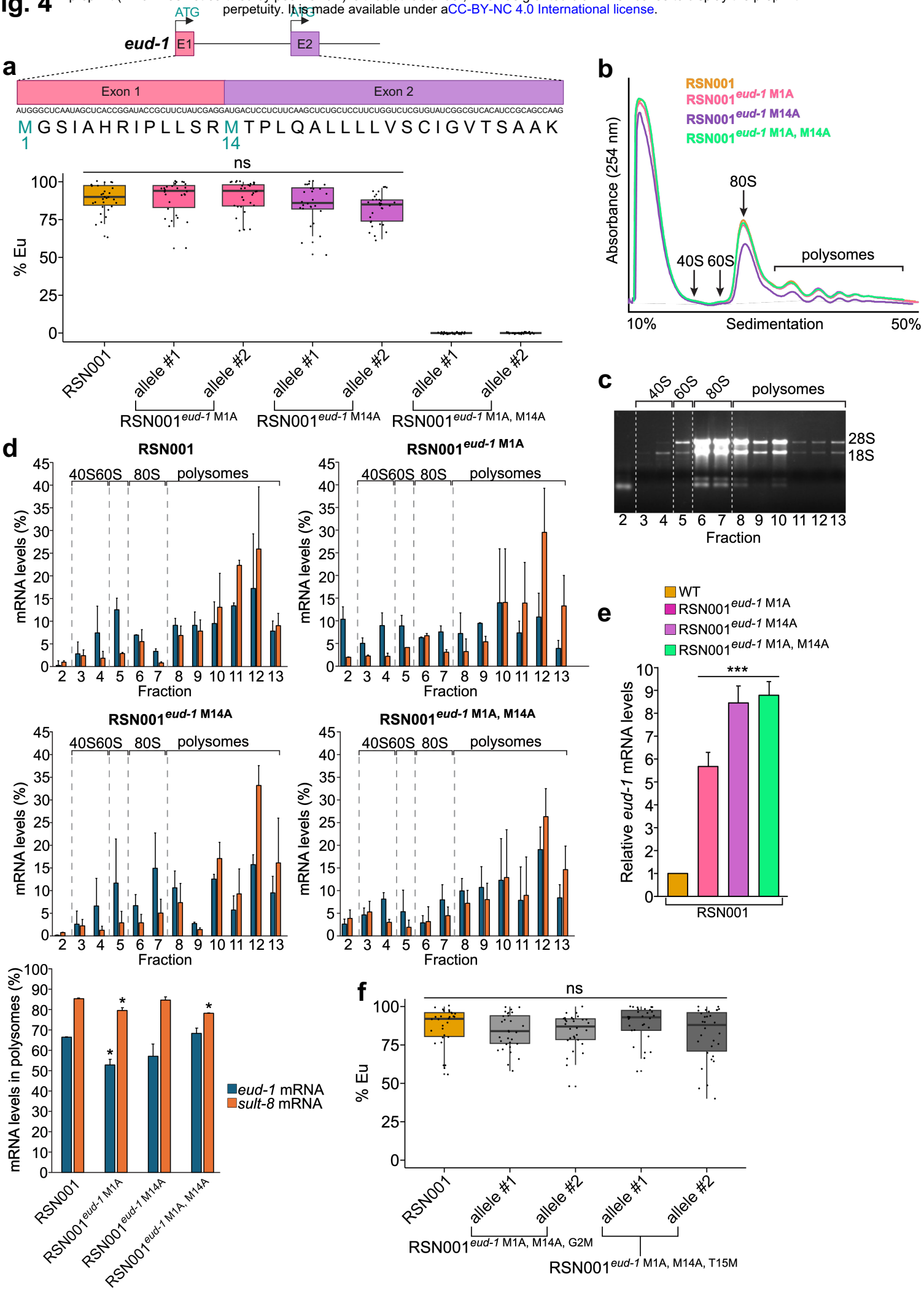
bioRxiv preprint doi: https://doi.org/10.64898/2026.03.27.714762; this version posted March 27, 2026. The copyright holder for this preprint (which was not certified by peer review) is the author/funder, who has granted bioRxiv a license to display the preprint in perpetuity. It is made available under aCC-BY-NC 4.0 International license.

Fig. 3



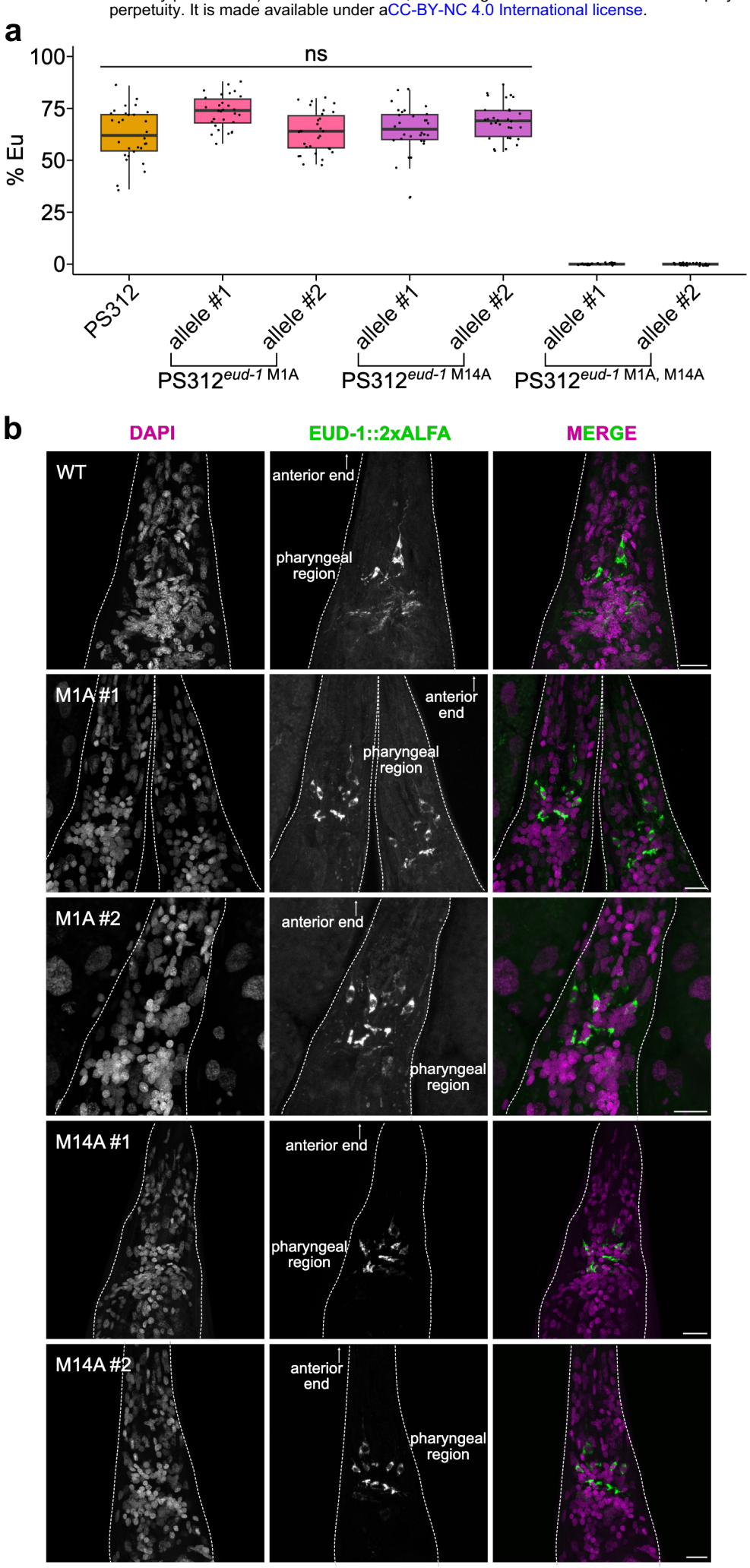
bioRxiv preprint doi: https://doi.org/10.64898/2026.03.27.714762; this version posted March 27, 2026. The copyright holder for this preprint (which was not certified by peer review) is the author/funder, who has granted bioRxiv a license to display the preprint in perpetuity. It is made available under aCC-BY-NC 4.0 International license.

Fig. 4



bioRxiv preprint doi: https://doi.org/10.64898/2026.03.27.714762; this version posted March 27, 2026. The copyright holder for this preprint (which was not certified by peer review) is the author/funder, who has granted bioRxiv a license to display the preprint in perpetuity. It is made available under aCC-BY-NC 4.0 International license.

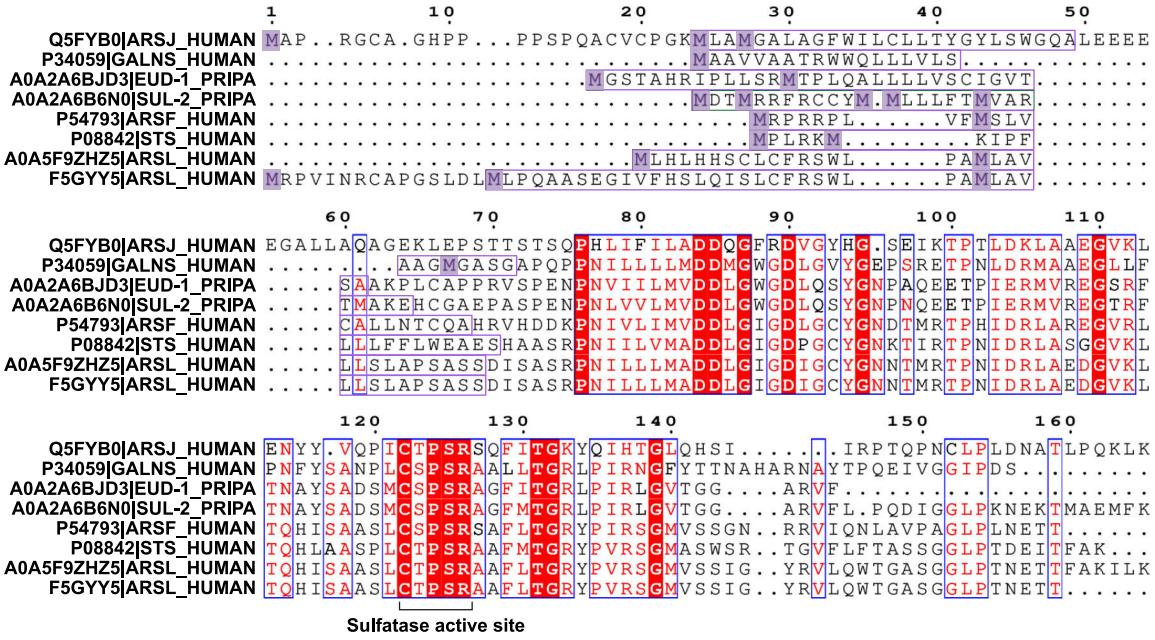
Fig. 5



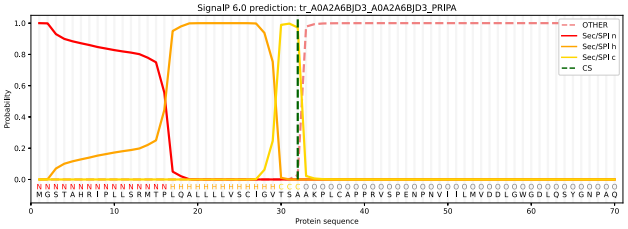
bioRxiv preprint doi: https://doi.org/10.64898/2026.03.27.714762; this version posted March 27, 2026. The copyright holder for this preprint (which was not certified by peer review) is the author/funder, who has granted bioRxiv a license to display the preprint in perpetuity. It is made available under aCC-BY-NC 4.0 International license.

Fig. 6

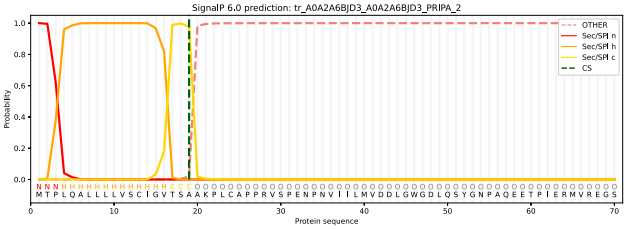
a



b EUD-1

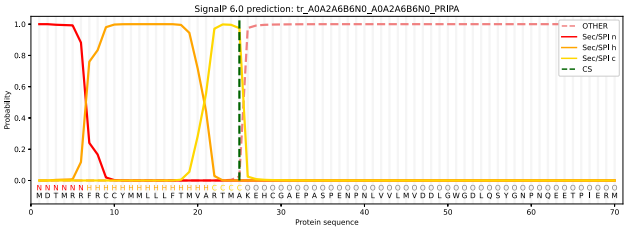


EUD-1_PRIPA - likelihood SP: 0.9991

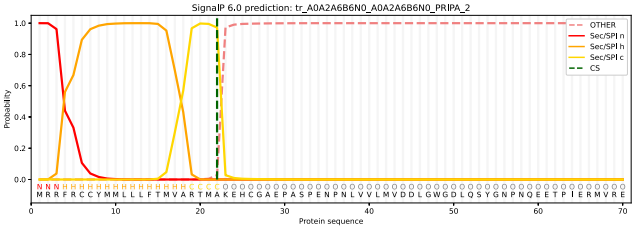


EUD-1_PRIPA Δ13- likelihood SP: 0.9992

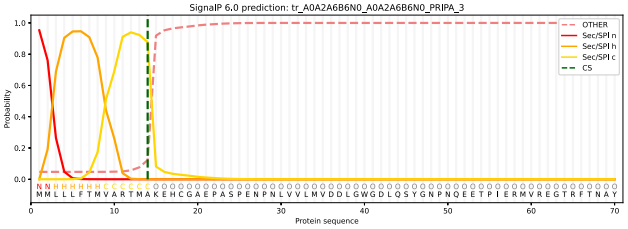
C SUL-2 (PPA21290/A0A2A6B6N0)



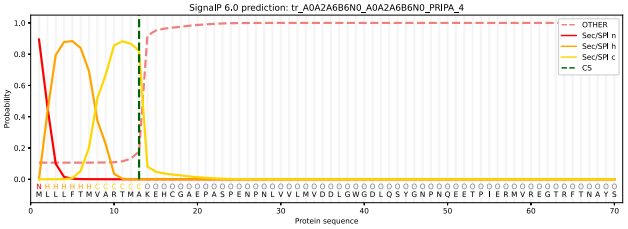
SUL-2_PRIPA - likelihood SP: 0.9991



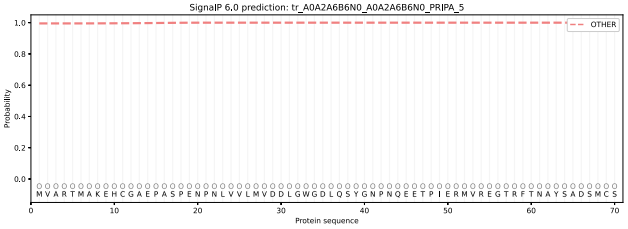
SUL-2_PRIPA Δ3 - likelihood SP: 0.9989



SUL-2_PRIPA Δ11 - likelihood SP: 0.9493



SUL-2_PRIPA Δ12 - likelihood SP: 0.8897

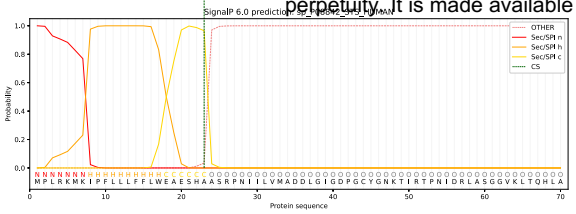


SUL-2_PRIPA Δ18 - likelihood SP: 0.004

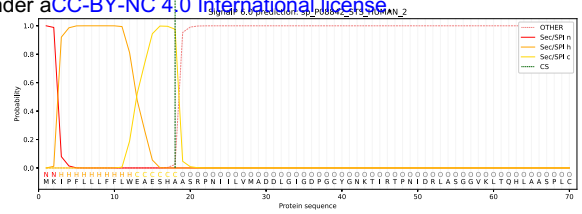
bioRxiv preprint doi: https://doi.org/10.64898/2026.03.27.714762; this version posted March 27, 2026. The copyright holder for this preprint (which was not certified by peer review) is the author/funder, who has granted bioRxiv a license to display the preprint in perpetuity. It is made available under aCC-BY-NC 4.0 International license.

Fig. 7

a STS (P08842 and A0A5F9ZHZ5)

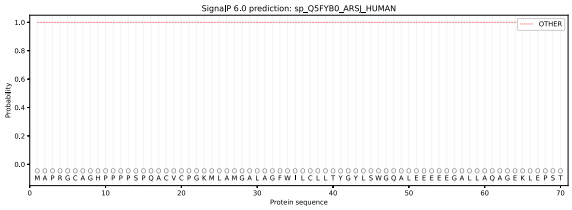


STS_HUMAN - likelihood SP: 0.9991

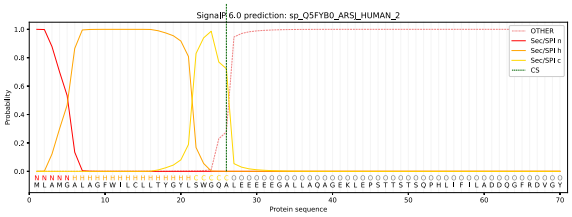


STS_HUMAN Δ5 - likelihood SP: 0.9992

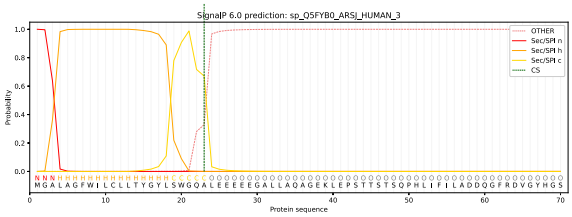
b ARSJ (Q5FYB0)



ARSJ_HUMAN - likelihood SP: 0

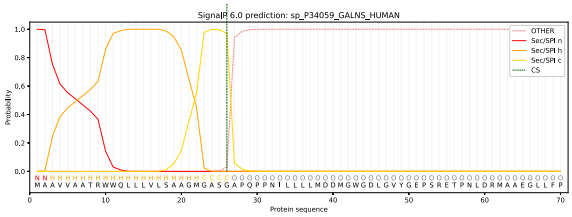


ARSJ_HUMAN Δ23 - likelihood SP: 0.9985

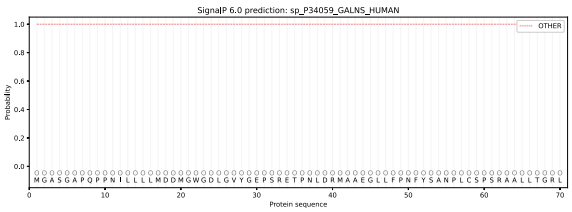


ARSJ_HUMAN Δ26 - likelihood SP: 0.9992

c GALNS (P34059)

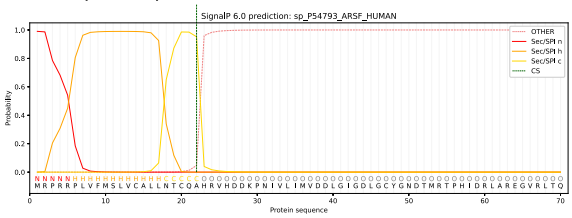


GALNS_HUMAN - likelihood SP: 0.9991

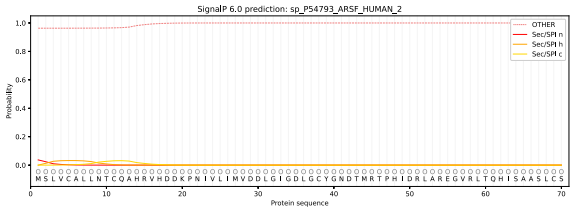


GALNS_HUMAN Δ21- likelihood SP:0

d ARSF (P54793)

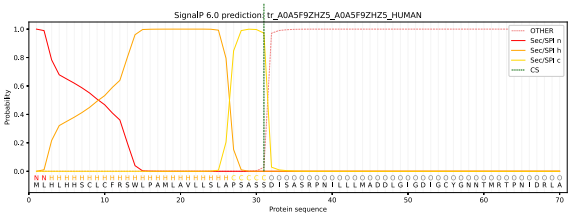


ARSF_HUMAN - likelihood SP: 0.9879

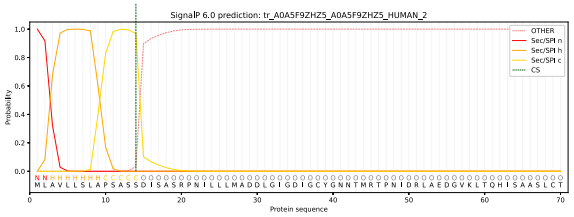


ARSF_HUMAN Δ9 - likelihood SP: 0.034

e ARSL - short isoform (A0A5F9ZHZ5)

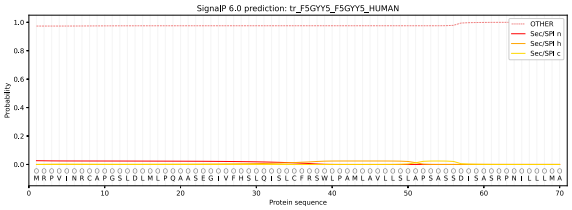


ARSL_HUMAN - likelihood SP: 0.9999

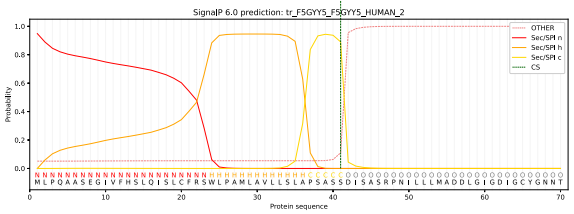


ARSL_HUMAN - likelihood SP: 0.9987

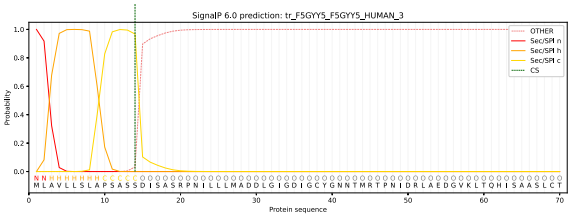
f ARSL - long isoform (F5GYY5)



ARSL_HUMAN - likelihood SP: 0.0001

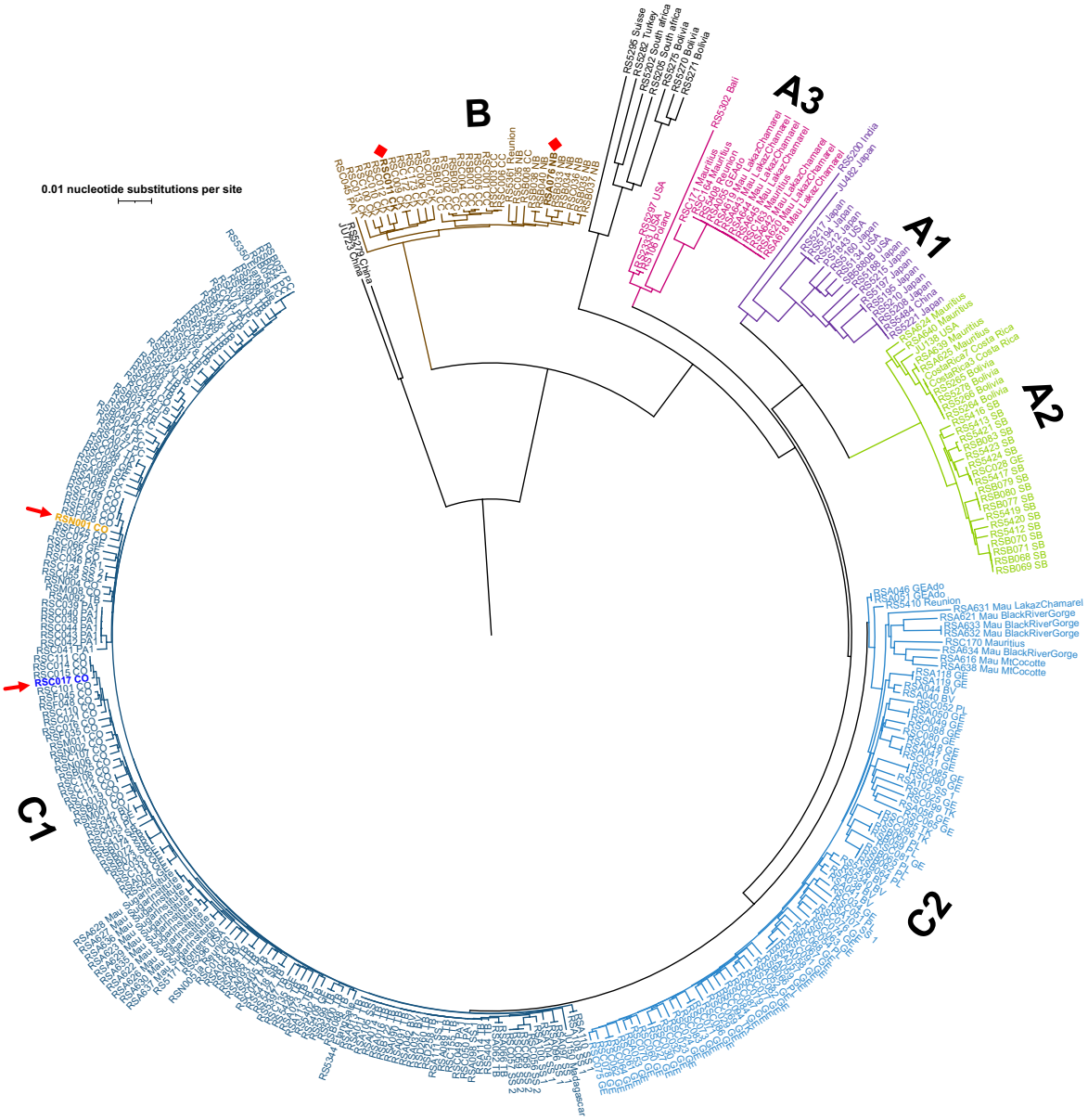


ARSL_HUMAN Δ15- likelihood SP: 0.9458

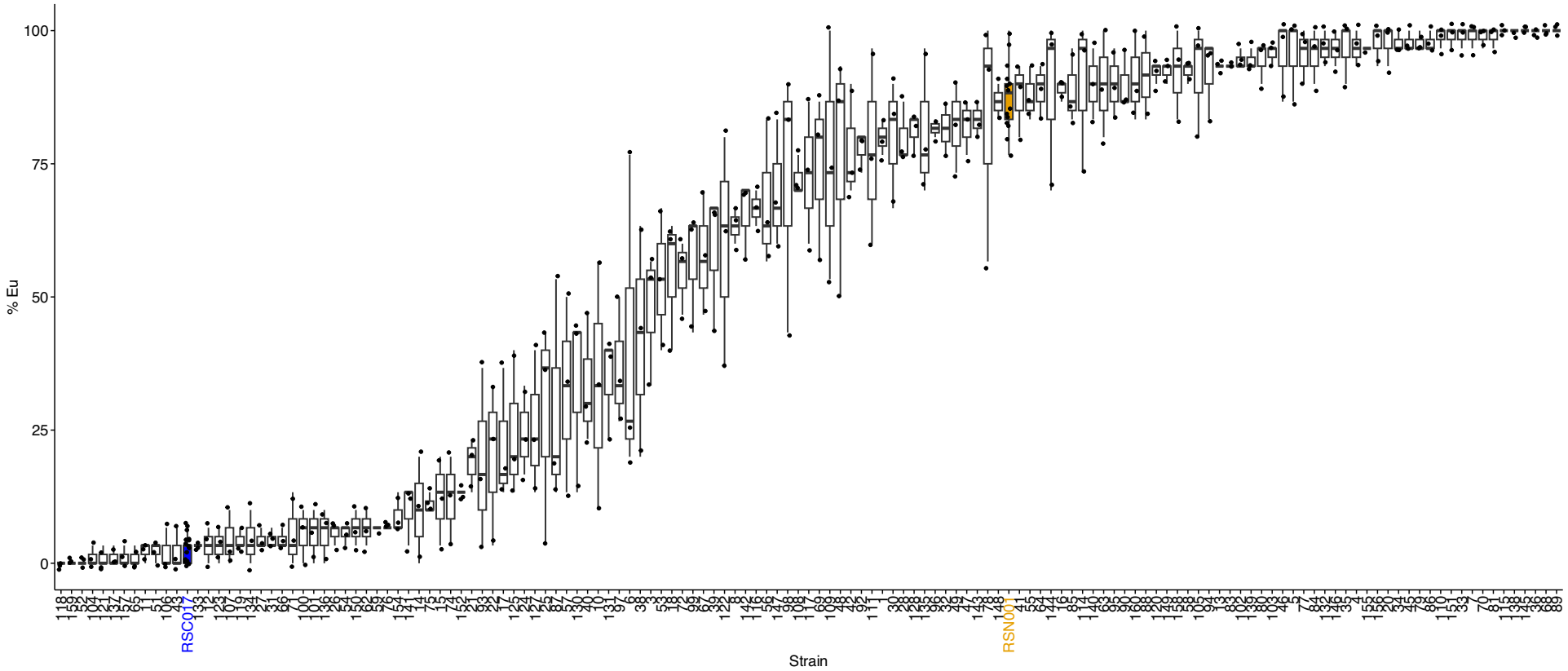


ARSL_HUMAN Δ42- likelihood SP: 0.9987

bioRxiv preprint doi: https://doi.org/10.64898/2026.03.27.714762; this version posted March 27, 2026. The copyright holder for this preprint (which was not certified by peer review) is the author/funder, who has granted bioRxiv a license to display the preprint in perpetuity. It is made available under aCC-BY-NC 4.0 International license.

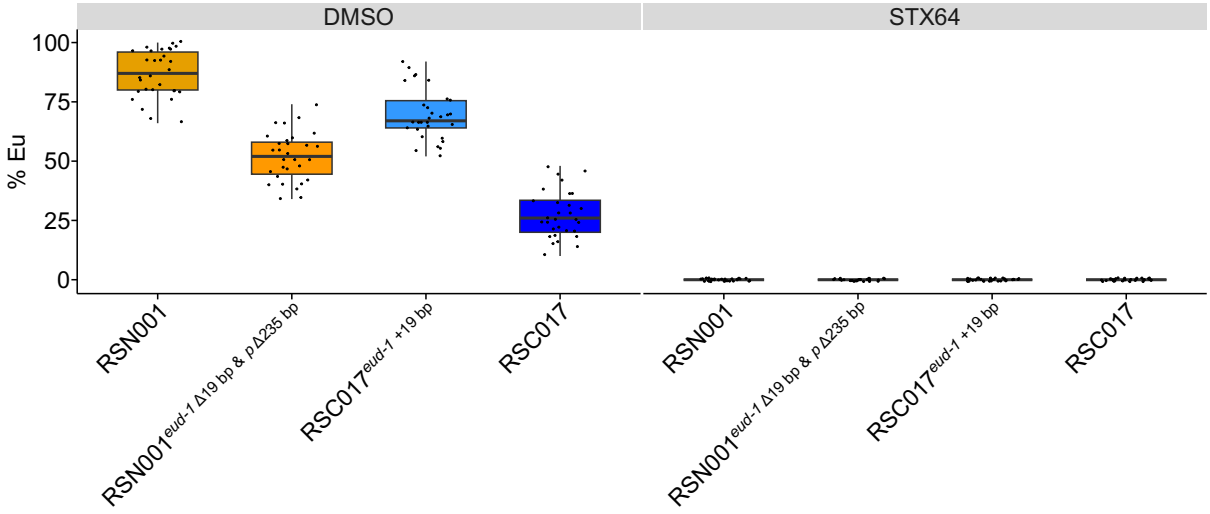


Suppl. Fig. 1 RSC017 and RSN001 strains are closely related. Both *Adoretus*-derived strains (indicated by red arrows) belong to the C1 clade of *P. pacificus* worldwide genotypes. *P pacificus* strains isolated from *Amneidus godefroyi* beetles and used in an earlier study[1] (indicated by red diamonds) belong to a separate clade: clade B. Scale bar: 0.01 nucleotide substitutions per site. *P. pacificus* clades follow an earlier nomenclature in Rödelsperger et al[2].



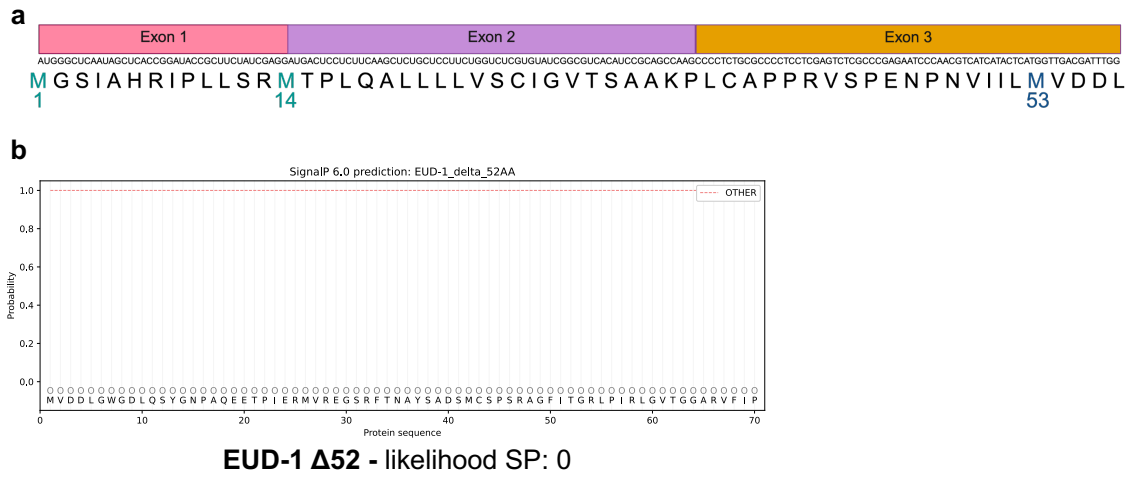
Suppl. Fig. 2 Mouth-form phenotype of RILs and the parental strains RSC017 (St-biased) and RSN001 (Eu-biased). Graph depicts the percentage of Eu animals in the different RILs, RSC017 (in blue) and RSN001 (in orange). Boxplots show the median (centre line), interquartile range (IQR; box), and whiskers extending to 1.5×IQR of mouth-form ratio. Source data are provided as a Source Data file.

bioRxiv preprint doi: https://doi.org/10.64898/2026.03.27.714762; this version posted March 27, 2026. The copyright holder for this preprint (which was not certified by peer review) is the author/funder, who has granted bioRxiv a license to display the preprint in perpetuity. It is made available under aCC-BY-NC 4.0 International license.



Suppl. Fig. 3 Eu morph in Δ19 bp nonsense variants in exon 1 of *eud-1* relies on EUD-1/sulfatase activity. Quantification of Eu animals in wild type and CRISPR-engineered *eud-1* variants in the absence and presence of the steroid sulfatase inhibitor STX64 (n = 30 replicates). Boxplots show the median (centre line), interquartile range (IQR; box), and whiskers extending to 1.5×IQR of mouth-form ratio. Source data are provided as a Source Data file.

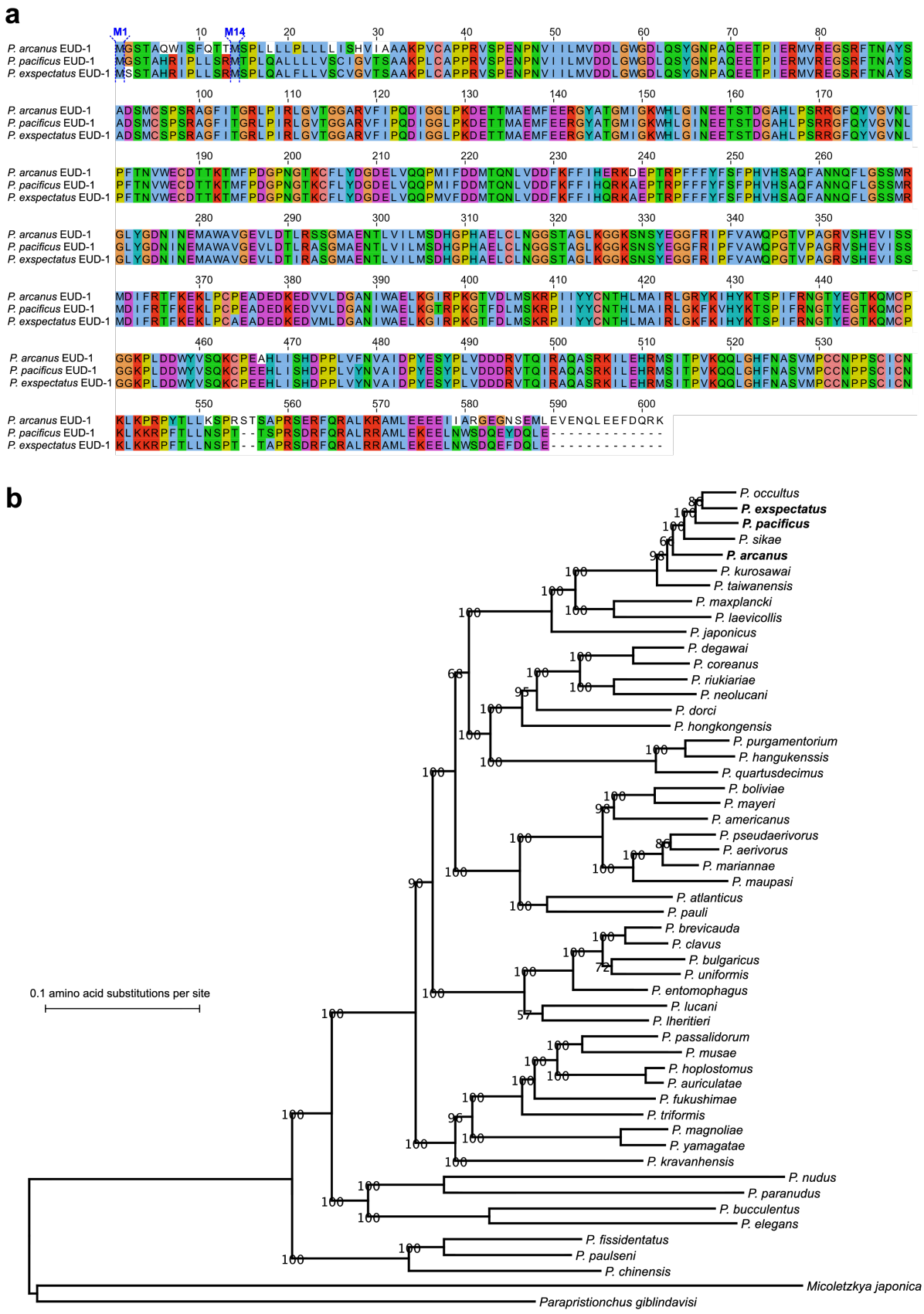
bioRxiv preprint doi: https://doi.org/10.64898/2026.03.27.714762; this version posted March 27, 2026. The copyright holder for this preprint (which was not certified by peer review) is the author/funder, who has granted bioRxiv a license to display the preprint in perpetuity. It is made available under aCC-BY-NC 4.0 International license.



EUD-1 Δ52 - likelihood SP: 0

Suppl. Fig. 4 *eud-1* exons 1 and 2 encode a signal peptide. a, Schematic representation of *eud-1* exons 1-3 nucleotide and amino acid sequences. Three in-frame Met are present in the first three exons: M1, M14 and M53. **b,** Prediction of signal peptide of a EUD-1 protein lacking the first 52 amino acids using SignalP 6.0. Likelihood value for the prediction is denoted below the graph.

bioRxiv preprint doi: https://doi.org/10.64898/2026.03.27.714762; this version posted March 27, 2026. The copyright holder for this preprint (which was not certified by peer review) is the author/funder, who has granted bioRxiv a license to display the preprint in perpetuity. It is made available under aCC-BY-NC 4.0 International license.



Suppl. Fig. 5 EUD-1 N-terminal proteoforms are present in other *Pristionchus* species. a, Alignment of EUD-1 protein sequences across three *Pristionchus* species, *P. pacificus*, *P. arcanus* and *P. exspectatus* highlighting the conservation of M1 and M14 (in blue). **b,**

bioRxiv preprint doi: https://doi.org/10.64898/2026.03.27.714762; this version posted March 27, 2026. The copyright holder for this preprint (which was not certified by peer review) is the author/funder, who has granted bioRxiv a license to display the preprint in perpetuity. It is made available under aCC-BY-NC 4.0 International license.

Phylogenetic relationships among *Pristionchus* congeners. *P. pacificus*, *P. arcanus* and *P. exspectatus* are highlighted in bold. Phylogenetic reconstruction adapted from Theam et al[3]. Scale bar: 0.1 amino acid substitutions per site.

bioRxiv preprint doi: https://doi.org/10.64898/2026.03.27.714762; this version posted March 27, 2026. The copyright holder for this preprint (which was not certified by peer review) is the author/funder, who has granted bioRxiv a license to display the preprint in perpetuity. It is made available under aCC-BY-NC 4.0 International license.

References

1. Dardiry, M. et al. Divergent combinations of *cis*-regulatory elements control the evolution of phenotypic plasticity. *PLoS Biol.* **21**, e3002270 (2023).
2. Rödelsperger, C. et al. Single-molecule sequencing reveals the chromosome-scale genomic architecture of the nematode model organism *Pristionchus pacificus*. *Cell Rep.* **21**, 834–844 (2017).
3. Theam, P. et al. *Pristionchus kravanhensis* n. sp., the first *Pristionchus* species reported from Cambodia. *Nematology* **27**, 651–663 (2025).